

Research Article

An Empirical Algorithm using Derivative Difference for Estimating Chlorophyll-A in Case-II Water

P. Murugan^{1,2}, R. Sivakumar¹, Savithri Bhat³

¹Department of Civil Engineering, SRM University, Kattankulathur, Tamilnadu, India

²ISRO Satellite Centre, Bangalore, India

³Department of Biotechnology, BMS College of Engineering, Bangalore

Correspondence should be addressed to P. Murugan, mu@isac.gov.in

Publication Date: 21 December 2019

DOI: <https://doi.org/10.23953/cloud.ijarsg.444>

Copyright © 2020. P. Murugan, R. Sivakumar, Savithri Bhat. This is an open access article distributed under the **Creative Commons Attribution License**, which permits unrestricted use, distribution, and reproduction in any medium, provided the original work is properly cited.

Abstract Water quality management includes measurement of quantity and quality. The abundance of phytoplankton in water body represents the physical condition and chemical constituents. As Chlorophyll-a exists in all types of phytoplankton, naturally the choice for water quality measurement is estimation of Chl-a concentration. The Chl-a concentration is estimated using various spectral reflectance algorithms such as single band regression, band ratio, three-band ratio, four-band ratio etc have been developed and is being used. Subsequently, the first order derivative ratio and second order derivative ratio methods are also used in some studies. Though such algorithms provide water quality measures, new algorithms are being introduced to improve estimation accuracy. In this paper, a new algorithm 'Derivative Difference' is proposed. It is based on the Chlorophyll concentration variation with shape of reflectance spectrum. The derivative data represents the slope of the reflectance data at different wavelength. The difference in derivative values at selected two different wavelengths were correlated with measured values to estimate Chl-a concentration. Obtained results were compared with the values obtained from band ratio method and derivative ratio methods. The algorithm is found to be better in some conditions.

Keywords *Remote sensing; Chlorophyll-a; Derivative; Spectroradiometer; Hyperspectral*

1. Introduction

The deterioration of water quality of inland water bodies is a serious ecological and social problem as they are the water resources for drinking, domestic, agricultural and industrial purposes. Management of quality of water bodies is essential to provide water to the ever increasing population and changing lifestyle. Water management activities usually include protecting water bodies from polluting elements, saving water and distributing it without wastage, i.e. managing the quality and quantity of water. While quantity management is maintaining capacity of water body by preventing encroachment and sedimentation, quality management is controlling the physical, chemical and bio-objects within the specified limit to enable usability of the water.

As the abundance of Chl-a content represents the physical and chemical characteristics of the water, Chlorophyll-a (Chl-a) concentration is a major indicator of eutrophic status and water quality (Moses et

al., 2009). In case of ocean water (Case-I), the reflectance is dominated by the chlorophyll and the variation of reflectance can be attributed to the Phytoplankton abundance variation only. In contrast, the reflectance of in-land water (Case-II) is considerably affected by the optical properties of inorganic suspended matter and Colored Dissolved Organic Matter (CDOM). Hence the algorithms with blue-green bands used in case-I water is not suitable to case-II water. As CDOM absorption and particulate scattering decrease with increase in wavelength and become negligible in Red-infrared region, Red and Near Infrared (NIR) spectral region is extensively used to estimate Chl-a in Case-II water (Yu et al., 2014). As the physical and chemical components vary from lake to lake, the spectral bands suitable to measure the Chl-a for a particular lake may not suit to another lake. For every lake, suitable spectral bands are to be selected by comparing the estimated values from spectral bands combinations with laboratory-measured values.

The conventional method of quantifying Chl-a measurement is collecting samples from different locations of water body and measuring the chlorophyll-a concentration using spectrophotometer. This method needs field sampling, usage of chemical etc, which are time consuming, so difficult to perform for large area water bodies. Measuring certain optical properties like reflectance in different wavelength provides the concentration of the chlorophyll instantly. The spectral reflectance methods are used to estimate Chl-a in Aerial, Satellite and in situ measurements. The aerial surveys collect the spectral reflectance of the water bodies of small area and study the relation between reflectance spectrum with the chlorophyll-a. The satellite remote sensing provides a near real time, large scale and spatially continuous data in fixed time frequency, at less cost.

Many algorithms are developed to estimate the abundance of these constituents in water bodies like ocean, coastal, lakes and rivers based on spectral reflectance. The Chl-a estimation algorithms can be divided into two different categories: (i) Multiband models in the forms of ratios of different band combinations which utilizes the absorption bands of Chl-a in the red and NIR spectral region (Ruddick et al., 2001); and (ii) algorithms that use the Chl-a fluorescence emission around 685 nm (Gower et al., 1999).

The first group of algorithms are based on multispectral imaging. In this group, many algorithms have been developed using Red and NIR region spectral bands to estimate Chl-a concentration in eutrophic and turbid case II waters (Huang et al., 2014; Han et al., 2014). It covers single band, band ratio model (Hoge et al., 1987), three band models (Sathyendranath et al., 1989; Chen et al., 2013; Duan et al., 2010a, Tian et al., 2014), four band model (Le et al., 2009), five band model (Gohin et al., 2002), normalised differential chlorophyll index (NDCI) (Mishra and Mishra, 2012) etc. Some band ratio algorithms developed for the Chlorophyll estimation in terrestrial vegetation have also demonstrated in estimating Chl-a in water (Dall'Demo et al., 2003). As multispectral imageries are collected with less number of wide spectral bands, they cannot reflect minute variations like intensity variation in particular wavelength, intensity maximum shifting from wavelength to wavelength. As their output is integrated reflectance, change in reflectance with respect to narrow spectral bands is submerged in wider band.

The second group of algorithms are mainly based on Hyperspectral data, which provides almost continuous spectral measurements with hundreds of narrow spectral bands. They are: peak position near 700 nm (Gitelson, 1992); peak magnitude above baseline; area above baseline; first order derivative (Rundquist et al., 1996), second order derivative (Shi et al., 2007) and derivative ratio model (Tsai and Philpot, 1998) etc. Artificial neural network based algorithm (Chauhan et al., 2005), spectral decomposition method (Zhang et al., 2014), weighted algorithm (Yi, 2013), Spectral Vector Machine (SVM) based model (Sun et al., 2009) and three-band reflectance difference model (Duan et al., 2010b) are also used to estimate the chlorophyll-a concentration.

In this paper, a new algorithm called Derivative difference is introduced to estimate the Chl-a in Case-II water. The effectiveness of this algorithm in case-II water bodies is demonstrated using spectroradiometer data.

2. Materials and Methods

2.1. Methods

Among many factors affect the reflectance values of water, atmospheric absorption, CDOM, Organic Substance Sediments (OSS) are important. When we calculate the derivative values from reflectance, the effect of slowly changing factors with respect to wavelength such as atmosphere and CDOM are eliminated (Philpot, 1991). The derivative values provide the slope of reflective spectrum. These derivative values and derivative ratio values are used to estimate chlorophyll in many studies.

In the present study, as a new measure, the difference of derivative values at two different wavelengths has been used to estimate the chlorophyll-a. Obtained results are compared with the estimated values from both band ratio and derivative ratio methods. The estimated values obtained using this algorithm using spectroradiometer data were verified with measured values as well. Method, study area and results are described in following sections.

2.2. Study Area

The study area selected for this purpose is the Halasuru Lake, which is located at the heart of Bangalore city, India spread over the latitudes of $12^{\circ} 58' 41''$ N and $12^{\circ} 59' 15''$ N and longitudes of $77^{\circ} 36' 57''$ E and $77^{\circ} 37' 22''$ E, respectively. The area of the lake is approximately 125 Acres and is 930 m above the sea level. The depth of the lake varies from 3 m to 15 m and average depth of the lake is 5m. The main source of water to this lake is rainwater. It also receives direct industrial and domestic wastewaters from the surrounding area after aerated. The increased settlements near the lake is the cause for the pollution of the Lake. The satellite view of Halasuru Lake is shown in Figure 1.



Figure 1: View of Halasuru Lake, Bangalore

2.3. In-situ Reflectance Measurement using Spectroradiometer

In-situ measurements were carried out with spectro-radiometer at different locations of the lake. Sacchi disk measurement was also carried out to measure the Sacchi depth to avoid bathymetry

radiation. The depth of lake at sample collection locations was much more than the Sacchi depth. The specular reflection from the water was avoided by carrying out the fieldwork between 9.30 AM and 11.00 AM local time. The locations of sample collection in Halasuru Lake are marked and shown in Figure 1.

Hyperspectral reflectance was measured using Analytical Spectral Devices, Field spec Pro spectro-radiometer with a spectral resolution of one nm and the spectral range from 350 nm to 1800 nm. During the measurement, the instrument was held 0.6 m above the water surface manually, 0.5 m away from the boat and the probe was directed vertically down towards water. During the measurement at each location, sampling of the radiance was carried out for 25 times and the final output is produced after averaging these values. Five such outputs were collected at each location. The radiance plots from those outputs from same locations were compared and the datasets with large errors were rejected. Good data sets were averaged to generate final radiance data. This procedure was followed for measurement of water radiance and reference plate (Lambertian reflector) radiance as well. When radiance of reference plate was measured, the reference plate was kept parallel to the water surface in sun light and the measurement probe was held normal to the surface. The Latitude and Longitude of sample collection location were recorded from a GPS system output.

The remote sensing reflectance spectra $R_{rs}(\lambda)$, were calculated as (Rundquist 1996; Han, 1997).

$$R_{rs}(\lambda)_{meas} = \frac{L_w(\lambda)}{L_{cal}(\lambda)} * R_{cal}(\lambda) \times 100 \dots (1)$$

Where $L_w(\lambda)$ water leaving radiance, $L_{cal}(\lambda)$ scattered by reference plate and $R_{cal}(\lambda)$ reflectance of reference panel. At each sampling location, both water leaving radiance and reference radiance were measured without time gap.

2.4. Laboratory Measurements

Water samples were collected at a depth of 10 to 15 cm below the surface immediately after the reflectance measurements. Chl-a in the water was measured using the laboratory method (Jeffrey and Humbrey, 1975; Arar, 1997).

3. Analysis

3.1. Reflectance Spectra Analysis

As the reflectance variation due to Chl-a concentration is found to be between 350 to 800 nm and the absorption of radiation by water is more beyond 800 nm, hence spectro-radiometer data with wavelength between 350 and 800 nm was selected for study. The spectral reflectance of the samples collected from different locations is shown in Figure 2.

The reflectance spectra magnitudes in the region of 350 to 450 nm are low due to the high absorption of water in this region. The maximum absorption is seen at 440 nm. The reflectance spectra show a clear reflectance peak in the green region between 550 nm and 570 nm. After 570 nm the reflectance comes down steadily upto 630 nm and at 640 nm, an inflection is observed. The red absorption is peak around 670 nm. This is due to the combined effect of absorption of chlorophyll and water. After this, the reflection steadily increases up to the region around 705 nm (NIR) and this high reflectance is due to the fluorescence of chlorophyll-a (Neville and Gower, 1997). After this, the reflection decreases to the lowest level due to the absorption of water. Also, around 760 nm a small peak is seen in reflection spectra.

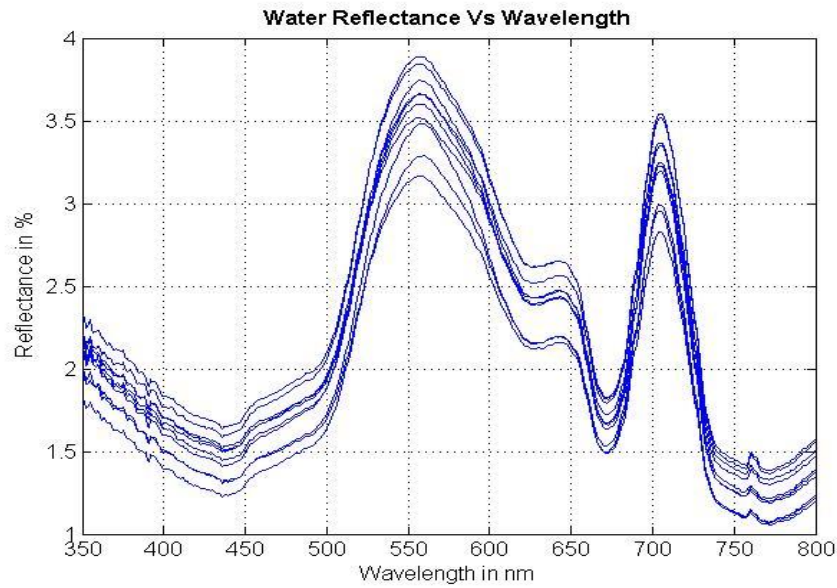


Figure 2: Reflectance spectra of all samples

3.2. Reflectance Band Ratio Methods

As the reflectivity in the NIR region R_{NIR} is due to the fluorescence of chlorophyll and is directly proportional to chlorophyll contents and the dip in reflectance in Red region R_{Red} is due to the absorption of Chl-a, and inversely proportional to reflectance in Red region, the Ratio R_{NIR}/R_{Red} will be directly proportional to the chlorophyll concentration. Hence, the ratio of NIR to Red reflectance will represent the chlorophyll-a concentration.

Table 1: Top ten-correlation values obtained using the reflectance band ratio method

	WL ₁	WL ₂	R ²
1	637	705	0.9042
2	637	703	0.9025
3	638	705	0.9017
4	637	702	0.9002
5	623	705	0.8995
6	637	706	0.8993
7	638	703	0.8981
8	629	709	0.8979
9	637	701	0.897
10	643	704	0.8957

3.3. First Order Derivative Values

The derivative values are calculated using following equation:

$$\text{Where, } R'_{\lambda n} = \frac{R_{\lambda n+1} - R_{\lambda n-1}}{\lambda(n+1) - \lambda(n-1)} \dots (2)$$

Where $R_{\lambda n+1}$, $R_{\lambda n-1}$ are the reflectance at $\lambda n+1$ and $\lambda n-1$. These values provide the change in reflection with respect to small change in wavelength (1 or 2 nm).

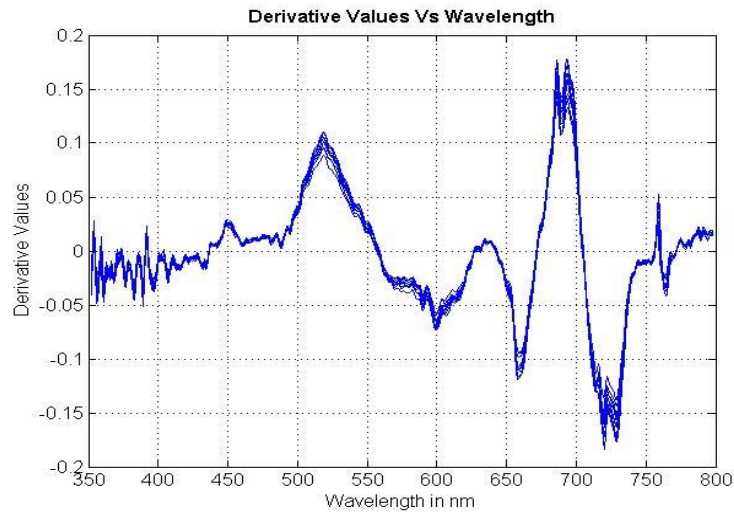


Figure 3: First order derivative data

Regression Analysis between Derivative Values and Chl-a

The derivative values of reflectance spectrums are correlated with measured chlorophyll values to estimate Chlorophyll-a (Huang et al., 2010). In this study, the derivative values are smoothed to reduce the noise and correlated with Chl-a values. The maximum correlation value 0.69 was found at wavelength of 678 nm. Smoothing was done with linear running mean filter with different window size. Following figure shows the derivative values smoothed by different window sizes.

Table 2: Top ten-correlation values obtained using derivative values

	Not smoothed		Smoothed with 1 x 3 windows		Smoothed with 1 x 5 windows		Smoothed with 1 x 7 windows	
	WI (nm)	R ²	WI (nm)	R ²	WI (nm)	R ²	WI (nm)	R ²
1	678	0.69	356	0.70	350	0.66	678	0.64
2	612	0.63	678	0.66	637	0.64	677	0.61
3	392	0.62	392	0.63	678	0.64	383	0.59
4	385	0.61	677	0.62	677	0.62	679	0.58
5	552	0.60	679	0.61	679	0.61	544	0.57
6	460	0.59	545	0.59	392	0.59	545	0.56
7	545	0.58	546	0.58	545	0.58	676	0.55
8	680	0.57	552	0.57	421	0.58	543	0.55
9	551	0.57	680	0.57	544	0.57	550	0.54
10	624	0.56	551	0.56	546	0.56	551	0.54

The maximum correlation value was achieved at 356 nm with 1 x 3 window smoothing. Many bands have shown better correlation in 678, 676nm range and 550-552 range. The R2 values are varying with the smoothing window size.

3.4. The First Order Derivative Ratio Method

The derivative ratio method combines the benefits of the ratio and derivative methods. In this method the ratio of first derivative at two different wavelengths is correlated with measured values of chlorophyll-a.

The ratio of first derivative can be computed as $P_{\lambda,mn} = R'_{\lambda,m} / R'_{\lambda,n} \dots (3)$

Where, $R'_{\lambda,n} = \frac{R_{\lambda,n+1} - R_{\lambda,n-1}}{\lambda(n+1) - \lambda(n-1)}$

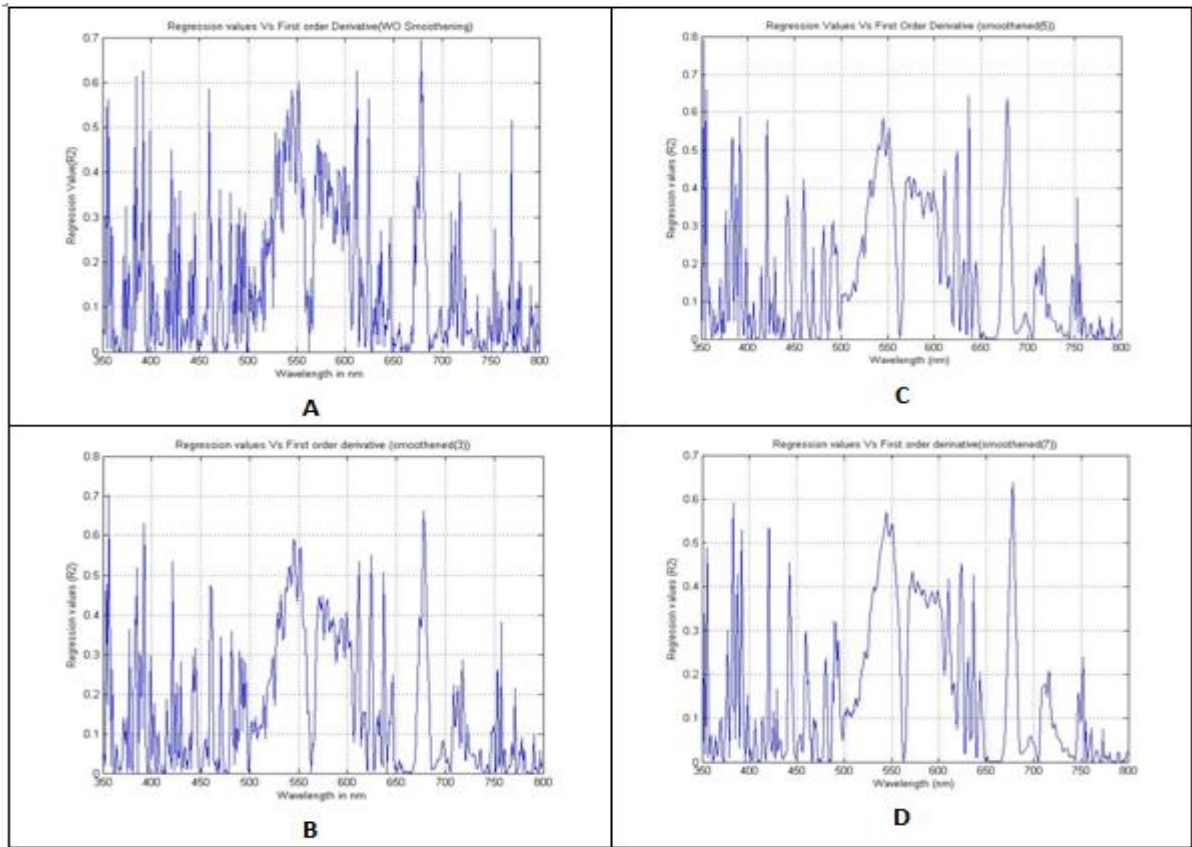


Figure 4: Correlation between first order derivative values and measured Chl-a values at different wavelengths: A-without smoothing; B, C & D are smoothed with 1 x 3, 1 x 5 and 1 x 7 window running linear mean filter

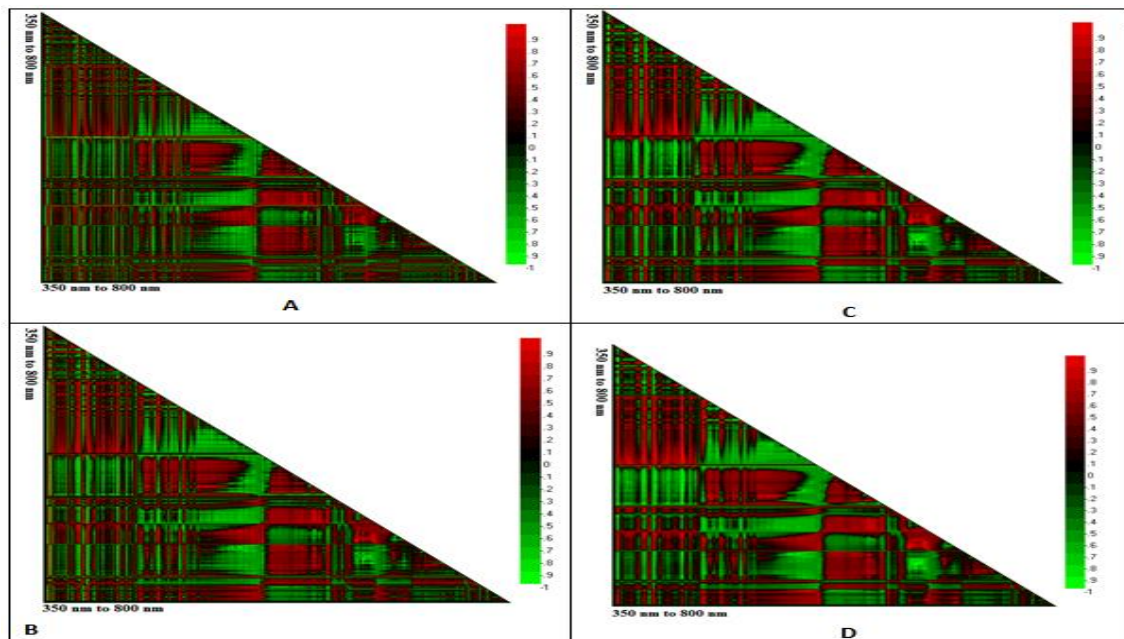


Figure 5: The correlation of ratio of first order derivative values with measured Chl-values at different wavelengths: A-without smoothing; B, C & D are smoothed with 3, 5 and 7 window running average algorithm

$P_{\lambda,m}$ is the ratio of first derivative, $R'_{\lambda,n}$ is the derivative at λ_n and $R'_{\lambda,m}$ is the derivative at λ_m . Computation of derivative, derivative ratio and regression between derivative ratio and the Chl-values were implemented in software. The correlation was calculated for all possible band combinations and results are presented in the Figure 5.

Table 3: Top ten-correlation values obtained using derivative ratio values

	Not smoothed			Smoothened with 1 x 3 values			Smoothened with 1 x 5 values			Smoothened with 1 x 7 values		
	B1	B2	R ²	B1	B2	R ²	B1	B2	R ²	B1	B2	R ²
1	460	473	0.9122	612	714	0.8925	421	460	0.9386	421	544	0.9667
2	460	486	0.8938	653	699	0.8885	356	376	0.9183	421	545	0.9645
3	612	715	0.8849	422	482	0.8823	421	539	0.8962	421	527	0.959
4	356	700	0.8778	356	796	0.8724	421	540	0.8923	420	545	0.959
5	356	703	0.8778	356	732	0.8506	653	696	0.8866	421	525	0.9559
6	612	683	0.8684	356	733	0.8481	421	611	0.8864	421	546	0.9553
7	356	649	0.8608	421	482	0.8398	421	749	0.8808	420	535	0.9495
8	356	758	0.8573	539	710	0.8374	421	543	0.8748	420	538	0.9487
9	356	720	0.8562	651	699	0.8323	355	615	0.8742	421	459	0.9399
10	666	735	0.8501	356	652	0.8317	421	546	0.8742	421	547	0.937

The high correlation was found with the wavelengths of 460 nm and 473 nm.

3.5. The Second Order Derivative Method

The higher order derivative methods for spectral analysis is proposed by Philpot (1991). The second order derivative values were used for chlorophyll estimation in many studies (Shi, 2007). The ratio of Second derivative is computed as

$$P_{\lambda,mn} = R''_{\lambda,m} / R''_{\lambda,n} \dots (4)$$

Where, $R''_{\lambda,n} = \frac{R'_{\lambda,n+1} - R'_{\lambda,n-1}}{\lambda(n+1) - \lambda(n-1)}$

$P_{\lambda,mn}$ is the ratio of second derivative, $R''_{\lambda,n}$ is the second derivative at λ_n and $R''_{\lambda,m}$ is the second derivative at λ_m . As the second order derivative values have noise and spikes, smoothing is recommended to get better results.

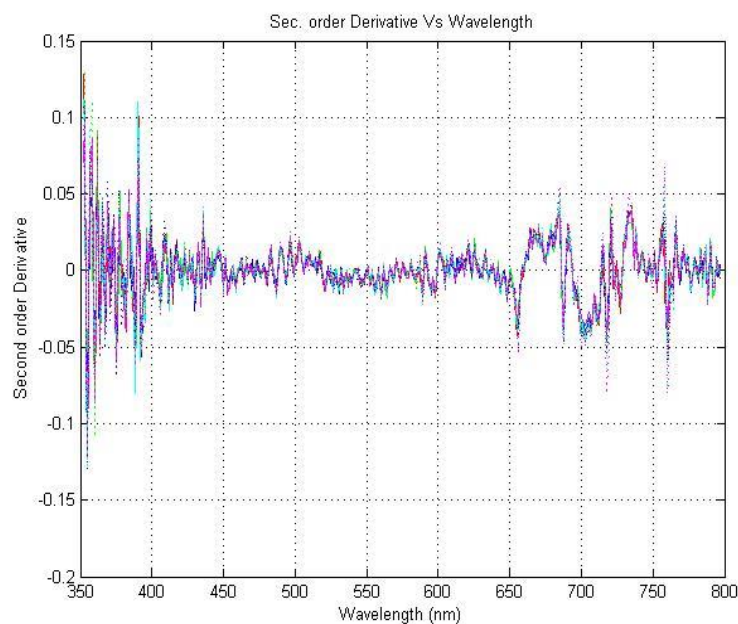


Figure 6: Second order derivative data

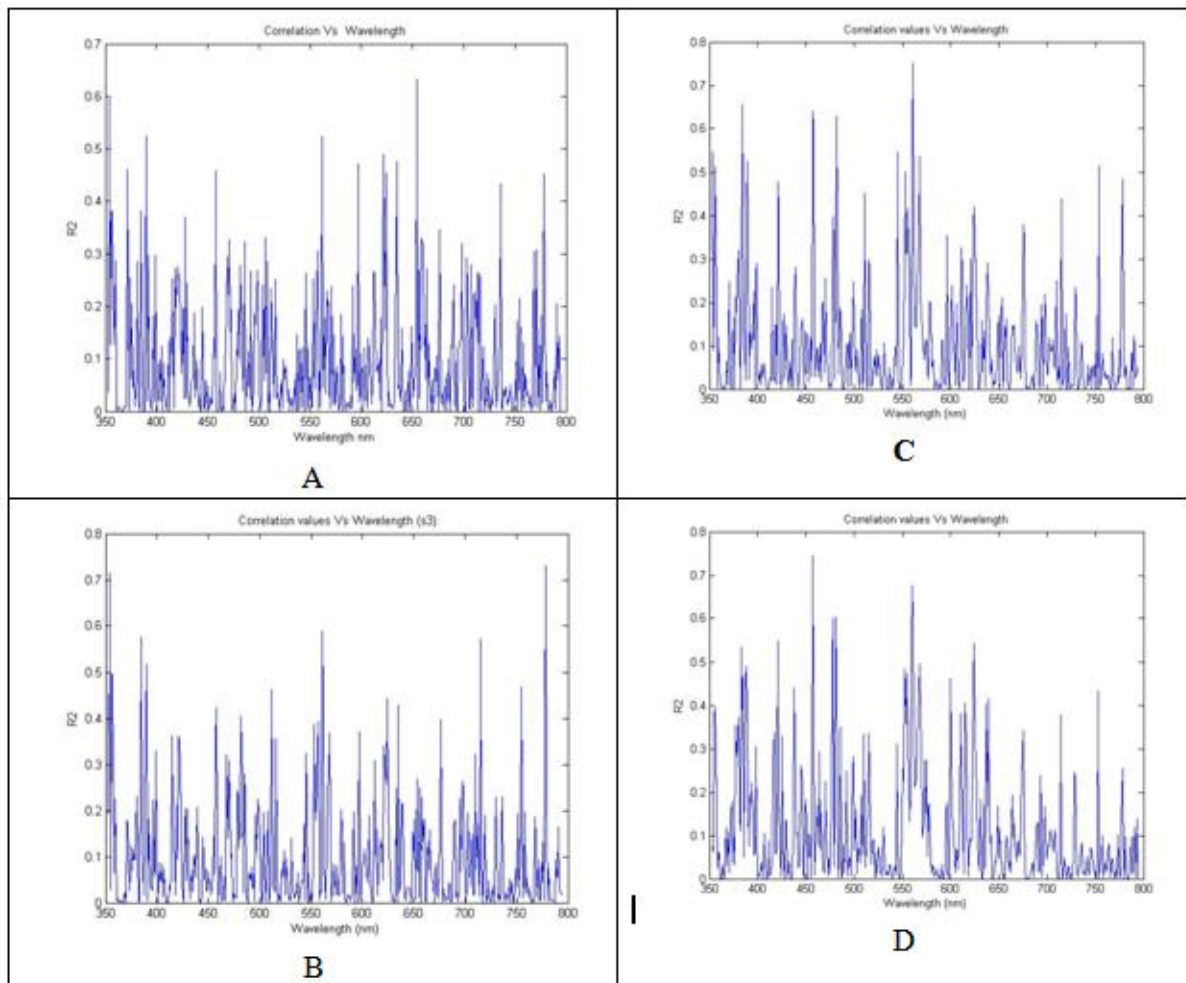


Figure 7: Correlation between second order derivative values and measured Chl-a values at different wavelengths: A-without smoothing; B, C & D are smoothed with 1 x 3, 1 x 5 and 1 x 7 window running linear mean filter

Table 4: The high correlation values with second order derivative values

	Not smoothed		Smoothened with 3 windows		Smoothened with 5 windows		Smoothened with 7 windows	
	WI (nm)	R ²	WI (nm)	R ²	WI (nm)	R ²	WI (nm)	R ²
1	654	0.6327	778	0.7312	565	0.752	457	0.7434
2	354	0.5963	354	0.7145	384	0.6561	560	0.6757
3	562	0.5246	561	0.5892	457	0.6402	481	0.6054
4	390	0.5243	385	0.5756	482	0.6276	561	0.5985
5	622	0.4892	715	0.5721	458	0.6064	478	0.5985
6	635	0.4750	390	0.5172	560	0.5887	421	0.5475
7	597	0.471	357	0.4966	545	0.5454	624	0.5423
8	372	0.4609	356	0.4952	353	0.5451	383	0.5335
9	458	0.4595	755	0.4683	568	0.5355	383	0.5027
10	624	0.4529	512	0.4614	389	0.5255	477	0.5012

3.6. The Second Order Derivative Ratio Method

The second order ratio method is used to estimate the chl-a Concentration.

The ratio of Second derivative is computed as $P_{\lambda_{mn}} = R''_{\lambda_m} / R''_{\lambda_n} \dots (5)$

Where, $R''_{\lambda,n} = \frac{R''_{\lambda,n+1} - R''_{\lambda,n-1}}{\lambda(n+1) - \lambda(n-1)}$

$P_{\lambda,mn}$ is the ratio of second derivative, $R''_{\lambda,n}$ is the second derivative at λ,n and $R''_{\lambda,m}$ is the second derivative at λ,m .

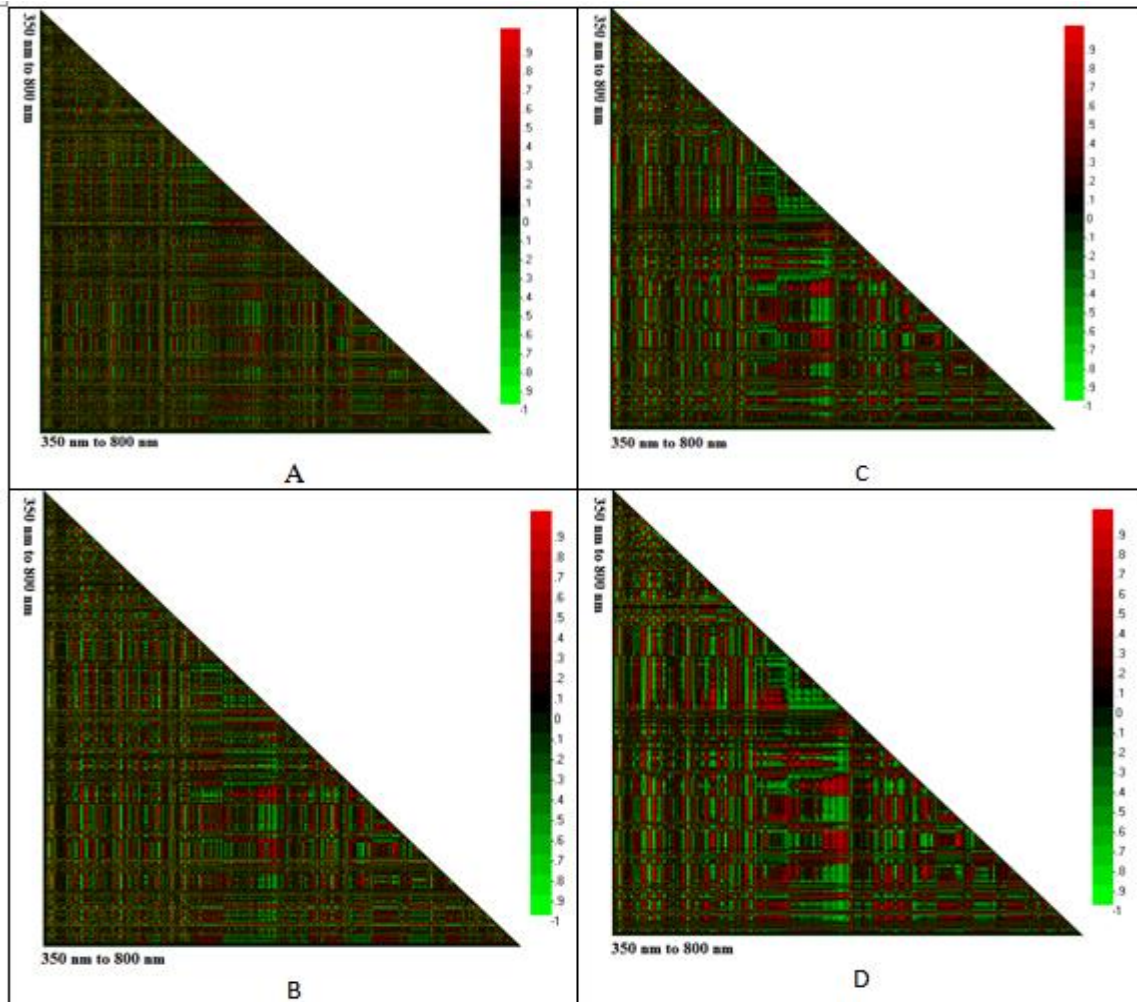


Figure 8: The Correlation between ratio of second order derivative values and measured Chl-a values at different wavelengths: A-without smoothing; B, C & D are smoothed with 3, 5 and 7 window running average algorithm

Table 5: High ten-correlation values obtained using second order derivative ratio values

2 nd rat	Not smoothed			Smoothened with 1 x 3 values			Smoothened with 1 x 5 values			Smoothened with 1 x 7 values		
	WL ₁	WL ₂	R ²	WL ₁	WL ₂	R ²	WL ₁	WL ₂	R ²	WL ₁	WL ₂	R ²
1	377	413	0.8675	708	735	0.8892	354	519	0.9314	681	709	0.9172
2	704	735	0.8578	355	501	0.8668	354	771	0.9160	399	647	0.8778
3	355	708	0.8490	355	562	0.8647	616	622	0.8997	447	500	0.8603
4	355	655	0.8328	355	677	0.8625	354	687	0.8953	681	708	0.8554
5	357	597	0.8325	386	398	0.8407	354	374	0.8849	399	497	0.8392
6	357	662	0.8286	355	712	0.8348	354	553	0.8819	353	545	0.8336
7	355	691	0.8277	355	704	0.8317	354	445	0.8765	556	696	0.8328
8	355	505	0.8219	386	527	0.8277	354	561	0.8757	497	616	0.8314
9	355	683	0.8098	355	734	0.8185	354	742	0.8696	458	553	0.831
10	424	577	0.8089	355	707	0.8181	459	562	0.8640	458	561	0.8301

3.7. Derivative Difference Method

In this study, a new algorithm called Derivative Difference method is introduced to estimate Chlorophyll-a. In this algorithm the difference between derivative values at different wavelengths were correlated with the measured Chl-a values.

Difference of First Order Derivative

The difference of first order derivative can be computed as $P'_{\lambda mn} = R'_{\lambda m} - R'_{\lambda n} \dots (6)$

Where, $R'_{\lambda n} = \frac{R_{\lambda n+1} - R_{\lambda n-1}}{\lambda(n+1) - \lambda(n-1)}$

$P'_{\lambda mn}$ is the Difference of first order derivative, $R'_{\lambda n}$ is the derivative at λn and $R'_{\lambda m}$ is the derivative at λm .

Difference of Second Order Derivative

The difference of Second order derivative can be computed as $P''_{\lambda mn} = R''_{\lambda m} - R''_{\lambda n} \dots (7)$

Where, $R''_{\lambda n} = \frac{R'_{\lambda n+1} - R'_{\lambda n-1}}{\lambda(n+1) - \lambda(n-1)}$

$P''_{\lambda mn}$ is the difference of second order derivative, $R''_{\lambda n}$ is the second order derivative at λn and $R''_{\lambda m}$ is the second order derivative at λm .

This method was used on raw data, first order derivative data and second order derivative data, individually. The results are tabulated and shown below in Table 6-8.

Table 6: High ten-correlation values obtained using difference method on raw data

	Not smoothened			Smoothened with 1 x 3 values			Smoothened with 1 x 5 values			Smoothened with 1 x 7 values		
	WL ₁	WL ₂	R ²	WL ₁	WL ₂	R ²	WL ₁	WL ₂	R ²	WL ₁	WL ₂	R ²
1	650	693	0.8167	650	693	0.8111	650	693	0.8064	650	693	0.8057
2	651	693	0.8066	651	693	0.8053	651	693	0.8043	648	694	0.8001
3	355	359	0.8032	632	694	0.8005	646	693	0.8005	651	693	0.7976
4	646	694	0.7989	652	693	0.7942	652	693	0.7875	645	693	0.7901
5	650	694	0.7901	642	694	0.7882	633	394	0.7875	649	694	0.788
6	647	693	0.7885	650	694	0.7866	645	693	0.7859	630	695	0.7868
7	652	693	0.7850	634	694	0.7809	650	694	0.7878	628	693	0.7813
8	633	694	0.7834	631	695	0.7799	641	694	0.7813	652	693	0.7806
9	639	695	0.7829	645	693	0.7792	637	694	0.7726	653	692	0.7802
10	642	694	0.7816	631	693	0.7681	632	695	0.7718	650	694	0.7783

Table 7: High ten-correlation values obtained using difference method on first order derivative data

	Not smoothened			Smoothened with 1 x 3 values			Smoothened with 1 x 5 values			Smoothened with 1 x 7 values		
	WL ₁	WL ₂	R ²	WL ₁	WL ₂	R ²	WL ₁	WL ₂	R ²	WL ₁	WL ₂	R ²
1	422	611	0.9266	475	482	0.9397	648	672	0.9283	379	677	0.9052
2	425	430	0.922	422	612	0.9199	610	671	0.8934	379	678	0.8904
3	392	401	0.9101	436	624	0.9122	611	671	0.8898	610	671	0.8752
4	428	678	0.9021	648	671	0.8949	356	379	0.8774	375	678	0.8591
5	624	678	0.8936	610	671	0.8898	648	673	0.8752	613	671	0.8529
6	399	545	0.8921	610	672	0.8815	376	678	0.8748	612	671	0.8527
7	666	736	0.8797	648	673	0.8780	611	672	0.8744	609	670	0.8512
8	476	624	0.8683	612	671	0.8709	609	671	0.8712	611	671	0.8477
9	385	625	0.8527	498	681	0.8573	421	749	0.8647	613	670	0.8462
10	356	732	0.8517	356	615	0.8569	427	678	0.8591	426	678	0.8440

Table 8: High ten-correlation values obtained using difference method on second order derivative data

	Not smoothened			Smoothened with 1 x 3 values			Smoothened with 1 x 5 values			Smoothened with 1 x 7 values		
	WL ₁	WL ₂	R ²	WL ₁	WL ₂	R ²	WL ₁	WL ₂	R ²	WL ₁	WL ₂	R ²
1	517	705	0.8836	512	562	0.9434	354	366	0.9628	433	566	0.8510
2	509	563	0.846	355	396	0.8707	354	397	0.9226	467	561	0.8420
3	609	691	0.8259	355	397	0.856	372	605	0.9101	422	616	0.8347
4	600	716	0.8199	355	385	0.8435	354	603	0.9071	562	778	0.8265
5	655	789	0.8174	505	562	0.8361	354	404	0.8974	458	562	0.8237
6	633	655	0.816	562	636	0.8225	354	604	0.8919	458	553	0.8226
7	459	655	0.815	513	623	0.8183	616	622	0.8879	601	640	0.8201
8	373	417	0.8147	386	626	0.8016	562	779	0.8776	458	482	0.8194
9	517	704	0.8141	355	456	0.7944	354	596	0.8770	459	561	0.8190
10	598	779	0.8104	562	779	0.7937	459	546	0.8739	353	545	0.8131

Table 9 compiles the effectiveness of the derivative difference methods w.r.t to derivative ratio and band ratio methods.

Table 9: Comparison of the derivative difference results with derivative ratio and band ratio

	Without Smoothing	Smoothened with 1 x 3 window	Smoothened with 1x 5 window	Smoothened with 1 x 7 window
Raw data Band Ratio	0.9042	0.8987	0.8945	0.8936
Raw data Band Difference	0.8167	0.8111	0.8064	0.8057
1 st order derivative ratio	0.9122	0.9139	0.9386	0.9667
1 st order Derivative Difference	0.9266	0.9397	0.9283	0.9052
2 nd order Derivative Ratio	0.8808	0.8945	0.9314	0.9172
2 nd order Derivative Difference	0.8836	0.9434	0.9628	0.8510

4. Conclusion

Chlorophyll concentration was estimated with band ratio, derivative ratio and derivative difference methods. The suitable wavelength sets vary slightly with smoothening window size. From Table 9, it is found the 1 x 5 window provides better correlation values. It is noticed that while proposed band difference method provided a poor correlation with raw data, it provides improved high correlation results with derivative data. The results of proposed difference method on derivative data has provided highest determination coefficient uniformly in 1st order and 2nd order derivative difference methods. It is to be noted from Tables 1-8, the correlation coefficients due to band ratio and derivative methods

are poorer and mostly effective for a narrow range of wavelengths; on the other hand the correlation coefficients due to derivative difference methods provide very good measure across all wavelength bands.

Acknowledgement

Authors thank the Management of SRM University and Indian Space Research Organisation for their encouragement and support during this study. Authors also thank Dr. Savithri Bhat, R & D Center of Department of Biotechnology, BMS college of Engineering, Bangalore for their support and suggestions.

References

- Chauhan, P., Nagamani, P.V. and Nayak, S. 2005. Artificial Neural Networks (ANN) based algorithms for chlorophyll estimation in the Arabian Sea. *Indian Journal of Marine Sciences*, 34, pp.368-373.
- Chen, J., Zhang, X.H. and Quan, W.E.T. 2013. Retrieval chlorophyll-a concentration from coastal waters: three band semi-analytical algorithms comparison and development. *Optical Express*, 21, pp.9024-9042.
- Dall'Demo, G., Gitelson, A.A. and Rundquist, D.C. 2003. Towards a unified approach for remote estimation of chlorophyll-a in both terrestrial vegetation and turbid productive waters. *Geophysical Research Letters*, 30, p.1938.
- Duan, H., Ma, R., Xu, J., Zhang, Y. and Zhang, B. 2010. Comparison of different semi-empirical algorithms to estimate chlorophyll-a concentration in inland lake water. *Environmental Monitoring and Assessment*, 170, pp.231–244.
- Duan, H., Ma, R., Zhang, Y., Loiselle, S.A., Xu, J., Zhao, C., Zhou, L. and Shang, L. 2010. A new three-band algorithm for estimating chlorophyll concentration in turbid inland lakes. *Environmental Research Letters*, 5, p.044009 .
- Gitelson, A.A. 1992. The peak near 700 nm in radiance spectra of algae and water: relationships of its magnitude and position with chlorophyll concentration. *International Journal of Remote Sensing*, 13, pp.3367-3373.
- Gohin, F., Druon, J.N. and Lambert, L. 2002. A five channel chlorophyll concentration algorithm applied to SeaWiFS data processed by SeaDAS in coastal waters. *International Journal of Remote Sensing*, 23, pp.1639-1661.
- Gower, J.F.R., Doerffer, R. and Borstad, G.A. 1999. Interpretation of the 685 nm peak in water-leaving radiance spectra in terms of fluorescence, absorption and scattering, and its observation by MERIS. *International Journal of Remote Sensing*, 20, pp.1771-1786.
- Han, L. and Rundquist, D. Comparison of NIR/RED ratio and first derivative of reflectance in estimating algal-chlorophyll concentration: a case study in a turbid reservoir. *Remote Sensing Environment*, 62, pp.253-261.
- Hoge, E.F., Wright, C.W. and Swift, R.N. 1987. Radiance ratio algorithm wavelengths for remote oceanic chlorophyll determination. *Applied Optics*, 26, pp.2082-2094.

- Huang, C., Zou, J., Li, Y., Yang, H., Shi, K., Li, J., Wang, J., Chena. X. and Zheng. F. 2014. Assessment of NIR-red algorithms for observation of chlorophyll-a in highly turbid inland waters in China. *Journal of Photogrammetry and Remote Sensing*, 93, pp.29-39.
- Huang, Y., Jiang, D., Zhuang, D. and Fu, J. 2010. Evaluation of hyperspectral Indices for Chlorophyll-a concentration estimation in Tangxun Lake (Wuhan, China). *International Journal of Environmental Research and Public Health*, 7, pp.2437-2451.
- Jeffrey, S.W. and Humphrey, G.F. 1975. New spectrophotometric equations for determining chlorophylls a, b, c1 and c2 in higher plants, algae and natural phytoplankton. *Biochemical Physiology Pflanzen*, 167, pp.191-194.
- Le, C., Li, Y., Zha, Y., Sun, D., Huang, C. and Lu, H. 2009. A four-band semi-analytical model for estimating chlorophyll a in highly turbid lakes: The case of Taihu Lake, China. *Remote Sensing Environment*, 113, pp.1175-1182.
- Mishra, S. and Mishra, D.R. 2012. Normalised difference chlorophyll index: a novel model for remote estimation of chlorophyll-a concentration in turbid productive waters. *Remote Sensing Environment*, 117, pp.394-406.
- Moses, W.J., Gitelson, A.A., Berdnikov, S. and Povazhnyy, V. 2009. Estimation of chlorophyll-a concentration in case ii waters using MODIS and MERIS data – successes and challenges, *Environment News Letters*.
- Neville, R.A. and Gower, J.F.R. 1977. Passive remote sensing of Phytoplankton via chlorophyll fluorescence. *Journal of Geophysical Research*, 82, pp.3487-3493.
- Philpot, W.D. 1991. The derivative ratio algorithm: avoiding atmospheric effects in remote sensing. *IEEE Transactions on Geoscience and Remote Sensing*, 29, pp.350-357.
- Ruddick, K.G., Gons, H.J., Rijkeboer, M. and Gavin Tilstone, G. 2001. Optical remote sensing of chlorophyll a in case 2 waters by use of an adaptive two-band algorithm with optimal error properties. *Applied Optics*, 40, pp.3575-3585.
- Rundquist, D.C., Han, L., Schelles, J.F. and Peake, J.S. 1996. Remote measurement of algal chlorophyll in surface waters: the case for the first derivative of reflectance near 690 nm. *Photogrammetric Engineering & Remote Sensing*, 62, pp.195-200.
- Sathyendranath, S., Prieur, P. and Morel, A. 1986. A three-component model of ocean color and its application to remote sensing of phytoplankton pigments in coastal waters. *International journal of Remote Sensing*, 10, pp.1373-1394.
- Shi, H., Xing, Q., Chen, C., Shi, P. and Tang, S. 2007. Using second derivative spectrum to estimate chlorophyll-a concentration in turbid estuarine waters. *Prec. of SPIE*. 6790, 679032-1.
- Sun, D., Li, Y. and Wang, Q. 2009. A unified model for remotely estimating chlorophyll a in lake Taihu, China, Based on SVM and in situ Hyperspectral Data. *Transaction on Geoscience and Remote Sensing*, 47, pp.2957-2965.
- Tian, H., Cao, C., Xu, M., Zhu, Z., Liu, D., Wang, X. and Cui, S. 2014. Estimation of chlorophyll-a concentration in coastal waters with HJ-1A HIS data using a Three-band Bio-optical model and validation. *International journal of Remote Sensing*, 35, pp.5984-6003.

Tsai, F. and Philpot, W. 1998. Derivative analysis of hyperspectral data. *Remote Sensing Environment*, 66, pp.41-51.

YI, C. 2013. A weighted algorithm for estimating chlorophyll – a concentration from turbid waters. *Journal of Indian Society of Remote Sensing*, 41, pp.957-967.

Yu, G., Yang, W., Matsushita, M., Li, R., Oyama, Y. and Fukushima, T. 2014. Remote estimation of chlorophyll-a in inland waters by a NIR-Red Based Algorithm: Validation in Asian Lakes. *Remote Sensing*, 6, pp.3492-3510.

Zhang, Y., Ma, R., Duan, H., Loiselle, S. and Xu, J. 2014. A spectral Decomposition Algorithm for Estimating Chlorophyll-a Concentrations in Lake Taihu, China. *Remote Sensing*, 6, pp.5090-5106.

Research Article

Land Use Landcover Change Monitoring and Projection in the Dano Catchment, Southwest Burkina Faso

Gloria C. Okafor¹, Thompson Annor², Samuel N. Odai¹, Isaac Larbi³

¹West African Science Centre on Climate Change and Adapted Land Use WASCAL, Department of Civil Engineering, Kwame Nkrumah University of Science and Technology, Kumasi, Ghana

²Department of Physics, Kwame Nkrumah University of Science and Technology, Kumasi, Ghana

³Climate Change and Water Resources, West African Science Centre on Climate Change and Adapted Land Use (WASCAL), Universite d'Abomey Calavi, Benin

Correspondence should be addressed to Gloria C. Okafor, gloriacokafor@yahoo.com

Publication Date: 21 December 2019

DOI: <https://doi.org/10.23953/cloud.ijarsg.445>

Copyright © 2020. Gloria C. Okafor, Thompson Annor, Samuel N. Odai, Isaac Larbi. This is an open access article distributed under the **Creative Commons Attribution License**, which permits unrestricted use, distribution, and reproduction in any medium, provided the original work is properly cited.

Abstract Burkina Faso has long been experiencing intense land-use landcover changes (LULCC) which have resulted in widespread land degradation. Hence, the need to obtain LULC information for improved land-use planning and sustainable management of land-resources cannot be overemphasized. This study examined the historical LULCC in the Dano catchment and projected the situation in 2050 for business-as-usual (BAU) and afforestation scenarios. Multitemporal Landsat images of 1990, 2000, 2010 and 2016 were classified with an overall accuracy of more than 90%. The Cellular-Automata Markov approach was used to project the future LULC pattern after identifying major driving forces of LULCC. The results revealed a substantial expansion in settlement and cropland area of about 62% and 6% respectively, which triggered a 15% decrease in forest cover, thus paving the way for severe soil degradation. The increase in cropland, settlement area, water bodies, and the decrease of forest were at an annual rate of 3.8%, 10.5%, 6.97% and 2.53% respectively within the past 26 years. The projected LULC under the BAU scenario revealed further forest loss from 46.72% in 2016 to 38.54%, owing to an extension in agriculture from 38.51% to 46.69%. The afforestation scenario projected a potential increase in forest by 2.13% and a decrease in cropland by 2.09% in the future relative to 2016. This study illustrates the accelerated land degradation and the challenges on ecosystem sustainability of the Dano landscape, hence, appropriate interventions like reforestation, protection measures and policy option in strategic land-use planning are needed to resolve the further loss of forest cover.

Keywords *Land degradation; Dano catchment; Markov-cellular automata; Projection; Remote sensing*

1. Introduction

Land-use landcover change (LULCC) concerns have become the frontier in global change, as realized from global research agenda on environmental change. A significant unprecedented combination of demography growth, migration, accelerated socio-economic activities and other human exploitations in recent time have intensified these environmental changes with profound effect of land-use change. According to the World Atlas of Desertification (WAD3), over 75% land area of the Earth is already degraded and by 2050, about 90% could turnout degraded (Reynolds et al., 2018). Globally, Africa is

the most affected and that accounts for 65% of the total extensive cropland degradation of the world, with semi-arid and dry sub-humid zones about 70% degraded land (Thiombiano & Tourino-Soto, 2007).

Burkina Faso has experienced rapid socioeconomic development under considerable population growth. Increasing agricultural areas, urban expansion and forest depletion in the last 40 years have become a norm in a way to meet the increasing demand of the surging populace. This increased pressure on the available land resources and anthropogenic activities in various sectors, especially the economic sector, lead to land degradation thereby affecting food security, rural livelihoods and ecological sustainability (Moges & Bhat, 2018). The unplanned urban expansion and the mining activities that are going on in the area have led to the loss of croplands to commercial use, forest to farmlands; water and soil erosion due to deforestation and water pollution from the discharge of municipal garbage and industrial waste. In this context, there is much need to assess and understand land use changes over time and its driving forces as well as projections into the future.

Nowadays, several evolved methods and techniques of land use change assessment under successive distinct periods at finer scales using remote sensing and spatially explicit data for modeling purposes cannot be overemphasized. Satellite observations provide valuable surrogates and can reveal conversions and modifications of land changes that are connected to the condition of ecosystem services. Considerable number of researches have been conducted within WA to detect and address LULCC problems such as degradation (Braimoh & Vlek, 2004; Obahoundje et al., 2017), deforestation and desertification (Baatuuwie, 2015), environmental change due to urbanization (Tewolde & Cabral, 2011) agriculture and mining (Awotwi et al., 2018). However, they are mostly either about temporal change detection of land use or classification. Among those few are studies who showed changes in natural vegetation, and a large increase in croplands with annually increased population density (Ruelland et al., 2010; Ouédraogo, 2010). Moreover, few efforts have been made to predict future changes or accurately investigate LULCC in hydrological context over a long time in the Black Volta Basin (BVB) environment (Akpoti et al., 2016), and such investigations remain rare, especially in semi-arid zones. Recently, land surface models e.g. Land change modeler (LCM) have been employed by researchers to forecast LULCC (Gibson et al., 2018) to improve impact assessment in order to aid planning and sustainable land management. An example study observed a growing trend in settlement expansion which could lead to significantly increased surface runoff and change in drainage geography (Mahmoud Ibrahim, 2016). Other earlier works have also reported LULCC differences under different scenarios (Han et al., 2015; Deng et al., 2013). In addition, the choice of appropriate scale for these models to support land-use development necessitates a trade-off involving spatial extent and detail.

Explicitly, the long-term historical evaluations and projections into the future land cover changes at catchment scales are needed to avoid potentially catastrophic damage and the effect of surface processes on regional climate and ecosystem services. Moreover, this is essential to enable understanding of the degree to which LULCC is a threat to water resources at the Dano catchment. To address this critical need by providing a better quantitative understanding of LULC changes, this study aimed to analyze the historical (1990 to 2016 period) LULCC and project future (2050) LULC patterns for two scenarios: business-as-usual (BAU) and afforestation using the Land Change Modeler (LCM).

2. Materials and Methods

2.1. Study Area

The Dano catchment with an area of 582 km² located in the loba province, Southwest of Burkina Faso is situated at latitudes 7°00' - 14°30'N and longitudes 1°30' - 5°30'W (Figure 1). The climate of the area is a tropical transition zone with a pronounced dry and rainy season. The mean annual rainfall is 943 mm, with nearly 80% concentrated in the months of July to September considering 1970 to 2013

period of the Burkina Faso National Meteorological Service data. The recent climate-change study has identified trends of warmer and drier conditions and moderate to severe drought years (Kasei et al., 2010). Geologically, the catchment is composed of Paleoproterozoic basement, largely flat with an average slope of 2.9% and elevation ranging between 229 m and 509 m above sea level. The catchment is drained by several intermittent streams that dry up during the dry season and has easily erodible soils that render the area sensitive to pronounced land-degradation processes (Duadze, 2004). Landcover such as woody savannahs and shrubs are also exploited for wood and intensive use to produce the local beer “dolo”. In the catchment, rain-fed agriculture constitutes the major land-use with the production of some staple crops like cassava, yam, groundnut, maize and sorghum dominating. The rural population density in southwest Burkina Faso is between 41-60 persons per km² (Knauer et al., 2017), and largely depend on water supply from surface water.

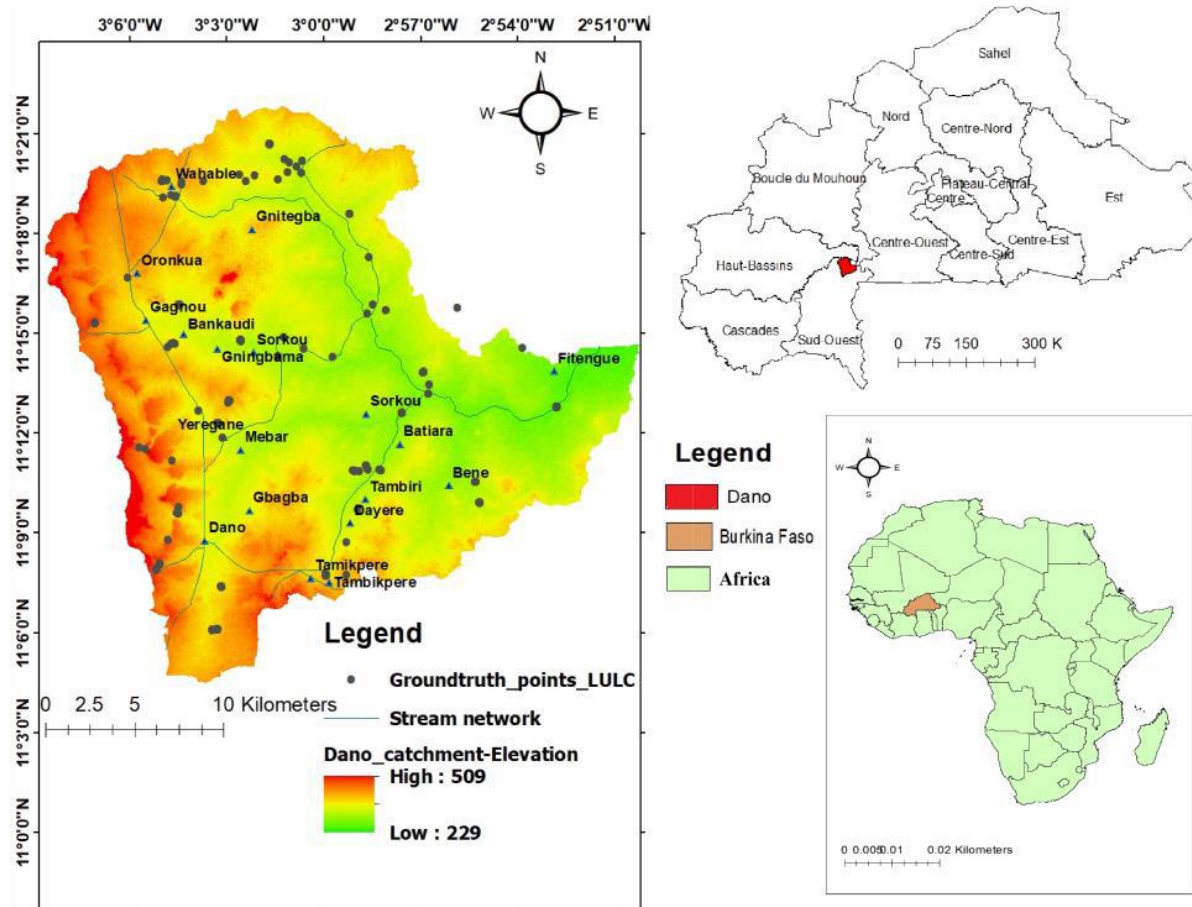


Figure 1: Map showing the location, Digital elevation and ground-truth LULC of Dano Catchment

2.2. Data

This research used four Landsat satellite images downloaded from the portal of EarthExplorer (<https://earthexplorer.usgs.gov/>) at no cost for the years 1990, 2000, 2010 and 2016 (Table 1). Scenes selections were based on the criteria of availability, acquisition dates and 10% cloud cover. In addition, ancillary data including slope and elevation derived from Digital Elevation Model (DEM) (<http://srtm.csi.cgiar.org/>) for modeling purposes were acquired. Field data were collected for training and as reference samples to validate the classified images. The field campaign was organized in the dry season of 2016 with a total of 150 GCPs (Ground Control Points) focused to ensure representative spatial locations for all readily mapped landcover types (e.g. grassland, etc.). Sixty per cent of these points were used for training and the remaining for validation of the 2016 LULC map. Other LULC reference samples for the year 1990, 2000 and 2010 were generated from Google Earth maps and

GLOBELAND30: a 30 m resolution global landcover dataset developed by the National Geomatics Centre of China (Chen et al., 2017) for training and validation.

Table 1: Spatial data description

Type	Dataset	Date	Source
Satellite images (30 m resolution, path/row 196/052)	Landsat 8 OLI-TIRS	Nov 27, 2016	EarthExplorer
	Landsat 5 TM	Nov 27, 2010	
	Landsat 7 ETM+ SLC-on	Nov 07, 2000	
	Landsat 5 TM	Dec 1990	
	DEM (30 m), road and river network		Shuttle Radar Topographic Mission
Reference data	Globeland30	2000, 2010	http://www.globallandcover.com/GLC30Download/index.aspx
	Ground control points (GCPs)	2016, 1990	Field campaign, GoogleEarth Image

(Sensor types: OLI: Operational Land Imager-Thermal Infrared Sensor; TM: Thematic Mapper, ETM+: Enhanced Thematic Mapper).

2.3. Classification and Accuracy Assessment

The methodology applied in this study is illustrated in a flowchart (Figure 2). First, standard image pre-processing through radiometric correction was performed on the images to remove atmospheric influences based on the metadata information and to uniquely decipher the direct relationship between the biophysical phenomena and acquired data (Coppin et al., 2004). This was followed by generating LULC maps via a step-by-step classification. The supervised classification method of Maximum Likelihood was used by incorporating ground surveys and information obtained from local knowledge (focus group discussion). The accuracy of the classification results obtained was checked using a confusion matrix created from comparing a classification result with a set of reference pixels or ground truth samples. In collecting reference points used for the accuracy assessment, the probability sampling method was followed to create the adjusted error matrix (Olofsson et al., 2013). The method involves three steps namely: sampling design, response design, and error-adjusted-area analysis. The technique allows computation of confidence interval estimates for statistical inferences and uncertainty measures. The sample design employed stratified random sampling in ArcGIS software for collecting sets of reference points to validate the LULC classification. Afterwards, the response design stage of determining the sampling unit of the reference data followed, in order to calculate the estimated area-adjusted matrix. Accordingly, bearing in mind at least a minimum sample of 60 per class in a total number of classes (Congalton, 1991), the stratified random points (Table 2) were created for 1990, 2000, 2010, and 2016 respectively.

Table 2. Sample Points for LULC Validation

LULC Category (Strata)	Sample sizes			
	1990	2000	2010	2016
Water Body	60	60	60	60
Settlement	60	60	60	60
Cropland	65	70	70	65
Forest	75	70	70	75
Grasslands	60	60	60	60
Total	320	320	320	320

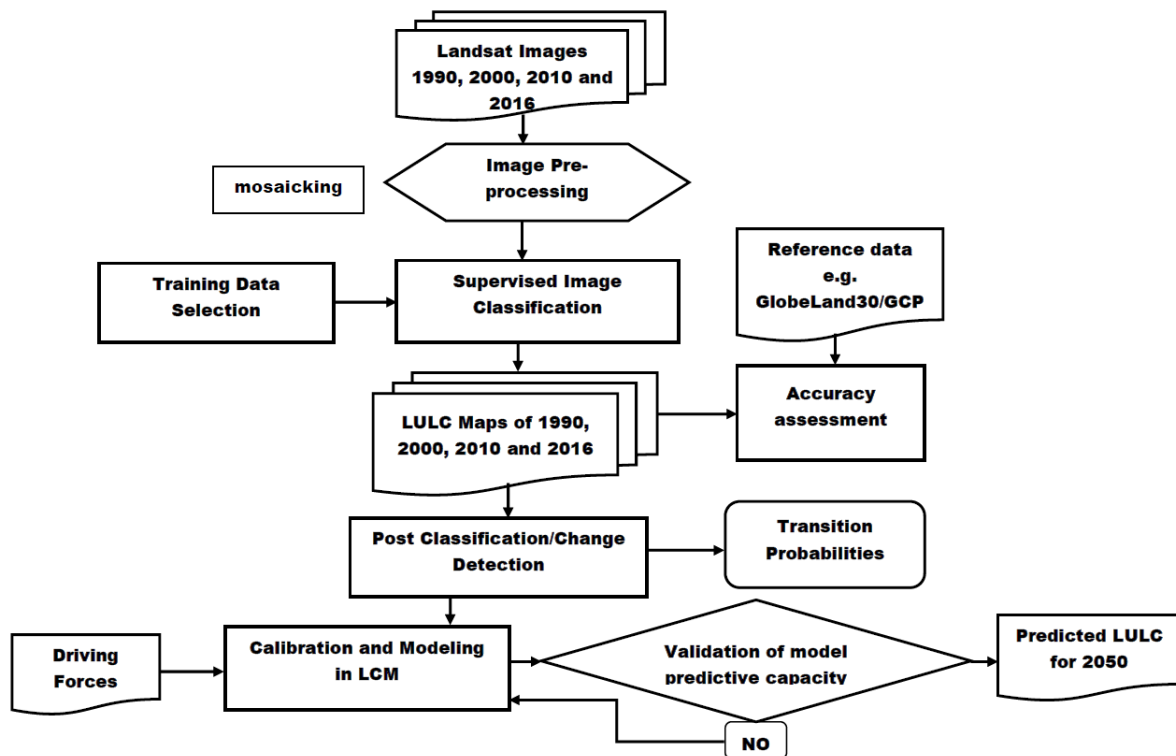


Figure 2. Methodology flowchart used in this study

2.4. LULCC Analysis and Indicators Identification

The LULC change analysis in this study was performed based on the widely used post-classification change analysis with the independently classified maps using Land Change Modeller (LCM). The change analysis aided the detection of LULC conversions by tracking the transition of each pixel between two-time steps of observation. The change detection module in LCM provides information on gains and losses by each LULC class, the net change of each class, contributors to the net change experienced by each class, and the transition of areas among LULC classes that has occurred between the two-time steps.

In addition, the quantification analysis of this spatiotemporal LULCC was realized through indicators like the spatial trend and Annual Land Use/Cover Change Rate (ALUCR) defined in equation 1:

$$ALUCR_{a,t} = \frac{LU_{a,t} - LU_{a,t-1}}{N_t - N_{t-1}} \times 100 \dots (1)$$

Where ALUCR (%) is the rate of LULCC per annum, $LU_{a,t}$ and $LU_{a,t-1}$ are the total land area of LULC category in hectares at current N_t and earlier time N_{t-1} . This also enabled change analysis on a class-wise basis.

2.5. LULC Model Implementation and Validation

The LCM was further used to predict LULC following the procedure: change detection, transition potential modeling and driving factors determination, change prediction, and model validation.

Change Detection - In this first step as earlier mentioned in section 3.3, mainly two-time categorical maps assessed between time-1 & time-2 enabled understanding of gains, losses and transition among the LULC classes as well as nature of change in the catchment from 1990 to 2016 (Figure 2). The changes from one class to another are imperative in identifying the dominant transitions and target

them for modeling. The change maps are created using the likelihood of transformation from one class to another - Evidence likelihood images. Landcover change between the years 1990 and 2000 were first analysed resulting in transition potential maps and probability matrix that illustrates the significant LULC transition at this phase. Emphasis was also given to the principal categories of change with areas more than 5000ha to limit the number of transitions to be modelled.

Transition Potential Modeling and Driving Factors Determination - Consequently, two major transitions were considered (forest to cropland and cropland to forest areas) in Transition Potential Tab. The Multi-layer Perceptron (MLP) neural network is a one direction network algorithm that flows from input to output with a hidden layer(s) in between (Nazzal et al., 2008) that allows for modeling multiple transitions at once. The transitions between the two timesteps are presented as a change matrix used for calibration and targeted for modeling into the future (Figure 2). In addition, major driving factors determined for modeling transition of historical change as predictor variables or constraints include slope, population (settlement), elevation, distance to roads and rivers. These were considered because they are noted to influence LULCC over time (Thorn et al., 2016). The LCM allows a quick look at the probable explanatory model power of the driving forces presented in the Cramer's V. The Cramer's V of 0.15 and above of any variable is useful, while values > 0.4 are good and preferred.

Change Prediction and Model Validation – The LCM uses the change rates from the change analysis and transition potential maps to predict the future LULC, in this case, 2010 (Figure 2). Ensuing Markov chain analysis, this step assists in determining the transition rates from one land-use type to another under certain intrinsic conditions. The hybrid cellular automata (CA)-Markov model is selected among several available and most commonly used land use modeling tools and techniques (such as Clue-S models, multi-agent models, or GEOMOD) because model is recognized as suitable to model the spatiotemporal dynamic changes in landscape patterns in the context of this paper and applied among many scientific communities (Mukhopadhaya, 2016).

Subsequently, the independently classified map of 2010 was compared to the predicted map from the initial two timesteps (1990 and 2000); a way of validating the land change model. The model validation is an important component in modeling aimed to ascertain the quality of the simulated 2010 map comparatively to a reference map (classified 2010 LULC map). The model when considered fit, after validation, was then used to predict LULC for the year 2050 using base maps of 1990 and 2016 LULC as illustrated in Figure 2. To show overall agreement between the observed and predicted maps, in three-dimensional space method (allocation disagreement and quantity disagreement based on Pontius & Millones (2011) techniques and Kappa Index of Agreement (KIA) are used. The following validation statistics of various Kappa indexes (Pontius, 2000) shows agreement between paired maps with variable LULC categories: Kappa for no information (Kno) giving the overall success of the simulation; Kappa for location (denoted as Klocation) showing agreement on location (Nadoushan et al, 2012). The KIA shown with Kstandard confounds disagreement of quantity with the disagreement of location (Hadi et al., 2014). In addition, comparisons of the simulated and the actual area extent of each LULC class were also performed.

2.6. Scenario Development

Scenario development is a recent prevalent practice in LULC research studies because it offers a possibility for assessing the present and future situations geared towards decision making. After the model predictive power assessment, this was then used to project for 2050 LULC with driving forces according to the underlying transition probabilities with years 1990 and 2016 as base maps. Two scenarios were developed and can be termed as (i) business-as-usual (BAU) based on the historical land-use changes between 1990 and 2016 and (ii) Afforestation-based scenario used to explore alternative environmental preservation pathways (Table 3). The afforestation scenario was created by altering the probability matrices for forest and cropland as predicted by the Markov model. This

scenario imbibed an increase in forest and grassland by 15% following the total annual LULC rate change.

3. Results

3.1. Spatial distribution and Accuracy of LULC

The independently classified images results of four different years are given in Figure 3. Five dominant LULC classes including Water body (rivers, lakes, ponds and reservoirs), settlement (mainly residential, roads, bare soils), Cropland (cultivated land - rain-fed or irrigated with partial tree cover < 10% and fallow lands), woody savannah (scattered trees – open savannah woodland and plantations with shrub undergrowth) and Grasslands (including temporarily flooded herbaceous vegetation (wetlands), murky water, dark soils and stones) were classified. Forest and cropland dominated the LULC classes while the lowest is water (Figure 4).

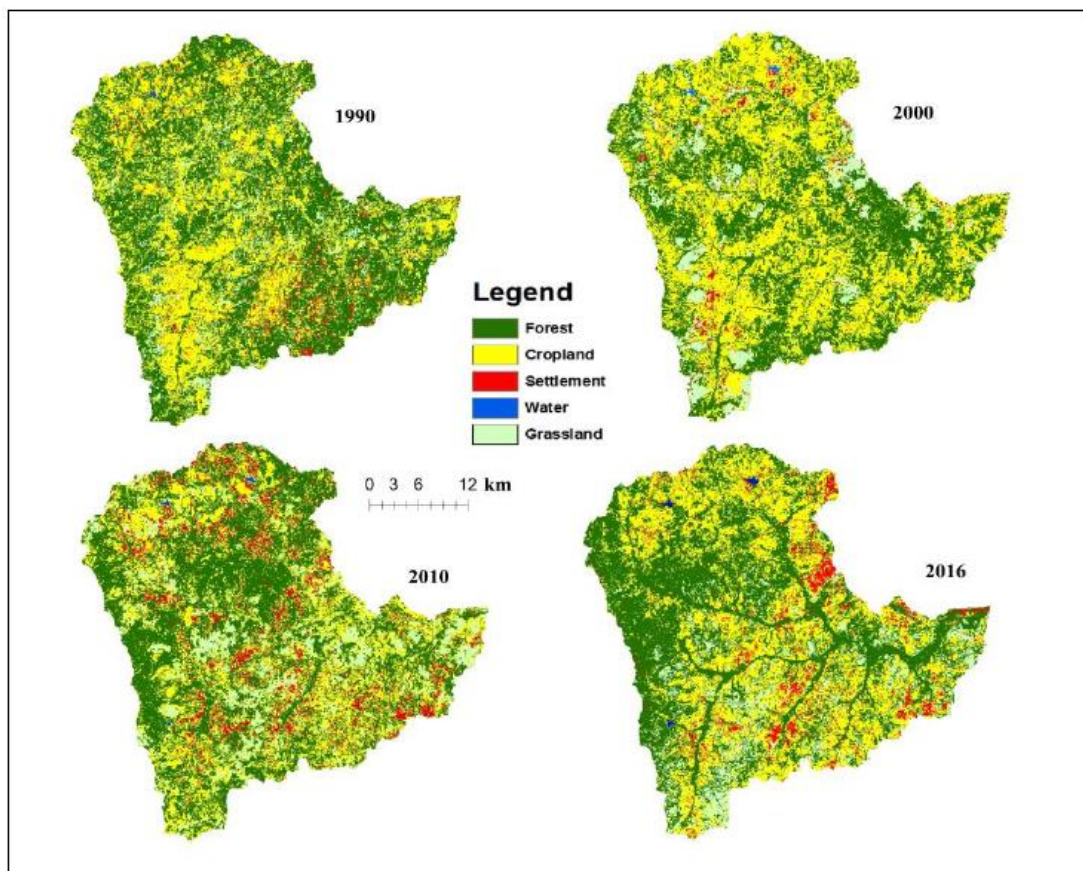


Figure 3: *Classified LULC maps of the Dano catchment*



Figure 4: Proportions of LULC types in Dano Catchment

Accuracy assessment of the classified maps was carried out in order to validate these results. Table 3 shows the results achieved based on pixel count matrix (Appendix 1) which yielded overall accuracies (OA) of 90%, 93%, 88%, and 90% for maps of years 1990, 2000, 2010, and 2016 respectively. While the error adjusted area matrix achieved 87%, 90%, 84% and 84% correspondingly. The error adjusted area (Table 4) shows a general drop in overall accuracy because it considered the error of omission while estimating the area proportions.

Table 3: Percentage user’s (UA) and producer’s accuracies (PA) for each LULC class for the years 1990, 2000, 2010 and 2016 based on the pixel count matrix

Landcover class	1990		2000		2010		2016	
	PA	UA	PA	UA	PA	UA	PA	UA
Forest (Nij)	91	84	77	95	78	87	88	79
Agric	77	91	76	76	87	79	80	86
Settlement	94	83	58	92	90	87	94	97
Water	100	100	60	100	100	100	100	100
Grassland	92	93	58	93	87	88	90	92
Overall accuracy	90		93		88		90	

The least accuracy observed for 2010 LULC map is as a result of major spectral confusion observed between categories cropland, settlement and grassland. However, the area distribution (Table 4) reveals that for all categories of LULC, the maps fell within 95% confidence interval of the estimated area indicating good agreement between the classified images and ground-truths as well as the reliability of the classified maps (Olofsson et al., 2014).

Table 4: Spatial analysis result of error adjusted area of LULC maps for 1990, 2000, 2010 and 2016

Year	Landcover	Mapped area (%)	Estimated area (%)	Conf. interval
1990	Forest	51.53	45.77	4.84
	Agric	37.25	38.70	4.17
	Settlement	2.05	3.66	2.21
	Water	0.07	0.07	0.00
	Grassland	9.09	11.80	2.93
	Total	100.00	100.00	

2000	Water	0.09	0.09	0.00
	Grassland	8.24	8.94	1.80
	Forest	42.18	43.88	3.67
	Artificial surfaces	2.07	3.72	2.06
	Cropland	47.42	43.36	4.13
Total		100.00	100.00	
2010	Grassland	11.19	14.79	3.46
	Forest	46.74	46.20	4.68
	Agric	36.61	30.83	4.04
	Artificial surfaces	5.37	8.08	2.76
	Water	0.09	0.09	0.00
	Total		100.00	100.00
2016	Grassland	9.97	12.65	2.85
	Forest	44.48	38.87	4.74
	Artificial surfaces	6.11	7.41	1.71
	Water	0.12	0.12	0.00
	Agric	39.31	40.96	4.88
	Total		100.00	100.00

3.2. Change detection and Quantification

Land use change analysis results in Table 5 apparently showed that during the 1990 to 2016 period across Dano catchment, the significant land changes that occurred was forest conversion to all other classes and all other classes to settlement. Forest lost about 4006.32 ha (15%) of its total area with a persistent change of 70% while settlement and water increased by 2184.93 ha (62%) and 26.10 ha (39%) respectively.

Table 5: Main LULC conversions using the estimated area statistics from 1990 to 2016 in the Dano Catchment

Class	1990-2000		2000-2010		2010-2016		1990-2016	
	Area change	ha	%	ha	%	ha	ha	
Forest		-1095.45	-4.1	1349.19	5.3	-4260.06	-15.8	-4006.32
Agric		2711.91	12.0	-7292.28	-28.9	5905.94	32.9	1325.58
Settlement		38.07	1.8	2537.34	117.0	-390.47	-8.3	2184.93
Water		12.69	31.0	1.53	2.9	11.88	21.5	26.10
Grassland		-1667.22	-2.9	3404.18	5.8	-1243.69	-2.1	493.27

Forest degradation, grassland decrease, settlement and agricultural land expansion can be seen from the presented LULC changes in Tables 5. To further buttress this, analysis of the annual rate of land-use change (ARLUC) is computed in Figure 5 to highlight the importance of LULC focus of the study. The following results were obtained: forest decreased at the rate of 4.3% and 18.8% per year in the periods 1990 to 2000 and 2010 to 2016 respectively; while cropland increased at the rate of 10.7% and 24.8% with areas greater than 5,000 ha at a similar timeframe. Grassland decreased yearly by 32% and 16.9% in 1990 to 2000 and 2010 to 2016 decades respectively. The reverse of these changes (cropland reduction: 40.6%; forest and grassland increase: 5.5% and 39.5%) are seen in the 2000 to 2010 period. Settlement and water consistently increased in the entire timestamp.

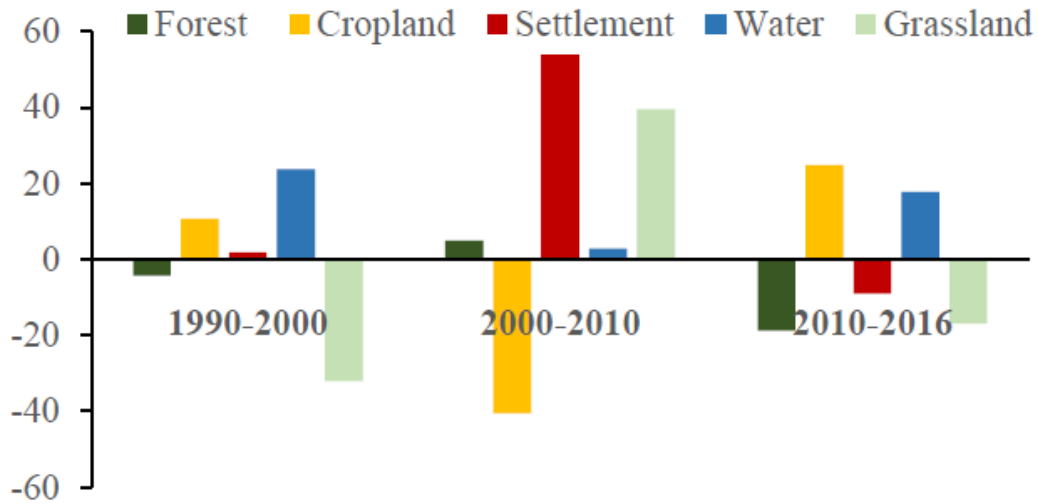


Figure 5: Annual Rate of Land-use Change (ARLUC in %/yr) from 1990 to 2016

3.3. Transition Probabilities and Driving Forces

The classified maps transition probabilities matrices are presented in Tables 6. The most important conversions were from forest to all other class: water, settlement, grassland and substantially to cropland – 5023 ha, hence, this is considered as the major transition in the land change model, since urban areas occupy less than 7% of the catchment. The diagonal values in the matrices represent the probability that each LULC class remains unchanged, while the off-diagonals represent the probability of transition to another class. In the period 1990 to 2000, forest and cropland had the highest probability of undergoing changes. The low unchanged transition in settlement class is from rapid development at that period and misclassification due to identical spectral signature with cropland in the catchment. The 1990 to 2016 period matrices show a general reduction in all classes except settlement (0.09) that increased. Cropland mostly reduced meaning that most conversions are within cropland. The high probability value for forest (0.47) can be attributed to forest recovery observed in the earlier change analysis (Figure 5).

Table 6: Markov chain matrix of LULC transition probabilities in different periods from 1990 to 2016 in the Dano Catchment

Period: from-to	LULC	Forest	Cropland	Settlement	Water	Grassland
1990-2000	Forest	0.5224	0.3833	0.0088	0.0003	0.0852
	Cropland	0.2986	0.6090	0.0003	0.0088	0.0586
	Settlement	0.1670	0.7132	0.0704	0.0088	0.0486
	Water	0.2396	0.1297	0.0022	0.5868	0.0418
	Grassland	0.4147	0.3852	0.0271	0.0040	0.1726
1990-2016	Forest	0.4787	0.3786	0.0514	0.0006	0.0906
	Cropland	0.4268	0.4185	0.0675	0.0015	0.0856
	Settlement	0.3573	0.4777	0.0908	0.0014	0.0727
	Water	0.3609	0.1438	0.0529	0.4214	0.0210
	Grassland	0.4895	0.3426	0.0385	0.0007	0.1287

The forest transition had a varying spatial trend over the catchment indicating a divergent predictor variable contributing to the change (Figure 6). The highest degree of forest area loss has occurred in the North and South sides of the catchment. Cramer's V values gave the correlation coefficient ranging from 0.0 to 1.0 signifying either a redundant variable or significant potential variable. Based on the values, settlement was a major player in the land use change followed by distance to water bodies, the

road and elevation factors. This implies that areas close by settlement have been cleared for food production so as to satisfy basic life needs. Taking these results into account to model land use change (agricultural land area increases and forest decrease); model calibration was performed for 2010 based on the transition probability grid from 1990 to 2000. These transitions were modelled in one sub-model using the produced transition map.

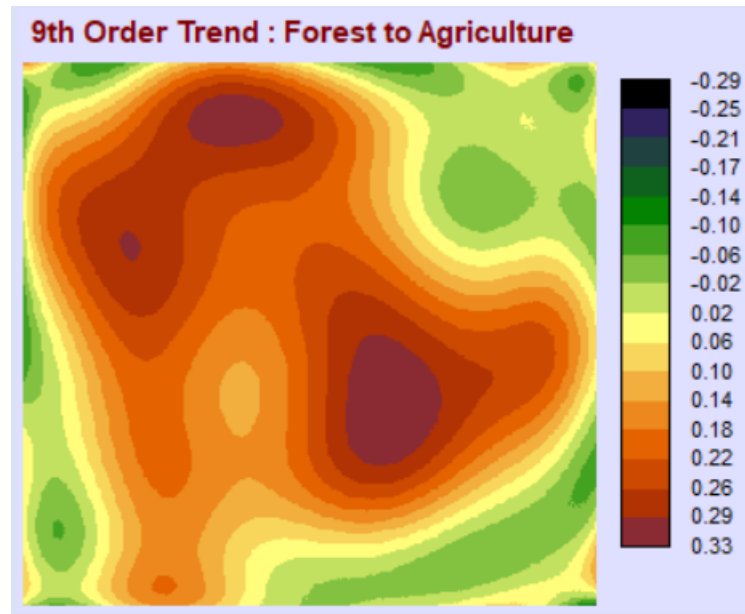


Figure 6: The Spatial trend of change from forest to cropland

3.4. Model Prediction and Performance Evaluation

Illustrated in Figure 7 is the comparison of the predicted 2010 agricultural expansion map and an independently classified map of the Dano catchment in 2010. Visual comparison of the simulated 2010 map with the classified map are reasonably similar and at a good confidence level (95%). However, over-prediction is seen for the forest at the far right (depicting the change of forest increase and cropland decrease that actually occurred between 2000 and 2010). This is due to models' less ability in capturing the random forest save interventions and newly developed areas. 41.67 and 47.92% in the extent of cropland and forest respectively were attained by the model (simulated) in 2010 while the actual map has an extent of 36.59% and 46.76%.

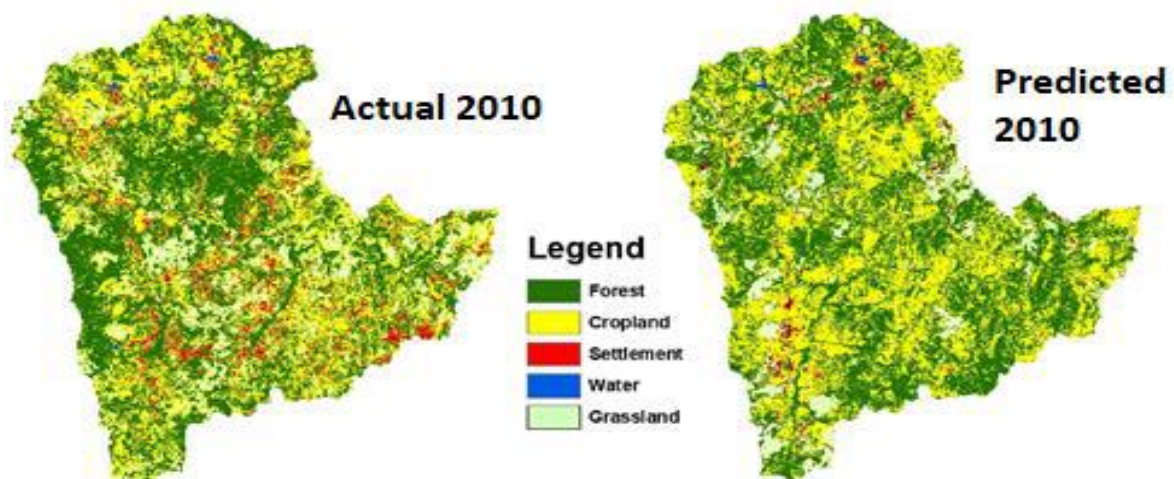


Figure 7: Comparison of the classified and predicted 2010 LULC maps

The model having attained an acceptable range of less of the observed, which can be emphasized on the inadequacy of forcing driver restrictions and poor model ability in capturing the randomly farming activities which occurred within settlement areas. Since statistical techniques are vital for model validation as visual validation remains subjective and misleading at times (Pontius and Chen, 2006), the Kappa for the projected and real map of 2010 is presented. Also, LULC mapping and analysis in this study was achieved using medium resolution images, therefore, detections using high-resolution satellite images could be more dependable.

Notwithstanding, the agreement and disagreement between the simulated and the classified maps of 2010 reveal Kno, Klocation and Kstandard values of 81%, 83% and 73% respectively. The model also showed quantity and location disagreement of 4.9% and 15.4%, respectively. The interpretation of these agreement values is that the most part of the study area experienced change, as the dominant classes of forest and cropland underwent changes during this period (Figure 8). The exchange is the largest component of error. Cropland and forest account for most of the exchange component while forest has the largest overall error in the quantity component. Likewise, LULCC is more pronounced (heterogeneous) at the local level and in areas of change, which indicates that CA_Markov model reasonably simulated the 2010 LULC patterns and thus, in a good position to predict future LULCC in the Dano catchment.

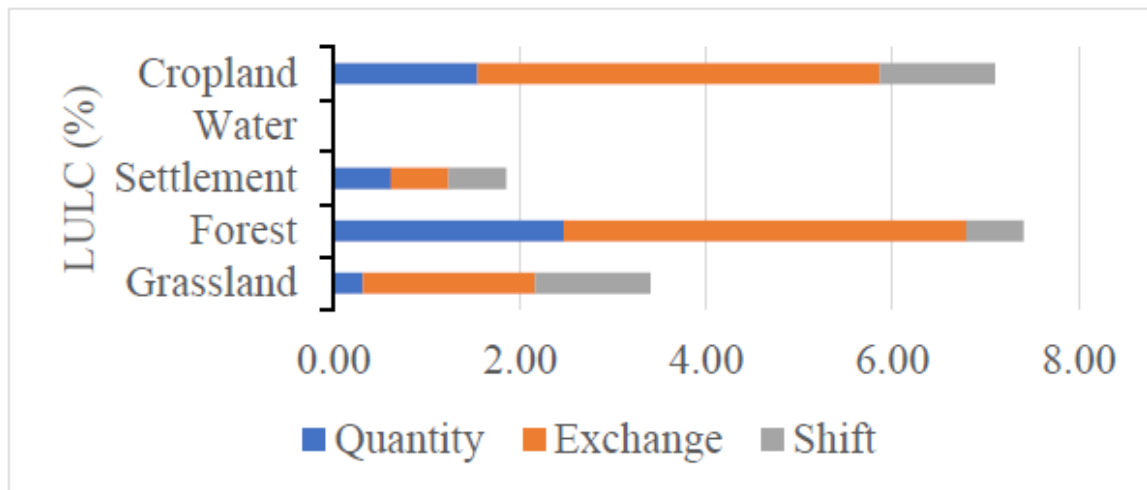


Figure 8: Quantity agreement (Quantity) and Allocation agreement (Exchange + Shift) of LULC map

After model validation, two scenarios LULC future projection into the year 2050 was simulated with 1990 and 2016 maps by applying the sub-model test implemented during the 2010 model calibration. The predicted 2050 maps in Figure 9 show that forest cover will decrease from 46.72% in 2016 to 38.54% and cropland area will expand from 38.51% to 46.69% under a business-as-usual scenario (Table 7). Contrarily to the BAU, the afforestation scenario projects forest increases by 2.13% compared to 2016.

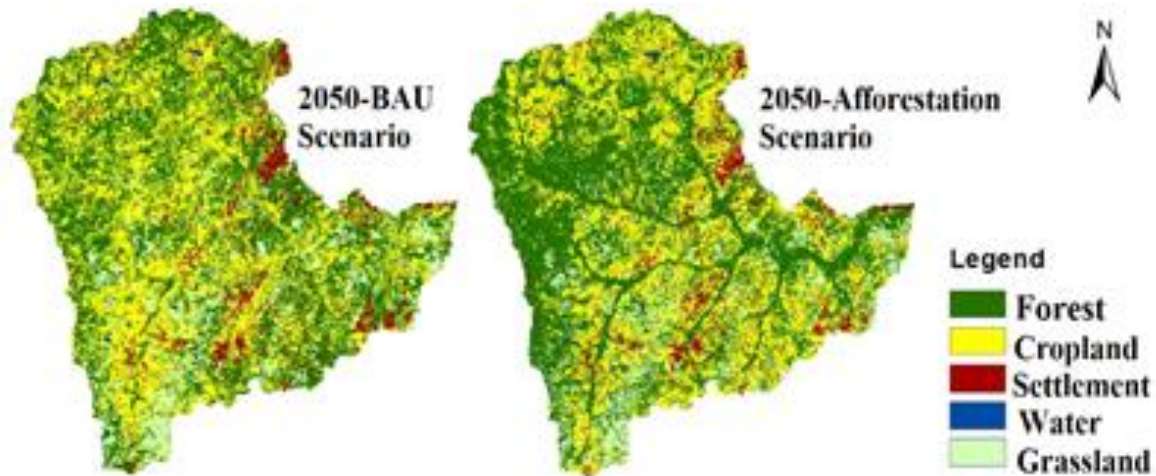


Figure 9: Trend and predicted (2050) LULC in Dano Catchment

Table 7: LULC change scenarios developed in this study

LULC	2016 Area in ha (%)	Scenario 1 (Current conditions or Business-as-usual) Area ha (%)	Scenario 2 (Afforestation) Area ha (%)
Forest	27211.05 (46.72)	22444.11 ha (38.54)	28437.66 (48.85)
Cropland	22427.82 (38.51)	27194.76 ha (46.69)	21201.21 (36.42)
Settlement	3149.46 (5.41)	3149.46 (5.41)	3149.46 (5.41)
Water	67.05 (0.12)	67.05 (0.12)	67.05 (0.12)
Grassland	5386.41 (9.25)	5386.42 (9.25)	5386.42 (9.25)

4. Discussion

4.1. LULCC Mapping in the Context of Hydrological Implications

Given the overall goal and framework of LULCC mapping, specific or targeted LULC can be monitored, which is mostly dynamic especially at a small scale. The quantified results provided clear evidence of substantial land-cover changes and forest cover degradation in the Dano catchment. Grassland has decreased between 1990 and 2000 by 2.43%, and between 2010 and 2016 by 17% while forest cover reduced by 4.3% and 18.8% of its area per year between 1990 to 2000 and 2010 to 2016 respectively (Table 7). There is an encroachment of settlement and farmland into water bodies, and forest occurred mainly along the river-lines as seen in Figure 4. A slight increase in Water body over the period analyzed was due to the creation of reservoirs for agriculture (irrigated) in the catchment.

Earlier studies in different parts of West Africa that investigated LULC changes and within similar timeframe have reported increases in cultivated land and shrubland areas in the periods investigated (Obahoundje et al., 2017). Results obtained from the historical Landsat classifications (Figure 4) confirmed the decrease in the extent of savannah woodland and grasses which is consistent with observation made by Yira et al. (2016) and revealed that the study catchment experienced interim losses in the cropland area between 2000 and 2010 (Forkuor et al., 2014). These local studies are illustrative of land-use change in small-scale farming communities.

The settlement class is seen to have tripled and hamlets of scattered houses are seen mostly surrounded by farmlands due to the rural nature of the catchment. But, in the recent decade (2010 and 2016), 9% decrease in the settlement class was observed which can be attributed to migration to cities

in search of better jobs and higher-quality education to improve their livelihoods as the area is close to the capital city and principal towns. If this settlement increase at a rapid rate, as observed continues, this would significantly decrease forest areas with the resultant effect on water yield (Akpoti et al., 2016) and further impact negatively via soil erosion. Forest has high capacities for regulating and supporting ecosystem services, such as carbon sequestration, the preservation of habitats and biodiversity. Increase deforestation rate also contributed to surface runoff increase and it is also responsible for downflow sedimentation (Yira, 2016). The rapid expansion of agricultural land use and urbanization are significant drivers of water quality degradation and inherently plays a leading role in water pollution.

4.2. Explaining the Driving Forces and Analyzing Connections at the Catchment Level

With increasing climate change impacts including variable rainfall and flood events, encroached water bodies used for farming make people and properties in those locations vulnerable. Uncontrolled lateral expansion of cultivated lands, deforestation, grassland degradation and loss of wetland in the area were the main forms of land change, which poses a direct and indirect threat to essential ecosystem especially water resources.

Numerous factors could account for the observed decrease in forest and cropland increase in the Dano catchment. The observed LULCC is governed by biogeographical and socio-economic factors and one obvious factor is rapid population growth. Several studies have noted that the growing population has often led to the expansion of the cultivated area in West Africa (Lambin et al, 2003, Ouédraogo, 2010). The population in the Ioba province (where Dano catchment is located) increased by 19% between 1996 and 2006 (INSD, 2007). Further insight into the agricultural expansion reveals significant strong correlations with population from 2001 and 2014 (Knauer et al., 2017), confirming a possible linkage between the observed cropland increase in the catchment from 2000 to 2016. The total rural population of Burkina Faso has also been reported to moderately increase up to 244,000 people at that time. Overall, cropland increased from 37 to 39 % during the study timeframe. Population growth increases the demand for more cultivated land, fuelwood, and infrastructural development; which invariably leads to vegetative cover losses. This can also be associated with certain agricultural and political policies in Burkina Faso (e.g. Community-Driven Development) which resulted in deforestation (Braumoh, 2009).

The distribution of rainfall is another determinant that was responsible for the observed changes in cropland area in the catchment during the period of investigation. For instance, the poor rainfall distribution in 2002/2008 (Figure 10) is a possible cause of the reduction in agricultural areas from 47% in the year 2000 to 37% in 2010. These inconsistent rainfall events which have been reported by other studies (Kabo-Bah et al., 2016; Tossou et al., 2017) cause drought events that contribute to land degradation. The increase in water bodies recorded for 2010 and 2016 can be linked to high precipitation events, reservoirs, and dam constructions.

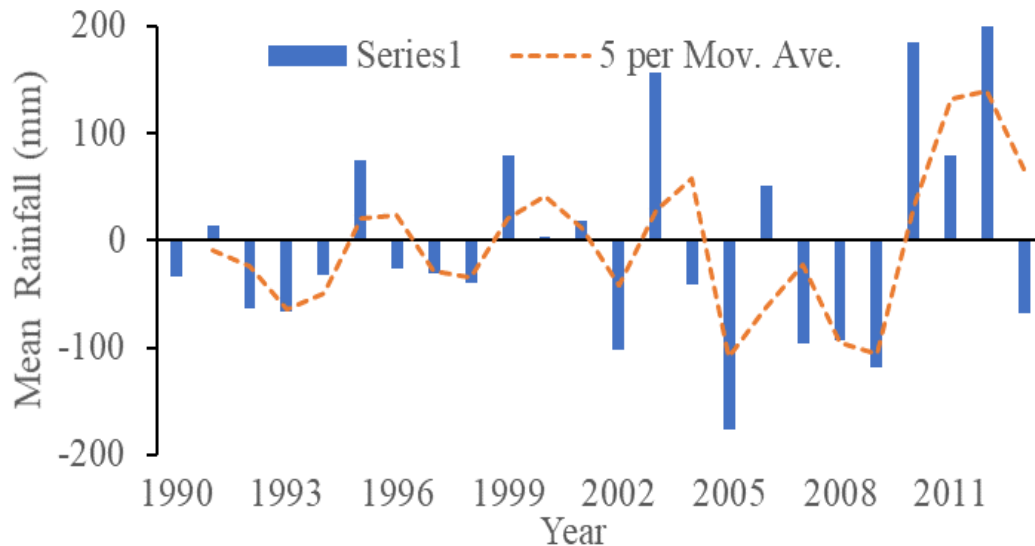


Figure 10: Long-term (1990 to 2013) annual rainfall (mm) anomaly in Dano

Further, this drastic decrease in the area of cropland is also likened to prevalent flooding in West Africa and other parts of Sub Saharan Africa (SSA) in 2007 which destroyed properties, eroded farmlands and led to the loss of lives (Levinson and Lawrimore, 2008). Although annual precipitation in Dano was low in the year 2007 as compared to 2006, careful examination of the mean monthly totals bared that anomalous rainfall amounts in July/August 2007 and little excess from the previous year (>50) mainly caused the flooding. Similarly, this analysis is supported by (Tazen et al., 2018) who investigated the relationship between flood trends and extreme precipitation events. The study concluded that especially in from the 2000s, the flood frequency increased from 2 to 3 per year since 1986. 40% loss of the cropland area consists of the total eroded areas. Soil erosion is widely experienced in the region. However, the percentage of cropland area increased at an annual rate of 24.8% in the last decade could be farmers' response to a possible farm loss in the previous years via agricultural intensification and extension.

In contrast to cropland decrease, forest increase observed at that period, in line with the recent study by Knauer et al. (2017) can be partly due to recovery, long-term fallow system, and reforestation via Reducing Emission from Deforestation and Forest Degradation (REDD) initiatives and policy on protected areas. In response to environmental concerns, a large number of restoration and protection measures have been implemented (enclosures of plantations, policy interventions, tree-planting campaigns). However, tree planting and assisted natural regeneration of indigenous trees are important drivers of regrowth/revegetation in this region (Bramoh, 2009).

Nevertheless, Dano experienced a decline in the forest resulting from deforestation for agriculture, bush burning, urban growth and possibly flood occurrence in the farming season of 2007. According to IUCN (2005), major accelerators of forest decline in the catchment's areas consist of human activities such as harvesting wood for cooking, the source of energy and poor forest management.

Also, low agricultural production has contributed to an increase in deforestation (Etongo, Djenontin, & Kanninen, 2016). Duaze (2004) observed that farmland soils were the lowest in fertility when compared to other land-use types. Generally, soils in this region are of low fertility and continuous farming will lead to degraded soils and low productivity. Upper soils are usually sandy and very susceptible to erosion and compaction. The declining soil fertility in farmlands in a combination of the growing population and other factors, put more pressure on land resources (Callo-Concha et al., 2013), therefore, leading to further land degradation. Moreover, the interrelation of this LULCC with climate change is expected to further lead to severe land degradation (Thiombiano and Tourino-Soto, 2007). As an important factor controlling a basin's hydrology, LULCC continuation in this area aid to

accelerate modification of the catchment's climate. Understanding these drivers at a small level is imperative to aid the formation of adequate policies.

4.3. Study Relevance to National and International Goals

This study results, even though on a small scale, are relevant in; 1) formulation and implementation of national development policies such as 'Politique Forestière Nationale' of Burkina Faso 2) achieving the United Nation's sustainable development goals (SDGs) and 3) decision making as input to biophysical and socioeconomic models. For instance, *Stratégie Nationale de Gestion des Feux en Milieu Rural* outlines policies and strategies aimed at sustainable forest and agricultural management so as to reduce the poverty of the rural areas and enhance the livelihoods of forest communities as outlined in Burkina Faso's national strategy for poverty reduction (MEF, 2004). These are to be adopted by the local government institutions (e.g. provinces, municipalities and departments) in Burkina Faso. As Dano catchment forms a substantial part of Ioba province, results obtained can contribute to achieving local scale targets in land use planning and climate change adaptation. Kalame et al, 2008 highlighted that the present forest policies in Burkina Faso, however, lacked clear objectives on climate change adaptation (and/or mitigation) but contain elements of risk management practice. In this regard, the objectives and result from this study, particularly the predicted LULC pattern, will assist relevant national authorities to develop specific strategies such as the development of pro-poor REDD policies that will ensure sustainable use of resources and attain economic opulence. On one hand, the predicted cropland expansion under the business as usual scenario (see section 3.4), will mean to encourage of agricultural management practices and policies that reduce GHG emissions and subsequent negative climate change effects. On the other hand, the pursuit of scenario 2 (afforestation), which predicted an increase in savannah woodland, will require promoting best practices and climate-smart agriculture (CSA) such that a reduction in cropland area will not necessarily lead to food insecurity.

In addition to national relevance, the study results can contribute to monitoring progress towards attaining SDG goals 6 (WASH) and 15 (Life on earth). For example, the historical and predicted LULC change pattern can provide indicators to address the different relevant targets as in the case of 15.1.1 & 15.2.1. Specifically, unsustainable LULC dynamics and land degradation observed in the catchment as cropland expansion and poor agricultural practices are indicators of ecosystem modifications such as the catchment water balance that will certainly lead to alteration of the hydrological regime. Similarly, LULC transition probabilities between the present state and predicted (2050) provide insight on the calculated indicator for forest area as a proportion of total land area (15.1.1). Trade-offs between agriculture and forest can be managed through spatial management and use of degraded lands. Land use intensification such as bush fallow should be encouraged as mitigation practices and incentives should be given to retaining tree cover. Equally, the outputs from this study can be used in ecohydrological models for decision making of ecological management. Combining the approach of hydrologic modeling and scenario analysis, (Bossa, Diekkrüger, & Agbossou, 2014) observed that savannah conversion to cropland intensified annual runoff with a high risk of flooding erosion rates. The predicted LULC pattern scenarios in this study can provide insight into how much the hydrological ecosystem (freshwater availability) will be impacted and an appreciation of whether or not SDG 6 can be achieved. Thus, climate change-related risks such as droughts and flood, recently found to have intensified as a result of LULC change (Sylla et al., 2016), can also be minimized when appropriate measures are taken based on results of such simulations.

5. Conclusion

This study examined the historical LULCC in the Dano catchment between 1990 and 2016 and projected the LULC patterns for two future (2050) scenarios using the CA-Markov chain model. Results revealed clear evidence of substantial land-cover changes and forest cover degradation in the catchment. The trend of decreasing in the forest and increasing cultivated land during the historical

period is expected to continue in 2050 under the BAU scenario, while under afforestation scenario a potential increase in vegetation was projected. Furthermore, the study findings provide solid evidence that deforestation reinforces land degradation across the catchment which poses a major threat to ecosystem sustainability of the landscape especially water resources for the future. To ensure food security and circumvent deforestation, a well-planned and sustainable land use practices would be desirable in the area. The outcome of this study is useful for the sustainable development of the future Dano watershed. The study recommends future research should pay more attention to the use of multiple socioeconomic predictors/drivers (e.g. Land policy data) of land degradation to improve the understanding of the environmental change effect caused by LUCC and the precision of the future projection.

Acknowledgement

This work was supported by Graduate Research Program in Climate Change and Adapted land use (GRP-CCLU) of the West African Science Centre on Climate Change and Adapted Land Use (WASCAL) funded by Federal Ministry of Education and Research (BMBF). We thank Heinmann and Barro for their assistance during the field work.

Funding

This work which is part of a doctoral study has been funded by the German Federal Ministry of Education and Research (BMBF) through West Africa Science Centre of Climate change and Adapted Land use (WASCAL).

Conflicts of Interest

The authors declare no conflict of interest

References

- Akpoti, K., Antwi, E. and Kobo-bah, A. 2016. Impacts of rainfall variability, land use and land cover change on stream flow of the Black Volta Basin, West Africa. *Hydrology*, 3(3), p.26.
- Awotwi, A., Anornu, G.K., Quaye-Ballard, J.A. and Annor, T. 2018. Monitoring land-use/land-cover changes due to extensive gold mining, urban expansion and agriculture in the Pra River Basin of Ghana, 1986-2025. *Land Degradation & Development*, pp.1–13.
- Baatuuwie, B.N. 2015. Multi-dimensional approach for evaluating land degradation in the Savanna belt of the White Volta Basin. PhD Dissertation, Kwame Nkrumah University of Science and Technology, Kumasi, Ghana.
- Bossa, A., Diekkrüger, B. and Agbossou, E. 2014. Scenario-based impacts of land use and climate change on land and water degradation from the meso to regional scale. *Water*, 6(10), pp.3152–3181.
- Braimoh, A.K. and Vlek, P.L.G. 2004. Land-cover change analyses in the Volta Basin of Ghana. *Earth Interactions*, 8(21), pp.1–17.
- Callo-Concha, D., Gaiser, T., Webber, H., Tischbein, B., Müller, M. and Ewert, F. 2013. Farming in the West African Sudan Savanna: insights in the context of climate change. *African Journal of Agricultural Research*, 8(38), pp.4693–4705.
- Chen, J., Cao, X., Peng, S. and Ren, H. 2017. Analysis and applications of GlobeLand30: a review. *ISPRS International Journal of Geo-Information*, 6(8), p.230.

- Congalton, R.G. 1991. A review of assessing the accuracy of classifications of remotely sensed data. *Remote Sensing of Environment*, 37, pp.35–46.
- Coppin, P., Jonckheere, I., Nackaerts, K., Muys, B. and Lambin, E. 2004. Digital change detection methods in ecosystem monitoring: a review. *International Journal of Remote Sensing*, 25 (9), pp.1565–1596.
- Deng, X., Liu, J., Lin, Y. and Shi, C. 2013. A framework for the land use change dynamics model compatible with RCMs. *Advances in Meteorology*, pp.1–7.
- Duadze, S.E.K. 2004. Land use and land cover study of the savannah ecosystem in the Upper West Region (Ghana) using remote sensing (Ecology and Development Series). Cuvillier Verlag, Inhaberin Annette Jentzsch-Cuvillier, Nonnenstieg 8, 37075 Göttingen, Germany. Retrieved from <https://cuvillier.de/de/shop/publications/3006%0ACopyright>.
- Etongo, D., Djenontin, I. N. S., & Kanninen, M. (2016). Poverty and Environmental degradation in Southern Burkina Faso: an assessment based on participatory methods. *Land*, 5(3), pp.1–23.
- Forkuor, G., Conrad, C., Thiel, M., Ullmann, T. and Zoungrana, E. 2014. Integration of optical and synthetic aperture radar imagery for improving crop mapping in northwestern Benin, West Africa. *Remote Sensing*, 6(7), pp.6472–6499.
- Gibson, L., Münch, Z., Palmer, A. and Mantel, S. 2018. Future land cover change scenarios in South African grasslands - implications of altered biophysical drivers on land management. *Heliyon*, 4(7), p.e00693.
- Hadi, S.J., Shafri, H.Z.M. and Mahir, M.D. 2014. Modelling LULC for the period 2010-2030 using GIS and remote sensing: A case study of Tikrit, Iraq. *IOP Conference Series: Earth and Environmental Science*, 20(1).
- Han, H., Yang, C. and Song, J. 2015. Scenario simulation and the prediction of land use and land cover change in Beijing, China, *Sustainability*, 7(4), pp.4260-4279.
- INSD. 2007. Re'sultats pre'liminaires du recensement ge'neral de la population et de l'habitat de 2006. Institut National des Statistiques et de la Demographie (INSD). Direction de la Demographie, Ouagadougou, Burkina Faso.
- INSD. 2014. Annuaire statistique 2013 du Burkina Faso. Direction de la Demographie, Ouagadougou, Burkina Faso.
- Kabo-Bah, A., Diji, C., Nokoe, K., Mulugetta, Y., Obeng-Ofori, D. and Akpoti, K. 2016. Multiyear rainfall and temperature trends in the volta river basin and their potential impact on hydropower generation in Ghana. *Climate*, 4(4), p.49.
- Kasei, R., Diekkrüger, B. and Leemhuis, C. 2010. Drought frequency in the Volta Basin of West Africa. *Sustainability Science*, 5(1), pp.89–97.
- Knauer, K., Gessner, U., Fensholt, R., Forkuor, G. and Kuenzer, C. 2017. Monitoring agricultural expansion in Burkina Faso over 14 years with 30 m resolution time series: The role of population growth and implications for the environment. *Remote Sensing*, 9(2).
- Lambin, E.F., Geist, H.J. and Lepers, E. 2003. Dynamics of land-use and land-cover change in tropical regions. *Annual Review of Environment and Resources*, 28(1), pp.205–241.

Levinson, D.H. and Lawrimore, J.H. 2008. State of the Climate in 2007. *Bulletin of the American Meteorological Society*, 89(7), pp.S1–S179.

Mahmoud Ibrahim, M. 2016. Integrating geoinformation and socioeconomic data for assessing urban land-use vulnerability to potential climate-change impacts of Abuja. PhD Thesis, Kwame Nkrumah University of Science and Technology, Kumasi, Ghana.

Minaei, M., Shafizadeh-Moghadam, H. and Tayyebi, A. 2018. Spatiotemporal nexus between the pattern of land degradation and land cover dynamics in Iran. *Land Degradation and Development*, pp.2854–2863.

Moges, D.M. and Bhat, H.G. 2018. An insight into land use and land cover changes and their impacts in Rib catchment, north-western highland Ethiopia. *Land Degradation & Development*, pp.1–14.

Mukhopadhyaya, S. 2016. Land use and Land Cover Change Modelling using CA-Markov case study deforestation analysis of Doon Valley. *Journal of Agroecology and Natural Resource Management*, 3(1). Available from:

https://www.researchgate.net/publication/303547816_Land_use_and_Land_Cover_Change_Modelling_using_CA-Markov_Case_Study_Deforestation_Analysis_of_Doon_Valley. Accessed Jul 11 2019.

Nadoushan, M.A., Soffianian, A. and Alebrahim, A. 2012. Predicting urban expansion in Arak Metropolitan Area using two land change models. *World Applied Science Journal*, 18, pp.1124–1132.

Nazzal, J.M. El-Emary, I.M. and Najim, S.A. 2008. Multilayer perceptron neural network (MLPs) for analysing the properties of Jordan oil shale. *World Applied Science Journal*, 5, pp.546–552.

Obahoundje, S., Ofori, E., Akpoti, K. and Kabo-bah, A. 2017. Land use and land cover changes under climate uncertainty: modelling the impacts on hydropower production in Western Africa. *Hydrology*, 4(1), p.2.

Olofsson, P., Foody, G.M., Herold, M., Stehman, S.V., Woodcock, C.E. and Wulder, M.A. 2014. Good practices for estimating area and assessing accuracy of land change. *Remote Sensing of Environment*, 148, pp.42–57.

Olofsson, P., Foody, G.M., Stehman, S.V. and Woodcock, C.E. 2013. Making better use of accuracy data in land change studies: Estimating accuracy and area and quantifying uncertainty using stratified estimation. *Remote Sensing of Environment*, 129, pp.122–131.

Ouedraogo, I., Tigabu, M., Savadogo, P., Compaoré, H., Odén, P.C. and Ouadba, J.M. 2010. Land cover change and its relation with population dynamics in Burkina Faso, West Africa. *Land Degradation and Development*, 21, pp.453-462.

Pontius, R.G. and Millones, M. 2011. Death to Kappa: Birth of quantity disagreement and allocation disagreement for accuracy assessment. *International Journal of Remote Sensing*, 32(15), pp.4407–4429.

Reynolds, J., Cherlet, M., Hutchinson, C., Hill, J., Von Maltitz, G. and Sommer, S. 2018. Rethinking land degradation and sustainable land management. EUR: KJ-07-17-008-EN-N.

Ruelland, D., Levvasseur, F. and Tribotté, A. 2010. Patterns and dynamics of land-cover changes since the 1960s over three experimental areas in Mali. *International Journal of Applied Earth Observation and Geoinformation*, 12(suppl. 1).

Sylla, M. B., Elguindi, N., Giorgi, F. and Wisser, D. 2016. Projected robust shift of climate zones over West Africa in response to anthropogenic climate change for the late 21st century. *Climatic Change*, 134(1–2), pp.241–253.

Tazen, F., Diarra, A., Kabore, R.F.W., Ibrahim, B., Bologo/Traoré, M., Traoré, K. and Karambiri, H. 2018. Trends in flood events and their relationship to extreme rainfall in an urban area of Sahelian West Africa: The case study of Ouagadougou, Burkina Faso. *Journal of Flood Risk Management*, pp.1–11.

Tewelde, M.G. and Cabral, P. 2011. Urban sprawl analysis and modeling in Asmara, Eritrea. *Remote Sensing*, 3(10), pp.2148–2165.

Thiombiano, L. and Tourino-Soto, I. 2007. Status and trends in land degradation in Africa. In *Environmental Science and Engineering (Subseries: Environmental Science)*. pp.39–53. Springer Berlin Heidelberg, Heidelberg, Berlin.

Thorn, A.M., Thompson, J.R. and Plisinski, J. 2016. Patterns and predictors of recent forest conversion in New England. Intended for “Land”. Available from: <http://Harvardforest.Fas.Harvard.Edu/Jt/Publications>, pp.1–17.

Tossou, E.M., Ndiaye, M.L., Traore, V. B., Sambou, H., Kelome, N.C., Sy, B.A. and Diaw, A.T. 2017. Characterisation and Analysis of Rainfall Variability in the Mono-Couffo River Catchment Complex, Benin (West Africa). *Resources and Environment*, 7(1), pp.13–29.

van de Giesen, N., Andreini, M., van Edig, A., Vlek, P., Giesen, N.V.N.D.E., Andreini, M. and Vlek, P. 2001. Competition for water resources of the Volta basin. In *Regional Management of Water Resources (Proceedings of a symposium held during the Sixth IAHS Scientific Assembly at Maastricht, The Netherlands, July 2001)*. IAHS Publication No. 268, 1964, pp.199–205.

Yira, Y., Diekkrüger, B., Steup, G. and Bossa, A.Y. 2016. Impact of climate change on water resources in a tropical West African catchment using an ensemble of climate simulations. *Hydrology Earth System Sciences*, 537, pp.187–199.

Research Article

Sugarcane mapping in Paraná State Brazil using MODIS EVI images

Clóvis Cechim Júnior^{1*}, Jerry Adriani Johann², João Francisco Gonçalves Antunes³ and Flávio Deppe⁴

^{1,2}Agricultural Engineering Department, State University of West Paraná (UNIOESTE), Cascavel, Paraná, Brazil

³Embrapa Agricultural Informatics (EMBRAPA), Campus of Unicamp, Campinas, São Paulo, Brazil

⁴Meteorological System of Paraná (SIMEPAR), Curitiba, Paraná, Brazil

Correspondence should be addressed to Clóvis Cechim Júnior, juniorcechim@hotmail.com

Publication Date: 7 April 2020

DOI: <https://doi.org/10.23953/cloud.ijarsg.451>

Copyright © 2020 Clóvis Cechim Júnior, Jerry Adriani Johann, João Francisco Gonçalves Antunes and Flávio Deppe. This is an open access article distributed under the **Creative Commons Attribution License**, which permits unrestricted use, distribution, and reproduction in any medium, provided the original work is properly cited.

Abstract Sugarcane cultivated in Brazil deserves attention because it makes the Country the world's largest producer of sugar and ethanol. The aim of this work was to develop and evaluate a methodology for sugarcane mapping in Paraná State, Brazil using temporal series of the MODIS EVI, for 2010/2011 to 2013/2014 crop seasons. The methodology included supervised classification Fuzzy ARTMAP, taking as input variables such as terms of harmonics amplitude and phase, and phenological metrics of culture. Area estimates indicated a moderate and strong correlation (r_s), ranging from 0.62 to 0.71 comparing with IBGE official data and from 0.79 to 0.87 with the Canasat data. To assess mapping accuracy, Canasat vector maps were used as reference to build the confusion matrix. The method developed based on Fuzzy ARTMAP proved efficient to map and estimate the acreage of sugarcane in the State of Paraná, due to digital processing techniques used in homogeneous samples, selection of phenological seasonal metrics, and decomposition of images in accordance with harmonics and supervised training. These together minimized the neural network forecast errors. Results indicate that the methodology is appropriate for sugarcane mapping.

Keywords *Annual agriculture; timeseries; vegetation index*

1. Introduction

Brazil is a key player in world agricultural crop production, due to its wide territorial extension and the adoption of high level crop technology. The availability of reliable and fast information is important for agricultural planning and management and also to ensure more stability of agricultural market prices. In this way, it becomes essential to adopt techniques which allow to systematically monitoring in short and medium time the cultivated areas of different agricultural crops. Many studies (Johann et al., 2012; Arvor et al., 2012; Victoria et al., 2012; Vicente et al., 2012; Grzegozewski et al., 2016) have showed that the use of satellite images and remote sensing techniques allow agricultural crop mapping and area estimates of different crops.

With the use of remote sensing agricultural crop mapping can be done in advance compared to the method adopted by official organizations which use indirect methodologies and take into account some subjective procedures, such as questionnaires that are sent to cooperatives, to equipment resellers and other agencies linked to each production chain (IBGE, 2002).

An example of sugarcane monitoring project is the Canasat (Rudorff et al., 2010). The aim of this project was to map sugarcane areas, initially in São Paulo State and subsequently to the other States in the South Brazil. The methodology used was visual interpretation of LANDSAT, CBERS and RESOURCESAT-I images for sugarcane mapping and area estimates. In this context it is necessary to search for new ways to monitor these areas.

Currently, TERRA and AQUA MODIS images are suitable for agricultural monitoring due to high temporal resolution and moderate spatial resolution (Galford et al., 2008; Sakamoto et al., 2010). MODIS images have been used in both mapping and monitoring agricultural crops (Xavier et al., 2006; Johann et al., 2012; Brown et al., 2013; Santos et al., 2014; Mengue and Fontana, 2015; Souza et al., 2015; Grzegozewski et al., 2016), and specifically for sugarcane which is a semi-perennial crop (Silva et al., 2010; Ordones et al., 2010; Fernandes et al., 2011; Adami et al., 2012; Alves et al., 2014; Duft et al., 2015; Antunes et al., 2015a).

The use of MODIS vegetation indexes products, such as EVI (Enhanced Vegetation Index) and NDVI (Normalized Difference Vegetation Index), allows to establish the default spectro-temporal data to identify different agricultural crops (Johann et al., 2016) and map large territorial extensions with repetitivity and low costs. The timeseries of vegetation indices, used in mappings, can also be used to examine the Earth's surface changes, finding evidence of changes in vegetation development and demonstrate standards of temporal dynamics (Jia et al., 2011).

To analyse multi temporal remote sensing images the harmonic analysis or Fourier Analysis has been used (Jakubauskas et al., 2001), as it allows the characterization of vegetation phenology based on temporal changes, allowing the understanding of temporal dynamics of vegetation cover (Jakubauskas, 2001; Lacruz, 2006). The oscillatory temporal behaviour throughout the timeseries can be associated to the vegetation productive cycles and seasonal variation of photosynthetic activity (Victoria et al., 2009).

In this context, the aim of this study was to map and estimate cultivated areas of sugarcane, in the State of Paraná, using timeseries MODIS EVI images and a supervised Fuzzy ARTMAP classification model for 2010/2011 to 2013/2014 crop years.

2. Study Area

Brazil is the largest sugarcane producer, with the average of 271.4 million tonnes (1961 to 2013 crop seasons), followed by India with around 207.5 million tonnes (FAOSTAT, 2016). Brazil is also the largest sugar producer, accounting for 20% of the world production and 40% of global sugar exports. It is the second largest producer of ethanol, accounting for 20% of world production and 20% of global exports (UNICA, 2015). The study area includes the Paraná State in Brazil's Southern region (Figure 1). Paraná State is the 5th largest national sugarcane producer, with an average (between 2010 to 2014) of 7.5 million tons of sugarcane per year, which represents 7.1% of the national production (IBGE, 2016). It has 399 municipalities; however, the concentration of sugarcane fields is in the mesoregions Northwest, Central North and Pioneer North.

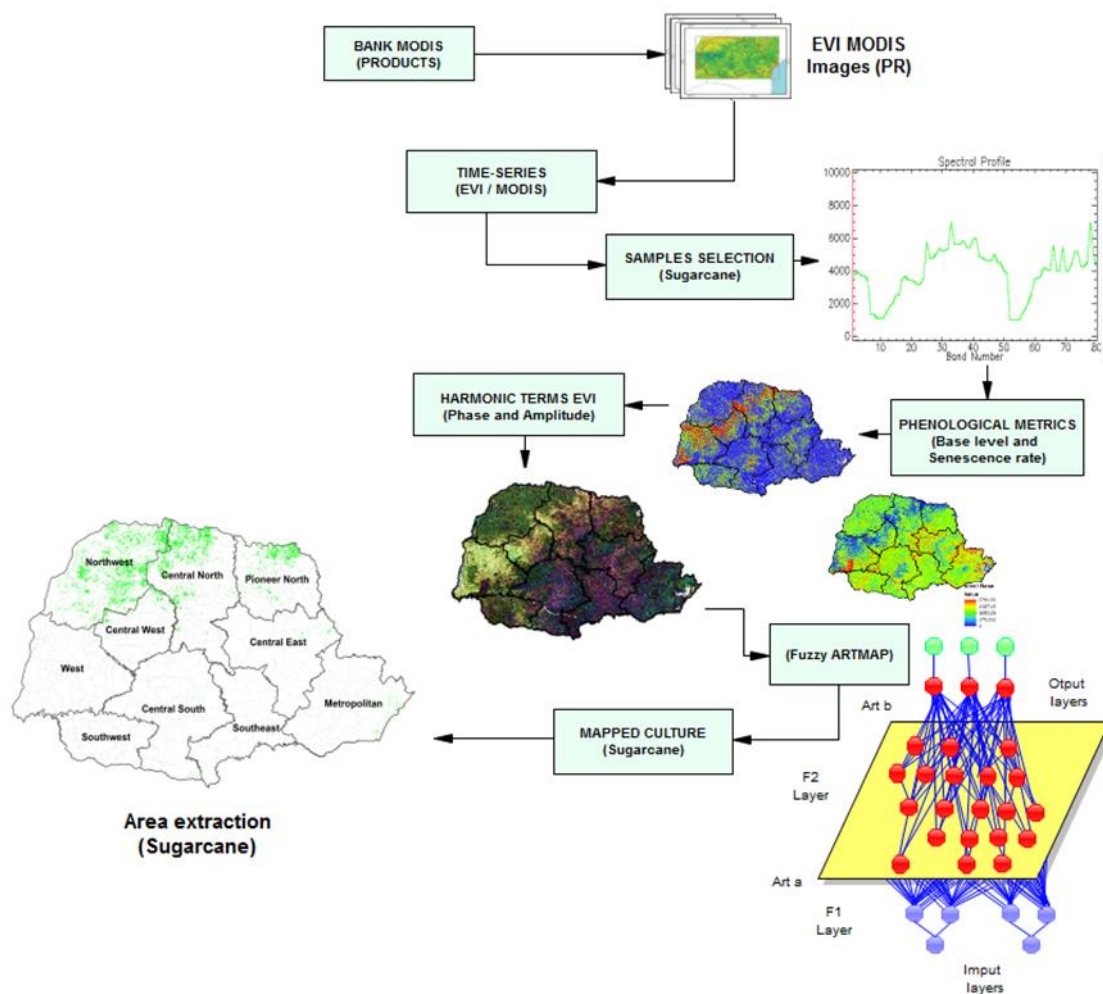


Figure 1: Methodological flowchart for generation of mapping in the Paraná state.

3. Data Used and Methods

The research method consisted of the following steps: (i) Acquisition of satellite images; (ii) Decomposition of EVI timeseries; (iii) Extraction of phenological seasonal metrics; (iv) Selection of sampling homogeneous sets; (v) Digital processing; (vi) Stratified random sampling; (vii) Fuzzy ARTMAP classification model; (viii) Accuracy analysis; (ix) Comparison analysis of area with official data of IBGE and Canasat.

3.1. Acquisition of satellite images

The timeseries TERRA and AQUA MODIS images were gathered from EMBRAPA (Brazilian Agricultural Research Corporation). The geodetic reference System is WGS-84, in geographical coordinates (latitude and longitude) and in GeoTIFF (Geographic Tagged Image File Format). The image source was the Land Processes Distributed Active Center (LP DAAC). Products available included EVI (Enhanced Vegetation Index) images with a spatial resolution of 250 meters, with 46 annual compositions from TERRA and AQUA satellites, updated every 16 days.

The vegetation index EVI proposed by (Huete et al., 1997), was developed to be used with MODIS sensor images. Applications include sugarcane mapping due the optimization of spectral response of vegetation, improving sensitivity in regions of higher densities of biomass, provide monitoring of vegetation by reducing canopy substrate and atmospheric influences (Huete et al., 1997; Huete et al., 1999; Huete et al., 2002).

3.2. Decomposition of EVI time series

Before running the algorithm, it was necessary to stack the timeseries images for the period used for sugarcane mapping (September to April) for each crop year. This is the period of greatest growth of sugarcane including tilling phase until the vegetative peak. For this procedure it was used an IDL (Interactive Data Language) routine developed by Esquerdo et al. (2011) which implements time series stacking of vegetation index images.

The second procedure consisted on decomposition of EVI time series in harmonic terms (composition of images of amplitude and phase), and variance calculation of each harmonic in each series, which was made from the application of HANTS algorithm (Harmonic Analysis of Time-Series NDVI) (Roerink et al. 2000).

The harmonics terms were generated on a per-pixel basis for each time series composition, which decompose the annual variation of the EVI and are represented by the average (0 harmonic), by phase that indicates the culture cycle and ranges from 0° to 360° and by amplitude (1 harmonic) which indicates the maximum mode of variation of vegetation for the entire period (Antunes et al., 2016).

The HANTS algorithm was implemented in IDL by De Wit and Su (2005) and it aims to eliminate high-frequency oscillations called noises. In addition to using the seasonal effect evidenced by the development of vegetation, turning them into low-frequency sine functions in different phases and amplitudes, it indicates the period of time series associated with the development cycles of the phenological stages, and also, perform as smoothing filter in the image time series.

3.3. Extraction of phenological metrics

The third procedure was to extract the phenological metrics "base level" and "rate of senescence" temporal series of EVI of sugarcane (Figure 1), using TIMESAT software (Eklundh and Jönsson, 2015). These metrics were extracted from 506 EVI images and the whole study area fit inside one MODIS tile (TERRA and AQUA) for the period of October 2004 through September 2014, after going through the procedure of noise filtering and smoothing by Savitzky-Golay filter (Savitzky and Golay, 1964; Luo et al., 2005). The metrics represent a synthesis (average) of the temporal series and assist on separability between land cover classes (Antunes, 2014).

3.4. Selection homogeneous pixel set

The selection and acquisition of the sample data set used Canasat maps as reference; the pixel selection was based on the homogeneity (pure pixels) of the sugarcane spectral response. However, the sample data set could also be gathered by analyzing the temporal spectrum profile of EVI characteristic of sugarcane directly on the MODIS images (Cechim Júnior et al., 2016). The pixels used as samples in the classifiers must represent homogeneously the cultivation of sugarcane and must eliminate the interference of different targets present in images.

The mesoregions Northwest, Pioneer North and Central North of Paraná State show greater concentration of sugarcane and high production relative to the rest of the state. Therefore, have a higher probability of occurrence of pure pixels, which make the spectrum-temporal profiles of EVI in this region more characteristic of areas of cultivation of sugarcane, compared to spectrum-temporal profiles of mesoregions West and Southwest where the presence of cultivated areas of sugarcane is not very significant because of the large amount of soybeans and corn cultivated.

3.5. Digital image processing

In order to build the sampling frame, actual Canasat polygons were used as reference and GIS processing techniques were used in order to convert the vector map to raster format. The spatial degradation was based on the technics used by Foody and Cox (1994) and Antunes (2014). A low pass 9 x 9 convolution filter and resampling by nearest neighbour method was applied to match with 250 meters spatial resolution and with the same projection system of MODIS images.

The digital image processing technics were necessary to separate and sort the class of sugarcane in homogeneous regions from the gray levels present in the images converted from vector format the Canasat. Therefore, field edges were eliminated in order to avoid spectral contamination with other targets in the selection of samples.

After this, the images were converted to 8 bit range from 0 to 255 digital numbers (DN) values. The DN's ranging from 200 to 255 included homogeneous areas of sugarcane, the DN's ranging from 2 to 199 represent transitions classes, and 0 to 1, no sugarcane classes (Antunes, 2014).

In order to establish the sample sets, a stratified random sampling technique was used. Therefore, intervals from 200 to 255 DN were label sugarcane and intervals from 0 to 1 DN were label not sugarcane. This was done for each crop year.

3.6. Random sampling

To obtain a classification error around 5%, Van Niel et al. (2005) suggests using the golden rule for minimum size set of samples, calculated by [Eq. 1]:

$$n = 30 \times N \times K \quad (1)$$

where n is the total number of training samples, N is the data size (7 harmonic terms (average plus amplitude and phase frequencies 1, 2, 3)) and 2 phenological metrics of EVI). K is the number of classes (2 classes: sugarcane and not sugarcane).

In this way, the minimum sample size was 810 pixels, 540 pixels for training samples (i.e., 2/3) and 270 pixels for test samples (i.e., 1/3) which were used to assess the accuracy of the mapping. With the purpose of increasing the number of pixels of the sample set a mathematical morphological filter was used, which is a non-linear method of digital image processing. The main purpose is the quantification of geometric structures. The expansion consists in filling up or expanding the growth of pixels in an image into binary or gray scale (Haralick et al., 1987).

These procedures end up with a homogeneous set of reference samples to assist and facilitate the processing of training the classifier, which was obtained from the algebra using the Canasat reference maps to eliminate overlapping classes of training samples with the application of morphological filter.

After processing MODIS EVI time series on harmonic terms using the HANTS and phenological metrics using software TIMESAT, these images were inserted into the Fuzzy ARTMAP classifier of the IDRISI Taiga 16.05, along with the set of samples obtained by stratified random sampling in raster format.

3.7. Fuzzy ARTMAP classification model

ARTMAP networks are commonly grouped into ART1 (binary inputs) and ART2 (real entries) with unsupervised training, and ARTMAP (for clustering) with supervised training. The advantage of this type of network is the ability for automatic generation of neurons in the output layer, present a very stable structure. Therefore, achieving high immunity against noises which can be added from new

entries. The ART networks training is independent from the order of presentation of input data (Rezende, 2003).

The classification of harmonic terms of time series of EVI together with phenological seasonal metrics was carried out with self-organizing neural network of Fuzzy ARTMAP grouping, which is a non-parametric model based on Adaptive Resonance Theory of cognitive processing of the human brain, for the approach of non-linear multidimensional functions. This architecture works repeatedly to solve the dilemma 'stability x plasticity', keeping an equilibrium to create new categories of recognition when unknown standards stimulate the network and the ability to group similar patterns in the same category, preserving previously acquired knowledge (Carpenter et al., 1991).

The parameterization of the Fuzzy ARTMAP classifier proceeded according to Antunes (2014). For ART_a, the "choice parameter" was set at 0.01, the training rate was equal to 0.93 and the vigilance parameter equal to 0.94. For ART_b, training rate and parameter vigilance 1.00 was used.

The mapping layer that connects ART_b to ART_a has the same dimension of the number of output classes. In this case, there are two classes formed: the class of sugarcane and not sugarcane.

3.8. Map accuracy Analysis

The analysis of spatial accuracy was carried out according to Pontius and Millones (2011), using Overall Accuracy (OA) and Kappa agreement index (KI) (Congalton, 1991; Congalton and Green, 1999), and Inclusion Errors (IE) and Omission Errors (OE), taking as reference the Canasat maps that have an excellent accuracy (Adami, 2012).

When using the KI, to calculate the accuracy based on randomness, emerges as an option for the Overall Disagreement (OD) analysis (Pontius and Millones, 2011). This is formed by the component "Quantity", considered as the classification of incorrect proportions of pixels in classes and by "Allocation" component, which refers to the spatial distribution of incorrect pixels in classes. These components provide complementary and additional information to assist in the explanation of the error. The method proposed by Pontius and Millones (2011) derives from a single confusion matrix, in which the input variables must be entered as sample reference collections classes, which are compared with the entire population of pixels of the classes in the generated map.

Band ratio represents a transformation technique that applies by dividing the digital numbers of one band by their corresponding pixels of another band (e.g., Mather, 2004). This helps to enhance the spectral differences between the variables on land surface (Goetz et al., 1983). This technique allowed discrimination between different rock types and highlighted areas rich in specific mineral compositions (Abrams et al., 1983; Sabins 1997; Abdelkareem and El-Baz, 2016; Gad and Kusky, 2006). In addition to band ratios, PCA was used to transform the components of the image into its principal components (Loughlin, 1991; Gomez et al., 2005). This transformation has the ability to highlight the similarities and differences in the used data. The output will be eigenvectors and eigen values of the matrix covariance.

Minimum noise transformation technique also was used to segregate noise from the VNIR-SWIR ASTER Data. The advantage of this technique is to filter or remove those bands that contribute most to noise (Green et al., 1988; Boardman and Kruse, 1994). It is better technique than PCA in compressing and ordering data in relationship of their image quality. Where the PCA technique is yields linear transformations of the input data which subsequently amplify their variance, and the Minimum Noise Fraction (MNF) transform yields linear transformation which subsequently reduce their noise fraction.

3.9. Area Comparison Analysis

In the post classification step was applied the filter Sieve Classes available in the Environment for Visualizing Images (ENVI, 2016) program, which allows to increase the resolution and accuracy of the parcels mapped, and thus avoiding contamination by isolated pixels that of sugarcane.

The last step consisted of extracting area of culture with a routine developed in IDL by Esquerdo et al. (2011). The municipal area information, obtained for each crop year were compared with the data of the project Canasat area and the official Brazilian Institute of Geography and Statistics (IBGE 2016).

As statistical indicators we used the Spearman's rank correlation coefficient (r_s), the Mean Error (ME) [Eq. 2] which measures the average number of errors, the Square Root of the Mean Squared Error (RMSE) [Eq. 3] that represents the size of the errors, the coefficient of concordance refined Willmott et al. (2012) [Eq. 4] which measures the accuracy of estimated values in relation to the line 1:1.

$$ME = \frac{1}{n} \sum_{i=1}^n (O_i - E_i) \quad (2)$$

$$RMSE = \sqrt{\frac{1}{n} \sum_{i=1}^n (O_i - E_i)^2} \quad (3)$$

$$dr = 1 - \frac{\sum_{i=1}^n |E_i - O_i|}{2 \sum_{i=1}^n |O_i - \bar{O}|} \quad (4)$$

where: E_i = cultivated area of sugarcane estimated by municipality; O_i = cultivated area of sugarcane observed of the municipalities; \bar{O} = average area cultivated of sugarcane observed in the municipalities; n = number of municipalities.

4. Results and Discussion

4.1. Result obtained by the Fuzzy ARTMAP

The results of the spatial distributions of the areas cultivated with sugarcane in Paraná state showed a greater concentration in themesoregions Northwest, Central North, and Pioneer North according to maps generated by Fuzzy ARTMAP classification model for the crop years from 2010/2011 to 2013/2014. In addition, it was observed a small concentration of this culture to the North of the region of Center Western (Figure 2).

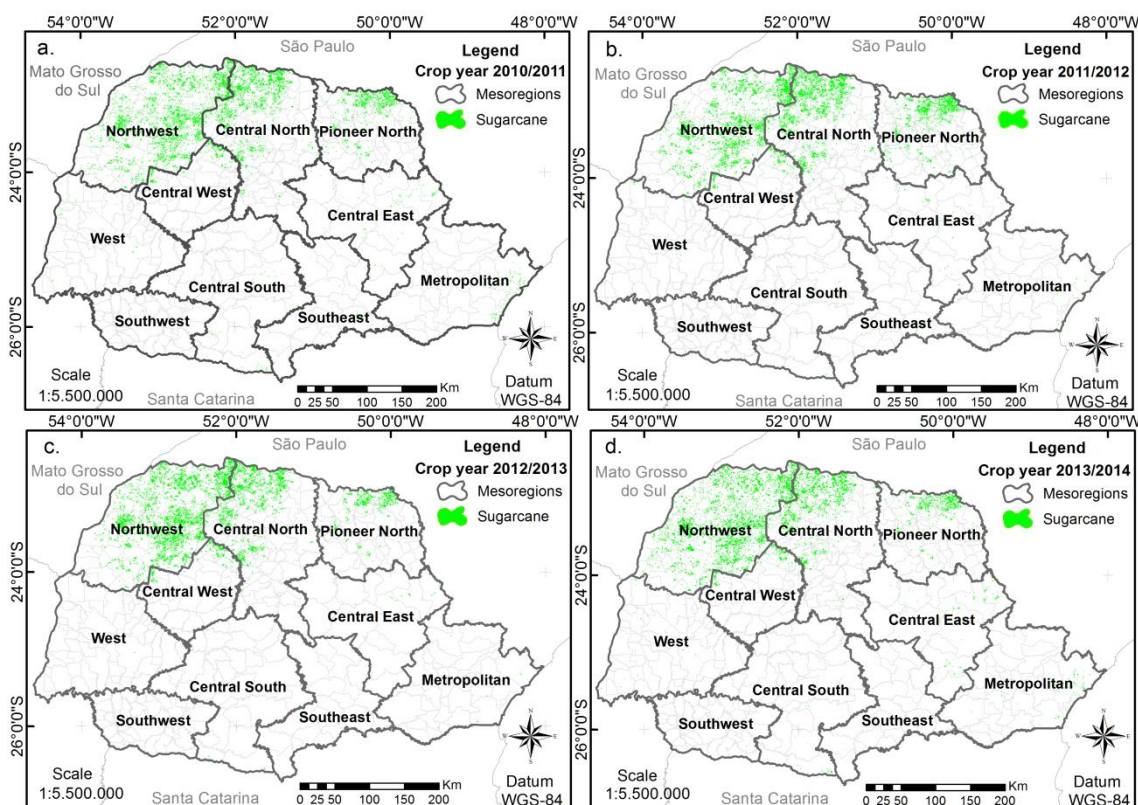


Figure 2: MODIS mappings for the cultivation of sugarcane in the Paraná state for the crop years: (a) 2010/2011; (b) 2011/2012; (c) 2012/2013; (d) 2013/2014.

4.2. Map accuracy analysis

With regards to the overall accuracy is desirable that a classification reach indexes over 85% (Foody, 2002), which was confirmed by average of the (OA) of 97.52% (Table 2) obtained by Fuzzy ARTMAP classification, which indicates a high accuracy of thematic maps generated.

The Kappa Index (KI) (Table 2) ranged from 0.81 (2013/2014) to 0.84 (2011/2012 and 2012/2013), which indicates an excellent quality of thematic classification ($KI \geq 0.81$) (Landis and Koch, 1977) generated from the Fuzzy ARTMAP classification.

In the work carried out by Antunes et al. (2015b), sugarcane mapping using classification of time series of MODIS data, obtained for the crop years from 2004/2005 to 2011/2012, KI values ranging from 0.80 to 0.85 and OA ranging from 95.09% to 95.80%. The OA reached 95.41% and average KI of 0.83.

Table 2: Indexes of accuracy obtained for Fuzzy ARTMAP mappings

Crop year	(KI)	OA (%)	Inclusion Errors (%)		Omission Errors (%)	
			Sugarcane	Not Sugarcane	Sugarcane	Not Sugarcane
2010/2011	0.83	97.53	11.35	1.99	20.56	0.99
2011/2012	0.84	97.65	8.98	2.14	23.08	0.30
2012/2013	0.84	97.69	10.19	1.63	17.35	0.89
2013/2014	0.81	97.21	9.46	2.34	24.68	0.76

The results are significant even if compared with works that use other methodologies for sugarcane mapping using MODIS data. The work by Duft et al. (2015) tested and evaluated the accuracy of maps

generated using the seasonal variation and amplitude of values of MODIS NDVI and EVI, applying HANTS harmonic analysis algorithm to smooth out the data and eliminate noise. This mapping was done for the crop year of 2009/2010 and obtained the best rating performance with a KI of 0.80 for the vegetation index EVI and KI of 0.66 for NDVI.

Similar results were found by Johann et al. (2012), with KIs varying from 0.85 to 0.90 and OA of 92.75% to 95% for summer crops in the Paraná State. The (EI) varied from 3.5% to 7.5% for summer crops and for not summer crops the variation was from 4.5% to 7.5%.

It was observed that the mappings generated from the model Fuzzy ARTMAP for class "Sugarcane" presented IE ranging from 8.98% (crop year 2011/2012) to 11.35% (crop year 2010/2011) (Table 2).

This indicates that the model classified erroneously these regions as sugarcane, but were other targets. To the class "Not-sugarcane" there was a variation of IE from 1.99% (crop year 2010/2011) to 2.34% (crop year 2013/2014). That were the targets of sugarcane not selected by the model classification. In this case, targets of pastures with spectrum-temporal profile similar to the cultivation of sugarcane contributed the representativeness of IE due to spectral confusion. The proportion of OE varied from 0.76% (crop year 2013/2014) to 0.99% (crop year 2010/2011); being this the proportion that was excluded from the class it belonged.

Although the training samples were homogeneous, the resulted higher level of error of omission of the Sugarcane class (Table 2) was the same dimension as found by Antunes et al. (2015b). In their work, they found that the error is associated with the inherent spectral variability of culture during the vegetation development cycle, which causes greater spectral confusion in the recognition of the standard spectral-temporal spectrum by the classifier.

The Overall Disagreement (OD) was used for additional accuracy assessment of Fuzzy ARTMAP mappings for 2010/2011 to 2013/2014 crop seasons. The quantity component had greatest value obtained in the crop year of 2014/2015 with 1.97%. While the lowest value registered was 1.22% in crop year 2012/2013. For the allocation component, the lowest observed value was 0.26% in the crop year of 2011/2012 and the greatest observed value was 0.75% in the crop year of 2010/2011 (Table 3).

Table 3: Overall disagreement classification models Fuzzy ARTMAP

Fuzzy ARTMAP Model	Overall Disagreement (%)	
	Quantity	Allocation
Crop years		
2010/2011	1.54	0.75
2011/2012	1.94	0.26
2012/2013	1.22	0.69
2013/2014	1.95	0.62

Antunes et al. (2015b) achieved an average total overall disagreement of 4.59%, with 2.72% of the component quantity and 1.87% of the disagreement of the allocation component. Very near and similar to the values of accuracy found in the mappings made with classification of time series of EVI/MODIS in the Paraná State, where the contribution quantity component of the total disagreement was greater than the allocation component, implying in larger proportions of incorrect pixels assigned in classes.

4.3. Comparison analysis of area

The comparison of the official IBGE data with those obtained in the mappings (Table 4), showed an average overestimation of 68,291 ha. The greatest difference was found for the crop year 2012/2013 (83,995 ha) and the lowest difference to the crop year 2013/2014 (42,354 ha), representing 13.02% and 6.22% respectively, of the total area of the State with the culture. Already comparisons of data mappings with the Canasat data had a minor difference of area in relation to comparison with the

official data of the IBGE, the largest difference for the crop year of 2010/2011 (14,464 ha), which is equivalent to 2.16%.

Table 4: Official sugarcane area IBGE and Canasat, and mappings generated by the models Fuzzy ARTMAP with regards (2010/11 to 2013/14)

Variables	Crop years			
	2010/2011	2011/2012	2012/2013	2013/2014
IBGE area (ha)	641,765	655,509	645,280	681,152
Mapping area (ha)	718,713	725,375	729,275	723,506
Difference (Map -IBGE) (ha)	76,948	69,866	83,995	42,354
Difference (%)	10.71	10.66	13.02	6.22
Canasat area (ha)	668,673	681,148	699,501	
Mapping area (ha)	683,137	694,114	701,650	
Difference (Map - Canasat) (ha)	14,464	12,967	2,148	
Difference (%)	2.16	1.90	0.31	

Data analysis compared through statistical metric (ME) indicated that State scale the area obtained by mapping was overrated between 106.15 ha (2013/2014) and 210.51 ha (2012/2013) (Figure 3).

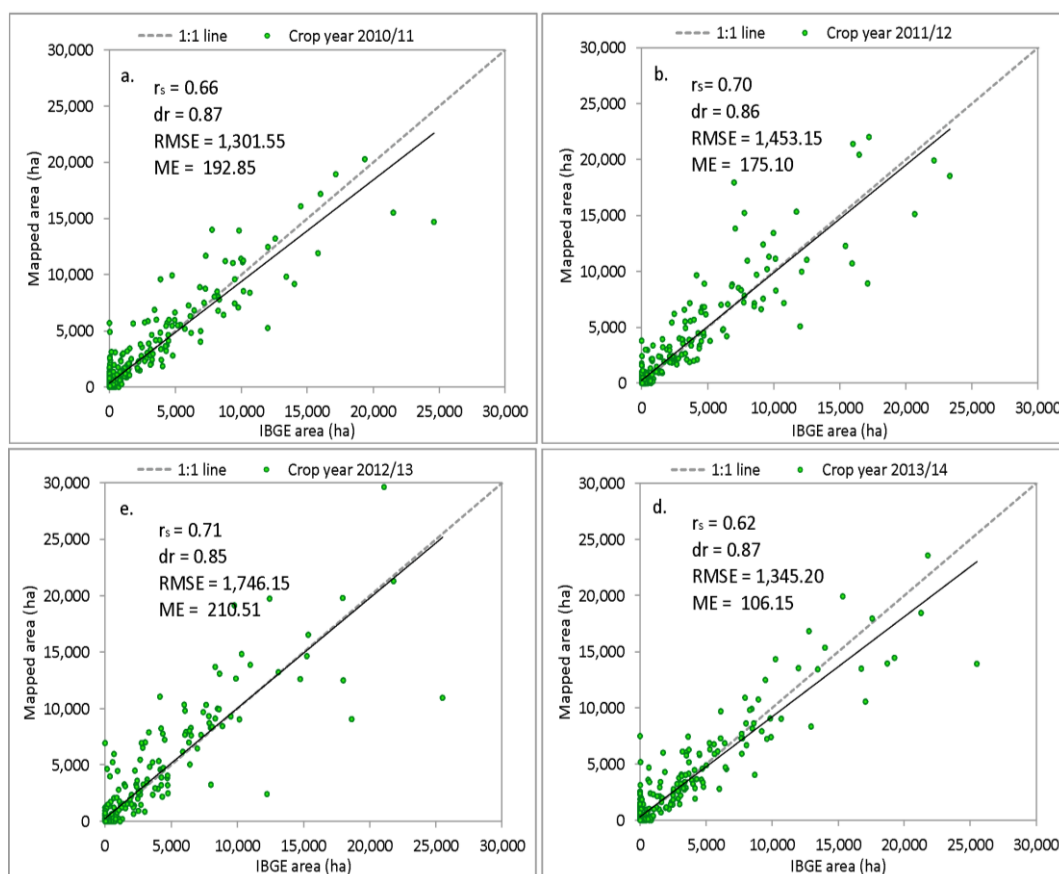


Figure 3: Relationship between the cultivated area of sugarcane of Fuzzy ARTMAP mapping and official data from IBGE for the crop years (a) 2010/2011; (b) 2011/2012; (c) 2012/2013; (d) 2013/2014

In this way, there was a trend of overestimation of cultivated area of sugarcane in the mappings generated by the Fuzzy ARTMAP classification compared to the official data of IBGE. In comparison with the Canasat data (ME) indicated that State scale the area obtained by mapping was overrated between 74.62 ha (2012/2013) and 125.41 ha (2010/2011) (Figure 4).

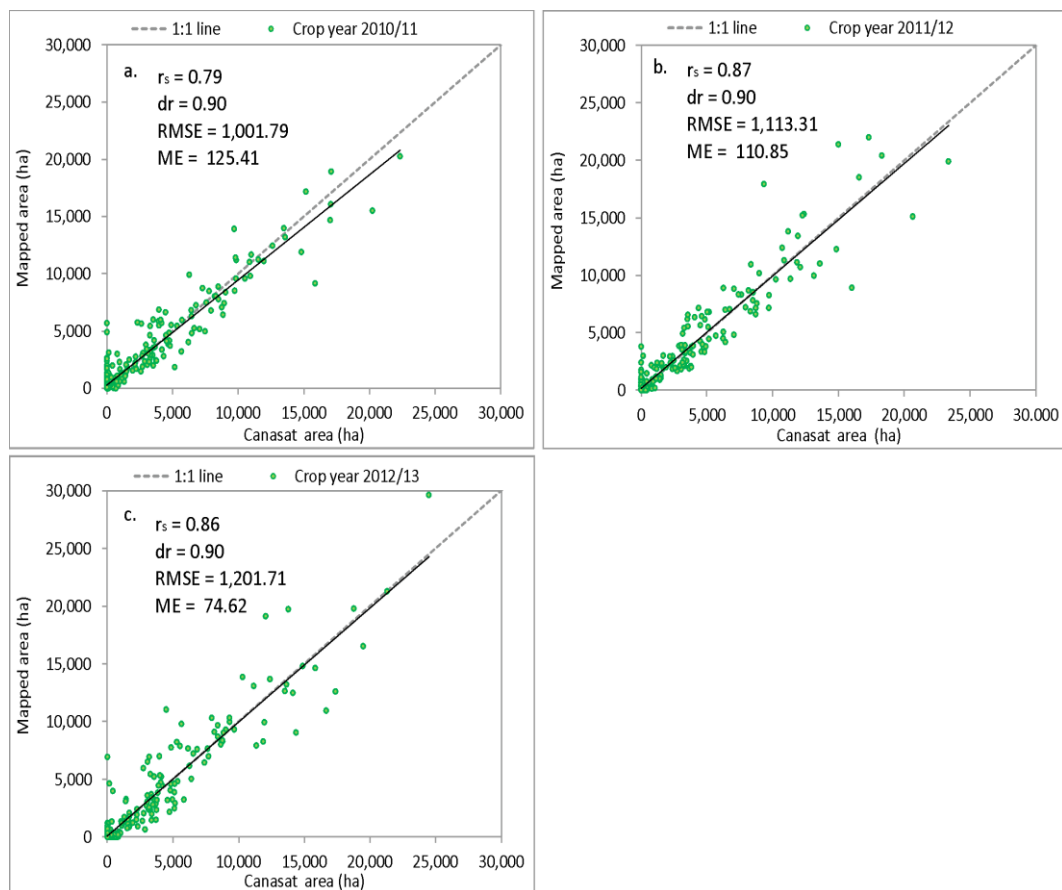


Figure 4: Relationship between the cultivated area of sugarcane of Fuzzy ARTMAP and mapping Canasat for the crop years (a) 2010/2011; (b) 2011/2012; (c) 2012/2013

Similar results were obtained by Grzegozewski et al. (2016) in their mapping of corn in the Paraná State using the MODIS sensor with overestimation of area 16% when compared with official data of the Agriculture and Supply Secretary of Paraná (SEAB). According to Santos et al. (2014) this overestimation of area with the MODIS sensor can be credited 250 m spatial resolution of the images. In virtue of this spatial resolution cultivated area estimated can be overrated or underrated. What depends on the size of the agriculture plots and the type of crop grown to be mapped.

Duft et al. (2015) in mapping of sugarcane with the NDVI also observed an overestimation with 8.3% justifying this due to problems of mistaken targets between sugarcane and grazing, which feature very similar physiology and the same type of photosynthetic metabolism. These results were also explained by Zanzarini et al. (2013) justification according to the saturation of the NDVI in the period of maximum vegetative development, where different targets feature similar spectral responses.

For the mappings of sugarcane with EVI in the Paraná State, saturation and confusion, with different targets were not observed, due to there is no large areas of pastureland and the procedure adopted in the acquisition of homogeneous samples of sugarcane, which minimize the spectral mixture that was observed by Duft et al., (2015) in the State of São Paulo in Brazil.

The RMSE showed that the size of the error produced between comparisons of estimates of area (Figure 3) had an average variation municipal from 1,311.55 ha (crop year 2010/2011) to 1,746.20 ha (crop year 2012/2013). For the Canasat data the RMSE showed that the size of the error produced between comparisons of estimates of area had an average variation municipal from 1,101.79 ha (crop year 2010/2011) to 1,201.71 ha (crop year 2012/2013).

The refined Willmott's index of agreement (dr) (Figure 3) measured the accuracy between the cultivated area estimated and observed data. In comparison with official data of IBGE varied from 0.84 (crop year 2012/2013) to 0.86 in the remaining crop years. For the Canasat data (dr) obtained was of 0.90 in all crop years the which indicates a great performance, having a high accuracy between estimates compared in all crop years evaluated.

For comparing between estimates of areas of official data of IBGE and the Fuzzy ARTMAP classifications the municipal level, was used the Spearman's correlation coefficient (r_s), because in the statistical analysis of the data showed no normalcy in the area estimates, the values obtained for the (r_s) coefficient ranged from 0.61 (crop year 2013/2014) to 0.71 (crop year 2012/2013), indicating that the estimates of cultivated area of sugarcane were moderately correlated with a positive association. Vicente et al., (2012) to compare data of cultivated area obtained between 2004 and 2009 by mappings of culture of sugarcane (generated with time series of NDVI Spot), in the State of São Paulo, with official data of IBGE, there were good correlation ($r = 0.89$), and the area estimates indicated good agreement in relation to the official data.

With regards to the municipal level comparisons with Canasat data (Figure 4), the values obtained for the (r_s) ranged from 0.79 (crop year 2010/2011) to 0.87 (crop year 2011/2012), indicating that the estimates of cultivated area of sugarcane were strongly correlated with a positive association. Ordonez et al. (2010) found that for the State of São Paulo the sugarcane cultivated area (generated with time series of MODIS NDVI images) for the crop year of 2008/2009, 75% of municipalities showed greater proximity in comparison of estimates of area with Canasat data than data from the IBGE. Therefore, indicating with what was observed in this work where the estimates of the area of sugarcane Fuzzy ARTMAP model generated were more close to Canasat than IBGE. Need to register that the methodology employed by the Canasat also make use of satellite images, resulting in better estimates with less errors due to subjective information.

The use of Fuzzy ARTMAP classification model in series spectro-temporal EVI/MODIS enabled mapping of areas under cultivation with the culture of sugarcane in municipal-scale in an efficient and objective way. This allowed generating area estimates in advance when compared to other methods analysed. This opens up possibilities of improving the estimates carried out by official bodies and use this information in state agricultural planning including crop production and transportation.

5. Conclusions

The decomposition of time series of EVI/MODIS allowed the understanding of dynamic spectro-temporal and phenological development of sugarcane.

The harmonic analysis proved to be a useful technique in the analysis of time series of vegetation index MODIS/EVI images, which along the phenological metrics obtained by TIMESAT allowed a better performance of Fuzzy ARTMAP classifier in the differentiation of agricultural areas with vegetation or pasture.

The use of images of amplitude, referring to the annual component time series of EVI, made it possible to establish the pixels that contain agricultural crops, and may also associate such images on the variance of the series that is most evident in pixels where there is the development of agricultural crops.

The spatial accuracy analysis generated by Pontius and Millones (2011) the methodology, presented greater representation when compared to the traditional method of analysis based on error matrix, since it considered a proportional sampling process.

In this way, as the classes evaluated are unbalanced (sugarcane and not-sugarcane), the method makes it possible to detect the reality of the phenomenon under study from the extrapolation of sampling sets used to assess the accuracy for the entire population in analysis, thus avoiding tendentious results.

In comparison with the data of the Canasat and official IBGE statistics, the mappings from sugarcane obtained presented a higher similarity with Canasat area estimates, despite having overrated the acreage of sugarcane.

Acknowledgments

This work was supported in part by grants from the Coordination of Improvement of Higher Education Personnel (CAPES), State University of Western Paraná (UNIOESTE) and Meteorological System of Paraná (SIMEPAR). And also for the technical-scientific partnership established by the co-author Dr. João Antunes, geotechnology researcher scientist of Embrapa Agricultural Informatics, with Ph.D. Zhe Li, currently senior remote sensing scientist in Center for Space Research of University of Texas at Austin, in support to the software for image classification used in this work.

References

- Adami, M., Mello, M. P., Aguiar, D. A., Rudorff, B. F. T., Souza, A. F. 2012. A web platform development to perform thematic accuracy assessment of sugarcane mapping in South-Central Brazil. *Remote Sensing*, 4, pp.3201-3214. <https://doi.org/10.3390/rs4103201>
- Alves, C. D., Florenzano, T. G., Alves, D. S., Pereira, M., N. 2014. Mapping land use land cover changes in a region of sugarcane expansion using TM and MODIS. *Revista Brasileira de Cartografia*, 66, pp.337-347.
- Aparecido, L. E. O., Rolim, G. S., Richetti, J., Souza, P. S., Johann, J. A. 2016. Koppen, Thornthwaite and Camargo climate classifications for climatic zoning in the State of Paraná, Brasil. *Ciência e Agrotecnologia*. Lavras:UFLA, pp. 405-4017. <http://dx.doi.org/10.1590/1413-70542016404003916>
- Arvor, D., Meirelle, M., Dubreuil, M., Dubreuil, V., Béngue, A., Shimabukuru, Y. E. 2012. Analyzing the agricultural transition in Mato Grosso, Brasil, using satellite-derived indices. *Applied Geography*, pp. 702-713. <https://doi.org/10.1016/j.apgeog.2011.08.007>
- Antunes, J. F. G. 2014. Classificação de séries temporais de dados MODIS baseada em redes neuro-fuzzy para o monitoramento sistemático do cultivo da cana-de-açúcar. 147 f. Tese (Doutorado em Engenharia Agrícola) – Faculdade de Engenharia Agrícola, Universidade Estadual de Campinas, Campinas.
- Antunes, J. F. G., Lamparelli, R. A. C., Rodrigues, L. H. A. 2015a. Avaliação da dinâmica do cultivo da cana-de-açúcar no estado de São Paulo por meio de perfis temporais de dados MODIS. *Journal of the Brazilian Association of Agricultural Engineering*, 35(6), pp. 1809-4430. <http://dx.doi.org/10.1590/1809-4430-Eng.Agric.v35n6p1127-1136/2015>
- Antunes, J. F. G., Lamparelli, R. A. C., Rodrigues, L. H. A. 2015b. Mapeamento do cultivo da cana-de-açúcar por meio da classificação de séries temporais de dados MODIS. Anais XVII Simpósio Brasileiro de Sensoriamento Remoto – SSBR, João Pessoa – PB, Brasil.
- Antunes, J. F. G., Lamparelli, R. A. C., Rodrigues, L. H. A. 2016. Representação de ciclos harmônicos de séries temporais Modis para análise do cultivo da cana-de-açúcar. *Revista Pesquisa Agropecuária Brasileira*, 5(11), pp.1868-1876. <http://dx.doi.org/10.1590/s0100-204x2016001100009>

Brown, J. C., Kastens, J. H., Coutinho, C. A., Victoria, D. C., Bishop, C. R. 2013. Classifying multiyear agricultural land use data from Mato Grosso using time-series MODIS vegetation index data. *Remote Sensing of Environment*, pp. 39-50. <https://doi.org/10.1016/j.rse.2012.11.009>

Canty, M. J. 2010. *Image analysis, classification and change detection in remote sensing: with algorithms for ENVI/IDL*. New York: CRC Press, Taylor & Francis, 2 ed., p.471.

Carpenter, G. A., Crossberg, S., Reynolds, J. H. 1991. ARTMAP: Supervised real-time learning and classification of nonstationary data by a self-organizing neural Network. *Neural Networks, Boston*, 4(5), pp. 565-588. [https://doi.org/10.1016/0893-6080\(91\)90012-T](https://doi.org/10.1016/0893-6080(91)90012-T)

Caviglione, J. H., Kiihl, L. R. B., Caramori, P. H., Oliveira, D. 2000. *Cartas climáticas do Paraná*. Londrina: IAPAR, CD-Rom.

Congalton, R.G. 1991. A review of assessing the accuracy of classifications of remotely sensed data. *Remote Sensing of Environment*, 37, pp.35-46. [https://doi.org/10.1016/0034-4257\(91\)90048-B](https://doi.org/10.1016/0034-4257(91)90048-B)

Congalton, R.G., Green, K. 1999. *Assessing the accuracy of remotely sensed data: principles and practices*. Boca Raton: CRC Press, p.160.

Cechim Júnior, C., Johann, J. A., Antunes, J. F. G. 2016. Mapping of sugarcane crop area in the Paraná State using Landsat/TM/OLI and IRS/LISS-3 images. *Revista Brasileira de Engenharia Agrícola e Ambiental*, 21(6), pp.427-432. <http://dx.doi.org/10.1590/1807-1929/agriambi.v21n6p427-432>

Grzegozewski, D. M., Johann, J. A., Opazo, M. A., Mercante, E., Coutinho, A. C. 2016. Mapping soya bean and corn crops in the State of Paraná, Brazil, using EVI images from the Modis sensor. *International Journal of Remote Sensing*, 37(6), pp.1257-1275. <https://doi.org/10.1080/01431161.2016.1148285>

De Wit, A. J. W., Su, B. 2005. Deriving phenological indicators from SPOT-VGT data using the HANTS algorithm. In: International SPOT-VEGETATION Users Conference, 2nd, Proceedings. Belgium: Antwerp, pp.195-201.

Duft, D. G., Picoli, M. C. M., Scarpore, F. V., Hernades, T. A. D., Galdos, M. V. 2015. Comparação do desempenho de índices de vegetação do sensor MODIS para mapeamento sistemático da cana-de-açúcar. SBSR - XVII Simpósio Brasileiro de Sensoriamento Remoto, João Pessoa-PB, INPE, pp.2727–2734.

Eklundh, L., Jonsson, P. 2015. TIMESAT: A software package for Time-Series Processing and Assessment of Vegetation Dynamics. In: Kuenzer, C.; Dech, S.; Wagner, W. Remote Sensing Time Series: Revealing Land Surface Dynamics. v. 22, Springer: New York, p.441. https://doi.org/10.1007/978-3-319-15967-6_7

EMBRAPA - Empresa Brasileira de Pesquisa Agropecuária. *Centro Nacional de Pesquisa de Solos. Sistema Brasileiro de Classificação de Solos*. Rio de Janeiro, 1999. 412 p.

ENVI (Exelis Visual Information Solutions). 2016. "Pós-classification". Accessed on 02 June 2016. <https://www.harrisgeospatial.com/docs/SievingClasses.html>.

Esquerdo, J. C. D. M., Antunes, J. F. G., Andrade, J. C. de. 2010. *Desenvolvimento do banco de produtos MODIS na Base Estadual Brasileira*. (Comunicado Técnico, 100) - Campinas: Embrapa Informática Agropecuária, p.7.

Esquerdo, J. C. D. M., Zullo Junior, J., Antunes, J.F.G. 2011. Use of NDVI/AVHRR time series profiles for soybean crop monitoring in Brazil. *International Journal of Remote Sensing*, 32(13), pp.3711- 3727. <https://doi.org/10.1080/01431161003764112>

FAOSTAT - *Food And Agriculture Organization of the United Nations Statistics Division*, 2014. Disponível em: < http://faostat3.fao.org/browse/Q*/S >. Acesso em: 3 jul. 2016.

Fernandes, J. L., Rocha, J. V., Lamparelli, R. A.C. 2011.Sugarcane yield estimates using time series analysis of spot vegetation images. *Scientia Agricola. (Piracicaba, Brazil.)* 68(2), pp.139-146. <http://dx.doi.org/10.1590/S0103-90162011000200002>

Foody, G. M. 2002.Status of land cover classification accuracy assessment. *Remote Sensing of Environment*, 80(1), pp.185-201. [https://doi.org/10.1016/S0034-4257\(01\)00295-4](https://doi.org/10.1016/S0034-4257(01)00295-4)

Foody, G. M., Cox, D. P. 1994.Sub-pixel land cover composition using a linear mixture model and fuzzy membership functions. *International Journal of Remote Sensing*, 15(3), pp.619-631, <https://doi.org/10.1080/01431169408954100>

Galford, G. L., Mustard, J. F., Melillo, J., Gendrin, A., Cerri, C. C., Cerri, C. E. P. 2008. Wavelet analysis of MODIS time series to detect expansion and intensification of row-crop agriculture in Brazil. *Remote sensing of environment*. pp.576-587. <https://doi.org/10.1016/j.rse.2007.05.017>

Haralick, R. M., Sternberg, S. R., Zhuang, X. 1987.Image Analysis Using Mathematical Morphology. *IEEE Transactions on Pattern Analysis and Machine Intelligence*, 9(4), pp.532-550. [doi: 10.1109/TPAMI.1987.4767941](https://doi.org/10.1109/TPAMI.1987.4767941)

Huete, A., Didan, K., Miura, T., Rodriguez, E. 2002. Overview of the radiometric and biophysical performance of the MODIS vegetation indices. *Remote Sensing of Environment*, 83(1-2), pp.195-213.[https://doi.org/10.1016/S0034-4257\(02\)00096-2](https://doi.org/10.1016/S0034-4257(02)00096-2)

Huete, A., Justice, C., Leeuwen, W. V. *MODIS vegetation index (MOD 13) algorithm theoretical basis document*. 1999. Disponível em: <http://modis.gsfc.nasa.gov/data/atbd_mod13.pdf>. Acesso em: 24 mar. 2016.

Huete, A., Liu, H. Q., Batchily, K., Leween, W. 1997.A comparison of vegetation indices over a global set of TM images for EOS-MODIS. *Remote Sensing of Environment*, 59, pp.440-451. [https://doi.org/10.1016/S0034-4257\(96\)00112-5](https://doi.org/10.1016/S0034-4257(96)00112-5)

IBGE - Instituto Brasileiro de Geografia e Estatística. *Banco de Dados Agregados: Sistema IBGE de Recuperação Automática – SIDRA*. 2014. Disponível em: <<http://www.sidra.ibge.gov.br>>. Acesso em: 06 mar. 2014.

IBGE - Instituto Brasileiro de Geografia e Estatística. *Banco de Dados Agregados: Sistema IBGE de Recuperação Automática – SIDRA*. 2016. Disponível em: <<http://www.sidra.ibge.gov.br>>. Acesso em: 24 fev. 2016.

IBGE - Instituto Brasileiro de Geografia e Estatística. *Relatórios metodológicos - Pesquisas Agropecuárias - Departamento de Agropecuária*. v. 6, 2.ed., Rio de Janeiro, 92 p., 2002.

Jakubauskas, M. E., Legates, D. R., Kastens, J. H. 2001. Harmonic analysis of time-series AVHRR NDVI data. *Photogrammetric Engineering and Remote Sensing*, 67(4), pp.461–470.

- Jia, L., Shang, H., Hu, G., Menenti, M. 2011. Phenological response of vegetation to upstream river flow in the Heihe River basin by time series analysis of MODIS data. *Hydrology Earth System Sciences*, 15(3), pp.1047-1064. <https://doi.org/10.5194/hess-15-1047-2011>
- Johann, J. A., Rocha, J. V., Duft, D. G., Lamparelli, R. A. C. 2012. Estimativa de áreas com culturas de verão no Paraná, por meio de imagens multitemporais EVI/Modis. *Pesquisa Agropecuária Brasileira*, 47(9) pp.1295-1306. <http://dx.doi.org/10.1590/S0100-204X2012000900015>
- Köppen, W., Geiger, R. 1928. *Klimate der Erde*, Justus Perthes, Gotha.
- Landis, J. R., Koch, G. G. 1977. The measurement of observer agreement for categorical data. *Biometrics*, 33(1), pp.159-174.
- Mengue, V. P., Fontana, D. C. 2015. Assessment of spectral-temporal dynamics for mapping the main summer crops in the Rio Grande do Sul State. *Bragantia, Campinas*, 74(3), pp.331-340. <http://dx.doi.org/10.1590/1678-4499.0452>
- Ordones, H. A. M., Rocha, J. V., Lamparelli, R. A. C. 2010. *Mapeamento de cana-de-açúcar para o ano-safra 2008/2009 no Estado de São Paulo por meio de índice de vegetação do sensor MODIS*. III SEEMI - Simpósio em Estatística Espacial e Modelagem de Imagens, Foz do Iguaçu - PR.
- Pontius, R. G., Millones, M. 2011. Death to Kappa: birth of quantity disagreement and allocation disagreement for accuracy assessment. *International Journal of Remote Sensing*, 32(15), pp.4407-4429. <https://doi.org/10.1080/01431161.2011.552923>
- Rezende, S. O. 2003. Sistemas inteligentes fundamentos e aplicações. *Manole*, p.525.
- Roerink, G. J., Menenti, M., Verhoer, W. 2000. Reconstructing cloud free NDVI composites using Fourier analysis of time series. *International Journal of Remote Sensing*, 21(9), pp.1911-1917. <https://doi.org/10.1080/014311600209814>
- Rudorff, B. F. T., Aguiar, D. A., Silva, W. F., Sugawara, L. M., Adami, M., Moreira, M. A. 2010. Studies on the rapid expansion of sugarcane for ethanol production in São Paulo State (Brazil) Using Landsat Data. *Remote Sensing*. <https://doi.org/10.3390/rs2041057>
- Sakamoto, T., Yokozawa, M., Toritani, H., Shibayama, M., Ishitsuka, N., Ohno, H. 2005. A crop phenology detection method using time-series MODIS data. *Remote Sensing of Environment*. p.366-374. <https://doi.org/10.1016/j.rse.2005.03.008>
- Santos, J. S., Fontana, D. C., Silva, T. S. F., Rudorff, B. F. T. 2014. Identificação da dinâmica espaço-temporal para estimar área cultivada de soja a partir de imagens MODIS no Rio Grande do Sul. *Revista Brasileira de Engenharia Agrícola e Ambiental, Campina Grande, PB*, 18(1), pp.54-63. <http://dx.doi.org/10.1590/S1415-43662014000100008>
- Silva, W. F., Aguiar, D. A., Rudorff, B. F. T., Sugawara, L. M. 2010. *Canasat project: Monitoring of the sugarcane cultivation area in south central Brazil*. ISPRS TC VII Symposium - 100 years, Vienna, Austria.
- Vicente, L. E., Gomes, D., Victoria, D. C., Garçon, E. A. M., Bolfe, E. L., Andrade, R. G., Silva, G. B. S. 2012. Séries temporais de NDVI de sensor SPOT vegetation e algoritmo SAM aplicados ao mapeamento de cana-de-açúcar. *Pesquisa Agropecuária Brasileira, Brasília*, 47(9), pp.1337-1345.

Victoria, D. C., Oliveira, A. F., Grego, C. R. 2009. Análise harmônica de séries temporais de imagens NDVI/MODIS para discriminação de coberturas vegetais. SBSR - XIV Simpósio Brasileiro de Sensoriamento Remoto, Natal, INPE, p.1589-1596.

Victoria, D. C., Paz, A. R., Coutinho, A. C., Kastens, J., Brown, C. 2012. Cropland área estimates using MODIS NDVI time serie in the state of Mato Grosso, Brazil. *Pesquisa Agropecuária Brasileira*, 47(9), pp.1270-1278. <http://dx.doi.org/10.1590/S0100-204X2012000900012>

Willmott, C. J., Roberson, S. M., Matsuura, K. 2012. A Refined Index of Model Performance. *International Journal of Climatology*, 32, pp.2088-2094. <https://doi.org/10.1002/joc.2419>

Xavier, A. C., Rudorff, B. F. T., Shimabukuro, E., Berka, L. M. S., Moreira, M. A. 2006. Multi-temporal analysis of MODIS data to classify sugarcane crop. *International Journal of Remote Sensing*, 27(4), pp. 755-768. <https://doi.org/10.1080/01431160500296735>

Zanzarini, F. V., Pissarra, T. C. T., Brandão, F. J. C., Teixeira, D. D. B. 2013. *Correlação espacial do índice de vegetação (NDVI) de imagem Landsat/ETM+ com atributos do solo*. Revista Brasileira de Engenharia Agrícola e Ambiental, Campina Grande, PB, 17(6), pp.608-614. <http://dx.doi.org/10.1590/S1415-43662013000600006>

Research Article

Groundwater Modeling of Huzur Tehsil, M.P Using GIS Techniques

Vimal Shukla*, Jyoti Sarup

Department of Civil Engineering, Center of Remote sensing and GIS, Maulana Azad National Institute of Technology Bhopal, Madhya Pradesh

Correspondence should be addressed to Vimal Shukla, vimalshukla.nitbpl@gmail.com

Publication Date: 22 April 2020

DOI: <https://doi.org/10.23953/cloud.ijarsg.455>

Copyright © 2020 Vimal Shukla, Jyoti Sarup. This is an open access article distributed under the **Creative Commons Attribution License**, which permits unrestricted use, distribution, and reproduction in any medium, provided the original work is properly cited.

Abstract Huzur Tehsil, district Bhopal city in the Madhya Pradesh state of India has faced the problem of groundwater availability in recent times believed largely due to rapid urbanization coupled with the presence of increasing Population and the urban sprawl increase the number of bores well in earth, which is the reason to the declination of groundwater level. That means water is very important for the sustained use of natural resources and is vital for the existence of mankind. Groundwater used for a variety of purposes, including irrigation, drinking, and manufacturing. For assessing the groundwater Level suitability zones through GIS techniques, this study was undertaken in the Huzur Tehsil, Bhopal district, Madhya Pradesh. Artificial recharge is expected to become increasingly necessary in the future as the growing population requires more water and thus, more storage is required to conserve water for use in times of shortage. Geospatial techniques employing Geographical information systems (GIS) are increasingly being used in the field of hydrology and water resources development. This is the greatest advantage of using GIS techniques for Groundwater level (bore well) investigations and monitoring is its ability to generate information in water level behavioral conditions, which is provided very critical for successful analysis, prediction, and validation. In the present study, the Kriging technique was used to interpolate the groundwater levels. Interpolation of pre and post-monsoon groundwater levels was carried out for the year 1996-2017. Finally, we generated the fluctuation maps were showing the fluctuation in the pre-post monsoon period between the years, 1996-2000, 2001-2005, -2010 and 2011-2017 and Long term trend fluctuation maps were generated showing, and finally, Feature Projected Groundwater Level map are generated 2018-2051 period, and showing the Groundwater Level trend (1996-2051) since. For visualization groundwater level depth (mbgl) and Fluctuation, in the pre and post-monsoon period, showing the 3D Surface modeling using Matlab tools.

Keywords *Groundwater level mapping; groundwater fluctuation; Geospatial Techniques; Kriging; 3D surface; GIS*

1. Introduction

Groundwater is subsurface water that occurs beneath the earth's surface. In a hydrologic water cycle, groundwater comes from surface waters (precipitation, lake, reservoir, river, sea, etc.) and percolates into the ground beneath the water table. Groundwater is a significant part of the hydrologic cycle, containing 21% of earth water. Growth in population, urbanization, and standards of living has resulted in increased demand for water. Groundwater has an important role in the environment: it replenishes

streams, rivers, and wetlands and helps to support wildlife habitat; it is used as the primary source of drinking water and also in agricultural and industrial activities. Around the world, groundwater resources are under increasing pressure caused by the intensification of human activities and other factors such as growing population and very fast Urban Sprawl. Many states in India use the water right process to manage groundwater quantity and to ensure that over drafting does not occur. Groundwater is the major source of drinking water in rural India. It is estimated that approximately one-third of the world's population use groundwater for drinking purpose (Nickson et al., 2005). In addition to rural households, public water supplies in various parts of the world depend on wells and groundwater. But due to increases, the number of population that means urban sprawl increases and demand for water are is required more in an urban area and which increasing number is of bore well every house holding in an urban area, which is the reason to decline the Groundwater Level. As we know groundwater is an important source of water supply throughout the world, its uses in irrigation, industry, municipality and domestic areas continue to increase. Therefore, greater emphasis is being laid for a planned and optimal utilization of water resources. Owing to the uneven distribution of rainfall both in time and space, the surface water resources are unevenly distributed. This has resulted in an increased emphasis on the development of groundwater resources. The simultaneous development of groundwater especially through bore wells a will decline water table. In such a situation, a severe problem is created resulting in the drying of bore wells. Modern techniques like GIS (Geographical information technology) are increasingly becoming important day by day in all real-world problems of geospatial nature. The field of hydrology and water resource development is also the area having an extensive scope of deriving benefits from these tools of geoinformatics (Krishna et al., 2005). One of the greatest advantages of using GIS for hydrological investigations and monitoring is its ability to generate information in groundwater fluctuation and condition of groundwater, which is very crucial for successful analysis, prediction, and validation (Kumar M.G. et al., 2008). GIS technology is becoming an important tool as a platform to efficiently manage large and complex information organized around its core. It also provides suitable alternatives for efficient management of large and complex databases.

1.1. Problem Identification

In see few years the Groundwater Level decline in Huzur Tehsil, district Bhopal, Madhya Pradesh, India. Due to increases in the high population and more urban sprawl that means increasing the number of bores well, which are affected by the groundwater level. And few bore well dry in the pre-monsoon period. This condition produces a continuous decline groundwater level in Huzur, Tehsil district Bhopal, Madhya Pradesh, India.

1.2. Objectives of the Study

The analysis of the declining groundwater levels and the factors responsible for it is the immediate need of the hour to assess the overall scenario concerning groundwater. The study includes the analysis of groundwater fluctuation (1996-2017) pre-post monsoon. The study includes the analysis of Long term trend groundwater fluctuation (1996-2017) pre-monsoon. The study includes the analysis of feature projected groundwater level fluctuation (2018-2051) and shows the trend pattern in Groundwater level fluctuation. With the help of MATLAB showing the groundwater level fluctuation visualization.

2. Study Area

Huzur Tehsil, Bhopal district, spanning over an area of about 1361.77 sq. km lies in the central part of the state of Madhya Pradesh. Before the independence of India, it was a part of the Bhopal state, which was founded by Nawab Dost Mohammad Khan in the year 1722. The reorganization of states in November 1956, made Bhopal the capital of Madhya Pradesh State, but it remained the part of Sehore district. In the year 1972 Bhopal became the new district under the Bhopal commissioner's division.

The district is bounded by Guna district on the north, Vidisha district on the northeast, Raisen district on the east and Sehore and Rajgarh district on the southwest and west respectively. There are 245 villages in the Huzur These, Bhopal District. Bhopal urban area is about 296 sq km. Bhopal city is the district as well as state headquarter. Bhopal is well connected with all parts of the country by Air, Rail, and roads. The location of the study area is shown in the map below (Figure 1). The area falls between North latitude $23^{\circ} 04'18''$ and $23^{\circ} 25'46''$ and East longitude $77^{\circ} 10'07''$ and $77^{\circ} 37'32''$. Show the Location map of Huzur Tehsil is given in (Figure 2).

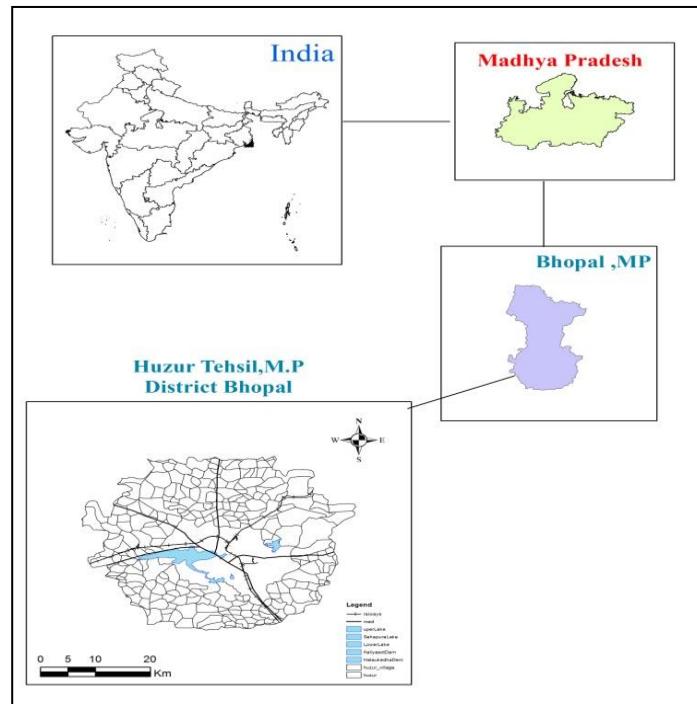


Figure 1: Location of the study area

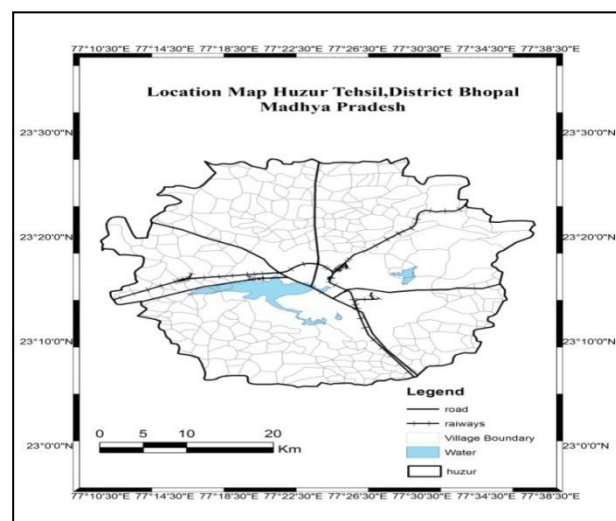


Figure 2: The Location Map of Huzur Tehsil, District Bhopal, Madhya Pradesh, India

2.1. Climate

Bhopal has consisted of the humid subtropical climate, with mild, dry winters, hot summer and a humid monsoon season. The summers start in late April and go on till mid-June, the average temperature is around 30 °C (86 °F), with the peak of summer in May, when the highs regularly exceed 40 °C (104 °F).

2.2. Rainfall

The monsoon starts in late June and ends in late September. IMD normal annual rainfall of Bhopal city is 1260.2 mm. The average temperature is almost around 25 °C (77 °F) and the humidity is quite high. The temperatures rise again up to late October when winter starts, which lasts up to early March. The winters in Bhopal are mild, sunny and dry, with average temperatures around 18 °C (64 °F) and little or no rain. The winter time peaks in January when temperatures may drop close to freezing on some nights. The daily normal temperature of Bhopal in May - 40.70 C and minimum - 26.40 C. rainfall analysis the monsoon time last June to September time Groundwater level is good Condition in the study are . The annual variation of rainfall is shown below (Figure 3).

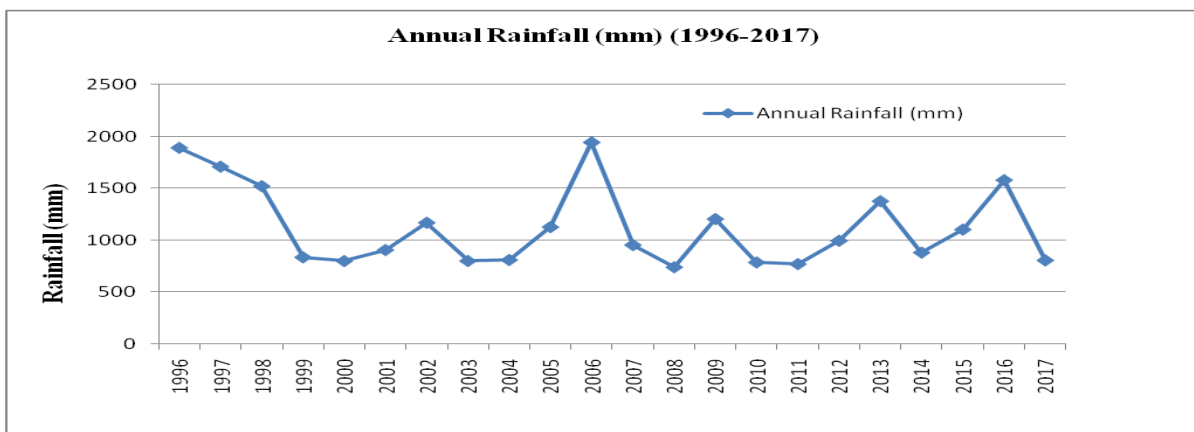


Figure 3: Rainfall Patter

2.3. Well Distribution

Above the study area to collect the 130 rural and 220 urban areas bore well point. Show in below location of well point in urban and rural area (Figure 4).

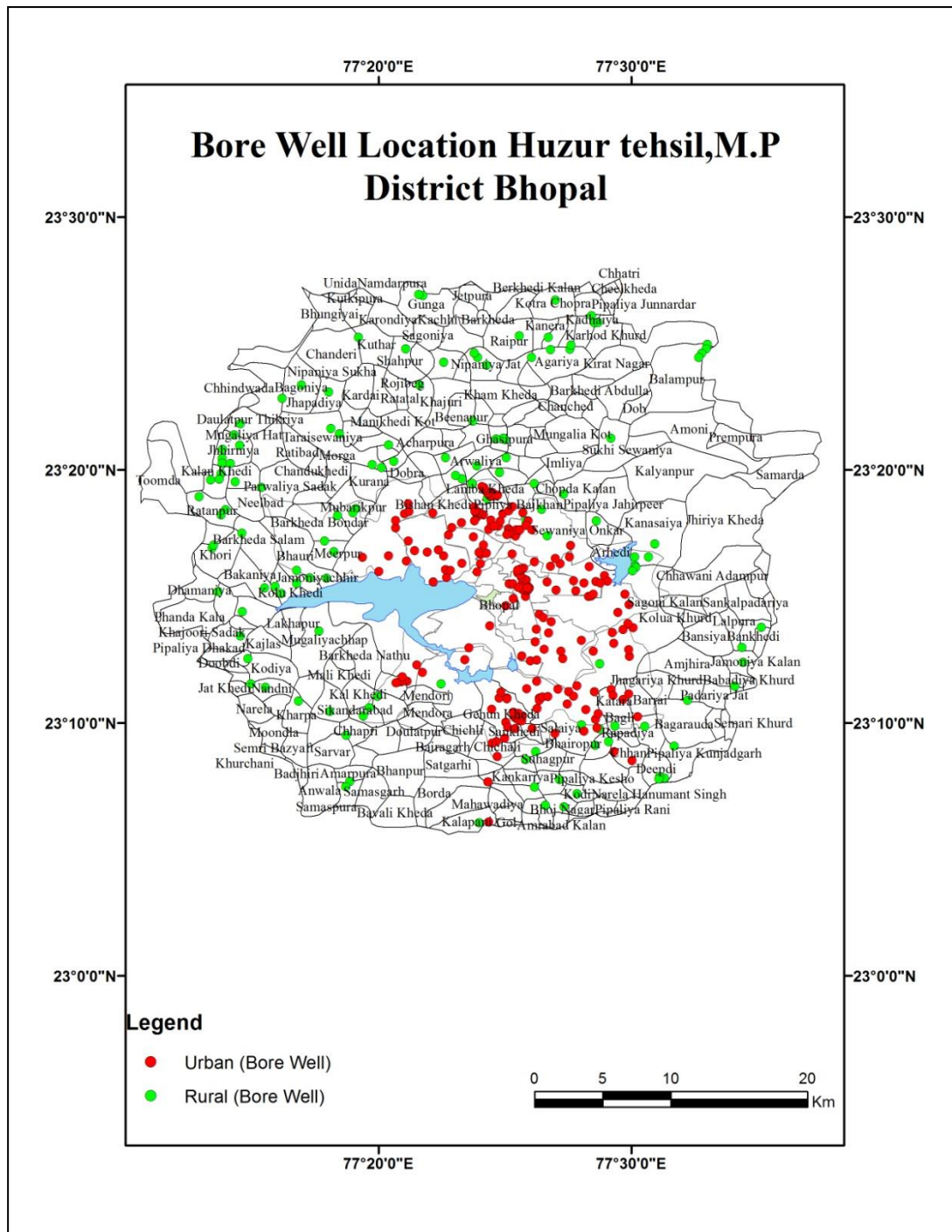


Figure 4: Location of well distribution in Huzur Tehsil District Bhopal, Madhya Pradesh, India

3. Data Collection and Methodology

3.1. Data collection

Central Ground Water Board (CGWB) maintains 350 wells Huzur Tehsil, Bhopal district for monitoring groundwater resources. We have collected a total of 350 bore wells data that are collected in Huzur tehsil, Bhopal District. They are identification of well Location Ground truths using the handhelds GPS. As shown in below the Well Location map in Huzur tehsil, District Bhopal, Madhya Pradesh (Figure 4). The collected urban and rural Groundwater Level Bore well (mbgl) data (1996-2017) Huzur Tehsil, District Bhopal, Madhya Pradesh as shown in two sample of Table 1, 2 (Source: Central Ground Water

Board, Ministry of Water Resources, Government of India, India, taken 2015). And Five year annual average groundwater level between the 1996-2000, 2001-2005, 2006-2010 shows in Table 3, 4, 5. And last seven year period lies 2011-2017 as shown in Table 6 (Source: Central Ground Water Board, Ministry of Water Resources, Government of India, India, taken 2015).

Table 1: List of Two Urban area Pre –Post Monsoon Groundwater Level (mbgl) in Huzur Tehsil (1996- 2017)

WL_ID	Lat	Long	Site_Type	Year_Obs	Pre-monsoon (mbgl)	Post-monsoon (mbgl)
UA101	23.26	77.43	Bore Well	1996	4.35	3
UA101	23.26	77.43	Bore Well	1997	7.42	3.05
UA101	23.26	77.43	Bore Well	1998	8.13	4.22
UA101	23.26	77.43	Bore Well	1999	9.92	5.14
UA101	23.26	77.43	Bore Well	2000	10.95	5.24
UA101	23.26	77.43	Bore Well	2001	12.83	5.35
UA101	23.26	77.43	Bore Well	2002	13.55	5.46
UA101	23.26	77.43	Bore Well	2003	14.78	7.13
UA101	23.26	77.43	Bore Well	2004	15.48	7.56
UA101	23.26	77.43	Bore Well	2005	15.78	7.65
UA101	23.26	77.43	Bore Well	2006	16.09	7.79
UA101	23.26	77.43	Bore Well	2007	16.54	7.86
UA101	23.26	77.43	Bore Well	2008	16.75	7.89
UA101	23.26	77.43	Bore Well	2009	16.89	7.95
UA101	23.26	77.43	Bore Well	2010	16.99	8.12
UA101	23.26	77.43	Bore Well	2011	17.15	8.45
UA101	23.26	77.43	Bore Well	2012	17.55	8.67
UA101	23.26	77.43	Bore Well	2013	17.79	8.96
UA101	23.26	77.43	Bore Well	2014	17.98	9.12
UA101	23.26	77.43	Bore Well	2015	18.11	10.36
UA101	23.26	77.43	Bore Well	2016	18.55	11.58
UA101	23.26	77.43	Bore Well	2017	18.78	12.8
UA102	23.26	77.43	Bore Well	1996	14.72	9.91
UA102	23.26	77.43	Bore Well	1997	15.79	10.45
UA102	23.26	77.43	Bore Well	1998	16.75	11.76
UA102	23.26	77.43	Bore Well	1999	33.16	19.51
UA102	23.26	77.43	Bore Well	2000	33.59	19.73
UA102	23.26	77.43	Bore Well	2001	33.68	20.35
UA102	23.26	77.43	Bore Well	2002	33.85	20.74
UA102	23.26	77.43	Bore Well	2003	33.95	20.98
UA102	23.26	77.43	Bore Well	2004	34.15	21.11
UA102	23.26	77.43	Bore Well	2005	34.98	22.27
UA102	23.26	77.43	Bore Well	2006	40.98	22.35
UA102	23.26	77.43	Bore Well	2007	42.52	28.25
UA102	23.26	77.43	Bore Well	2008	45.84	32.24
UA102	23.26	77.43	Bore Well	2009	47.25	36.52
UA102	23.26	77.43	Bore Well	2010	49.33	39.2
UA102	23.26	77.43	Bore Well	2011	52.15	42.13
UA102	23.26	77.43	Bore Well	2012	54.35	44.02

UA102	23.26	77.43	Bore Well	2013	56.48	46.05
UA102	23.26	77.43	Bore Well	2014	60.25	48.15
UA102	23.26	77.43	Bore Well	2015	65.28	50.25
UA102	23.26	77.43	Bore Well	2016	68.15	52.15
UA102	23.26	77.43	Bore Well	2017	70.55	54.55

Table 2: List of Two Rural area Pre –Post Monsoon Groundwater Level (mbgl) in Huzur Tehsil (1996- 2017)

WL_ID	Lat	Long	Site_Type	Year_Obs	Pre-monsoon (mbgl)	Post-monsoon (mbgl)
R201	23.28	77.51	Bore Well	1996	7.56	4.57
R201	23.28	77.51	Bore Well	1997	7.75	6.15
R201	23.28	77.51	Bore Well	1998	8.05	6.25
R201	23.28	77.51	Bore Well	1999	8.45	7.10
R201	23.28	77.51	Bore Well	2000	8.65	6.98
R201	23.28	77.51	Bore Well	2001	11.32	10.86
R201	23.28	77.51	Bore Well	2002	12.66	11.34
R201	23.28	77.51	Bore Well	2003	14.32	12.11
R201	23.28	77.51	Bore Well	2004	16.10	17.66
R201	23.28	77.51	Bore Well	2005	17.10	17.76
R201	23.28	77.51	Bore Well	2006	17.76	11.45
R201	23.28	77.51	Bore Well	2007	17.80	10.54
R201	23.28	77.51	Bore Well	2008	20.22	17.76
R201	23.28	77.51	Bore Well	2009	24.38	17.76
R201	23.28	77.51	Bore Well	2010	26.30	18.32
R201	23.28	77.51	Bore Well	2011	27.00	17.76
R201	23.28	77.51	Bore Well	2012	27.31	13.91
R201	23.28	77.51	Bore Well	2013	27.42	14.00
R201	23.28	77.51	Bore Well	2014	27.52	14.10
R201	23.28	77.51	Bore Well	2015	27.73	14.60
R201	23.28	77.51	Bore Well	2016	28.65	22.55
R201	23.28	77.51	Bore Well	2017	30.48	23.46
R202	23.28	77.50	Bore Well	1996	8.82	2.50
R202	23.28	77.50	Bore Well	1997	15.30	10.18
R202	23.28	77.50	Bore Well	1998	16.12	12.60
R202	23.28	77.50	Bore Well	1999	19.14	12.23
R202	23.28	77.50	Bore Well	2000	19.24	13.52
R202	23.28	77.50	Bore Well	2001	16.66	13.54
R202	23.28	77.50	Bore Well	2002	16.98	12.82
R202	23.28	77.50	Bore Well	2003	19.65	13.20
R202	23.28	77.50	Bore Well	2004	17.90	13.90
R202	23.28	77.50	Bore Well	2005	18.40	13.92
R202	23.28	77.50	Bore Well	2006	17.23	13.98
R202	23.28	77.50	Bore Well	2007	18.10	14.06
R202	23.28	77.50	Bore Well	2008	18.25	13.15
R202	23.28	77.50	Bore Well	2009	19.70	13.04
R202	23.28	77.50	Bore Well	2010	19.80	12.71

R202	23.28	77.50	Bore Well	2011	19.95	12.45
R202	23.28	77.50	Bore Well	2012	20.00	12.52
R202	23.28	77.50	Bore Well	2013	20.12	12.92
R202	23.28	77.50	Bore Well	2014	20.25	13.12
R202	23.28	77.50	Bore Well	2015	22.86	20.72
R202	23.28	77.50	Bore Well	2016	24.38	22.25
R202	23.28	77.50	Bore Well	2017	24.38	22.25

Table 3: Five year annual average groundwater level sample rows from Bore well point of Huzur Tehsil, M.P, Bhopal (1996-2000)

WL_ID	YEAR	Pre-monsoon (mbgl)	Post-monsoon(mbgl)	LAT	LON	Fluctuation
UA101	1996-2000	8.154	4.13	23.25	77.43	4.024
UA102	1996-2000	22.802	14.272	23.25	77.43	8.53
UA103	1996-2000	8.092	6.21	23.25	77.43	1.882
R201	1996-2000	8.092	6.21	23.27	77.51	1.882
R202	1996-2000	15.724	10.206	23.27	77.50	5.518
R203	1996-2000	8.706	3.954	23.27	77.50	4.752

Table 4: Five year annual average groundwater level sample rows from Bore well point of Huzur Tehsil, M.P, Bhopal (2001-2006)

WL_ID	YEAR	Pre-monsoon (mbgl)	Post-monsoon(mbgl)	LAT	LON	Fluctuation
UA101	2001-2005	14.484	6.63	23.25	77.43	7.854
UA102	2001-2005	34.122	21.09	23.25	77.43	13.032
UA103	2001-2005	14.3	12.31	23.25	77.43	1.99
R201	2001-2005	14.3	12.236	23.27	77.51	2.064
R202	2001-2005	17.918	13.476	23.27	77.50	4.442
R203	2001-2005	10.924	6.606	23.27	77.50	4.318

Table 5: Five year annual average groundwater level sample rows from Bore well point of Huzur Tehsil, M.P, Bhopal (2006-2010)

WL_ID	YEAR	Pre-monsoon (mbgl)	Post-monsoon (mbgl)	LAT	LON	Fluctuation
UA101	2006-2010	16.652	7.922	23.25	77.43	8.73
UA102	2006-2010	45.184	31.712	23.25	77.43	13.472
UA103	2006-2010	21.292	15.166	23.25	77.43	6.126
R201	2006-2010	21.292	15.166	23.27	77.51	6.126
R202	2006-2010	18.616	13.388	23.27	77.50	5.228
R203	2006-2010	12.13	7.842	23.27	77.50	4.288

Table 6: Five year annual average groundwater level sample rows from Bore well point of Huzur Tehsil, M.P, Bhopal (2011-2017)

WL_ID	YEAR	Pre-monsoon (mbgl)	Post-monsoon(mbgl)	LAT	LON	Fluctuation
UA101	2010-2017	17.987	9.991	23.25	77.43	7.995
UA102	2010-2017	61.03	48.185	23.25	77.43	12.844
UA103	2010-2017	31.905	20.507	23.25	77.43	11.398
R201	2010-2017	28.015	17.197	23.27	77.51	10.818
R202	2010-2017	21.705	16.604	23.27	77.50	5.101
R203	2010-2017	13.468	8.322	23.27	77.50	5.145

3.2. Population data

These are collected the Population of Huzur Tehsil, District Bhopal, Madhya Pradesh as per Census 2001 (1429132) & 2011 (1834493) out of a total population, 89.5% people live in urban areas while 10.5% lives in the rural areas. As shown in below the total population of Huzur Tehsil, district Bhopal, M.P in Figure 5. As per Census 2011, the number of total 211 Villages in Huzur Tehsil of Bhopal district, Madhya Pradesh. Show the Table 7 and 8 lists of cities and villages in Huzur Tehsil of Bhopal district, Madhya Pradesh (Source: As per Census 2011).

Table 7: List of population in Huzur tehsil, District Bhopal (censusindia.gov.in)

S.NO	Name	Population 2001	Population 2011	Density -2001 (per sq.km)	Density -2011 (per sq.km)
1	Bhopal(M Corp)	1260038	1598197	4031	5113

Table 8: List of Villages population in Huzur Tehsil (censusindia.gov.in)

S.NO.	Name	Population 2001	Population 2011	Density 2001 (per sq.km)	Density 2001 (per sq.km)
1	Toomda	5033	5413	387	416
2	Ratanpur	1815	6208	320	1096
3	Bangrasia	2530	4946	838	1639
4	Hatai Khedi	188	247	230	302

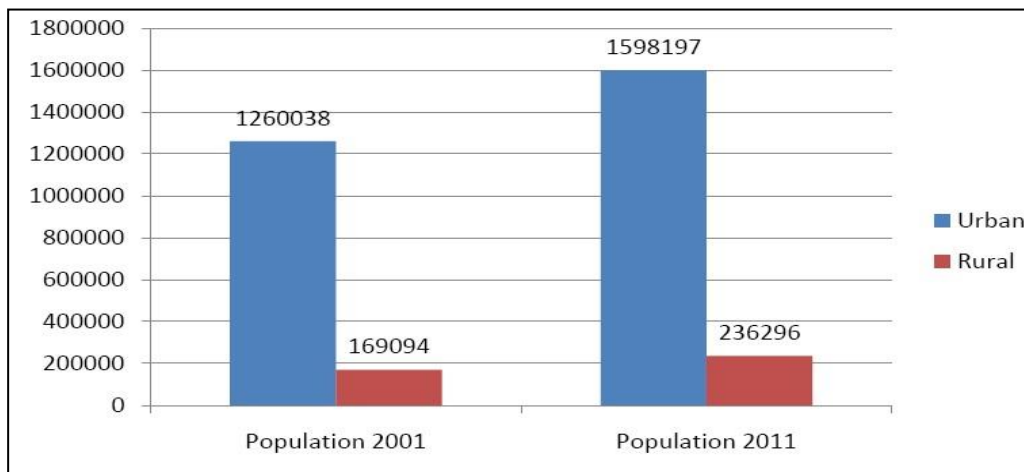


Figure 5: Show the total population of Huzur, Tehsil, district Bhopal.

As per Census 2001 and 2011, the water demanded are increasing in 2011, and more water demand day to day, and increase the number of bores well. These causes see the behavioral of groundwater level decline. Apply the Arithmetical Increase Method to find out the projected population. The projected population Huzur tehsil, district Bhopal in 2051.the total projected population is (5503477). As shown in below the total Actual Population & Projected Population in Huzur Tehsil, District Bhopal, Madhya Pradesh (Figure 6). As the city is developing rapidly, there is a huge increase in the migration of people from nearby villages and towns. The source of Groundwater Level refilling depends upon the monsoon in Huzur tehsil. Which is seeing every person uses about 80-100 gallons of water per day (according to USGS). And 1 gallon is approximately Values in 3.78 Liter that means the Population of Huzur, Tehsil, District Bhopal Madhya Pradesh 2001 is 1429132 and 2011 population is 1834493. And every day Water requirement is 540211896 Liter/day (Figure 7). That means Groundwater Level decline yearly by yearly, as show the Water utility of Liter per day in actual and projected Population in the study area (Figure 7). The total area of Huzur is 1,361.77 sq.km with population density in 2001 is

1,049 and 2011 is 1347 (per sq.km). Used the GIS tools to provide information on population and density in Huzur Tehsil, district Bhopal, Madhya Pradesh. And generate the population and density (area per sq. Km) map of Huzur area in (2001 & 2011).

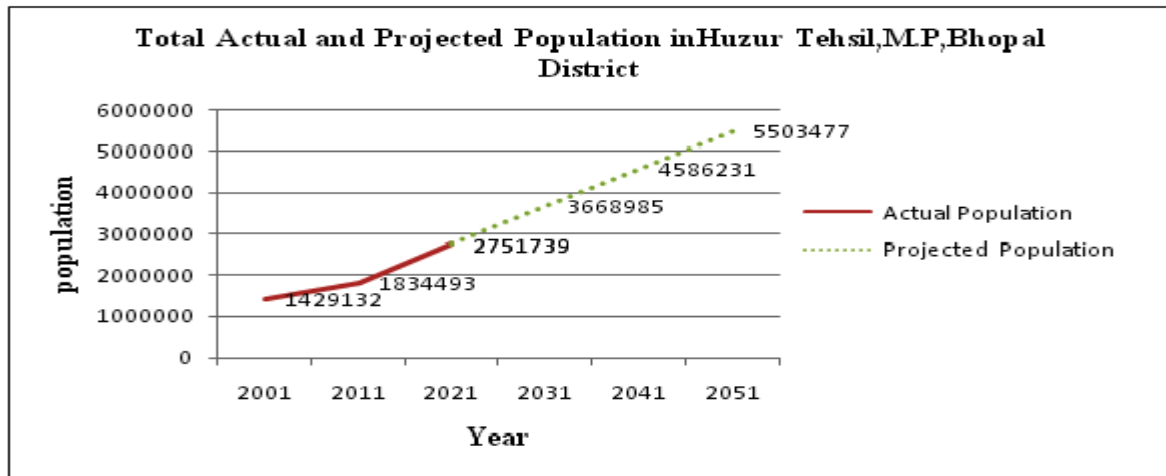


Figure 6: The total Actual Population & Projected Population in Huzur Tehsil, District Bhopal, Madhya Pradesh

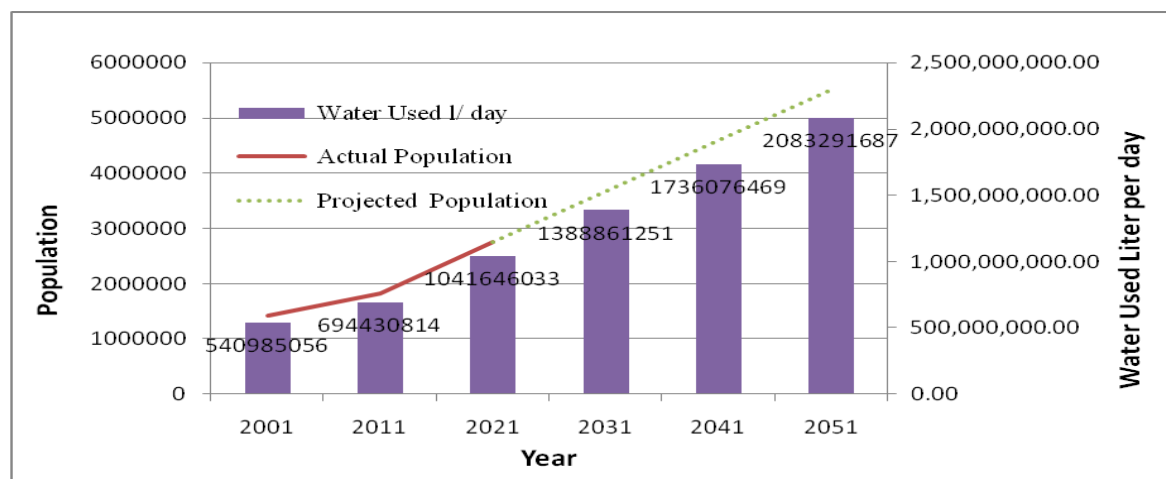


Figure 7: Water utility of Liter per day in actual and projected Population

3.4. Methodology

The base map of the study area was prepared using a survey of India topographical maps (Figure 9). The bore well observation data were plotted on to the map by using location (latitude & longitude) of each well. In total 350 observations, wells were selected for further processing of the data for Groundwater Level analysis. Based on above collection these are prepared the GIS map with the help of the Kriging interpolation model technique in Arc GIS Software. In this study, the Kriging technique was used for the spatial distribution of Groundwater level fluctuation (mbgl) for pre and post-monsoon on the five-year average interval (1996-2000, 2001-2005, 2006-2010, 2002-2006, 2006-2010), and one seven year interval (2011-2017). And long term trend fluctuation (1996-2017). Using the Matlab to the analysis of Groundwater Level in bore well, and Generate the Groundwater-Surface Modeling in Pre and Post Monsoon. And find out the Groundwater Level feature Projected (2018- 2022, 2023-2027, 2028-2032, 2033-2037, 2038-2042, 2043-2047, 2048-2051) and long trend in (2018-2051) using GIS technique and prepared the map. Show the flow chart of the methodology in Figure 8.

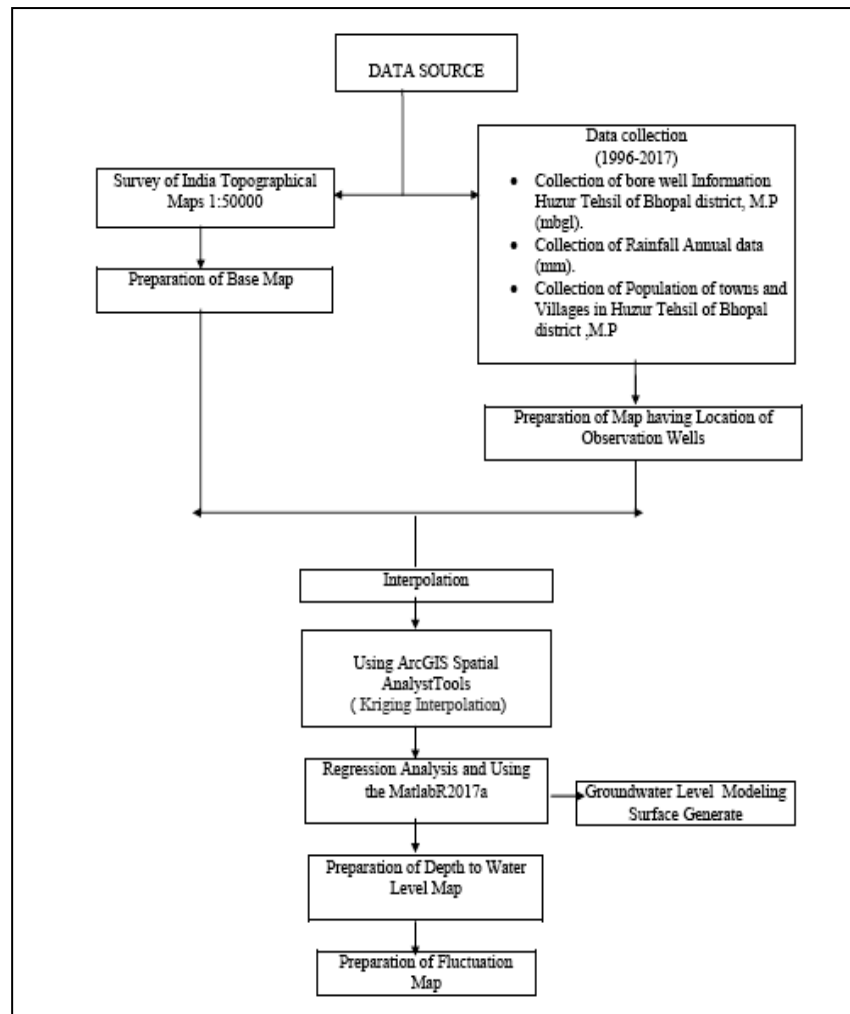


Figure 8: Flow chart of Methodology

3.4.1. Kriging Interpolation model

Kriging is named after D.G. Krige, a South African mining engineer and pioneer in the application of statistical techniques to mine evaluation. The Kriging technique is derived from the theory of regionalized variables (Krige, 1966; Matheron, 1963). An advantage of Kriging (above other moving averages like inverse distance) is that it provides a measure of the probable error associated with the estimates. Kriging can be seen as a point interpolation, which requires a point map as input and returns a raster map with estimations and optionally an error map. The estimated or predicted values (Z) is thus a linear combination known input point values (zi) and have a minimum estimation error.

Thus,

$$Z = \sum (w_i * z_i) \text{-----1}$$

Where wi is weight factors. In case the value of an output pixel would only depend on three input points, this would read:

$$Z = w_1 * z_1 + w_2 * z_2 + w_3 * z_3 \text{-----2}$$

Thus, to calculate one output pixel value Z, first, three weight factors w1, w2, w3 have to be found (one for each input point value z1, z2, z3), then, these weight factors can be multiplied with the

corresponding input point values and summed. In Kriging, the weight factors are calculated by finding the semi-variance values for all distances between input points and by finding semi-variance values for all distances between an output pixel and all input points; then a set of simultaneous equations has to be solved. The weight factors are calculated in such a way that the estimation error in each output pixel is minimized. All semi-variance values are calculated by using a user-specified semi-variogram model. The model describes the expected variance in value between pairs of samples with a given relative orientation. One of the best semi-variogram models like Spherical, Exponential, and Gaussian, etc. is selected and values for the sill, range, and nugget are chosen for best fit. Thus, the semi-variogram model and values for sill, range, and nugget have been finalized, and the Kriging operation has been continued.

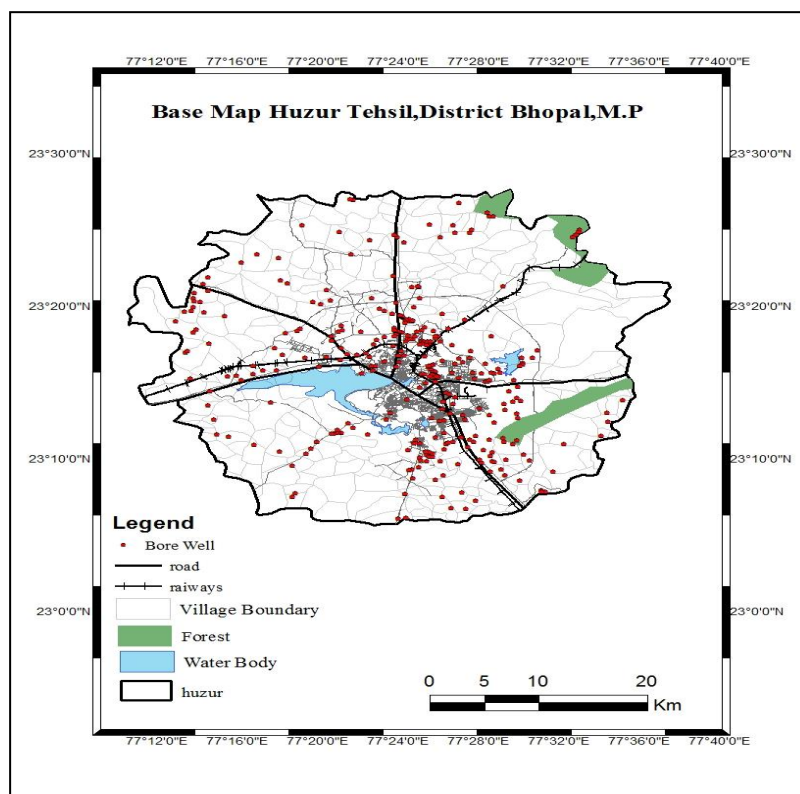


Figure 9: Classification of base map Huzur tehsil, District Bhopal, Madhya Pradesh

4. Results and Discussion

It has taken all twenty two year annual rainfall (1996-2017) and each well point groundwater level in pre-post seasons of the year. And analysis of population 2001 and 2011 based on that analysis to project the population in 2051 year. That means the population are increase yearly to yearly, the water demand are increases in Huzur tehsil, district Bhopal, which effected the declination of water level. The Groundwater is not in underground lakes, nor is it water flowing in underground rivers. It is simply water that fills pores or cracks in subsurface rocks. When rain falls or snow melts on the surface of the ground, some water may run off into lower land areas or lakes and streams. What is left may be absorbed by the soil, seep into deeper layers of soil and rock, or evaporate into the atmosphere.

4.1. Groundwater System Behavior

Groundwater System Behavior which is that will help in a better understanding of the Huzur tehsil groundwater system. And water depth in bore well and fluctuation of water level in bore well in the same village and urban area, and long trend of water level.

4.1.1. Depth to water level

The groundwater level is an important parameter to understand the existing groundwater potential of an area. The groundwater potential can be estimated by the depth of the water found. It can be inferred that if the depth to the water level from ground level is shallow, then the Groundwater condition is good. But if the depth is deep then the groundwater level is poor. Water level mainly depends upon rainfall, sub-surface geological nature, weathering condition, depth to bedrock, etc. but few years saw declination of groundwater level which is Urban sprawl or suburban sprawl. To understand the water level of the study area, groundwater level data for both pre-monsoon and post-monsoon, was data collected for 360 bore wells which are monitored by Central Ground Water Board Water Resource Data Centre, Bhopal. The groundwater level of the study for pre-monsoon, the post-monsoon season has been calculated from 1996-2017. Above the (Table 1, 2, 3, 4) data collection in groundwater Level bore well in the study area. To show the average value of depth to water level (mbgl) for different year Pre-monsoon in (1996-2000, 2001-2005, 2006-2010, 2011-2017) (Figure 10). Using the ArcGIS10.5 generates the Groundwater Level depth map Pre-monsoon between 1996-2000, 2001-2005, 2006-2010, and 2011-2017. During pre-monsoon (period 1996-2000, 2001-2005, 2006-2010, 2011-2017), the depth to the water level in the district varied largely from between 6.56 - 13.79, 12.55-20.65, 16.06-26.44, and 22.87-49.19 mbgl (Figure 12). The Average value of depth to water level (mbgl) for different year Post-monsoon is (1996-2000, 2001-2005, 2006-2010, and 2011-2017) (Figure 11). Using the ArcGIS10.5 generates the Groundwater Level Depth Map Post-monsoon 1996-2000, 2001-2005, 2006-2010, and 2011-2017 (as shown in Figure13). During post-monsoon (Period 1996-2000, 2001-2005, 2006-2010, 2011-2017), the depth to water level in the district varied largely from between 4.34 - 9.49, 8.47- 14.15, 11.76- 17.50, 16.11- 24.94 (mbgl) (Figure 13).

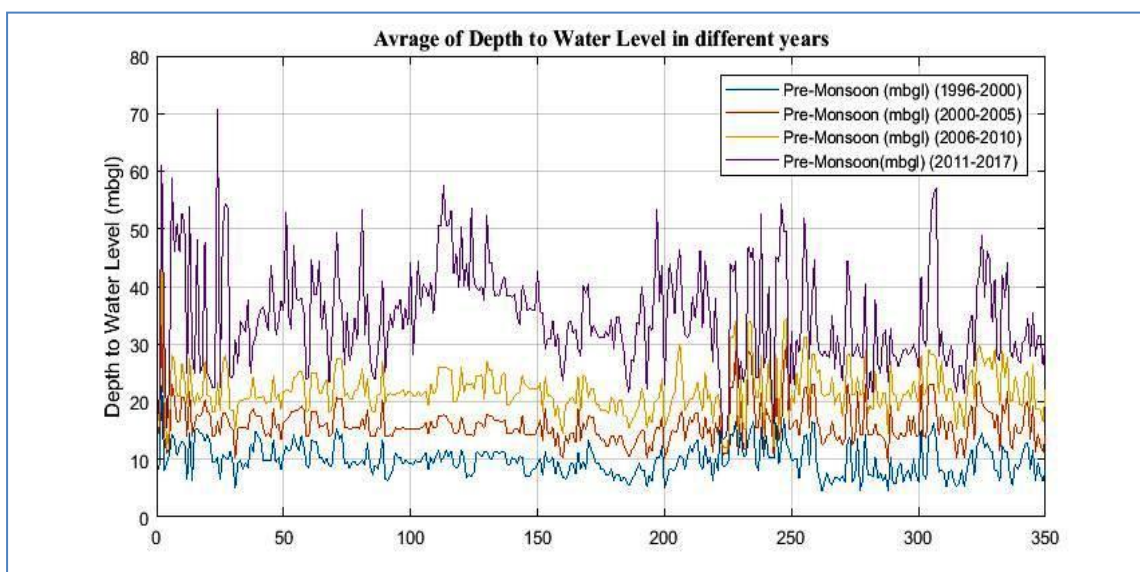


Figure 10: Pre-monsoon Average depth to the water level in Huzur, M.P, Bhopal District for Years 1996-2000, 2001-2005, 2006-2010 and 2011-2017

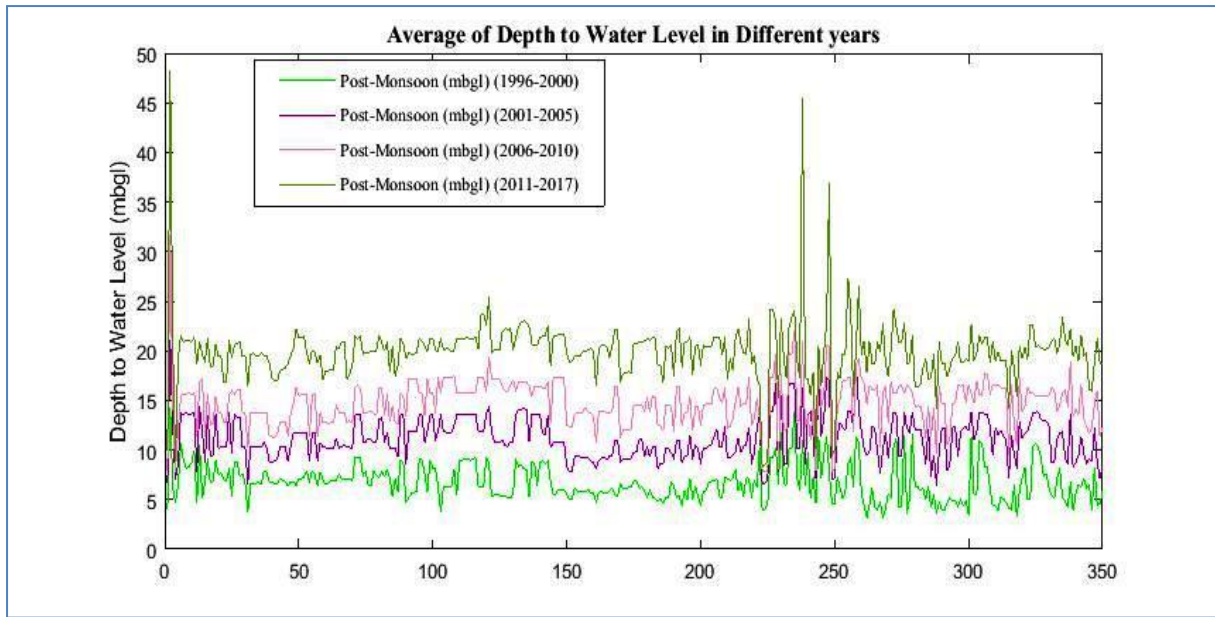
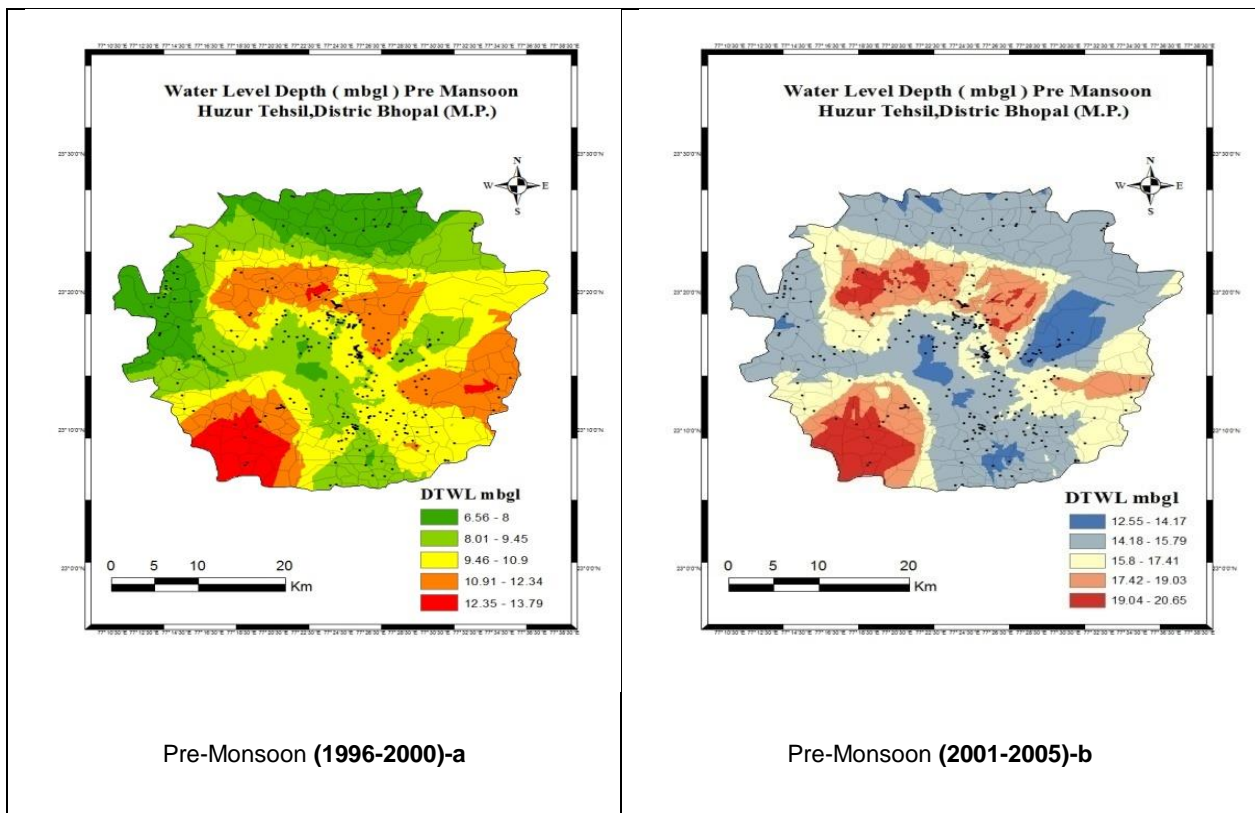


Figure 11: Post-monsoon Average depth to the water level in Huzur Tehsil, M.P, Bhopal District for Years 1996-2000, 2001-2005, 2006-2010 and 2011-2017



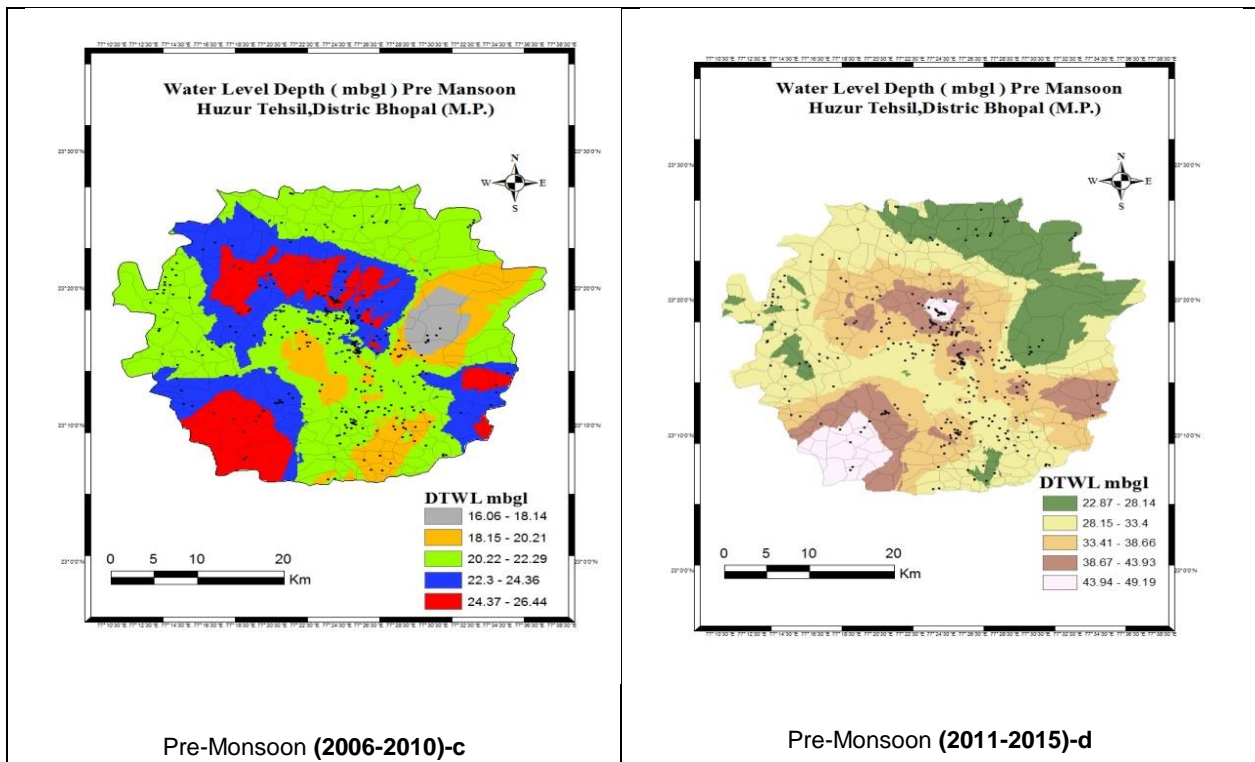
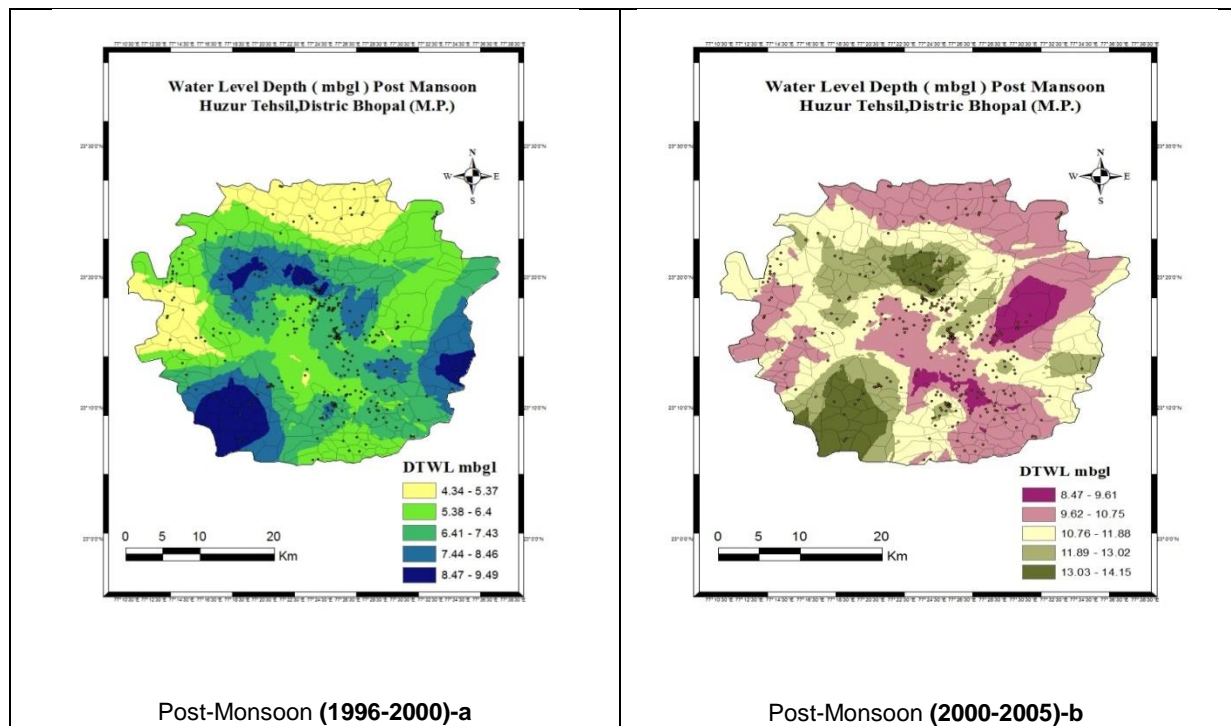


Figure 12: Pre-Monsoon Depth to water level maps for the years 1996-2000, 2001-2005, 2006-2010 and 2011-2017



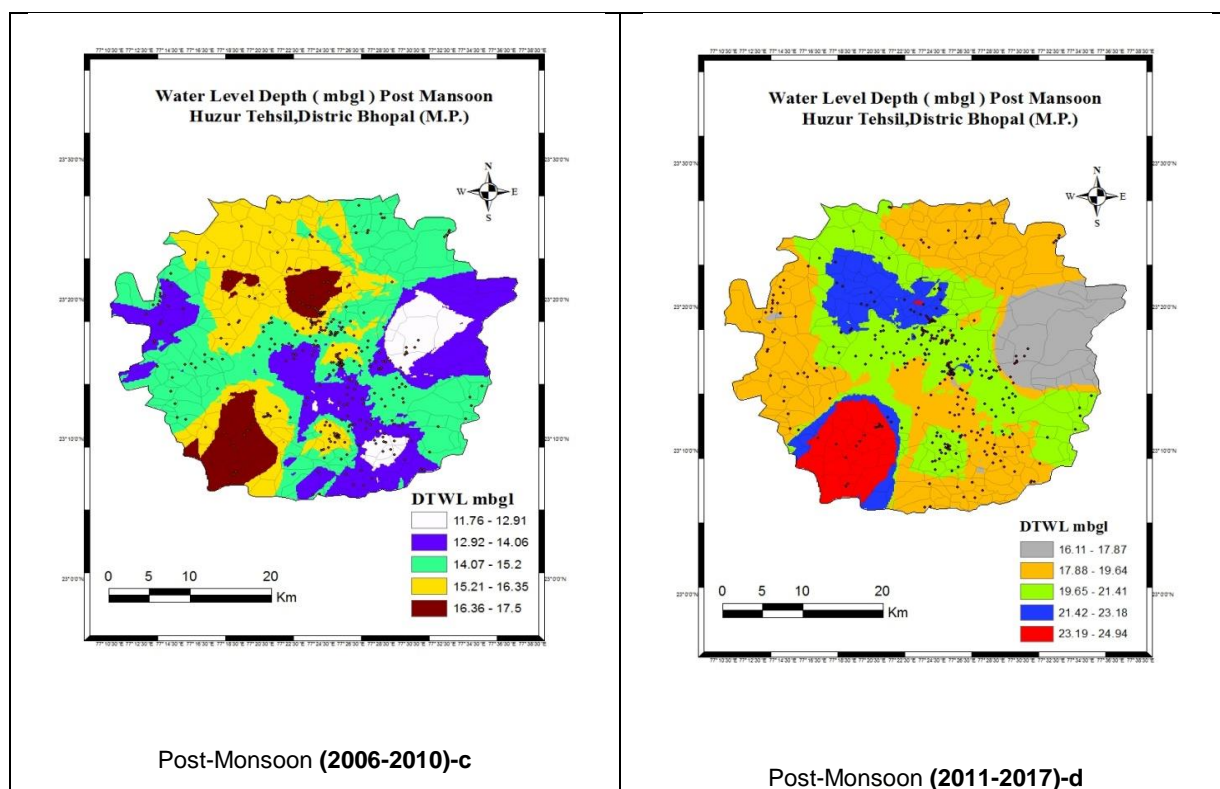


Figure 13: Post-Monsoon Depth to water level maps for the years 1996-2000, 2001-2005, 2006-2010 and 2011-2017

4.1.2. Water Level Fluctuation

The water level fluctuation of 1996-2000, 2001-2005, 2006-2010, 2011-2017 that the groundwater level between lies 1.63-4.76, 2.73-7.97, 4.26-10.92, 6.58-27.40 (mbgl). The analysis of water level fluctuation of the Pre-monsoon and Post-monsoon period during 1996- 2000, 2001-2005, 2006-2010 indicates the bores well are good condition. But after (2011-2017) indicates that 70% of the bore wells are dried. That means Groundwater Level decline. As shown in the graph of average interval Groundwater level fluctuation Period 1996-2000, 2001-2005, 2006-2010 and 2011-2017 (Figure 14). And after the analysis to find out the since (2011-2017) is groundwater Level fluctuation more decadal. Using the ArcGIS10.5 generates the Groundwater Level depth fluctuation map as shown the water level fluctuation maps in Huzur Tehsil, M.P, Bhopal District for Years 1996-2000, 2001-2005, 2006-2010 and 2011-2017(Figure 15).

4.1.3. Long term water level fluctuation

Analysis of decadal pre-monsoon water level data for the period 1996- 2017 indicates that, in general, the declining trend in water levels has been in most parts of Huzur, Tehsil, District Bhopal, Madhya Pradesh. The Groundwater Level maximum decline was in an urban area while the minimum in decline was rural areas. The declining trend ranges from 13.71 to 37.96 m/year (Figure 16).and generates the Long Trend of Groundwater Level modeling in pre-monsoon (1996-2017) and Water level contour map created from the model results as shown in Figure 17.

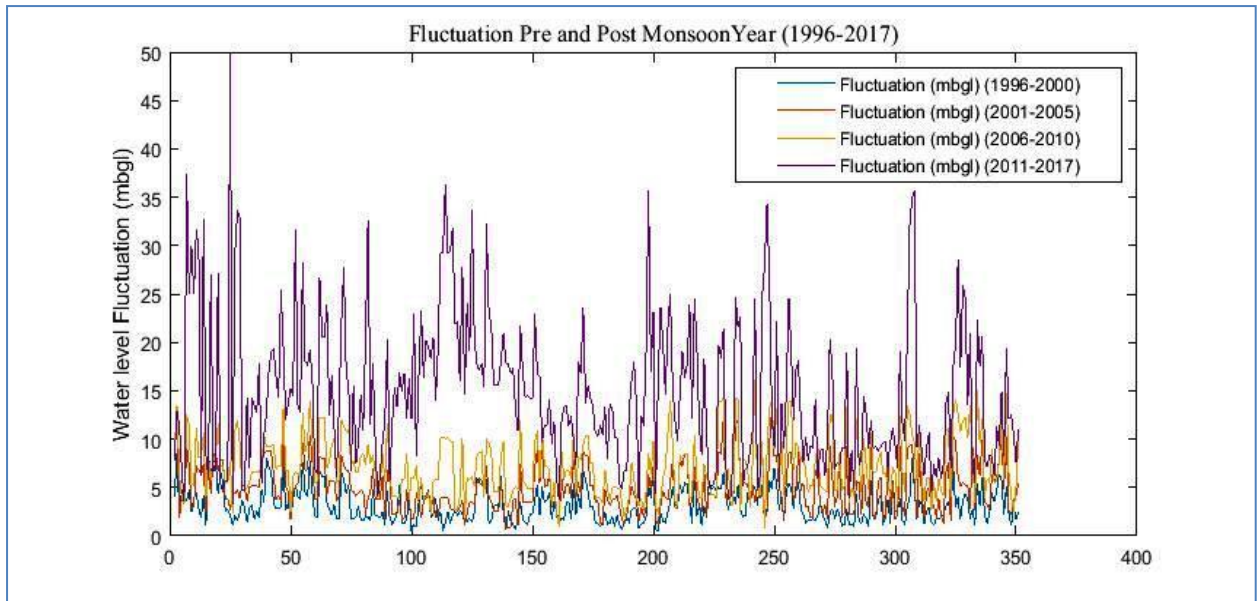
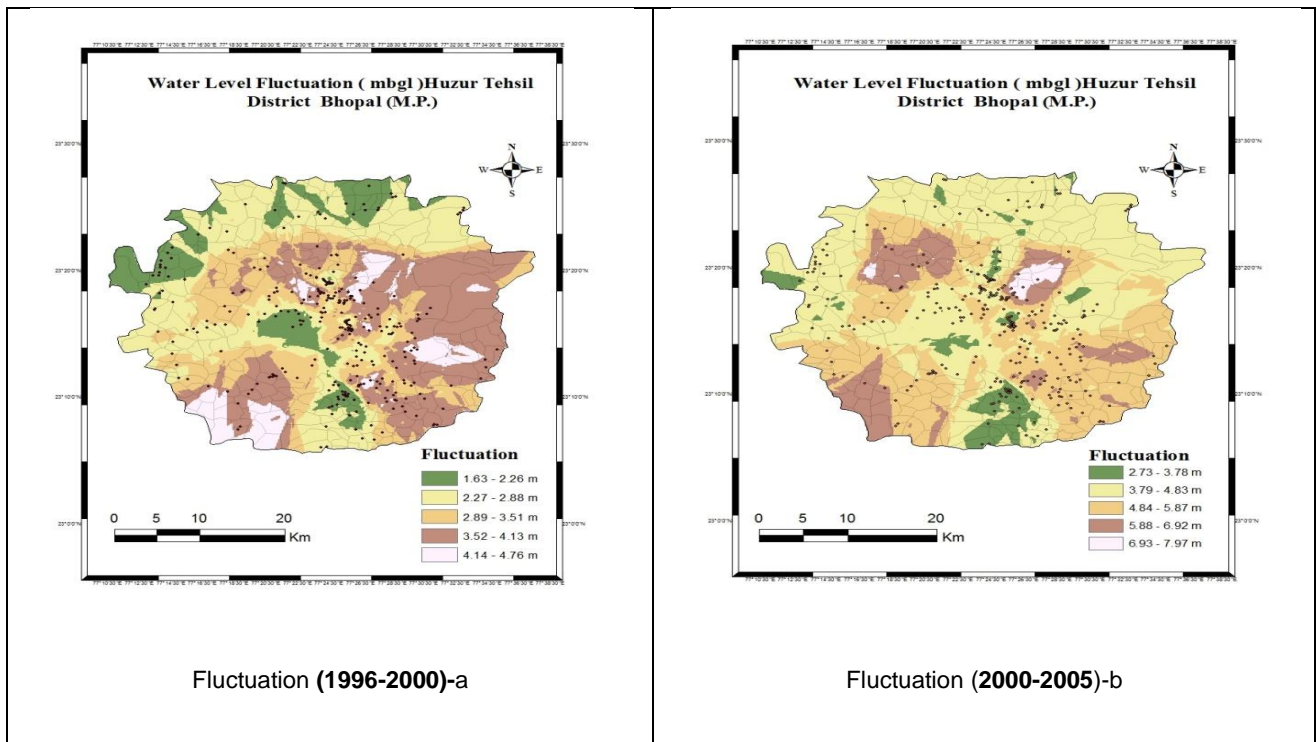


Figure 14: Fluctuation of Groundwater Level in Huzur Tehsil, M.P, Bhopal District for Years 1996-2000, 2001-2005, 2006-2010 and 2011-2017



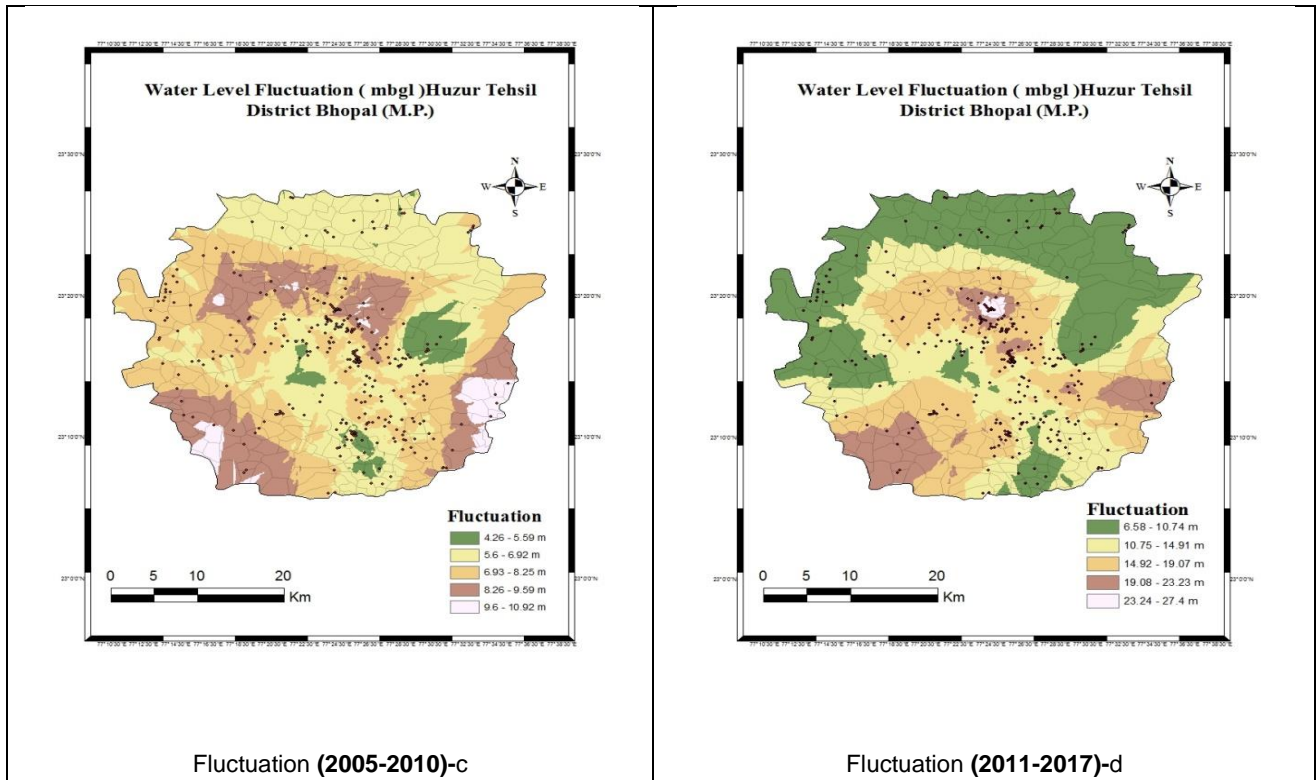


Figure 15: Fluctuation of water level maps for the years 1996-2000, 2001-2005, 2006-2010 and 2011-2017

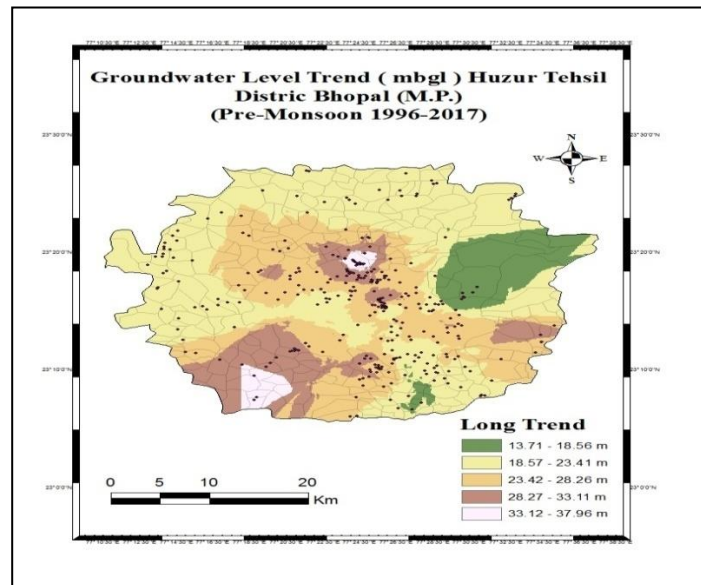


Figure 16: Decadal pre-monsoon water level Long trend map (1996– 2017)

Using MATLAB R2017b Curve Fitting Toolbox provides an app and functions for fitting curves and surfaces to data. The toolbox lets you perform exploratory data analysis, preprocess and post-process data, compare candidate models. The library provides optimized solver parameters and starting conditions to improve the quality of your fits. The toolbox also supports nonparametric modeling techniques, such as spines, interpolation, and smoothing. Using the MATLAB to show the Long trend of Groundwater Level modeling in pre-monsoon (3d Surface) (Figure 17).

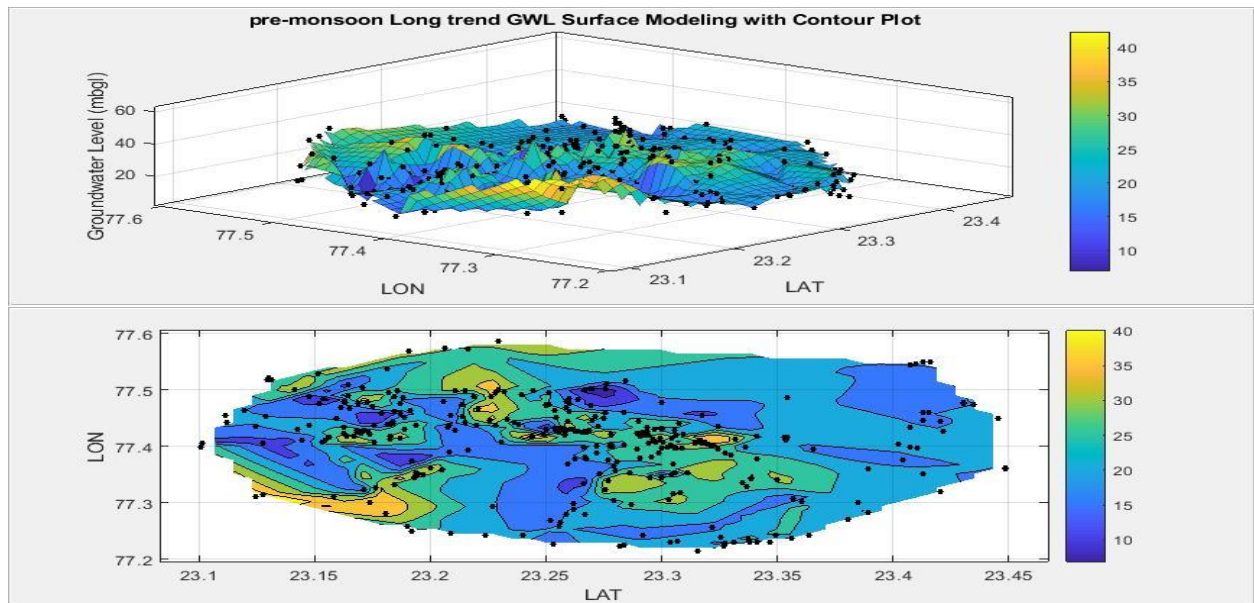


Figure 17: Long Trend of Groundwater Level modeling in pre-monsoon and Water level contour map created from the model results (3d Surface) (1996-2017)

4.1.4. Projected Feature Forecast Trend Groundwater Level

Based on the above analysis groundwater level (1996 - 2017) in Huzur tehsil, District Bhopal, deal with the provided the feature projected Ground water Level in Huzur tehsil, District Bhopal (2018-2051).Theses section analysis of Projected Feature Groundwater Level in Huzur Tehsil, District Bhopal. These are using FORECAST Function is categorized under Statistical functions. It will calculate or predict future value using existing values.

Formula=FORECAST(x, known_y's, known_x's) -----3

The FORECAST function uses the following arguments:

1. **X** (required argument) – It is a numeric x-value for which we want to forecast a new y-value.
2. **Known_y's** (required argument) – It is the dependent array or range of data.
3. **Known_x's** (required argument) – It is the independent array or range of data that is known to us.

The equation for FORECAST function will calculate a new y-value using the simple straight-line equation:

$$y=a+bx,$$

Where:

$$a = \bar{y} - b\bar{x}$$

And:

$$b = \frac{\sum (x - \bar{x})(y - \bar{y})}{\sum (x - \bar{x})^2}$$

And the values of x and y are the sample means (the averages) of the known x - and the known y -values. Based on the above Table 1 & 2 with reacted to find out the feature projected values in ground water level in study area (2018-2051) as shown in Table 9 and 10 two urban and rural pre-post monsoon data list. As shown in below the Projected Feature Forecasting Groundwater Level Fluctuation (Table 11). After the analysis Feature Projected Forecast Groundwater Level Fluctuation since 2018-2022, 2023-2027, 2028-2032, 2033-2037, 2038-2042, 2043-2047, 2048-2051. The Groundwater Level fluctuation was between 7.69 - 36.59, 9.41 - 49.13, 10.93 - 60.9, 12.27 - 70.49, 13.76 - 81.9, 15.22 - 92.83, 17.17 - 102.28 (mbgl) (Figure 18, 19, 20).

Table 9: List of Two Urban areas Pre –Post Monsoon Feature projected Groundwater Level (mbgl) in Huzur Tehsil (2018- 2051)

WL_ID	YEAR_OBS	Pre-monsoon (mbgl)	Post-monsoon (mbgl)
UA101	2018	21.17	11.67
UA101	2019	21.29	11.98
UA101	2020	21.53	12.24
UA101	2021	21.70	12.55
UA101	2022	21.92	12.92
UA101	2023	22.13	13.26
UA101	2024	22.43	13.58
UA101	2025	22.74	13.86
UA101	2026	23.12	14.26
UA101	2027	23.53	14.69
UA101	2028	23.96	15.13
UA101	2029	24.39	15.56
UA101	2030	24.85	15.99
UA101	2031	25.31	16.40
UA101	2032	25.77	16.78
UA101	2033	26.20	17.14
UA101	2034	26.62	17.49
UA101	2035	27.04	17.81
UA101	2036	27.45	18.11
UA101	2037	27.82	18.36
UA101	2038	28.16	18.66
UA101	2039	28.47	19.05
UA101	2040	28.75	19.54
UA101	2041	29.19	19.92
UA101	2042	29.63	20.31
UA101	2043	30.07	20.68
UA101	2044	30.50	21.05
UA101	2045	30.93	21.42
UA101	2046	31.35	21.79
UA101	2047	31.75	22.15
UA101	2048	32.15	22.50
UA101	2049	32.54	22.85
UA101	2050	32.93	23.20
UA101	2051	33.32	23.55

UA102	2018	70.52	55.57
UA102	2019	72.69	57.97
UA102	2020	74.64	60.26
UA102	2021	76.31	62.50
UA102	2022	79.24	65.31
UA102	2023	82.18	68.10
UA102	2024	85.08	70.87
UA102	2025	87.89	73.56
UA102	2026	90.55	76.12
UA102	2027	93.02	78.48
UA102	2028	95.29	80.66
UA102	2029	97.84	82.53
UA102	2030	100.32	84.58
UA102	2031	102.86	86.73
UA102	2032	105.32	89.02
UA102	2033	107.71	91.36
UA102	2034	110.10	93.78
UA102	2035	112.43	96.21
UA102	2036	114.69	98.63
UA102	2037	117.01	101.06
UA102	2038	119.58	103.50
UA102	2039	122.25	105.92
UA102	2040	124.97	108.36
UA102	2041	127.52	110.68
UA102	2042	130.05	112.99
UA102	2043	132.53	115.27
UA102	2044	134.92	117.52
UA102	2045	137.32	119.77
UA102	2046	139.73	122.06
UA102	2047	142.17	124.37
UA102	2048	144.63	126.72
UA102	2049	147.11	129.10
UA102	2050	149.59	131.50
UA102	2051	152.06	133.91

Table 10: List of Two Rural areas Pre –Post Monsoon Feature projected Groundwater Level (mbgl) in Huzur Tehsil (2018- 2051)

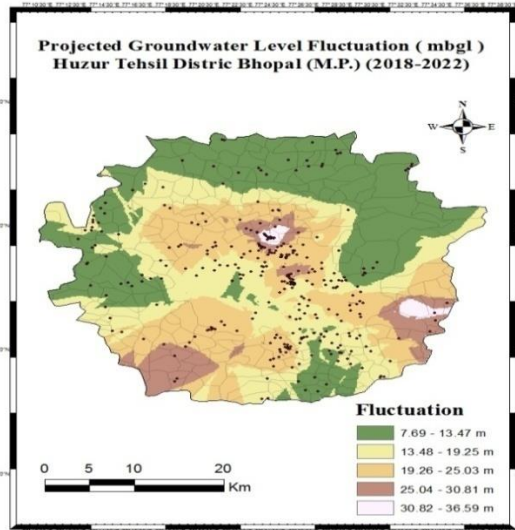
WL_ID	YEAR_OBS	Pre-monsoon (mbgl)	Post-monsoon (mbgl)
R201	2018	33.02	21.17
R201	2019	34.42	21.63
R201	2020	35.77	22.13
R201	2021	37.05	22.53
R201	2022	38.24	22.89
R201	2023	39.30	23.10
R201	2024	40.45	23.54

R201	2025	41.58	23.95
R201	2026	42.73	24.36
R201	2027	43.91	25.26
R201	2028	45.07	26.25
R201	2029	46.16	26.67
R201	2030	47.10	26.88
R201	2031	48.10	27.67
R201	2032	49.35	28.49
R201	2033	50.73	29.38
R201	2034	52.13	30.24
R201	2035	53.51	30.71
R201	2036	54.83	31.06
R201	2037	56.06	31.27
R201	2038	57.18	31.35
R201	2039	58.24	32.05
R201	2040	59.30	32.87
R201	2041	60.46	33.47
R201	2042	61.64	34.09
R201	2043	62.83	34.72
R201	2044	64.04	35.34
R201	2045	65.26	35.96
R201	2046	66.47	36.55
R201	2047	67.68	37.13
R201	2048	68.89	37.68
R201	2049	70.11	38.21
R201	2050	71.33	38.75
R201	2051	72.55	39.33
R202	2018	23.43	18.66
R202	2019	23.24	18.40
R202	2020	23.50	18.68
R202	2021	23.79	19.15
R202	2022	24.35	19.59
R202	2023	24.96	20.15
R202	2024	25.34	20.74
R202	2025	25.73	21.28
R202	2026	26.35	21.85
R202	2027	26.82	22.49
R202	2028	27.32	23.15
R202	2029	27.68	23.82
R202	2030	28.07	24.51
R202	2031	28.42	25.09
R202	2032	28.85	25.63
R202	2033	29.26	26.07
R202	2034	29.64	26.40
R202	2035	29.98	26.61

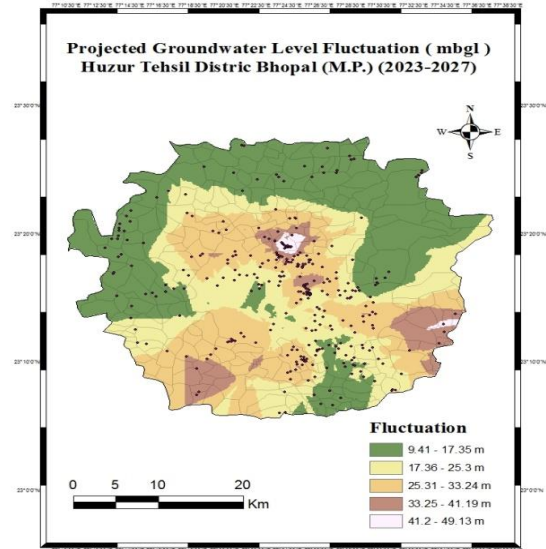
R202	2036	30.26	26.73
R202	2037	30.48	26.71
R202	2038	30.89	27.30
R202	2039	31.42	28.08
R202	2040	31.97	28.94
R202	2041	32.43	29.50
R202	2042	32.84	30.00
R202	2043	33.23	30.48
R202	2044	33.61	30.95
R202	2045	33.98	31.41
R202	2046	34.37	31.85
R202	2047	34.75	32.30
R202	2048	35.13	32.73
R202	2049	35.51	33.16
R202	2050	35.91	33.60
R202	2051	36.31	34.04

Table 11: Analysis of Projected Feature Forecasting Groundwater Level Fluctuation values

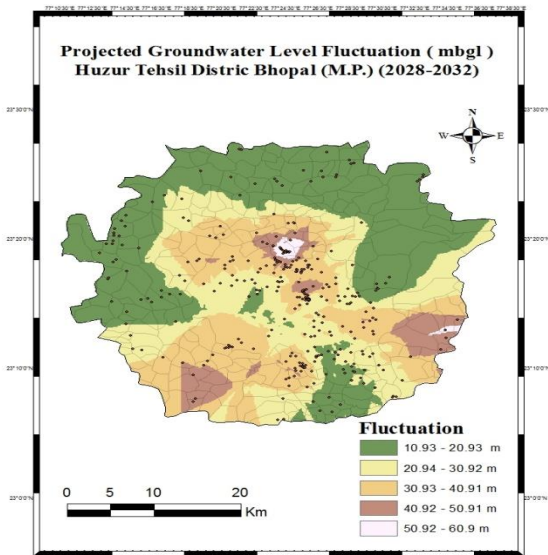
Fluctuation (1996-2000)	Fluctuation (2000-2005)	Fluctuation (2006-2010)	Fluctuation (2011-2017)	Projected Fluctuation (2018-2022)	Projected Fluctuation (2023-2027)	Projected Fluctuation (2028-2032)	Projected Fluctuation (2033-2037)	Projected Fluctuation (2038-2042)	Projected Fluctuation (2043-2047)	Projected Fluctuation (2048-2051)
1.63	2.73	4.26	6.58	7.69	9.41	10.93	12.27	13.76	15.22	17.17
2.27	3.79	5.6	10.75	13.48	17.36	20.94	23.92	27.4	30.75	34.21
2.89	4.84	6.93	14.92	19.26	25.31	30.93	35.57	41.03	46.27	51.23
3.52	5.88	8.26	19.08	25.04	33.25	40.92	47.21	54.66	61.8	68.25
4.14	6.93	9.6	23.24	30.82	41.2	50.92	58.85	68.29	77.32	85.27
2.26	3.78	5.59	10.74	13.47	17.35	20.93	23.91	27.39	30.74	34.2
2.88	4.83	6.92	14.91	19.25	25.3	30.92	35.56	41.02	46.26	51.22
3.51	5.87	8.25	19.07	25.03	33.24	40.91	47.2	54.65	61.79	68.24
4.13	6.92	9.59	23.23	30.81	41.19	50.91	58.84	68.28	77.31	85.26
4.76	7.97	10.92	27.4	36.59	49.13	60.9	70.49	81.9	92.83	102.28



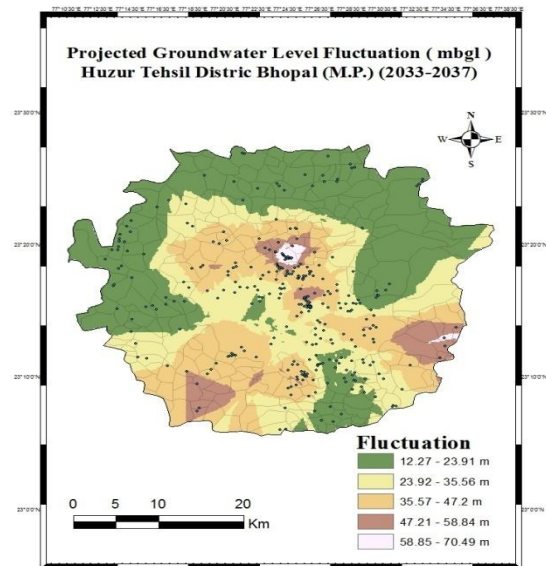
Projected GWL Fluctuation (2018-2022)-a



2-Projected GWL Fluctuation (2023-2027)-b



3-Projected GWL Fluctuation (2028-2032)-c



4-Projected GWL Fluctuation (2033-2037)-d

Figure 18: Feature Projected Forecast Groundwater Fluctuation of water level maps for the years (2018-2022, 2023-2027, 2028-2032 and 2033-2037)

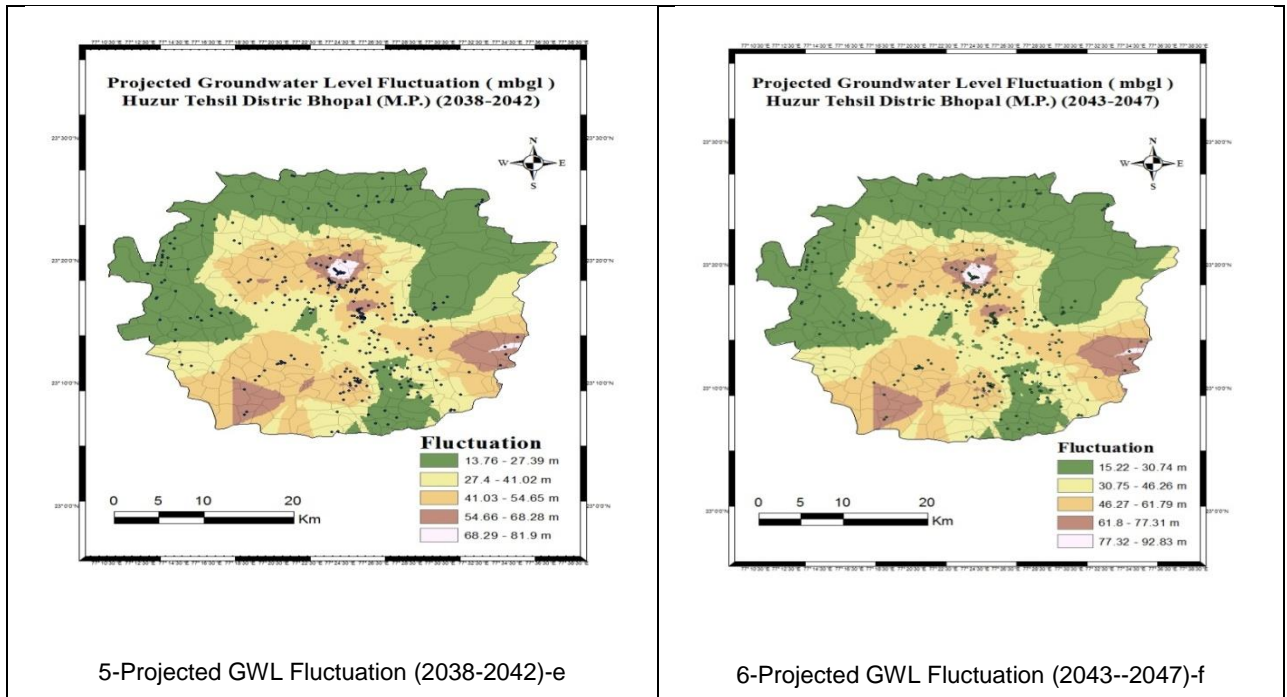


Figure 19: Feature Projected Forecast Groundwater Fluctuation of water level maps for the years (2038-2042, 2043-2047)

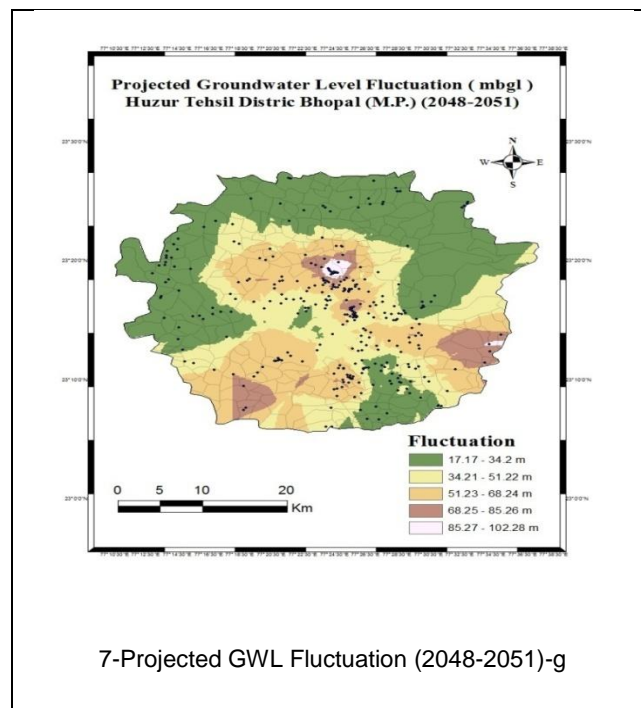


Figure 20: Feature Projected Forecast Groundwater Fluctuation of water level maps for the years (2048-2051)

4.1.5. Long term projected water level fluctuation

Analysis of Projected decadal pre-monsoon water level data for the period 2018- 2051 indicates that, in general, the declining trend in water levels has been in most parts of Huzur, Tehsil, District Bhopal, Madhya Pradesh. The Groundwater Level maximum decline was in an urban area while the minimum in decline was a rural area. The declining trend ranges from 27.65 to 91.58 m/year (Figure 21) and generate the Projected Feature Long Trend of Groundwater Level GIS map in pre-monsoon (2018-2051) as shown Figure using Matlab to projected 3d surface and Water level contour map created from the model results (Figure 22).

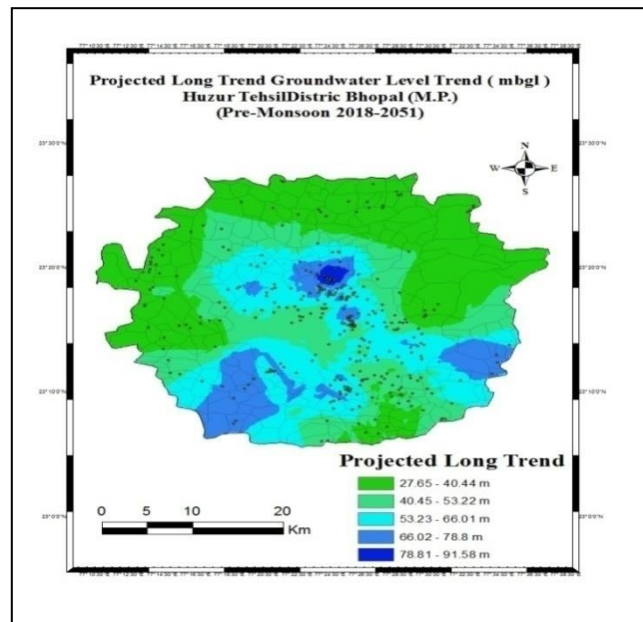


Figure 21: Projected Feature Long trend decadal pre-monsoon water level trend map (2018– 2051)

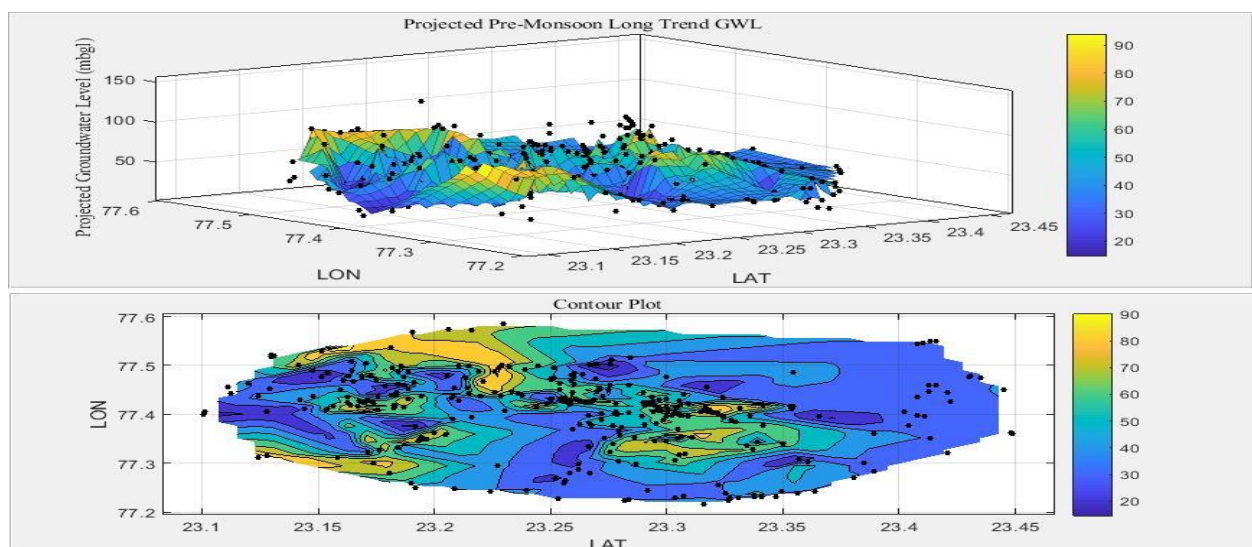


Figure 22: Projected Long Trend of Groundwater Level modeling in pre-monsoon and Water level contour map created from the model results (3d Surface) (2018-2051)

After the analysis of groundwater trend in pre-monsoon actual and projected feature shown the decline in the groundwater level. If we can do not stop the population growth and Urban sprawl such that after 20 or 30-year water level much more decline. And water will be not getting on the earth. Which is generated the drought condition in more area India? That means the Groundwater Level trend is increasing order (Figure 23).

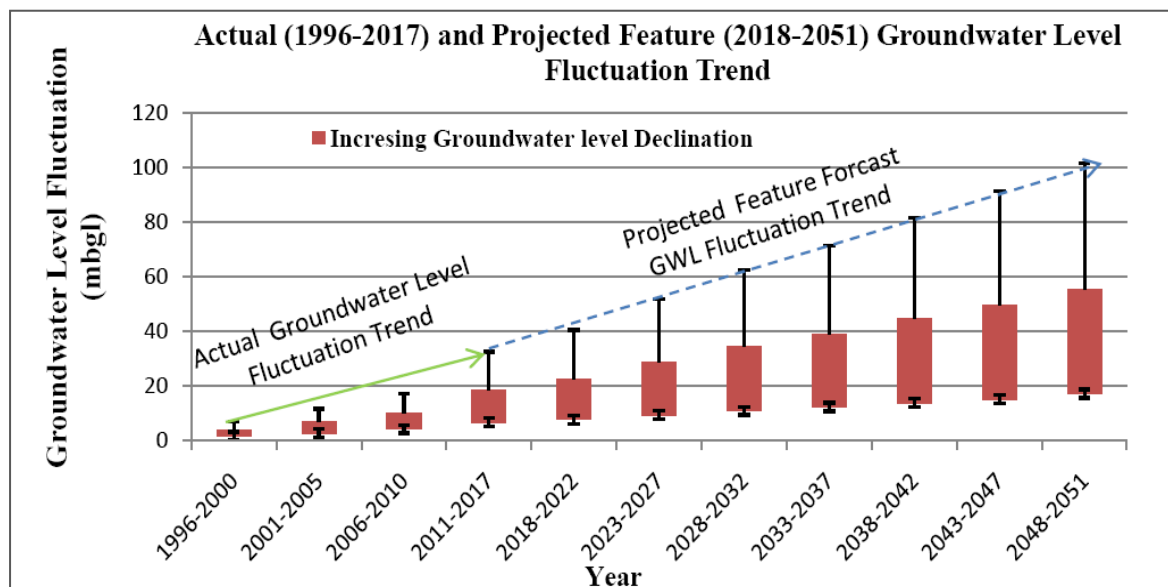


Figure 23: Increase decline Groundwater Level Fluctuation Trend (1996 -2017 to 2018-2051)

5. Conclusions

The study reflects an overall inclining trend of depth to groundwater level over the study period. In general, the results show that the district is facing the problem of declining groundwater Level in the recent past, after the year 2011. In 2011 to 2017 Huzur tehsil District Bhopal, Madhya Pradesh Groundwater level at the time of pre-monsoon time most of the area decline. And an increasing number of bore well drought. The areas showing inclining trend on a long -term bases (1996-2017 to 2018-2051) are the areas having decline groundwater level. Since 1996-2017 the Groundwater Level fluctuation was between lies 1.63-27.40 (mbgl). And the period 2018-2051 feature projected groundwater level fluctuation since 2018- 2051 feature projected Groundwater Level fluctuation was between 7.69 -102.28 (mbgl) and after analysis of pre-long trend Groundwater Level Fluctuation period 1996-2017. The declining trend ranges from 13.71 to 37.96 m/year. And the projected feature pre-long trend declining trend ranges from 27.65 to 91.58 m/year (period 2018-2051). That means increasing the population, in urban sprawl, the effect of the increasing decline of groundwater. The study demonstrates the subtle use of GIS in spatial distribution mapping and monitoring for groundwater Level in the area. The overall status of groundwater level fluctuations has received very little attention in our study area. The behavior of groundwater level fluctuations is, however, is in the initial phases for the development and management of groundwater resources as an alternative resource for drinking and domestic purposes for future demand. Groundwater level decline shows an increasing trend from 1996 to 2017 and 2018 to 2051.

References

- Agarwal Rajat, Garg, P.K. 2016. Statistical Assessment of Groundwater Resources and long trend using geospatial techniques, *doi: 10.1109/IGARSS.2016.7729464*.
- Adnan, S., Iqbal, J. 2014. Spatial analysis of the groundwater quality in the Peshawar districts Pakistan. *Procedia Engineering*, 70, pp.14-22.
- Balakrishnan, P., Saleem, Abdul, Mallikarjun, N.D. 2011. Groundwater quality mapping using geographic information system (GIS): A Case Study of Gulbarga city, Karnataka, India. *African Journal of Environmental Science and Technology*, 5, doi: 10.3390/w6010068.
- Sivapragasam, C., Kannabiran, K., Karthik, G., Raja, S. 2015. Assessing Suitability of GP Modelling for Groundwater Level. *Aquatic Procedia*, 4, pp. 693-699. <https://doi.org/10.1016/j.aqpro.2015.02.089>.
- Chia Yeeping, Chiu, J. Jessie, Chiang Yi-Hsuan, Lee Tsai-Ping, Chen-Wuing Liu. 2008. Spatial and Temporal Changes of Groundwater Level Induced by Thrust Faulting, *Pure appl. geophys.*, 165, pp. 5-16. <https://doi.org/10.1007/s00024-007-0293-5>
- Hamid Seyed Ahmadi, Sedghamiz Abbas. 2007. Geostatistical Analysis of Spatial and Temporal Variations of Groundwater Level. *Environ Monit Assess*, 129, pp.277-294 <https://doi.org/10.1007/s10661-006-9361-z>
- Jat Mahesh K., Khare Deepak., Garg, P. K. 2009. Urbanization and its impact on groundwater: a remote sensing and GIS-based assessment approach. *The Environmentalist*, 29, pp.17-32 <https://doi.org/10.1007/s10669-008-9176-2>
- Kaminska Agnieszka., Grzywna Antoni. 2014. Comparison of Deterministic Interpolation Methods for the Estimation of Groundwater Level. *Journal of Ecological Engineering*, 15, pp. 55-60 <https://doi.org/10.12911/22998993.1125458>.
- Khazaz Lamiaa, Qulidi Jarar Hassane, Moutaki Saida El., Ghafiri Abdessamad. 2015. Comparison and Evaluating Probabilistic and Deterministic spatial Interpolation Method for Groundwater Level of Haouz in Morocco. *Journal of Geographic Information System*, 7, pp. 631-642. <http://dx.doi.org/10.4236/aces.2011.13015>
- Krishna A.P., 1996. Remote Sensing Approach for Watershed Based Resources Management Priorities in the Sikkim Himalaya - A Case Study. *J. Indian Soc. Remote Sens.*, 24, pp.69-83.
- Krishna A.P., 2005. Snow and Glacier Cover Assessment in the High Mountains of Sikkim Himalaya. *Hydrological Processes*, 19, pp.2375-2383. <https://doi.org/10.1002/hyp.5890>
- Krige, D.G., 1966. Two-dimensional weighted moving average trend surfaces for ore valuation. In: Proceedings of the Symposium on Mathematical Statistics and Computer Applications in Ore Valuation, Johannesburg, pp.13-38.
- Kumar M.G., Agarwal A.K., Bali R. 2008. Delineation of potential sites for water harvesting structures using remote sensing and GIS. *J Indian Soc Remote Sens.*, 36, pp.323-334.
- Lohani A.K., Krishan G. 2015. Application of Artificial Neural Network for Groundwater Level Simulation in Amritsar and Gurdaspur Districts of Punjab, India. *J Earth Sci Clim Change*, 6, p.274.

Matheron, G.F. 1963. Principles of Geostatistics. *Economic Geology*, 58, pp.1246-1266. <http://dx.doi.org/10.2113/gsecongeo.58.8.1246>

Manjurul Hussain Md., Bari Hefzul Sheikh., Tarif Ehsanul Mohammed. 2016. Temporal and spatial variation of groundwater level in Mymensingh district, Bangladesh. *International Journal of Hydrology Science and Technology*, 6, pp.188-197.

Narany, Sheikhy, Tahoor, Ramli, Firuz, Mohammad, Aris, Zaharin, Ahmad, Sulaiman, Nor, Azmin, Wan, Fakharian, Kazem. 2014. Spatial Assessment of Groundwater Quality Monitoring Wells Using Indicator Kriging and Risk Mapping, Amol-Babol Plain, Iran. *Water*, 6, pp.68-85.

Nickson R., McArthur J.M., Shrestha B., Kyaw-Myint T.O., Lowry D. 2005. Arsenic and other drinking water quality issues, Muzaffargarh district, Pakistan. *Appl Geochem*, 20, pp.55-68.

Reeta Rani, Chaudhary, B.S. 2016. GIS Based Spatio-temporal Mapping of Groundwater Depth in Hisar District, Haryana State, India. *International Journal of Advanced Remote Sensing and GIS*, 5, pp. 1971-1980.

Jones Wayne R., Spence Michael J., Bowman Adrian W., Evers Ludger, Molinari Daniel A. 2014. A software tool for the spatiotemporal analysis and reporting of groundwater monitoring data. *Environmental Modelling & Software*, 55, pp.242-249.

Xiao, Yong, Gu, Xiaomin, Shiyang, Yin, Jingli, Shao, Yali Cui, Qiulan, Zhang, Yong, Niu. 2016. Geostatistical interpolation model selection based on ArcGIS and spatio-temporal variability analysis of groundwater level in piedmont plains, northwest China. *SpringerPlus* 5, p.425. <https://doi.org/10.1186/s40064-016-2073-0>

Yan Jinfeng, Guo Quanjun, Min Ji, Zhao Xiangwei. 2009. Model Simulation of Groundwater Level under the Effects of Land Use in an Oasis. 2009 First International Conference on Information Science and Engineering. Nanjing, China. <https://doi.org/10.1109/ICISE.2009.750>

Research Article

New Fusion Algorithm for Improving Secondary Forest Cover Mapping

Jwan Al-doski, Shattri B. Mansor, Zailani Khuzaimah

Department of Civil Engineering, Faculty of Engineering, Universiti Putra Malaysia 43400, Serdang, Selangor, Malaysia

Correspondence should be addressed to Jwan Al-doski, Aldoski-Jwan@hotmail.com

Publication Date: 22 April 2020

DOI: <https://doi.org/10.23953/cloud.ijarsg.456>

Copyright © 2020 Jwan Al-doski, Shattri B. Mansor, Zailani Khuzaimah. This is an open access article distributed under the **Creative Commons Attribution License**, which permits unrestricted use, distribution, and reproduction in any medium, provided the original work is properly cited.

Abstract Secondary forests play a central role in recovering earlier lost carbon and biodiversity via deforestation and degradation, yet little data is applicable to the magnitude of numerous succession phases. Such information is considered a priority in tropical regions with elevated past and current disturbance rates; however, regrowth in the area is rapid. Focusing on Kuala Krai district, Kelantan state, Malaysia, this paper offer a new fusion algorithm by using the clustering method (fuzzy k-means (FKM)) and Vector Supporting Machines (SVM) procedures. The methodology scheme applied was split into two phases, a clustering map firstly was acquired using FKM from the Sentinel-2A MSI (10 m) image; at the same time, the initial image used to extract Green Normalized Vegetation Index (GNDVI) layer. Using SVM classifier, the classification map was created. Second, SVM and FKM fusion as a hybrid classifier were tested, verified and compared to MLC-parametric and SVM-nonparametric classification algorithms. The study results reveal the effectiveness of the GNDVI layer and FKM segmentation map to enhance SVM classification through applying the Sentinel-2A MS image by approximately 8 % and 14 %, respectively, as opposed to SVM and MLC. Thus this study is inspiring as it is extremely difficult to generate a reliably map land cover in heterogeneous areas, especially in tropical areas, and yet this job is crucial for conservation projects, climate change mitigation strategies, and expansion plans and regional development policies.

Keywords *Secondary Forest Mapping; Vector Supporting Machines; Fuzzy K-Means; Sentinel-2A MS Image*

1. Introduction

Whereas tropical deforestation and degradation, always correlated with forest fragmentation and biodiversity loss, proceed at high levels, certain tropical regions are undergoing secondary forest expansion that performs a minimizing roles in the disappearance of species (Hansen et al., 2013; Haro-Carrión and Southworth, 2018). These complicated forest dynamics cover regions and area changes, and related environmental consequences become even more complicated when agricultural land modifications, including forest plantations, and other procedures of land change are integrated (Haro-Carrión and Southworth, 2018; Lambin, Geist and Lepers, 2003). Detailed forest cover regions and their changes using remote sensing methodologies are still required to strengthen our understanding of the true effects of human operations in certain tropical areas (Lambin, Geist and

Lepers, 2003; Frédéric Achard et al., 2010). In humid tropics like Malaysia, mapping forest cover area and changes utilizing remote sensing technologies have been successfully predicted (Maxwell, Warner, and Fang, 2018). Distinct satellite images were applied and examined using various techniques of image classification to map secondary forest land cover in the tropics (Frédéric Achard et al., 2010; Gibbs et al., 2010). The most prevalent parametric land algorithms involve maximum likelihood and linear discriminant analysis (Lu and Weng, 2007; Yonezawa, 2007). In regard to classify satellite data (single or multi-date images) of heterogeneous land cover spectral signatures, non-parametric algorithms such as Artificial Neural Networks (ANN), Decision Tree Classifiers (DTC) and Vector Supporting Machines (SVM) have demonstrated enhanced efficiency over more traditional classification methods (Lu and Weng, 2007; Immitzer, Atzberger, and Koukal, 2012).

However, Machine learning algorithms have been commonly used over the previous centuries as classification algorithms and maybe some evaluations of their comparative results compared to other classifiers have been carried out in the tropical region (Carreiras, Pereira, and Shimabukuro, 2006). Among these algorithms, SVMs have proved their classification accuracy. Precisely, elevated accuracies in land cover mapping and outperforming other algorithms have been demonstrated by SVMs (Schulz, Hänsch, and Sörgel, 2011). The accomplishment of SVM is linked to SVM classifier's inherent characteristics, which can manage unplaced issues, and to the dimensionality curse, this offers strong, scarce solutions and defines non-linear limits between classifications of land cover decisions (Hughes, 1968). It aims to distinguish secondary forest class from other land cover classifications by detecting a plane in a multidimensional characteristic room that optimizes its separation, rather than using stats to define such classes (Awad and Khanna, 2015). SVM classifiers do not need decent training sets, but only samples of training. Foody and Mathur (2006) stated use of small training sets of intentionally chosen mixed pixels with support vectors, as this technique does not lose classification accuracy and would save considerable time (Foody and Mathur, 2006).

The other very well-developed classification algorithm is Fuzzy k-means (FKM) clustering algorithm is a technique of multivariate units in different research of vegetation, soil and forestry (Tapia, Stein, and Bijker, 2005; He, T. et al., 2014]. The algorithm FKM was used mainly to resolve the class overlap concern, but its viability can be reduced if the data sets are massive (He, T. et al., 2014; Shaikh and Patil, 2017]. The fundamental issue for increasing the classification accuracy of SFC mapping is the appropriate selection of algorithms as suggested by some researchers. For example, (Nguyen and Pham, 2016] incorporated a NDVI and DEM with Landsat 8 image spectral bands to reduce the influence of shadows on image classification, differentiate between natural and planted forests, and generate a forest inventory support LCM from Hoa Binh Province. A precision classification was conducted on a multi-source dataset (bands 1–7, and 9, NDVI, and DEM) compared to spectral picture outcomes. Generally speaking, general precision increased by 5.23% (from 84.51 to 89.74%) The multisource classification with SVM was used by (Watanachaturaporn, Arora and Varshney, 2008) distinct textural measures are a significant source of ancillary data and their advantages for classifying land cover mapping were outlined in research using various techniques and classifiers.

We implemented a combination approach to deal with Secondary Forest Cover (SFC) mapping in Sentinel-2A MSI image in order to use certain the advantages of SVM and FKM clustering. The SVM classifier has been shown to produce a spectral classification map, while the FKM clustering algorithm has been implemented to get a segmentation map ensemble. SVM and FKM algorithm fusion proposes to minimize class sorting problems by achieving the feature vector and realizing the optimal nonlinear classification boundaries with SVM.

2. Develop New Fusion Algorithm

A parametric MLC, a non-parametric SVM as well as a hybrid as integration of unsupervised, SVM and FKM fusion classifiers were used to compare different classifiers. Since extensive definitions have been

stated by many researchers (Awad and Khanna, 2015; Deilmay, Ahmad and Zabihi, 2014; Zhang, Ren and Jiang, 2015), we will not explain how the algorithms MLC and SVM operate here.

2.1. Gaussian- RBF Based SVM Classifier

After defining the Sentinel-2A MSI data set which is used for SFC mapping, for just the supervised classification stage, a robust classifier should be selected (He, T. et al., 2014). The linear SVM classifier is selected because of its inherent robustness to high-dimensional information sets and unplaced issues. The initial suggested SVM algorithm by (Vapnik and Lerner, 1963). The SVM's fundamental concept is to map multidimensional information into such a higher-dimensional space where there is a hyperplane that can be used to linearly distinguish the initial information, maximizing the margin between distinct classifications (Awad and Khanna, 2015; Zhang H., et al., 2015) and (Boser, Guyon and Vapnik, 1992) suggested a technique by introducing the kernel trick to the maximum-margin hyperplane to generate nonlinear classifiers. The classifier seeks to establish a separation rule linear type among instances caused by a higher-dimensional sample space mapping feature (Nisbet, Elder and Miner, 2009)

A linear separation in a certain space corresponds in the initial input space to a nonlinear separation. An instance is shown in Figure 1. The kernel key is the foundation of such an algorithm: since mapped tests tend only in the form of dot items in the SVM formulation, such procedures can be replaced by valid kernel functions $K(.,.)$, going back specifically to the internal product value in that space, Eq. (1). The solution is provided by the maximum margin width hyperplane, which ensures the highest generalization capability on earlier unknown data. It is necessary to optimize the dual optimized formulation.

$$\max_{\alpha} \sum_{i=1}^N \alpha_i - \frac{1}{2} \sum_{i=1}^N \sum_{j=1}^N \alpha_i \alpha_j \omega_i \omega_j k(x_i, x_j), \quad s.t. 0 \leq \alpha_i \leq cand \sum_{i=1}^N \alpha_i \omega_i = 0, \quad (1)$$

Where a user-identified parameter is C, that regulates the trade-off between the difficulty of the system and the training error, the coefficients outlining are α_i the key of the optimization and (binary case) $\omega_i \in \{+1; -1\}$ are sample-related class labels x_i . When the answer to Eq. (2) is discovered, the unknown sample label x' is provided sign of decision function, i.e. its location on the separating hyperplane

$$\omega' = sign[\sum_{i=1}^N \alpha_i \omega_i k(x_i, x') + b] \quad (2)$$

Experiments are performed in this study using a kernel Gaussian -RBF:

$$k(x_i, x_j) = exp(-\|x_i - x_j\|^2 / 2\sigma^2)$$

Where σ is the user-identified bandwidth of the Gaussian function. Typically The Gaussian RBF is used in several environmental and LC mapping applications for its computational complexity. The one-against-all system is implemented to fix multi-class issues

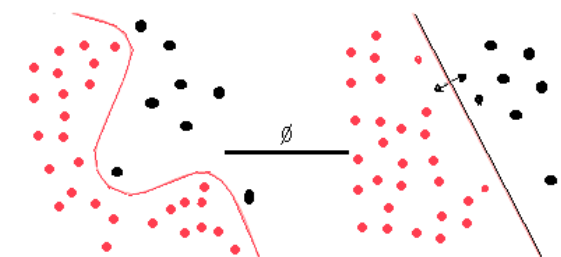


Figure 1: SVM- Kernel Machine

2.2. FKM Clustering for Forest Cover Segmentation

A fuzzy segmentation is introduced to pre-classify land cover for mapping. There is plenty of motivation for this decision. First, no set objects can be acknowledged as the concept for ground coverings was intrinsically vague, and therefore no valid, quantitative statuses are available. Second, many units between limits are intersected (He, T. et al., 2014). In an FKM cluster, the degree to which an object belongs to all contestant classes requires to retain a record (He, T. et al., 2014). Exactly, a true figure is classified in the range for all items [0, 1] considered a membership value [referred to as $\mu(Xc)$] is enrolled in all c classes where a value of $\mu(Xc)=0$ clarifies that the object does not reside to the class or set, Xc , and $\mu(Xc)= 1$ Specifies that it belongs completely to the set or class, Xc , and thus can be considered a replica of the set. Values among $\mu (Xc) = 0$ and $\mu (Xc) = 1$ stipulate the comparative power of the degree to which product has group Xc 's classic elements. Consequently, the outcome of FKM clustering is a register of the degree to which the object belongs to each class becoming considered each object getting evaluated. The FKM clustering algorithm is used for four sentinel 2A (10 m) image pixel values. This method offers a range of units recognized by the largest subscription value class, based on the degree of fuzziness provided by the parameter fuzziness φ and the number of land cover classes (k). In this research, sighted N data, φ , and the highest partition coefficient F will be used for k [Eq. (3)] and H (entropy parameter) [Eq. (4)]

$$F = \frac{F' - \frac{1}{k}}{1 - \frac{1}{k}}, \text{ s. t. } F' = \frac{1}{N} \sum_{i=1}^N \sum_{c=1}^k (m_{ic})^2 \quad (3)$$

$$H = \frac{H' - 1 + F}{\log k - 1 + F}, \text{ s. t. } H' = -\frac{1}{N} \sum_{i=1}^N \sum_{c=1}^k m_{ic} \log(m_{ic}) \quad (4)$$

m_{ic} is pixel i to category c , $c = 1, \dots, k$ Both F' and H' depends entirely on the number of categories k . In the fuzzy method, categorization for a range of class numbers and parameters was reiterated for the (k) and φ . Sentinel 2A image (10 m), we tried k 2 to 15 and reached the greatest accuracy when $k=4$ (Figure 2). As shown in the observation of different writers, the φ was set to 2.0.

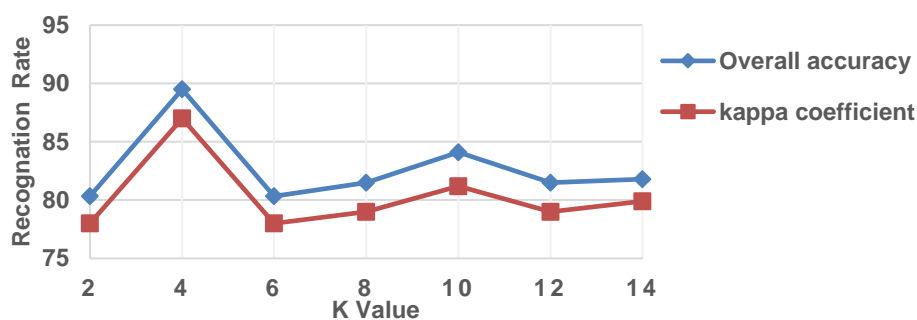


Figure 2: Choose the optimal k for FKM

2.3. Green Normalized Difference Vegetation Index (GNDVI)

In addition to the choice of image classifiers, it is acknowledged that the use of ancillary data is essential for image classification performance. Ancillary data were effectively used to enhance the classification of images, in particular by including topographical measurements (elevation and slope), NDVI, GNDVI and texture measurements in the image classification manner in addition to spectral information to separate characteristics with comparable spectral features (Coburn and Roberts, 2004). GNDVI has become a standard land cover remotely sensed product (Xue and Su, B., 2017; Dzieszko, M., Dzieszko, P., and Królewicz, 2012) for discrimination and interpretation of mapped vegetation units it has been commonly used see Figures 5 (b) and 6 (b). GNDVI has been calculated from (Gitelson, Kaufman and Merzlyak, 1996).

$$\text{GNDVI} = \text{NIR} - \text{G} / \text{NIR} + \text{G} \quad (5)$$

Where NIR and G were used for near-infrared and green data bands.

2.4. Classification Architectures of SVM and FKM Fusion

An appropriate technique must be identified to take benefit of the FKM and SVM algorithms. The architectures of the classification are provided: (i) clustering of FKM and (ii) classification of SVM. Figure 3 shows the main scheme. Using FKM clustering algorithm, the Sentinel-2A MSI image is classified and clustering maps are produced. At the same time, the initial image extracts GNDVI layer. The original image is added to both the clustering map and the GNDVI layer. The SVM classifier is then used for classification. SFC map is finally acquired.

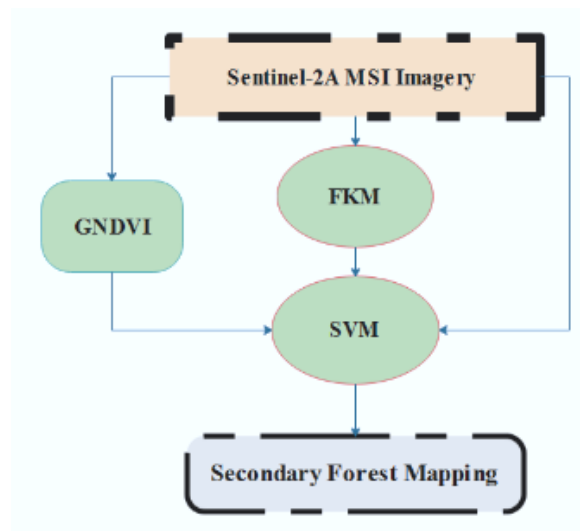


Figure 3: The main scheme for a new fusion technique (SVM and FKM algorithms)

3. Material

3.1. Study Area

The test regions selected is the district Kuala Krai, Kelantan state, Malaysia. The co-ordinates are between longitudes 102.280105°E and 102.229727°E and latitudes 6.202459°N and 5.882407°N (Figure 4). The annual average rainfall is over 6,000 mm. The temperature is 27.5 C0 per month. The rainy, equatorial climate suits oil palm plantations, making oil palm one of the region's largest cash crops. Test research elevation progressively raises from 400 -900 m above sea level so our research region is comparatively flat.



Figure 4: Location of Kuala Krai, Malaysia

3.2. Sentinel-2A Data and Pre-processing

Sentinel-2A is launched in June 2015; Sentinels Data can be downloaded from (<https://scihub.copernicus.eu/>) for free. The Sentinel-2A MS data is distinguished by a 13 spectral bands with a ground spatial resolution between 10 and 60 m (Table 1). Sentinel-2A MS imagery acquired on 3 July 2017 at Level L1C geocoded (solar azimuth 1270, solar elevation 660) with standard product of TOA reflectance and then was pre-processed. Firstly, the image atmospherically corrected with sen2cor software version 2.3 (Telespazio VEGA Deutschland GmbH, Darmstadt, Germany) to generate and BOA reflectance corrected Level-2A bands on the Anaconda Python platform using the Sen2Cor processor (version 2.3) (J r me et al., 2016). The format of the output product is a compilation of TIFF images with three distinct resolutions (10, 20 and 60 m) reproduced bands. In this research, we used 10-meter bands to obtain SFC map. The Sentinel-2 MSI image was then geometrically corrected (Lima et al., 2019; Baillarin et al., 2012) using 15 GCPs from main features like roads and DEM to attain enhanced geodetic accuracy (Habib et al., 2017). The first-order polynomial function and the nearest protocol was enacted to correct systematic variations between neighboring images in a few instances. The total transformation RMSE equal 0.07 which was less than a pixel was attained. Then the Sentinel-2 MS image re-projected to UTM coordinating scheme, WGS 1984 datum and 47 south zone using the nearest neighbours resampling method. The data were spatially subset with ENVI 5.1 software to the study area.

Table 1: Sentinel-2 MSI spectral bands information

Sentinel-2 Bands	Central Wavelength (μm)	Resolution (m)	Bandwidth (nm)
Band 1—Coastal aerosol	0.443	60	20
Band 2—Blue	0.490	10	65
Band 3—Green	0.560	10	35
Band 4—Red	0.665	10	30
Band 5—Vegetation Red Edge	0.705	20	15
Band 6—Vegetation Red Edge	0.740	20	15
Band 7—Vegetation Red Edge	0.783	20	20
Band 8—NIR	0.842	10	115
Band 8A—Narrow NIR	0.865	20	20
Band 9—Water Vapor	0.945	60	20
Band 10—SWIR—Cirrus	1.380	60	30
Band 11—SWIR	1.610	20	90
Band 12—SWIR 20	2.190	20	180

To decrease complexity calculation and enhance classification accuracy, two sample images were clipped after topographical correction by DEM, see (Figure. 5(a)) for sample 1 image, and (Figure 6(a)) for sample 2. By visual inspection, image interpretation in both sample images emphasized a total of five LC classes of interested areas. Finally, sample 1 image labeled 3367 pixels (Figure 5(b)) and sample 2 image labeled 2919 pixels (Figure 6(b)). Water bodies, primary forests, secondary forests, urban areas and other classes were the sort of land cover. Careful attention has been given to scatter training areas across each image to ensure that they are indicative of the whole image and to collect as many samples of practice for each land cover class (Table 2) as proposed criteria have been met to determine the appropriate minimum sample size. The Jeffries – Matusita transformed divergence index was used to evaluate the separability of sample information. This study separability confirmed, it was rather high for water bodies, urban regions, and other regions, but for primary forest and secondary forest classes, it is much smaller. All of these pixels were used to train and validate classifiers for SVM supervision.

Table 2: Size of land cover samples (# pixels) collected for develop new fusion approach

No	Land Cover Classes	Sample pixels	Sample 1	Sample 2
1	Water Bodies	398	242	
2	Primary Forest	568	460	
3	Secondary Forest	784	860	
4	Urban Area	825	774	
5	Other	792	583	
Total	3367		2919	

3.3. Experimental Setup

The MLC, SVM, SVM and FKM fusion classifiers were used to explore different types of algorithms. All algorithms have been initiated in Windows 10 using ENVI+IDL 5.1. The combination of both algorithms was mainly split into two phases in this research. First, by means of Eq (5), the GNDVI layer was calculated utilizing Sentinel-2A MS red and near-infrared bands; the clustering FKM algorithm was applied to generate a division map with 10 m imagery across all four bands. The GNDVI layer and division map were then piled onto the original MS image of the Sentinel-2A. Second, in order to calculate and generate the SFC map, the SVM classifier was lastly set up. A 3 x 3 pixel majority filter was introduced after map manufacturing to minimize salt and pepper noise to improve accuracy. Reference data collection for precision assessment was based on stratified random sample selection, with sample units being collected at a minimum of 1 m to avoid future effects of spatial autocorrelation.

From the pictures themselves, the information was field-truthed by specialist understanding. For the aggregate and accuracy assessment obtained by each class, a confusion matrix was developed, and this is the most common method for remote sensing classification accuracy assessment.

4. Results and Discussions

Figures 5 and 6 demonstrate the MLC, SVM and FKM and SVM classifier fusion classification maps. In Figure 5, all classification techniques recognized secondary class forest as the land cover class taking over half of the entire area of the region, accompanied by primary class forest. Entirely techniques recognized classes of urban areas and water bodies as smallest region of the land cover class. Other class, on the contrary, represented the biggest percentage in Figure 6.

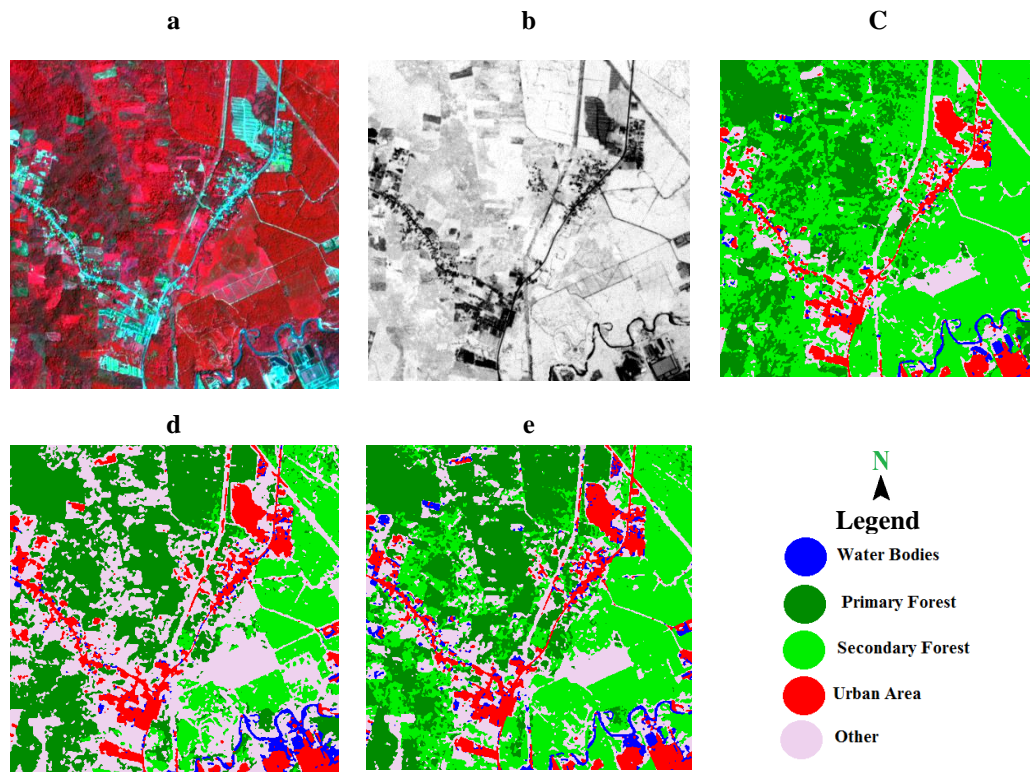


Figure 5: Multispectral high resolution Sentinel-2A MS image acquired over Kota Bharu city, Kelantan state, Malaysia (sample 1 image). (a) RGB image structure (b) GNDVI (c) MLC map (d) SVM map (e) SVM and FKM Fusion map.

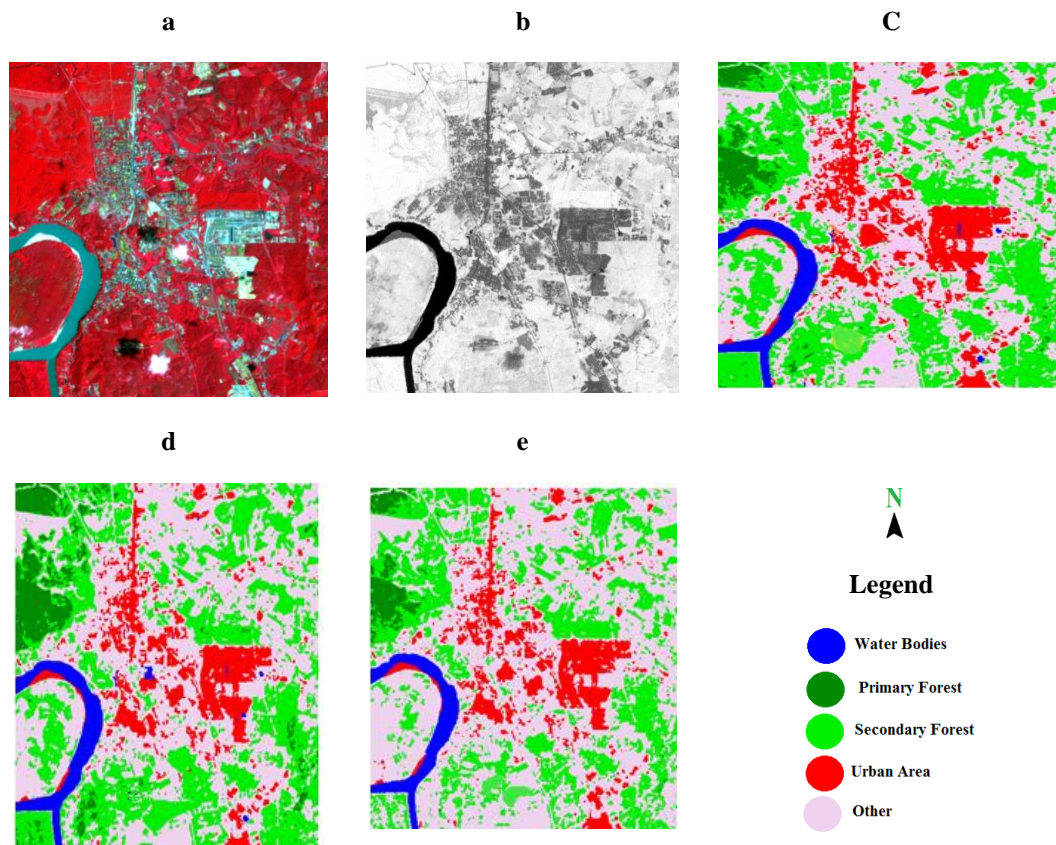


Figure 6: Multispectral high resolution Sentinel-2A MS image acquired over Kota Bharu city, Kelantan state, Malaysia (sample 2 image). (a) RGB image structure (b) GNDVI (c) MLC map (d) SVM map (e) SVM and FKM Fusion map

To evaluate the separation efficiency of classes, confusion matrices were generated per each classification algorithm. In the sample 1 image, each algorithm with OV evaluated 78.05%, 86%, and 93.8%, respectively, of MLC, SVM, and SVM and FKM fusion (Table 3). Whereas for sample 2 image, the MLC, SVM, FKM and SVM fusion classifiers OA was 85.2%, 90.4%, and 98.6% (Table 4). From both tables, the MLC technique developed accuracy for the individual classes of the smallest producer and user. The most details were on the MLC map, while the least details were on the SVM classification map. It is due to the subsequent translation of the SVM algorithm into a convex issue of optimization that can ensure the ideal global. MLC is focused, however, on addressing the resident issue and guaranteeing the local optimal. Tables 3 and 4 show that in SFC maps from SVM classifier is more profitable than MLC. It also coincides with the fact that in SFC maps, the SVM algorithm is better than MLC which was denoted from (Zhang, Ren and Jiang, 2015; Mondal et al., 2012). Amongst other classifiers, the fusion of the SVM and FKM algorithms had the largest OA. In this research, the greatest OA accuracy produced by FKM and SVM fusion suggests that our strategy is beneficial in carrying out SFC maps. The outcome was significantly affected by the samples of training although there were some shadows in urban area and samples of water bodies training. In splitting secondary forest and primary forest classes, the suggested technique was less efficient. It might be due to the Sentinel-2A MS image date.

Table 3: Sample 1 image land cover accuracy % of MLC, SVM and fusion classifiers

Land Cover Classes	MLC		SVM		SVM and FKM	
	PA%	UA%	PA%	UA%	PA%	UA%
Water Bodies	73.68	100	97.22	100	94	98.95
Primary Forest	72.50	94.57	95.33	96.62	94	94
Secondary Forest	65	71.23	67	83.87	97	92.38
Urban Area	86.59	87.57	86.9	94.51	93	92.08
Other	90.41	58.67	91.2	65.35	91	91.92
OA%	78.05		86		93.8	
K Coefficient	0.72		0.82		0.92	

PA, Producer accuracy; UA, User accuracy

Table 4: Sample 2 image land cover accuracy % of MLC, SVM and fusion classifiers

Land Cover Classes	MLC		SVM		SVM and FKM	
	PA%	UA%	PA%	UA%	PA%	UA%
Water Bodies	81	100	92	98.92	98	100
Primary Forest	65	100	98	72.59	96	98.97
Secondary Forest	100	64.52	63	96.92	99	100
Urban Area	100	100	100	100	100	100
Other	100	84.3	100	92.52	100	94.34
OA%	85.2		90.4		98.6	
K Coefficient	0.81		0.88		0.98	

PA, Producer accuracy; UA, User accuracy

The FKM and SVM algorithms fusion for sample 1 image confusion matrix is shown in Table 5. Despite the extremely accurate general outcomes achieved by the fusion of SVM and FKM algorithms, it was significantly less efficient in acknowledging secondary forest, urban area, and others. Approximately 3% of the secondary forest was confused as the primary forest, whilst also 6% of the others class was wrongly marked as the class of the urban region. Table 6 also demonstrates the sample area 2 mage confusion matrix of FKM and SVM algorithms fusion. In highlighting primary forest, others, and water bodies, the algorithm was less efficient. Approximately 4% of primary forest was confused as others and 2% of others were wrongly marked as the class of water bodies.

Table 5: Confusion matrixes representing the highest overall classification using SVM and FKM fusion in sample

1

Land Cover Classes	Ground truth (%)					
	Water Bodies	Primary Forest	Secondary Forest	Urban Area	Other	Total
Water Bodies	94	0	0	1	0	19
Primary Forest	0	94	3	0	3	20
Secondary Forest	0	3	97	0	5	21
Urban Area	6	1	0	93	1	20.20
Other	0	2	0	6	91	19.80
Total	100	100	100	100	100	

The size of surface objects relative to a sensor's spatial resolution is strongly associated with the divergence of the image. There have been some errors between primary and secondary forest classes. Approximately 3% of primary forest category pixels were regarded as secondary forest classes and around 5% of secondary forests were incorrectly categorized as other classes (Table 6), only 2% of other classes were erroneously categorized as primary forests and 6% were confused as urban areas, which can also be caused by the urban area training study. The reasons are as follows for the bad decision that distinguishes urban, other, and water bodies. First, the urban area on the

Sentinel-2A MS image was smaller than the other land cover classes, and some trees, grasses, and bare surface were included in urban area class sample. Second, the urban area and other class had comparable houses. It can also be discovered that factories were constructed on hills and that the urban area was positioned close to leakage from the classification map resulting from the policy of local land use.

Table 6: Confusion matrixes representing the highest overall classification using SVM and FKM fusion in sample 2

Land Cover Classes	Ground truth (%)					Total
	Water Bodies	Primary Forest	Secondary Forest	Urban Area	Other	
Water Bodies	98	0	0	0	0	19.60
Primary Forest	0	96	1	0	0	19.40
Secondary Forest	0	0	99	0	0	19.80
Urban Area	0	0	0	100	0	20
Other	2	4	0	0	100	21.20
Total	100	100	100	100	100	

5. Summary

This paper suggested a combination of classification techniques for SVM and FKM. When dealing with RS images as data sets for land cover mapping, this technique can enhance effectiveness the accuracy. The effectiveness of the GNDVI layer and FKM segmentation map has been illustrated in this studies to improve SVM classification in the Sentinel-2A MS image by approximately 8% compared to SVM and 14% compared to MLC. Experiments on the issue of classification of the Sentinel-2A MSI image showed excellent outcomes and inspired future and in-depth studies on the classification of land cover. This is the first time that we have infused SVM and FKM algorithms to classify SFC. Attention to greater resolution images and combine more data is the most important asset. Our findings are encouraging since it is highly hard to reliably map land cover in heterogeneous fields, particularly in tropical regions, and yet this task is essential for preservation initiatives, climate change mitigation strategies, and the design of development plans and rural development strategies. Our current strategy to fusion offers the benefit of being simple to enforce, as both GNDVI measurement and SVM classifier existence are readily available and price-effective in common and affordable remote sensing software, as SVM classifiers can use bigger training databases without compromising the precision of classification. Importantly, the very accurate findings gained from this method indicate its excellent potential for land cover mapping in tropical regions.

Acknowledgements

Authors wish to gratefully acknowledge Prof. Shattri B. Mansor, Director of GIS Research Centre at Universiti Putra Malaysia, and Dr. Zailani Khuzaimah for the financial support, recommendations and guidance through this study. The authors wish to acknowledge the helpful comments and advise from both anonymous reviewers.

References

- Awad, M. and Khanna, R. Support Vector Machines for Classification in *Efficient Learning Machines: Theories, Concepts, and Applications for Engineers and System Designers* Berkeley, CA: Apress, 2015, pp.39-66.
- Baillarin, S. J., Meygret, C., Dechoz, B., Petrucci, S., Lacherade, Tremas, T., Isola, C., Martimort, P., Spoto, F. Sentinel-2 level 1 products and image processing performances, in: *2012 IEEE international geoscience and remote sensing symposium*, 2012, pp.7003-7006: IEEE.

Boser, B. E., Guyon, I. M., and Vapnik, V. N. A training algorithm for optimal margin classifiers, in: *Proceedings of the fifth annual workshop on Computational learning theory*, 1992, pp.144-152: ACM.

Carreiras, J., Pereira, J., and Shimabukuro, Y. E. 2006. Land-cover mapping in the Brazilian Amazon using SPOT-4 vegetation data and machine learning classification methods. *Photogrammetric Engineering & Remote Sensing*, 72(8), pp.897-910.

Coburn, C., and Roberts, A. C. 2004. A multiscale texture analysis procedure for improved forest stand classification. *International journal of remote sensing*, 25(20), pp.4287-4308.

Deilmai, B. R., Ahmad, B. B., and Zabihi, H. Comparison of two classification methods (MLC and SVM) to extract land use and land cover in Johor Malaysia in *IOP Conference Series: Earth and Environmental Science*, 2014, 20(1), p.012052: IOP Publishing.

Dzieszko, M., Dzieszko, P., and Królewicz, S. 2012. Digital aerial images land cover classification based on vegetation indices. *Quaestiones Geographicae*, 31(3), pp.5-23.

Foody, G.M. and Mathur, A. 2006. The use of small training sets containing mixed pixels for accurate hard image classification: Training on mixed spectral responses for classification by a SVM. *Remote Sensing of Environment*, 103(2), pp.179-189.

Frédéric Achard, Hans-Jürgen Stibig, Hugh D. Eva, Erik J. Lindquist, Alexandre Bouvet, Olivier Arino and Philippe Mayaux. 2010. Estimating tropical deforestation from Earth observation data. *Carbon Management*, 1(2), pp.271-287.

Gibbs, H. K., Ruesch, A. S., Achard, F., Clayton, M. K., Holmgren, P., Ramankutty, N. and Foley, J. A. 2010. Tropical forests were the primary sources of new agricultural land in the 1980s and 1990s. *Proceedings of the National Academy of Sciences*, 107(38), pp.16732-16737.

Gitelson, A. A., Kaufman, Y. J., and Merzlyak, M. N. 1996. Use of a green channel in remote sensing of global vegetation from EOS-MODIS. *Remote sensing of Environment*, 58(3), pp.289-298.

Habib, A., Akdim, N., Labbassi, K., Khoshelham, K., and Menenti, M. 2017. Extraction and accuracy assessment of high-resolution DEM and derived orthoimages from ALOS-PRISM data over Sahel-Doukkala (Morocco). *Earth Science Informatics*, 10,(2), pp.197-217.

Hansen, M. C., Potapov, P. V., Moore, R., Hancher, M., Turubanova, S. A., Tyukavina, A., Thau, D., Stehman, S. V., Goetz, S. J., Loveland, T. R., Kommareddy, A., Egorov, A., Chini, L., Justice, C. O., Townshend, J. R. G. 2013. High-resolution global maps of 21st-century forest cover change. *Science*, 342 (6160), pp.850-853.

Haro-Carrión, X. and Southworth, J. 2018. Understanding Land Cover Change in a Fragmented Forest Landscape in a Biodiversity Hotspot of Coastal Ecuador. *Remote Sensing*, 10(12), p.1980.

He, T., Sun, Y.-J., Xu, J.-D., Wang, X.-J., and Hu, C.-R. 2014. Enhanced land use/cover classification using support vector machines and fuzzy k-means clustering algorithms. *Journal of Applied Remote Sensing*, 8(1), p.083636.

Hughes, G. 1968. On the mean accuracy of statistical pattern recognizers. *IEEE transactions on information theory*, 14(1), pp.55-63.

Immitzer, M., Atzberger, C. and Koukal, T. 2012. Tree species classification with random forest using very high spatial resolution 8-band WorldView-2 satellite data. *Remote Sensing*, 4(9), pp.2661-2693.

Jérôme Louis, Vincent Debaecker, Bringfried Pflug, Magdalena Main-Knorn, Jakub Bieniarz, Uwe Mueller-Wilm, Enrico Cadau, Ferran Gascon. Sentinel-2 sen2cor: L2a processor for users, in: *Proceedings of the Living Planet Symposium, Prague, Czech Republic*, 2016, pp.9-13.

Lambin, E. F., Geist, H. J. and Lepers, E. 2003. Dynamics of land-use and land-cover change in tropical regions. *Annual review of environment and resources*, 28(1), pp.205-241.

Lima, T. A., Beuchle, R., Langner, A., Grecchi, R. C., Griess, V. C., and Achard, F. 2019. Comparing Sentinel-2 MSI and Landsat 8 OLI Imagery for Monitoring Selective Logging in the Brazilian Amazon. *Remote Sensing*, 11(8), p.961.

Lu, D. and Weng, Q. 2007. A survey of image classification methods and techniques for improving classification performance. *International journal of Remote sensing*, 28(5), pp.823-870.

Maxwell, A. E., Warner, T. A. and Fang, F. 2018. Implementation of machine-learning classification in remote sensing: An applied review. *International Journal of Remote Sensing*, 39(9), pp.2784-2817.

Mondal, A., Kundu, S., Chandniha, S. K., Shukla, R., and Mishra, P. 2012. Comparison of support vector machine and maximum likelihood classification technique using satellite imagery. *International Journal of Remote Sensing and GIS*, 1(2), pp.116-123.

Nguyen, T. T. H., and Pham, T. T. T. 2016. Incorporating ancillary data into Landsat 8 image classification process: a case study in Hoa Binh, Vietnam. *Environmental Earth Sciences*, 75(5), p. 430.

Nisbet, R., Elder, J., and Miner, G. 2009. *Handbook of statistical analysis and data mining applications*. Academic Press.

Schulz, K., Hänsch, R., and Sörgel, U. Machine learning methods for remote sensing applications: an overview in *Earth Resources and Environmental Remote Sensing/GIS Applications IX*, 2018, 10790, p. 1079002: International Society for Optics and Photonics.

Shaikh, A. H. and Patil, M. E. 2017. Enhancing the Performance of K-Means Clustering by using Fuzzy Partitioning Matrix. *International Journal of Computer Applications*, 166(4).

Tapia, R., Stein, A., and Bijker, W. 2005. Optimization of sampling schemes for vegetation mapping using fuzzy classification. *Remote Sensing of Environment*, 99(4), pp.425-433.

Vapnik, V., and Lerner, A. Y. 1963. Recognition of patterns with help of generalized portraits. *Avtomat. i Telemekh*, 24(6), pp.774-780.

Watanachaturaporn, P., Arora, M. K., and Varshney, P. K. 2008. Multisource Classification Using Support Vector Machines. *Photogrammetric Engineering & Remote Sensing*, 74(2), pp.239-246.

Xue, J., and Su, B. 2017. Significant remote sensing vegetation indices: A review of developments and applications. *Journal of Sensors*, 2017.

Yonezawa, C. 2007. Maximum likelihood classification combined with spectral angle mapper algorithm for high resolution satellite imagery. *International Journal of Remote Sensing*, 28(16), pp.3729-3737.

Zhang, H., Weng, Q., Lin, H., and Zhang, Y. 2015. *Remote sensing of impervious surfaces in tropical and subtropical areas*. CRC Press.

Zhang, Y., Ren, J., and Jiang, J. 2015. Combining MLC and SVM classifiers for learning based decision making: Analysis and evaluations. *Computational intelligence and neuroscience*, 2015, p.44.

Research Article

Environmental-economic Approach to Analysis of Agriculture Land Suitability Using Spatial Modelling

Wang Shuangao¹, Liu Zhixiong¹, Liu Yi¹, Li Huafeng¹ and Mohamed Shamsudeen²

¹Business School, China University of Political Science and Law, Xueyuan Road Campus: 25 Xitucheng Lu, Haidian District, Beijing, China

²Independent Researcher

Correspondence should be addressed to Wang Shuangao, wangshuangao@outlook.com

Publication Date: 20 April 2020

DOI: <https://doi.org/10.23953/cloud.ijarsg.457>

Copyright © 2020 Wang Shuangao, Liu Zhixiong, Liu Yi Li Huafeng and Mohamed Shamsudeen. This is an open access article distributed under the **Creative Commons Attribution License**, which permits unrestricted use, distribution, and reproduction in any medium, provided the original work is properly cited.

Abstract Agriculture is a predominant factor economic and Gross Domestic Product (GDP) for any country. However, the agriculture land was changed into urban area and built-up land due to population growth and rapid urbanization. For last two decades, 25% of agriculture lands were converted into other purposes, which lift the economic value for land using and impact the ecosystem economic service value. While comprehensive and continuous valuation of identifying suitable economic and feasible agricultural land are vital for agriculture planning and maintain food security, they typically time consuming and exclusive field studies. We demonstrated using of spatial data to identify the suitable agricultural land integrating economic, physical, biological and chemical parameters. We identified the suitable and economical agriculture land during 2019-2020 in Thanjavur district in Cauvery delta protected agricultural zone. We used spatial analysis to understand the agriculture suitability land into three categories as highly suitable, moderately suitable and low suitable. Our study identifies 1027.2 sq.km areas of Peravurani, Thanjavur, Thiruvaiyaru, Papanasam, Thiruvaidaimaruthur are highly suitable for pearl millet cultivation. The 754.12-sq.km areas of Orathanadu, near Thanjavur and near Pattukkottai are suitable for maize. The 1896.28-sq.km areas of Pattukkotai, Peravurani and the small portion of Thanjavur and Papanasam are suitable for sorghum cultivation. The 754.12-sq.km highly suitable areas of Thanjavur and near Orathanadu are suitable for rice cultivation. The 178.42 sq.km areas of Orathanadu are mainly high suitable for cotton. The 745.12-sq.km areas of Thanjavur and near Orathanadu are highly suitable for pulses. The 712.19-sq.km areas of Peravurani and Thanjavur are more suitable for sesame cultivation. Our results provide information to economist, agriculture planning department and urban planners for appropriate methodology to identify the agricultural land.

Keywords *Remote Sensing; GIS; Economic Value; Agriculture; Land suitability; Physical, Chemical and Biological parameters; Ecosystem services*

1. Introduction

Agriculture is a predominant factor economic and Gross Domestic Product (GDP) for any country (Palaniswami, Gopaldasundaram and Bhaskaran, 2011). However, the agriculture lands were changes into urban area and built-up land due to population growth and rapid urbanization (Mohammad Shah Nawaz Khan and Mohd. Mazhar Ali Khan, 2014). The quality of agriculture land various depends on the physical, chemical and biological parameters of the soil (Appala Raju, 2015). The economic value of the productive lands associated with the variation of these parameters. However, due to the conversation of land and anthropogenic activities reduces the quality of these parameters influences the economic value of agriculture land (Gizachew Ayalew, 2015).

The investigation of the landuse and landchanges associated with agriculture land changes is momentarily increasing significantly, as human activities transform ecosystem in urban and urban near rural land (Jadab Chandra Halder, 2013). Besides, the greatest level of a population has been increasing in the developing countries (Jadab Chandra Halder, 2013). By 2030, world's population is expected to increase by 72%, though landuse of cities of 100,000 could upsurge by 175% (Appala Raju, 2015). The surpassing expansion of city causes urban sprawl that is an extension of settlement decreases the agriculture land, water bodies, and forestland. The study on agriculture land supports different fields of science such as agriculture planning, landscape architecture studies, urban planning, land-use planning, economics and ecosystem services (Jadab Chandra Halder, 2013).

The developing country like India, the people from every part of the villages move towards the cities for better social life, education and income. The increasing population of cities directly consequences of land-cover and land-changes (Jadab Chandra Halder, 2013). High growth of population causes land transformation, land scarcity and deforestation (Jadab Chandra Halder, 2013). The development of city consequences the movement of urban and rural poor onto bordering lands of cities (Appala Raju, 2015). The great movement of urban poor and extension of cities and sudden development of industries and IT sectors cuts of the bordering productive agriculture land, encroachment on water bodies and transformation of wild lands (Jadab Chandra Halder, 2013). There is an essential of greater attention on the urban growth of emerging cities in India (Gizachew Ayalew, 2015). India faces major problems of urbanization and population growth are declining agriculture land, urban sprawl, air pollution, housing, overcrowding, encroachment, slums, disposal of waste, increasing settlements, water scarcity, water pollution and sewage problems (Jadab Chandra Halder, 2013). The urbanization also leads to various environmental impacts, such as higher energy utilization, disturbance of diversity of species, flood risk and ecosystem fragmentation (Gizachew Ayalew, 2015). The predictable growth of urban sprawl, agriculture land suitability and ecosystem services aid to provide better urban planning and eco-friendly cities without major consequence (Gizachew Ayalew, 2015). Meanwhile, the greater dimension of measurement for accessing and monitoring urban sprawl and ecosystem services associated with agriculture land is always needed. The availability of remotely sensed data always gives greater extent to improve the agriculture land, urban modeling, urban landscape pattern analysis (Gizachew Ayalew, 2015), urban growth (Jadab Chandra Halder, 2013) and urban sprawl studies (Jadab Chandra Halder, 2013).

The spatial and physical characteristic of urban and agriculture land features patterns and its form are quantified using spatial metrics. Additional modeling based on the spatial metrics would help in evaluating future variations in urban and agriculture land. These indices measurable can be obtained by computing directly from thematic maps. Recent studies landscape urban model and analysis have employed from spatial metrics and this term called as landscape metrics, which is derived from landscape ecology. These improved studies on landscape feature can facilitate to integrate the physical structure of a landscape, urban and agriculture land situation, and development. However, the precision and validation of these landscape metrics in the urban model can be achieved from spatiotemporal pattern examination and land suitability prediction.

Globally, different studies on urban growth pattern analysis associated with agriculture land suitability and model were achieved but the developing country like India has a limited examination on rapid urbanization. India is one of the fast growing urban in last three decades has resulted in declining

agriculture land. Thus, the urban planners need to understand the spatiotemporal changes with addressing these environmental problems and ensure to provide the basic infrastructure and facilities without a disturbing ecosystem.

The present study focused on suitability analysis of economic and parameter based agriculture land for future land-use allocation. Land evaluation can be predominantly based on soil resources inventories commonly called soil survey (Palaniswami, Gopaldasundaram and Bhaskaran, 2011). For the purpose of maintaining and developing agricultural land use at a delta region on spatially (Mohammad Shah Nawaz Khan and Mohd. Mazhar Ali Khan, 2014), it is avital to identify the levels and geographic patterns of biophysical constraints for the purpose of land suitability (Appala Raju, 2015). Land suitability analysis is a prerequisite for sustainable agricultural practices (Gizachew Ayalew, 2015). It can be evaluated based on the parameters of physical and chemical characteristic (Appala Raju, 2015). Land suitability is a function of crop requirements and soil/land characteristics (Jadab Chandra Halder, 2013). Thus, the physical and chemical parameters can be measured and tested in the laboratory (Joseph Kihoro, Njoroge J. Bosco and HunjaMurage, 2013). By matching the land characteristics with the crop, requirements that can be analyzed suitability of land (Joshua Jonah Kunda, Anyanwu Nneoma C. and Ahmed Abubakar Jajere, 2013). The main objective of this paper is to create the physiographic map, which is used to identify the soil physical and chemical characteristics to classify the suitable land for different crop agriculture.

2. Study Area

The study area is Thanjavur district, which has a seven taluks such as Kumbakonam, Thiruviyaru, Papanasam, Thiruvidadimaruthur, Orathanadu, Pattukkottai and Peravurani (Figure 1). It is bounded by North latitude $10^{\circ}08'$ to $11^{\circ}12'$ and West longitude $78^{\circ}48'$ to $79^{\circ}38'$ on the northeast by Nagapattinam district, on the east by Thiruvarur district, on the south by Bay of Bengal on the west by Pudukkottai district and the north by river Kollidam (Khwanruthai Bunruamkaew and Yuji Murayama, 2012). The district lies at the Cauvery delta region, the most fertile region in the state. The Cauvery River and its tributaries irrigate the district (Lefteri DUSHAJ et al., 2009). The climate condition is tropical with average annual rainfall of 938 mm and temperature usually ranges $25-35^{\circ}\text{C}$. Thanjavur district had a population of 2,405,890 (Malay Kumar Pramanik, 2016).

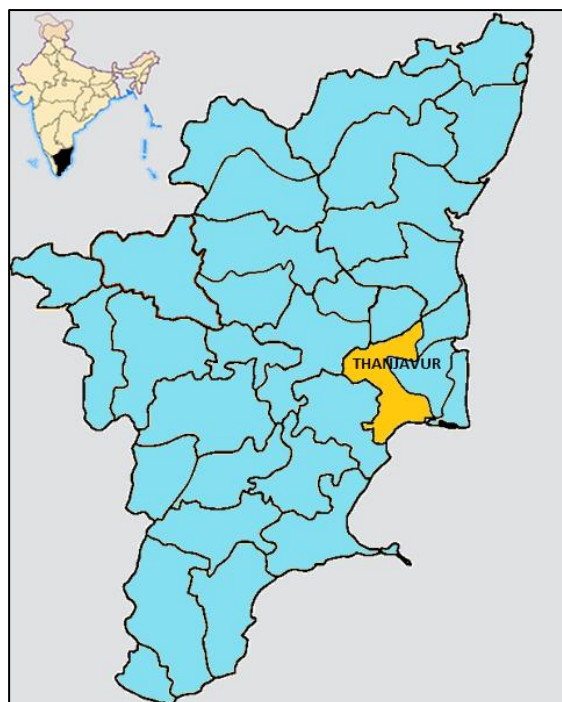


Figure 1: Map shows the study area, Thanjavur district

3. Methodology

The Figure 2 depicts the flowchart, which has the methods to generate the socio-economic land suitability for agriculture. There are 20 samples collected from the study area. The soil samples are collected using the GPS instrument.

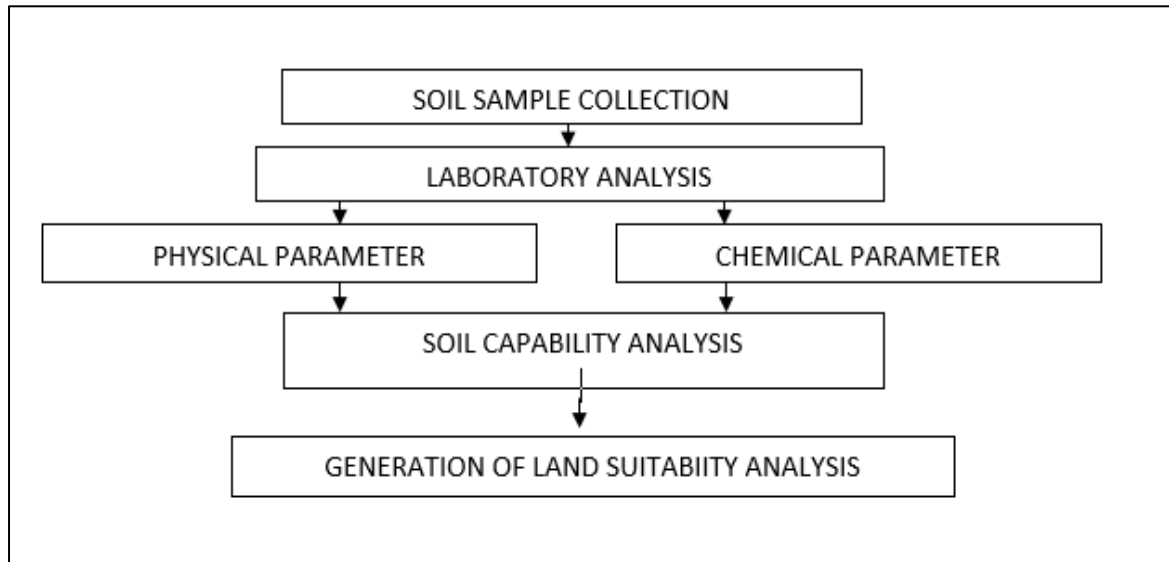


Figure 2: Flow chart of Land suitability

3.1. Laboratory Analysis

The collected samples from the specific area are analyzed in the laboratory, which provided the numerical data from the soil parameters as shown in the Table 1. The physical land properties of the study area are evaluated, including the soil texture and water holding capacity. The chemical properties of soil like pH, EC, Potassium, Phosphorus, Organic Carbon and Nitrogen are also taken for soil site suitability analysis.

Table 1: Numerical data from the Laboratory Analysis

NAME	TEXTURE	pH	WATER HOLDING CAPACITY	EC	OC	N	P	K
Vallam	SL	7.2	27.396	0.7	0.91	127.4	9	265
Nanjikottai	SL	7.9	53.078	0.74	0.96	144.2	4.51	245
Punnainallur	SL	7.2	56.675	0.66	0.88	130.2	3.85	245
Soorakkottai	L	7.7	43.671	0.88	0.97	134.2	8.5	270
Ullur	L	7.8	18.05	0.7	0.85	128.8	5.75	310
Darasuram	SCL	7.5	23.407	0.72	0.88	130.2	3.85	295
Sathyamangalam	SL	8.1	31.309	0.89	0.97	112	4.5	270
Poondi	SL	6.9	24.201	0.19	0.58	110	5.5	300
Thirupuvanam	SL	6.1	22.51	0.38	0.55	125.2	6.7	288
Madukkur	L	7	25.357	0.25	0.78	140.8	8.55	278
Alathur	L	7	24.01	0.35	0.72	123.5	4.8	340
Pattukkottai	L	7.5	61.851	0.3	0.95	128.5	7.5	325

Peravurani	L	7.4	50.321	0.3	0.85	138.7	9.1	312
Ambalapattu	L	7.3	22.3	0.63	1.27	203	5.25	295
Kanjanur	SCL	8.2	32.654	1.1	0.87	130.2	5.35	265
Ullikadai	SCL	7.5	31.885	0.19	0.85	140.3	5.83	320
Narasingampettai	SCL	8.2	31.885	0.79	0.82	124.6	6	255
Nallavanniyankudikadu	SL	7.1	15.545	0.8	0.95	126	8.5	315
Sendakadu	L	7.8	26.341	0.3	0.85	135.2	7.5	325
Kurungulam	L	6.7	41.11	0.6	0.8	138.7	9.1	312

3.2. Land Suitability Analysis

Land suitability analysis has been performed by the assessment method to assess land suitability for an existing and potential uses. The soil suitability can be mainly analyzed based on the physical and chemical characters of soil (Martine Nyeko, 2012). By using overlay analysis function, the suitability index can be formed for crop requirement (Mohammad Reza Yousefi and Ayat Mohammad Razdari, 2015). Then land characteristics can be evaluated for grouping of specific areas of land in terms of their suitability for agricultural usage as shown in the Table 2. Regarding land suitability, other factors can also be considered in the account such as economics, requirements, farmer access, water and energy access, conflicting and complementary land uses.

Table 2: Agriculture Land Suitability Criteria

MAP LAYER	AGRICULTURE LAND SUITABILITY CRITERIA
Soil	Clayey soil Loamy Soil
pH	6.9 to 7.2 - Highly suitable 7.2 to 7.5 - Moderately suitable 7.5 to 8.1 – Low suitable
Electrical conductivity	0.19 to 0.48 – Highly suitable 0.48 to 0.78 – Moderately suitable 0.78 to 1.0 - Low suitable
Organic Carbon	0.55 to 0.75 – Highly suitable 0.75 to 0.85 – Moderately suitable 0.85 to 1.26 – Low suitable
Nitrogen	140 to 171– Highly suitable 110 to 140 – Moderately suitable 171 to 200 – Low suitable
Phosphorus	3.85 to 5.95 – Highly suitable 5.95 to 6.9 – Moderately suitable 6.9 to 9 –Low suitable
Potassium	245 to 271 – Highly suitable 271 to 308 – Moderately suitable 308 to 340 Low suitable
Water Holding Capacity	33 to 48 – Highly suitable 15 to 33 – Moderately suitable 40 to 60 – Low suitable
Texture	Sandy Clay Loamy – Highly suitable Sandy Clay – Moderately suitable Loamy – Low suitable

4. Results and Discussions

The physical and chemical properties of the land are major determinants for crop suitability of agriculture land. The physical land properties of the study area are evaluated, including the soil texture and water holding capacity. The chemical properties of soil are also evaluated such as pH, EC, Potassium (K), Phosphorus (P), Organic Carbon (OC) and Nitrogen (N) that are also taken for soil site suitability analysis. Land suitability index has been calculated by applying the overlay analysis function with crop requirement and land characteristics involving the evaluation. Then the grouping of specific areas of land in terms of their suitability for defined agricultural use. The suitability land categorized into highly suitable, moderately suitable and low suitable.

4.1. Sample Collection

The soil sample collection is the most important step in any nutrient/soil amendment management program. Soil sampling should reflect tillage, past soil alteration placement, cropping pattern, soil type, old field boundaries.

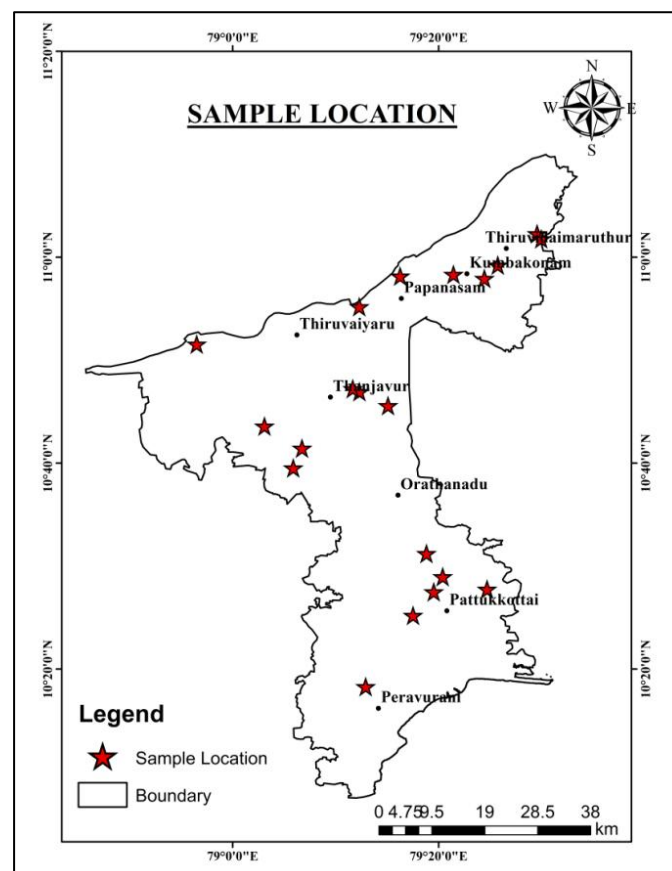


Figure 3: Sample Location Map

The soil samples are collected from the various area based on the soil type. The position of sample location is determined using GPS as shown in Figure 3. As of total 20 samples are collected from the study area.

4.2. Generation of Thematic Maps of Soil Parameters

Thematic maps were generated for each of the soil physical and chemical parameter using IDW interpolation provided in Arc GIS 10.2 software. Inverse Distance Weighted (IDW) interpolation determines cell values using a linearly weighted combination of a set of sample points. The weight is a function of inverse distance. IDW lets the user control the significance of known points on the interpolated values, based on their distance from the output point.

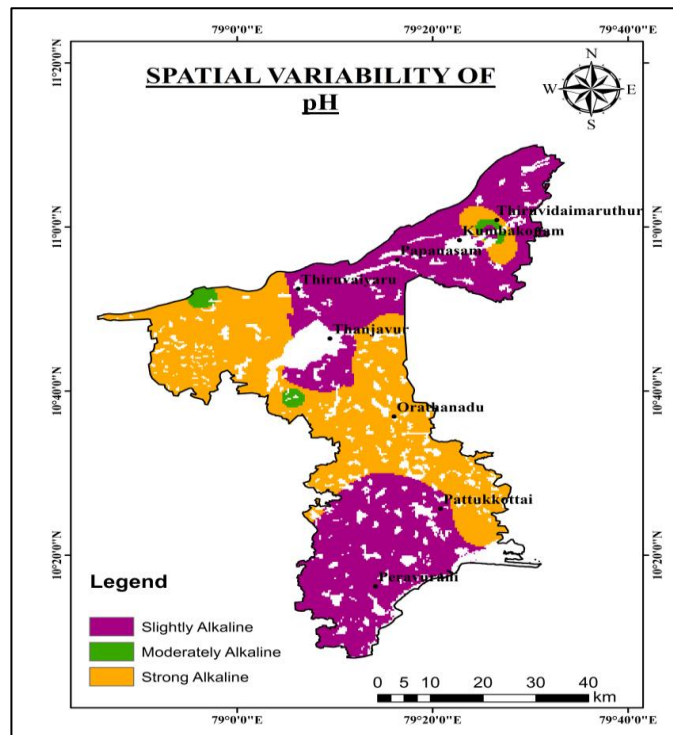


Figure 4: Spatial variability of pH Map

The purple color shows the slightly alkaline it is mainly suitable for the agricultural land and its covered area from 1477.7 sq.km as shown in Figure 4.

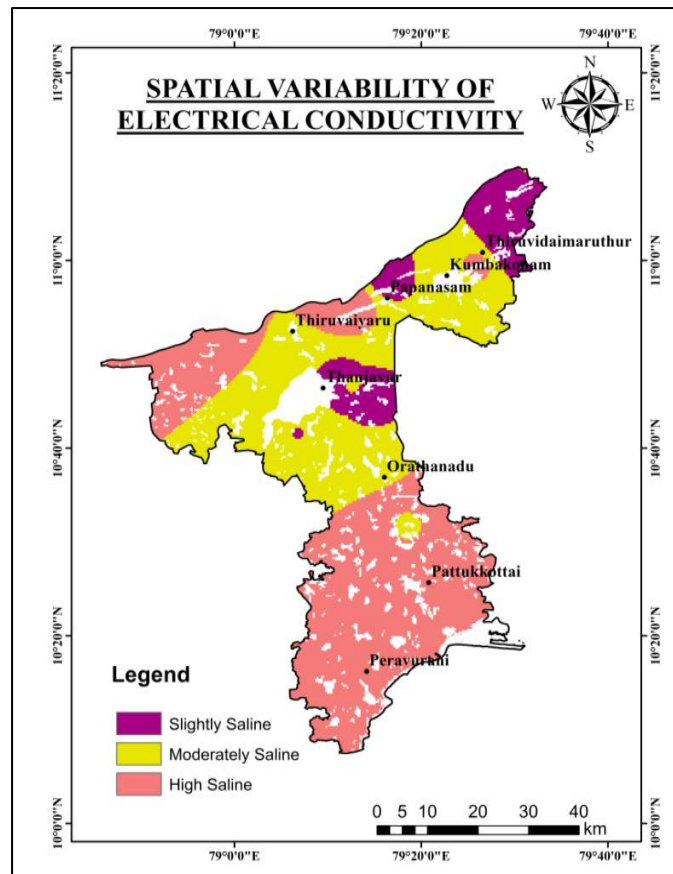


Figure 5: Spatial variability of Electrical Conductivity Map

The ranges slightly saline consider from the agricultural land. The slightly saline areas present in the purple color from the map its covered area from 401.18 sq.km as shown in Figure 5. The range of EC is .48 to .78 highly saline and .19 to .48 is slightly saline and .78 to 1.08 is moderately saline.

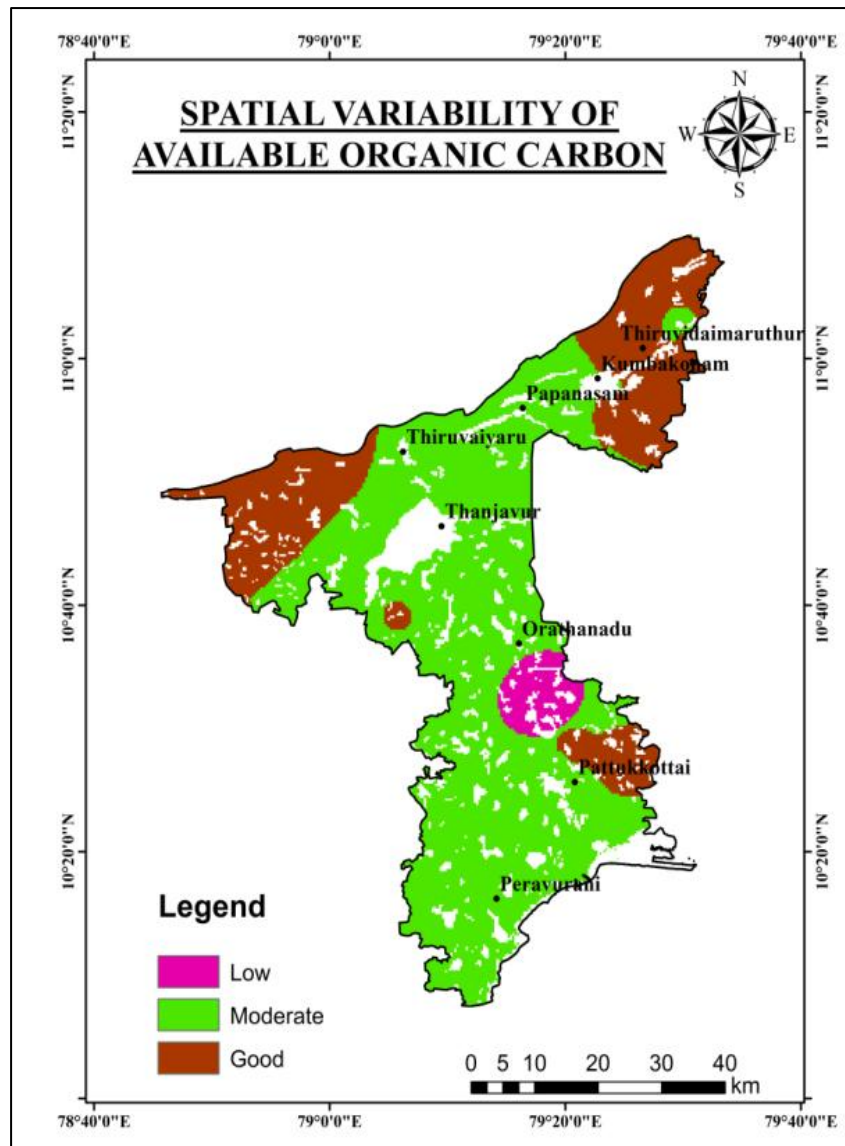


Figure 6: Spatial variability of Available Organic Carbon map

The normally the agriculture land ranges from 0.5-0.75 covered area from 825.23 sq.km as shown in Figure 6.

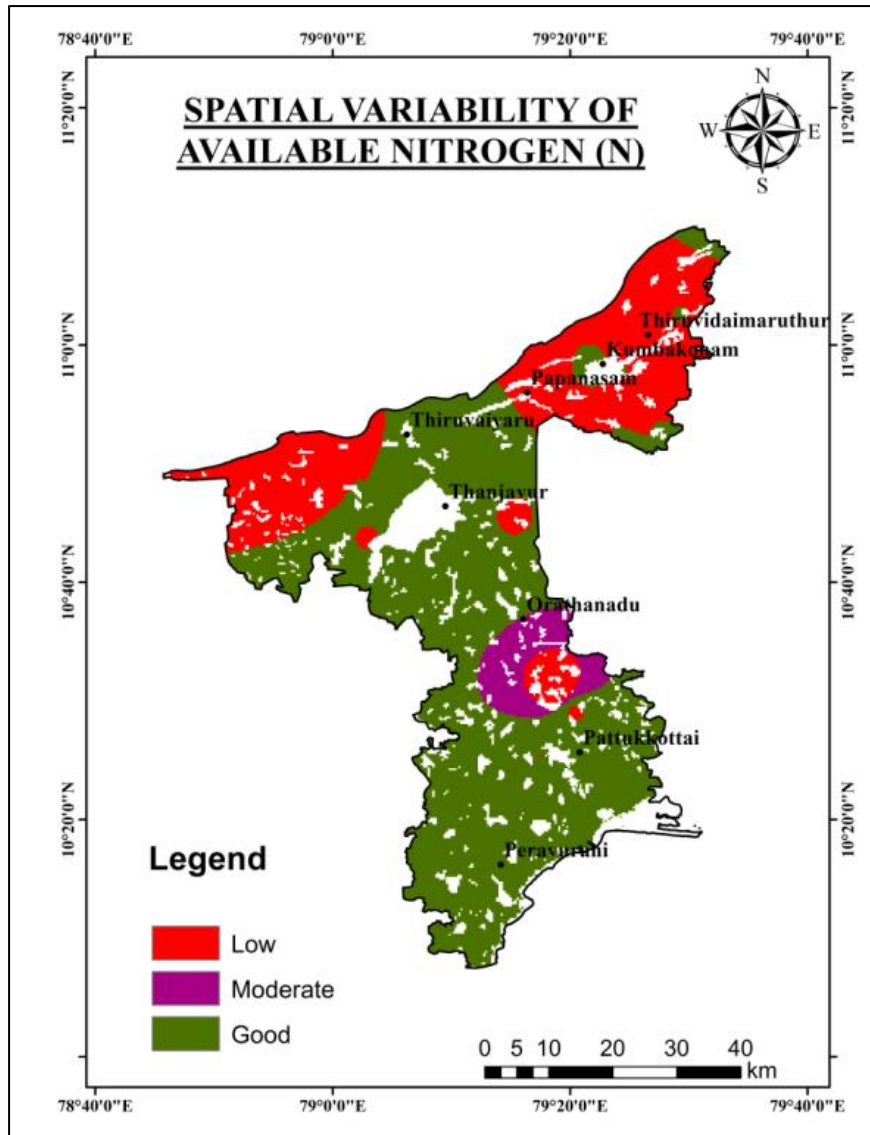


Figure 7: Spatial variability of Nitrogen Map

The range of the nutrients limitation for the agriculture land is 140-171 considered as Good and its covered area about 2256.38 sq.km as shown in Figure 7.

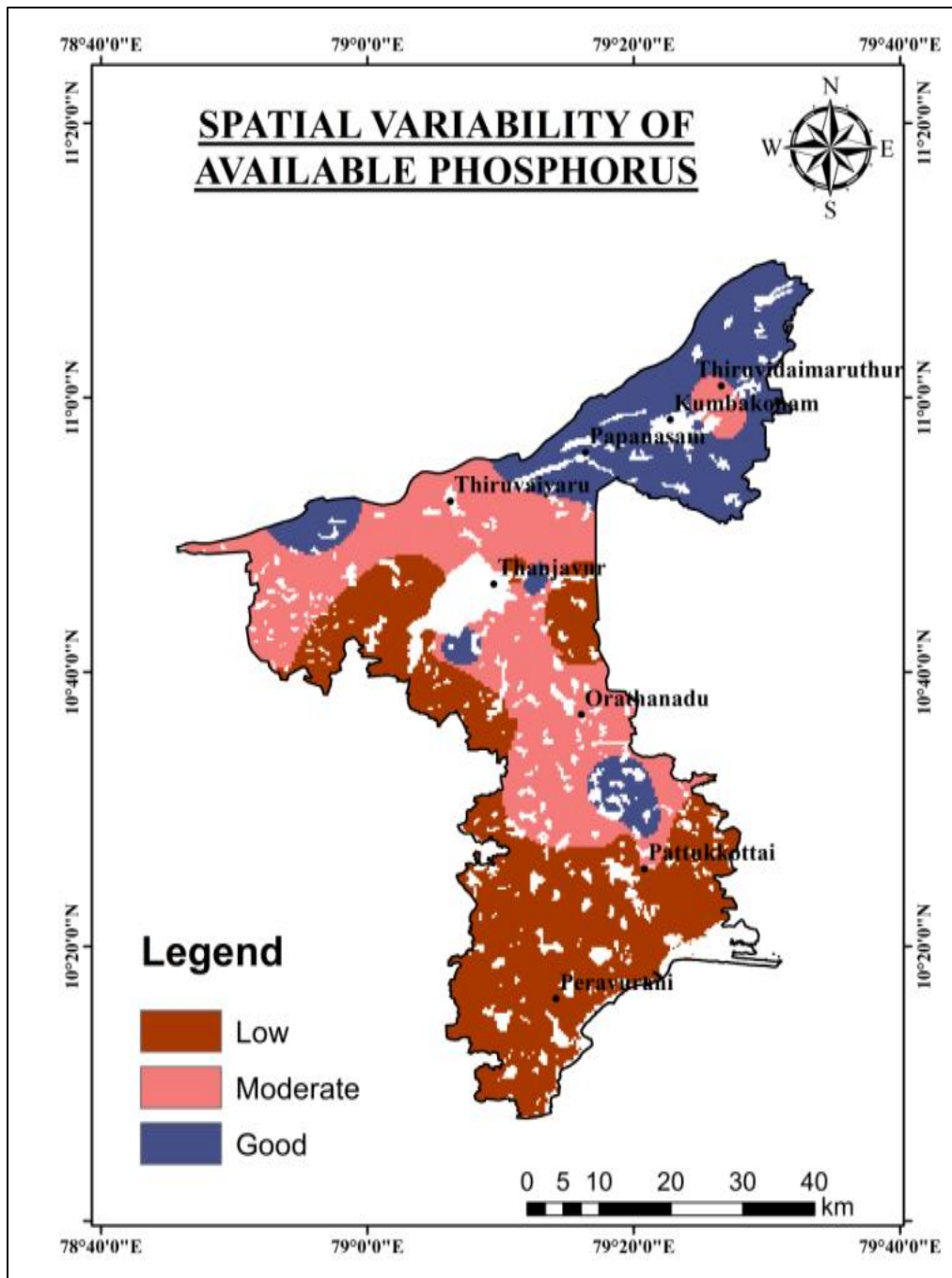


Figure 8: Spatial variability of phosphorus Map

The high available P content might possibly be due to the confinement of crop cultivation. The good condition of agricultural land ranges from 3.85-5.95 and its covered area about 787.99 sq.km as shown in Figure 8.

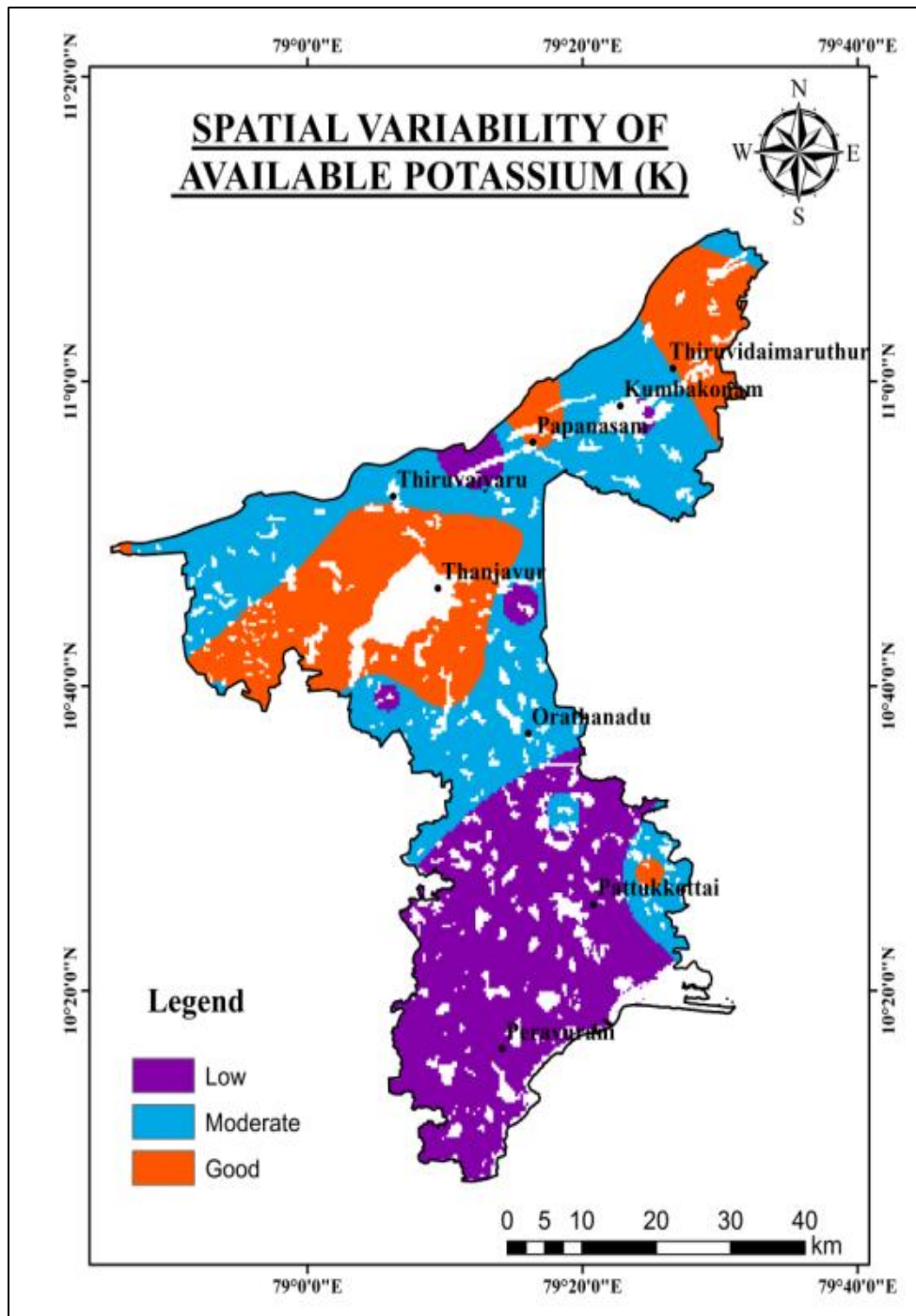


Figure 9: Spatial variability Potassium Map

The ranges of K from 245 to 276 which is suitable for agricultural land and its covered area from 1219.82 sq.km as shown in Figure 9.

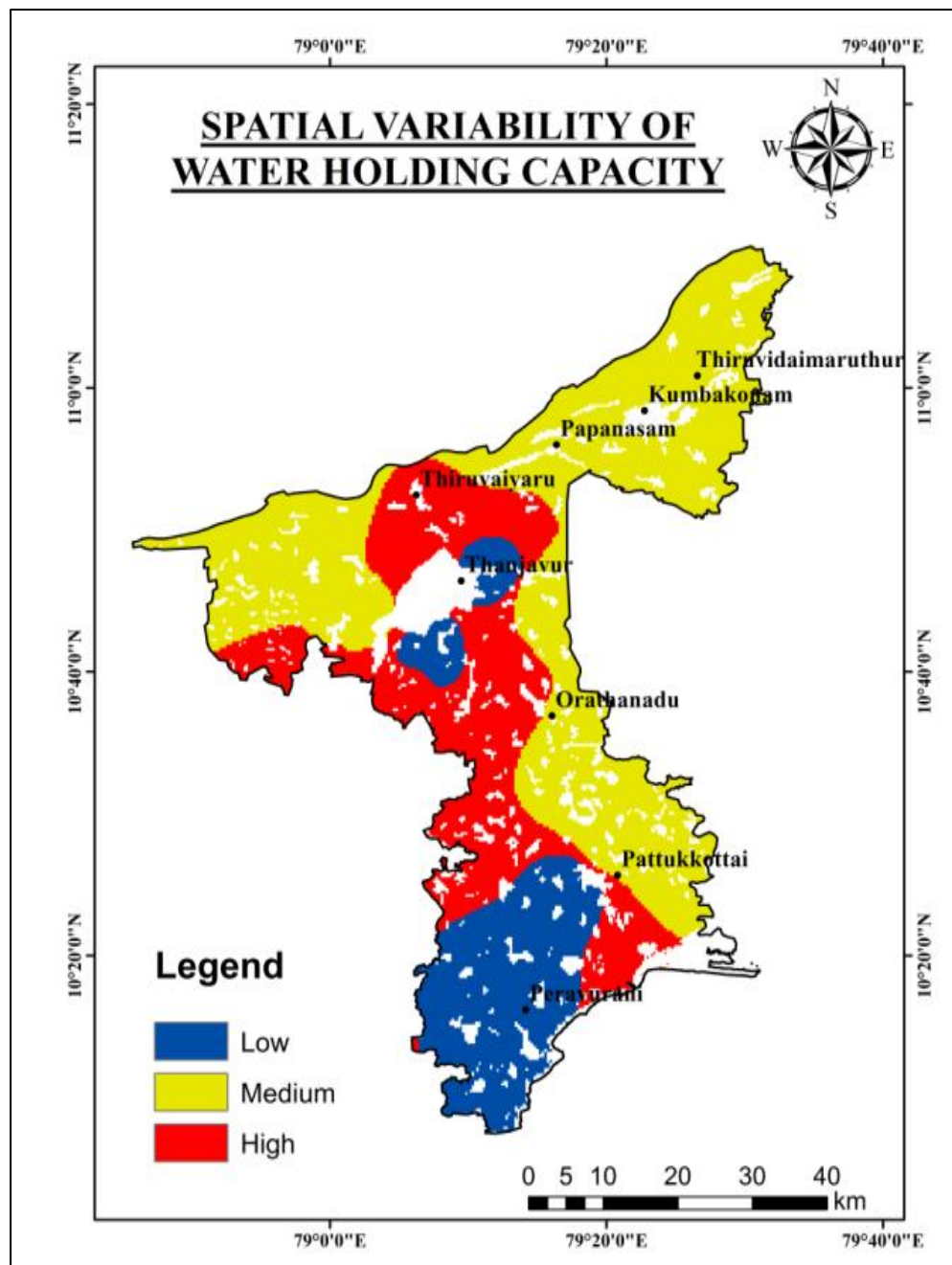


Figure 10: Spatial variability Water Holding Capacity map

Soils that hold generous amounts of water are less subject to leaching losses of nutrients or soil. The agriculture land water holding capacity generally ranges from is 33.18-40.2 covered area from 1459.3 sq.km as shown in Figure 10.

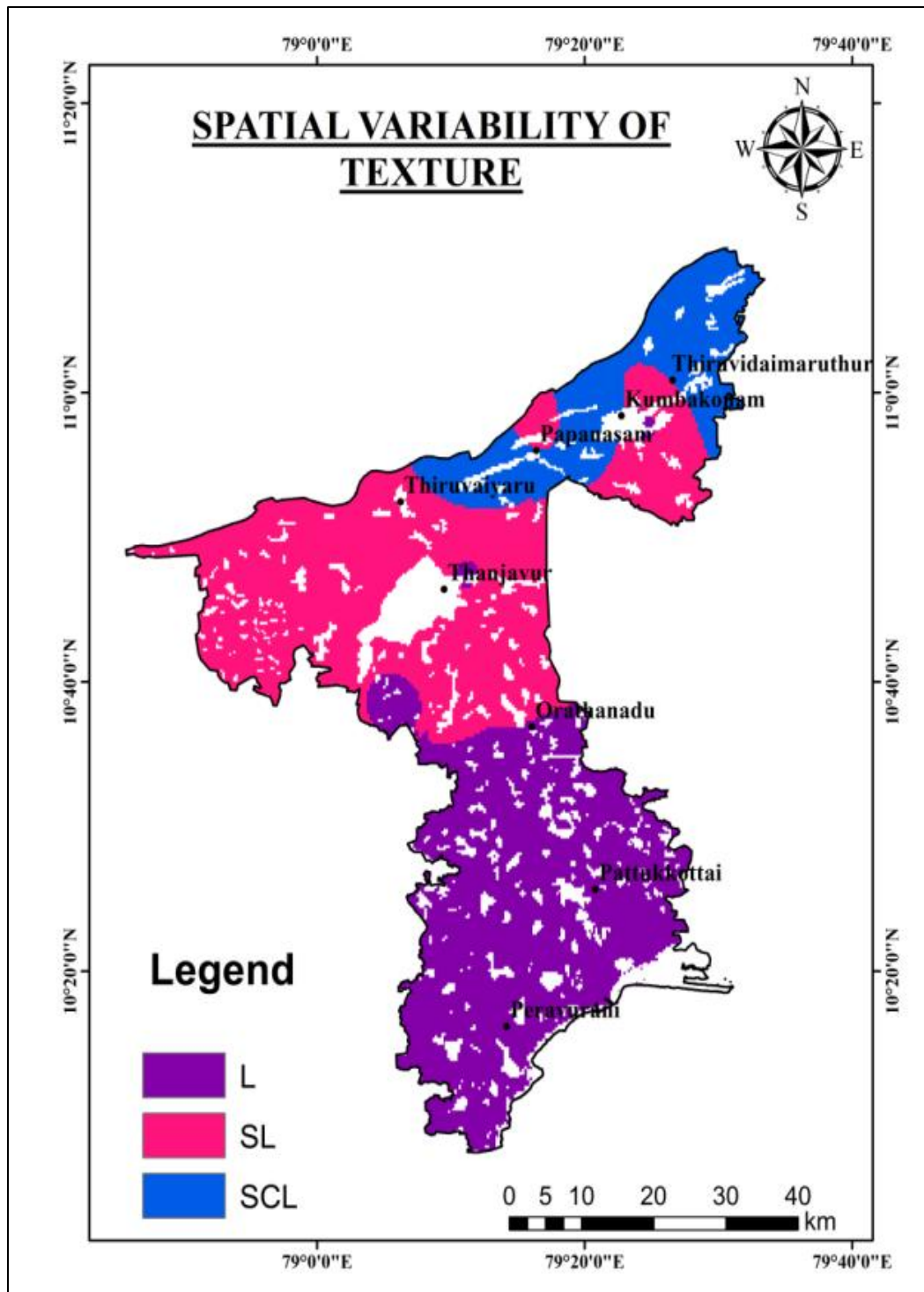


Figure 11: Spatial variability of Texture Map

The SCL texture type mainly suitable for agricultural land and its covered area about 481.92 sq.km as shown in Figure 11.

4.3. Overlay Analysis

Land suitability evaluation, on basis of soil conditions requires criterion mostly from the soil attributes. It represents the main soil parameters used for generation of the thematic map layers which used in weighted overlay process for generating the final suitability map for each crop. Once the standardized

thematic layers and their weights were assigned for each crop and soil parameter, the weighted sum overlay within Arc GIS was applied to produce the crop suitability map.

4.4. Land Suitability for different crops

A total of 7 crops were evaluated from the for growing in the study area such as pearl millet, maize, cotton, rice and sorghum. With the suitable parameters the *kharif* crops can be identified as shown in Table 3. The quality of each land category was assessed by the ratings highly suitable, moderately suitable and Low suitable that refer to the effects of the individual land qualities on production of the crop. The crop land-use requirements and land qualities were matched for each of the soil series and the final land-suitability maps for each selected crop were made.

Table 3: Suitable Land Parameter for Each Crops

CROP	SUITABLE LAND PARAMETER
PEARL MILLET	High pH Electrical Conductivity
MAIZE	Low Organic Carbon Nitrogen Potassium High pH
SORGHUM	Low Potassium Low Organic Carbon Nitrogen High pH
RICE	Organic Carbon Nitrogen Potassium
COTTON	Low Organic Carbon Low Available Nitrogen Low Potassium
PULSES	Organic Carbon Nitrogen Potassium
SESAME	Low Water Holding Capacity Sandy Loamy Soil Texture

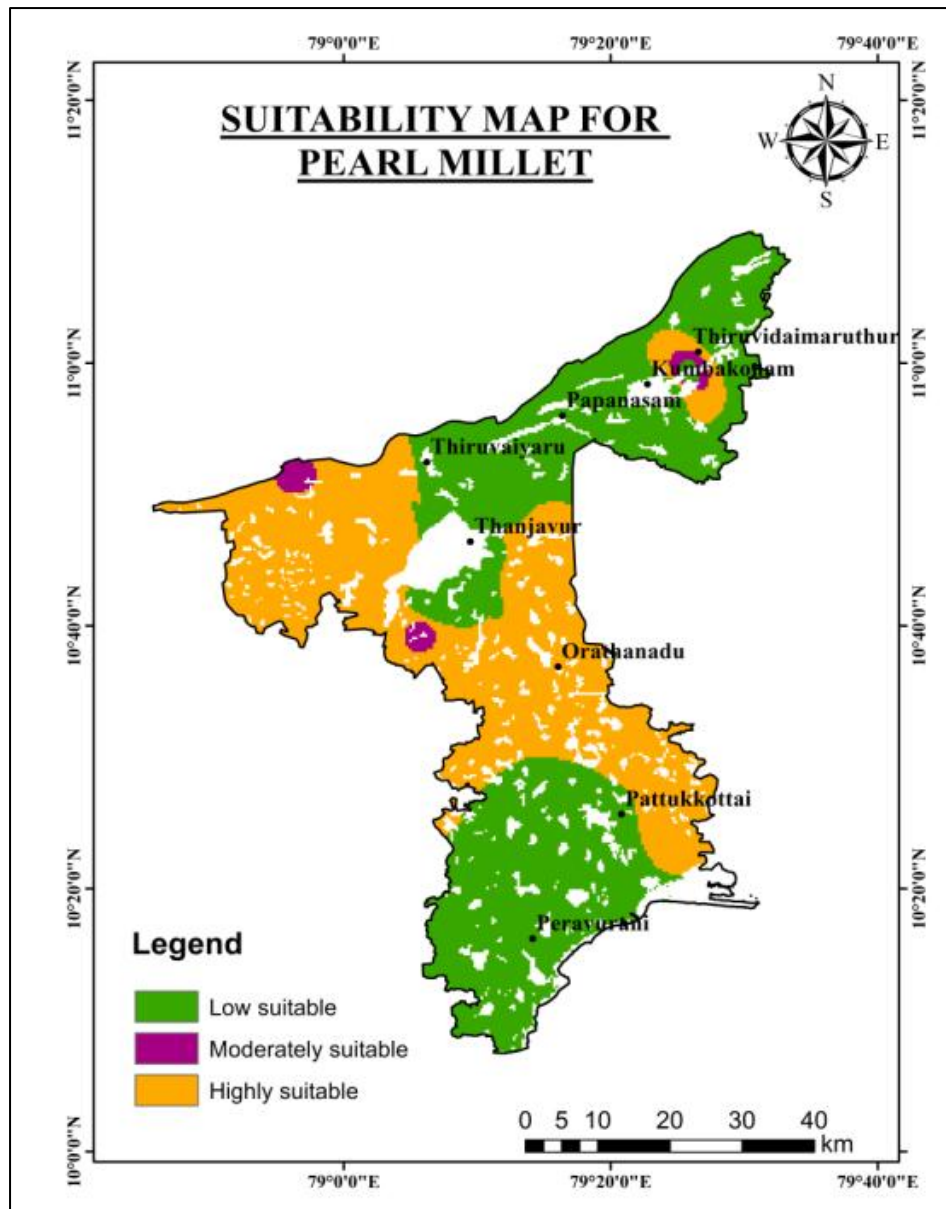


Figure 12: Suitability Map for Pearl Millet

Pearl millet is the most widely grown type of millet. High pH and EC are the major limitations. About 43.7 sq.km area of Poondi and near Kumbakonam is moderately suitable whereas 1027.2 sq.km and 1859 sq.km of area are highly suitable areas of Peravurani, Thanjavur, Thiruvaiyaru, Papanasam, Thiruvaidaimaruthur and nearly Kumbakonam. Marginally suitable areas of Orathanadu, Kumbakonam, Vallam and near Pattukkottai as shown in Figure 12.

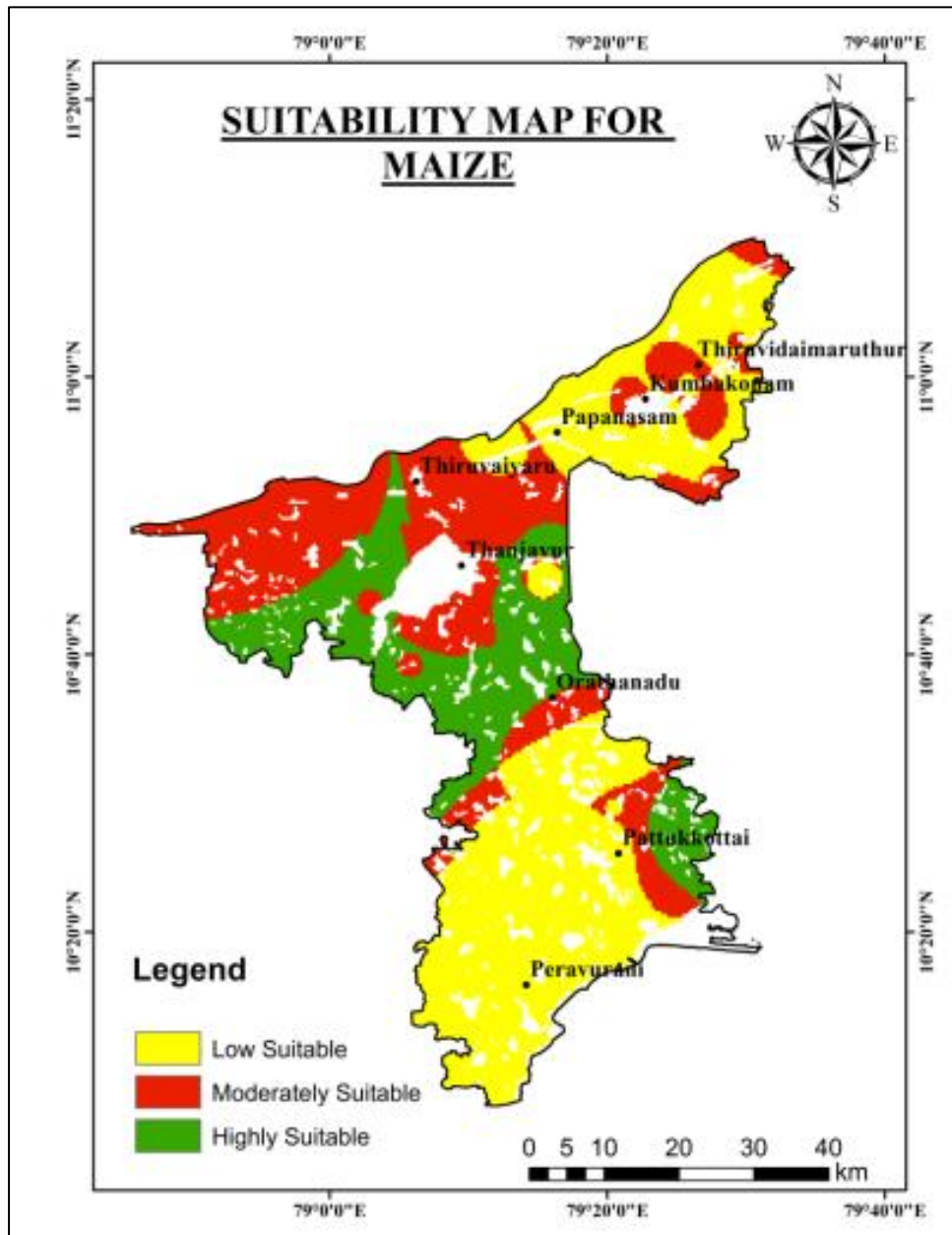


Figure 13: Suitability Map for Maize

The major limitations are low organic carbon, nitrogen, potassium and high pH. Around 754.12 sq.km areas of Peravurani, Papanasam and near Pattukkottai are marginally suitable for maize cropping while 652.32 sq.km areas of Orathanau, near Thanjavur and near Pattukkottai and 1000.53 sq.km areas of Thanjavur, near Tiruvaimaruthur, Papanasam, Kumbakonam are highly and moderately suitable area as shown in Figure 13.

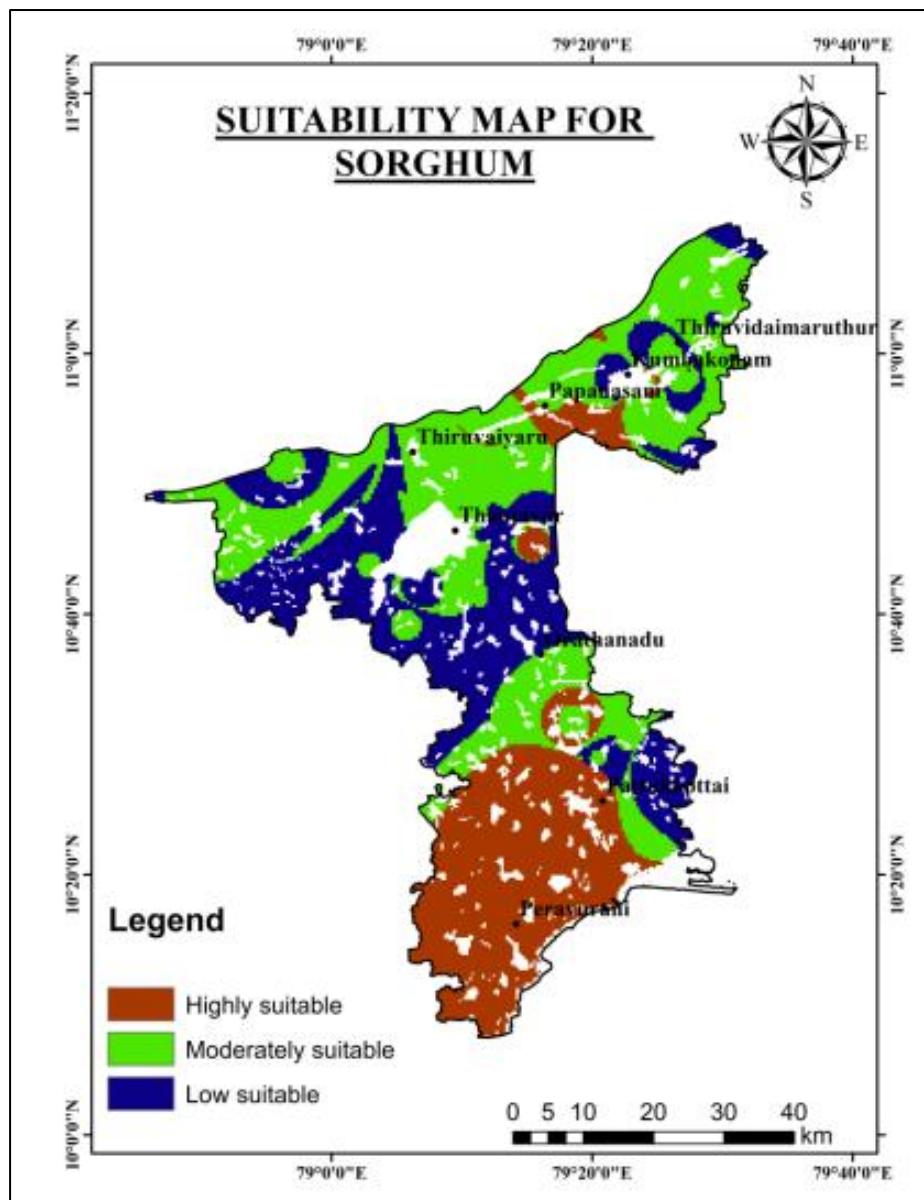


Figure 14: Suitability Map for Sorghum

The 1896.28 sq.km areas of Pattukkottai, Peravurani and the small portion of Thanjavur and Papanasam are suitable for sorghum cultivation. The low suitable area of 709 sq.km are present in the Pooni, Thanjavur, Orathanadu and near Pattukkottai as shown in Figure 14.

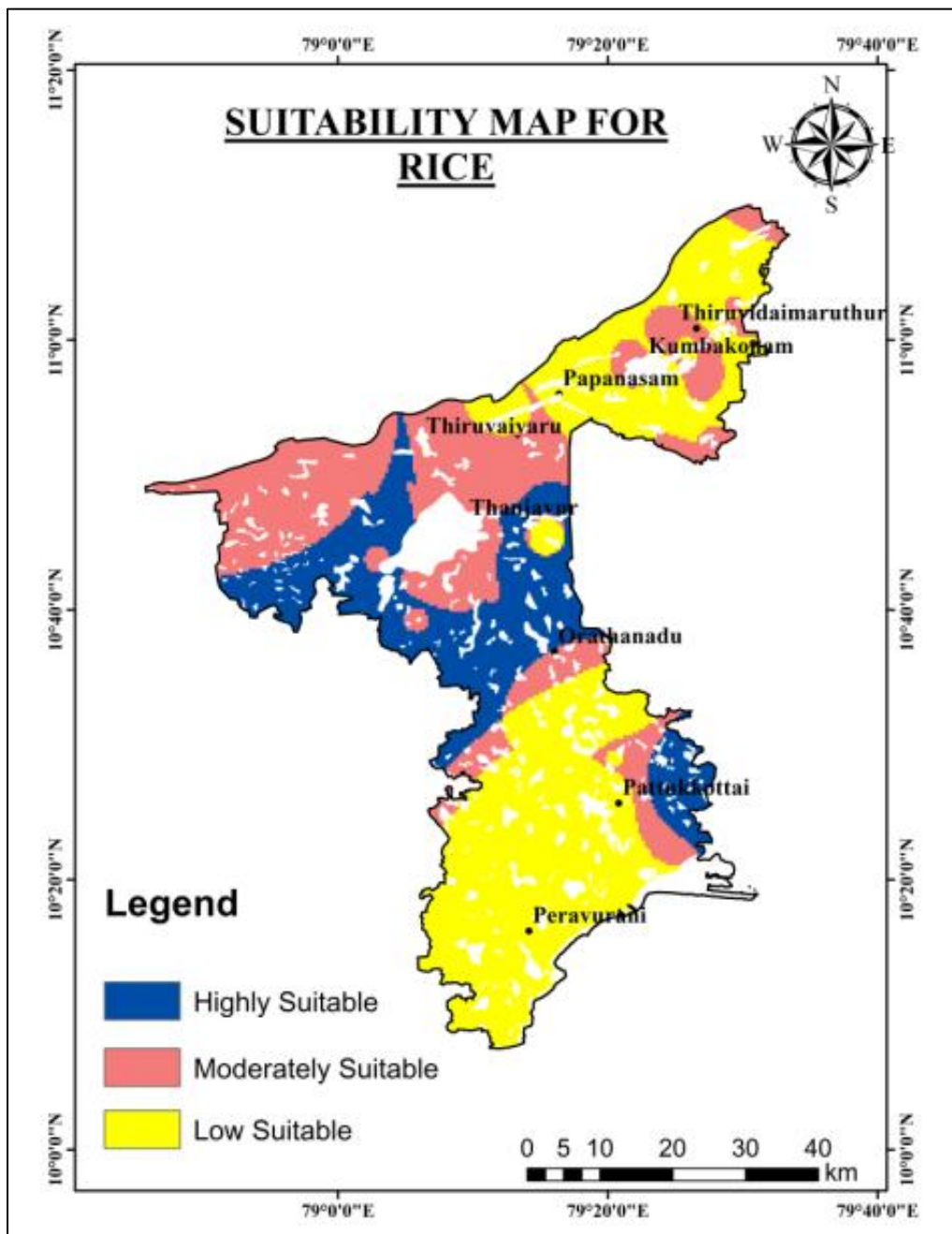


Figure 15: Suitability Map for Rice

The area from 754.12 sq.km highly suitable areas of Thanjavur and near Orathanadu and 1000.53 sq.km moderately suitable areas of Thiruvaiyaru, Kumbakonam and Nearorathanadu as shown in Figure 15.

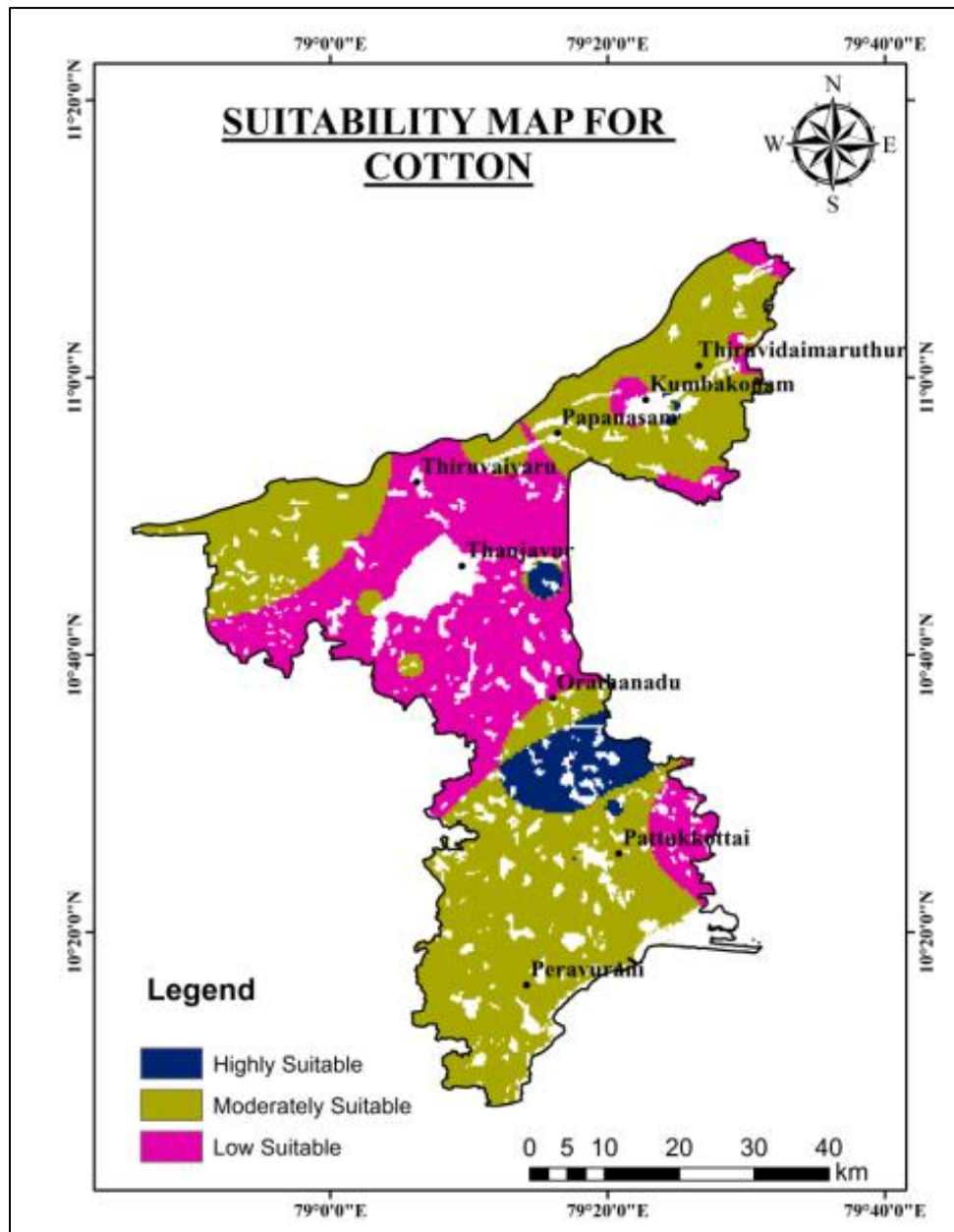


Figure 16: Suitability Map for Cotton

The 178.42 sq.km areas of Orathanadu are mainly high suitable, 1804.51 sq.km moderately suitable area from Peravurani, Pattukkottai, Poondi, Papanasam, Kumbakonam and Thiruvaidaimaruthur as shown in Figure 16.

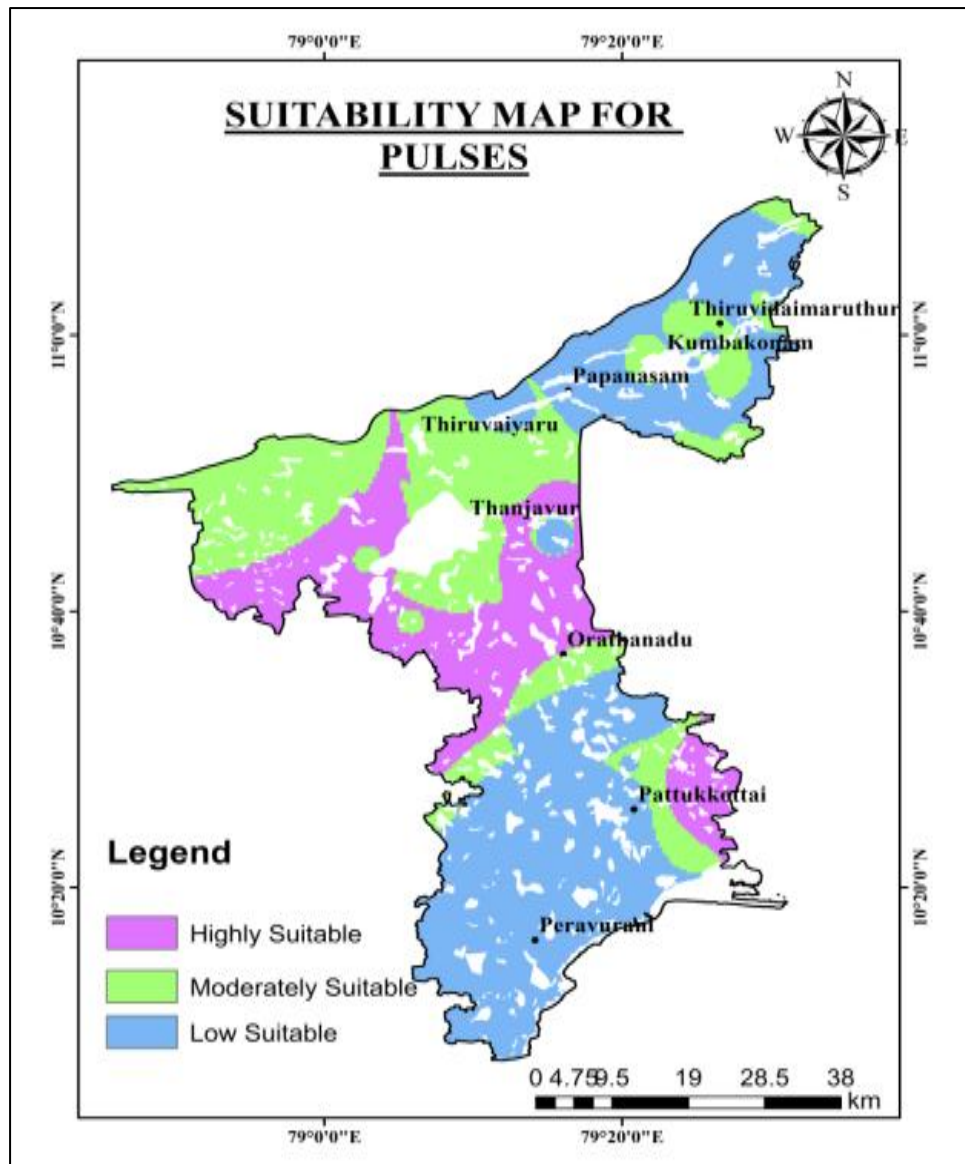


Figure 17: Suitability Map for Pulses

The 745.12 sq.km areas of Thanjavur and near Orathanadu are highly suitable and 1000.52 sq.km moderately suitable areas of Thiruvaiyaru, Kumbakonam and near Orathanadu as shown in Figure 17.

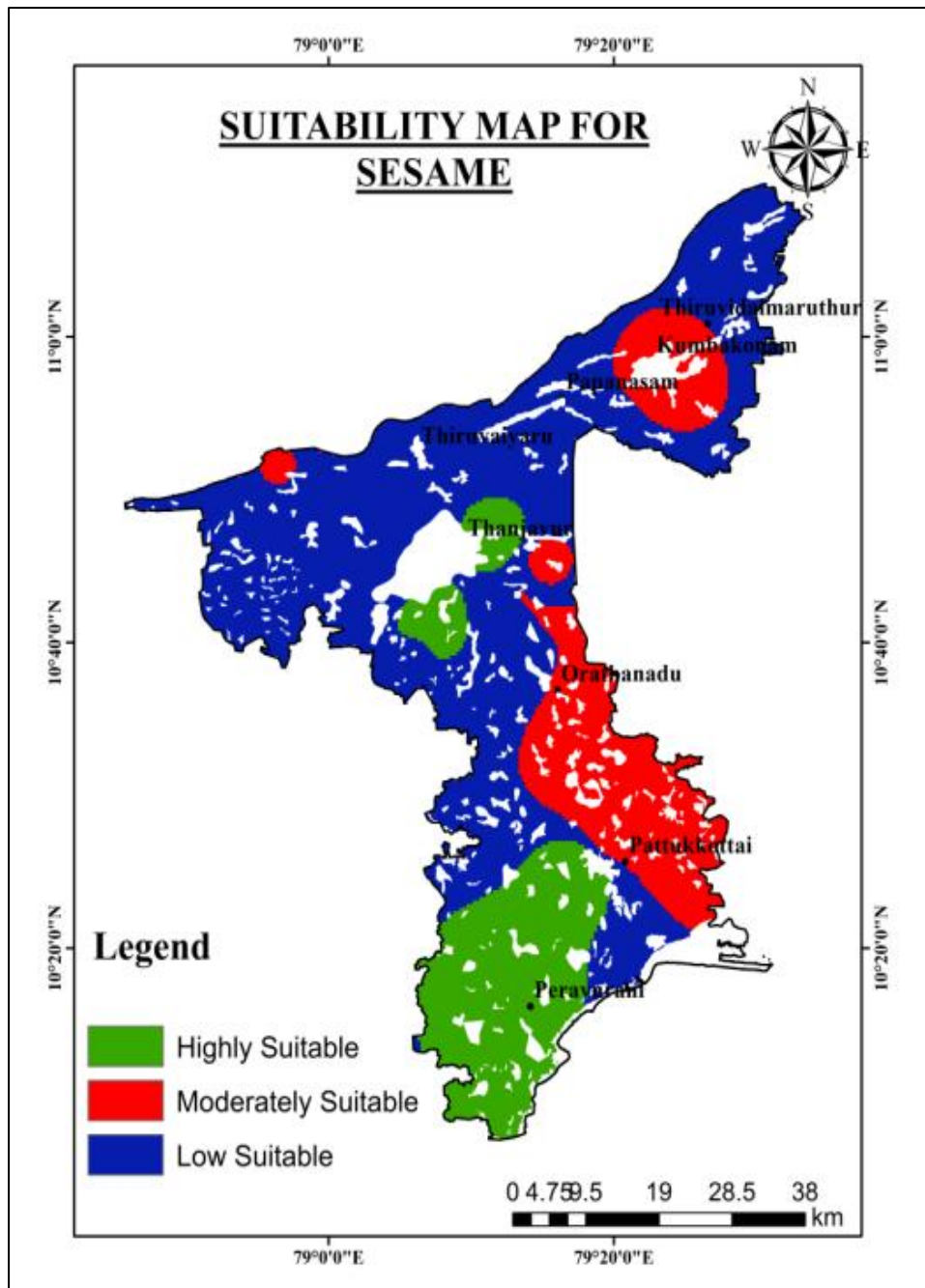


Figure 18: Suitability Map for Sesame

The 712.19.37 sq.km areas of Peravurani and Thanjavur are more suitable, 658.76 sq.km areas of Orathanadu, Pattukkottai and Kumbakonam moderately suitable for sesame cultivation as shown in Figure 18.

5. Conclusion

The study indicates the highly suitable economical areas for agriculture production. The moderately and low suitable areas required little investment in fertilizer and agrochemicals for a meaningful production and maintain the economic value. The overlay analysis method commonly used in multi-criteria decision-making exercises was found to be a useful method to determine the weights, in terms of parameters and economic concern. The GIS is found to be a technique that provides greater flexibility and accuracy for handling digital spatial data. The GIS in our experiment proves it is a powerful combination to apply for land-use suitability analysis. The land suitability classes are divided

into three categories as highly suitable, moderately suitable and low suitable. The soil-site suitability for kharif crops in Thanjavur district represents that soil suitability class area for pearl millet, maize, sorghum, rice, cotton, pulses and sesame. The 1027.2 sq.km areas of Peravurani, Thanjavur, Thiruvaiyaru, Papanasam, Thiruvaidaimaruthur are highly suitable for pearl millet cultivation. The 754.12 sq.km areas of Orathanadu, near Thanjavur and near Pattukkottai are suitable for maize. The 1896.28 sq.km areas of Pattukkottai, Peravurani and the small portion of Thanjavur and Papanasam are suitable for sorghum cultivation. The 754.12 sq.km highly suitable areas of Thanjavur and near Orathanadu are suitable for rice cultivation. The 178.42 sq.km areas of Orathanadu are mainly high suitable for cotton. The 745.12 sq.km areas of Thanjavur and near Orathanadu are highly suitable for pulses. The 712.19 sq.km areas of Peravurani and Thanjavur are more suitable for sesame cultivation. The selected areas are more suitable to left the economic value of the region and maintain the ecosystem services.

References

- Appala Raju, N. 2015. Land Capability and Suitability in Vizianagaram district of Andhra Pradesh using Remote sensing and GIS Techniques. *IOSR Journal of Humanities and Social Science*, 20, pp.56-64.
- Avvannavar, S.M. and Shrihari, S. 2008. Evaluation of water quality index for drinking purposes for river Netravathi, Mangalore, South India. *Environmental Monitoring and Assessment*, 143(1-3), pp.279-290.
- Azeez, P.A., Nadarajan, N.R. and Mittel, D.D. 2000. The impact of monsoonal wetland on groundwater chemistry. *Pollut Res.*, 19(2), pp.249-255.
- Bhargava, D.S. 1983b. Most rapid BOD assimilation in Ganga and Yamuna Rivers. *J. Environ. Eng. Am. Soc. Civ. Eng.*, 109(1), pp.174-188.
- Bhargava, D.S. 1983c. Use of water quality index for river classification and zoning of Ganga River. *Environ. Pollut. Ser. B (England)*, 6(1), pp.51-67.
- BIS. 2012. *Indian Standards Specification for Drinking Water, B.S. 10500*. Government of India, New Delhi.
- Chandra, D.S. and Asadi, S. 2017. Estimation of water quality index by weighted arithmetic water quality index method: a model study. *International Journal of Civil Engineering and Technology*, 8(4), pp.1215-1222.
- CPCB. 2008. Guideline for water quality management. Central Pollution Control Board, Parivesh Bhawan.
- Cude, C.G. 2001. Oregon water quality index: A tool for evaluating water quality management effectiveness. *Journal of the American Water Resources Association*, 37(1), pp.125-137.
- Gizachew Ayalew. 2015. Land Capability Classification using Geographical Information System in Guang Watershed, Highlands of Ethiopia. *International Journal of Research Studies in Agricultural Sciences*, 1, pp.17-20.
- Jadab Chandra Halder. 2013. Land Suitability Assessment for Crop Cultivation by Using Remote Sensing and GIS. *Journal of Geography and Geology*, 5, pp 64-74.
- Joseph Kihoro, Njoroge, J. Bosco and HunjaMurage. 2013. Suitability analysis for rice growing sites using a multicriteria evaluation and GIS approach in great Mwea region, Kenya. *SpringerPlus*, 2, 265.
- Joshua Jonah Kunda, Anyanwu Nneoma C. and Ahmed Abubakar Jajere. 2013. Land suitability analysis for agricultural planning using GIS and multi criteria decision analysis approach in Greater Karu Urban Area, Nasarawa State, Nigeria. *African Journal of Agricultural Science and Technology*, 1, pp.14-23.

Khwanruthai Bunruamkaew and Yuji Murayama. 2012. Land Use and Natural Resources Planning for Sustainable Ecotourism Using GIS in Surat Thani, Thailand. *Journal of Sustainability*, 4, pp.412-429.

Lefteri DUSHAJ, Ilir SALILLARI Valentina SULJOTI, Majlinda CENAMERI, Fatbardh SALLAKU 2009. Application on GIS for Land Use Planning: A Case Study in Central Part of Albania. *Research Journal of Agricultural Science*, 41, pp 104-111.

Li, Z. and Fang, Y. 2009. Temporal and spatial characteristics of surface water quality by an improved universal pollution index in red soil hilly region of South China: A case study in Liuyanghe River watershed. *Environmental Geology*, 58(1), pp.101-107.

Maciunas, J. and Deininger, R.A. 1976. A comparison of several indexes quality. *Water Environment Federation*, 48(5), pp.954-958.

Munafò, M. and Cecchi, G. 2005. River pollution from non-point sources: A new simplified method of assessment. *Journal of Environmental Management*, 77(2), pp.93-98.

Malay Kumar Pramanik. 2016. Site suitability analysis for agricultural land use of Darjeeling district using AHP and GIS techniques. *Model Earth System Environment*, 2, pp 2-22.

Martine Nyeko. 2012. GIS and Multi-Criteria Decision Analysis for Land Use Resource Planning. *Journal of Geographic Information System*, 4, pp 341-348.

Mohammad Reza Yousefi and Ayat Mohammad Razdari. 2015. Application of GIS and GPS in Precision Agriculture. *International Journal of Advanced Biological and Biomedical Research*, 3, pp 7-9.

Mohammad Shah Nawaz Khan and Mohd. Mazhar Ali Khan. 2014. Land Suitability Analysis for Sustainable Agricultural Land Use Planning in Bulandshahr District of Uttar Pradesh. *International Journal of Scientific and Research Publications*, 4, pp.1-11.

Mas, J.F. 2005. Monitoring land-cover changes: a comparison of change detection techniques. *International Journal of Remote Sensing*, 20(1), pp.139-152.

Nickson, R. and Sengupta, C. 2007. Current knowledge on the distribution of arsenic in groundwater in five states of India. *Journal of Environmental Science and Health - Part A Toxic/Hazardous Substances and Environmental Engineering*, 42(12), pp.1707-1718.

Palaniswami, C., Gopalasundaram, P., and Bhaskaran, A. 2011. Application of GPS and GIS in Sugarcane Agriculture. *Sugar Technology*, 4, pp 360-365.

Rajasekhar, M., Sudarsana R., Siddi Raju, R. and Imran, B.U. 2017. Landuse and Landcover analysis using Remote Sensing and GIS: A case study in Uravakonda, Anantapur District, Andhra Pradesh, India. *International Research Journal of Engineering and Technology*, 4(09), pp.780-785.

Shalaby, A. and Tateishi, R. 2007. Remote sensing and GIS for mapping and monitoring land cover and land-use changes in the Northwestern coastal zone of Egypt. *Applied Geography*, 27, pp.28-41.

Sherrard, J. J. and Erskine, W.D. 1991. Complex response of a sand-bed stream to upstream impoundment. *Regulated Rivers: Research & Management*, 6(1), pp.53-70.

Shin, J.J. and Mellano, C. 2014. Treatment of glenoid chondral defect using micronized allogeneic cartilage matrix implantation. *Arthroscopy Techniques*, 3(4), pp.e519-e522.

Simsek, C. and Gunduz, O. 2007. IWQ Index: A GIS-integrated technique to assess irrigation water quality. *Environmental Monitoring and Assessment*, 128(1–3), pp.277-300.

Singh, P.K. and Panigrahy, B.P. 2018. Evaluation of the surface water quality index of jharia coal mining region and its management of surface water resources. *Environmental Pollution*, pp.429-437.

Research Article

Identification of Groundwater Potential Zones Using Analytical Hierarchy Process (AHP) and GIS-Remote Sensing Integration, the Case of Golina River Basin, Northern Ethiopia

Hindeya Gebru^{1,2}, Tesfamichael Gebreyohannes², and Ermias Hagos²¹Department of Earth Sciences, Samara University, Samara, Ethiopia²School of Earth Sciences, Mekelle University, Mekelle, EthiopiaCorrespondence should be addressed to Hindeya Gebru, hindualem@gmail.com

Publication Date: 6 May 2020

DOI: <https://doi.org/10.23953/cloud.ijarsg.460>

Copyright © 2020 Hindeya Gebru, Tesfamichael Gebreyohannes, and Ermias Hagos. This is an open access article distributed under the **Creative Commons Attribution License**, which permits unrestricted use, distribution, and reproduction in any medium, provided the original work is properly cited.

Abstract Groundwater is the main source of water both for domestic and irrigation purposes in the study area, Golina basin. The Golina basin is located in the North Wollo Administration, Amhara regional state, Northern Ethiopia. The study area has a surface area of 916.77 km² and is a semi-arid environment with an annual mean precipitation of 913 mm/year. Because of its presumed groundwater potential, the area has recently received significant attention from the regional and federal governments as well as investors. As a result, 81 wells have been drilled for groundwater extraction mainly for irrigation purposes. About 182 springs and hand-dug wells have been developed for domestic purposes. However, little has been done to know the overall groundwater potential, the groundwater potential zonation and the sustainability of the current and planned groundwater extraction in the basin. Thus, the main objective of this work is to delineate groundwater potential zones of the area using an integrated method of AHP, GIS, and Remote sensing. A total of 10 thematic layers are used for the groundwater potential zone assessment. Based on the AHP method, the priority of the thematic layers with their weight are as follows: geology (0.22), geomorphologic landform (0.22), lineament density (0.17), slope (0.12), drainage density (0.09), soil (0.07), land use land cover (0.04), precipitation (0.04), normalized difference vegetation index (NDVI) (0.02) and topographic wetness index (TWI) (0.02). The groundwater potential zones of the area are computed using raster calculator in spatial analyst tool in GIS software and divided into five classes as very poor, poor, moderate, good and very good with area coverage of 93 km² (10%), 265 km² (29%), 175 km² (19%), 221 km² (24%) and 162 km² (18%) of the total area, respectively. The result is validated using the existing spring, hand-dug wells and borehole yields. Accordingly, the high yield boreholes are drilled and concentrated in very good groundwater potential zones whereas the low yield springs are developed in the very poor. Out of 263 water points 74, 72, 48, 59 and 10 water points are located in very good, good, moderated, poor and very poor groundwater potential zones, respectively. Mainly the very good groundwater potential fall in the alluvial deposit, plain and valley landforms, very low slope (flat), high lineament density, low drainage density, coarse soil textures, and water body and cultivated lands with high precipitation, NDVI and TWI. The result of this study can be used for the planning of new groundwater-based projects and the expansion of the existing irrigation project in the basin.

Keywords *Analytical Hierarchy Process; geographic information system; remote sensing; groundwater potential; Golina River Basin*

1. Introduction

1.1. General

Globally, groundwater is the source of one-third of all freshwater withdrawals (Taylor et al., 2013). It is a crucial natural resource for any economic development in arid and semi-arid countries that have a scarcity in their water resources (Kuisi et al., 2014). All development activities are directly and indirectly depend on groundwater resources. However, this resource is highly affected by existing geology, degree of chemical weathering, quality of recharge, level of groundwater, some surface element sources, etc. whereas surface water is normally affected by surface pollutants (Kaur et al., 2017). Naturally, surface water has less mineral content as compared to groundwater; however, because of its exposure to the surface. It is highly susceptible to pollution through anthropogenic activities. In addition to this, the construction of surface water harvesting structures for different purposes are costly and covers a larger area than groundwater points. Because of all these advantages the groundwater demand for domestic, irrigation, industrial, etc. increasing from year to year. In countries like Ethiopia, the demand for groundwater is enhanced because of fast population growth, urbanization and continued economic development of the nation in general. Likewise, groundwater is the most common resource utilized for domestic water supply, agriculture, and livestock in the present study area.

The common techniques of groundwater exploration using geophysical methods are expensive and time-consuming (Fenta et al., 2014; Fetter, 1994; Nsiah et al., 2018; Roscoe, 1990; Sener et al., 2005). These problems have forced people to use other technologies that can help investigate large areas in a short period of time with limited resources. These methods, including GIS and remote sensing, have been adapted to delineate groundwater potential zones. It is very easy and faster method for mapping groundwater potential zone in different geology conditions (Adji and Sejati, 2014; Nair et al., 2019; Siva et al., 2017). The RS and GIS approaches have been applied to delineate groundwater potential zones throughout the globe by various researchers (Agarwal et al., 2009; Al-Shabeeb-Shabeeb et al., 2018; Das et al., 2018; Fenta et al., 2014; Murmu et al., 2019; Pinto et al., 2017; Sar et al., 2015; Singh et al., 2019; Siva et al., 2017; Thapa et al., 2017; Yeh et al., 2016). The exploration for and locating groundwater potential using RS and GIS directly or indirectly depend on geology, geomorphology (landforms), slope, soil type, rainfall, landuse and drainage parameters (Murasingh et al., 2018; Thapa et al., 2017). Locating the groundwater potential zone is very essential for sustainable utilization of the resources. It supports planners, decision makers and policymakers to protect the groundwater resource from any quantity and quality impacts. The analytic hierarchy process (AHP) approach is one of the most extensively used multi-criteria decision-making models (Arulbalaji et al., 2019; Murmu et al., 2019). Basically, AHP is considered as a simple, transparent, effective, and reliable system (Ishizaka and Labib, 2011; Machiwal et al., 2011), and hence can be used for delineating groundwater potential zones (Patra et al., 2018). In this study, the groundwater potential zones are delineated by RS, GIS and AHP techniques using geology, geomorphology (landforms), slope, soil type, lineament density, drainage density, rainfall, landuse/landcover, Normalized differences vegetation index (NDVI), and Topographic wetness index (TWI) parameters. The findings are validated with the specific yield of the existing boreholes and discharge amount of the springs located in the particular areas. The main objective of this study is to map and delineate groundwater potential zones using the integrated approaches which support sustainable development, planning, and utilization with proper management of groundwater for irrigation and drinking purposes.

1.2. Study area

Golina river basin is located in North Wollo Administration, Amhara Regional State, and Northern Ethiopia. It is bounded between 540810 and 585122m East longitude and 1352908 and 1318433m North latitude (*Figure 1*). It has a total of 916.77 km² areal coverage and an elevation variation from 1326 to 3970 m above mean sea level. The basin is southwestern part of the Danakil depression, the northwestern Ethiopian plateau, and the marginal valley. It is surrounded by Raya Valley from the North, from the South by the Alwuha basin, from the East by the Gudina basin and from the West by the Nile basin. It is drained by Golina, Hormat and Kelkel rivers which are merged together near the outlet and exit the basin through the Golina outlet in the eastern part. The Golina River is perennial while the other two are intermittent streams. The Golina river basin is characterized by semi-arid climate conditions. The spatial distribution of the annual mean maximum and annual mean minimum temperatures of the basin varies from 18 – 30°C and 5 – 15°C, respectively. The spatial distribution of the annual mean precipitation of the basin ranges from 764 to 1092mm per year.

Groundwater is the main source of water for the community, even if they used the river in some places for irrigation. The local community uses groundwater from developed springs and hand-dug wells in the mountainous area while boreholes are used in the lowland.

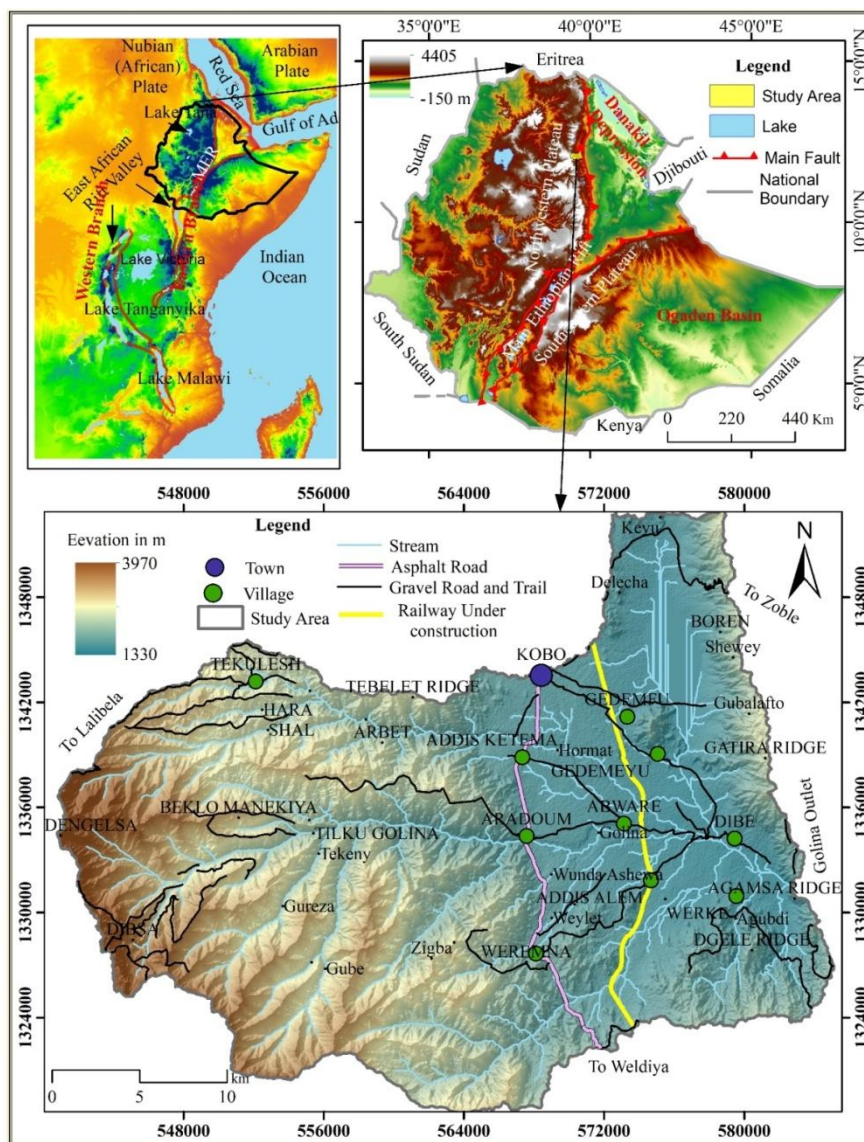


Figure 1: Location map of the study area

2. Methods

2.1. Thematic layers preparation

The groundwater potential of the area is delineated using ten thematic layer parameters namely geology, geomorphology (landforms), lineament density, drainage density, slope, soil, land use/cover, rainfall, normalized difference vegetation index (NDVI) and topographic wetness index (TWI). The boundary and the streams of the basin are extracted from DEM using the graphical user interface ArcSWAT in GIS software. The digital elevation model is downloaded from Advanced Land Observing Satellite (ALOS) Phased Array type L-band Synthetic Aperture Radar (PALSAR) with 12.5m spatial resolution (ASF DAAC, 2008). The geological map is prepared in the field. The main lithology and geological structures of the area are described in the field. The geomorphologic landform of the area is prepared using SAGA GIS software. The landform is classified using TPI based landform classification. Lineaments are extracted from hillshade using PCI Geomatics software. The hillshade also prepared from the digital elevation model (DEM) of the basin using surface in the spatial analyst tool in GIS software. The drainage and lineament densities are developed from streams and lineaments using line density in spatial analyst tool in GIS software. Landsat 8 OLI imagery was downloaded from the Earth Explorer, U.S. Geological Survey website (www.earthexplorer.usgs.gov). The NDVI is prepared from Landsat 8-OLI with 30m resolution using raster calculator in spatial analysis tool in GIS software. The slope of the area is prepared from DEM using surface in spatial analyst tool in ArcGIS 10.2 software. The daily rainfall of the study area is collected from 1992 to 2016 in 11 stations from the Ethiopian National Meteorological Agency (ENMA). The stations used for the analysis Alamata, Chercher, Dilb, Kobo, Korem, Lalibela, Sanka, Sirinka, Waja, Robit, Muja, Woldia, and Zobel. Among these, Kobo and Robit are located within the boundary of the study area while Alamata, Chercher, Dilb, Korem, Lalibela, Sanka, Sirinka, Waja, Muja, Woldia, and Zobel are located outside of the basin. The mean annual rainfall is interpolated using an inverse distance weighting (IDW) technique in GIS software. The TWI is calculated from the flow accumulation and slope of the basin using the raster calculator in Map algebra in GIS software. Land use/cover is developed from the Landsat 8-OLI using supervised image classification in ArcGIS 10.2 software. It is validated by comparing with sample training that is collected from the ground during the field visits and from Google earth. The soil map of the area is prepared from a raw data gathered by Metaferia contractor engineer (MCE) consult (2007) and data downloaded from Soil grid with 2.5 km resolution (for the area which is not covered by MCE consult). The groundwater point data are collected from different governmental and non-governmental organizations. The general flow chart of the methodology is given in Figure 2.

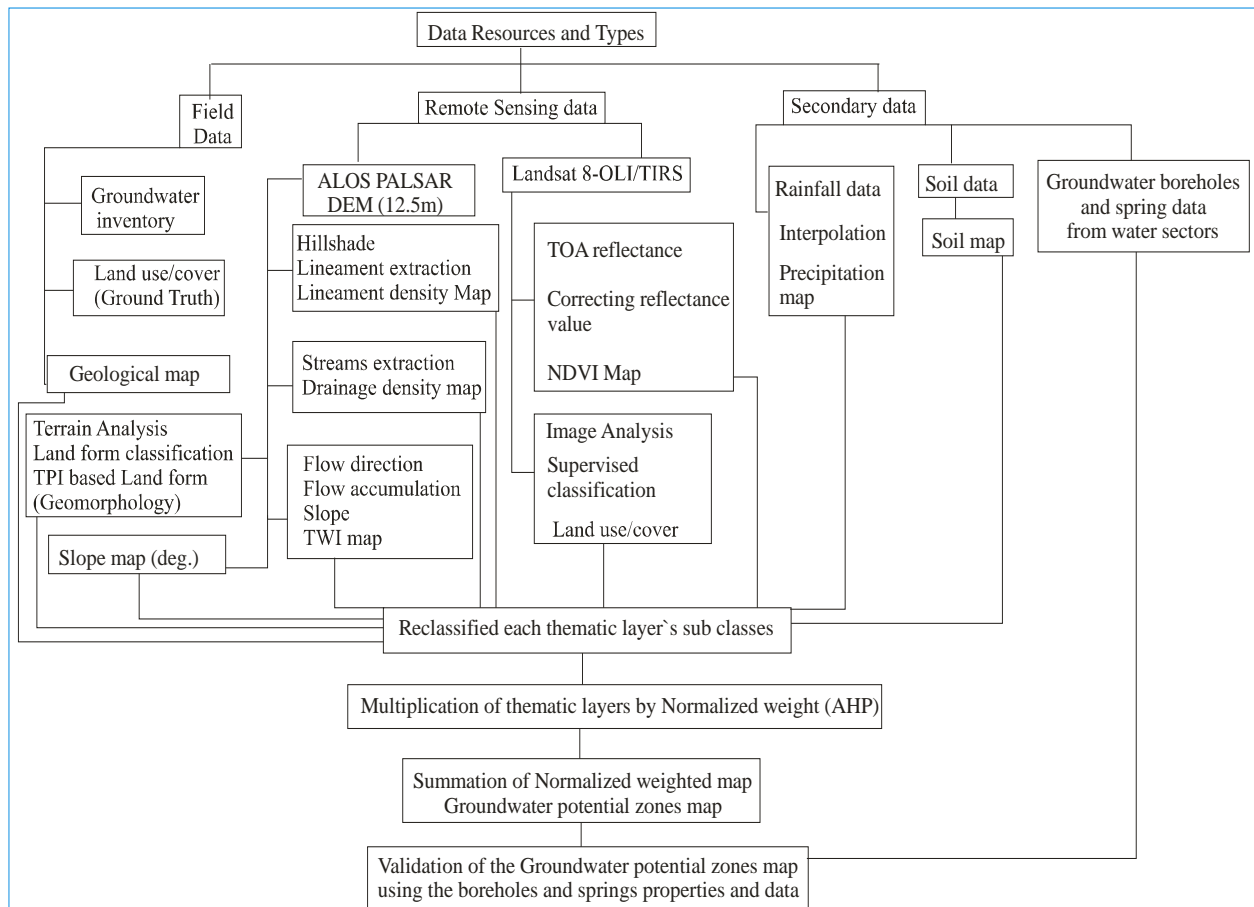


Figure 2: Flow chart of the methodology

2.2. Multi-criteria decision analysis using AHP

According to Arulbalaji et al. (2019), multi-criteria decision analysis using Analytical Hierarchical Process (AHP) is the most common GIS-based method for demarcating groundwater potential zones. The AHP method is used to generate and integrate all thematic layers based on their importance and influences for groundwater potential. In this study, a total of 10 thematic layers are used. These thematic layers are selected based on their importance for groundwater storage and transmissivity. The first procedure of this approach is to assign (Saaty, 2005, 1980) scales for pairwise comparison of the thematic layer's matrix. The two thematic layers which have equal importance for groundwater potential are assigned 1 but for the extreme importance of the pairs are given 9 (Table 1). The analytical hierarchical process (AHP) method is used for both the class of the layers and the thematic layers to identify their ranks and priority for the groundwater potential. Hence, the total weight (TW) in Table 3 is determined from the total scale weight divided by a total number of parameters for all thematic layers and classes of layers. Then, the normalized weight is derived from the assigned weight of a parameter feature class divided by the corresponding geometric mean (Kaliraj et al., 2014; Nair et al., 2019). The thematic layer with a higher normalized weight value shows a higher influence where as a lower value illustrates a less important on the groundwater potential zones (Magesh et al., 2012). The principal Eigenvalues of the parameters and class are derived from the total weight and normalized weight factors.

Table 1: Saaty's Scale of Relative Importance (Saaty, 2005)

Scale	Numerical rating	Reciprocal
Equal importance	1	1
Equal to moderate importance	2	1/2
Moderate importance	3	1/3
Moderate to strong importance	4	1/4
Strong importance	5	1/5
Strong to very strong importance	6	1/6
Very strong importance	7	1/7
Very strong to the extreme importance	8	1/8
Extreme importance	9	1/9

The λ_{max} values of the thematic layer and classes are computed from the largest Eigen values to check the decision consistency of the pair wise comparison as shown in the equation below. It is the summation of the product of total weight and normalized weight of the parameters in the matrix.

$$\lambda_{max} = \sum_{i=1}^n TW_i * NW_i \tag{Eq. 1}$$

Where λ_{max} for the largest Eigen values, TW_i for the total weight and NW_i for the Normalized weight of the thematic layers.

Saaty (1980) defines the consistency index, the measure of consistency, deviation or degree of variation of consistency and computed using the following formula (Eq.).

$$CI = \frac{\lambda_{max} - n}{n - 1} \tag{Eq. 2}$$

Where CI denoted for consistency index, λ_{max} for the largest Eigen values and n is n^{th} number of thematic layers

He proposed to use the consistency index by comparing with the appropriate consistency index so-called Random consistency index (RI) which is given in Table 2.

Table 2: Random consistency index (Saaty, 1980)

n	1	2	3	4	5	6	7	8	9	10
RI	0	0	0.58	0.9	1.12	1.24	1.32	1.41	1.45	1.49

The comparison between the consistency index (CI) and random consistency index (RI) is called consistency ratio (CR) which is computed using the following equation:

$$CR = \frac{CI}{RI} \tag{Eq. 3}$$

Where CR denoted for consistency ratio, CI for consistency index and RI for random consistency index According to Saaty (1980), the value of the Consistency Ratio should be smaller or equal to 0.1 to accept in the consistency, otherwise, it needs to revise the judgment.

Table 3: shows the assigned weights, the total weights of the thematic layers and Normalized weights (CI = 0.11 and CR = 0.08)

TL	GMLF	Geo	LD	SP	DD	SL	LUC	PPT	NDVI	TWI	NW
GMLF	1	2	3	2	2	3	4	5	6	7	0.22
Geo	1/2	1	2	3	4	5	6	7	7	7	0.22
LD	1/3	1/2	1	2	3	4	5	6	7	7	0.17
SP	1/2	1/3	1/2	1	2	3	4	5	6	3	0.12
DD	1/2	1/4	1/3	1/2	1	2	3	5	4	5	0.09
SL	1/3	1/5	1/4	1/3	1/2	1	2	3	5	4	0.07
LUC	1/4	1/6	1/5	1/4	1/3	1/2	1	0.5	2	3	0.04
PPT	1/5	1/7	1/6	1/5	1/5	1/3	2	1	2	3	0.04
NDVI	1/6	1/7	1/7	1/6	1/4	1/5	1/2	1/2	1	2	0.02
TWI	1/7	1/7	1/7	1/3	1/5	1/4	1/3	1/3	1/2	1	0.02
TW	3.93	4.88	7.74	9.78	13.48	19.28	27.83	33.33	40.5	42	1.00

Where: TL – Thematic Layers, GMLF – Geomorphologic Landform, Geo – Geology, LD – Lineament Density, SP – Slope, DD – Drainage Density, LUC – Land Use/Cover, PPT – Precipitation, NDVI – Normalized Difference Vegetation Index, TWI – Topographic Wetness Index, TW – Total Weight and NW – Normalized Weight.

2.3. Groundwater Potential calculation

The weight map of the thematic layer feature classes is prepared using ArcGIS to compute the groundwater potential zones of the study area using the following equation. The normalized weights of the themes multiplied by the normalized weights of the class are applied to evaluate the groundwater potential index using the raster calculator in ArcGIS 10.2 software.

$$GWPI = GM_w * GM_{wi} + Geo_w * Geo_{wi} + LD_w * LD_{wi} + SP_w * SP_{wi} + DD_w * DD_{wi} + SL_w * SL_{wi} + LULC_w * LULC_{wi} + PPT_w * PPT_{wi} + NDVI_w * NDVI_{wi} + TWI_w * TWI_{wi} \quad \text{Eq. 4}$$

Where: GWPI refers to groundwater potential index, GM for geomorphologic landform, Geo for geology, LD for lineament density, SP for slope, DD for drainage density, SL for soil texture, LULC for land use land cover, PPT for precipitation, NDVI for normalized difference vegetation index, TWI for Topographic wetness index, and the subscribes of w and wi are for the normalized weights of the themes and normalized weights of the feature class, respectively.

Table 4: Class of thematic layers with normalized weights

Thematic layer (w)	Classes	wi	Thematic layer (w)	Classes	wi
Geo (0.22)	CI = 0.082, CR = 0.062		SL (0.07)	CI = 0.046, CR = 0.035	
	Alluvial deposit	0.36		Sand	0.35
	Tarmaber formation	0.21		Sandy Loam	0.24
	Alaje formation	0.16		Sandy Clay	0.16
	Aiba formation	0.11		Loam	0.11
	Ashangi formation	0.10		Clay Loam	0.07
	Rhyolite	0.04		Silty Clay	0.05
	Granite	0.02		Clay	0.03

GM (0.22)	CI = 0.094, CR = 0.063	LUC (0.04)	CI = 0.085, CR = 0.064
Plains	0.29	Waterbody	0.42
Valley	0.21	Agricultural land	0.21
open slopes	0.15	Glass land	0.14
Upper slopes	0.11	Forest land	0.09
Mid slope Drainage	0.08	Shrub	0.07
Stream	0.06	Bare land	0.04
Upper Drainage	0.04	Residential	0.02
Local Ridges	0.03	PPT (0.04)	CI = 0.022, CR = 0.020
Mid slope ridges	0.02	1095.0-1025.0	0.42
High ridges	0.02	1025.1-960.0	0.26
LI (0.17)	CI = 0.03, CR = 0.027	960.1-895.0	0.16
Very high (4.0-5.15)	0.42	895.1-825.0	0.10
High (3.0-4.0)	0.26	825.1-760.0	0.06
Medium (2.0-3.0)	0.18	NDVI (0.02)	CI = 0.023, CR = 0.020
Low (1.0-2.0)	0.09	Very high (>0.50)	0.42
very low (0.0-1.0)	0.05	High (0.30-0.50)	0.26
SI (0.12)	CI = 0.046, CR = 0.041	Intermediate (0.10-0.30)	0.16
Flat (0-8.0)	0.45	Low (0-00-0.10)	0.10
Gentle slope (8.1-16)	0.29	Very low (<0)	0.06
Medium slope (17.1-30.0)	0.15	TWI (0.02)	CI = 0.024, CR = 0.021
Steep slope (30.1-45)	0.07	Very low SM (-8) - (-2.5)	0.05
Very steep (45.1-78)	0.04	Low SM (-2.6) - 4	0.10
DD (0.09)	CI = 0.006, CR = 0.01	Medium SM (4.1) - (8)	0.15
Low (<1)	0.54	High SM (8.1) - (12)	0.26
Medium (1 - 2)	0.30	Very high SM (12.1) -(22)	0.44
High (>2)	0.16		

3. Results and Discussions

3.1. Thematic layers preparation

3.1.1. Geology

The geology of the Golina river basin is part of the Tertiary flood basalts of the northwestern Ethiopian plateau which is formed in the Cenozoic era before 30Mya (Hofmann et al., 1997). The northwestern Ethiopian plateau volcanic rocks are classified by Blandford (1870) as a lower Ashangi group unconformity overlain by the Magdala group. Later, these volcanic formations are regrouped by Zanettin and Justin Visentin (1973) and Gregnanin and Piccirillo (1974) as Ashangi and Aiba basalts, Alaje Rhyolites, and Termaber basalts.

The North-East part of the study area is covered with flow banded rhyolite rock. This rock unit is characterized by greenish, fine-grained, slightly weathered, ridge forming, compacted and associated with ignimbrite, tuffs, and Ash. The rock is porphyritic and composed of phenocrysts of K-feldspar, quartz, and plagioclase. The rhyolite rock is in contact with Ashangi formation as a result of northeast-striking sinistral strike-slip fault. Granite occurs as a ridge and hill forming intrusive rocks in the central valley. The granite rock has pinkish and greyish in fresh color, yellowish weathered color, medium to coarse-grained. It consists of quartz, k-feldspar, and pyroxenes. The alluvial deposits are exposed in the graben formed by western and eastern ridges. These sediments contain gravels, sand, silt, and sediments. The flow direction of the sediments shows from the western ridge towards the eastern part

of the graben. The grain size of the sediments is coarse near the mountainous while it is fine-grained in the central part of the graben. The stratigraphy of the sediments indicates that there were a series of sedimentation cycles.

From a hydrogeological point of view, areas covered with the alluvial deposits are the main groundwater potential areas. Thus, most of the boreholes drilled for domestic and irrigation purposes are concentrated in the alluvial deposits. According to Kebede (2013), the basal sequence (Ashangi basalt) is low permeability and low productive aquifer than the upper sequences (Aiba-Termaber-Alaje formations) of the Ethiopian volcanic plateau. The ridge forming rhyolite and granite rocks are impervious and nonproductive formations in the study area. Therefore, the normalized weight of the geology is arranged from high in alluvial deposits to low in granite (Figure 3).

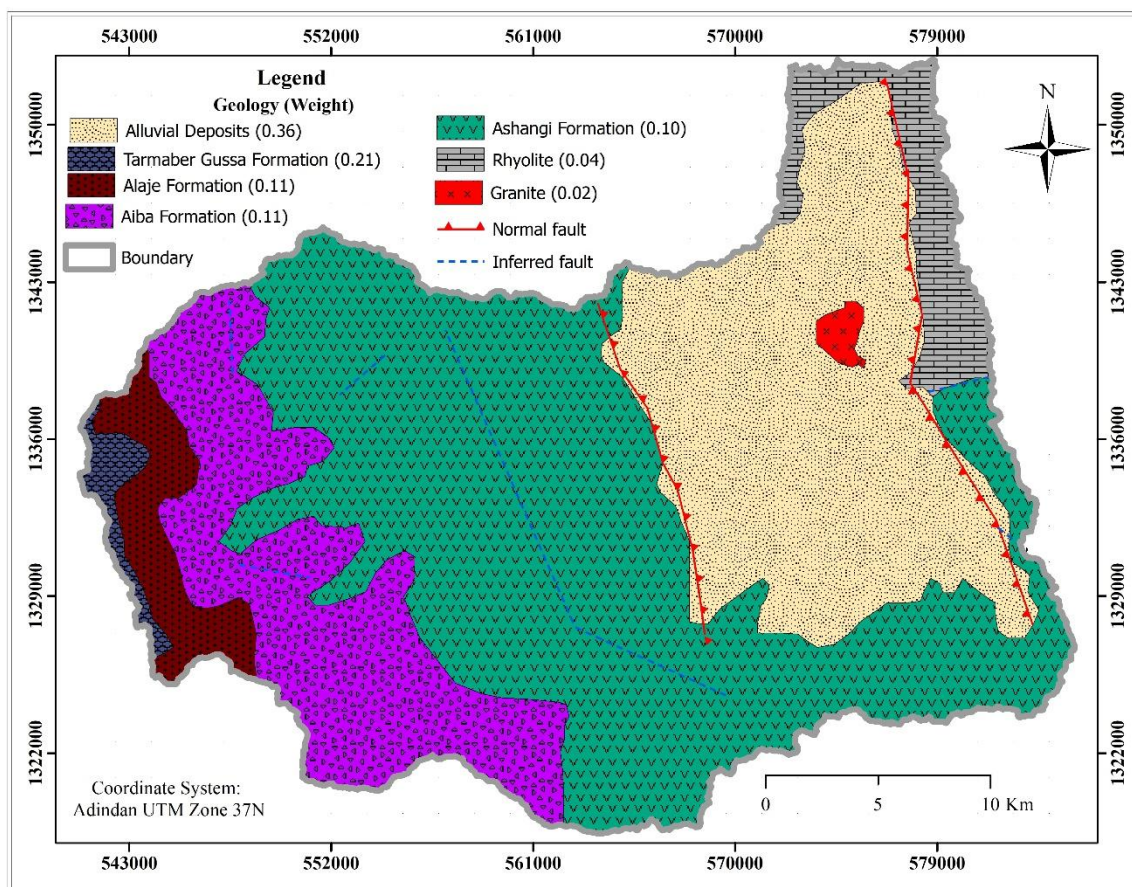


Figure 3: Geological map.

3.1.2 Geomorphologic Landform

The topographic terrain index-based landforms of the basin are prepared using SAGA GIS software from the digital elevation model (Conrad et al., 2015). The landform using topographic position index (TPI) is the difference between the elevation value of each cell in a digital elevation model (DEM) and the average elevation of the specified neighborhood around that cell (Weiss, 2001). Negative values (valley) mean the cell is lower than its surroundings while Positive values (ridge) mean it is higher. Accordingly, the area is classified into plain, valley, open slope, upper slope, midslope drainage, stream, upland drainage, local ridge, midslope ridge, and high ridges. The normalized weight value of plain and valley landforms are higher than the others for groundwater potential. But the ridge types are lower for groundwater potential as shown in (Figure 4). The graben part of the normal fault is dominated by plain and valley landform classes. The landforms of the western and eastern parts include all classes that indicate a rugged and rough topography.

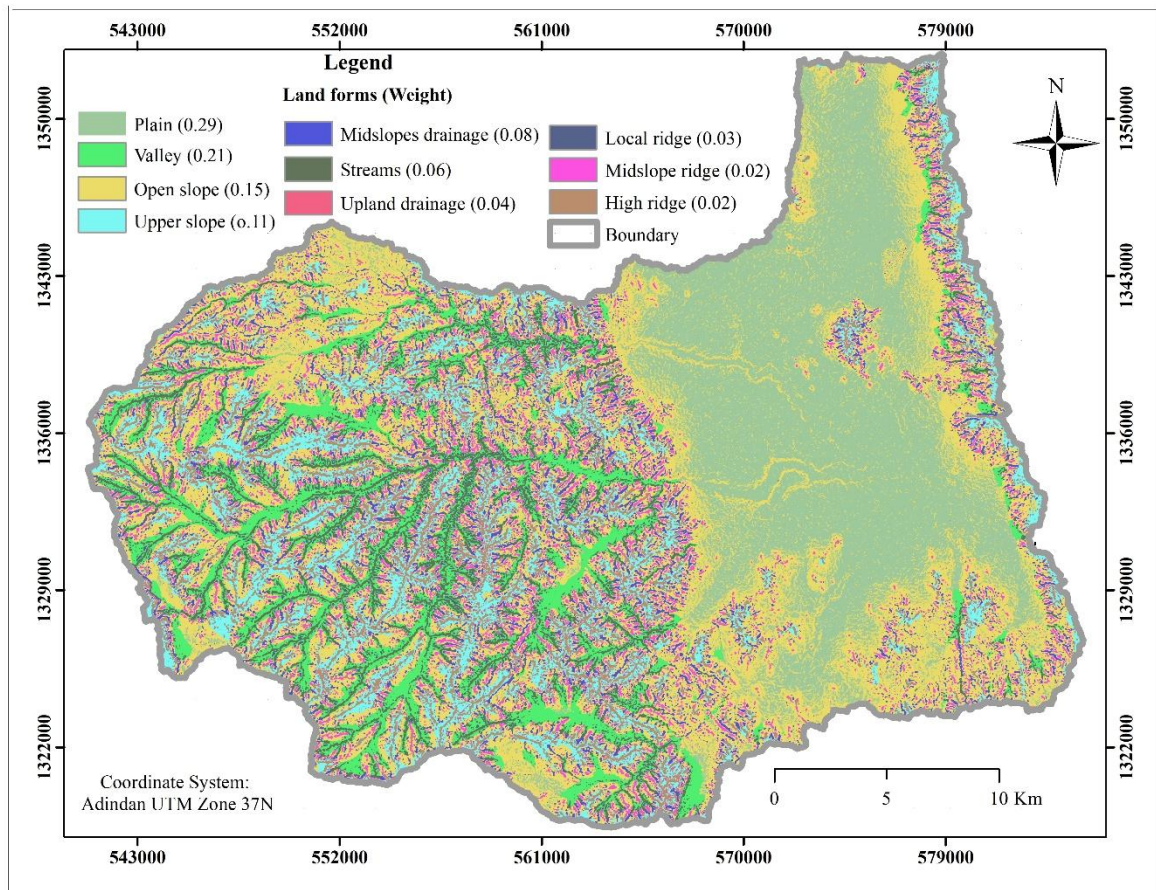


Figure 4: Geomorphologic landforms map.

3.1.3 Lineament and Lineament density

Lineament features are sources secondary porosity and permeability in hard rocks. They are very important for groundwater movement and storage. These lineaments are the linear features such as fault, joint, and fractures which serve as a container and conduit for groundwater storage and movement (Mukherjee et al., 2012; Obi Reddy et al., 2000). The groundwater movement and storage in hard rocks are controlled by lineaments and discontinuities because they are considered as subsurface secondary porosity. The intersection of various lineaments are areas where groundwater storage is possible keeping other parameters favorable for groundwater infiltration and storage. Lineament density map is important to reveal the groundwater recharge, flow, and development (Nag and Saha, 2014); (Murasigh et al., 2018). The lineament density is the ratio of the total lineament lengths and the unit area which expressed as Km per Km². The higher lineament density area have high groundwater potential especially when they are associated with the other parameters like landform and slope. The lineaments are extracted automatically from hillshade using line extraction in PCI Geomatics 2017 and the lineament density is also mapped using line density tool in ArcGIS 10.2. The dominant lineament orientation of the area is NE – SW as shows in the rose diagram (Figure 5). The lineament orientation has an impact on the groundwater flow direction of the area. The mountainous area has concentrated lineament and lineament density but sparsely dense in the lowland. The lineament density map is classified into five classes: less than 1 (very low), 1 – 2 (low), 2 – 3 (medium), 3 – 4 (high) and greater than 4 km/km² (very high) (Figure 5). The plain landform of the area has very low lineament density whereas very high is assigned in the high ridge and slope areas. Therefore, the weight for groundwater potential zone delineation is high in the high lineament density as shown in (Table 4).

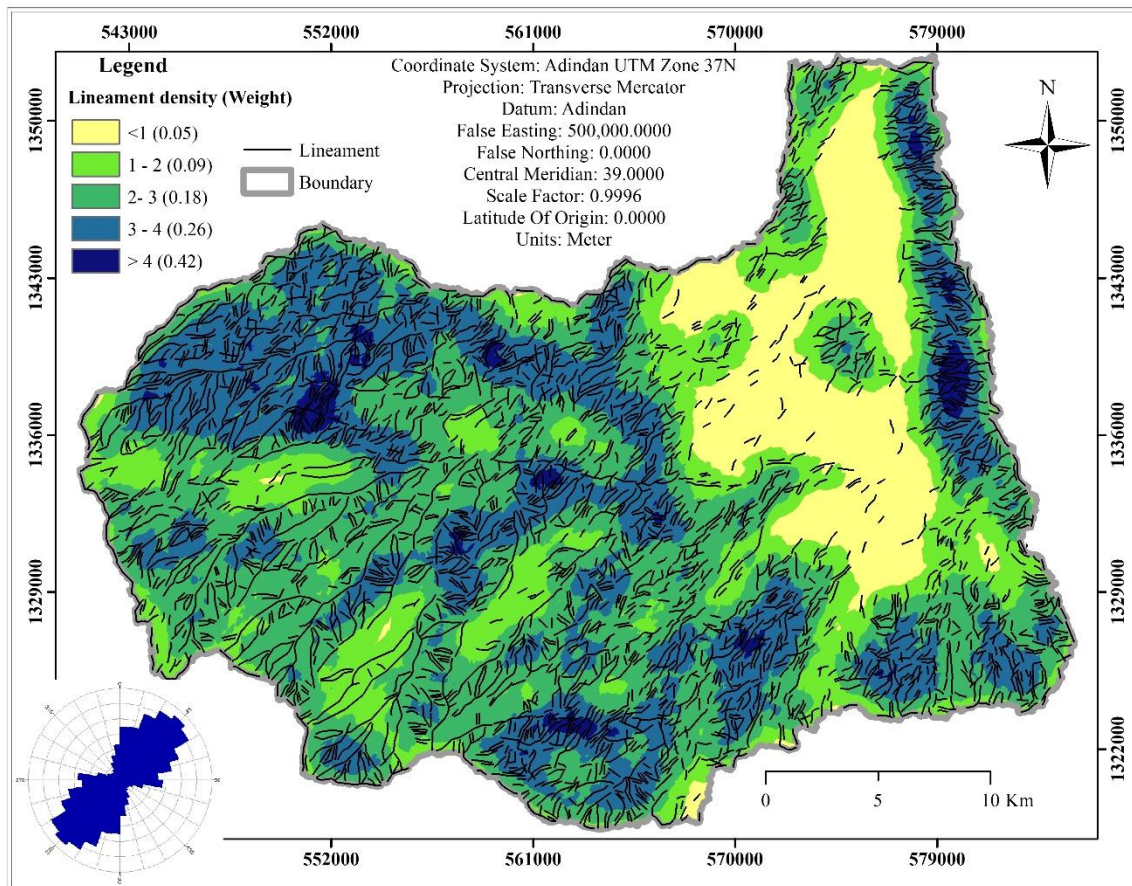


Figure 5: Lineaments, Rose diagram, and lineament density.

3.1.4 Slope

Slope is one of the factors controlling the processes of infiltration of surface water into the subsurface (Morbidei et al., 2018). Slope has a vital role for the groundwater potential of the drainage basin because the infiltration rate increased with a decreasing slope angle. The study area is classified into five slope classes as below 7 degrees (flat plain), 7 to 15 degrees (gentle slope), 15 to 25 degrees (intermediate), 25 to 35 degrees (steep) and above 35 degrees (highly steep). The lower slope angle is very important for groundwater percolation whereas the highly steep is good for surface runoff. The rain that falls on the flat area with a small slope angle has a chance to join the groundwater table of the basin but on the highly steep area, it flows directly to the streams of the basin. Therefore, the western and eastern part of the basin is dominated by a variety of slope types which indicates a rugged topography and is susceptible to runoff rather than infiltration. The plains and valley landforms associated with a low slope is preferable for groundwater potential. So that the high weight is assigned for low slope (flat plain) whereas low weight is given for the very steep slopes due to their relative importance for groundwater potential (Figure 6).

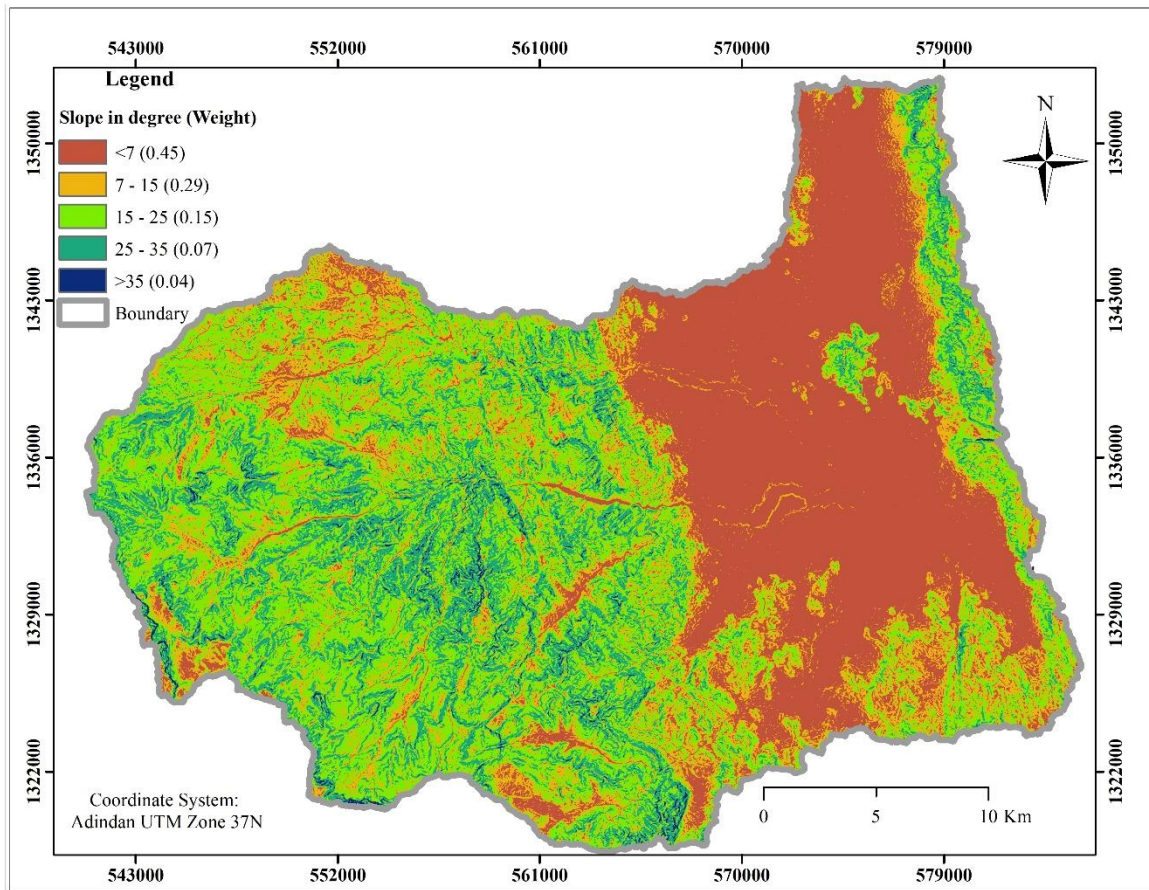


Figure 6: Slope map.

3.1.5 Drainage Pattern and Drainage Density

Drainage characteristics of a basin provided an indirect clue to the hydrogeological characteristics of the area and are useful for groundwater resources assessment (Singhal and Gupta, 1999). The main drainage characteristics are drainage patterns and drainage density. The drainage pattern of the basin is systematically arranged as dendritic. This arrangement indicates the homogeneity of the lithology of the area which is dominated with a variety of basalt formations. Drainage density is the ratio of the total channel length of the streams within a basin to the area of the basin.

$$Dd = \frac{L}{A} \quad \text{Eq. 5}$$

Where Dd is drainage density, L is the length of the streams, and A is an area of the basin.

According to the scale of the drainage map of the study area (Figure 7), the total length of the basin is 414.26 km within a total basin area of 916.77 km² and therefore, the drainage density of the basin is 0.45 km/km².

The drainage density of a basin shows the nature of relief, climate, resistance to erosion and permeability of the rock materials (Singhal and Gupta, 1999). Moreover, the area with high drainage density indicates the high relief, low resistant to erosion, low permeability, high surface runoff, and very low groundwater recharge but the reverse nature is true for low drainage density area. The drainage density is high in the area where more streams joined together. The streams of the study area flow from the west to the east and are merged at the lower elevation near the outlet (Figure 7). An area with zero drainage density and without stream network is a potential for groundwater occurrence.

Therefore, the drainage density is divided into three main classes as less than 1 for low, 1 to 2 for medium and greater than 2 for high drainage density. Very low weight is given for high drainage density while the very high weight is given for the low drainage density of the area (Figure 7).

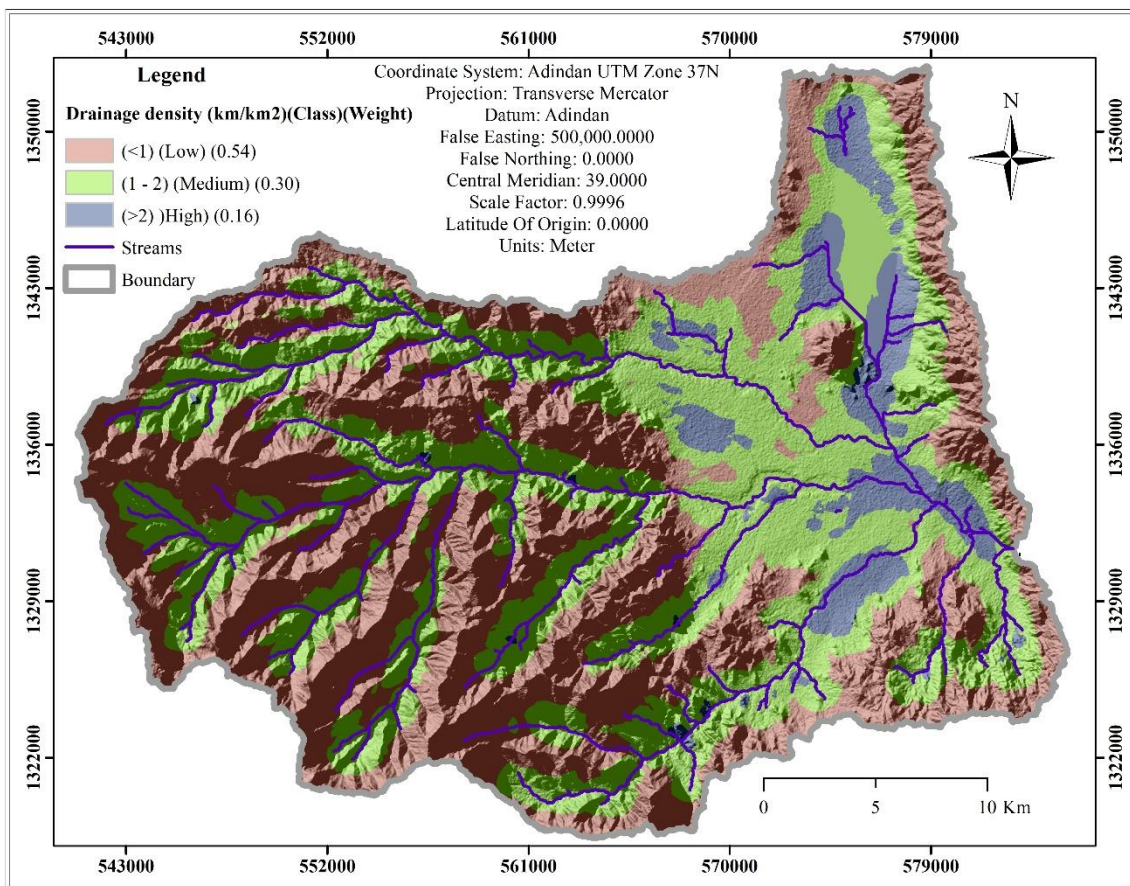


Figure 7: Drainage density and streams.

3.1.6 Soil Types

Groundwater recharge zones are places where the ground surface allows water infiltration and percolation through the soil (Chowdhury et al., 2009). The rate of water infiltration is directly depending on the grain size of the soils. Soil textures are a valuable thematic layer for groundwater potential and recharge assessment. Soil texture, the percentage of sand, silt, and clay, is an inherent factor affecting infiltration, percolation, and recharge. Water moves more quickly through large pores of sandy soil than through clayey soil. The sandy soils have a high infiltration rate than clayey soils. The coarse textures (e.g. Sand) is high permeability but the fine textures (e.g. Clay) show very low permeability. So that soil texture is strongly affecting the movement and storage of the groundwater. Based on the soil data derived from the literature, the study area has sand, sandy loam, sandy clay, loam, clay loam, silty clay, and clay soils. Accordingly, weights are given to the different soil classes in the area as indicated in Figure 8 (high for sand but low for clay).

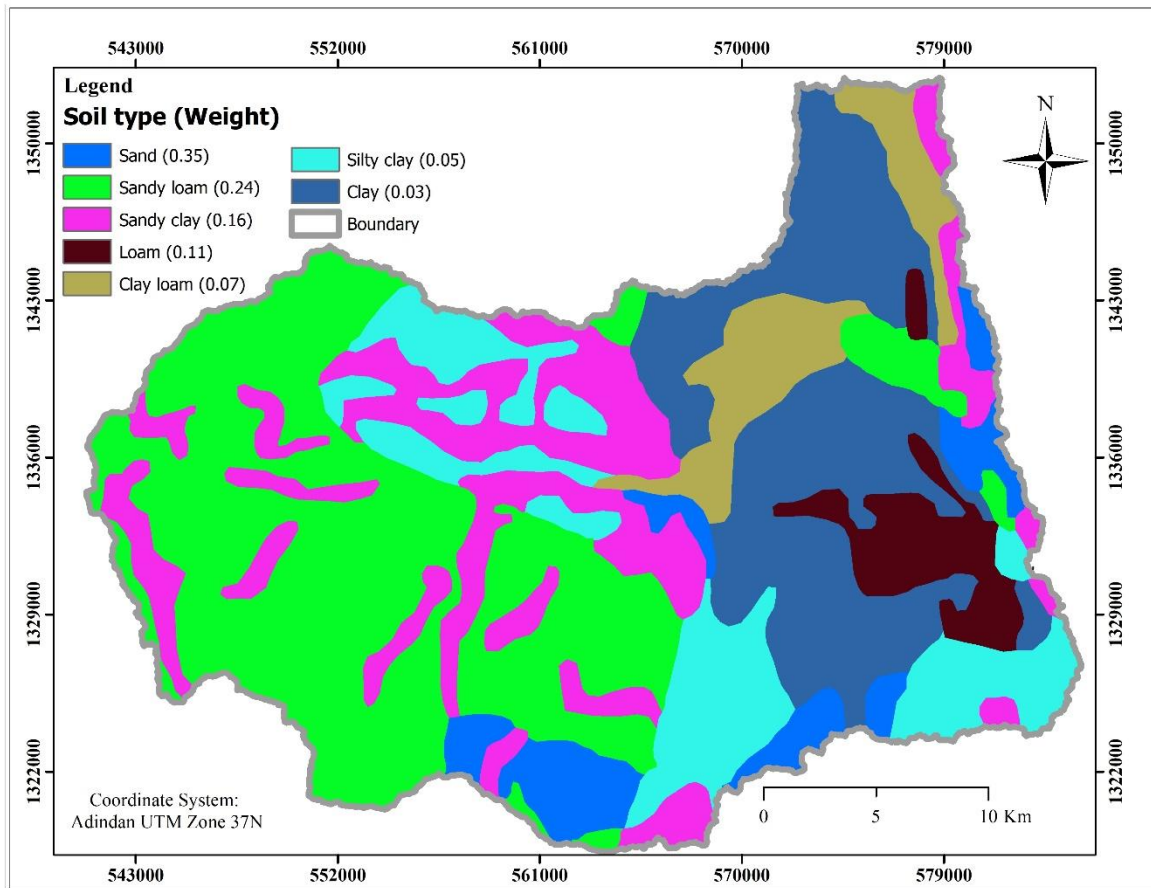


Figure 8: Soil texture map.

3.1.7 Land use/cover (LULC)

Understanding the effect of LULC on groundwater recharge and surface runoff is very interested in sustainable water resource management (Owuor et al., 2016). Moreover, accurate and reliable information about the present and future LULC will support in the management of resources (Murmu et al., 2019; Singh et al., 2018). The water addition from the unsaturated zone to the saturated zone of the water-bearing formation is affected by land use land cover. Even change in land use land cover will have an influence on the groundwater recharge, evaporation and surface runoff. The precipitation tends to infiltrate in the forest, vegetated and agricultural lands but tends to directly flow on the bare land and residential area as surface runoff. The land use land cover of the basin is categorized into a water body, cultivated land, natural forest, shrubland, bare land, and residential land and their groundwater recharge capacity decreases accordingly. So the highest weight is given to the water body and cultivated land and the lowest to residential and bare land (Figure 9).

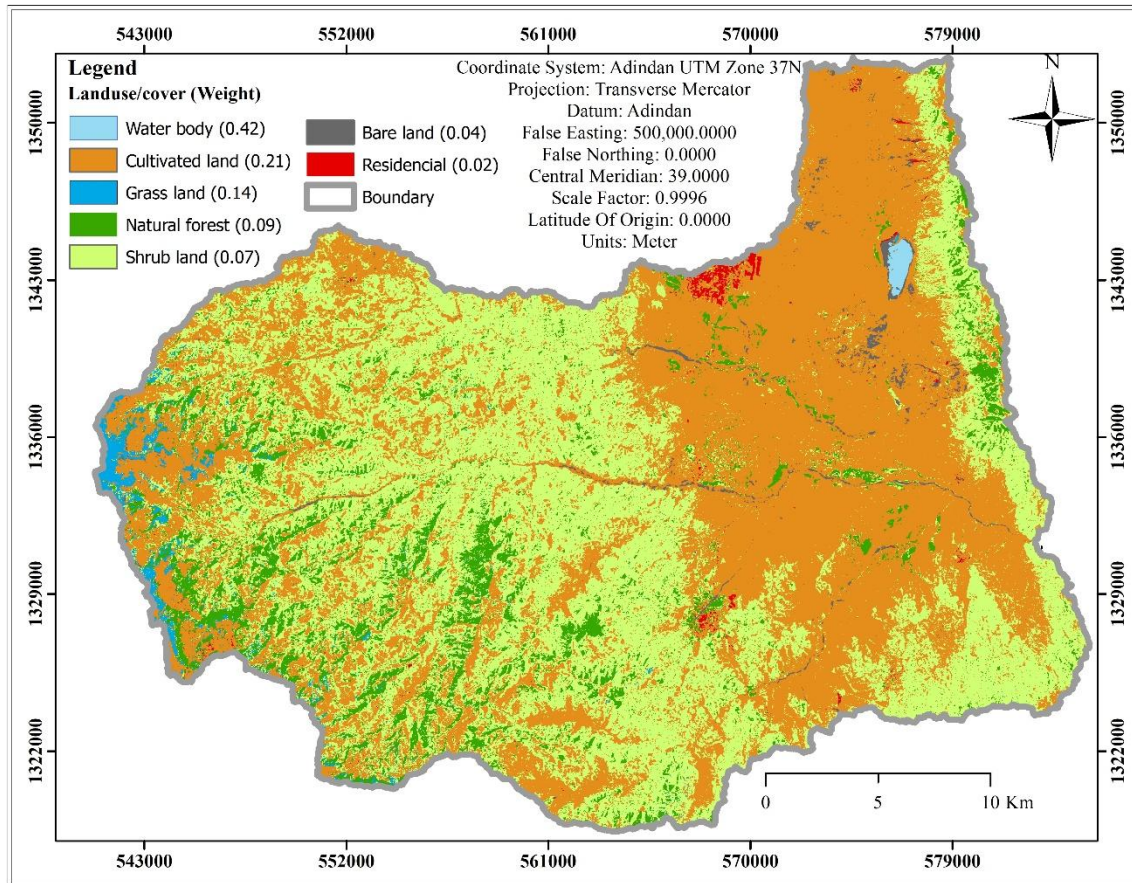


Figure 9: Land use/cover map.

3.1.8 Precipitation

Precipitation is the main source of groundwater recharge (Agarwal et al., 2009). The spatial distribution of precipitation of the study area is produced using the inverse distance weight interpolation method in ArcGIS software. The southwestern part of the basin receives high precipitation while the northeastern part receives low precipitation, relatively. The high-altitude area of the basin recorded high precipitation when compared with the low land altitude due to the orographic effect. As elevation decreases towards the east the precipitation also decreases. The mean annual precipitation of the study area ranges from 760 to 1095 mm/year with an average value of 913 mm/year. The precipitation distribution in the basin can be grouped into five classes as 760 to 825, 825 to 895, 895 to 960, 960 to 1025 and 1025 to 1095 mm/year (Figure 10). The class with low precipitation is assigned low weight because of its less importance for groundwater potential. The class with high precipitation is assigned a higher weight. The area that received high precipitation has a chance to get more percolated water than the area that received low precipitation, keeping all other factors constant.

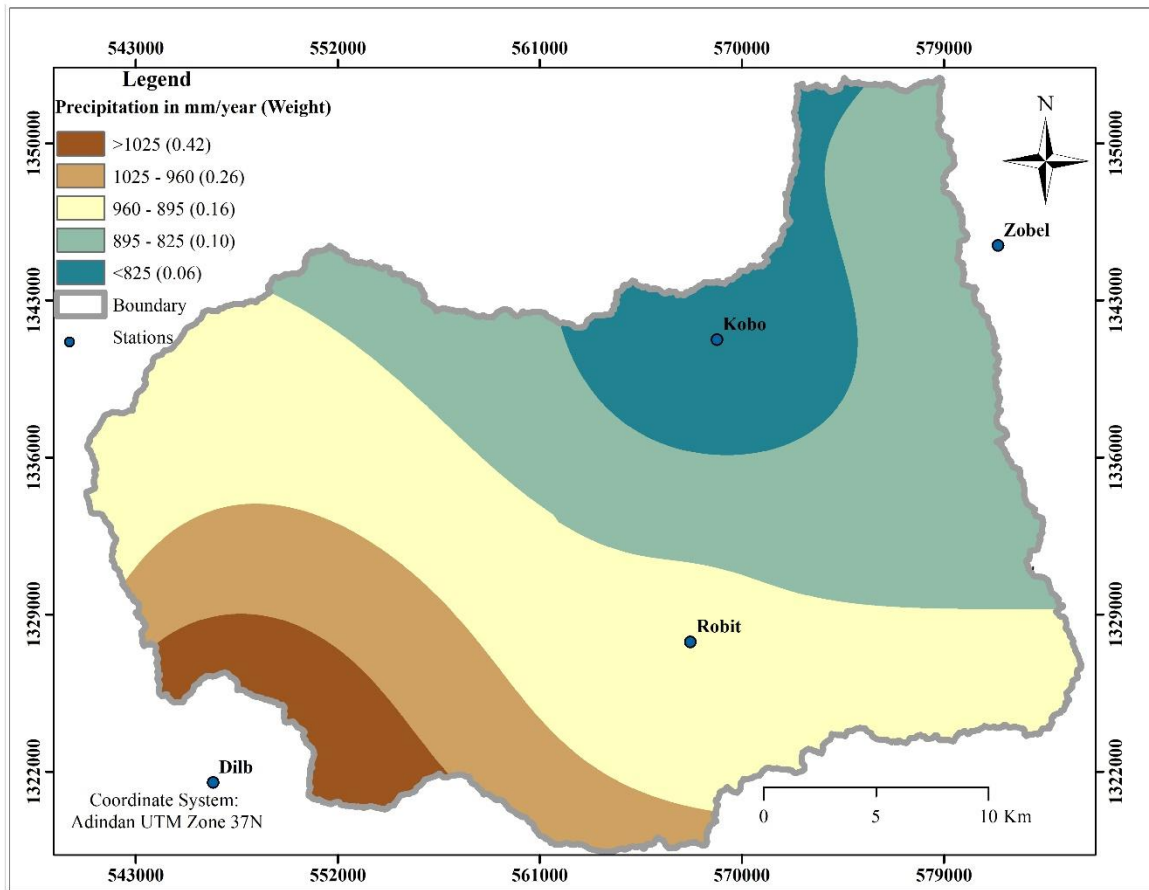


Figure 10: Spatial distribution of precipitation

3.1.9 Normalized Difference Vegetation Index (NDVI)

The normalized difference vegetation index is very essential for the delineation of groundwater potential zones (Sar et al., 2015). It is very important to assess the distribution of vegetation and the crop stage condition in the basin. The value with elevated vegetation area serves for infiltration rather than surface runoff because of the densely vegetated conditions. This is a method developed to easily distinguish between plants, water, and bare lands (Allestro and Parente, 2015).

The NDVI is counting vegetation by computing the difference between the near-infrared band and visible red band from Landsat 8 OLI using the following equation.

$$NDVI = \frac{(NIR - Red)}{(NIR + Red)} \quad \text{Eq. 8}$$

Where NDVI is normalized difference vegetation index, NIR is near-infrared (band 4) and Red is visible red (band 3) in Landsat 8 OLI.

Accordingly, the study area is reclassified into five NDVI classes as less than zero (very low vegetation coverage), 0 to 0.1 (low), 0.1 to 0.3 (intermediate), 0.3 to 0.5 (high) and greater than 0.5 (high vegetation coverage) (Figure 11). The area covered with high vegetation is assigned a high weight and the area covered with low vegetation is assigned low weight according to their importance for recharge (Table 4).

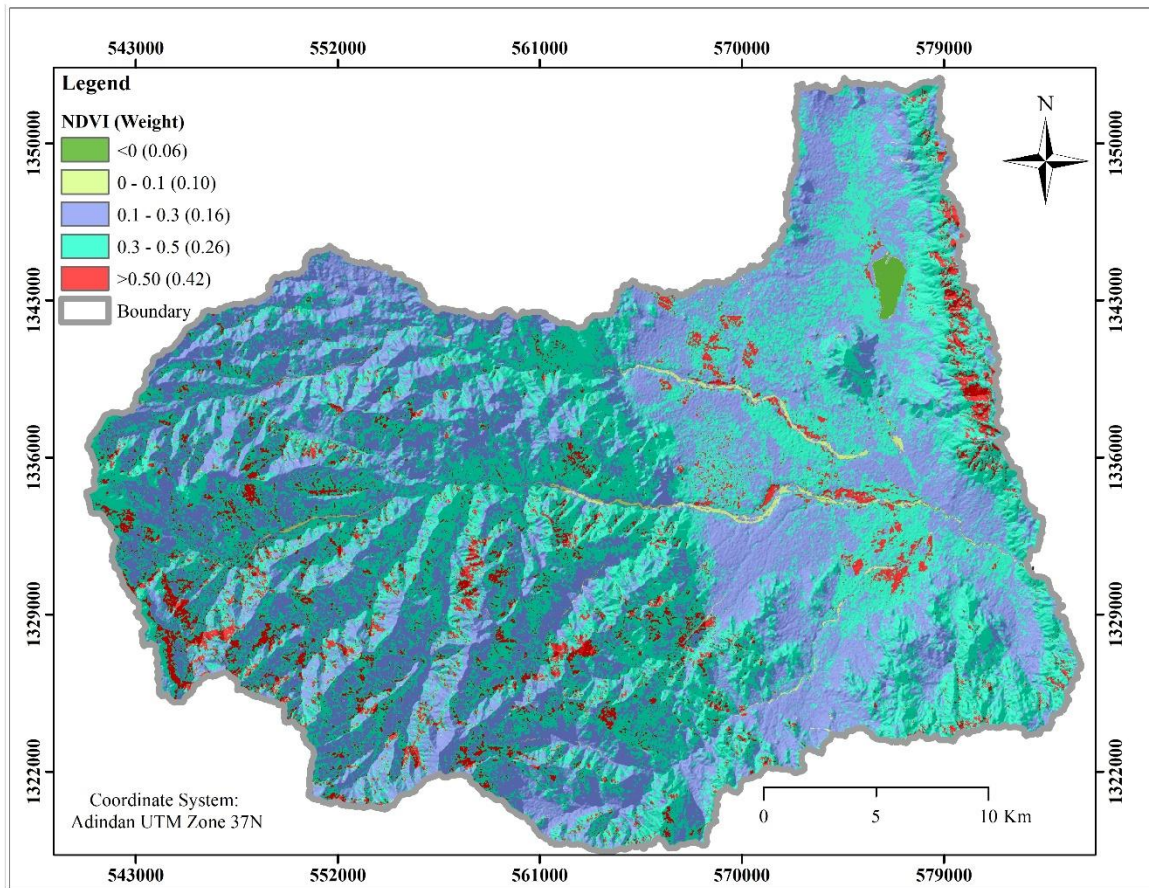


Figure 11: Normalized difference vegetation index (NDVI) map.

3.1.10 Topographic Wetness Index (TWI)

The topographic wetness index quantifies the tendency of soil water distribution, which is affected by topography (Beven and Kirkby, 1979; Raduła et al., 2018). It reflects the potential groundwater infiltration caused by the effects of topography (Arulbalaji et al., 2019; Mokarram et al., 2018). TWI is computed in SAGA GIS software using the following formula from DEM.

$$TWI = \ln \left(\frac{\alpha}{\tan \beta} \right) \quad \text{Eq. 9}$$

Where α is the upslope contributing area while β is the topographic gradient (slope). The upslope contributing area was estimated from the flow accumulation of the basin and the slope is in degree. The TWI value of the basin ranges from -8 to 22. These values are reclassified into five TWI classes from -8 to -2.5, -2.6 to 4, 4.1 to 8, 8.1 to 12 and 12.1 to 22 (Figure 12). The highest value indicates the presence of high soil moisture but the low value is soil without moisture or water. The highest class is assigned with high weight for groundwater potential and vice-versa. The lowland part of the area is found to be of high soil moisture area than the high lands. TWI indicates the soil moisture content and the groundwater storage are affected by the topography of the area. The water body and streams have the highest values of TWI.

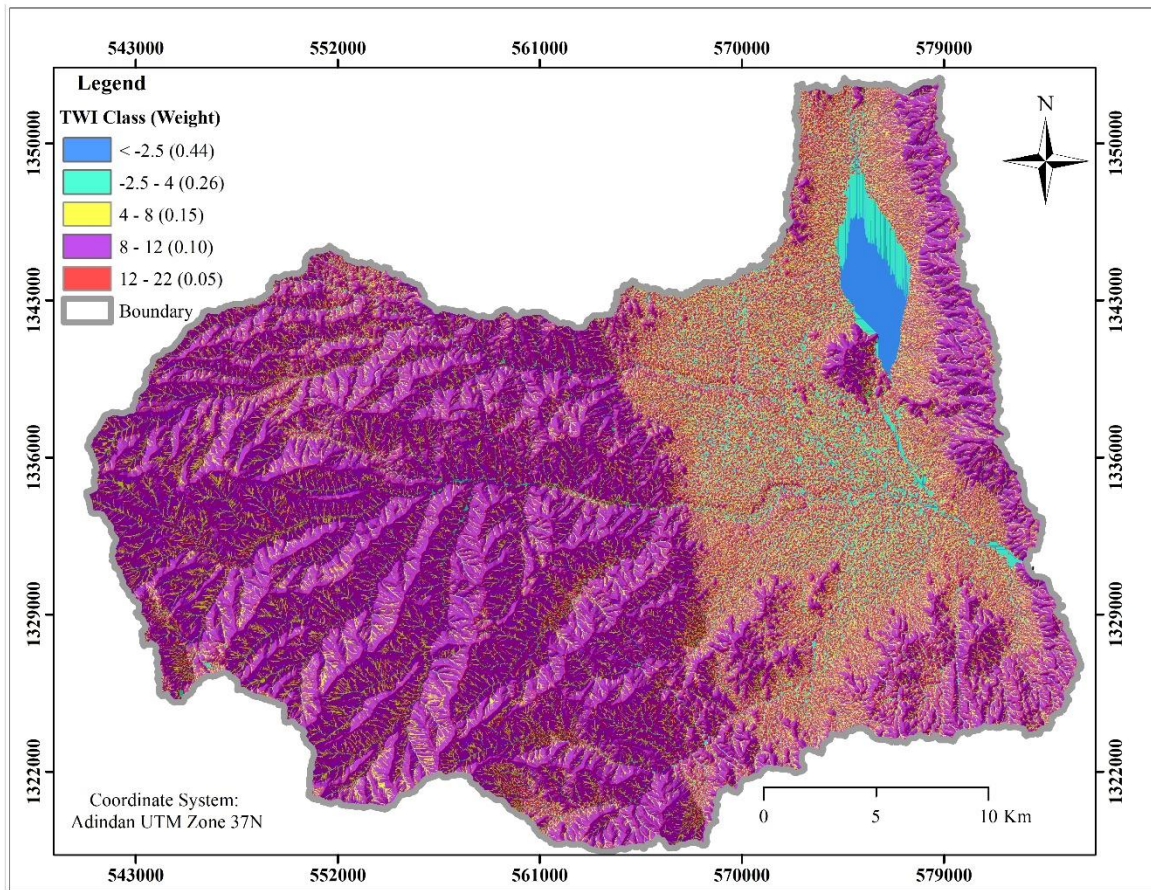


Figure 12: Topographic wetness index (TWI) map.

3.2 Groundwater Potential Zone and Validation

The resulting groundwater potential map of the study area indicated five discrete zones representing very good, good, moderate, poor and very poor groundwater potential areas (Figure 13). The total areal extent of the very good groundwater potential is 162 km² (18%). Most of the very good groundwater potential is found in the eastern part of the study area which is an alluvial deposit, very low slope (flat), plain and valley geomorphologic landforms. Similarly, the area extent of good, moderate, poor and very poor are 221 km² (24%), 175 km² (19%), 265 km² (29%) and 93 km² (10%), respectively (Table 5).

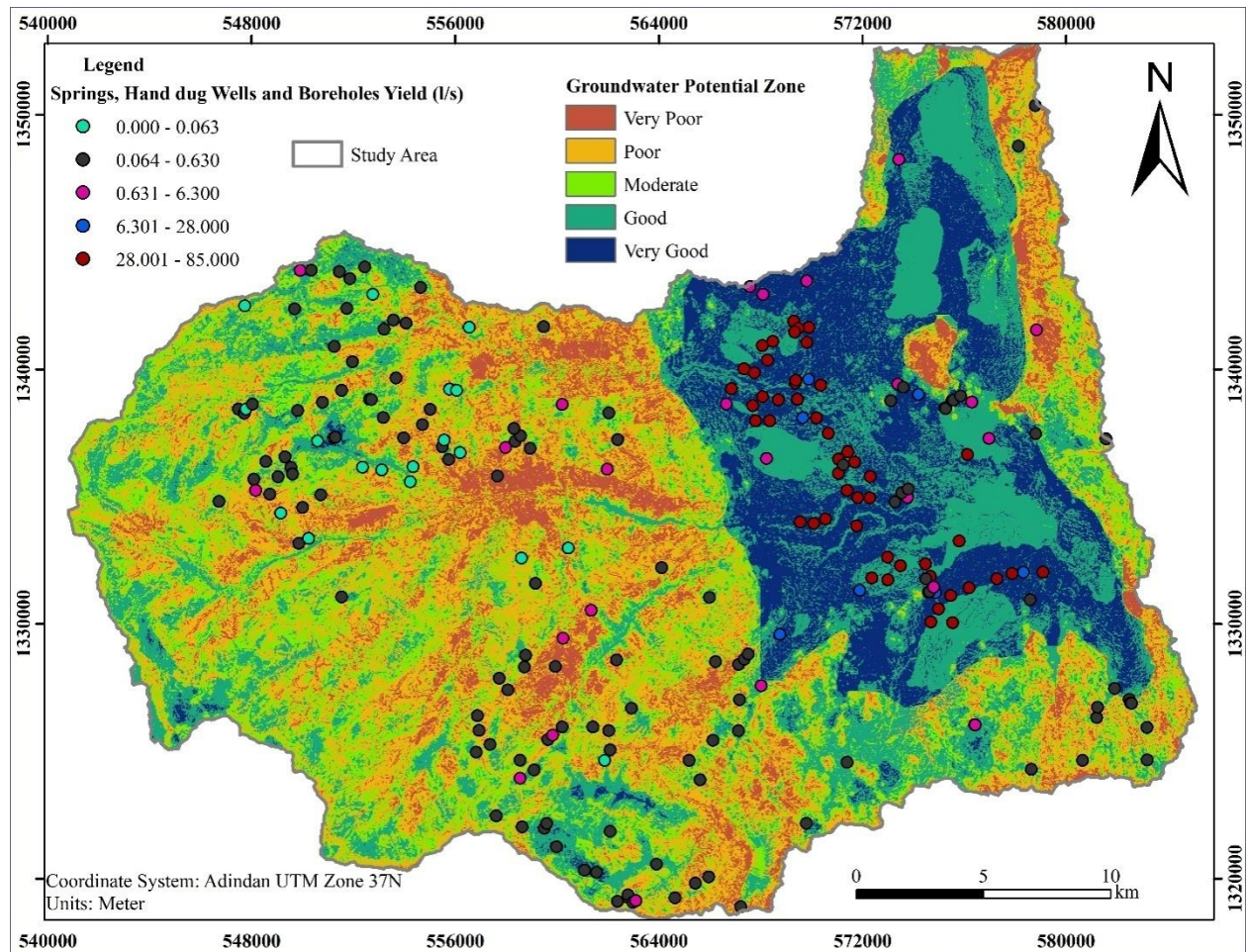


Figure 13: Groundwater potential zones.

The good and moderate groundwater potential zones are found in the alluvial deposits and Termaber formations, at the bottom of the ridges, in the intermountain valleys, near streams and around dense lineaments. The poor and very poor groundwater potential areas are mainly visible in Ashangi formation, granite, and rhyolite, ridges, sparsely lineament density and steep slope areas. The result shows that the central and western parts of the area are not suitable for groundwater potential.

Table 5: Groundwater potential zones

S.No.	Groundwater potential zone	Area (Km ²)	% of the total area	No. of water points
1	Very good	162	18	74
2	Good	221	24	72
3	Moderate	175	19	48
4	Poor	265	29	59
5	Very poor	93	10	10

The groundwater potential map of the study area is validated with the existing groundwater borehole and springs yield. Most of the deep boreholes which serve for irrigation purposes are concentrated in the very good and good groundwater potential zones. The yields of the boreholes are greater than 28 l/s. The groundwater points (springs, hand-dug wells, and boreholes) of the area are classified based on their magnitude of yields into five groups as those with a yield less than 0.063, 0.063 to 0.63, 6.3 to 28 and greater than 28 l/s (Figure 13). The springs and hand-dug wells with very low yield are located in the very poor, poor and moderate groundwater potential. The low yield springs are mainly concentrated in the poor groundwater potential zone of the area. About 50 boreholes with a yield greater than 28 l/s are drilled in the area and 39 of them are concentrated in the very good

groundwater potential zone (Table 6). Only 10 springs are found on the very poor groundwater potential zone.

Table 6: The number of springs, hand-dug wells, and boreholes in groundwater potential zones

Groundwater Potential zones	< 0.063 l/s	0.063 - 0.63 l/s	0.63 – 6.3 l/s	6.3 – 28 l/s	> 28 l/s
Very Good	4	18	7	6	39
Good	12	37	11	1	11
Moderate	5	39	4	-	-
Poor	14	42	3	-	-
Very Poor	2	6	2	-	-

4. Conclusion and Recommendations

In this study, an attempt was made to delineate the different groundwater potential zones in the Golina River Basin where groundwater is used as a source of water for both supplementary and complementary domestic and irrigation using the integrated methods of the analytical hierarchy process (AHP), GIS and remote sensing. The result indicated that the groundwater potential of the area can be divided into five zones as very poor, poor, moderate, good and very good covering 10%, 29%, 19%, 24% and 18% of the total area of the basin, respectively. The results are validated using the existing springs, hand-dug wells, and borehole yields. Out of total 50 boreholes, 11 and 39 boreholes serving for irrigation are drilled in the good and very good groundwater potential zones, respectively (Table 6), while the low yield springs and hand-dug wells are developed and drilled in the very poor, poor, moderate and in the good types of groundwater potential zones. This indicates that the AHP-GIS-Remote sensing integrated approach for groundwater potential identification gives an acceptable result. Hence, it is fair to conclude that this result can be used for the planning of new groundwater-based projects and expansion of the existing irrigation project in the basin.

Acknowledgment

The authors wish to thank Samara University and Mekelle University for funding the research work. We would also like to extend our appreciation to the Ministry of Water, Irrigation, and Electricity of Ethiopia and the Water Resource Office of Kobo Wereda for providing us with the borehole and spring data.

References

- Adji, T.N., Sejati, S.P., 2014. Identification of groundwater potential zones within an area with various geomorphological units by using several field parameters and a GIS approach in Kulon Progo Regency, Java, Indonesia. *Arab. J. Geosci.* 7, pp.161–172. <https://doi.org/10.1007/s12517-012-0779-z>
- Agarwal, E., Agarwal, R., Section, G., 2009. Delineation of Groundwater Potential Zone : An AHP / ANP approach Abstract : pp.887–898.
- Al-Shabeeb, A.A.R., Al-Adamat, R., Al-Fugara, A., Al-Amoush, H., AlAyyash, S., 2018. Delineating groundwater potential zones within the Azraq Basin of Central Jordan using multi-criteria GIS analysis. *Groundw. Sustain. Dev.* 7, pp.82–90. <https://doi.org/10.1016/j.gsd.2018.03.011>
- Allestro, P.D., Parente, C., 2015. Gis application for ndvi calculation using landsat 8 oli images. *Int. J. Appl. Eng. Res.* 10, pp.42099–42102.
- Arulbalaji, P., Padmalal, D., Sreelash, K., 2019. GIS and AHP Techniques Based Delineation of Groundwater Potential Zones: a case study from Southern Western Ghats, India. *Sci. Rep.* 9, pp.1–17. <https://doi.org/10.1038/s41598-019-38567-x>

ASF DAAC, 2008. ALOS PALSAR_Radiometric_Terrain_Corrected_high_res [WWW Document]. asf.alaska.edu. <https://doi.org/DOI: 10.5067/Z97HFCNKR6VA>

Beven, K.J., Kirkby, M.J., 1979. A physically based, variable contributing area model of basin hydrology. *Hydrol. Sci. Bull.* 24, pp.43–69. <https://doi.org/10.1080/02626667909491834>

Chowdhury, A., Jha, M.K., Chowdary, V.M., 2009. Delineation of groundwater recharge zones and identification of artificial recharge sites in West Medinipur district, West Bengal, using RS, GIS and MCDM techniques. *Environ. Earth Sci.* <https://doi.org/10.1007/s12665-009-0110-9>

Conrad, O., Bechtel, B., Bock, M., Dietrich, H., Fischer, E., Gerlitz, L., Wehberg, J., Wichmann, V., Böhner, J., 2015. System for Automated Geoscientific Analyses (SAGA) v. 2.1.4. *Geosci. Model Dev.* 8, pp.1991–2007. <https://doi.org/10.5194/gmd-8-1991-2015>

Das, B., Pal, S.C., Malik, S., Chakraborty, R., 2018. Modeling groundwater potential zones of Puruliya district, West Bengal, India using remote sensing and GIS techniques. *Geol. Ecol. Landscapes* 00, pp.1–15. <https://doi.org/10.1080/24749508.2018.1555740>

Fenta, A.A., Kifle, A., Gebreyohannes, T., Hailu, G., 2014. Spatial analysis of groundwater potential using remote sensing and GIS-based multi-criteria evaluation in Raya Valley, northern Ethiopia. *Hydrogeol. J.* 23, pp.195–206. <https://doi.org/10.1007/s10040-014-1198-x>

Fetter, C.W., 1994. Applied hydrogeology. Upper Saddle River, N.J. : Prentice Hall.

Hofmann, C., Courtillot, V., Féraud, G., Rochette, P., Yirgu, G., Ketefo, E., Pik, R., 1997. Timing of the Ethiopian flood basalt event and implications for plume birth and global change. *Nature*. <https://doi.org/10.1038/39853>

Ishizaka, A., Labib, A., 2011. Review of the main developments in the analytic hierarchy process. *Expert Syst. Appl.* <https://doi.org/10.1016/j.eswa.2011.04.143>

Kaliraj, S., Chandrasekar, N., Magesh, N.S., 2014. Identification of potential groundwater recharge zones in Vaigai upper basin, Tamil Nadu, using GIS-based analytical hierarchical process (AHP) technique. *Arab. J. Geosci.* 7, pp.1385–1401. <https://doi.org/10.1007/s12517-013-0849-x>

Kaur, T., Bhardwaj, R., Arora, S., 2017. Assessment of groundwater quality for drinking and irrigation purposes using hydrochemical studies in Malwa region, southwestern part of Punjab, India. *Appl. Water Sci.* 7, pp.3301–3316. <https://doi.org/10.1007/s13201-016-0476-2>

Kebede, S., 2013. Groundwater in Ethiopia: Features, Numbers and Opportunities. Springer Berlin Heidelberg, Verlag Berlin Heidelberg. <https://doi.org/10.1007/978-3-642-30391-3>

Kuisi, M. Al, Mashal, K., Al-Qinna, M., Hamad, A.A., Margana, A., 2014. Groundwater Vulnerability and Hazard Mapping in an Arid Region: Case Study, Amman-Zarqa Basin (AZB)-Jordan. *J. Water Resour. Prot.* 06, pp.297–318. <https://doi.org/10.4236/jwarp.2014.64033>

Machiwal, D., Jha, M.K., Mal, B.C., 2011. Assessment of Groundwater Potential in a Semi-Arid Region of India Using Remote Sensing, GIS and MCDM Techniques. *Water Resour. Manag.* 25, pp.1359–1386. <https://doi.org/10.1007/s11269-010-9749-y>

Magesh, N.S., Chandrasekar, N., Soundranayagam, J.P., 2012. Delineation of groundwater potential zones in Theni district, Tamil Nadu, using remote sensing, GIS and MIF techniques. *Geosci. Front.* <https://doi.org/10.1016/j.gsf.2011.10.007>

Mokarram, M., Shaygan, M., Sathyamoorthy, Di., 2018. Using DEM and GIS for evaluation of groundwater resources in relation to landforms in the Maharlou-Bakhtegan watershed, Fars province, Iran. *J. Water L. Dev.* 37, pp.121–126. <https://doi.org/10.2478/jwld-2018-0031>

Morbidelli, R., Saltalippi, C., Flammini, A., Govindaraju, R.S., 2018. Role of slope on infiltration: A review. *J. Hydrol.* <https://doi.org/10.1016/j.jhydrol.2018.01.019>

Mukherjee, P., Singh, C.K., Mukherjee, S., 2012. Delineation of Groundwater Potential Zones in Arid Region of India-A Remote Sensing and GIS Approach. *Water Resour. Manag.* <https://doi.org/10.1007/s11269-012-0038-9>

Murasingh, S., Jha, R., Adamala, S., 2018. Geospatial technique for delineation of groundwater potential zones in mine and dense forest area using weighted index overlay technique. *Groundw. Sustain. Dev.* 7, pp.387–399. <https://doi.org/10.1016/j.gsd.2017.12.001>

Murmu, P., Kumar, M., Lal, D., Sonker, I., Singh, S.K., 2019. Delineation of groundwater potential zones using geospatial techniques and analytical hierarchy process in Dumka district, Jharkhand, India. *Groundw. Sustain. Dev.* 9, p.100239. <https://doi.org/10.1016/j.gsd.2019.100239>

Nag, S.K., Saha, S., 2014. Integration of GIS and Remote Sensing in Groundwater Investigations: A Case Study in Gangajalghati Block, Bankura District, West Bengal, India. *Arab. J. Sci. Eng.* <https://doi.org/10.1007/s13369-014-1098-3>

Nair, N.C., Srinivas, Y., Magesh, N.S., Kaliraj, S., 2019. Assessment of groundwater potential zones in Chittar basin, Southern India using GIS based AHP technique. *Remote Sens. Appl. Soc. Environ.* 15, p.100248. <https://doi.org/10.1016/j.rsase.2019.100248>

Nsiah, E., Appiah-Adjei, E.K., Adjei, K.A., 2018. Hydrogeological delineation of groundwater potential zones in the Nabogo basin, Ghana. *J. African Earth Sci.* 143, pp.1–9. <https://doi.org/10.1016/j.jafrearsci.2018.03.016>

Obi Reddy, G.P., Chandra Mouli, K., Srivastav, S.K., Srinivas, C. V., Maji, A.K., 2000. Evaluation of ground water potential zones using remote sensing data - a case study of Gaimukh watershed, Bhandara district, Maharashtra. *J. Indian Soc. Remote Sens.* <https://doi.org/10.1007/BF02991858>

Owuor, S.O., Butterbach-Bahl, K., Guzha, A.C., Rufino, M.C., Pelster, D.E., Díaz-Pinés, E., Breuer, L., 2016. Groundwater recharge rates and surface runoff response to land use and land cover changes in semi-arid environments. *Ecol. Process.* 5. <https://doi.org/10.1186/s13717-016-0060-6>

Patra, S., Mishra, P., Mahapatra, S.C., 2018. Delineation of groundwater potential zone for sustainable development: A case study from Ganga Alluvial Plain covering Hooghly district of India using remote sensing, geographic information system and analytic hierarchy process. *J. Clean. Prod.* 172, pp.2485–2502. <https://doi.org/10.1016/j.jclepro.2017.11.161>

Pinto, D., Shrestha, S., Babel, M.S., Ninsawat, S., 2017. Delineation of groundwater potential zones in the Comoro watershed, Timor Leste using GIS, remote sensing and analytic hierarchy process (AHP) technique. *Appl. Water Sci.* 7, pp.503–519. <https://doi.org/10.1007/s13201-015-0270-6>

Raduła, M.W., Szymura, T.H., Szymura, M., 2018. Topographic wetness index explains soil moisture better than bioindication with Ellenberg's indicator values. *Ecol. Indic.* 85, pp.172–179. <https://doi.org/10.1016/j.ecolind.2017.10.011>

- Roscoe, M.C., 1990. Handbook of Groundwater Development, 1st edn. ed. Wiley-Interscience.
- Saaty, T.L., 2005. Analytic Hierarchy Process. Hoboken, NJ Wiley Online Libr. Encycl. Biostat. <https://doi.org/10.1002/0470011815.b2a4a002>
- Saaty, T.L., 1980. The Analytic Hierarchy Process, Decision Analysis. <https://doi.org/10.3414/ME10-01-0028>
- Sar, N., Khan, A., Chatterjee, S., Das, A., 2015. Hydrologic delineation of ground water potential zones using geospatial technique for Keleghai river basin, India. Model. *Earth Syst. Environ.* 1, pp.1–15. <https://doi.org/10.1007/s40808-015-0024-3>
- Sener, E., Davraz, A., Ozcelik, M., 2005. An integration of GIS and remote sensing in groundwater investigations: A case study in Burdur, Turkey. *Hydrogeol. J.* 13, pp.826–834. <https://doi.org/10.1007/s10040-004-0378-5>
- Singh, S.K., Laari, P.B., Mustak, S., Srivastava, P.K., Szabó, S., 2018. Modelling of land use land cover change using earth observation data-sets of Tons River Basin, Madhya Pradesh, India. *Geocarto Int.* <https://doi.org/10.1080/10106049.2017.1343390>
- Singh, S.K., Zeddies, M., Shankar, U., Griffiths, G.A., 2019. Potential groundwater recharge zones within New Zealand. *Geosci. Front.* 10, pp.1065–1072. <https://doi.org/10.1016/j.gsf.2018.05.018>
- Singhal, B.B.S., Gupta, R.P., 1999. Applied hydrogeology of Fractured rocks, 2nd edn. ed. Springer Science+Business, London New York. <https://doi.org/10.1007/978-90-481-8799-7>
- Siva, G., Nasir, N., Selvakumar, R., 2017. Delineation of Groundwater Potential Zone in Sengipatti for Thanjavur District using Analytical Hierarchy Process. *IOP Conf. Ser. Earth Environ. Sci.* 80. <https://doi.org/10.1088/1755-1315/80/1/012063>
- Taylor, R.G., Scanlon, B., Döll, P., Rodell, M., Van Beek, R., Wada, Y., Longuevergne, L., Leblanc, M., Famiglietti, J.S., Edmunds, M., Konikow, L., Green, T.R., Chen, J., Taniguchi, M., Bierkens, M.F.P., Macdonald, A., Fan, Y., Maxwell, R.M., Yechieli, Y., Gurdak, J.J., Allen, D.M., Shamsudduha, M., Hiscock, K., Yeh, P.J.F., Holman, I., Treidel, H., 2013. Ground water and climate change. *Nat. Clim. Chang.* 3, pp.322–329. <https://doi.org/10.1038/nclimate1744>
- Thapa, R., Gupta, S., Guin, S., Kaur, H., 2017. Assessment of groundwater potential zones using multi-influencing factor (MIF) and GIS: a case study from Birbhum district, West Bengal. *Appl. Water Sci.* 7, pp.4117–4131. <https://doi.org/10.1007/s13201-017-0571-z>
- Weiss, a, 2001. Topographic position and landforms analysis. Poster Present. ESRI User Conf. San Diego, CA. https://doi.org/http://www.jennessent.com/downloads/TPI-poster-TNC_18x22.pdf
- Yeh, H.F., Cheng, Y.S., Lin, H.I., Lee, C.H., 2016. Mapping groundwater recharge potential zone using a GIS approach in Hualian River, Taiwan. *Sustain. Environ. Res.* 26, pp.33–43. <https://doi.org/10.1016/j.serj.2015.09.005>

Research Article

Analysis of Melt and Freeze in Shyok Sub-Basin, Indus Basin of Indian Himalaya using Ku Band Scatterometer SCATSAT-1

Mehanaz Fathima J.¹, Rajashree V. Bothale¹ and P. Jagadeeswara Rao²

¹Outreach Facility, National Remote Sensing Centre, Hyderabad, India

²College of Engineering, Andhra University, Visakhapatnam

Correspondence should be addressed to Mehanaz Fathima J., mehanaz123@gmail.com

Publication Date: 29 May 2020

DOI: <https://doi.org/10.23953/cloud.ijarsg.467>

Copyright © 2020 Mehanaz Fathima J., Rajashree V. Bothale and P. Jagadeeswara Rao. This is an open access article distributed under the **Creative Commons Attribution License**, which permits unrestricted use, distribution, and reproduction in any medium, provided the original work is properly cited.

Abstract The spatio temporal evaluation of melting snow and ice is important, among other things for studying climatological and hydrological applications. The knowledge of melting and freezing cycles of the seasonal snow cover is essential for water resources management and flood forecasting. Microwave remote sensing is a promising tool to characterise the melt and freeze over a large spatial scale and frequent temporal basis. This study attempts to use the Ku band dual polarization satellite SCATSAT-1 launched by ISRO with a scatterometer on-board with an enhanced spatial resolution of 2.2 Km to analyse the melt and freeze conditions in the Shyok basin, which is a sub-basin of the Indus river basin. The backscatter measurements from SCATSAT are helpful in identifying melt and freeze due to its sensitivity to the water present in the illuminated region. This study aims to adopt an adaptive threshold technique to identify the melt and freeze conditions, where the winter mean and maximum standard deviation and drop in backscatter due to the water content in the snow forms the basis to identify the melt and freeze conditions of the snow covered area. Spatio-temporal variability was observed in melt onset with 18% area under melt onset in the month of June, 2018. Onset in the month of April and May was less in comparison to June. Melt incidence maps were generated for major melt months of April, May and June and were categorised into 5 categories. April observed melt for 1 – 5 days, whereas a part of the study area was in melt condition throughout the month of June. A derived snow cover map was validated with Soumi_NPP derived snow cover with correlation of 0.96, indicating that SCATSAT can be used for snow cover retrieval over Himalayas by observing melt/freeze. Availability of daily SCATSAT data makes it possible to generate daily melt incidence maps.

Keywords *Adaptive threshold; Indian Himalayas; Melt and Freeze Onset*

1. Introduction

The cryosphere represents the important part of the Earth's climate system. The presence of ice and snow on the Earth is significant over a wide range of spatial and temporal scales and seasonal snow cover occurrence is a significant water resource in mountainous regions of the globe. Many global models of climate change predict that substantial changes occur at higher altitudes, so it is important

to monitor these portions of the Earth. Among the several processes, monitoring the melting snow and ice is crucial for climatological and hydrological applications. For example, melting and refreezing cycles are responsible for increased snow grain size through constructive metamorphism, thereby affecting the albedo and the surface energy balance through the amount of solar radiation absorbed by the snow pack (Tedesco, 2015). The presence of snow and ice affects the heating and cooling disturbing the energy balance, the variation in the status of snow is the indicator of climate change (Bothale et al., 2015). The knowledge about the melt onset dates is fundamental for water resource management and helps in flood forecasting. Researchers are interested in knowing the seasonal accumulation of snow and the length of the melt period. The Himalayas, which are also considered as the 'third pole', contain the world's largest reserves of ice and snow outside the poles. Understanding the melt and freeze cycles of the Himalayas is very important as they act as the source for many important rivers. Knowing the melt and freeze conditions in the Himalayas will also help in avalanche monitoring.

In historic times the observations of weather and the physical state of the snow covered regions were possible by in situ measurements. Melting is the outcome of various connected processes, which are influenced by the surface energy balance. The ground measurements of these components are difficult to collect and are not cost effective. The remoteness of these snow covered regions from the centres of population and its hostile environment means that the investigation by means of remote sensing methods particularly satellite remote sensing is desirable (Derksen et al., 2002 and Bothale et al., 2017). Because of the long heritage of spaceborne data, especially those collected in the microwave spectrum, it is possible to study the trends in melting for longer than 30 years. This information can be used to relate the melting features with climate drivers (Tedesco et al., 2009). Furthermore, remote sensing technique has proved to be promising for analysing the melt and freeze over a large area with spatio-temporal frequency.

1.1. Background

Microwave remote sensing can be used as a reliable approach due to its capability to operate in all weather conditions. Consequently, microwave sensors can detect melt even when the surface is frozen and near-surface temperature is below freezing. A large number of studies have been conducted using passive microwave sensors to detect surface melt. The use of active microwave sensors in these types of studies is given major importance these days. The active microwave measurements obtained from the scatterometer are useful in determining the melt season for a snow covered area. Scatterometer are active microwave sensors that observe the normalised radar backscatter coefficient σ° of the Earth's surface; these scatterometer measurements are particularly sensitive to water present in the illuminated surface and it is a function of incidence angle and surface roughness and the surface's electrical properties. The backscatter signatures observed from snow covered terrain and liquid water are markedly different (Carsey, F.D., 1992). As the amount of liquid water increases the wet snow causes a decrease in backscatter (Ulaby, F.T. et al., 1981). This response of the microwave region helps the researchers in identifying the melt duration and ice layer formation (Wang et al., 2008 and Oza et al., 2011). Compared to optical data, microwave sensors have much greater ground instantaneous field of view in the order of 10's of kilometres depending on the frequency, which makes the data suitable for large spatial scale studies. Also, the large swath width of microwave sensors together with their small sensitivity to the atmosphere provides information over the Earth on a daily basis. SCATSAT-1 satellite launched by India with the scatterometer sensor on board provides the microwave measurements on a daily basis, this dual polarization Ku band scatterometer is helpful in monitoring the melt and freeze conditions over a large spatial scale. For Ku band microwave radiation the backscatter for dry snow is stronger than that of wet snow (Sites and Ulaby, 1981). There are a lot of studies, which were carried out using active microwave backscatter measurements to analyse the freeze and thaw cycles (Hillard et al., 2003 and Bothale et al., 2015).

2. Materials and Methods

2.1. Study Area

The study is carried out for Shyok river basin which is a sub-basin of Indus river basin of the Indian Himalayas (Figure 1). The Shyok which flows generally north westward is fed by melt water from numerous glaciers on its way.

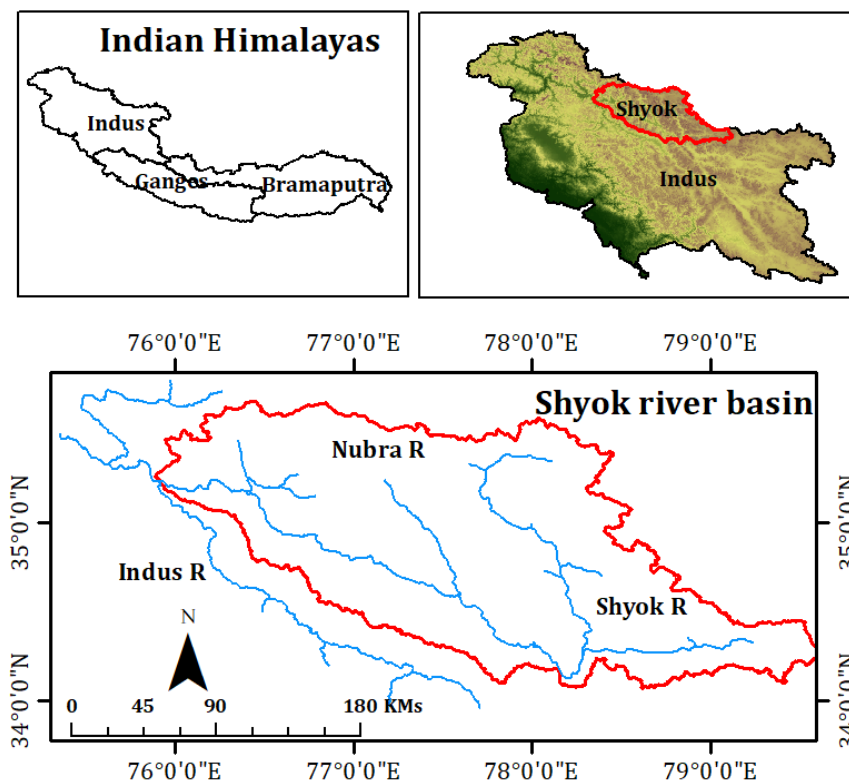


Figure 1: Study area map with location of point for backscatter response

The Shyok River originates from the Rimo glacier, which is one of the tongues of Siachen glacier. It rises in the Karakoram Range in the Himalayas. After originating from the Rimo glacier, the river flows in a south easterly direction. After merging with the Pangong range, the river takes a U turn and flows east-North westerly direction and after joining the Pangong it takes a north western turn, flowing parallel to its previous path. Shyok flows through one of the main Tectonic fault lines that separate the Himalayas from the Karakorams. The river widens at the confluence with the Nubra River. The Shyok runs in a wide valley, instantly stepping into a narrow gorge after Chalunka, continuing through Turtuk and Tyakshi before crossing into the state of Pakistan. The climate of Shyok sub-basin is semi-arid with annual precipitation less than 200 mm. The maximum temperature reaches to around 30°C in June. The velocity of the river is high, causing river erosion. Winter temperature reaches as low as -10°C.

2.2. Data used

The study uses the data from Indian satellite **SCATSAT -1** launched by Indian space Research organisation in 2016 with a scatter meter on board. It is a dual polarization pencil beam scatterometer, which operates in Ku band and gives both HH and VV images at a daily basis. The instrument has an incidence angle of 57° in VV and 49° in HH polarisation. SCATSAT –1 enhanced resolution images are available in 2.2 Km and same were downloaded from the MOSDAC website (www.mosdac.gov.in). The analysis in the present study was carried out for the year 2018.

2.3. Methodology

The methodology adopted in the study is given in the Figure 2.

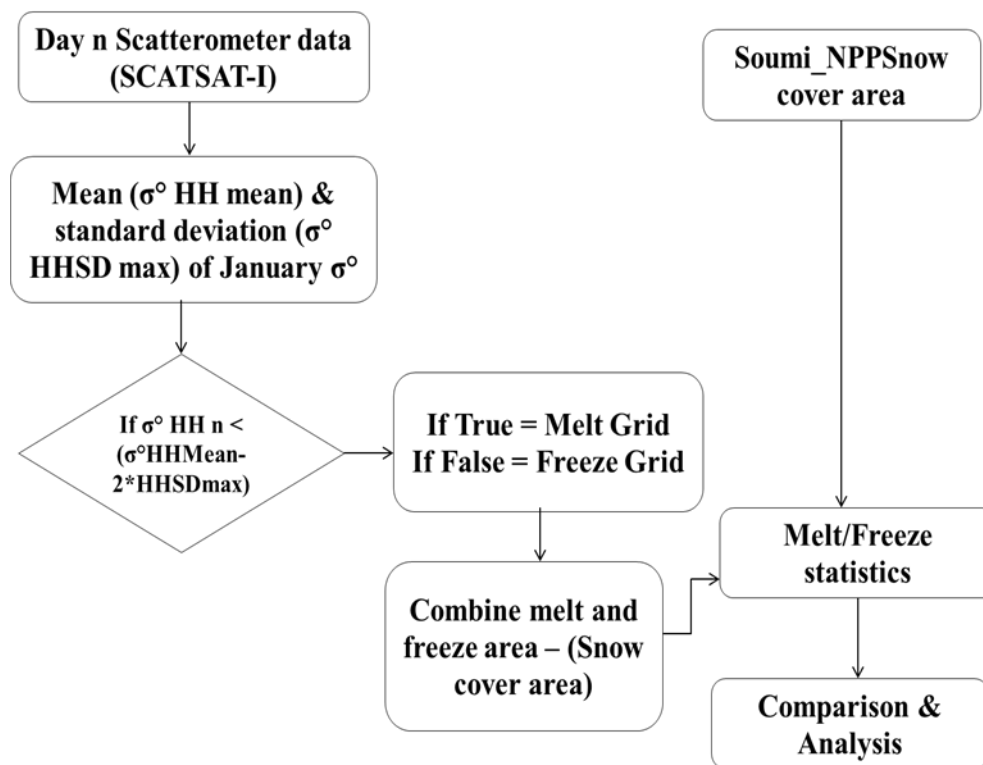


Figure 2: Methodology

Analysis of the backscatter response

As mentioned earlier, the backscatter from the scatterometer is sensitive to water content present in the illuminated region (Ulaby and Sites, 1981). The backscatter response of some points as shown in the Figure 3 from the study area was observed and it was observed that, as the water content increases, there is a sudden drop in backscatter which relates to the increase in temperature and the melt occurrence. The backscatter response of both HH and VV polarisation was analysed and it was observed that due to lower incidence angle the σ° from HH is more sensitive to the liquid water content (Wang et al., 2007) and hence it was used in the further analysis.

2.4. Melt / Freeze detection

Detecting the melt condition of snow covered areas is very crucial for monitoring and managing water resources. Previous researchers have carried out the analysis by applying a fixed threshold methodology to detect whether the pixel is in melt or freeze (Bothale et al., 2015 and Pandey et al., 2011). But the spatial variability of the Himalayan terrain makes the approach of using fixed threshold limited. This study adapts the adaptive threshold technique to detect the melt and freeze conditions. The backscatter values are higher for the month of January in winter season due to the increase in snow cover. The accumulating snow increases the backscatter values due to the strong volume scattering within the snow pack. In this study, an adaptive threshold was calculated for each pixel location based on the winter mean and the standard deviation. This technique helps in incorporating the variability in terrain and its response to backscatter. Based on the winter mean, standard deviation and drop in the backscatter due to the water content in the snow, the condition, which is used to satisfy the melt and freeze grid is as follows;

$$\text{If } \sigma_{HHn}^0 < (\sigma_{HH\text{Mean}}^0 - 2 * \sigma_{HH\text{SDmax}}^0), \text{ MG} = \text{True} \quad (1)$$

$$\text{If } \sigma_{HHn}^0 \geq (\sigma_{HH\text{Mean}}^0 - 2 * \sigma_{HH\text{SDmax}}^0), \text{ MG} = \text{False} \quad (2)$$

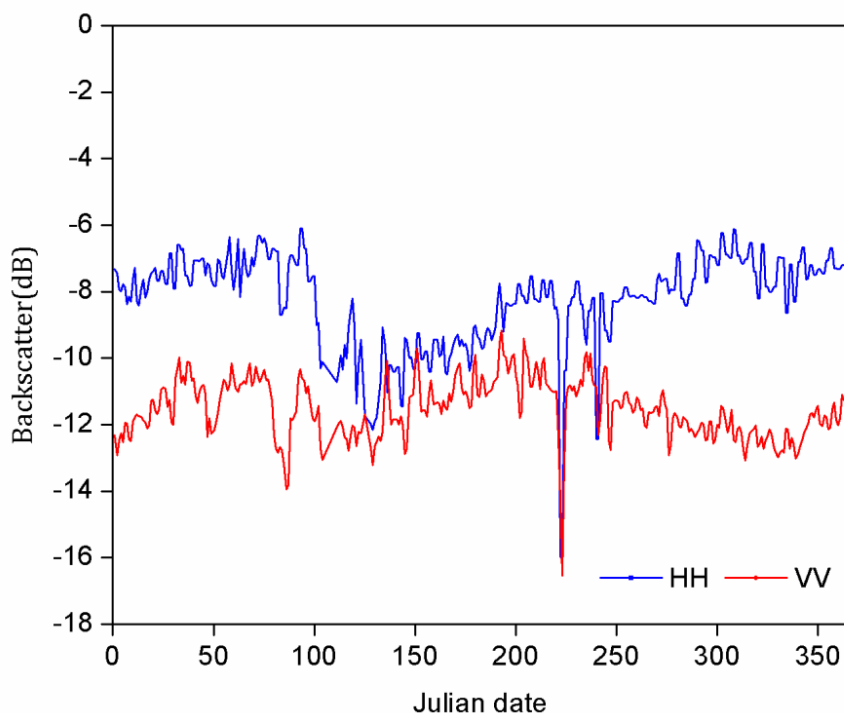


Figure 3: Scatsat-1 backscatter response for HH and VV polarisation over point shown in Figure 1

2.5. Detecting onset of melt and freeze

Based on the melt and freeze and freeze analysis, the onset of melt and freeze was identified in the study area. Whenever the backscatter of HH is lower than the adaptive threshold on the four consecutive images, the first day was considered as the onset of melt. Similarly, the onset of freeze was detected when the σ^0 of HH is higher than the threshold on 4 consecutive images. To understand the melt conditions over the entire study area, the total number of melt days was generated by counting the number of pixels under the melt throughout the year.

3. Results and Discussions

3.1. Melt and Freeze onset

The melt and freeze onset for the Shyok basin is shown in the Figure 4. The year 2018 observed 18% area under melt onset in the month of June, followed by 14% in the month of April. Lower areas observed melt in the month of March itself with 13% area under melt onset. Some areas observed melt and freeze in the same month, indicating they are predominantly in freeze condition with one or two days of melt. In places of higher elevation, where the snow is present throughout the year, the melt and freeze onset variations are more. 15% of the area received freeze onset in the month of April and 8% in the month of March itself. Majority of non-snow areas depicted by white colour, follow the river valley of Shyok and Nubra. The North-Eastern region of the basin area is devoid of snow cover. The melt/freeze status maps were generated daily as the SCATSAT data is available on daily basis. Figure 4 shows day-wise number of pixels under melt for the study area. Majority of the area is under melt onset in June as shown in the Figure 5.

3.2. Melt Incidence

The total melt incidence output generated for Shyok basin is shown in the Figure 6. Melt incidence map was generated by counting the number of pixels, which are in melt status, in the respective month. The melt incidence was classified in 5 melt categories, viz.; melt for 1-5 days, 6-15 days, 16-20 days, 21-25 days and 26-30 days. During the months of April & May, pixels were not in melt condition throughout the month. Part of the study area was in 1-5 days melt and remaining area was in 6-15 days melt. Major melt was observed in the North-North-West of the basin where the pixels were in melt state throughout the month as shown in the Figure 6c. In the month of June, the same area falls in the category of 26-30 days. The total number of melt days also vary depending upon the elevation range in the study area. This type of output helps in understanding the spatio-temporal variability of the melt conditions in the study area.

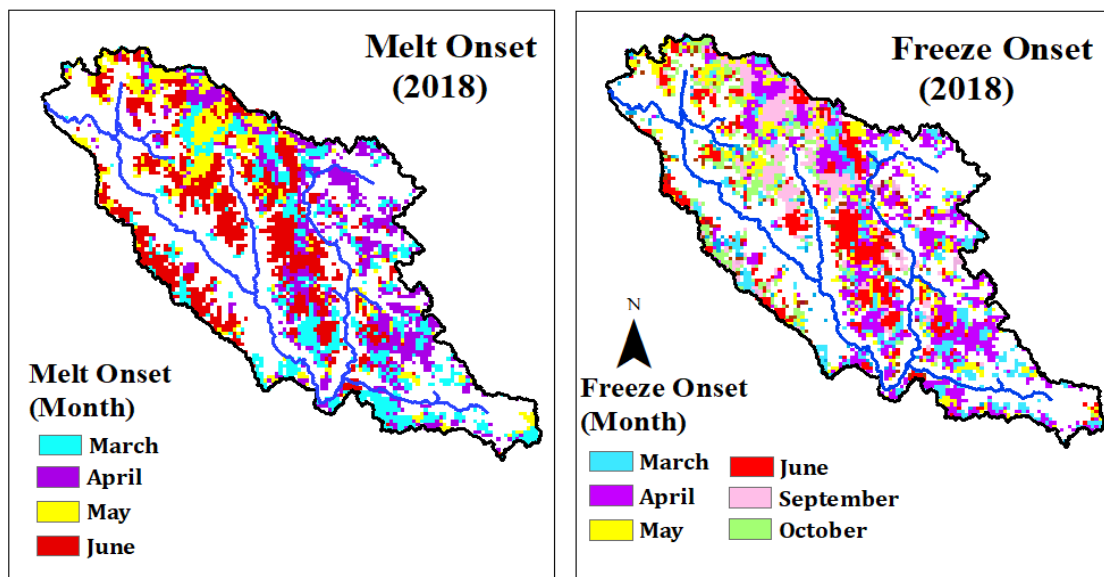


Figure 4: Melt Onset and Freeze onset in Shyok basin for the year 2018

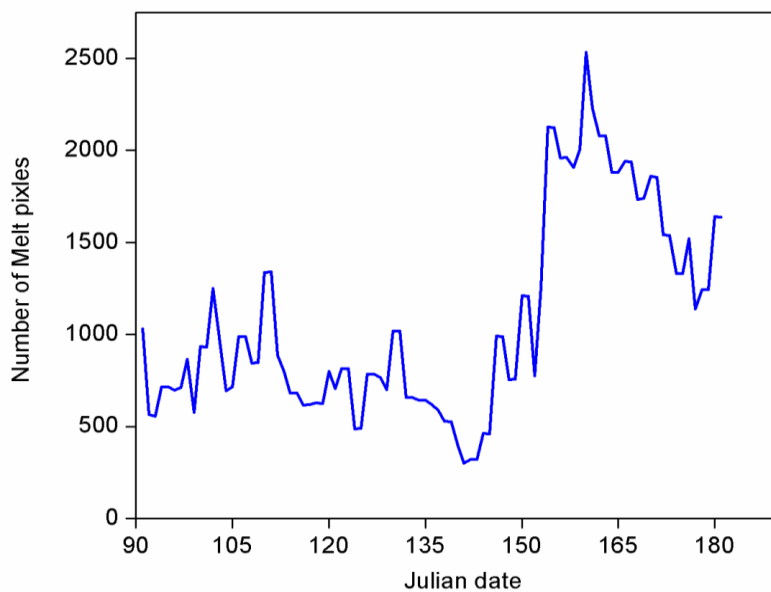


Figure 5: Day wise melt pixels over Shyok Basin

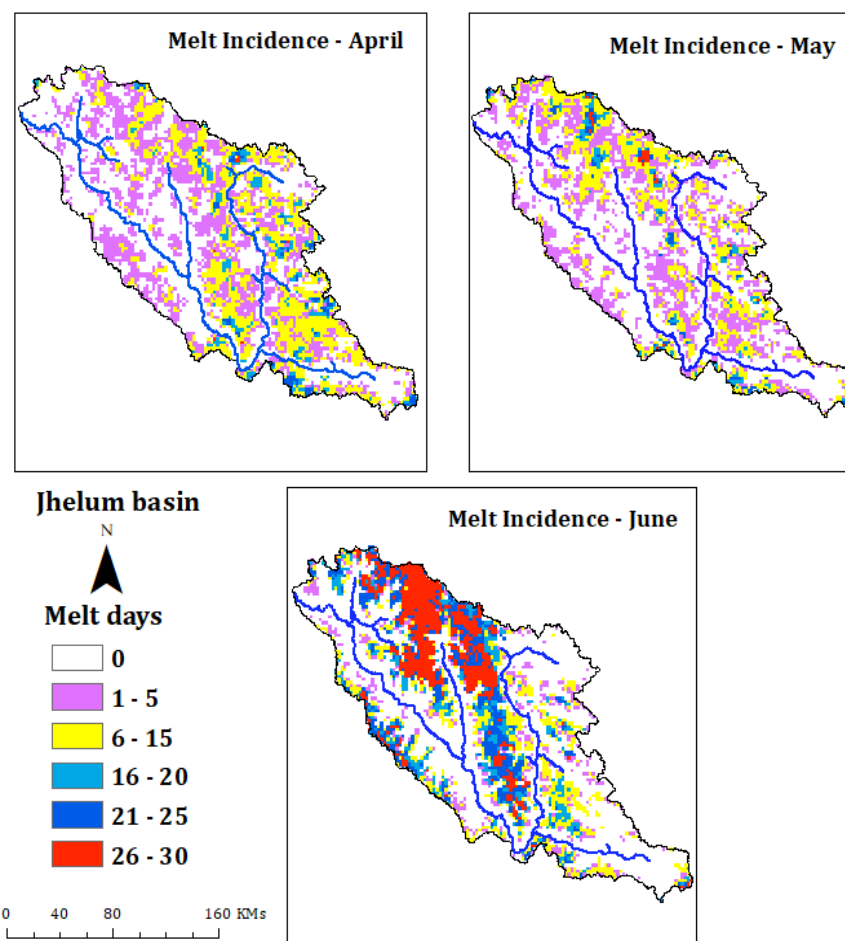


Figure 6: Melt Incidence in Shyok basin a) for April, b) May and c) June

3.3 Validation

From the generated daily melt and freeze outputs, the snow cover area was calculated by adding up the pixels in melt and freeze conditions. The generated snow cover area map was compared with the snow cover area map generated using Soumi_NPP data, which is already available. The comparison was made for the major melt months of April, May and June. Figure 7 shows the comparison of the snow cover areas generated using two different datasets of SCATSAT and Soumi-NPP. A correlation of 0.96 was obtained between both, which indicates that by observing melt/freeze status of snow area through active microwave scatterometer data, snow cover retrieval is also possible. Munoz et al (2013) in their study mentioned the sensitivity of scatterometer to melt/freeze and Naglar, T. & Rott, H. (2000) used Synthetic Aperture Radar (SAR) data to map wet snow in mountainous terrain, which showed very good correlation with existing snow cover retrievals.

4. Conclusion

This study shows the efficiency of the SCATSAT-1 scatterometer operating in Ku band in knowing about the melt and freeze conditions of the snow covered regions in India on a daily basis. This analysis also shows the variability in the melt and freeze onset in the Shyok basin. It also shows the efficacy of SCATSAT data in snow cover retrieval. Monitoring the melt and freeze conditions is crucial for monitoring and managing water resources. Thus the data from the scatterometer is proved to be a powerful tool for monitoring melting at multiple spatial and temporal resolutions.

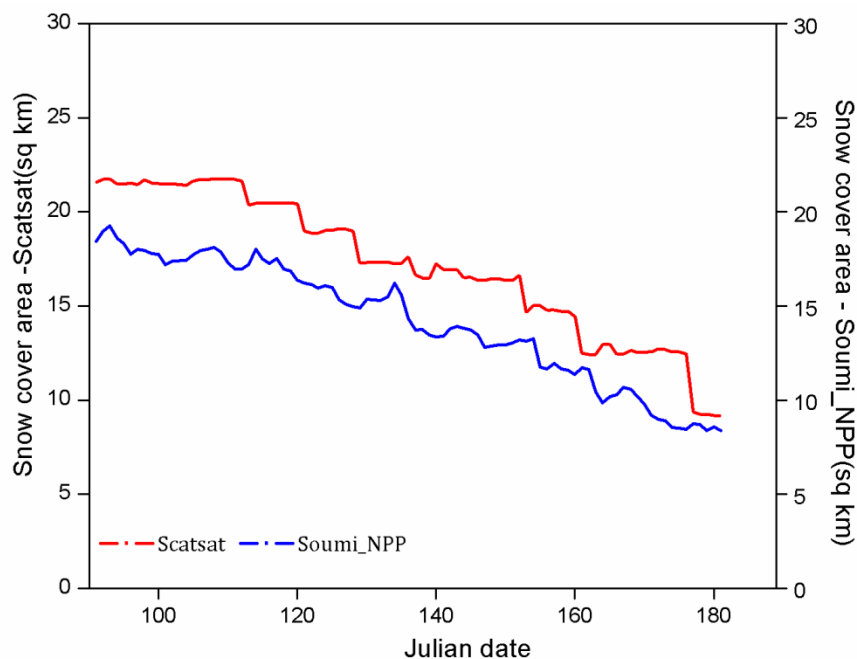


Figure 7: Comparisons between snow cover area from SCATSAT and Soumi-NPP

Acknowledgement

Authors are thankful to Director NRSC for constant encouragement & support. We also thank SCATSAT-1 utilisation project of SAC/ISRO. Meteorological & Oceanographic Satellite Data Archival Centre (MOSDAC), Space Applications Centre is acknowledged for SCATSAT data.

References

- Carsey, F.D. 1992. *Microwave remote sensing of sea ice*. Washington DC Geophysics Union, 455.
- Derksen, C and Brown, R. 2012. *Spring snow cover extent reductions in the 2008-2012 period exceeding climate model predictions*. Geophysical Research Letters. 39.
- Hillard, U. and Sridhar, V., and Lettenmaier, D.P. and McDonald, K.C. 2003. *Assessing snowmelt dynamics with NASA scatterometer NSCAT data and a hydrologic process model*. Remote Sensing of Environment, 86, pp. 52-69.
- Jonathan Munoz Barreto, Jose Infante, Tarendra Lakhankar, Reza Khanbilvardi, Peter Romanov, Nir Krakauer and Alfred Merrill Powell. 2013. *Synergistic Use of Remote Sensing for Snow Cover and Snow Water Equivalent Estimation*. *British Journal of Environment and Climate Change*, 3(4), pp.612-627.
- Nagler, T. and Rott, H. 2000. *Retrieval of wet snow by means of multitemporal SAR data*. *IEEE*, 38(2), pp.754-765.
- Oza, S.R., Singh, R.K., Vyas, N.K. and Sarkar, A. 2011. *Study of inter-annual variations in surface melting over Amery Ice Shelf East Antarctica, using space-borne scatterometer data*. *Journal of Earth System Sciences*, 120(2), pp.329-336.

Prajjwal K. Panday, Karen E. Frey and Bardan Ghimire. 2011. Detection of the timing and duration of snow melt in the Hindu Kush–Himalaya using QuickSCAT, 2000-2008. *Environmental Research Letters*, 6, 024007.

Rajashree V. Bothale, P.V.N., Rao and C.B.S., Dutt and Dhadhwal, V.K. 2015. *Detection of snow melt and freezing in Himalaya using OSCAT data. Journal of Earth System Sciences*, 124(1), pp.101-113.

Rajashree V. Bothale, Anoop S. Rao, Dhadhwal, V.K. and Y.V.N., Krishnamurthy. 2017. Understanding relationship between melt/freeze conditions derived from space-borne scatterometer and field observations at Larsemann hills, East Antarctica during austral summer 2015-16. *Current Science*, 113(4), pp.733-742.

Tedesco, M. 2009. Assessment of snow retrieval algorithms over Antarctica from K-band space borne brightness temperature (1979-2008). *Remote Sensing of Environment*, 113(5), pp. 979-997.

Tedesco, M. 2015. *Remote Sensing of the Cryosphere*. John Wiley and Sons. p.403.

Ulaby, F.T. and Stiles, W.H. 1981. Microwave response of snow. *Advances in Space Research*, 1(10), pp.131-149.

Wang, L. and Derksen, R. Brown. 2008. Detection of pan-Arctic terrestrial snowmelt from QuickSAT, 2000-2005. *Remote Sensing of Environment*, 112, pp.3794-805.

Research Article

Morphometric Analysis and Prioritization of Sub-watersheds for Management of Natural Resources using GIS: A Case Study of Rajasthan, India

S. Sangita Mishra, Krutarth Patel, Srinivas Pendem, and Neel Shrivatra

Department of Civil Engineering, Amity School of Engineering and Technology, Amity University Mumbai, Panvel-410206, Maharashtra, India

Correspondence should be addressed to S. Sangita Mishra, dr.sushreemishra80@gmail.com

Publication Date: 2 July 2020

DOI: <https://doi.org/10.23953/cloud.ijarsg.471>

Copyright © 2020 S. Sangita Mishra, Krutarth Patel, Srinivas Pendem, and Neel Shrivatra. This is an open access article distributed under the **Creative Commons Attribution License**, which permits unrestricted use, distribution, and reproduction in any medium, provided the original work is properly cited.

Abstract Natural resources management is crucial in water scarce semi-arid regions because of scanty rainfall and over exploitation of ground water resources. The watershed chosen in this study is drained by Bandi River having area of 2162.7 km² and located in Pali district of Rajasthan, India. Incessant rainfall, continuous exploitation of ground water results in the reduction of ground water level and recurrent drought conditions in this area. Hence, the watershed had been further divided into 5 sub-watersheds represented as SWS-1 to SWS-5 with geographical area ranging from 98 km² to 265 km² and perimeter ranging from 47 km to 79 km. These sub watersheds were then prioritized based on morphometric analysis considering the linear, areal and relief aspects of the drainage system in GIS environment using ArcGIS 10.5.5. The analysis showed that the drainage density of sub-watersheds varies between 1.351 km/km² to 2.513 km/km² and the lowest drainage density was found in SWS-4 that indicated the presence of impermeable sub-soil system with dense vegetation cover and low relief in the sub-watershed. The sub-watershed, SWS-2 has high circularity ratio of 0.6 that indicated the topography at the late maturity stage. Similarly, the Elongation Ratio varied from 0.4007 to 0.9340 in the sub-watersheds indicated comparatively steep ground slope and high relief. After the computation of all morphometric parameters of the sub watersheds, the compound parameter values were calculated and the sub-watershed having the lowest compound parameter value was given the highest priority for conservation measures. In this study, the sub-watershed SWS-1 was found to have the lowest compound value of 1.875 and hence considered for immediate soil conservation and water management measures.

Keywords *Bandi River; Soil Conservation; Drainage density; Elongation ratio; Circularity ratio*

1. Introduction

Natural Resources i.e. water and soils are scanty and their optimum usage is imperative, especially in developing countries like India, wherein the population density has been increasing alarmingly. The catchment areas, watersheds, sub watersheds, mini and micro watersheds are the hydrological units considered to conserve natural resources. The river basin management concept recognizes the interrelationships among the hydrological response units like low lands, highlands, land use and land

cover, slope, aspect, geomorphology, and soil. However, it may not be feasible to consider the entire watershed or river basin area at once for management of land and water resources. Hence the river basin is usually divided into numerous smaller units, as sub watersheds, mini watersheds or micro watersheds, by considering its drainage system. Geo morphological analysis or morphometric analysis of the watersheds is very important in this regard.

Morphometric analysis requires measurement of the linear, areal and relief features, slope of the drainage network, ground slopes and aspect of the drainage basin. Many researchers have carried out studies on the morphometric analysis of watersheds or sub watersheds using GIS and remote sensing techniques (Ahmed and Rao, 2015; Nag et al., 1998; Thakkar and Dhiman, 2007). Mishra and Nagarajan (2010) had researched on the management of natural resources in Tel River Basin of Odisha, India using morphometric analysis and prioritization of 12 sub-watersheds. They had concluded that the sub watershed having the highest priority based on compound parameters should be provided with soil conservation measures. Srinivasa et al., (2004) had carried out a study on morphometric analysis of sub watersheds of Pawagada area, Tumkur district, Karnataka using GIS software. Shrimali et al., (2001) had studied on the 42km² Sukhana lake catchment in the Shiwalik hills to prioritize the regions facing soil erosion of soil using remote sensing and GIS. Chopra et al., (2005) had conducted a study on morphometric analysis of Bhagra Phungotri and Hara maja sub watersheds of Gurdaspur district, Panjab. Khan et al., (2001) had used remote sensing and GIS for prioritization of watershed in the Guhiya basin, India. Nookaratnam et al., (2005) had conducted a study on the positioning of check dams by prioritization of micro watersheds using a sediment yield index (SYI) model and morphometric analysis in GIS environment. Mundetia et al., (2018) had analyzed morphometric parameters of the Khari River basin and prioritized the sub-watersheds on the basis of ground water potential using GIS approach. In this study, a part of the Bandi River Basin had been taken up as the study area and morphometric analysis and prioritization of sub watersheds were carried out.

2. Study Area

The area selected in this study is one of the watersheds of Bandi River covering 2162 km² and lies between 25° 15' and 25° 49' N latitude and 73° 17' and 73° 54' E longitude in Marwar area of Pali District, Rajasthan (Figure 1). It is a sixth order watershed having nearly dendritic to sub-dendritic drainage pattern with non-perennial streams of Someshar river, Mithri river, Khari river and Sukri river (Tributaries of Bandi River). Besides natural streams, the watershed area is also occupied by many surface canals namely Jawai canal, Mandiya canal, Betwa canal, Sumer Samand canal and large number of lakes which are almost dry in all the seasons. Rainfall at Pali is very less all year long and average temperature is 26.6 °C. The rainfall throughout a year is around 462 mm, due to less rainfall most of the part of year there is water scarcity and very less forest area (Figure 2). In order to cope with the surface water scarcity, the ground water resource is over exploited resulting in the reduction of ground water level as shown in Figure 3. Incessant rainfall, continuous exploitation of ground water is the main reasons of recurrent drought conditions in this area.

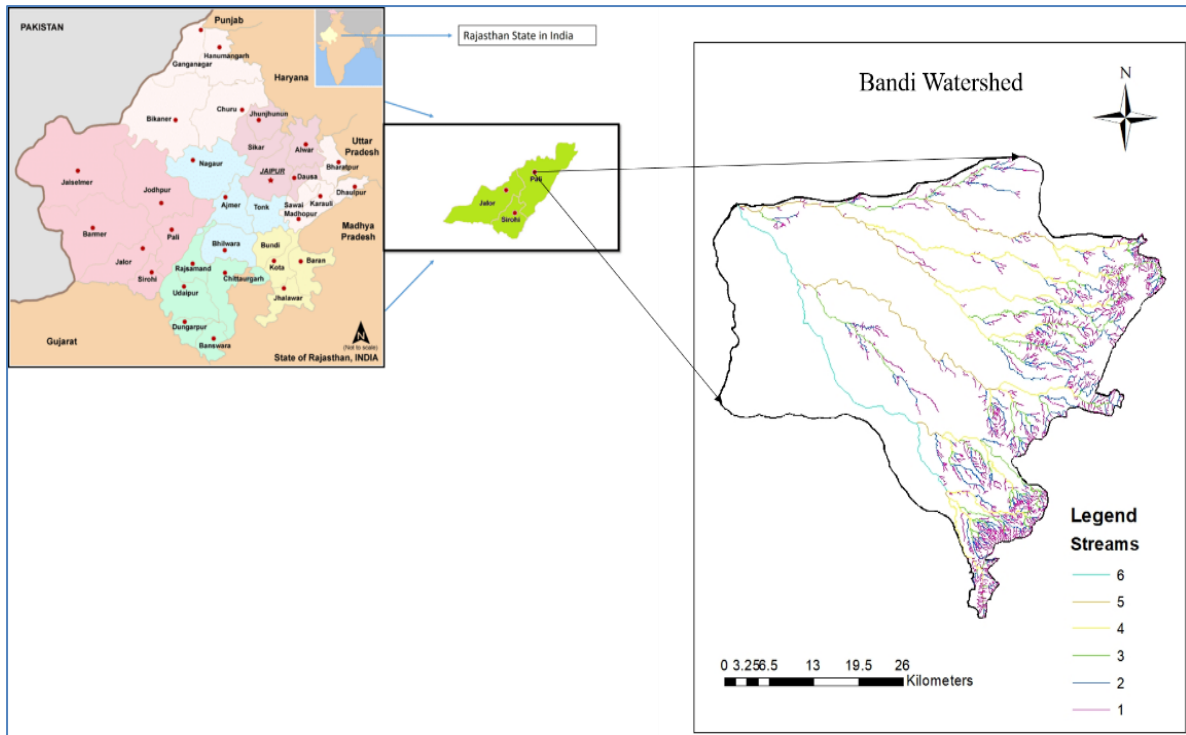


Figure 1: Index map of Bandi watershed

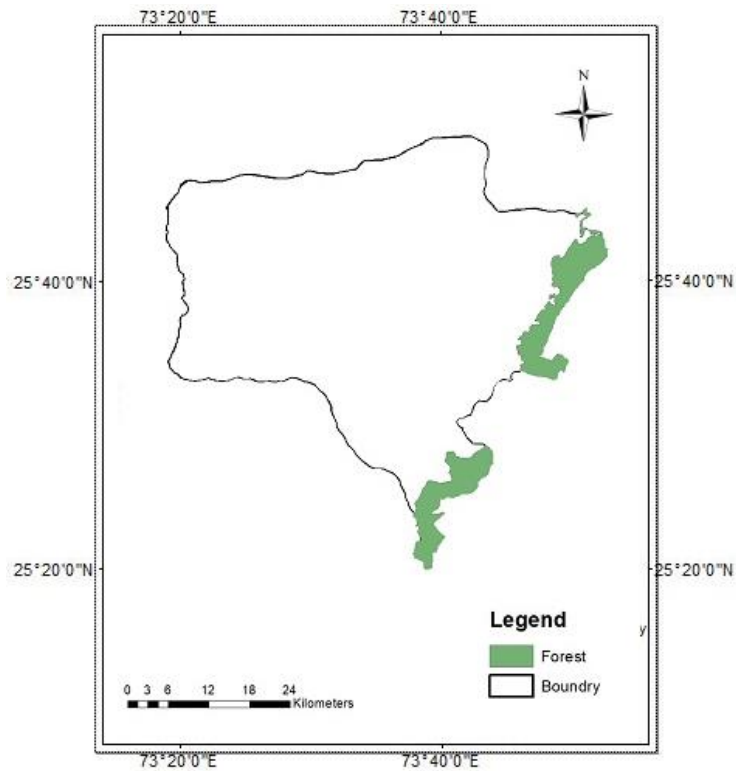


Figure 2: Forest area Cover in Bandi Watershed

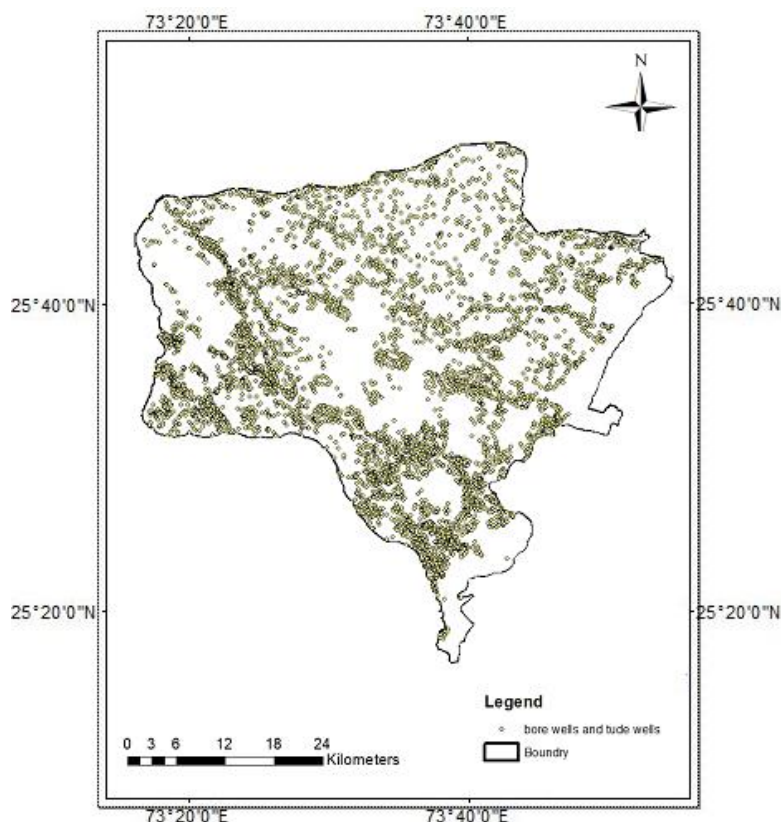


Figure 3: Groundwater resources in Bandi Watershed

3. Methodology

The study area i.e. a part of Bandi watershed was divided into 5 sub-watersheds for Morphometric analysis. The main watershed and sub watersheds were delineated using the toposheet from the survey of India in GIS environment. For digitization of the drainage pattern of the watershed and sub-watersheds, ArcGIS 10.5.5 was used and all the fundamental parameters like perimeter, area, basin length, stream length and number of streams were extracted from the drainage map. The morphometric parameters were computed using the formulae given by (Horton, 1945), (Schumm, 1956) and (Miller, 1953). Several other morphometric parameters viz. circularity ratio, bifurcation ratio, stream order, elongation ratio, drainage frequency, stream length, drainage density and compactness constants were calculated using the formulae mentioned in Table 1. Rank was provided to each sub watershed based on these parameters. At last the compound parameter value of all sub-watersheds was computed and the sub watershed having the least compound parameter value was given the highest priority. The detailed procedure adopted in this study is explained in the methodology flow chart (Figure 4).

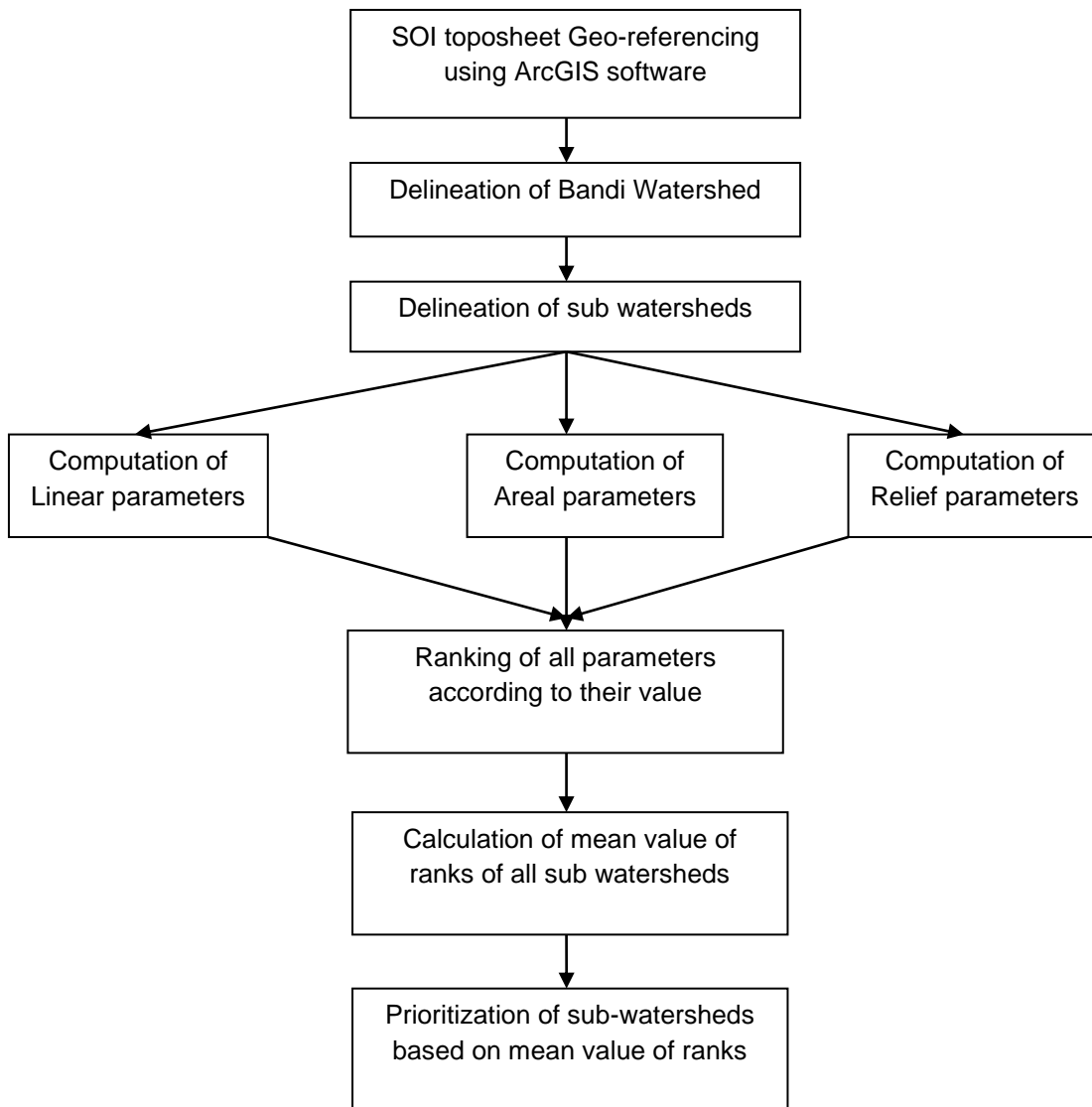


Figure 4: Methodology flow chart

Table 1: Formula for computation of Morphometric parameters

Morphometric Parameters	Formula	Reference
Stream order	Hierarchical rank	Strahler (1964)
Stream length (L _u)	Length of the stream	Horton (1945)
Mean stream length (L _{sm})	$L_{sm} = L_u / N_u$ where L _u = Total stream length of order 'u' N _u = Total number of stream segments of order 'u'	Strahler (1964)
Stream length ratio (R _l)	$R_l = L_u / L_{u-1}$ where L _u = Total stream length of order 'u' L _{u-1} = The total stream length of its next lower order	Horton (1945)
Bifurcation ratio (R _b)	$R_b = N_u / N_{u+1}$ where N _u = Total no. of stream segments of order 'u' N _{u+1} = Number of segments of the next higher order	Schumm (1956)

Drainage density (D_d)	where	$D_d = L_u / A$ D_d = drainage density L_u = total stream length of all orders A = area of the basin(km^2)	Horton (1945)
Stream frequency (F_s)	where	$F_s = N_u / A$ F_s = stream frequency N_u = total number of streams of streams of all orders A = area of the basin, km^2	Horton (1945)
Circulatory ratio (R_c)	where	$R_c = 4 * \pi * A / P^2$ R_c = circularity ratio π = π value i.e., 3.141 A = area of the basin, km^2 P^2 = square of the perimeter, km	Miller (1953)
Elongation ratio (R_e)	where	$R_e = (4 * A / \pi)^{0.5} / L_b$ R_e = elongation ratio A = area of the basin, km^2 π = π value i.e., 3.141 L_b = basin length, m	Miller (1953)
Form factor (F_f)	where,	$F_f = A / L_b^2$ F_f = form factor A = area of the basin, km^2 L_b = basin length	Schumm (1956)
Drainage texture (T)	where	$T = N_u / P$ N_u = total no. of streams of all orders P = basin perimeter, km	Horton (1945)
Compactness constant (C_c)	where	$C_c = 0.2821 P / A^{0.5}$ C_c = Compactness Ratio A = Area of the basin , km^2 P = basin perimeter, km	Horton (1945)

4. Results and Discussion

As mentioned in the methodology section, the Bandi watershed was divided into five sub-watersheds named as SWS-1 to SWS-5. It was found from the analysis that the drainage pattern is irregular in all the sub watersheds.

Linear aspects

Stream Length (L_u): The stream length was calculated using Horton’s law (Horton, 1945), for all five sub-watersheds. Usually, the total length of all the stream segments decreases as the stream order increase (Table 2). Sub-watershed SWS-2, SWS-3 and SWS-4 follows Horton’s law, but SWS-1 and SWS-5 has variation in stream segments. This might have happened due to moderately steep slopes, and lithological variations.

Stream Length ratio (R_l): According to Horton’s law of stream length, the mean stream length segments of each of the successive orders of a basin tends to approximate a direct geometric series with stream length increasing towards higher order of streams. All the five Sub-watersheds SWS-1 to SWS-5 has irregular pattern from one order to another order indicating the late geomorphic development.

Stream order (U): The Bandi river is a long River having many streams and this river is a 6th order stream covering an area of 2162.7 km^2 . The Bandi River is further divided into Sub-watersheds SWS-1, SWS-2, SWS-3, SWS-4, and SWS-5 covering an area of 115.427 km^2 , 106.704 km^2 , 160.153 km^2 , 264.422 km^2 and 98.643 km^2 respectively. The SWS-1 is having 6th order streams while the SWS-2, SWS-3, SWS-4, and SWS-5 are 5th order streams. Geomorphologic pattern for Bandi Basin is observed as dendritic to semi-dendritic pattern that exhibits homogeneous underlain material.

Stream frequency (F_s): Mostly low stream frequency indicates less slope and high permeability of the subsurface material, which may result in less runoff. Whereas high frequency indicates high slope and low permeability of subsurface material, which may result in more runoff. Sub-watersheds SWS-1, SWS-2, SWS-3 and SWS-5 has high stream frequency which shows that there is less slope, high permeability and less runoff, whereas SWS-4 has less frequency which shows that there is high slope, less permeability and more runoff. These result shows that this area has more dense forest.

Table 2: Stream analysis

Sub-watersheds	Stream numbers in different orders						Order wise total stream lengths (km)						Stream length ratio				
	1	2	3	4	5	6	1	2	3	4	5	6	2/1	3/2	4/3	5/4	6/5
SWS-1	20 1	3 9	17	7	1	1	167.69	51.1 7	29.3 4	36.7 4	1.26	3.92	0.31	0.57	1.25	0.03	3.10
SWS-2	0	0	0	0	0	0	86.44	45.6 6	33.9 8	19.6 4	5.15	0.00	0.53	0.74	0.58	0.26	0.00
SWS-3	13 3	4 0	14	4	2	0	129.87	65.2 8	25.9 7	19.4 0	17.76	0.00	0.50	0.40	0.75	0.92	0.00
SWS-4	15 6	5 1	27	9	1	0	162.28	77.0 2	63.4 4	50.5 8	3.84	0.00	0.47	0.82	0.80	0.08	0.00
SWS-5	10 4	2 7	19	11	1	0	87.25	21.6 8	16.6 2	26.2 0	2.92	0.00	0.25	0.77	1.58	0.11	0.00

Dimensionless factors

Circularity Ratio (R_e): The high, medium and low value of circularity ratio usually indicates young, mature and old stage of basin respectively. Values close to 0 indicates elongated basin and values close to 1 indicates circular basin. All the sub-watersheds have circularity ratio values ranging from 0.32 to 0.7 which indicated that all basins come under young to medium stage (Table 3). It was also observed that SWS-1 and SWS-3 are more elongated than SWS-2, SWS-4 and SWS-5. Based on these results, it can be assumed that the SWS-2, SWS-4 and SWS-5 have more diversity of slope, less permeable subsoil and high runoff.

Form Factor (F_f): All sub-watersheds have form factor varies from 0.12 to 0.69. This parameter defines basin shape and its value always varies from 0 to 1. Its indication is almost same as Circularity ratio but has different parameter of analysis. So values indicate that SWS-4 is more circular than others which has highest value 0.685. Flood flow is difficult to manage in circular shape basin than elongated shape basin.

Elongation Ratio (R_e): Elongation ratio value usually varies from 0 to 1 and it indicates the shape of the basin. Depending on the elongation ratio, the sub watersheds can be classified as elongated (<0.7), Oval (0.8 - 0.9) and circular (>0.9). Elongation ratio of all sub-watersheds varies from 0.4 to 0.94, in which SWS-4 has value 0.934 indicate circular shape basin, and all others has value less than 0.7 indicates elongated shaped basins.

Table 3: Morphometric parameters of sub watersheds Bandi watershed

Sub-watersheds	Area (Km ²)	Stream frequency (F_s) (km/km ²)	Basin Length (Km)	Form Factor (F_f)	Elongation Ratio (R_e)	Circularity Ratio (R_c)	Compactness constant (C_c)
SWS-1	115.427	2.304	18.416	0.340	0.658	0.321	1.764
SWS-2	106.704	1.415	29.090	0.126	0.401	0.603	1.288
SWS-3	160.153	1.205	27.813	0.207	0.513	0.323	1.758
SWS-4	264.422	0.923	19.648	0.685	0.934	0.594	1.298
SWS-5	98.6431	1.642	20.160	0.243	0.556	0.527	1.377

Measurement of intensity of dissection

Drainage density (D_d): Drainage density indicates how loosely the channels are spaced in the watershed/sub-watersheds. It is a ratio between total length of streams and total area of the basin (Horton, 1945). It also gives physiographic classifications, runoff potential, land cover, rock type, and climate and basin shape. Drainage density can be characterized as low (<2km⁻¹), moderate (2-4km⁻¹), high (4-6km⁻¹) and very high. All Sub-watersheds has drainage density varies from 1.35 to 2.52 (Table 4). SWS-1 has D_d (2.513km⁻¹) which indicates moderate and other sub-watersheds has D_d less than 2. As per the analysis, it can be determined that all the watersheds had relatively low Drainage density which indicates that subsoil material of all sub-watersheds is highly permeable, having good vegetation cover and low slope because of that runoff is less and soil has coarse drainage texture which improves infiltration.

On the basis of all these parameters, ranks are given to all watersheds from 1 to 5. Then a compound parameter is computed taking the average of the ranks for prioritization shown in Table 5. The Sub-watershed SWS-1 with compound parameter value 1.875 was given the highest priority followed by SWS-5. Basin with highest priority shows greater degree of erosion and becomes important unit for soil conservation measures. The prioritized map of the sub watersheds are represented in Figure 5.

Table 4: Values of Perimeter, drainage density, texture and bifurcation ratios

Sub-watersheds	Perimeter	Drainage Density	Drainage Texture (T)	Bifurcation ratios					Mean R _b
				R _{b1}	R _{b2}	R _{b3}	R _{b4}	R _{b5}	
SWS-1	67.163	2.513	3.960	5.153	2.294	2.429	7	1	3.575
SWS-2	47.170	1.788	3.201	3.413	1.933	2.143	7	0	2.898
SWS-3	78.883	1.612	2.446	3.325	2.857	3.500	2	0	2.336
SWS-4	74.801	1.350	3.261	3.058	1.889	3.000	9	0	3.389
SWS-5	48.491	1.567	3.340	3.851	1.421	1.727	11	0	3.600

Table 5: Estimation of compound parameters of Sub watersheds

Sub- watersheds	R _b	D _d	F _s	T	F _f	R _c	C _c	R _e	Compound parameter	Final priority
SWS-1	2	1	1	1	2	5	1	2	1.875	1
SWS-2	4	2	3	4	5	1	5	5	3.625	4
SWS-3	5	3	4	5	4	4	2	4	3.875	5
SWS-4	3	5	5	3	1	2	4	1	3	3
SWS-5	1	4	2	2	3	3	3	3	2.625	2

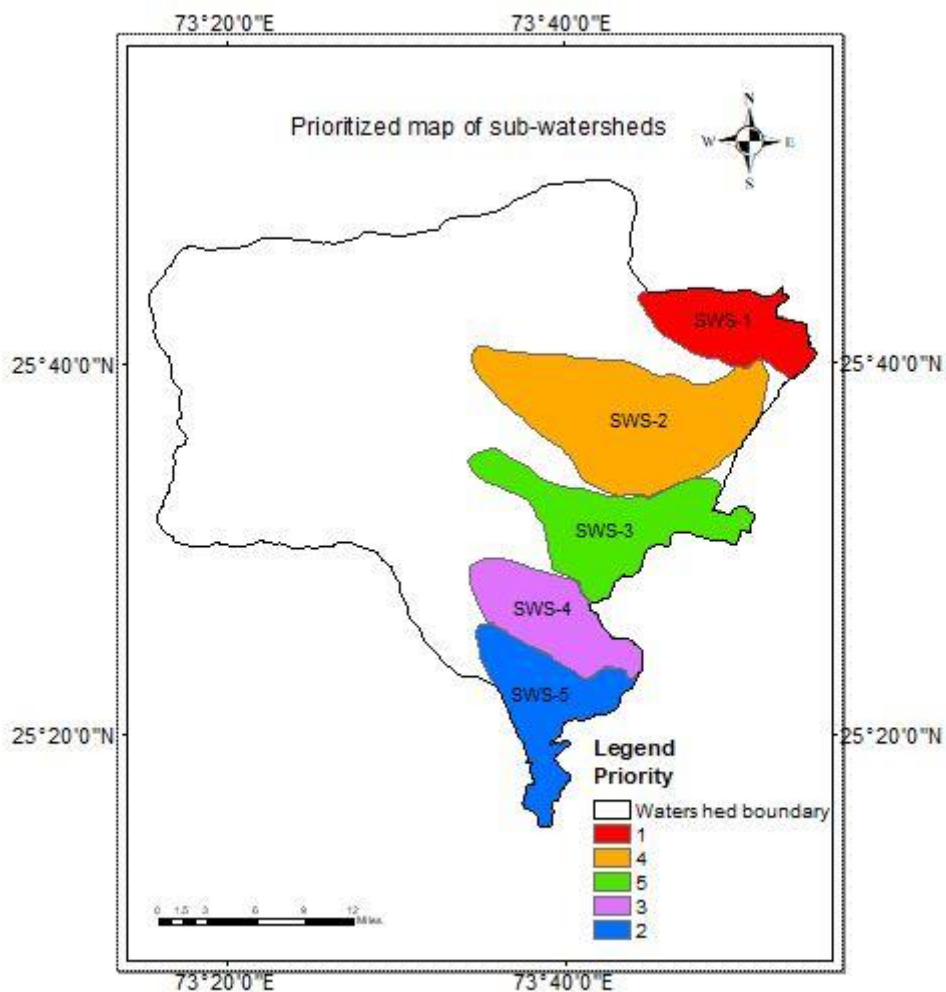


Figure 5: Prioritization map of Sub Watershed

5. Conclusion

Management of water resources is given utmost importance now days; hence study of prioritization of watersheds is an important aspect of planning for conservation and management of natural resources. The present study demonstrates the applicability of GIS techniques for prioritization of watershed based on Morphometric analysis which helps in management of water resources. For region like Pali, water management is most important because it was found that most of the underground water of these areas was exploited by bore wells or tube wells. So, analysis of different Morphometric parameters like drainage density, elongation ratio, stream length, stream frequency, land use etc. can help in decision making process for water resource management. From the results of prioritization of sub-watersheds, it can be determined that the sub-watersheds SWS-1 and SWS-5 should be given immediate attention to reduce soil erosion and sedimentation in these sub watersheds.

References

- Ahmed, F. and Rao, K.S. 2015. Prioritization of Sub-watersheds based on Morphometric Analysis using Remote Sensing and Geographic Information System Techniques. *International Journal of Remote Sensing and GIS*, 4(2), pp. 51-65.
- Chopra, R., Dhiman, R., and Sharma, P.K. 2005. Morphometric analysis of sub-watersheds in Gurdaspur District, Punjab using Remote Sensing and GIS techniques. *Journal of Indian Society of Remote Sensing*, 33(4), pp. 531-539.

Horton, R.E. 1945. Erosional development of streams and their drainage basins; Hydrological approach to quantitative morphology. *Geological Society of American Bulletin*, 56, pp. 275-370.

Khan, M. A., Gupta V.P., and Moharana P.C. 2001. Watershed prioritization using remote sensing and geographical information system: a case study from Guhiya, India. *Journal of Arid Environments*, 49, pp. 465-475.

Miller, V.C. 1953. A quantitative geomorphic study of drainage basin characteristics in the Clinch Mountain area. *Technical report-3*, Department of Geology, Columbia University.

Mishra. S.S., and Nagarajan, R. 2010. Morphometric analysis and prioritization of sub-watersheds using GIS and Remote Sensing techniques: a case study of Odisha, India. *International Journal of Geomatics and Geosciences*, 1(3), pp. 501-510.

Mundetia, N. 2018. Morphometric assessment and sub-watershed prioritization of Khari River basin in semi-arid region of Rajasthan, India. *Arabian Journal of Geosciences*, 11(18), pp. 530.

Nag, S.K. 1998. Morphometric analysis using remote sensing techniques in the Chaka sub-basin, Purulia district, West Bengal. *Journal of Indian Society of Remote Sensing*, 26(1-2), pp. 69-76.

Nookaratnam, K., Srivastava, Y.K., Venkateswarao, V., Amminedu, E. and Murthy, K.S.R. 2005. Check dam positioning by prioritization of micro-watersheds using SYI model and morphometric analysis – Remote sensing and GIS perspective. *Journal of the Indian Society of Remote Sensing*, 33(1), pp. 25-28.

Schumm, S.A. 1956. Evolution of drainage systems and slopes in Badlands at Perth Amboy, New Jersey. *Geological Society of America Bulletin*, 67, pp. 597-646.

Shrimali, S.S., Aggarwal S.P., and Samra, J.S. 2001. Prioritizing erosion-prone areas in hills using remote sensing and GIS – a case study of the Sukhna Lake catchment, Northern India. *Journal of Agricultural engineering*, 3(1), pp. 54-60.

Srinivasa, V.S., Govindaonah, S. and Home Gowda, H., 2004. Morphometric analysis of sub-watersheds in the Pawagada area of Tumkur district South India using remote sensing and GIS techniques. *Journal of Indian Society of Remote Sensing*, 32(4), pp. 351-362.

Strahler, A N. 1964. Quantitative geomorphology of drainage basins and channel networks. Section 4-II, In: *Handbook of Applied Hydrology* (Ed.: VT Chow). McGraw-Hill, pp. 4-39.

Thakkar, A.K. and Dhiman, S.D. 2007. Morphometric analysis and prioritization on miniwatersheds in Mohr watershed, Gujarat using remote sensing and GIS techniques. *Journal of Indian Society of Remote Sensing*, 35(4), pp. 313-321.

Research Article

Usage of Geographic Information System for Management of Soil Fertility, Egypt

Ganzour Shimaa, K.¹, Shendi, M. M.², Abdallah, A. E. M.¹ and Ismail, M.¹

¹Soils, Water and Environment Research Institute (SWERI), Agriculture Research Center (ARC), Egypt

²Soils and Water Department, Faculty of Agriculture, Fayoum University, Egypt

Correspondence should be addressed to Ganzour Shimaa K., sh.ganzour82@gmail.com

Publication Date: 9 July 2020

DOI: <https://doi.org/10.23953/cloud.ijarsg.473>

Copyright © 2020 Ganzour Shimaa K., Shendi M. M., Abdallah A. E. M. and Ismail M. This is an open access article distributed under the **Creative Commons Attribution License**, which permits unrestricted use, distribution, and reproduction in any medium, provided the original work is properly cited.

Abstract The current work was implemented to introduce an exclusive description for fertilization of an area equivalent to 50459.04 hectare situated along El Bahria Oasis Road – Giza Governorate, Egypt. GIS and GPS techniques were implicated in this study. Soil survey was carried out where the main physical, chemical properties and fertility parameters were engaged. The studied area was classified into two orders; Aridisols and Entisols. Geographic database for the soil properties and nutrients under study were built up and digital maps were produced. Land evaluation was done according to Storie & Sys and others; Land capability of the studied area showed four classes namely; II, III, IV and V with respect of storie). The land suitability for some crops (winter crops, summer crops and orchard trees) were appraised for the area under investigation and exported to GIS to be displayed in digital maps. Taking into account the contents of the nutrients present in soil the Fertilizer requirements for suitable crops were estimated; spatial analyst tools in Arc/GIS were used to create digital maps for the requirements of key figures nutrients (N, P, K) calculated in kg /hectare; The resulted map for fertilizers needs could be considered of enormous potential for precision farming application.

Keywords *Soil nutrients status; land capability and suitability; crop fertilizer requirements; fertilization maps; Arc/GIS technical*

1. Introduction

Global demand for food is tremendously rising due to higher population growth rate and the developing countries would share the highest percentage of such demand. Therefore, they should swiftly shift from conventional farming to precision one even at the rural districts and land reclamation; in order to boost the cultivation production. Land evaluation provides essential information on land resource, landform, land use, vegetation, climate and soil properties for a defined area. Concepts, definitions and case studies of land evaluation can be found in numerous publications such as (Storie, 1932 and 1978; Sys and Verheye, 1978 and Sys, *et al.*, 1991 and 1993). Land capability classification: USDA, (1973) has provided specific guidelines for land capability classification. This system has been adopted to include eight classes of land designated by Roman numerals. The risks of soil damage or limitations in use become progressively from class I to VIII. Capability grouping of soils is designed 1)

to help landowners and others to use and interpret the soil maps; 2) to introduce users to the details of the soil map itself and 3) to make possible broad generalizations based on soil potentialities, limitations in use and management problems. The capability classification provides three major categories of soil groupings: I. capability unit, II. capability subclass and III. Capability class according to USDA, (1961 and 2015) and Office of Environment and Heritage, (2012). The third and broadest category in the capability classification places all soils in eight capability classes. Tideman, (1990) confirmed that land capability is governed by the different land attributes such as types of soil "depth and texture, underlying geology, topography, hydrology... etc." land has a limited resource and with increasing population the demands for land become more competitive. Any given area of land can have a multitude of potential uses and all may need to be considered in planning and management of land resources. As for land suitability classification; Beek and Bennema, (1972) stated that it is a function of crop requirements and land characteristics *i.e.*, it is a measure of how well qualities of land unit match the requirements of a particular form of land use (FAO, 1976 and Sys *et al.*, 1991 & 1993). Suitability analysis can answer the question (what is to grow where?), in order to define suitability of an area for a specific practice, several criteria need to be evaluated (Belka, 2005). Depending on the land use limitations FAO, (1976) classified land suitability into two orders and 4 classes. Land suitability orders indicate whether land is assessed as suitable or not suitable for the use under consideration; Order S suitable "land of which having sustained use and expected to yield benefits which justify inputs, without unacceptable risk of damage to land resources", Order N suitable "land of which have qualities that appear to rule out sustained use". Nonetheless, the 4 classes are class; S1 "highly suitable", class S2 "moderately suitable", class S3 "marginally suitable", class N1 "not suitable" and class N2 "permanently not suitable". Evaluation of land capability for reclamation an area requires data include, chemical and/or physical soil properties and topographic level. One of the sustainable agricultural indicator is to cultivate crops that physically suitable for the soils. Land suitability analysis for crops is a prerequisite to achieve optimum utilization of available land resources for sustainable agricultural production.

Combination of GIS, geospatial mapping and RS technologies is a very powerful tool to achieve such task. Moreover, it helps in building up geographical database, in form of digital maps, for plant nutrients needed for relevant crops. Thereafter, appraisal the actual amounts of various fertilizers needed for the yields would be grown therein; taking into consideration the nutrient levels in soils, the grown plant needs and soil characteristics. Such specific digital maps can rationalize the consumption of the mineral fertilizers used. Egypt pays great attention to the development of its agricultural resources, either through the land reclamation or through maximizing the productivity of soil unit. The current study area is a part of the future promising governmental land reclamation and for developing modern rural districts to interact with the state development plan the current work was accomplished. The ultimate goal of this study is mainly to contribute in achieving the strategic objectives of such plan. In more specific words, this work aims to achieve the following objectives:

- To execute soil survey for an area suitable for agricultural development of Egypt being incorporated in land reclamation plan.
- To build up a geographic soil database for the main soil physical, chemical properties and nutrient contents of study area and depicting digital maps for the different soil characteristics and nutrients contents.
- To perform the land capability classification and land suitability for some crops.
- To establish a framework of geographical database for calculating fertilizer requirements based on soil characteristics and land use types.

2. Material and Methods

2.1. Study Area

The study area is virgin; it located at the Giza Governorate, Egypt and situated in the Western Desert, at El Baharia Oasis Road, It is in the extend of the south western direction of Wadi El Fargh. The area is bounded by the following four points:

- 1) 30° 38' 32.64" E 29° 51' 19.71" N
- 2) 30° 23' 18.22" E 29° 49' 23.30" N
- 3) 30° 40' 59.10" E 29° 40' 50.69" N
- 4) 30° 25' 10.88" E 29° 38' 37.38" N



Map (1): General location of the study area in Egypt

Map (2): Location map of the tested soil profiles

2.2. Soil survey execution for identifying the main soil physical, chemical properties and Nutrient status in the study area

A grid system was overlaid on the study area with a lag of 3 km distance to identify the location of the observation points. This was followed by a field work to collect representative soil samples; fifty seven soil profiles were allocated to represent the study area, Map (2). The soil profiles were dug to a depth of 150 cm unless opposed by bedrock or extremely hard layer. A total number of 178 soil samples were collected from the layers in order to determine the main soil physical and chemical characteristics as well as nutrients levels. The definite locations of the study soil profiles were recorded using GPS (*MODEL GARMYN*), which exported to ARC/GIS. A point map was created to represent the locations of the study soil profiles and used to create the geographic database for the different soil attributes.

2.2.1. Physical and chemical soil properties

- Particle size distribution was estimated using the International Pipette Method, described by Piper, (1950).
- Total calcium carbonate content was determined volumetrically using Scheibler's Calcimeter (Wright, 1939).
- Organic matter was determined using the Walkley and Black method (Jackson, 1967).
- Soil pH was measured in 1:2.5 soil water suspensions by using a pH meter (Van Reeuwijk, 1993).
- Soil paste extract was prepared for each soil sample, where determinations, Electrical conductivity (ECe), (CONDUCTANCE METER- YSI MODEL 35)&Soluble anions and cations (Jackson, 1967).
- The Gypsum content of soil was determined by precipitation with acetone according to Schoonover, (1952).
- Sodium Adsorption Ratio (SAR) a ratio for soil extracts used to express the relative activity of sodium ions in exchange reactions with soil according to Bower *et al.*, (1952). "SAR=Na/Ca+Mg /2"

- Exchangeable Sodium Percentage (ESP), it calculated by the formula according to Allison *et al.*, (1954).

$$\text{"ESP}=100(-0.0126+0.01475\text{SAR})1+(-0.0126+0.01475 \text{ SAR})"$$

2.2.2. Nutrient status

- Total nitrogen was determined by Kjeldahl methods using sodium hydroxide and boric acid according to Jackson, (1973).
- Total contents of macronutrients (P and K) in soil samples were extracted through digestion with perchloric-hydrofluoric acids (Hesse, 1971).
- Total phosphorus was determined using ascorbic acid method described by Houba *et al.* (1995). Where light absorbance was measured by Spectro-Photometer at 882 nm. (Model SPECTRONIC 21D).
- Total potassium was measured using Flame Spectro-Photometer (Model JENWAY PFP7).
- Available nitrogen was extracted from 5.0 g soil with 50 mL 2 M KCl (Page *et al.*, 1982), and determined using Kjeldahl methods (Jackson, 1973).
- Available phosphorus in soil was extracted using sodium bicarbonate solution, 0.5 M at pH 8.5 according to Olsen *et al.*, (1954) and determined used ascorbic acid (Van Reeuwijk, 1993). Absorbance was detected using Spectro-Photometer at 882 nm. (Model SPECTRONIC 21D).
- Available potassium in soil was extracted using 1 N ammonium acetate solution" NH₄OAC "at pH 7 according to Page *et al.*, (1982) and determined using flame spectrophotometer (Model JENWAY PFP7).
- Available Fe, Mn, Zn and Cu were extracted using DTPA method (Lindsay and Norvell, 1978). Available tested micronutrients were determined by Atomic Absorption Spectrophotometer, (Model GBC 932).

2.3. Coding soil database attributes and obtaining digital map

Results of physical, chemical properties and nutrient contents of the tested soils were entered as soil attributes for the soil profiles map. The attributes were coded using Arc/GIS (V., 10.3) as a geographic database. IDW Interpolation type was executed to produce the different soil properties and nutrient contents digital maps.

2.4. Soils classification

Soil classification is carried out according to USDA, (2014).

2.5. Land capability classification maps

Land capability was done using the rating suggested by Storie, (1932 and 1978) where, application in this equation: $Ci = \frac{A}{100} \times \frac{B}{100} \times \frac{C}{100} \times \frac{X1}{100} \times \frac{X2}{100} \times \frac{X3}{100} \times 100$

Where; Ci= Capability index, A= Soil depth, B= Texture, C= Slope, X1= Salinity, X2= CaCO₃ content and X3= Gypsum content.

2.6. Mapping land suitability for some crops

Land suitability was done using the rating tables suggested by Sys *et al.*, (1993) for alfalfa and sugar beet (winter crops); where, maize and sorghum (summer crops); olives and citrus (orchard trees).

Current and potential "land capability" and/ or "land suitability for crops" was calculated for the study area. The current "land capability" and/ or "land suitability for crops" indicates that "capability" and/ or "suitability for selected crops" of the area under the prevailing conditions of the soil. Whereas, the

potential "capability" and/ or "suitability" reflects the "land capability" and/ or "suitability for the same selected crops " of the area but after curbing and improving limiting factors such as salinity.

The evaluation is carried out by comparing the land characteristics with the limitation levels of the requirement tables. In addition, "capability index" and "suitability index for selected crops" were calculated using Stories equation and were added as open attributes table for the soil profiles point map. The attributes were coded using Arc/GIS as a geographic database for the profiles point map were used for interpolation (natural neighbor) activities then create symbolical/classified to produce capability and suitability digital map of different classes.

2.7. Framework of fertilizer requirements calculation

The fertilizer requirements of the study area were calculated using the geographical database through the capabilities of Arc/GIS then fertilizer requirement maps were produced according to the prevalent soils characteristics and the proposed land use type.

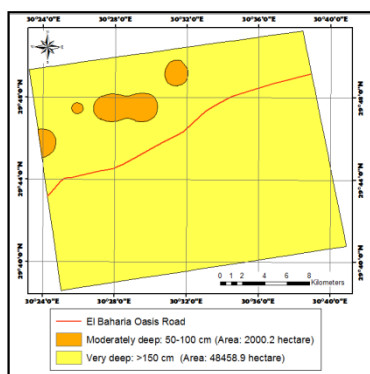
3. Results and Discussion

*All Maps represent physical, chemical and nutrient content for average surface and subsurface layers of the study area.

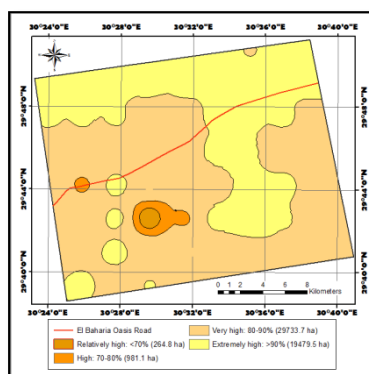
3.1. Descriptions of study soils physical and chemical properties

3.1.1. Soil depth: The study area is considered in terms of land use as virgin area with flat to undulating desert formations. Some of normal faults with strike slip movements seem to have affected the location. As indicated from Map (3), an area of approximately 2000 hectare there are moderately deep profiles, e.g., profiles 7, 13, 14, 15 and 21. According to the proposed limits after FAO (1990), while, 96.04% of the study area is considered very deep soils that could be suitable for either shallow and deep rooted cultivation.

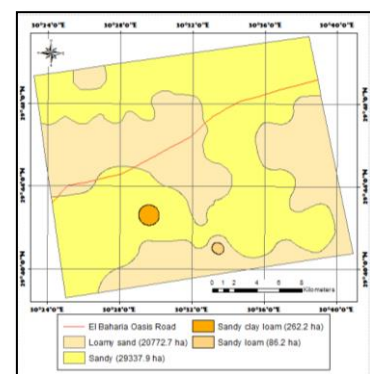
3.1.2. Soil texture: Soil texture is considered one of the most important soil criteria affecting soil behavior and land management, and it influences a number of physical and chemical soil characteristics. The obtained results showed that sand fractions dominated the soil particles in all the study soil samples, Map (4). Particle size distributions for the study soils are presented in Maps (5). The results revealed that most of the study area exhibits coarse sand texture, especially in the surface layers samples, and sometimes with medium to coarse textured as the texture varies between sand to sandy loam excluding profile 40 which possess sand clay loam due to the occurrence of shale deposits in that location. It appears that the soils under consideration may reflect multi- depositional regimes throughout soil profile layers. Desert pavement is commonly observed in the study area as high gravel contents were concentrated on the soil surface.



Map (3): Depth of soils in the study area



Map (4): Sand contents

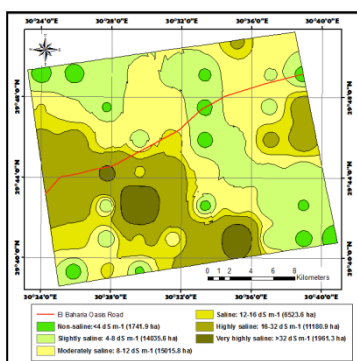


Map (5): Distribution pattern of textural classes

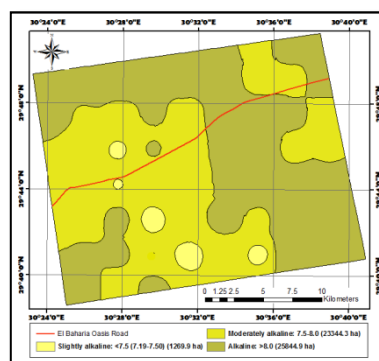
3.1.3. Soil salinity and alkalinity: Salinity is one of the main factors which limits the distribution of plant communities in their natural habitats and is causing increasingly severe agricultural problems. The study soils are characterized by different salinity levels ranged between non-saline (0.79 dS m^{-1}) to extremely highly saline (110.40 dS m^{-1}). The highly saline values may be related mostly to salinity inherited from dominating Eocene limestone. Whereas, the lowest EC values were more related to the permeable coarse textural soils. The distribution pattern of soil salinity in the study area, Map (6) shows that more than 31% of the area is non-saline, 1741.86 hectare to slightly saline soils, 14035.59 hectare. This confirms the potentiality of the study area for agriculture. The highly saline and very highly saline soils constitute only 22.16 % and 3.89 %, respectively.

3.1.4. Soil reaction- pH: Having the correct soil pH is crucial for the healthy plant growth as it affects the amount of nutrient available to plants (Nur *et al.*, 2014). Soil pH is considered as one of the most essential factors influencing plant uptake of trace element (Kabata-Pendias, 2001). The variation in soil pH usually is related to parent material, rainfall, topography and organic matter. From the obtained pH data in the current study, Map (7), the study soils are slightly alkaline to alkaline with pH values between 7.23 to 9.16. The alkaline pH values indicate that the soils are saturated with basic exchangeable cations besides the occurrence of free CaCO_3 in the soil. The most majority of the investigated soils have pH values in the range of 8.00 to 8.38.

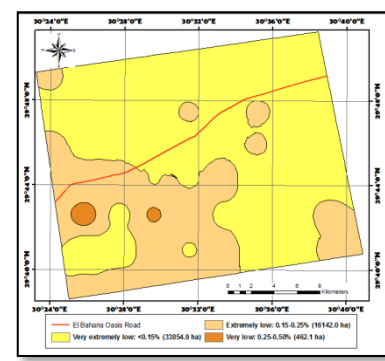
3.1.5. Organic matter content: Organic matter influences many soil characteristics including color, nutrient retaining or turnover and stability, holding capacity and soil aggregations (Tagwirg *et al.*, 1992). The data of OM% exhibited in, Map (8), show that the study area have general extremely low content of organic matter as the values are ranged from 0.02 to 0.34%. This is mainly could be related to the non-arable desert nature with no vegetation cover due to scarcity of precipitation and to the common coarse texture prevailing in the area.



Map (6): Soil salinity "ECe"



Map (7): Soil pH levels



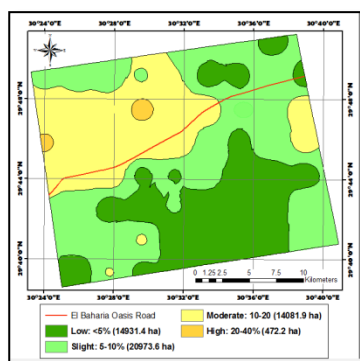
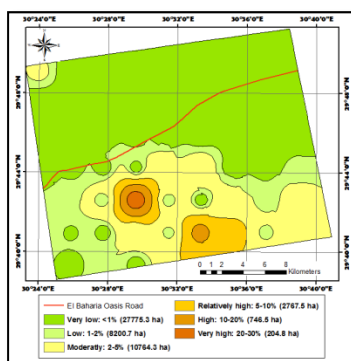
Map (8): Total organic matter

3.1.6. Calcium carbonate content: Soil CaCO_3 is an important soil criterion for agricultural cultivation of crops. This criterion affects soil moisture regime and availability of nutrients to plants, pH and organic matter stabilization (Schoeneberger *et al.*, 2011). Generally, calcium carbonate contents are mostly associated with coarse and moderately coarse textured soils. The data illustrated in Map (9) revealed that calcium carbonate values ranged between 0.17 to 31.39%; suggesting a possible relationship between CaCO_3 content and soil parent material in the area. It could be inferred from this Map, approx. 99% of the study area has low, slight and moderate CaCO_3 contents. There three categories cover 14931.36, 20973.60, 14081.85 hectare, respectively, whereas the highly calcareous soils (20-40 %) constitute only approx. 1% of the study area (472.23 hectare).

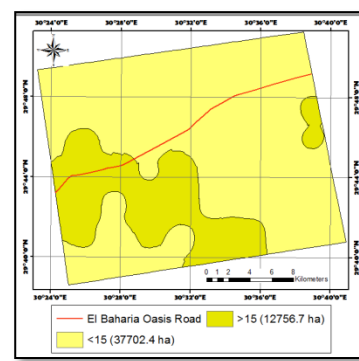
3.1.7. Gypsum content: Gypsum presence imparts to soils properties and affects soil development including soil morphology, water holding capacity, nutrient, water availability for plants, root growth and the standard concepts of soil texture and rapture resistance, (Susan *et al.*, 2014).

Gypsum accumulates in soil in a process similar to carbonate accumulation. However, since $\text{CaSO}_4 \cdot 2\text{H}_2\text{O}$ is more soluble than CaCO_3 and SO_4 is not as abundant as carbonate, gypsum deposits are less common and generally found in drier climates where very little leaching occurs (Lindsay, 1979). Soil gypsum contents in the study area are presented in Map (10). It ranged between < 0.01 to 33.11%. However, it could be classified into 6 classes: very low $<1\%$ (27775.20 hectare); low content 1-2% (8200.71 hectare); moderate content 2-5% (10764.27 hectare); relatively high content 5-10% (2767.50 hectare); high content 10-20% (746.46 hectare) and very high content 20-30% (204.84 hectare).

3.1.8. Exchangeable Sodium Percentage (ESP): The detrimental effect of sodium in soils has been widely investigated. It has been reported, for example that high ESP may enhance chemical dispersion of soils, which leads to crust formation and decreases infiltration rate (Robinson and Phillips, 2001). Soils ESP and SAR are positively related because soils solution cations and exchangeable cations are nearly always in equilibrium with each other (Singer and Munns, 1996). Dispersion problems may appear at a greater ESP or SAR. A limit beyond which the ESP is harmful to the soil structure is difficult to assess especially in sandy soils. In general, no problems are experienced in soils with $\text{ESP} < 15$ under arid climate. However, the ESP is not the only indicator of soil stability because the salt concentration of the soil solution also affects soil dispersion. The distribution pattern of the obtained ESP values is illustrated in Map (11). It is clear, approx. 74.7% of the study area, (37702.35 hectare), have low ESP values < 15 while the remaining parts possess higher ESP values. The highest values are associated with high salinity and dominance of soluble sodium in the soil paste extract.

Map (9): Total CaCO_3 contents

Map (10): Gypsum contents



Map (11): ESP

3.2. Nutrients contents in the study soils

3.2.1. Total macronutrients contents: Many investigators concluded that a soil system is a function of soil potentiality for essential plant nutrients, which was usually, related to the nature of soil parent material. This may result from combination of compositional differences between the physical and chemical conditions in soils (Officer *et al.*, 2006). The soil factors which influence the contents of the primary macronutrients (NPK) are mineralogical composition, soil texture, organic matter content, soil reaction, calcium carbonate and soil depth. The following discussion will be devoted to discuss the contents of NPK; the key players for the plant product.

a. Nitrogen; The obtained results are illustrated; the soils are very poor in total N content as it ranges between 30.5 to 140.0 mg kg^{-1} , apart from profile 40 that recorded 350 mg kg^{-1} , in top soil. The lowest total N value (0.02%) was recorded in a profile bottom, whereas the highest value (0.34%) was recorded in a profile surface.

b. Phosphorus; Values of total P differed widely in the study soils depending on the type of deposits. Total P contents mostly vary between 88.7 to 191.6 mg kg^{-1} , apart from the shale deposits in profile 40 that have 327.5, 356.2 and 342.3 mg kg^{-1} in its successive layers respectively. In general it seems that

marine and lacustrine deposits present in the study area played a substantial role in elevating total P content in the soils.

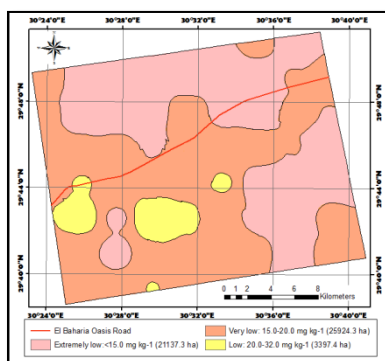
c. Potassium; Concerning the data of total K recorded in the different study soil, it ranged between 1160.2 to 9431.6 mg kg⁻¹ with no obvious distribution pattern trend through the profiles depth. The majority of study area soils possess total K values ranged between 3000-5000 mg kg⁻¹. Such higher value could be ascribed to the mineralogical composition. In this respect Ibrahim (2001) demonstrated that higher K value could be related to occurrence of feldspars arising from the recent lacustrine sediments.

3.2.2. Available macronutrients contents: Macronutrients status of the soils is an important aspect in context of sustainable agriculture production and it play a vital role in maintaining soil health and also productivity of crops. Regarding the available N, P and K data presented in the following is a brief description.

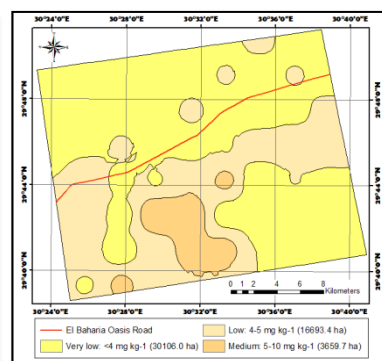
a. Nitrogen; Data of available N show that the available contents are generally low and do not exceed 18.8% of the total contents and it tends to decrease in coarse textured soils and organic matter. Data demonstrate that the distribution of available N range between 6.58 to 33.76 mg kg⁻¹. As clear from Map (12), the whole study area has low contents of available nitrogen that are grouped into one class, low (<40 mg kg⁻¹) and the maximum recorded value is 33.76 mg kg⁻¹.

b. Phosphorus; Data of the available P values, revealed that they did not exceed 3.8% of the total content, presumably due to either adsorption on the surface of CaCO₃ particles and/or precipitation due the reaction with soluble Ca that may available from the relatively high gypsum contents in the study area. This finding is consistent with the results reported by (Borhamy, 2001) as he indicated that the available content of P usually do not exceed 5% of the total content. The relatively high values of soil pH and adsorption of P on Mn and Fe oxides may also reduce P availability in the study area. As indicated in Map (13), the recorded values of available P in the study area ranged between 1.60 to 7.23 mg kg⁻¹ and allocated in different categories; low content (<5 mg kg⁻¹), and medium content (5-10 mg kg⁻¹) occupied 46799.37 and 3659.67 hectare, respectively.

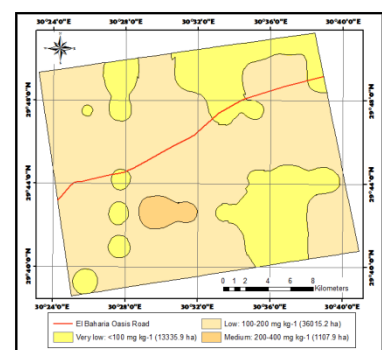
c. Potassium; Data in Map (14) show that the available K does not exceed 4.3% of the total K contents, the values ranged between 52.24 to 367.8 mg kg⁻¹. However, only limited area possess medium available K values range between 200-400 mg kg⁻¹ (2.19 % of total area), while the majority of study area possess low available K values less than 200 mg kg⁻¹ (97.80 % of total area).



Map (12): Available nitrogen.



Map (13): Available phosphorus.



Map (14): Available potassium.

3.2.3. Available micronutrients contents: There are many essential factors that may affect the contents of such micronutrients among them organic matters, soil pH, lime content, sand, silt and clay contents.

a. Iron; Fe is largely present in soils as insoluble Fe (III) oxides and its solubility greatly affected by the redox potential. The obtained data indicated that more than 99% of the study soils possess very low to low available Fe; ranged between 1.02 to 5.56 mg kg⁻¹.

b. Manganese; Available amounts of Mn ranged between 0.36 to 2.19 mg kg⁻¹. The lowest available Mn values are associated with the coarse texture higher content of CaCO₃ in similar results were obtained by (Ibrahim, 2001). However, the study area has low in available Mn content.

c. Zinc; Available Zn values in most of the study area are very low to low, these values ranged between 0.16 to 1.33 mg kg⁻¹. Approx. 78.66% of the study area has very low value <0.5 mg kg⁻¹.

d. Copper; The obtained data revealed that 97.85 % of the study soils possess very low to low amounts that range from 0.10 to 0.94 mg kg⁻¹. The lowest values attributed to the relatively coarse skeletal texture grade with low OM contents being of a very poor ability for Cu retention.

3.3. Soil classification

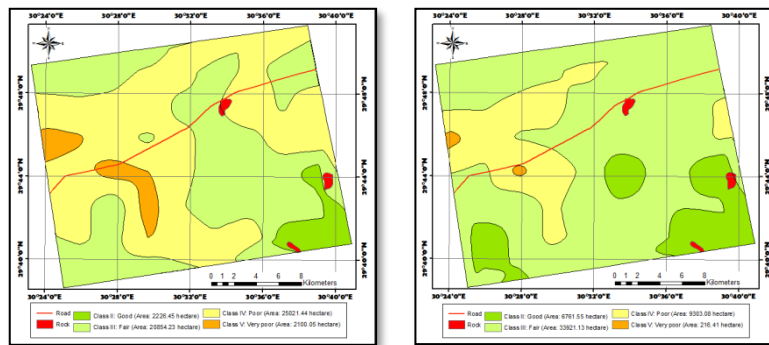
The purpose of soil classification is to provide basis for grouping and memorizing, to integrate knowledge of soils, to relate soils to each other and to their environments and to enable predictions of the soils behavior and response to anthropogenic intervention in its natural development. In the light of these results it could be concluded that the study area possesses two main soil Orders namely; Aridisols and Entisols covering 21168.49 and 29031.14 hectare; respectively, in addition, rock is covering 259.33 hectare.

3.4. Land capability assessment

3.4.1. Current land capability: Land capability assessment is considered one of the most important outputs of soil studies. Estimation of current land capability is illustrated in Map (15). The results revealed that the studied area possesses 48102.12 hectare of capable soils with classes II, III, IV, *i.e.* 95.33 % of the studied area, whereas the remaining areas are of very poor capability and/or of rocky in nature. The capability of the studied area varies from "good to very poor "according to some existing limiting factors as salinity, coarse texture, gravels content, calcium carbonate content, gypsum content and shallow soil depth. Part of these limiting factors could be corrected with time as salinity and gypsum while, texture, gravels content, calcium carbonate and shallow soil depth are considered economically not correctable. Results show that 2226.45 hectare, (4.41% of the evaluated soils) have good capability, Class II (without serious limiting factors). Fair capability class III is recorded in 20854.23 hectare, *i.e.* 41.33% of the studied area, with one limiting factor; texture in most cases and salinity or gravels in some soil profiles. Poor capability (class IV) is recorded in 25021.44 hectare, *i.e.* 49.59% of the studied area. These soils exhibit more limiting factors as; salinity, texture, gravels, soil depth and calcium carbonate content. Very poor capability Class V, 2100.05 hectare, constitutes approx. 4.16% of the studied area with more limiting factors as salinity, texture, gravels, depth and calcium carbonate.

3.4.2. Potential land capability: Land capability of the studied area is governed by different limiting factors. Some of these factors can be improved through appropriate soil management practices to enhance its land capability, Map (16). These management practices include leaching of salinity of some profiles where salinity leaching could drop soil salinity to 4 dS m⁻¹ as these of profiles having coarse fraction and very deep besides they are lacking the impact of higher gypsum or calcium carbonate aggregate in their layers. While other profiles are affected by gypsum and calcium

carbonate content so prediction for salt leaching is moderate. On the other hand, the presence of petrocalcic horizon sand layers with high gypsum content are expected to hinder salt leaching process in four profiles. By applying salt leaching management, the potential capability classes of the studied area are expected to be developed as Potential Class II, III, IV and V as presented in Map (16). Potential class II covers an area of approx. 6761.55 hectare (13.40% of the studied soils). This area is located in the eastern south and western south of the studied area. Potential class III covers an area of approx. 33921.13 hectare (67.22% of the studied area). Potential class IV covers an area of approx. 9303.08 (18.43% of the studied area). Very poorly potential class V covers a limited area of approx. 216.41 (0.43% of the studied area).



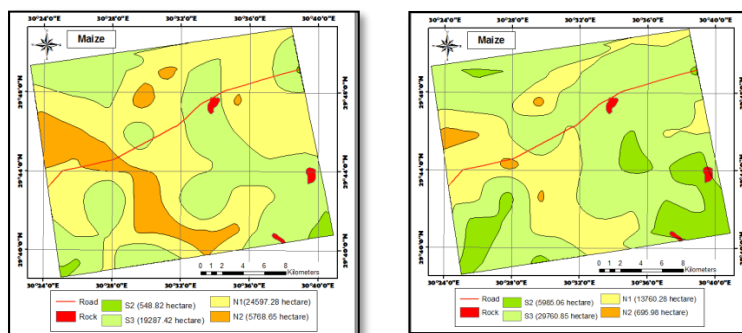
Maps (15, 16): Current and potential land capability classes in studied area

3.5. Land suitability for crops

Land suitability for crops is considered a very important issue in the reclamation of desert area and predicts the suitable land use in the area. Physical land suitability emphasizes the potential success of cultivating a specific crop in this area. Therefore, current and potential land suitability digital maps were produced for the studied soils. Current land suitability maps reflecting the soil suitability for selected crops under the current soil properties. While, the potential suitability is representing the crops suitability for the area after leaching salinity. Brief discussion of the tested crops is given below:

Maize (*Zea Mays L.*): Current suitability areas for maize is shown in Map (17), which indicate that, small area; approx. 548.82 hectare (1.09%) have moderate suitability due to the coarse texture limiting factor; approx. 19287.42 hectare (38.22%) have marginally suitable; limiting factors mostly; texture and salinity, approx. 24597.28 hectare (48.75%) are currently not suitable, approx. 5768.65 hectare (11.43%) are permanently not suitable due to presence of more limiting factors for agricultural use.

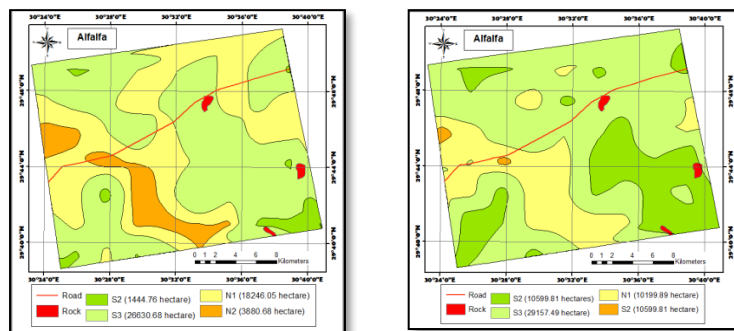
While, the potential suitability shown in Map (18); approx. 5985.06 hectare (11.86%) have moderately suitable, approx. 29760.85 hectare (58.98%) have marginally suitable, approx. 13760.28 hectare (27.27%) have currently not suitable and small area of approx. 695.98 hectare (1.38%) are permanently not suitable



Maps (17, 18): Current and Potential suitability classes for maize

Alfalfa (*Medicago Sativa L.*): The statistics manipulation of current suitability for Alfalfa, Map (19) indicate that approx. 1444.76 hectare (2.86%) are classified as moderately suitable S2, approx. 26630.68 hectare (52.78%) are classified as marginally suitable S3, approx. 18246.06 hectare (36.16%) are considered currently not suitable N1, approx. 3880.68 hectare (7.69%) are permanently not suitable N2. The observed limiting factors were mainly salinity and coarse texture.

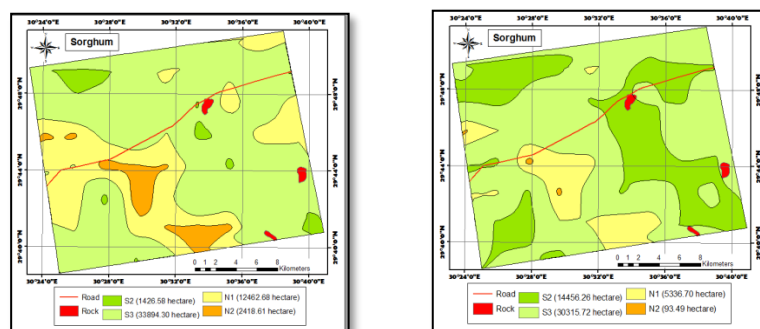
As shown in Map (20), the potential suitability shows that, moderately suitable class (S2) covers an area of approx. 10599.81 hectare, *i.e.* 21.01% of the studied area whereas, the marginally suitable areas (S3) constitute approx. 29157.49 hectare (57.78% of the studied area). On the other hand, the currently not suitable class (N1) covers approx. 10199.89 hectare, *i.e.* 20.21% of the tested soils and the permanently not suitable areas constitute small area of approx. 244.98 hectare (0.49 %).



Maps (19, 20): Current and potential suitability classes for alfalfa

Sorghum (*Sorghum Bicolor L.*): The current suitability for sorghum, Map (21) indicate that a small area of approx. 1426.58 hectare (2.83%) have moderate suitability with texture as a limiting factor, approx. 33894.30 hectare (67.17%) have marginally suitability (with salinity and/or texture as mostly limiting factors), approx. 12462.68 hectare (24.70%) are currently not suitable (with salinity and texture limiting factors), approx. 2418.61 hectare (4.79%) are permanently not suitable with more limiting factors.

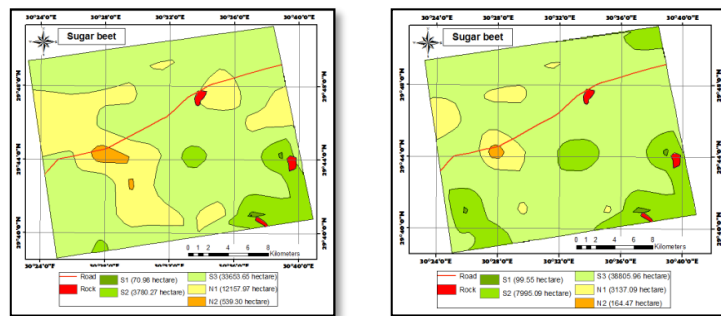
The potential suitability for sorghum, Map (22) indicate that approx. 14456.26 hectare (28.65 %) have moderately suitable class, approx. 30315.72 hectare (60.08%) have marginally suitable class, approx. 5336.70 hectare (10.58 %) are considered currently not suitable and limited area approx. 93.49 hectare (0.18 %) are considered permanently not suitable.



Maps (21, 22): Current and potential suitability classes for sorghum

Sugar beet (*Beta Vulgaris*): Distribution of current suitability is exhibited in, Map (23). A very limited area is approx. 70.98 hectare (0.14%) have highly suitable without limiting factor, approx. 3780.27 hectare (7.49%) have moderately suitable without limiting factor or salinity, the most majority of area approx. 33653.65 hectare (66.69%) have marginally suitable, approx. 12157.97 hectare (24.09%) is currently not suitable and small areas (approx. 539.30 hectare, 1.07%) have permanently not suitable with several limiting factors.

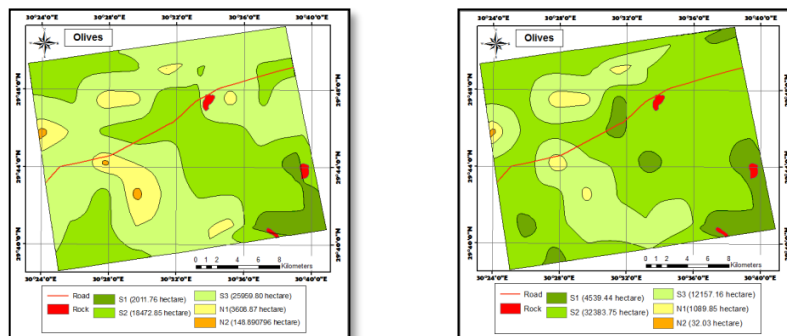
Potential suitability could be categorized into five classes, Map (24). Approx. 99.55 hectare (0.20%) have highly suitable, approx. 7995.09 hectare (15.84%) have moderately suitable one. However, the most majority of area approx. 38805.96 hectare (76.91%) have marginally suitable, approx. 3137.09 hectare (6.22%) have currently not suitable one and small area approx. 164.47 hectare (0.33%) are permanently not suitable.



Maps (23, 24): Current and potential suitability classes for sugar beet.

Olives (*Olea Europaea*): Results of current suitability for olive are presented in Map (25) which indicate that; 2011.76 hectare (3.99 % of the area) have highly suitable, 18472.85 hectare (36.61%) are moderately suitable due to texture or salinity limiting factors, 25959.80 hectare (51.45%) are marginally suitable (with limiting factors from texture and/or salinity), 3608.87 hectare (7.15%) are currently not suitable (with salinity and/or texture limiting factors;) and 148.89 hectare (0.30%) are permanently not suitable.

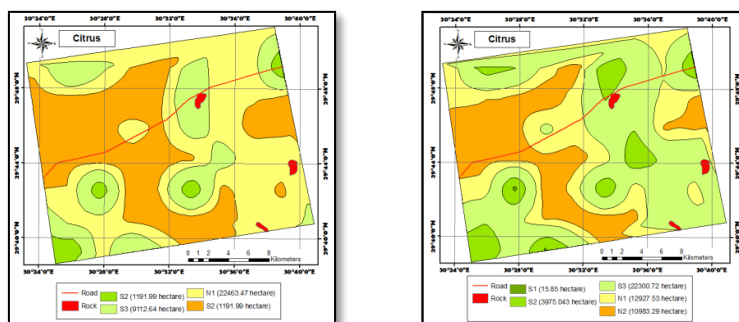
Potential suitability for olive is shown in Map (26) indicating that 4539.44 hectare have highly suitable class and the majority of the area, (32383.75 hectare) are classified as moderately suitable, 12157.16 hectare have marginally suitable class, 1089 hectare are currently not suitable and only approx. 32.03 hectare are permanently not suitable.



Maps (25, 26): Current and potential suitability classes for olives

Citrus (*Citrus Spp*): The spatial distribution of current suitability is illustrated in Map (27). Approx. 1191.99 hectare (2.36%) has moderately suitable. Approx. 9112.64 hectare (18.06%) have marginally suitable one and mostly salinity is the limiting factor. Nonetheless, approx. 22463.47 hectare (44.52%) are currently not suitable; approx. 17434.07 hectare (34.55%) are permanently not suitable due to the effect of salinity and CaCO_3 as limiting factors.

Potential suitability could be divided into four classes as shown in Map (28). Very small area approx. 15.85 hectare is of highly suitable, approx. 3975.04 hectare (7.88%) have moderately suitable one, approx. 22300.72 hectare (44.20%) are marginally suitable. However, approx. 12927.53 hectare (25.62%) has currently not suitable and areas approx. 10983.29 hectare (21.77%) are permanently not suitable for agricultural use.



Maps (27, 28): Current and potential suitability classes for citrus

3.6. GIS fertilizer requirements digital maps for the selected crops

The resulted available nutrients status maps (expressed in mg kg^{-1}) were used later for the calculation of fertilizer requirements for the proposed crops according to the recommended fertilizer requirements for each specific crop. This was done by simple subtract operation between the existing nutrients contents map and the recommended quantity of fertilizers to the proposed crops. The resulted fertilizers needs digital maps could be multiplied by simple conversion factors to have maps displaying the needed fertilizers in any commercial fertilizer forms.

3.6.1. Fertilization maps for some winter crops.

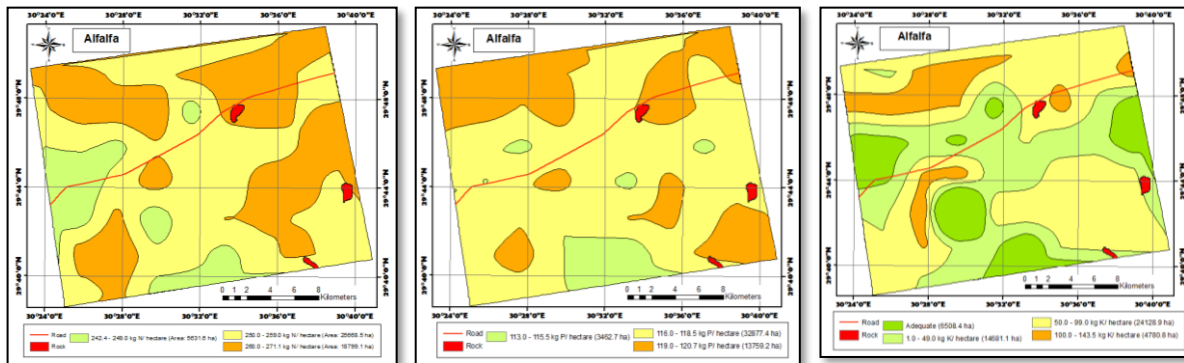
Alfalfa (*Medicago Sativa L.*):

➤ Blanket N fertilizer for alfalfa grown in the newly reclaimed soil is 285.60 kg N/hectare (ARC-Ministry of Agriculture-Egypt, brochure No.764). The N fertilization needs is displayed in Map (29). It indicates that approx. 5631.6, 25668.5 and 18799.1 hectare in need for N fertilization requirements equivalent to 242.4-249.0, 250.0-259.0 and 260-271.1 kg N/hectare, respectively; needed to be applied for one year to the studied soil .

➤ P fertilization, as super phosphate is added at a rate of 833 kg/hectare just prior cultivation starting then added at a rate of 357 kg/hectare every 4 months. In Map (30), more than 32877 hectare of the studied area is in a need approx. 116- 189.5 kg P/hectare, whereas approx. 3462.7 hectare show needs approx. 113-115.5 kg P/hectare. The recorded average needed for phosphorus fertilization reached to 117.6 kg P/hectare.

➤ K fertilizer is added at a rate of 238 kg/ hectare of potassium sulfate with land preparation before planting, then being added 119 kg/ hectare every 4 months. The distributions of potassium fertilization requirements in the studied area is exhibited in, Map (31). More than 6508 hectare of the studied soils

show adequate potassium contents for alfalfa requirements, whereas, approx. 14681.1, 24128.9 and 4780.8 hectare need potassium fertilization ranges from 1.0-49.0, 50.0-99.0 and 100.0-143.5 kg K/hectare, respectively.



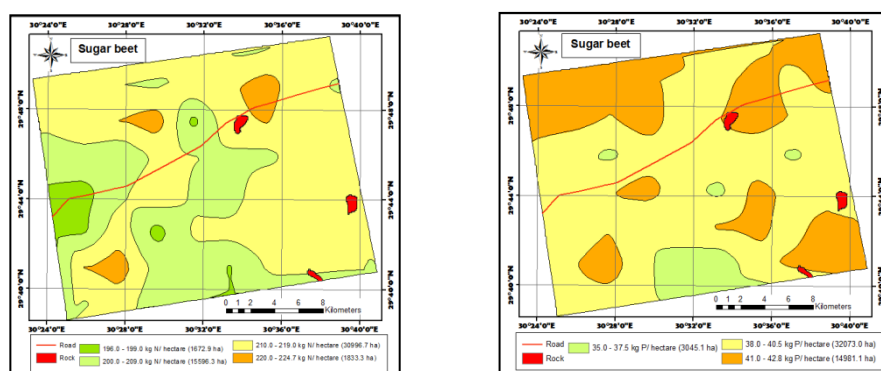
Maps (29, 30, 31): Nitrogen, phosphorus and potassium fertilizer requirements (kg N, P, K /hectare) for alfalfa.

Sugar beet (*Beta Vulgaris*)

➤ N fertilization is considered as one of the limiting factors for sugar beet crop. It needs approx. 714 kg/hectare of ammonium nitrate 33.5% in the reclaimed lands and sandy soils. Applying of N should not be delayed for 90 days of plant age as it causes the delay in the maturation of the crop and also reduces sugar (ARC- Ministry of Agriculture-Egypt, brochure No.696). As shown in Map (32), the distribution pattern of N fertilization needs is exhibited for the studied area. The maximum estimated value is 224.7 kg N/hectare, while the average value is 210.3 kg N/hectare. Approx. 15596.3 hectare of soils is in need to 200.0-209.0 kg N/hectare. Whereas, approx. 30996.7 hectare need fertilization with a rate ranged from 210.0-219.0 kg N/hectare.

➤ We should pay attention to P fertilization of the reclaimed land. The estimated need for this land is approx. 714 kg/hectare in the form of superphosphate (15.5%). The spatial distribution of the needed P fertilization is exhibited in Map (33). P fertilization map shows that the maximum needed P reached 42.8 kg P/hectare, whereas the average need for the whole studied area 39.7 kg P/hectare. Most of the studied area in needs to P fertilization 38.0-40.5 kg P/hectare (32073.0 hectare).

➤ K fertilization is recommended to be added at a rate of 238 kg/hectare of potassium sulfate (48%) during servicing or with the first batch of adding nitrogen fertilizer. However, the total studied soils show adequate potassium contents for sugar beet requirements; only just bio-fertility could be utilized.

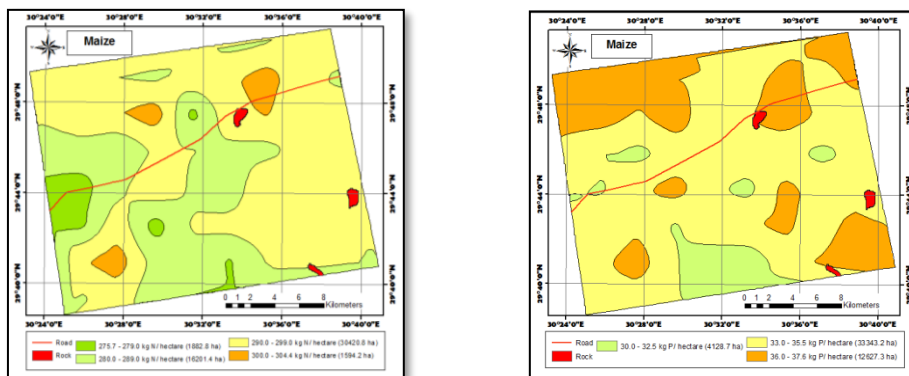


Maps (32, 33): Nitrogen and phosphorus fertilizer requirements (kg N, P, /hectare) for sugar beet

3.6.2. Fertilization maps for some summer crops.

Maize (*Zea Mays L.*)

- N fertilization needed is 952 kg/ hectare in the form of ammonium nitrate 33.5%. In three doses they should be applied the first at cultivation, the second after thinning and the third batch before the second irrigation (ARC- Ministry of Agriculture-Egypt, brochure No.962). The distribution pattern of N fertilization needs of the studied area is shown in Map (34). The maximum estimated value is 304.4 kg N/hectare, while the average value is 290.0 kg N/hectare. Approx. 1882.8 hectare of area is needed 275.7-279.0 kg N/hectare. While, approx. 30420.8 hectare need N fertilization at a rate ranged from 290.0-299.0 kg N/hectare.
- P fertilization in the form of super phosphate (P_2O_5 15%) is recommend to be added at a rate of 714 kg P/hectare before plowing. The spatial distribution of the needed P fertilization is confirmed in Map (35). P fertilization map show that the maximum needed P reached 37.6 kg P/hectare, whereas the average (66.6%) need for the whole studied area is 34.5 kg P/hectare. Most of the studied area (66.6 %) in need to P fertilization ranges 33.0-35.5 kg P/hectare.
- As for high-yield varieties or in the reclaimed land Addition of 238 kg potassium sulfate (48% K_2O) per hectare is recommended after thinning the plants. However, total studied area show adequate potassium contents for maize cultivation, only just bio-fertility could be utilized.

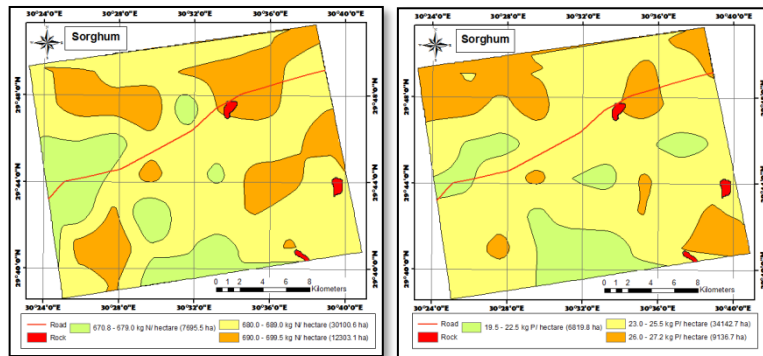


Maps (34, 35): Nitrogen and phosphorus fertilizer requirements (kg N, P, /hectare) for maize

Sorghum (*Sorghum Bicolor L.*)

- Sorghum needs 143 N-units/hectare in beginning of cultivation, to be added at the first irrigation, then application of 143 N-units/ hectare after the second irrigation. More 72 units of nitrogen would be added after each cut (ARC- Ministry of Agriculture-Egypt, brochure No.907). As for the organic fertilizers it is also recommended to add 48-72 m³/hectare composted organic manure with the land preparation. The calculated nitrogen fertilization need is illustrated in Map (36). Data indicate that the maximum fertilization need is 699.5 kg N/hectare (12303.1 hectare). Most of the studied area (60.1%) is in need to 680.0-689.0 kg N/hectare. The estimated average of nitrogen fertilization needs for sorghum if it would be cultivated in the studied area reached to 685.1 kg N/hectare.
- Recommended addition of P fertilization in the form of super phosphate is approx. 476 kg/hectare during land preparation for planting. As indicated in Map (37), in the studied area, approx. 34142.7 hectare (68.15%) needs approx. 23.0-25.5 kg P/hectare. The recorded average needed of phosphorus fertilization reached to 24.1 kg P/hectare.

➤ The recommended addition of potassium sulfate during the land preparation is a rate of 238 kg/hectare. The total studied soils show adequate amounts potassium for sorghum cultivation.



Maps (36, 37): Nitrogen and phosphorus fertilizer requirements (kg N, P, /hectare) for sorghum.

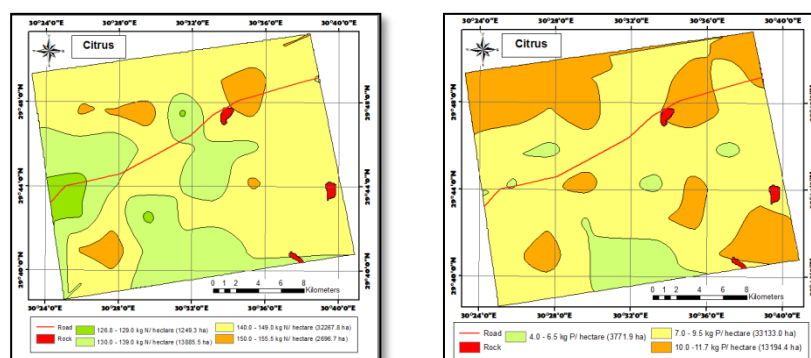
3.6.3. Fertilization maps for some orchard trees.

***Citrus (*Citrus Spp*)**: The following is a proposed program to fertilize citrus trees of age 1-3 years in the reclaimed lands (ARC- Ministry of Agriculture-Egypt, brochure No.366).

➤ Trees need N fertilization is 833 kg ammonium sulfate (20.5%) per hectare, for one year, where this amount is added through 21 dosages added from the second half of February and ending June. In addition, is recommending to be added 47.6-59.5 m² of manure per hectare. As Map (38), illustrates the distribution pattern of N fertilization needs for the studied soils. The maximum estimated value is 155.5 kg N/hectare for year, while the average value is 141.1 kg N/hectare. A few areas approx. 1249.3 hectare of soils is needed 126.8-129.0 kg N/hectare. Whereas most of studied soils, approx. 32267.8 hectare, need fertilization at a rate ranged from 140.0-149.0 kg N/hectare for year.

➤ P fertilization at a rate of 238 kg super phosphate (15.5%) per hectare is recommended. The spatial distribution of the needed P fertilization is illustrated in Map (39). P fertilization map show that the maximum needed P reached 11.7 kg P/hectare for one year, whereas the average need for the whole studied area 8.5 kg P/hectare. Most of the studied area (13194.4 hectare). in need to P fertilization ranges 7-9.5 kg P/hectare.

➤ Recommendation for K fertilization is adding 190 kg/ hectare of potassium sulfate per year divided into two batches, the first installment in March and the second in August. However, the total studied soils show adequate potassium contents for citrus cultivation; only just bio-fertility could be applied.



Maps (38, 39): Nitrogen and phosphorus fertilizer requirements (kg N, P, /hectare) for citrus

It is worthy to mention that digital maps for micronutrients fertilizer requirements to the selected crops could be produced. But, it should be bearing in mind that it is not advisable to correct deficiency of micronutrients dominating in sandy and calcareous soils through soil addition but through foliar application.

4. Conclusions

The current study concluded that: Incorporation of GIS methodology could be very helpful to produce accurate digital maps for the different soil characteristics, total and available nutrients status, land capability, land suitability for crops and the adequate fertilizer recommendation requirements for them. The resulted fertilizers needs maps are considered very potential for precision farming application. Therefore, it is recommended to apply such scientific methodology, depending on the most advanced recent technology, on the other new agricultural extension areas. Furthermore, in order to achieve much more benefit of the current work or similar one, it is advisable to monitor and update the available nutrients status for the tested point (that identified by GPS). This is suggested to be done twice a year before winter and summer cultivations to retrieve updated fertilization maps. This guide could be used by the decision makers for strategic fertilization plans.

References

- Allison, L., Richards, L., Reeve, R., Bernstem, L., Bower, A., Brown, J., Fireman, M., Hatcher, J., Hayward, H., Pearson, G. and Wilcox, L. 1954. Diagnosis and improvement of saline and alkali soils. United staff salinity laboratory staff. L.A. Richards (Editor). Agriculture Handbook: 60. U.S. Department of Agriculture.
- Beek, K.J. and Bennema. 1972. Land evaluation for agricultural, land use planning. An ecological methodology. pp: 61. (Memeograph). Dept. Soil Sci. and Geol., Agric. Univ., Wageningen, the Netherlands.
- Belka, K.M. 2005. Multi criteria analysis and GIS application in the selection of sustainable motorway corridor. Master's thesis submitted to Linkopings University Institutional for data vetenskap.
- Borhamy, S.E. 2001. Pedo-genetic aspects as related to soil fertility status at El-Fayoum. Egypt. Ph. D. Thesis. Fac. Agric. El-Fayoum, Cairo Univ., Egypt.
- Bower, C., Reitemeyer, R. and Fireman, M. 1952. Exchangeable cation analysis of saline and alkaline soils. Soil Sci., 73, pp.251-261.
- FAO. 1976. A framework for land evaluation. Soils Bulletin 32. Rome, Italy.
- FAO. 1990. Guidelines for Soil Description. 3rd (Ed.) Revised, Soil Resources, Management and Conservation Service Land and Water Development Division, Rome, Italy.
- Hesse, P.R. 1971. A Text book of Soil Chemical Analysis. John Murray Publ., William Clowes and Sons Limited, London, Beccels and Colchester.
- Houba, V.J., Van Der Lee, J.J. and Novozamsky, I. 1995. Soil and Plant Analysis. Part 5 B., 6th Ed., Dept. of Soil Sci. and Plant Nutrition, Wageningen Agricultural Univ.
- Ibrahim, S.E. 2001. Pedo- genetic aspects as related to soil fertility status at EL Fayoum, Egypt. Ph. D. Thesis, Fac. of Agric. El Fayoum, Cairo Univ., Egypt.
- Jackson, M.L. 1967. Soil chemical analysis. Prentic Hall, Ladia Private, LTD., New Delhi.

- Jackson, M.L. 1973. Soil chemical analysis. Prentice-Hall, Inc., Englewood Cliffs, New Jersey, U.S.A.
- Kabata-Pendias, A. 2001. Trace elements in soil and plants. 3rd (Ed). CRC Press, Boca Roton, FL. USA.
- Lindsay, W. 1979. Chemical equilibrium in soils. John Wiley and Sons, Inc. New York. p.449.
- Lindsay, W.L. and Norvell, W.A. 1978. Development of a DTPA soil test for zinc, iron, manganese, and copper. *J. Soil Sci. Soc. Amer.*, 42, pp.42-428.
- Nur, A., Ezrin, M. and Aimrun, W. 2014. Relationship between soil apparent electric conductivity and pH value of Jawa series in oil palm plantation. 2nd International Conference on Agricultural and Food Engineering. 2, pp.199-206.
- Office of Environment and Heritage. 2012. The land and soil capability assessment scheme second Approximator. Dep. of Premier and Cabinet NSW. www.environment.nsw.gov.au
- Officer, S; Tillman, R.; Palmer, A. and Whitton, J. 2006. Variability of clay mineralogy in two New Zealand steep-land top soils under pasture. *Geoderma*, 132, pp.13-28.
- Olsen, S.R., Cole, C.V., Watanable, F.S. and Dean, L.A. 1954. Estimation of available phosphorus in soils by extraction with sodium bicarbonate. U.S. Dept. Agric. Circular No. 939.
- Page, A.L., Miller, R.H. and Keeney, D.R. 1982. Methods of Soil Analysis. Part 2. Chemical and Microbiological Properties. 2nd (Ed.) Amer. Soc. of Agronomy. Madison, Wisconsin, USA.
- Piper, C.S. 1950. Soil and Plant Analysis. International Science Publisher, Inc., New York, USA.
- Robinson, D. and Phillips, C. 2001. Crust development in relation to vegetation and agricultural practice on erosion susceptible, dispersive clay soils from central and southern Italy. *Soil and Tillage Research*, 60, pp.1-9.
- Schoeneberger, P., Wysocki, D. and Benham, E. 2011. Field book for describing and sampling soils, Version 3.0. Natural Resources Conservation Service, National Soil Survey Center, Lincoln, NE.
- Schoonover, W. 1952. Examination of soils for alkali. University of California Extension Service, Berkeley, California (Mimeographed).
- Singer, M. and Munns, D. 1996. Soils: an introduction. 3rd ed. Prentice- Hall. Saddle River, NJ.
- Storie, R.E. 1932. An index for rating the agricultural values of soil. Bulletin 556, Berkeley: California Agricultural Experiment Station.
- Storie, R.E. 1978. Storie index soil rating (revised). Special Publication 3203, Division of Agricultural Science, University of California, Berkeley, CA.
- Susan, C., Juan, H. and Nelson, A. 2014. Gypsum soils their morphology, classification, function and land scaps. Chapter 4 Advances in Agronomy, 130.
- Sys, C. and Verheye, W. 1978. An Attempt to the Evaluation of Physical Land Characteristics for Irrigation According to the FAO Framework for Land Evaluation. International Training Center for Post Graduate Soil Scientists, Chent, Belgium, pp.66-78.

Sys, C., Van Ranst, E., Debaveye, J. and Beernaert, F. 1993. Land Evaluation Part III: Crop requirements. Agricultural Publication No. 7. GADC, Brussels, Belgium, pp.12-173.

Sys, C., Van Ranst, E. and Debaveye, J. 1991. Land Evaluation. Part 1: Principles in Land Evaluation and Crop Production Calculations; Part 2: Methods in Land Evaluation; Part 3: Crop Requirements (in press). Agricultural Publications no. 7, General Administration for Development Cooperation, Brussels.

Tagwira, F., Piha, M. and Mugwira, L. 1992. Effect of pH, phosphorus and organic matter contents on zinc availability and distribution in two Zimbabwean soils. *Commun. Soil Sci. Plant Anal.*, 23, pp.1485-1500.

Tideman, T.N. 1990. Integrating land value taxation with the internalization of spatial externalities. *Land Econ.* 66, pp.341-355.

USDA. 1961. Soil survey Stanton County, Kansas. Soil Conservation Service in Cooperation with Kansas Agricultural Experiment Station. Series 1958, pp.1-41.

USDA. 1973. Soil conservation service, land capability classification, Agriculture Handbook No. 210.

USDA. 2014. Keys to Soil Taxonomy. Soil Survey Staff, Natural Resources Conservation Service (NRCS). Twelfth Edition, 2014.

USDA. 2015. Soil study and land evaluation handbook. Natural resources conservation service. <https://websoilsurvey.sc.egov.usda.gov/App/HomePage.htm>

Van Reeuwijk, L.P. 1993. Procedures for soil analysis. CIP-Gegevens Koninklijke Bibliotheek, Den Haag: international soil reference and information centre. (Technical Paper/ International Soil Reference and Information Centre. ISSN 0923-3792: No.9) Trefw: Bodemkunde. ISRIC. Fourth Edition.

Wright, C. 1939. Soil Analysis. Thomas Murby Co., London.

Research Article

Effect of Landscape Changes on the Water Quality of Murchison Bay

Balaji Bhaskar Maruthi Sridhar^{1*} and Anthony Gidudu²

¹Department of Environmental and Interdisciplinary Sciences, Texas Southern University, Houston, Texas 77004, USA

²Department of Geomatics and Land Management, Makerere University, Kampala, Uganda

Correspondence should be addressed to Balaji Bhaskar Maruthi Sridhar, bhaskarm@tsu.edu

Publication Date: 22 July 2020

DOI: <https://doi.org/10.23953/cloud.ijarsg.474>

Copyright © 2020 Balaji Bhaskar Maruthi Sridhar and Anthony Gidudu. This is an open access article distributed under the **Creative Commons Attribution License**, which permits unrestricted use, distribution, and reproduction in any medium, provided the original work is properly cited.

Abstract The water quality in Murchison Bay of Lake Victoria, the Africa's largest fresh water lake, is on decline due to rapid urban sprawl, decrease in vegetative surface and increase in impervious surface of the drainage area resulting in eutrophication of the lake. The objectives of our study are 1) to analyze the nutrient and metal concentrations in the Murchison Bay; 2) to identify and map the long-term landscape changes in Murchison Bay Watershed (MBW); 3) to analyze the impact of the landscape changes on the water quality of Murchison Bay. Water samples were collected from Miami Beach (MB), Ggaba Beach (GB) and Mulungo Beach (MuB), along the Murchison Bay and analyzed for various metal and nutrient concentrations. Landsat satellite imagery, sampled over three decades (1995-2019) of the MBW were analyzed for the land cover changes. The chemical analysis of the water samples showed that the P concentrations were above the critical limits while the As and Pb concentrations were higher but remained below the critical limits in water. The remote sensing analysis reveal that the impervious surface in the MBW increased by about 21.9% while the vegetative surface decreased by 4.2% during the period of 1995 to 2019. The Chlorophyll a concentration in the Murchison Bay increased over the period of time resulting in deterioration of water quality. Integration of environmental chemical analysis along with geospatial data aids in understanding the impact of landscape changes on the Murchison Bay water quality and to identify the areas vulnerable to change.

Keywords *Urban Watershed; Lake Victoria; Wetlands; Remote Sensing; Landsat and Geographic Information Systems (GIS)*

1. Introduction

Lake Victoria is the largest freshwater body in Africa, with an area of about 68,800 km² and a mean depth of around 40 m and lies in a catchment area of 184,000 km² (Oyoo-Okoth et al., 2013). The lake is surrounded and bordered by three countries Kenya, Tanzania and Uganda and is the source for the Nile River. Lake Victoria is a fresh water ecosystem of high socio-economic importance in Africa, as it is the predominant source of irrigation and drinking water, large quantity of fish and provides water for various agricultural, industrial and transportation purposes (Juma et al., 2014; Orata et al., 2009) in East Africa.

Kampala, the capital city of Uganda is located in the Northern catchment area of Lake Victoria. The Kampala urban and suburban regions and the surrounding wetlands, including Nakivubu wetland system (area 31 km²) to the East of Kampala constitute a natural drainage network which flows into Murchison Bay and then further into the Lake Victoria (Richard, 2009). The wetlands around Kampala, receive industrial and domestic wastewater from the surroundings (Fuhriemann et al., 2015) and surface water runoff from the city of Kampala. These wetlands are under considerable pressure due to rapid urbanization, industrial expansion, increased highway and road networks, agricultural and human encroachment (Mbabazi et al., 2010; Kayima et al., 2008; Dalahmeh et al., 2018).

Kampala is one of the fastest growing city with an annual population growth rate of 4.03% over the period of 2006 to 2020 (City Mayors Foundation 2020; UBOS 2018), this rapid increase in population is mainly attributed to high fertility rate, increase in migration of rural communities to urban areas in search of employment, livelihood and better standard of living. This large expansion of urban areas is resulting in loss of natural habitat such as wetland and forests to human encroachment. As only 10% of the urban residents are connected to the sewage network (O'Brien et al., 2017), most of the Kampala residents and several small businesses and industries dispose wastewater into open streams and drainage channels. This is mainly attributed to lack of planning and poor financial resources for construction of sewage network especially within the suburban and poorer areas of the city (O'Brien et al., 2017; UN-Habitat, 2007; Kulabako et al., 2010).

Lake Victoria is composed of several shallow gulfs and bays, especially in the northern parts of the lake, which receive point source pollutants from municipal and industrial centers along with the non-point source pollutants from agriculture and other informal settlements. Murchison Bay, located in the northern part of the lake (Figure 1), has been affected by several anthropogenic influences such as encroachment, conversion and degradation of wetlands, overfishing, increased industrial pollution, and decline in water level (Hecky et al., 2010; Scheren et al., 2000; Akurut et al., 2017). Several studies reported continuous occurrences of blue green algal blooms such as cyanobacteria and water hyacinth infestation in Murchison Bay due to increase in nutrient contamination to the lake (Cózar et al., 2007; Haande et al., 2011).

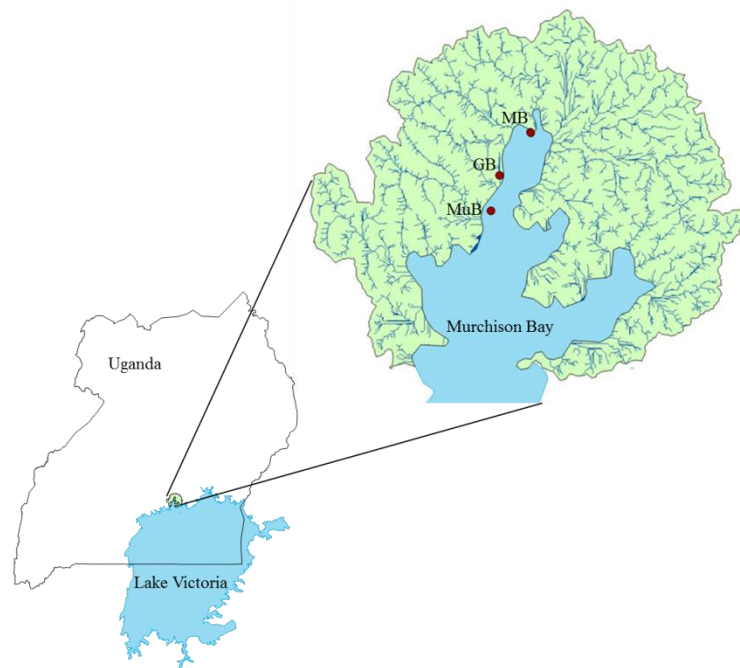


Figure 1: Murchison Bay along with its surrounding watersheds and the water flow lines that drain into the bay. Also shown are the water sampling locations at Miami Beach (MB), Ggaba Beach (GB) and Mulungo Beach (MuB) in the Murchison Bay of Lake Victoria. The subset image shows the location of Murchison Bay in the NorthWestern part of Lake Victoria in Uganda.

The water quality in Murchison Bay is on steady decline, due to increased nutrient runoff from agricultural and industrial areas, intense urban runoff from vast impervious surfaces of the watershed drainage area, poor domestic sewage disposal, resulting in eutrophication of the bay (Selman et al., 2008; Thamaga et al., 2018). Urban growth, population dynamics, industrial expansion has significant impact on the decline in the Murchison Bay water quality. Hence, it is important to monitor and study the long-term land cover and water quality changes of the Murchison Bay.

Water sample collection and monitoring the continuous land cover changes using traditional techniques is very expensive and time-consuming. The traditional methodology includes systematic field collection of the water samples, followed by acid digestion of the samples and then analyzing the chemical concentrations using various analytical instruments. Remote sensing is a cost effective, technologically sound monitoring technique that can be used for continuous monitoring of the landscape and water quality changes at a large scale and to quantify its effect on the extent of environmental contamination and the subsequent impact of the natural resources. The goal of this study is to analyze the long-term water quality changes in the Murchison Bay, in Uganda. The landscape changes in the surrounding watersheds draining into the Murchison Bay of Lake Victoria and its impact on the water quality changes was investigated in this research. Specific objectives of the study are: 1) to analyze the nutrient and metal concentrations in the Murchison Bay; 2) to identify and map the long-term landscape changes in Murchison Bay Watershed (MBW) and; 3) to analyze the impact of the landscape changes on the water quality of Murchison Bay.

2. Materials and Methods

2.1. Sampling Locations along Murchison Bay

The locations of the surface water samples and their distribution across the Murchison Bay is shown in Figure 1. Twelve water samples were collected from three different sampling locations namely, Miami beach (MB), Ggaba beach (GB) and Mulungo beach (MuB) along the Bay, which are popular publicly accessible locations for recreation, tourism, fishing, business and other day to day activities. Water samples from every location were collected in triplicate and the GPS coordinates of the sampling sites were recorded by using a portable Global Positioning System (GPS) receiver (Trimble Inc., Sunnyvale, CA). Samples were immediately transported to the laboratory in US, and kept refrigerated until further chemical analysis was performed.

2.2. Chemical Analysis

Water samples collected were microwave (Mars 6, CEM, Matthews, NC) acid digested using a microwave digestion unit using EPA 3015a method. About 45 ml of water sample was mixed with 5 ml of nitric acid for acid digestion in the sealed microwave vessels. The vessel contents were further cooled and filtered using Whatman 1 Filter paper. The samples were analyzed for of Al, As, B, Ba, Ca, Cd, Co, Cr, Fe, K, Mg, Mn, Mo, Na, P, Pb, S, Sr and Zn concentrations by using Inductive Coupled Plasma Mass Spectrometry (ICP-MS, Agilent 7500 Series, Santa Clara, CA). Results of water samples were statistically analyzed using the MINITAB statistical software (MINITAB Inc., State College, PA, USA).

2.3. GIS Analysis

The watershed and the hydrological stream network of the study area were delineated based on the Digital Elevation Models (DEM) using the hydrology tools of the spatial analyst extension of the ArcMap (ESRI, 2014). The Shuttle Radar Topographic Mission (SRTM) DEM data at 30 m resolution for Uganda was downloaded from the RCMRD website (<http://opendata.rcmrd.org/datasets/uganda-srtm-dem-30-meters>). All these data were used to create stream network and delineate watersheds for the Murchison Bay study area.

The spatial data for the study area was collected from various public and freely available datasets. These include, Energy sector GIS working group of Uganda (<http://www.energy-gis.ug/gis-data>), World Resources Institute (<https://www.wri.org/resources/data-sets/uganda-gis-data>), Uganda Bureau of Statistics (<https://www.ubos.org/data-portals-2/>), Humanitarian Data Exchange (<https://data.humdata.org/>) and from RCMRD Geoportal (<http://geoportal.rcmrd.org/>). Study areas of Murchison Bay, Lake Victoria and other geographical data were extracted and separated to derive the watershed study areas. Water sampling points of the study area were imported into GIS as separate vector layer. A 100m spatial buffer was created along the streams (with 50m on each side) within the study area and the land cover changes within the buffer was also evaluated from the downloaded satellite imagery.

2.4. Satellite Data Analysis

Four Landsat imagery from the time periods of 1) Jan 19, 1995, 2) Jan 28, 2010, 3) Feb 27, 2015, and 4) Jan 5, 2019, all having zero percent cloud cover, were chosen for this study. No cloud free Landsat imagery of study area prior to 1995 were found. Landsat imagery were downloaded from USGS Earth Explorer (<https://earthexplorer.usgs.gov/>) website, and processed using the ER Mapper V16.6 software (Hexagon Geospatial, 2020). Several single band and spectral ratio combinations were derived from the Dark Object Subtracted (DOS) values from each of the 7 bands in case of Landsat 5 imagery and from each of the 11 bands in case of Landsat 8 imagery. A DOS value of a spectral band is defined as one value less than the minimum digital number found in all pixels of that particular image for that spectral band (Vincent et al., 2004; Sridhar et al., 2009; 2011).

The vector data layers of Murchison Bay Watershed (MBW) study area was overlaid, clipped and the extracted study area from each of the Landsat imagery was then used for subsequent analysis. The land cover changes were evaluated by mapping the vegetative and impervious surface characteristics as environmental indicators to map and monitor the landscape changes in MBW. Normalized Difference Vegetation Index (NDVI) was calculated by using Equation 1 (Rouse et al., 1974) for Landsat 5 imagery and using equation 2 for Landsat 8 imagery, to map the green vegetation in the study area. An NDVI value of greater than 0.2 was applied as a mask to map only the vegetation. A Water Index (WI), equation 3 in case of Landsat 5 Imagery and equation 4 in case of Landsat 8 was used to map the water content of the study area. An Impervious Surface Area Index (ISAI), equation 5 was used to map the impervious surface areas in the Landsat 5 imagery while equation 6 is used for the Landsat 8 imagery. The spatial and temporal changes in impervious surface, water and vegetative surface areas from 1995 to 2019 were mapped and quantified individually for each of the selected images of MBW.

The changes in the Chlorophyll a concentration in the Murchison Bay water was visualized by applying the Landsat model developed to map the changes in the Chlorophyll a concentration in the water. The Chlorophyll a model that was applied to Landsat 5 imagery is given in equation 7 and for Landsat 8 imagery is given in equation 8 (Sridhar, 2019). Finally, the chemical analysis data, spatial and temporal data were integrated to analyze the overall landscape change pattern, in Murchison Bay and MBW.

$$NDVI = \frac{Band\ 4 - Band\ 3}{Band\ 4 + Band\ 3} \quad \text{Equation 1}$$

$$NDVI = \frac{Band\ 5 - Band\ 4}{Band\ 5 + Band\ 4} \quad \text{Equation 2}$$

$$WI = \frac{Band\ 2}{Band\ 5} \quad \text{Equation 3}$$

$$WI = \frac{Band\ 1}{Band\ 6} \quad \text{Equation 4}$$

$$ISAI = \sqrt{Band\ 6 \times Band\ 3} \quad \text{Equation 5}$$

$$\text{ISAI} = \sqrt{\text{Band } 10 \times \text{Band } 3} \quad \text{Equation 6}$$

$$\text{Chl a (mg/l)} = 14.39 - 78.5 \text{ R}_{21} + 34.49 \text{ R}_{52} - 17.87 \text{ R}_{73} \quad \text{Equation 7}$$

$$\text{Chl a (mg/l)} = -42.2 + 39.7 \text{ R}_{32} - 83.1 \text{ R}_{52} + 105.9 \text{ R}_{53} + 56.8 \text{ R}_{72} - 75.3 \text{ R}_{73} \quad \text{Equation 8}$$

Where $\text{R}_{xy} = \text{Band } x / \text{Band } y$

3. Results and Discussion

The water samples collected from the Miami Beach (MB), Ggaba Beach (GB) and Mulungo Beach (MuB) of Murchison Bay showed profound spatial heterogeneity in terms of the concentrations of different elements. The concentrations of As and Si were significantly higher in MB compared to other locations. The concentration of Al was significantly higher in GB and MuB while the concentration of Pb was significantly higher in MB and MuB compared to other location. The concentration of P was significantly higher in MB and GB compared to MuB (Table 1). The concentrations of all the other elements were below the proposed critical limits of WHO and EPA for drinking water (WHO, 2017; USEPA, 2018). The concentration of As in MB and the concentration of Pb in MB and MuB were high and almost close to the proposed maximum critical limit of 10 ppb (Table 1). The P concentrations in the MB and GB were well above the recommended maximum level of 100 ppb which is the proposed critical limit of EPA for algal bloom occurrence in surface water (Table 1).

Table 1: Heavy metal and nutrient elemental concentration in water samples collected from Murchison Bay of Lake Victoria. Miami Beach (MB), Ggaba Beach (GB) and Mulungo Beach (MuB) represents sampling locations along the bay. Given are mean values ($n = 3$) of three replicates. Also given are the proposed critical limits of WHO and EPA for drinking water (WHO, 2017; USEPA, 2018).

Elemental Concentrations (ppb)	Miami Beach (MB)	Ggaba Beach (GB)	Mulungo Beach (MuB)	WHO	EPA
Al	2.8	20.8*	25.6*	200	200
As	8.8*	0.1	0.6	10	10
B	11.2	11.8	10.6	2400	1000
Ba	23.6	22.5	22.3	1300	2000
Ca	8320	7596	6573	-	-
Cd	0.6	0.2	0.2	3	5
Co	1.0	0.2	0.3	-	-
Cr	0.5	0.6	0.4	50	100
Fe	25.6	25.6	25.8	-	300
K	4657	4207	3369	-	-
Mg	2838	2673	2461	-	-
Mn	3.3	0.8	0.1	400	50
Mo	2.6	2.1	2.1	70	-
Na	10553	9565	8261	-	20000
P	120.9*	152.7*	35.8	-	-
Pb	7.0*	3.2	8.0*	10	10
Si	1600*	1152	887	-	-
Sr	80.9	76.7	71.4	-	-
Zn	10.7	8.0	11.3	-	5000

† Means followed by asterisk (*) for the same element are significantly different at the 0.05 probability level.

The pseudo color Landsat imagery of the watershed areas that drain into the Murchison Bay shows that the urban impervious surface increased significantly from 1995 to 2019 at the expense of the vegetative cover (Figure 2). The gradual progression of the urban sprawl all along the western part of

the Murchison Bay can be seen distinctly. An unsupervised classification of the Landsat imagery with the ratio inputs of WI, NDVI and ISAI showed that the western part of the bay was significantly covered with impervious surface compared to the eastern part of the bay (Figure 3). The impervious surface area in the watershed increased by 21.9 % from 1995 to 2019 while the vegetative cover decreased by 4.2 % over the same period (Figure 4).

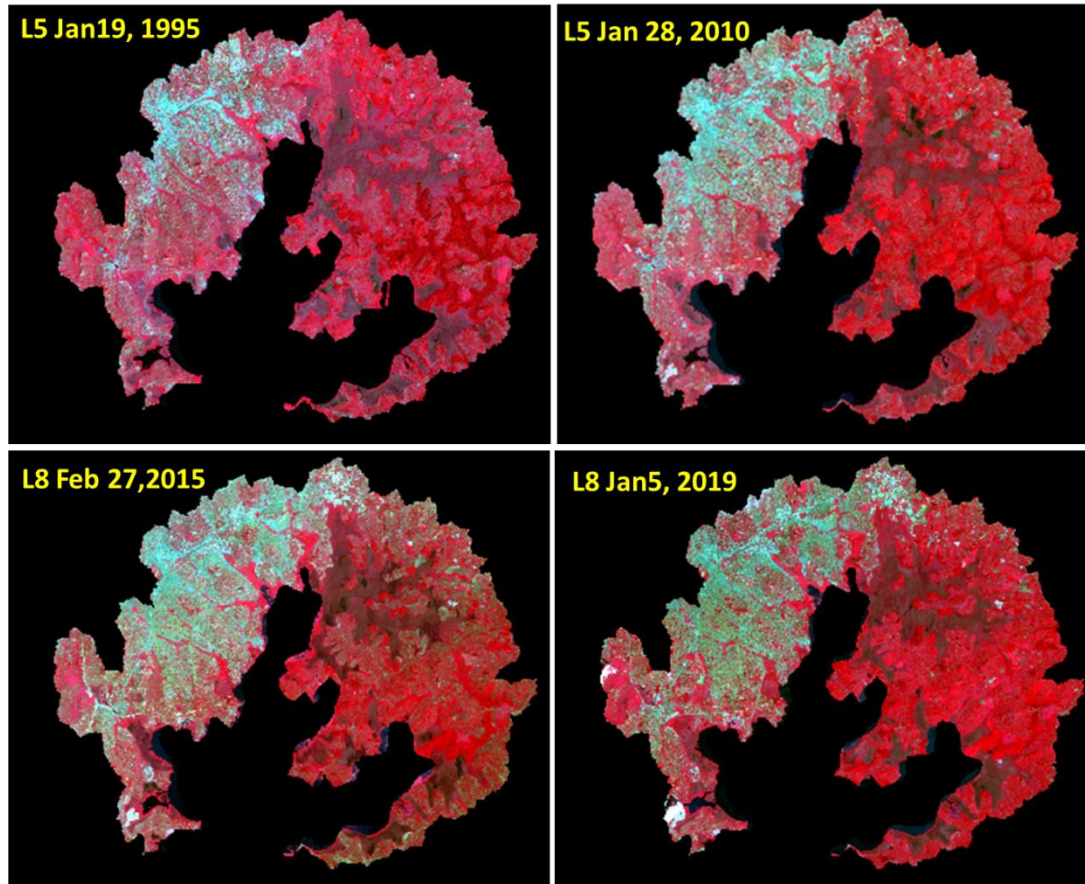


Figure 2: The pseudo color image of the Murchison Bay watershed where Landsat 5 bands 2, 3, 4 were shown in blue, green and red, respectively, while the Landsat 8 bands 3, 4, 5 were shown in blue, green and red, respectively. The vegetation appears in shades of red while the urban areas appear in pale white to lighter shades, the wetland areas and water appear dark. The western part of the study area is dominated by urban impervious surface while the eastern part by vegetation.

To identify the extent of land cover changes along the stream buffers within the watershed that drain into the Murchison Bay, a 100 m buffer zone along the streams were created and analyzed. All along the stream buffer zones, impervious surface area has increased and the vegetative surface area has decreased (Figure 5; Figure 6). The loss of vegetation along the stream buffer zone is distinct along the western and northwestern areas of the Murchison Bay compared to the eastern areas. The impervious surface area increased by 119 % from 1995 to 2019 while the vegetative cover decreased by 12 % over the same period along the stream buffer zones (Figure 5). The Chlorophyll a concentration in the Murchison Bay increased significantly from 1995 to 2019 (Figure 6), the algal blooms seem to arise from the Inner Murchison Bay, which is located in the northern part of the bay and spread towards the Outer Murchison Bay in the south.

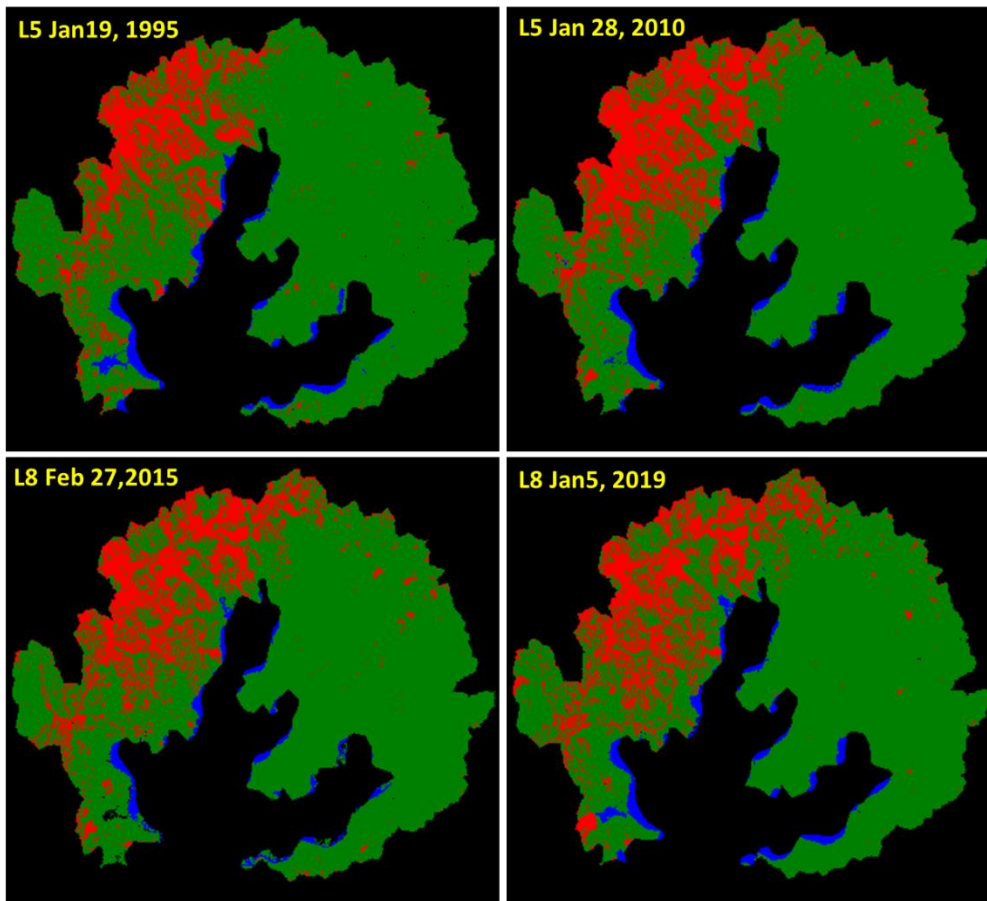


Figure 3: The unsupervised classification images of the study area where the areas covered with vegetative surface, impervious surface and water are shown in green, red and blue, respectively. The impervious surface areas increased at the expense of the vegetative cover during the period of 1995-2019.

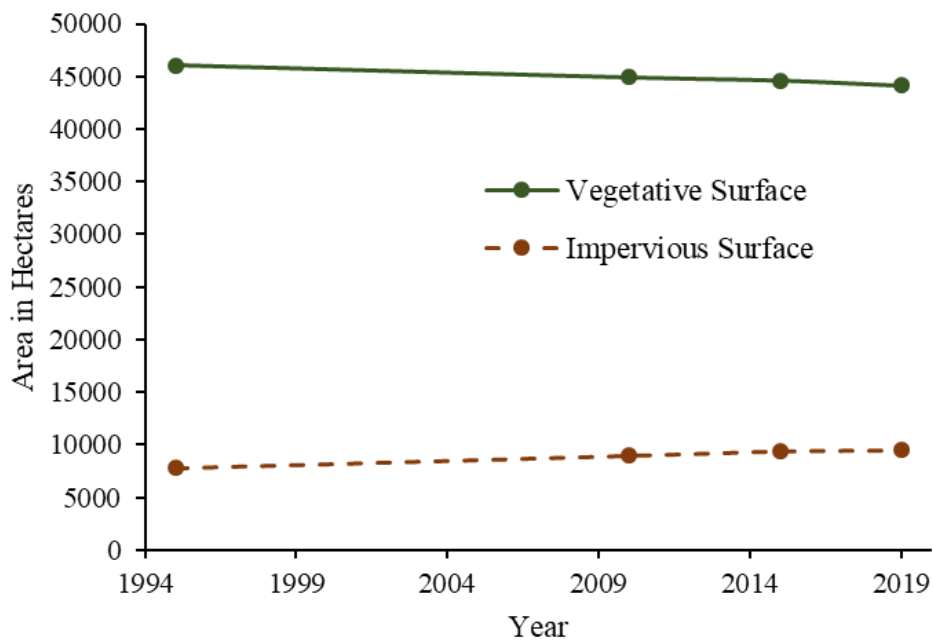


Figure 4: Change in the acreage of impervious and vegetative surface over the period of 1995-2019 in the Murchison Bay Watershed (MBW).

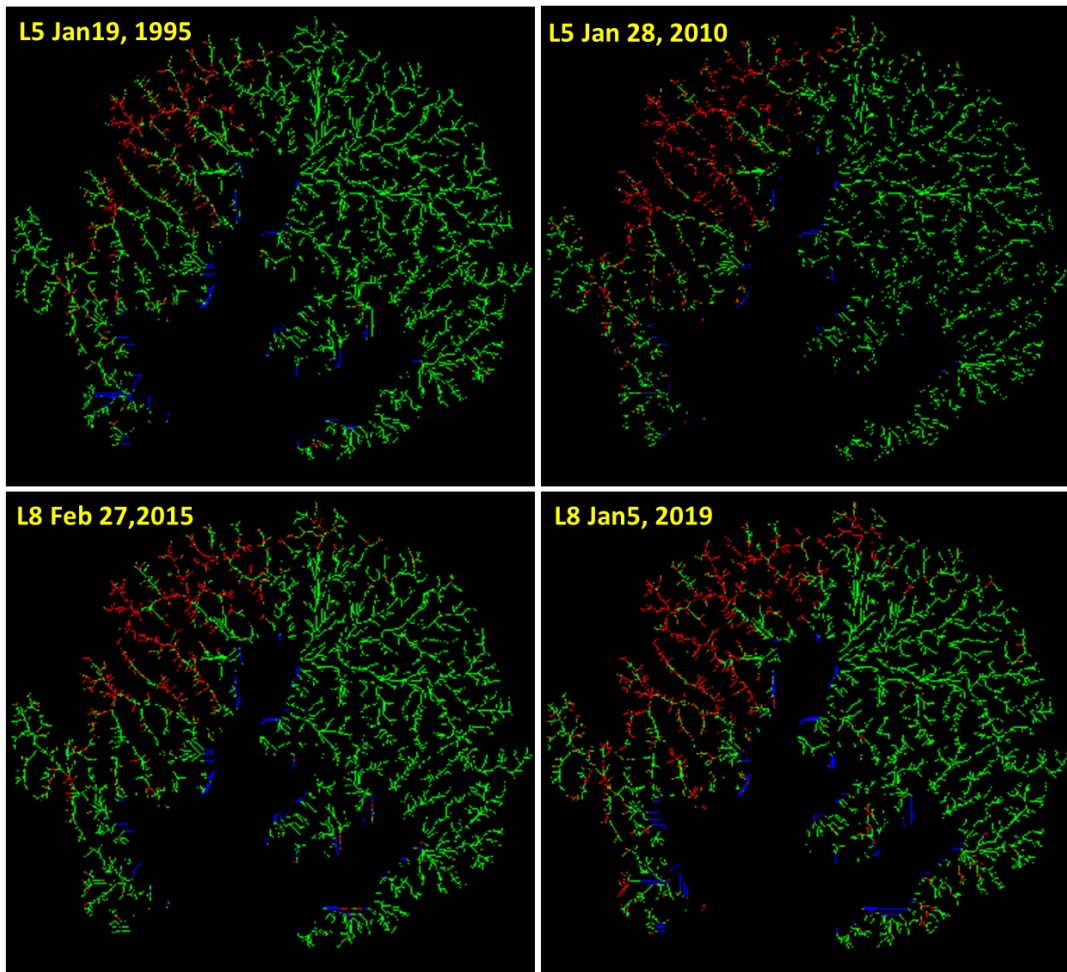


Figure 5: The unsupervised classification images of the study area along the stream buffers within the watershed where the areas covered with vegetative surface, impervious surface and water are shown in green, red and blue, respectively. The impervious surface areas along the stream buffers increased at the expense of the vegetative buffers during the period of 1995-2019.

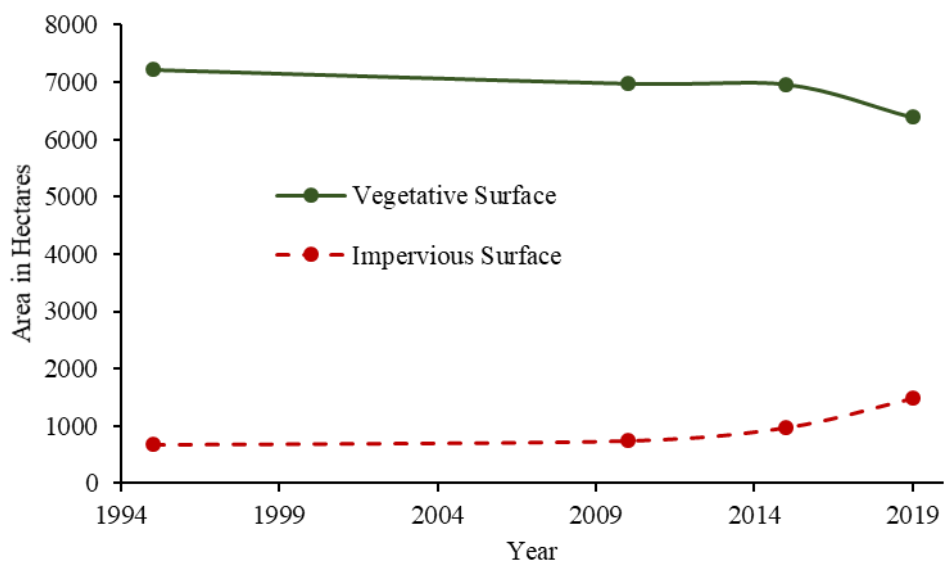


Figure 6: Change in the acreage of impervious and vegetative surface along the stream buffers in the Murchison Bay Watershed (MBW) over the period of 1995-2019.

The phosphorus concentration in the MB and GB are at more than the recommended maximum level of 100 ppb for the surface water. The Total P in the range of 10 to 75 ppb is the appropriate level to control the nuisance algal blooms in fresh water (USEPA, 2002). This high P concentration in the bay can be attributed mainly to the domestic and municipal waste and waste water disposal as well as intensification of agricultural and industrial activities within the watersheds draining into Murchison Bay, which causes lake eutrophication resulting in massive algal blooms and consequently spread of aquatic weeds such as water hyacinth (Selman et al., 2008). Water hyacinth affect the lake ecology by changing the habitat, interrupting the nutrient cycle, causing fish kills, and affecting the water transportation networks (Brendonck et al., 2003; Toft et al., 2003; Coetzee et al., 2014; Wasige et al., 2013; Thamaga et al., 2018).

Phosphorus also serves as an essential nutrient promoting algal growth such as cyanobacteria (*Microcystis*), which produce microcystin, a hepatotoxin, which impacts the human and animal health upon consumption of water contaminated with microcystins. From time to time, Murchison Bay and several other parts of Lake Victoria experience widespread algal blooms across the lake. Murchison Bay is heavily eutrophic (Haande et al., 2011; Ssebiyonga et al., 2013) and a major improvement can only be expected if the P inputs into the lake are controlled and the total P concentrations are brought down. Also the Murchison Bay is the water withdrawal point of the water treatment plant for the distribution of potable water for Kampala City. In recent years, with increase in surface runoff, industrial and municipal waste and sewage effluent into the bay, the water withdrawal points were extended to deeper and further portions of Lake Victoria (Akurut et al., 2017). The ammonia concentration in the surface waters of the bay is above the recommended standard criteria of 0.06 ppm (Richard, 2009), which also contribute the production of algal blooms along with the increase in P concentrations. The increase in the concentration of the algal blooms over the bay is clearly evident during the last three decades (Figure 7), which can be attributed to increase in the nutrient run off into the bay.

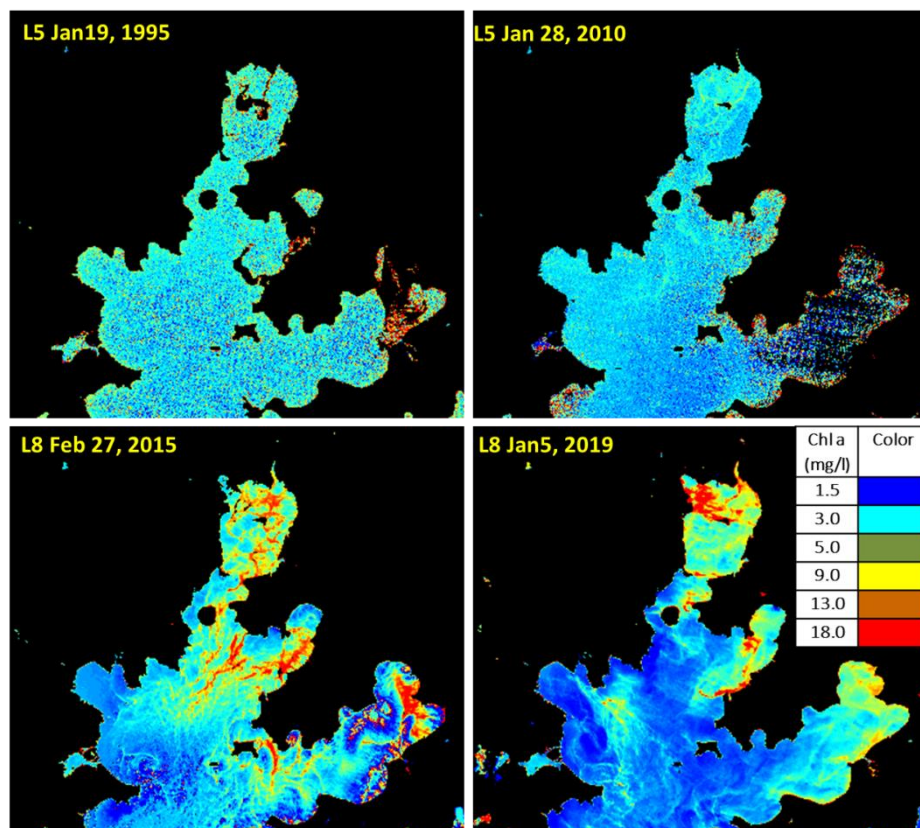


Figure 7: The changes in the Chlorophyll a concentration in the Murchison bay water during the period of 1995-2019. The Chlorophyll a concentration increased significantly and covered most of the bay with time.

The concentration of As in MB is significantly higher compared to other locations and is also higher than the general range of As in natural water which is 1-2 ppb (Hindmarsh and McCurdy, 1986; USNRC, 1999; WHO, 2011a). Long term exposure of high As concentration in drinking water increases the risk of cancer to the skin, lung, bladder and kidney (IPCS, 2001). The concentration of Pb in MB and MuB are getting close to the proposed maximum critical limit of 10 ppb which is higher than the average Pb levels of 2.8 and 2 ppb found in drinking water of US (WHO, 2011b) and Canada (Dabeka et al., 1992). High concentration of Pb over 10 ppb in water is poisonous affecting the health of infants, children and the fetus of pregnant women. The high concentration of metal and nutrient concentration in Murchison bay can be attributed to the presence of several large and small-scale industries within the drainage watershed. The partially treated or untreated effluents from upstream flows into the Nakivubu Channel, which further drains into the Murchison Bay (Richard, 2009). Apart from this, waste disposal from several systems such as pit latrines, waste water treatment plants and agricultural activities make its way into the bay (Richard, 2009).

The land cover change analysis revealed that the impervious surface increased by 21.9 % and the vegetative surface decreased by 4.2 % in the watershed areas during the period of last three decades. According to Akurut et al. (2017) the pollutant loading into streams of MBW has tremendously increased due to rise in population, wetland conversion, commercial growth, and industrialization in Kampala City. Urban sprawl, population increase and wetland loss around Murchison Bay is leading to land degradation and thus increasing the sediment and nutrient loading into the lake system from point and non-point sources of pollution (Machiwa, 2003). Pollutants originating from non-point sources was reported to be higher than that of point sources around Murchison Bay (Banadda et al., 2009) due to decrease in vegetation along the stream buffer zones and reduction in the wetlands. This claim can be justified by our land cover analysis along the 100 m stream buffers within the watershed where the vegetative cover decreased and impervious surface increased at a faster rate of 12% and 119%, respectively, than the rest of the watershed (Figure 5; Figure 6). Land cover change due to human activities is an important parameter that impacts the global environmental and ecological change by changing complex biophysical processes at global, regional and local scales (Wasige et al., 2013; Wu et al., 2003).

4. Conclusions

We compared and analyzed the Landsat satellite imagery of the last three decades (1995 to 2019) to identify the land cover changes of the Murchison Bay Watershed (MBW) and found that the vegetative surface decreased by 4.2 % and the impervious surface increased by 21.9 %. The land cover changes along the 100 m stream buffers within the watershed showed that the vegetative surface decreased and impervious surface increased by 12% and 119%, respectively, which is more intense than the rest of the watershed within the same period time. The increase in impervious surface of MBW is contributing to more surface water runoff and nutrient load into Murchison Bay resulting in more algal blooms. Consequently, the Chlorophyll a concentration increased significantly and covered most of the bay during the course of time in the last three decades based on the satellite imagery. Our water quality analysis reveal that the P, As and Pb concentrations were higher in Miami Beach (MB) followed by Ggaba Beach (GB) and Mulungo Beach (MuB), which are aligned accordingly in the north to south direction along which the influent water flows into the Murchison Bay. The chemical and image analysis data indicates that the nutrient and Chlorophyll a concentration increased along the gradient from the Outer Murchison Bay (OMB), to the Inner Murchison Bay (IMB), which are geographically located in the south and north of the Murchison Bay, respectively. This study improves the understanding of the land cover change in MBW which is recognized as a critical gap in the knowledge of wetland and forest loss, soil and water degradation, and eutrophication of Murchison Bay. Further research involving the use of high resolution satellite and aerial imagery along with a comprehensive water analysis for extensive inorganic and organic contaminants covering the entire bay will be greatly beneficial. Urban growth with environmental sustainability is key to the future economic growth in the region where urban development should be planned by conserving the natural resources.

Conservation of the wetland areas, reducing the inflow of domestic sewage and industrial effluents, developing and preserving the vegetative buffer strips around the drainage streams, along with the control of point and non-point source pollution is crucial to prevent the decline in the water quality of Murchison Bay and to reduce the proliferation of harmful algal blooms and floating aquatic weeds.

Acknowledgements

We thank the help of Mr. Musubula Edwards in water sampling and Ms. Djene Keita and Ms. Titilope for their help in chemical analysis of the samples. We would like to acknowledge the faculty and staff of CEDAT at Makerere University for their support. This work was supported by the Fulbright Faculty Scholar Award to Uganda to the primary author and the National Science Foundation (NSF) grants for Texas Southern University (TSU) under the award numbers HRD-1622993 and BCS-1831205.

References

- Akurut, M., Niwagaba, C.B. and Willems, P. 2017. Long-term variations of water quality in the Inner Murchison Bay, Lake Victoria. *Environmental Monitoring and Assessment*, 189, pp. 1-22.
- Banadda, E. N., Kansime, F., Kigobe, M., Kizza, M. and Nhapi, I. 2009. Land use-based nonpoint source pollution: a threat to water quality in Murchison Bay, Uganda. *Water Policy*, 11, pp. 93–104.
- Brendonck, L., Maes, J., Rommens, W., Dekeza, N., Nhwatiwa, T., Barson, M., Callebaut, V., Phiri, C., Moreau, K., Gratwicke, B., Stevens, M., Alyn, N., Holsters, E., Ollevier, F. and Marshall, B. 2003. The impact of water hyacinth (*Eichhornia crassipes*) in a eutrophic subtropical impoundment (Lake Chivero, Zimbabwe). II. Species diversity. *Archives of Hydrobiology*, 158, pp. 389–405.
- City Mayors Foundation, 2020. The world's fastest growing cities and urban areas from 2006 to 2020. [Online]. [Accessed Feb 15, 2020]. Available from: http://www.citymayors.com/statistics/urban_growth1.html.
- Coetzee, J.A., Jones, R.W. and Hill, M.P. 2014. Water hyacinth, *Eichhornia crassipes* (Mart.) Solms-Laub. (Pontederiaceae) reduces benthic macroinvertebrate diversity in a protected subtropical lake in South Africa. *Biodiversity and Conservation*, 23, pp. 1319–1330.
- Cózar, A., Bergamino, N., Mazzuoli, S., Azza, N., Bracchini, L., Dattilo, A. M. and Loisele S. A. 2007. Relationships between wetland ecotones and inshore water quality in the Ugandan coast of Lake Victoria. *Wetlands Ecology and Management*, 15, pp. 499– 507.
- Dabeka, R.W., McKenzie, A.D. and Lacroix, G.M.A. 1987. Dietary intakes of lead, cadmium, arsenic and fluoride by Canadian adults: a 24-hour duplicate diet study. *Food Additives and Contaminants*, 4, pp. 89–101.
- Dalahmeha, S., Tirgania, S., Komakech, A.J., Niwagaba, C.B. and Ahrens, L. 2018. Per- and polyfluoroalkyl substances (PFASs) in water, soil and plants in wetlands and agricultural areas in Kampala, Uganda. *Science of the Total Environment*, 631–632, pp. 660 –66.
- ESRI. 2014. Arc GIS Desktop-Environmental Systems Research Institute (Release 10.3). [ESRI Arc GIS] Redlands, CA, USA. [Accessed Feb 15, 2020].
- Fuhrmann, S., Stalder, M., Winkler, M.S., Niwagaba, C.B., Babu, M., Masaba, G., Kabatereine, N.B., Halage, A.A., Schneeberger, P.H., Utzinger, J. and Cisse, G. 2015. Microbial and chemical contamination of water, sediment and soil in the Nakivubo wetland area in Kampala, Uganda. *Environmental Monitoring and Assessment*, 187 (7), pp. 475.

Haande, S., Rohrlack, T., Semyalo, R. P., Brettum, P., Edvardsen, B., Lyche-Solheim, A., Sorensen, K. and Larsson, P. 2011. Phytoplankton dynamics and cyanobacterial dominance in Murchison Bay of Lake Victoria (Uganda) in relation to environmental conditions. *Limnologia*, 41, pp. 20–29.

Hecky, R., Mugidde, R., Ramlal, P., Talbot, M. and Kling, G. 2010. Multiple stressors cause rapid ecosystem change in Lake Victoria. *Freshwater Biology*, 55(s1), pp. 19–42.

Hexagon Geospatial. 2020. ERDAS ER Mapper Software (Version- 16.6.0.630). Madison, AL, USA. [Accessed Feb 15, 2020].

Hindmarsh, J.T. and McCurdy, R.F. 1986. Clinical and environmental aspects of arsenic toxicity. *CRC Critical Reviews in Clinical Laboratory Sciences*, 23, pp. 315–347.

IPCS. 2001. *Arsenic and arsenic compounds*. Geneva, World Health Organization, International Programme on Chemical Safety, Environmental Health Criteria 224. [Online]. [Accessed Feb 1, 2020]. Available from: https://www.who.int/ipcs/publications/ehc/ehc_224/en/.

Juma, D.W., Wang, H. and Li, F. 2014. Impacts of population growth and economic development on water quality of a lake: case study of Lake Victoria Kenya water. *Environmental Science and Pollution Research*, 21 (8), pp. 5737–5746.

Kayima, J., Kyakula, M., Komakech, W. and Echimu, S.P. 2008. A study of the degree of pollution in Nakivubo channel, Kampala, Uganda. *Journal of Applied. Sciences and Environmental Management*, 12, pp. 93–98.

Kulabako, R.N., Nalubega, M., Wozzi, E. and Thunvik, R. 2010. Environmental health practices, constraints and possible interventions in peri-urban settlements in developing countries: A review of Kampala, Uganda. *International Journal of Environmental Health Research*, 20, pp. 231-257.

Machiwa, P. K. 2003. Water quality management and sustainability: the experience of Lake Victoria Environmental Management Project (LVEMP)—Tanzania. *Physics and Chemistry of the Earth, Parts A/B/C*, 28(20), pp. 1111–1115.

Mbabazi, J., Kwetegyeka, J., Ntale, M. and Wasswa, J. 2010. Ineffectiveness of Nakivubo wetland in filtering out heavy metals from untreated Kampala urban effluent prior to discharge into Lake Victoria, Uganda. *African Journal of Agriculture Research*, 5 (24), pp. 3431–3439.

O'Brien, E., Munir, M., Marsh, T., Heran, M., Lesage, G., Tarabara, V.V. and Xagorarakis, I. 2017. Viral diversity and abundance in polluted waters in Kampala, Uganda. *Water Research*, 127, pp. 41-49.

Orata, F., Quinete, N., Werres, F. and Wilken, R.D. 2009. Determination of perfluorooctanoic acid and perfluorooctane sulfonate in Lake Victoria Gulf water. *Bulletin of Environmental. Contamination and Toxicology*, 82 (2), pp. 218–222.

Oyoo-Okoth, E., Admiraal, W., Osano, O., Manguya-Lusega, D., Ngure, V., Kraak, M.H.S., Chepkirui-Boit, V. and Makwali, J. 2013. Contribution of soil, water and food consumption to metal exposure of children from geological enriched environments in the coastal zone of Lake Victoria, Kenya. *International Journal of Hygiene and Environmental Health*, 216, pp. 8–16.

Richard, O. 2009. Deteriorating Water Quality in the Lake Victoria Inner Murchison Bay and its impact on the drinking water supply for Kampala, Uganda. The 13th World Lake Conference, Wuhan, China. [Accessed Feb 17, 2020]. Available from: <https://www.semanticscholar.org/paper/Deteriorating-Water-Quality-in-the-Lake-Victoria-on-Oyoo/c9991f0a3eac47985eaa19409ac4fd70b3efe69f>.

Rouse, J.W., Haas, R.H., Schelle, J.A., Deering, D.W. and Harlan, J.C. 1974. Monitoring the vernal advancement and retrogradation (green wave effect) of natural vegetation. Type III Final Report, NASA Goddard Space Flight Center, Green belt, Maryland.

Scheren, P., Zanting, H. and Lemmens, A. 2000. Estimation of water pollution sources in Lake Victoria, East Africa: application and elaboration of the rapid assessment methodology. *Journal of Environmental Management*, 58(4), pp. 235–248.

Selman, M., Greenhalgh, S., Díaz, R. and Sugg, Z. 2008. Eutrophication and Hypoxia in Coastal Areas: a Global Assessment of the State of Knowledge 1. World Resources Institute Policy Note, Washington D.C, p. 6.

Sridhar, B. B. M., Vincent, R.K., Witter, J.D. and Spongberg, A.L. 2009. Mapping the total phosphorus concentration of biosolid amended surface soils using LANDSAT TM data. *Science of the Total Environment*, 407, pp. 2894-2899.

Sridhar, B.B.M., Vincent, R.K., Roberts, S.J. and Czajkowski, K. 2011. Remote sensing of soybean stress as an indicator of chemical concentration of biosolid amended surface soils. *International Journal of Applied Earth Observation*, 13, pp. 676-681.

Sridhar, B.B.M. 2019. Geospatial informatics for environmental and natural resource management. Fulbright US Scholar Research Report.

Ssebiyonga, N., Erga, S.R., Hamre, B., Stamnes, J.J. and Frette, O. 2013. Light conditions and photosynthetic efficiency of phytoplankton in Murchison Bay, Lake Victoria, Uganda. *Limnologia*, 43(3), pp. 185–193.

Thamaga, K.H. and Dube, T. 2018. Remote sensing of invasive water hyacinth (*Eichhornia crassipes*): A review on applications and challenges. *Remote Sensing Applications: Society and Environment*. 10, pp. 36–46.

Toft, J.D., Simenstad, C.A., Cordell, J.R. and Grimaldo, L.F. 2003. The effects of introduced water hyacinth on habitat structure, invertebrate assemblages and fish diets. *Estuaries*. 26 (3), pp. 746–758.

UBOS. 2018. Statistical Abstract - Uganda Bureau of Statistics. [Online]. [Accessed Feb 15, 2020]. Available from: https://www.ubos.org/wp-content/uploads/publications/05_2019STATISTICAL_ABSTRACT_2018.pdf.

UN-Habitat. 2007. Situation Analysis of Informal Settlements in Kampala. HS/873/06E. [Online]. [Accessed Feb 15, 2020]. Available from: <http://www.rrojasdatabank.info/kampala.pdf>.

U.S.EPA. 2002. Summary table for the nutrient criteria documents. [Online]. [Accessed Feb 15, 2020]. Available from: <https://www.epa.gov/sites/production/files/2014-08/documents/criteria-nutrient-ecoregions-sumtable.pdf>.

U.S.EPA. 2018. 2018 Edition of the Drinking Water Standards and Health Advisories. EPA 822-F-18-001. [Online]. [Accessed Feb 15, 2020]. Available from: <https://www.epa.gov/sites/production/files/2018-03/documents/dwtable2018.pdf>.

USNRC. (1999). *Arsenic in drinking water*. Washington, DC, United States National Research Council, National Academy Press. [Online]. [Accessed Feb 15, 2020]. Available from: <https://www.nap.edu/catalog/6444/arsenic-in-drinking-water>.

Vincent, R. K., Qin, X., McKay, R. M. L., Miner, J., Czajkowski, K., Savino, J. and Bridgeman, T. 2004. Phycocyanin detection from LANDSAT TM data for mapping cyanobacterial blooms in Lake Erie. *Remote Sensing of Environment*, 89, pp. 381-392.

Wasige, J.E., Groen, T.A., Smaling, E. and Jetten, V. 2013. Monitoring basin-scale land cover changes in Kagera Basin of Lake Victoria using ancillary data and remote sensing. *International Journal of Applied Earth Observation*, 21, pp. 32–42.

WHO. 2017. Guidelines for drinking-water quality: fourth. Geneva: World Health Organization, License: CC BY-NC-SA 3.0 IGO. [Online]. [Accessed Feb 15, 2020]. Available from: <http://apps.who.int/iris>.

WHO. 2011a. Arsenic in drinking water. WHO/SDE/WSH/03.04/75/Rev/1. [Online]. [Accessed Feb 15, 2020]. Available from: https://www.who.int/water_sanitation_health/publications/arsenic/en/.

WHO. 2011b. Lead in drinking water. WHO/FWC/WSH/16.53. [Online]. [Accessed Feb 1, 2020]. Available from: https://www.who.int/water_sanitation_health/water-quality/guidelines/chemicals/lead-background-feb17.pdf.

Wu, J., David, J.L. and Jenerette, G.D. 2003. Linking land use change with ecosystem processes: a hierarchical patch dynamics model. In: Guhathakurta, S. (Ed.), *Integrated Land Use and Environmental Models*. Springer, New York.

Research Article

Irrigation Potential Utilization Estimation using Time-Series Satellite Data

Sobhan Mishra¹, Shankar Muthyam², Raju, P.V.¹, Annie Maria Issac¹, Rao, V.V.¹

¹National Remote Sensing Center, Hyderabad 50037, India

²Formerly with National Remote Sensing Center

Correspondence should be addressed to Sobhan Mishra, sobhanmishra91@gmail.com

Publication Date: 23 July 2020

DOI: <https://doi.org/10.23953/cloud.ijarsg.475>

Copyright © 2020 Sobhan Mishra, Shankar Muthyam, Raju, P.V., Annie Maria Issac, Rao, V.V. This is an open access article distributed under the **Creative Commons Attribution License**, which permits unrestricted use, distribution, and reproduction in any medium, provided the original work is properly cited.

Abstract In India, significant irrigation potential has been created to increase the agricultural crop intensity and its production. However, these irrigation systems, built with huge financial investments, exhibit significant gap in potential created and utilized. The contributing factors are multi fold and State & Central Governments initiated many programs to bridge the gap in irrigation potential created & utilized under command areas. Objective assessment of actual irrigation utilization in command areas is prerequisite for planning appropriate interventions to bridge the gap. Conventional field-based data collection mechanism is tedious and do not provide spatial patterns of irrigation utilization. Satellite data with multi-spectral and temporal dimensionality provides opportunities to estimate irrigation utilization and thus to derive its spatial patterns quantifying the gap between created and utilized. In this study, the irrigation potential utilized, as against the potential created was analyzed for Krishna basin using multi-temporal satellite data. Seasonal and annual crop map was derived from times series Advanced Wide Field Sensor (AWiFS) data through unsupervised classification. The crop area identified from the remote sensed information was separated into irrigated and rainfed classes based on temporal profiles of Normalized Differential Vegetation Index (NDVI) with in a crop season. Irrigation Potential Utilized (IPU) was determined as the gross irrigated area.

Keywords *Satellite data; Irrigation Potential Utilization; Ground truth*

1. Introduction

In India, irrigation potential has been created to increase the agricultural crop intensity and its production. However there is a significant gap between the irrigation potential created and utilized (Ramanayya et al., 2008). This may be due to lack of canals at field levels, improper design of irrigation projects, etc. Conventionally Irrigation Potential Utilized is assessed from the data collected by Irrigation Department, Revenue Department and Agricultural Department on periodic basis. This method has the limitations of data gaps and subjectivity errors. These conventional methods are highly manpower and time intensive.

Satellite remote sensing offers a great potential for routine monitoring of irrigated area due to better spatial coverage and readily available archives of satellite imagery (Jonna et al., 1992; Murali, K.G. et al. 2011). It is used for mapping out cropped areas with its source of irrigation. The images with high spectral and temporal frequencies can be used for identification of the crop type and its condition. The

historic data that span from many years allow comparison of cropping pattern change, thus revealing changes in cultivation pattern in coherence through time. Estimation of cropped area from remote sensing data provides spatial distribution of cultivated area and is useful for assessing irrigation performance, improving irrigation intensities, quantifying environmental impacts and assessing irrigation water use. Crop maps generated from satellite imagery through the season on a near real time basis can be used for estimating sown areas and there by estimation of irrigation water requirement, which in turn is helpful in water resource planning and management (Raju et al., 2008).

Remote Sensing indices like green vegetation index and leaf area index can be used for estimation of land cover types (Gutman et al., 1998.). Remote sensing also is a potential tool to provide spatial and temporal information for precession crop management (Myneni et al., 1995). Many studies had summarized the approach and techniques of remote sensing based crop discrimination and area estimation including single date approach based on maximum likelihood classification as well as use of hierarchical growth profile of classification of multiple crops like paddy, wheat, sorghum, groundnut, mustard and cotton (Dadhwal et al., Navalgund et al., 2000). Studies have also demonstrated the utility of multi date remote sensing derived indices like Normalized Difference Vegetation Index (NDVI) in estimation of Irrigation Potential Utilization within a command area (Shanker, M. et al., 2017)

NDVI band ratio of Near Infra-Red (NIR) and Red (R) (Rouse et al., 1974) is a remote sensing derived indicator of the crop stage and condition. The temporal profile of the of remote sensing derived vegetation indices like Normalized Difference Vegetation Index (NDVI), is used to capture the phonological development of the crop and there by identification of the crop progress through a season. The temporal profile of NDVI though exhibits a similar pattern; the quantitative values vary depending on the condition of the crop. A crop in a good condition presumed to be in irrigated condition, exhibits higher value of NDVI, there by facilitating a demarcation between the irrigated and rainfed condition within a crop type (Thenkabail et al., 2011)

In this study an attempt was made to separate cropped area seasonally with its irrigation source from time series optical datasets based on their temporal profile of NDVI. Unsupervised method of classification was adopted with set of decision rules for achieving the objective.

1.1. Study Area

The Krishna Basin extends over the states of Andhra Pradesh (10.07%), Telangana (19.74%), Maharashtra (26.34%) and Karnataka (43.82%). The basin has a maximum length and width of about 701 km and 672 km and lies between 73°17' to 81°9' East Longitudes and 13°10' to 19°22' North Latitudes. The basin is roughly triangular in shape and is bounded by Balaghat range on the North, Eastern Ghats on the South and Bay of Bengal on the east and Western Ghats on the West as illustrated in Figure 1. The basin falls under division-All drainage flowing into Bay of Bengal and Region-Rivers draining in Bay of Bengal, delineated primarily based upon drainage of rivers to outlet. Figure 2 shows the distribution of basin area over the three states. Krishna Basin is having a total area of 254746 sq. km which is nearly 8% of the total geographical area of the country.

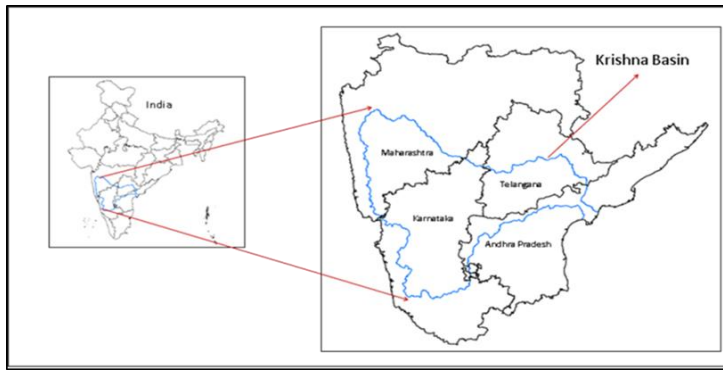


Figure 1: Location of Krishna Basin

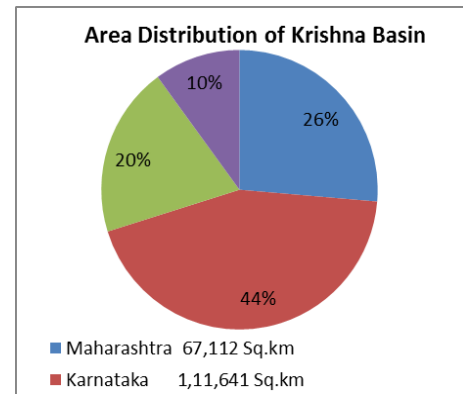


Figure 2: Distribution of Geographical Area

2. Materials and Methods

Obtaining seasonal and annual crop area maps with the help of remote sensing derived geospatial database is an age old practice for irrigation engineers and hydrologists. Recent studies have shown the utilization of remote sensing derived data for identification of crop types in a study area with its irrigation sources. In this paper decision rule based approach of unsupervised classification of time series monthly and fortnightly NDVI was adopted for identification of different crop types and its irrigated condition as illustrated in Figure 3. The datasets used in the study are discussed in the following sections.

2.1. Datasets Used

2.1.1. Satellite Imagery

Advanced Wide Field Sensor (AWiFS) optical datasets derived from Resourcesat were used in this study. It has a temporal frequency of 5 days, spatial resolution of 56m and has four bands in Visible and NIR (VNIR). The datasets were obtained from National Remote Sensing Center (NRSC) archives for two water years spanning from 2015 June to 2017 May.

2.1.2. Geospatial Datasets

Command area boundary and sub basin boundary was collected from India WRIS. Command area boundaries were digitized from high resolution datasets and the sub-basin boundaries were obtained from terrain processing of Digital Elevation Models.

2.1.3. Ground Truth Samples

Geo-Tagging of fields was done by using mobile application developed indigenously by National Remote sensing Center. The objective was to collect field information such as crop types, its growth stage, sowing and harvesting date and irrigation source. Around 800 ground truth points were collected in the projects of Krishna River Basin in two years 2015-16 and 2016-17.

2.1.4. Ancillary Datasets

The Land Use Land Cover information from generated in the Natural Resources Census (NRC) from AWiFS 56m for entire India for the year 2010-11 (Scale: 1: 250,000) was used for deriving the agriculture mask over which the classification was done.

2.2. Procedure

2.2.1. Generating Data Base

Top of atmospheric corrected AWiFS datasets were downloaded from archives of NRSC for the areas covering Krishna River basin. The datasets were preprocessed and corresponding NDVI images were generated. A temporal series of maximum NDVI at a time step of 15 days and one month was generated throughout the season.

The mask of non-agriculture areas was identified from the land use land cover map discussed in Section 2.1.4. The classification and its following analysis were carried out only on the agriculture area to avoid the error due to mixed pixels. A reference NDVI profile of different land covers were established in conjunction with the ground truth information. In order to avoid the possible inaccuracies inherent with multiple spectral reference profiles for multiple crops, the crops having similar temporal profile were aggregated and reference profiles for general crop groups were generated through out a year comprising of two seasons as seen in Figure 3.

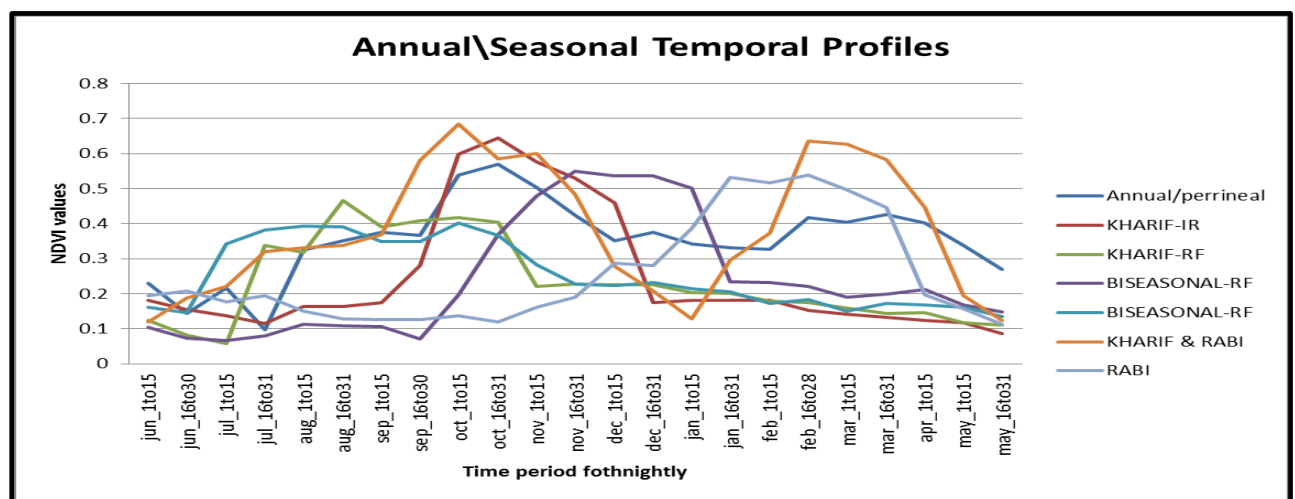


Figure 3: Temporal signatures for different seasonal crop groups collected from ground truth data

2.2.2. Decision Rule based Classification

Krishna basin was divided in to 8 sub basis as seen in Table 4. Classification was carried out sub basin wise to account for the spatial variation in crop calendar. The time series NDVI image was subjected to unsupervised classification. The image was classified into multiple classes and the classes were assigned with the general crop groups based on similarity with the reference signature (obtained from the ground truth). The categorization of the classes into crop groups was done by visual judgment. The criteria followed for classification is as described in Table 1.

Table 1: Criteria for Categorization

General Crop Group	No. of Peaks	Duration of the Profile (Base Period)	Trend of Peaks
Kharif – Irrigated	1	June- October	High
Kharif - Rainfed	1	June - October	Low
Bi-seasonal- Irrigated	1	June - February	High
Bi-seasonal- Rainfed	1	June - February	Low
Double Crop	2	June- May	High
Rabi	1	November - May	High
Annual/Perennial	1(Consistent)	June- May	High

2.2.3. Irrigation Potential Utilization Estimation

After classifying the time series NDVI image into the above crop classes, the area of each class was obtained. The Irrigation Potential Utilized (IPU) was estimated as the Gross Irrigated Area (GIA). Also, the Net Irrigated Area (NIA), Gross Sown Area (GSA) and Net Sown Area (NSA) were also estimated sub basin wise taking into consideration the crop areas as described in Table 2.

Table 2: Estimation of GIA, NIA, GSA and NSA

	Kharif-Irrigated	Kharif-Rainfed	Bi- seasonal Irrigated	Bi- seasonal Rainfed	Rabi	Double Crop	Annual/ Perennial
GIA / IPU	x		x		x	x (Twice)	x
NIA	x		x		x	x	x
GSA	x	x	x	x	x	x (Twice)	x
NSA	x	x	x	x	x	x	x

2.2.4. Accuracy Assessment by Kappa Statistics

800 ground truth samples were collected during two study years 2015-16 and 2016-17. Ground truth points were overlaid on the thematic map generated and compared for the accuracy of the classification with respect to the crop type, crop season and source of irrigation. The accuracy was estimated by computing the Kappa Statistics. Kappa statics is an inter observer variation that can be measured in any situation in which two or more independent variables are evaluating the same classes (Anthony J.V., and Joanne M.G., et al., 2005). The agreement of the classification with the reality is estimated by the Kappa value as described in Table 3.

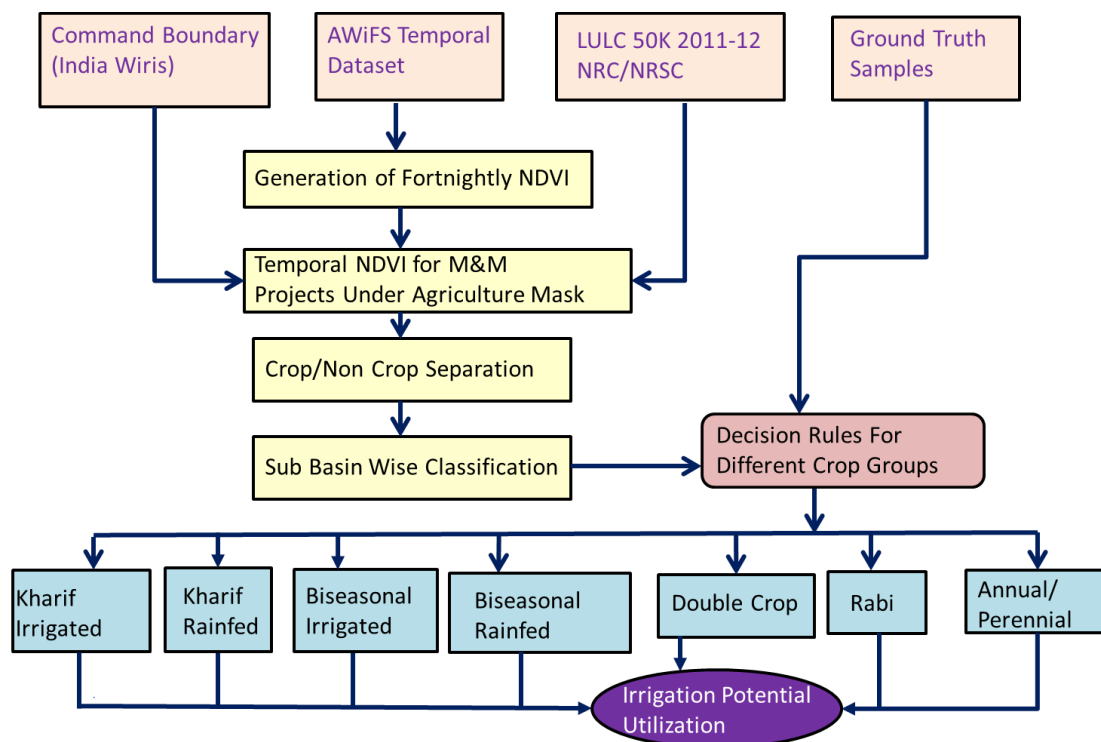


Figure 4: Flow chart showing the methodology for carrying out classification and obtaining IPU

Table 3: Range of Kappa Values and the Agreement

Kappa	Agreement
< 0	Less than chance agreement
0.01–0.20	Slight agreement
0.21– 0.40	Fair agreement
0.41–0.60	Moderate agreement
0.61–0.80	Substantial agreement
0.81–0.99	Almost perfect agreement

3. Results and Analysis

The classified map of Krishna basin showing irrigated / rainfed classes is shown in Figure 5 & 6 for 2015-16 and 2016-17 respectively. Sub-basin wise IPU (GIA) along with NIA, GSA, NSA are presented in Table 4 & Table 5 for the years 2015-16 and 2016-17. There was an increase in irrigated areas for Bhima Lower, Tungabhadra Lower and Tungabhadra Upper in the later year. This can be attributed to the increase in the implementation of lift irrigation schemes in these sub basins in the years under study.

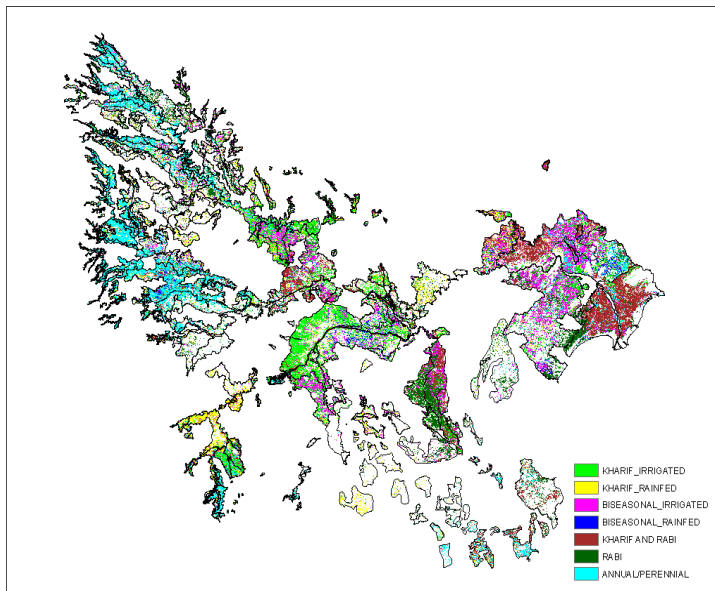


Figure 5: Crop classes present in Krishna Basin for the year 2015-16

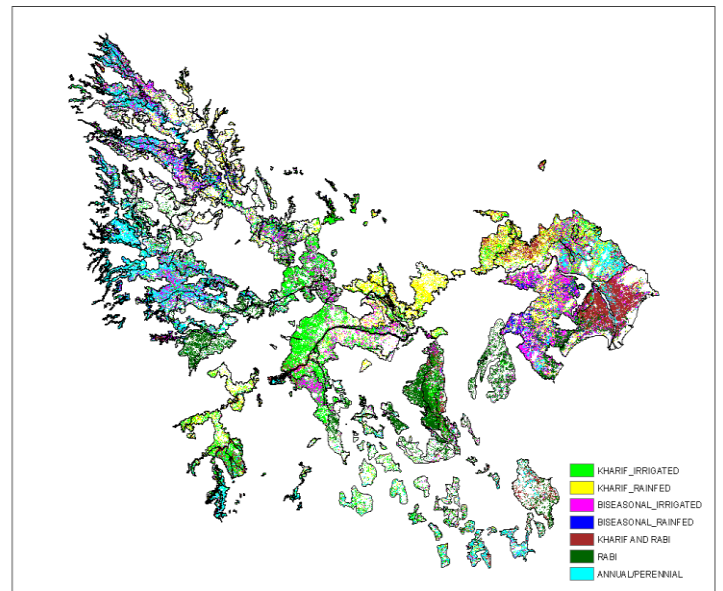


Figure 6: Crop classes present in Krishna Basin for the year 2016-17

Table 4: Sub-basin wise IPU, NIA, GSA and NSA for 2015-16

Sub Basin	2015-16 (Area in ha.)			
	Irrigation Potential Utilized (IPU)	Net Irrigated Area (NIA)	Gross Sown Area (GSA)	Net Sown Area (NSA)
Bhima Lower	2,38,873	2,38,873	3,04,968	3,04,968
Bhima Upper	8,36,385	7,73,509	10,91,260	10,28,384
Krishna Lower	18,81,481	14,54,291	24,04,275	19,77,085
Krishna Middle	89,701	72,602	2,67,148	2,50,049
Krishna Upper	15,64,168	14,96,245	16,23,029	15,55,106
Tungabhadra Lower	6,85,652	6,39,821	7,53,899	7,08,068

Tungabhadra Upper	3,42,907	2,80,230	4,19,441	3,56,764
Projects Outside Krishna basin	12,32,010	10,87,467	12,74,290	11,29,747
Net Area	68,71,177	60,43,038	81,38,310	73,10,171

Table 5: Sub-basin wise IPU, NIA, GSA and NSA for 2016-17

Sub Basin	2016-17 (Area in ha.)			
	Irrigation Potential Utilized (IPU)	Net Irrigated Area (NIA)	Gross Sown Area (GSA)	Net Sown Area (NSA)
Bhima Lower	3,77,287	3,67,375	4,65,206	4,55,294
Bhima Upper	8,91,144	8,24,984	10,14,505	9,48,346
Krishna Lower	22,10,477	15,97,151	23,50,571	17,37,246
Krishna Middle	1,97,166	1,53,940	2,43,995	2,00,769
Krishna Upper	14,60,818	12,58,367	16,29,996	14,27,545
Tungabhadra Lower	6,60,336	6,24,563	7,79,149	7,43,376
Tungabhadra Upper	3,08,085	2,42,785	4,32,659	3,67,360
Projects Outside Krishna basin	9,40,123	7,49,294	10,20,042	8,29,213
Net Area	70,45,436	58,18,459	79,36,125	67,09,149

3.1. Irrigation Potential Utilization (IPU) for Krishna Basin

The details of Irrigation Potential Utilization (IPU), Net Irrigated Area (NIA), Gross Sown Area (GSA), Net Sown Area (NSA) during 2015-6 and 2016-17 in Krishna basin is shown in Figure 7. The seasonal distribution of irrigated / rainfed classes is shown in Figure 8. There is an increase in the irrigated and sown area in the year 2016-17 as compared to the earlier year. The irrigated area increased by 4% in the later year due to the reduced rainfall in the year.

The Irrigation Potential Utilization (IPU) of Krishna basin is assessed as 68.71 Lakh ha. and 70.45 Lakh ha., Whereas Net Irrigated Area (NIA) is assessed as 60.43 Lakh ha. and 58.18 Lakh ha. during the study years of 2015-16 and 2016-17 respectively. Hence, it is observed that IPU and NIA are more or less same during both the years. However, the annual rainfall in the Krishna basin decreased by 18.75% from 2015-16 to 2016-17. Therefore, the stable IPU, in spite of reduction in annual rainfall, could be due to increased ground water utilization during 2016-17 compared to 2015-16. The marginal increase in IPU (2.53%) and a marginal decrease in NIA (3.72%) from 2015-16 to 2016-17, may be attributed to an increase in kharif and rabi irrigated area (double crop irrigated) from 11% to 18%.

3.2. Accuracy Assessment

The user's accuracy producer's accuracy for the season specific crop class classification was calculated for both the years are shown in the Table 6 and Table 7. The classification of the season specific crop class for the year 2016-17 was found to be more accurate as compared to the preceding year. The kappa statistics were computed for both the years. For the year 2015-16 the value is 25.33 and for the year 2016-17 the value is 34.22. This can be attributed to the fact that the later year had more number of satellite data sets which resulted in a smoother profile of NDVI and better classification.

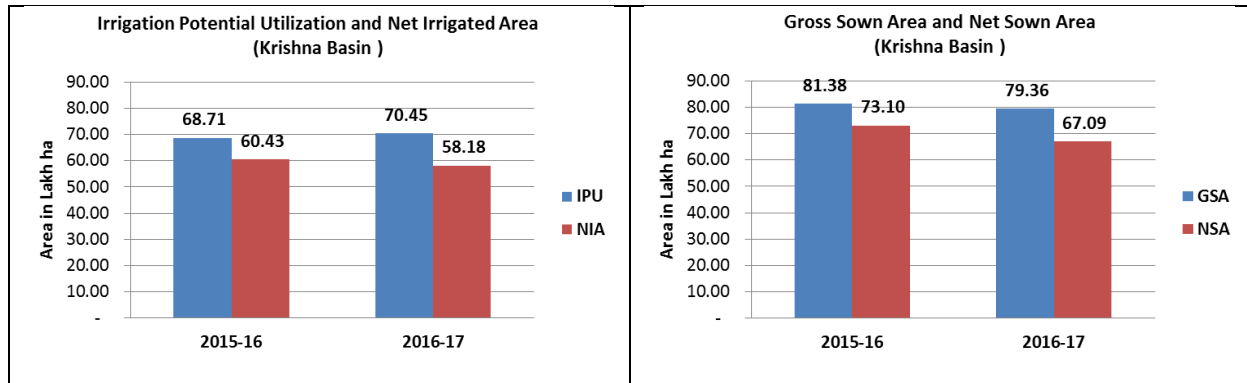


Figure 7: Status of IPU, NIA, GSA, NSA during 2015-16 & 2016-17

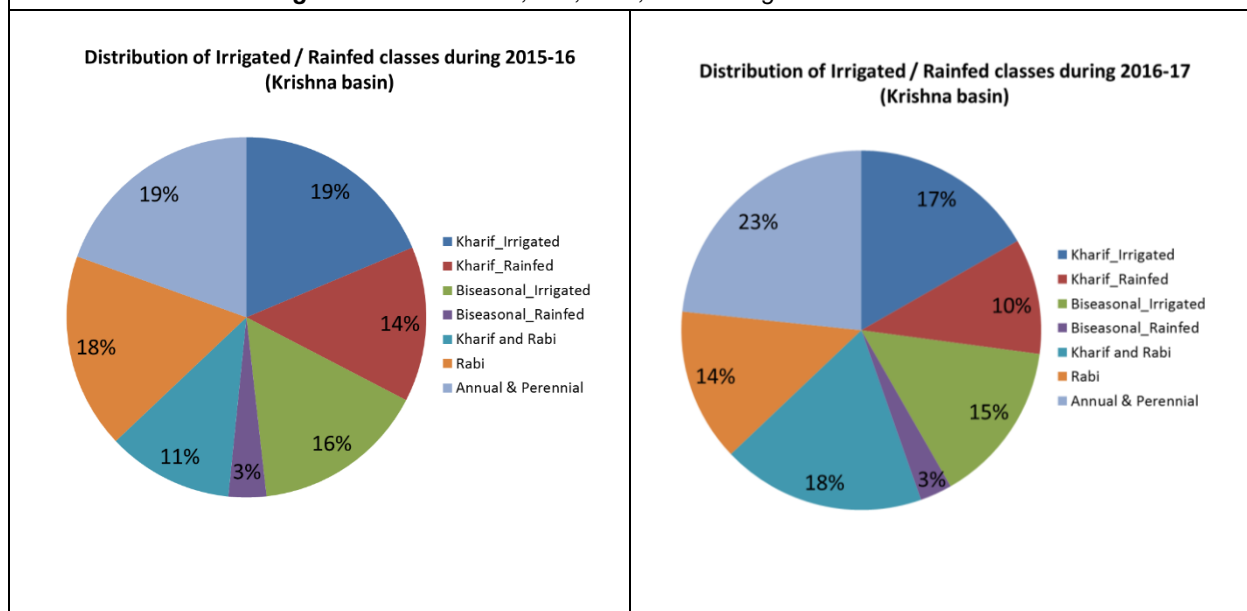


Figure 8: Seasonal distribution of Irrigated / Rainfed classes during 2015-16 & 2016-17

Table 6: Accuracy assessment for seasonal crop group for the year 2015-16

		Crop class obtained by Classification					Total	Users accuracy
Crop group		Kharif	Rabi	Biseasonal	Annual	Unclassified		
Crop Class obtained by Ground truth	Kharif	91	20	17	14	22	164	55.5
	Rabi	20	39	19	4	3	85	45.9
	Biseasonal	26	8	24	1	2	61	39.3
	Annual	17	23	15	35	8	98	35.7
	Total	154	90	75	54	35	408	
Producers Accuracy		59.09	43.33	32	64.8			
Kappa								25.33

Table 7: Accuracy assessment for seasonal crop group for the year 2016-17

		Crop class obtained by classification						
Crop Group		Kharif	Rabi	Biseason al	Annual	Unclassified	Total	Users accuracy
Crop class based on ground truth	Kharif	117	10	22	6	23	178	65.73
	Rabi	11	85	17	6	12	131	64.88
	Biseason al	35	11	45	2	27	120	37.5
	Annual	18	15	17	28	19	97	28.86
	total	181	121	101	42	81	526	
Producers Accuracy		64.64	70.24	44.55	66.66			
Kappa								34.22

4. Conclusions

The study aimed at assessment of Irrigation Potential Utilized in command areas of Krishna basin using temporal satellite data. Irrigation Potential Utilized was estimated as the Gross Irrigated Area in a water year using season specific crop types, irrigated and rainfed categories. The study used a vegetation phenological approach, derived using time-series satellite data for separating season specific crop types, irrigated and rainfed categories in Krishna river basin. Time series maximum NDVI was generated on monthly and fortnightly basis. Reference temporal profiles of NDVI were generated for different crops in different season using ground truth collected. The irrigated or rainfed condition of the crop in Kharif and Rabi season was identified based on the peak of NDVI temporal profile and comparing with reference profiles. The Irrigation Potential Utilized in Krishna Basin was 68, 71,177 ha and 70, 45,436 ha during 2015-16 and 2016-17, respectively. The accuracy of the crop area estimates were carried out by deriving the Kappa statistic indicating fair agreement with the ground observations. Incorporating more intensive ground truth on crop type, irrigation jurisdiction maps, actual irrigation deliveries would help in improving the discrimination of irrigated and rainfed regions with improved accuracies. Also, using additional multi-spectral indices derived water absorption & thermal spectral regions would also improve the accuracy of irrigated area mapping.

References

- Anthony, J.V., and Joanne, M.G. 2005. Understanding Inter observer Agreement: The Kappa Statistic. *Family Medicine*, 7(5), pp.360-3.
- Brian, D. Wardlow, Stephen L. Egbert, and Jude, H.K. 2006. Analysis of time-series MODIS 250 m vegetation index data for crop classification in the U.S. Central Great Plains. *Remote Sensing of Environment*, 108(3), pp.290-310.
- Dadhwal, V.K., Singh, R.P., Dutta, S., and Parihar, J.S. 2002. Remote sensing based crop inventory: A review of Indian experience. *Tropical Ecology*, 43(1), pp.107-122.
- Dadhwal, V.K. and Ray, S.S. 2000. Crop assessment using remote sensing- Part-II: Crop condition assessment and yield forecasting. *Indian Journal of Agriculture Economics*, 55(2), pp.55-67.
- Government of India. 2015. Web based land use statistics information system of India. District wise crop production statistics, <http://lus.dacnet.nic.in/>
- Government of India. 2015. Web based land use statistics information system of India. District wise land use statistics, <http://lus.dacnet.nic.in/>

- Gutman, G., Ignatov, A. 1998. The derivation of the green vegetation fraction from NOAA/AVHRR data for use in numerical weather prediction models. *Journal of Remote Sensing*, 19(8), p.1543.
- Husak, G.J, Marshall, M.T., Michaelsen J., Pedreros, D., Funk C., Galu. G. 2008. Crop area estimation using high and medium resolution satellite imagery in areas with complex topography. *Journal of Geophysical Research*, 113(d14) p.112.
- Jonna, S., and Chari, S.T. 1992. *Irrigated command area inventory using IRS 1A LISS I data*. Proceedings of International Space Year Conference on Remote Sensing and GIS, Feb 26-28, JNTU, Hyderabad, India.
- Kalpana, R., Natarajan, S., Mythili, S., Shekinah, D.E., Krishnarajan, J. 2003. Remote Sensing for Crop Monitoring- A Review. *Agric. Re*, 24(1), pp.31-39.
- Malik, R.P.S. and Briscoe, J. 2006. Handbook of water resources in India: development, management and strategies. Handbook of water resources in India: development, management and strategies.
- Moran, M.S., Inoue, Y., Barnes, E.M. 1997. Opportunities and Limitations for Image-Based Remote Sensing in Precision Crop Management. *Remote Sensing and Environment*, 61; pp.319-346.
- Murali, K.G., Thenkabail, P.S., Nelson, A. 2011. Mapping Irrigated Areas Using MODIS 250 Meter Time-Series Data: A Study on Krishna River Basin (India). *Water*, 3; pp.113-131.
- Myneni, R.B., Hall, F.G., Sellers, P.J., and Marshak, A.L. 1995. The interpretation of spectral vegetation indexes. *IEEE Transactions on Geoscience and Remote Sensing*, 33, pp.481-486.
- Navalgund, R.R. and Ray, S.S. 2000. Geomatics in natural resource management. In proceedings of geomatics-2000, Pune, India NR1-NR14.
- Raju, P.V., SessaSai, M.V.R., and Roy, P.S. 2008. In-season time series analysis of Resourcesat-1 AWiFS data for estimating irrigation water requirement. *International Journal of Applied Earth Observation and Geoinformation*, 10(2), pp. 220-228.
- Ramanayya, T.V., Nagadevara, V., Roy, S. 2008. Study Related to Gap between the Irrigation Potential Created and Utilized. Indian Institute of Management Bangalore.
- Rouse, B.V., Haas, R.H., Scheel, J.A., Deering, D.W. 1974. *Monitoring Vegetation Systems in the Great Plains with ERTS*. Proceedings, 3rd Earth Resource Technology Satellite (ERTS) Symposium, 1, p.48-62.
- Sandholt, I, Rasmaseen, K., Andersan, J. 2002. A simple interpretation of the surface temperature vegetation index space for assessment of soil moisture status. *Remote Sensing of Environment*, 79; pp.213-224.
- Shanker, M. 2017. Assessment of Irrigation Potential Utilization in Major Irrigation Project Using Geospatial Data. *International Journal of New Technology and Research*, 3(4), pp.95-99.
- Weicheng, W. and Eddy, D.P. 2011. *A Simple Algorithm to Identify Irrigated Croplands by Remote Sensing*. In Proceedings of 34th International Symposium on Remote Sensing of Environment, At Sydney, Australia.
- Wim, G.M.B., David, J.M. and Ian, W.M. 2000. Remote sensing for irrigated agriculture: examples from research and possible applications. *Agricultural Water Management*, 46(2), pp.137-155.

Research Article

Spatial Mapping of *Prosopis juliflora* (Swartz) DC in Pudukkottai District, Tamil Nadu, India

Anuja Hiregoudar, A. Rajasekaran and Monika Singh

Forest Ecology and Climate Change Division, Institute of Forest Genetics and Tree Breeding Coimbatore-641002, Tamil Nadu, India

Correspondence should be addressed to Anuja Hiregoudar, anuja.goudar@gmail.com

Publication Date: 25 September 2020

DOI: <https://doi.org/10.23953/cloud.ijarsg.479>

Copyright © 2020 Anuja Hiregoudar, A. Rajasekaran and Monika Singh. This is an open access article distributed under the **Creative Commons Attribution License**, which permits unrestricted use, distribution, and reproduction in any medium, provided the original work is properly cited.

Abstract Invasive Alien Species are serious threat to the natural ecosystem of the world. *Prosopis juliflora* (Swartz) DC is one such species introduced in India as a solution for desertification and to meet the fuel wood demand, but it has spread to various habitats and competes with the native species. The present study focuses on the spatial mapping of *P. juliflora* using Resourcesat – 2 Linear Self Scanning LISS (IV) Imagery through supervised classification and recoding methods. The influence of water bodies and road network on the distribution of *P. juliflora* and the variation in NDVI values of *P. juliflora* from various distances from the water body was assessed using buffer analysis. The results showed that .94% (4404.37 ha) of total geographical area of the district is occupied by *P. juliflora* with Viralimalai taluk contributing highest area (1083.49 ha) among the various taluks. Of the 4404 ha area under *P. juliflora* in the district, 2386 ha falls within the 1 km distance from rivers and streams while 1705 ha area falls within the 1 km distance from road. The percentage of *Prosopis* patches falling in higher NDVI category showed a decreasing trend when the distance to the water body and streams increased.

Keywords *Supervised Classification; Remote Sensing and Geographic Information System*

1. Introduction

Prosopis juliflora (Swartz) DC is an invasive alien species which has become one of the world's 100 most dominant invasive species (Walter and Armstrong, 2014; Becker et al., 2016). It spreads through the transportation of seeds along water courses and through animal dispersal, replacing native plant communities (Pasiiecznik, 2001) and causing negative implications on ecosystem including loss of biodiversity, impact on bird's diversity and habitat, reduction of water resources, loss and degradation of grasslands, farmlands and rangelands, change in plant community composition and plant mortality (Tiwari, 1999; Robbins, 2001; Gorgens and Wilgen, 2004; Scott et al., 2006; Zimmermann et al., 2006; Maundu et al., 2009; Kaur et al., 2012; Schachtschneider and February, 2013; Chandrasekaran et al., 2014).

Information on spatial extent is considered necessary for developing policies regarding invasive species management (Wittenberg and Cock, 2001). Efforts have been made to map the *P. juliflora* invasion in different parts of the world using remote sensing data (Mohamed, et al., 2011; Hoshino, et

al., 2012; Van den Berg, 2013; Mustafa Mirik, et al., 2012 & 2014; Amboka, et al., 2015; Michele Meroni, et al., 2016). However, quantitative assessments of the area invaded by *P. juliflora* and its probable distribution have not been studied adequately in India (Ramachandra, 2010; Pasha et al., 2014; Ragavan, 2015; Vidhya et al., 2017). Keeping this in view the present study focuses on the spatial mapping of the *P. juliflora* in the Pudukkottai district of Tamil Nadu, India.

2. Study Area

Pudukkottai district of Tamil Nadu state lies between the 78° 25' and 79° 15' East longitude and between 9° 50' and 10°40' of the North latitude has been selected for the study (Figure 1). It covers 4663 km² area with a coastline of 39 km, the district accounts for 3.58 percent of the total geographical area of the State. The district is further subdivided into 12 taluks such as Pudukkottai, Kulathur, Tirumayam, Gandarvakottai, Illupur, Karambakudi, Alangudi, Ponnamaravati, Viralimalai, Aranthangi, Avudayarkovil and Manamelkudi. The district comes under hot dry semi-arid agro-climatic zone and the climate is semi-arid tropical monsoonal type.

Generally, a dry and hot climate prevails in this district with the temperature ranges from a maximum of 40.49⁰ C (104.9⁰ F) to minimum of 22.63⁰ C (72.7⁰ F). April to June are the hottest months while December to January are the coldest months. The annual rainfall was 978.8 mm. The soil of the district can be classified into black, red, ferruginous, lateritic, alluvial and beach soils. Vellar is the main river and Agniyar, Pambar and Korai are the seasonal rivers which flows in the district. Apart from these rivers, a number of water bodies like tanks, lakes etc. are available in the district. Most of the fallow lands, dry water bodies and waste lands in the district are invaded by *P. juliflora*. However, there is no information on the spatial extent of *P. juliflora* invasion in the district. (District office website)



Figure 1: Pudukkottai district of Tamil Nadu, India (Study Area)

3. Methodology

Mapping the spread of *P. juliflora*.

Resourcesat-2 Linear Imaging Self Scanning Scanner (LISS- IV) images having 5.8-meter spatial resolution procured from the National Remote Sensing Centre (NRSC), Hyderabad were used for mapping the spread of *P. juliflora* in the district. Data from field survey, toposheets of Survey of India, information from Google Earth and GPS points were used for the mapping. The procured satellite images were georeferenced and supervised classification was done using Maximum Likelihood Classifier (MXL) in ERDAS IMAGINE 2014. Signatures for seven different classes (*Eucalyptus*, *Casuarina*, *P. juliflora*, Water body, Agriculture fields, Coconut and Barren land) were created. Multiple signatures have been collected to help the software for accurate classification.

The accuracy of the supervised classification was assessed with random points and producer accuracy, user accuracy and kappa statistics were calculated based on error matrix. Misclassified pixels were recorded by comparing with False Colour Composites and Google Earth images which highly improved the accuracy of classified images. The recoded raster images were converted into vector layers for assessing the spatial extent of the *P. juliflora* in ESRI ArcGIS 10.1.

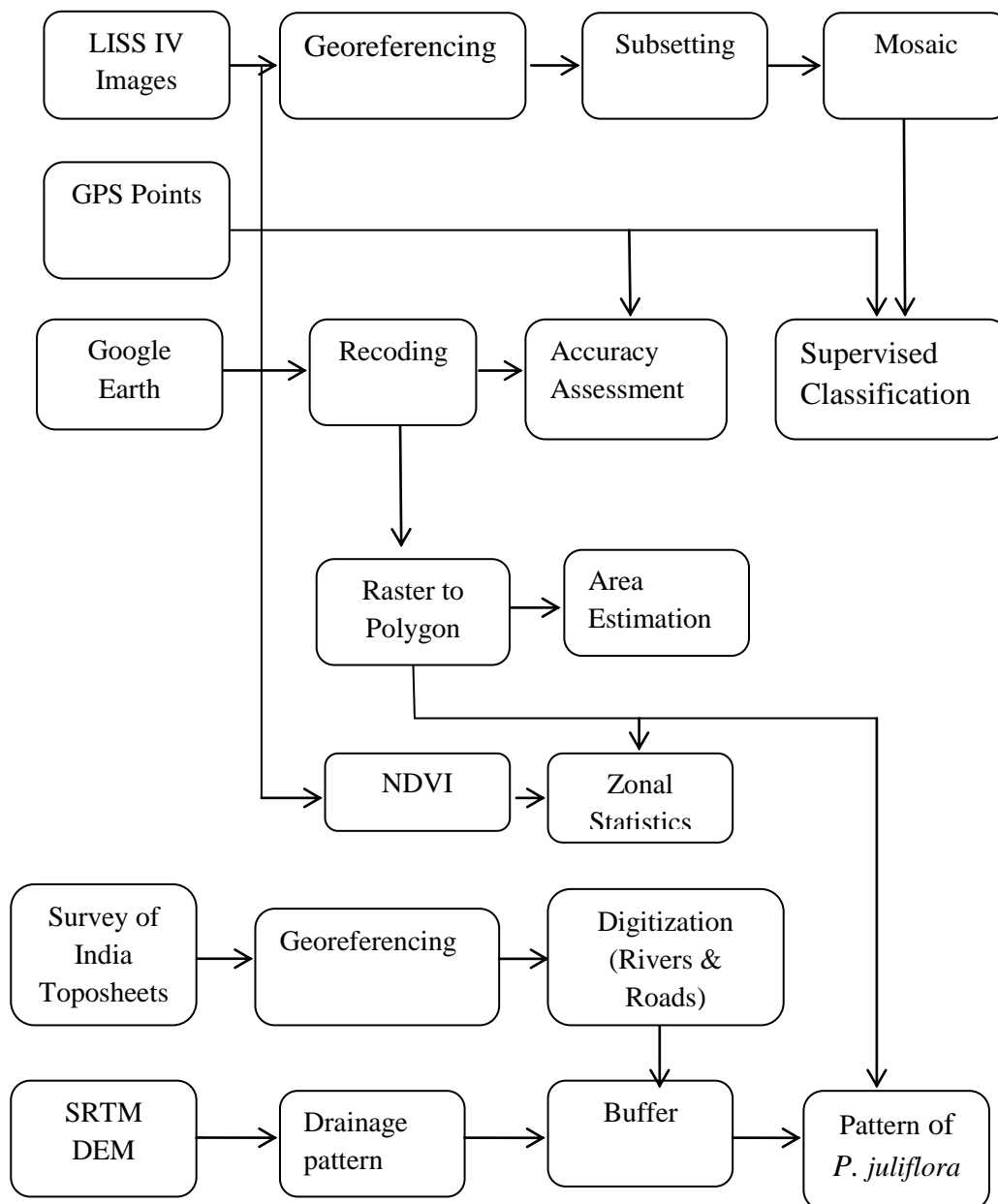
Buffer analysis

The influence of water bodies and road network on the distribution of *P. juliflora* was assessed using buffer analysis. The Shuttle Radar Topography Mission (SRTM) Digital Elevation Model for the study area downloaded from the website (<http://earthexplorer.usgs.gov>) was used for preparation of drainage map by conducting watershed analysis. The river/stream and major roads for the study area digitized from the Survey of India toposheets were superimposed on the drainage maps to identify the rivers/streams of the study area. Buffer of 100, 250, 500, 750 meters and 1 kilometre for the major rivers and roads of the study area were created to analyse the influence of water bodies and road network in ESRI ArcGIS 10.1.

Variation in Normalized Difference Vegetation Index (NDVI) values

Normalized Difference Vegetation Index (NDVI) was computed for the study area to assess the variation in NDVI values across various *P. juliflora* patches. The mean NDVI values for various *P. juliflora* polygons were extracted to vector layer using Zonal Statistics method in ERDAS IMAGINE 2014. The variation in NDVI values of *P. juliflora* polygons in 1 km buffer zones was also studied to assess the role of the water bodies in the growth and health of the *P. juliflora*.

Flow chart of Methodology followed



4. Results and Discussion

Extent of *Prosopis* distribution

In this study, the spatial extent of *P. juliflora* invasion in Pudukkottai district was mapped using Remote Sensing and GIS. The study revealed that 4404.37 ha area of the district has been invaded by *P. juliflora* which is .94% of total geographical area of the district (Table 1). Among the various taluks, Viralmalai has the highest area (1083.49 ha) under *P. juliflora* invasion. The largest and smallest patches of *P. juliflora* are also found in Viralmalai taluk with 141.4 and 0.0074 ha area respectively. About 2 % total geographic area of the Viralmalai taluk is invaded by *P. Juliflora* while 1.65% of total geographic area of the Avudayarkovil taluk is invaded by *P. juliflora* (697 ha area). Though, Kulathur and Pudukkottai taluks have higher area under *Eucalyptus* and *Casuarina* plantations, only 0.96% and 0.89% of their geographical area under *P. juliflora* invasion respectively. Among the various taluks, Manamelkudi has very less area under *P. juliflora* with 86.07 ha (0.34%). Viralmalai and

Avudayarkovil taluks are being drained by Korai and Pambar rivers also have more area under *P. juliflora* invasion.

Table 1: Extent of *P. juliflora* invasion in various taluks of Pudukkottai District

Taluk names	Area of Taluk (ha)	No of patches	Extent (ha)
Viralimalai	49822.5	356	1083.49 (2.1%)
Avudayarkovil	42039.2	233	697.59 (1.6%)
Kulathur	47923.7	145	462.03 (0.96%)
Tirumayam	56667.9	106	376.76 (0.66%)
Gandarvakottai	31700.6	97	310.46 (0.97%)
Pudukkottai	33807.3	167	303.91 (0.89%)
Ponnamaravati	32822.2	142	292.11(0.88%)
Aranthangi	44176.05	80	264.99 (0.59%)
Alangudi	38916.5	66	218.28 (0.56%)
Illupur	35383.5	39	129.12 (0.36%)
Karambakudi	25962.8	51	102.21 (0.39%)
Manamelkudi	25120.3	35	86.07 (0.34%)
Total	464542.98	1566	4404.37 (.94%)

Values in parentheses are % of geographical area.

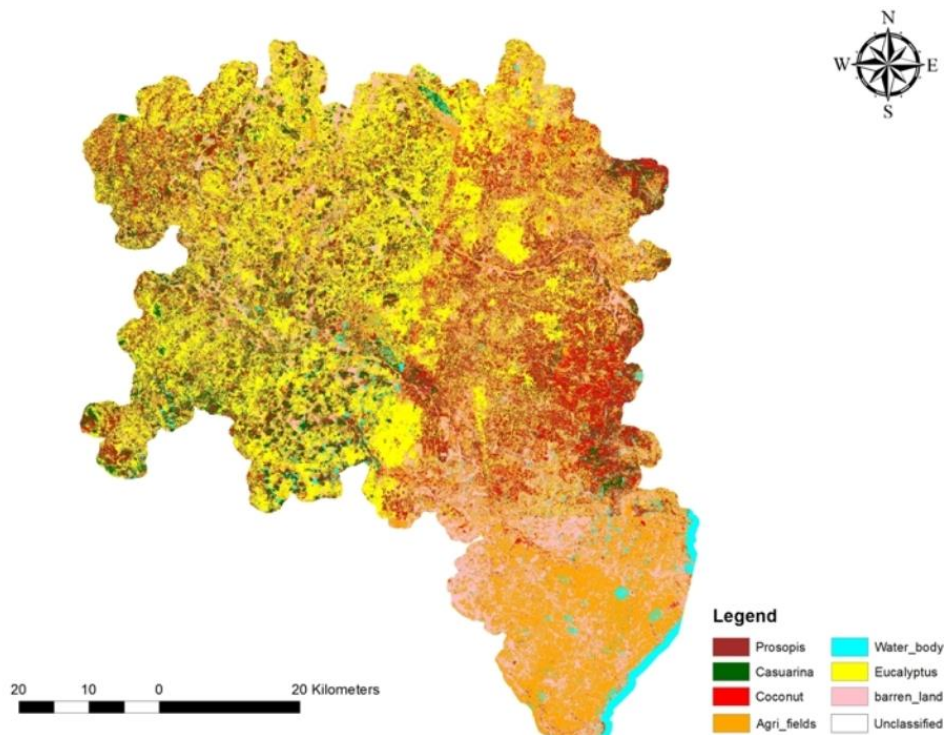


Figure 2: Extent of various landuse in Pudukkottai district

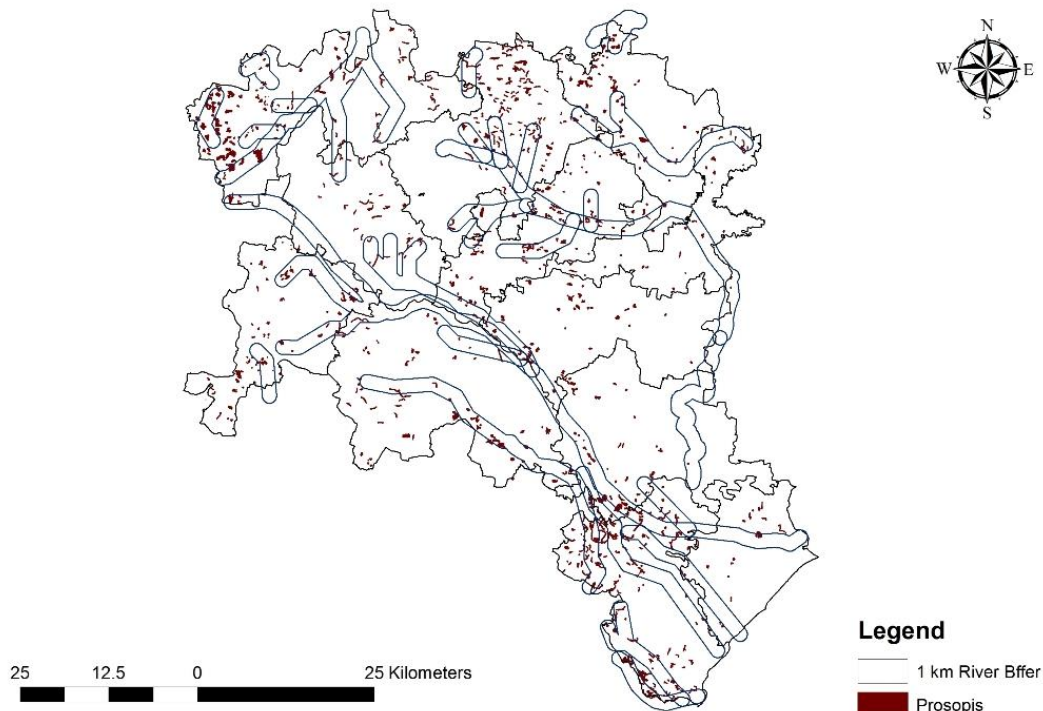


Figure 3: *P. juliflora* invasion near water bodies in Pudukkottai district

There are three zones of *P. juliflora* invasion in the district along the river banks in 1) Viralimalai 2) Kulathur and 3) Avudayarkovil taluks (Figure 3). The river Pambar which also flows through the neighbouring Sivagangai district showed higher *P. juliflora* invasion. It may also be noted that most of the *P. juliflora* invasion has been observed in areas which lies very near to adjacent districts such as Sivagangai, Tiruchirapalli and Ramanathapuram. The output of supervised classification showed that most of the *P. juliflora* occur along the water bodies and in the agricultural fallow lands (Figure 2). The Eastern and the Southern part of the study area showed the highest extreme *P. juliflora* invasion.

Buffer analysis of *P. juliflora* spread

In the present study an attempt was made to assess the influence of water bodies and road network on the distribution of *P. juliflora* using buffer analysis. The study revealed that out of 4404 ha mapped area during study, 2386 ha of area (54%) found within the 1 km buffer of rivers and streams (Figure 3 and Table 2) while 1705 ha area (38%) of *P. juliflora* falls within the 1km buffer of major roads (Figure 4) of the district.

The extent of *P. juliflora* varied across the different buffer zones of the river and roads. 100 m buffer around the river and roads have 12% and 17% of the total area of *P. juliflora* invasion in the district while at the 250 m buffer of river and roads the *P. juliflora* invasion is 16% and 25% respectively. The study indicates that the invasion of the species is more along the water bodies than along the roads. The *P. juliflora* patches are also found near smaller water bodies such as tanks, lakes and minor roads etc. Hence, the buffer analysis along these smaller water bodies and roads will also give more information on the distribution of *P. juliflora*. Since the number of smaller water bodies and minor roads in the district are more, due to paucity of time and non-availability of spatial data on these water bodies and roads, the same could not be included in the analysis.

Table 2: NDVI values of *P. juliflora* in different distances from water bodies

NDVI values	<i>P. juliflora</i> extent (ha)	Distance from water body (m)				
		100	250	500	750	1000
1.000 - 0.500	2005 .15 (45)	470 (59.6)	556 (48.9)	773 (46.1)	938 (44.1)	1006 (42.2)
0.499 - 0.300	2239.19 (50.9)	304 (38.5)	551 (48.5)	823 (49.1)	1087 (51.1)	1270 (53.2)
0.299 - 0.156	160.01 (3.6)	15 (1.9)	29 (2.6)	79 (4.7)	104 (4.9)	110 (4.6)
Total	4404	789	1136	1675	2129	2386

Values in parentheses are % to total

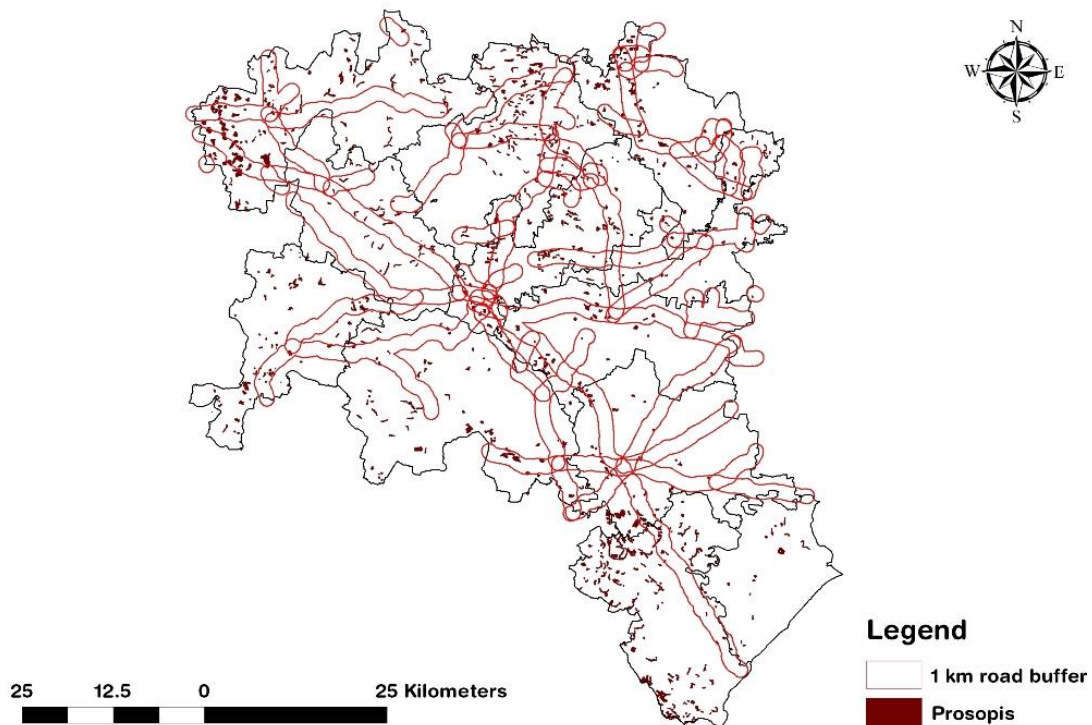


Figure 4: *P. juliflora* invasion near major roads in Pudukkottai district

Variation in Normalized Difference Vegetation Index (NDVI) values

The study showed that 50% of the *P. juliflora* recorded in the study area have NDVI values between 0.499 - 0.300, 45.5% between 1.00 - 0.500 while only 3.6% of *P. juliflora* in 0.299 - 0.156 category of NDVI values (Table 2). This variation in NDVI values could be due to various growth stages of *P. juliflora*, edaphic and topographic factors. Since about 45% of the patches have higher NDVI values than the surrounding vegetation, the NDVI values can also be used to distinguish the distribution of Prosopis and health in terms of biomass and leaf chlorophyll. Similarly, Gunawardena et.al, 2014 assessed NDVI values of Prosopis in Sri Lanka. However, time series analysis of NDVI and other vegetation indices along with field data may provide additional information.

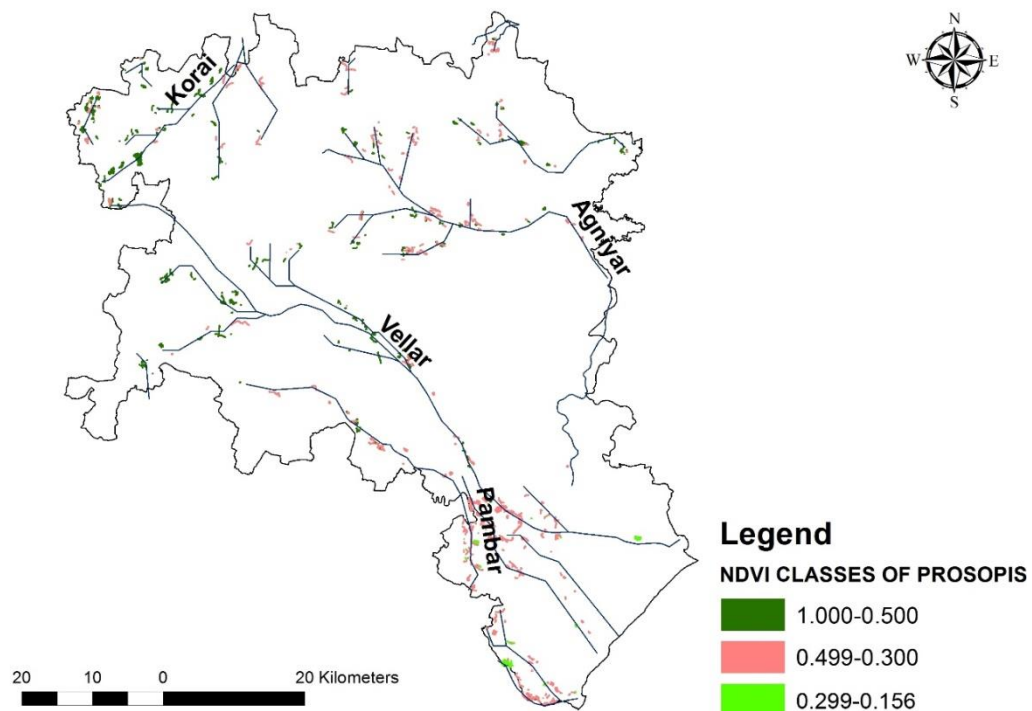


Figure 5: Variations in NDVI values of *P. juliflora*

The assessment of influence of water bodies and streams on the variation in NDVI values of *P. juliflora* using buffer analysis revealed that the percentage of Prosopis patches falling in higher NDVI category showed a decreasing trend when the distance to the water body and streams increased. Of the total 789 ha of Prosopis recorded (Table 2) within 100 m distance from the water body and streams in the study, about 470 ha (59 %) falling in higher NDVI value category (0.5 to 1.0), 38.5 % to the medium NDVI category (0.300 - 0.499) and only 1.9 % is low NDVI value category. However, of the 2386 ha of Prosopis recorded within 1 km distance from the water body and streams in the study, only 42.2% falling in higher NDVI value category (1.00 - 0.5), 53.2% to the medium NDVI category (0.499 - 0.300) and only 4.6 % is low NDVI value category (Table 2). However, NDVI values may vary in different growth stages of the plant, season and years. Hence time series analysis of satellite images is required to get additional information on the influence of water bodies and streams on the variation in NDVI.

5. Conclusion

The present study has quantified the extent of *P. juliflora* in the Pudukkottai district and found variation in spatial extent of *P. juliflora* cover in different distances from water bodies and roads. The spatial information generated will further help the land managers and policy makers in formulating preventive, control or eradication measures. However, the time series analysis of vegetation indices and spread of invasion is required to get additional information for effective management of *P. juliflora*.

Acknowledgements

We would like to thank Institute of Forest Genetics and Tree Breeding, Coimbatore for necessary logistical support in completing this research work. The authors are grateful to the editors and reviewers for their valuable comments and suggestions which have greatly improved the manuscript quality.

References

- Amboka, A.A. and Ngigi, T.G. 2015. *Mapping and monitoring spatial-temporal cover change of P. juliflora species colonization in Baringo Central, Kenya. International Journal of Engineering Science Invention*, 4(3), pp.50-55.
- Becker, M., Alvarez, M., Heller, G., Leparmarai, P., Maina, D., Malombe, I., Bollig M. and Vehrs, H. 2016. Land-use changes and the invasion dynamics of shrubs in Baringo. *Journal of Eastern African Studies*, 10; pp.111-129.
- Chandrasekaran, S., Saraswathy, K., Saravanan N.S., Kamaladhasan, N. and Arunnagendran. 2014. Impact of *P. juliflora*. on nesting success of breeding wetland birds at Vettangudi Bird Sanctuary, South India. *Current Science*, 106(5), pp.676-678.
- Felix Rembold, Ugo Leonardi, Wai-Tim Ng, Hussein Gadain, Michele Meronia, Clement Atzberger. 2015. Mapping areas invaded by *P. juliflora* in Somaliland with Landsat 8 imagery. *Remote Sensing for Agriculture, Ecosystem and Hydrology*, XVII; pp.9637.
- Gorgens, A., and van Wilgen, B. 2004. Invasive alien plants and water resources in South Africa: current understanding, predictive ability and research challenges. *South African Journal of Science*, 100; pp.27-33.
- Gunawardena, A.R, Fernando, T.T. Nissanka, S.P. and Dayawansa, N.D.K. 2014. Assessment of spatial distribution and estimation of biomass of *Prosopis juliflora* (Sw.) DC. in Puttlam to Mannar Region of Sri Lanka using Remote Sensing and GIS. *Tropical Agricultural Research*, 25(2), pp.228–239.
- Hoshino, B., Karamalla, A., Abd Elbasit, M., Manayeva, K., Yoda, K., Suliman, M., Elgamri, M., Nawata, H. and Yasuda, H. 2012. Evaluating the invasion strategic of mesquite (*P. juliflora*) in Eastern Sudan using remotely sensed technique. *Journal of Arid Land Studies*, 4; pp.1–4.
- Kaur, R., Gonzáles, W.L., Llambi, L.D., Soriano, P.J., Callaway, R.M., and Rout, M.E. 2012. Community impacts of *Prosopis juliflora* invasion: biogeographic and congeneric comparisons. *PLOS ONE*, 7(9), e44966.
- Maundu, P., Kibet, S., Morimoto, Y., Imbumi, M., and Adeka, R. 2009. Impact of *Prosopis juliflora* on Kenya's semi-arid and arid ecosystems and local livelihoods. *Biodiversity*, 10; pp.33–50.
- Mohamed, A.H., Holechek, J.L., Bailey, D.W., Campbell, C.L. and DeMers, M.N. 2011. Mesquite encroachment impact on southern New Mexico rangeland: remote sensing and geographic information systems approach. *Journal of Applied Remote Sensing*, 5; pp.1-11.
- Mustafa Mirik, Sriroop Chaudhuri, Brady Surber, Srinivasulu Ale and R. James Ansley. 2013. Detection of two intermixed invasive woody species using colour infrared aerial imagery and the support vector machine classifier. *Journal of Applied Remote Sensing*, 7(1); 073588.
- Pasha, S.V., Satish, K.V., Reddy, C.S., Prasada Rao, P.V.V. and Jha, C.S. 2014. Satellite image-based quantification of invasion and patch dynamics of mesquite (*P. juliflora*) in Great Rann of Kachchh, Kachchh Biosphere Reserve, Gujarat, India. *Journal of Earth System Science*, 123(7), pp.1481-1490.
- Pasiecznik, N., Felker, P., Harris, P., Harsh, L. and Cruz, G. 2001. *The P. juliflora – P. pallida complex: A monograph. Forest Ecology and Management*, 174(1-3), p.605.

Pudukkottai District Administration, 2020. <https://pudukkottai.nic.in/>

Ragavan, K. and Johnny, J.C. 2015. Quantification of invasive colonies of *P. juliflora* using remote sensing and GIS techniques. *International Journal of Engineering and Technical Research*, 3(5), pp.110-115.

Ramachandra, T.V. 2010. Mapping of fuel wood trees using geoinformatics. *Renewable and Sustainable Energy Reviews*, 14; pp.642–654.

Robbins, P. 2001. Tracking invasive land covers in India, or why our landscapes have never been modern. *Annals of the American Association of Geographers*, 91; pp.637-659.

Schachtschneider, K. and February, E. C. 2013. Impact of *Prosopis* invasion on a keystone tree species in the Kalahari Desert. *Plant Ecology*, 214(4), pp.597–605.

Scott, R., Huxman, T., Williams, D. and Goodrich, D. 2006. Eco-hydrological impacts of woody-plant encroachment: seasonal patterns of water and carbon dioxide exchange within a semiarid riparian environment. *Global Change Biology*, 12; pp.311-324.

Tiwari, J.W.K. 1999. Exotic weed *P. juliflora* in Gujarat and Rajasthan, India: boon or bane. *Tiger paper*, 26; pp.21-25.

Van den Berg, E.C., Kotze, I. and Beukes, H. 2013. Detection, quantification and monitoring of *P. juliflora* in the Northern Cape Province of South Africa using remote sensing and GIS. *South African Journal of Geomatics*, 2(2), pp.68-81.

Vidhya, R., Vijayasekaran, D. and Ramakrishnan, S.S. 2017. *Mapping invasive plant P. juliflora in arid land using high resolution remote sensing data and biophysical parameters*. *Indian Journal of Geo Marine Sciences*, 46(6), pp.1135-1144.

Walter, K.J. and Armstrong, K.V. 2014. Benefits, threats and potential of *P. juliflora* in South India. *Forests, Trees and Livelihoods*, 23; pp.232-247.

Wittenberg, R. and Cock, M.J.W. 2001. *Invasive alien species: A toolkit of best prevention and management practices*, CAB International; Wallingford, UK.

Zimmermann, H., Hofmann, J. and Witt, Arne. 2006. A South African perspective on *Prosopis*. *Biocontrol News and Information*. 27; pp.6-9.

Research Article

An Open Source Free Downloadable GUI Based Image Processing Software for Performing Various Mathematical and Statistical Operations on Remote Sensing Images

Hari Shanker Srivastava¹, Santvana Nigam²

¹ Indian Institute of Remote Sensing (ISRO), Dehradun – 248 001, India

² Department of Computer Science, Banasthali Vidyapith, Tonk – 304 022, India

Correspondence should be addressed to Dr. Hari Shanker Srivastava, hari.isro@gmail.com

Publication Date: 29 September 2020

DOI: <https://doi.org/10.23953/cloud.ijarsg.480>

Copyright © 2020 Hari Shanker Srivastava, Santvana Nigam. This is an open access article distributed under the **Creative Commons Attribution License**, which permits unrestricted use, distribution, and reproduction in any medium, provided the original work is properly cited.

Abstract Effective interpretation of remote sensing images acquired by space borne and air borne sensors requires various mathematical and statistical operations to be applied to them. Importance of use of various mathematical and statistical operations on Remote Sensing Images enhances manifold if the research/project work requires analysis of large number of these images. A large number of commercial image processing software are available in the market to support the requirement of implementation of various Mathematical and Statistical operations on remote sensing images. However, the cost of commercial software is very high; therefore, they are not affordable by schools and few institutes where sufficient funding is not available. Looking at the requirement of a freely available image processing software to perform various mathematical and statistical operations on large number of remote sensing images or a multi-band image, a GUI based image processing software has been developed to help those who want to work and explore remote sensing data but doesn't have sufficient funds to purchase costly software. Based upon the objective of the software, the name of the software has been decided as MASC (Mathematical and Statistical Calculator). This paper is about 'MASC' GUI which performs operations similar to 'mathematical and statistical operations on various bands' tool of some of the commercially available software. 'MASC' software is very useful in image enhancement and interpretation. The aim of this paper is to explain the various features of 'MASC' software. It is developed in MATLAB 2013a along with some java libraries whose functions are incorporated with the MATLAB code to enhance the look and field of the GUI and make it user friendly.

Keywords *Band Calculator; Binary Image Formats; Expression Evaluator; gain and offset; MASC Software; MATLAB*

1. Introduction

Remote Sensing is the science and art of obtaining information about an object or target without touching it. The images which are captured can be digital or analog. The analog images are mainly taken via aircraft associated with a sensor and the digital images are taken from satellites. A digital

image is a two-dimensional array of pixels. Each pixel has an intensity value (represented by a digital number) and a location address (referenced by its row and column numbers) [1].

The intensity value represents a physical quantity such as solar radiance, emitted infrared radiation or backscattered radar intensity. The intensity value is basically a digital number and the number of bits is the measure of the radiometric resolution of the image. For example, a 16-bit number ranges from 0 to 65535 (i.e. $2^{16} - 1$). The image band is two dimensional and the location address of the pixel is denoted by the row and column coordinates [1].

Image bands are a collection of images taken simultaneously of the same area in multiple regions of the electromagnetic spectrum. Human vision is able to detect three wavelengths: red, blue and green. All the colours that humans can perceive can be created by mixing these three colours [2].

Images can be displayed as grey scale images or colour composite images popularly known as False Colour Composite (FCC). Grey scale images comprise of only a single band whereas a FCC is a combination of three bands at a time. Associating each spectral band to a separate primary colour, results in a colour composite image. Colour composite images can be mainly of two types. First type of composite is known as **True Colour Composite**, which consists of three visual primary colour bands in such a way that the images resemble the original view. Second but commonly used composite is known as False Colour Composite (FCC) in which three bands are assigned arbitrary colours in such a manner that the image does not resemble the original view and is therefore known as False Colour Composite image [3].

Remote sensing data (images) acquired from various sensors and platforms have already proved its importance for the assessment, monitoring and management of natural resources in the entire globe. However, effective interpretation of remote sensing images acquired by space borne and air borne sensors requires various mathematical and statistical operations to be applied to them. Importance of use of various mathematical and statistical operations on Remote Sensing Images enhances manifold if the research/project work requires analysis of large number of Remote Sensing Images. A large number of commercial image processing software are available in the market to support the requirement of implementation of various Mathematical and Statistical operations on remote sensing images. However, in general, the cost of various commercial software are very high. Therefore, they may not be affordable by many schools and few institutes where sufficient funding is not available.

Looking at the requirement of a freely available image processing software to perform various mathematical and statistical operations on large number of remote sensing images or a multi-band image, a GUI based image processing software has been developed to help those who want to work and explore remote sensing data but doesn't have sufficient funds to purchase costly software. Based upon the objective of the software, the name of the software has been decided as MASC (Mathematical and Statistical Calculator). This paper is about 'MASC' GUI which performs operations similar to 'mathematical and statistical operations on various bands' tool of some of the commercially available software. These software are very useful in image enhancement and interpretation. The aim of this paper is to explain the various features of 'MASC' software. It is developed in MATLAB 2013 along with some java libraries whose functions are incorporated with the MATLAB code to enhance the look and field of the GUI and make it user friendly [4-5].

The 'MASC' software is developed to handle optical images of 8-bit, 16-bit, 32-bit and double data. If user wants to apply mathematical and/or statistical operations on multi-band remote sensing data, the input image files should be layer stacked with any number of bands, user can use any interleave format [6]. However, user is required to keep an associated '.hdr' file in the same folder where he is keeping the input image data. The input images are loaded into the GUI's central panel. These images can be grey scale or colour composite images (both true and false colour composite).

2. Conceptualization of MASC Software

This GUI will be used for better and effective interpretation of an image. It performs various arithmetic, exponential, logarithmic, trigonometric and statistical functions on image bands. When an image is taken it has a certain DN (digital number) value associated with each pixel. This DN value contains useful information about the target. Interpretation of single band remote sensing data is very easy but use of single band to extract useful/meaningful information about a target is not always possible. Therefore, it is a common practice in remote sensing to exploit multi-frequency or multi-temporal images of same area to extract detailed and meaningful/useful information about a target. However, interpretation of multi-band (multi-frequency and/or multi-temporal) remote sensing data is difficult, especially when number of input bands are more than three. In case of large number of input bands user needs to apply many mathematical and/or statistical operations on the set of images under consideration. Looking at the huge requirement of various mathematical and statistical operations on multi-band data "An Open Source Free Downloadable GUI Based Image Processing Software for Performing Various Mathematical and Statistical Operations on Remote Sensing Images" has been developed for the benefit of students of those schools where sufficient funding is not available. The software may also be useful for those researchers who are not getting scholarship or funding but willing to explore freely available remote sensing data. 'MASC' GUI which performs operations similar to 'mathematical operations on various bands' tool of some of the commercially available software, is also very useful in image enhancement and interpretation.

This GUI is built using MATLAB 2013a along with some java libraries whose functions and classes are incorporated with the MATLAB code to enhance the look and field of the GUI and make it user friendly [7]. MATLAB comes with a bunch of libraries which comprise of mathematical functions. Along with that MATLAB also has an image processing toolbox which makes working on images easier in comparison to other software [8-9]. In order to read and perform operations on optical images, MATLAB's 'ENVI file reader/writer' library is used [10-11].

In order to implement 'mathematical/statistical operations on various bands' tool, several mathematical/statistical functions have been used along with user defined functions. In addition to this, an expression evaluator algorithm has been developed which is capable of solving a valid mathematical/statistical expression on image bands and provides the output.

Along with 'mathematical/statistical operations on various bands' tool, this software also provides the user various other features like adjusting gain and offset values, pixel value display box, spatial sub setting and spectral profile in order to enhance user experience. These features shall be discussed further in detail.

3. Software Design

The name of the software is coined as 'MASC', which is abbreviation of 'Mathematical and Statistical Calculator'. Figure 1 shows the GUI with two opened images. At the top of the GUI is a menu bar followed by a toolbar. The tool bar consists of all the options present in the menu bar for the quick access of the user. Various shortcut keys have been provided to use the GUI tools effectively. The help option in the menu bar or  button in the toolbar provides all the necessary indications to use the 'MASC' software and information about the various components of 'MASC' software.

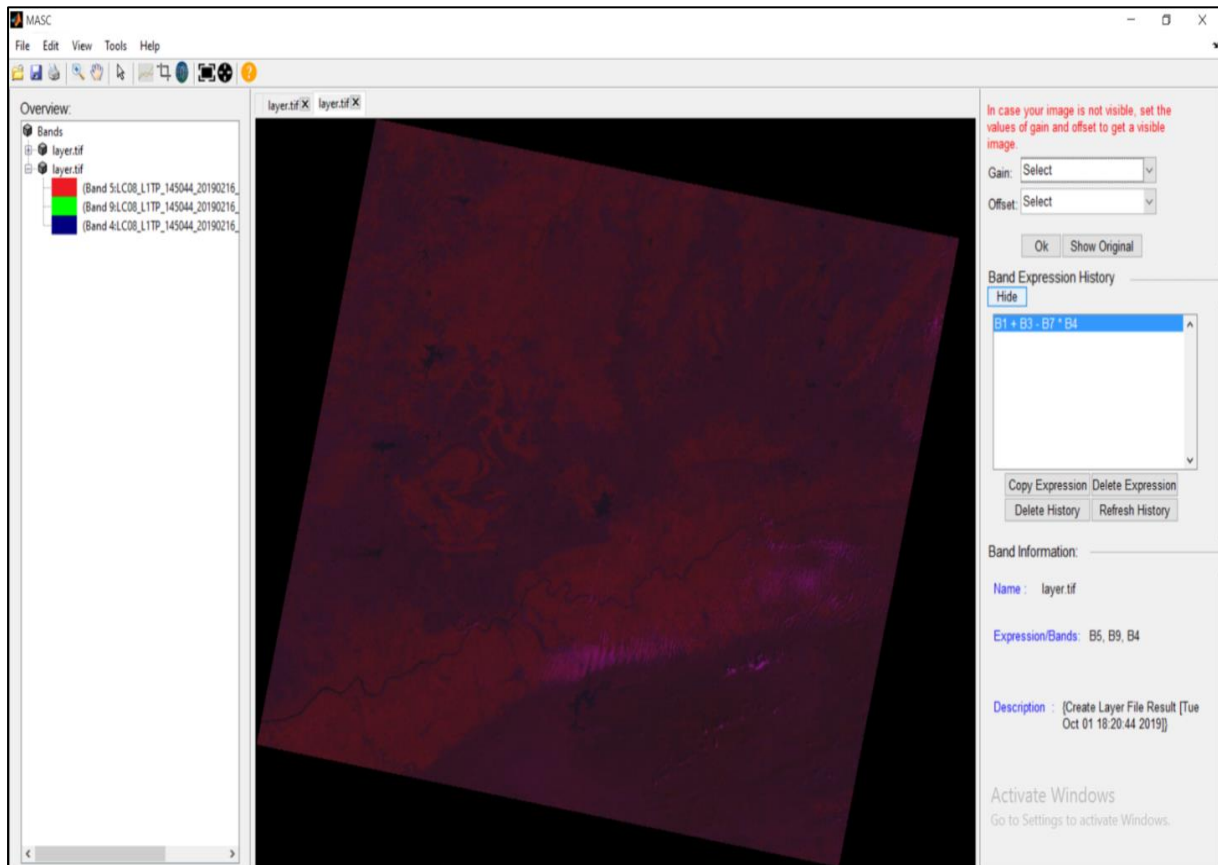


Figure 1: GUI with two opened images

Below the toolbar the GUI window is divided into three parts: the overview, the display panel and the panel which comprises of gain and offset option, the band expression history and the band information. The overview displays all the currently opened images in the central panel along with names of their respective bands. This is displayed in the form of a tree structure. The central panel is a java based tabbed panel where each new image opens in a new tab. The right panel is divided into following three parts (viz. the gain and offset, the band expression history and the band information)

- 3.1. **The gain and offset** adjusts the grey scale image level of brightness and contrast. The gain and offset values are obtained when the user selects them from the drop down list and clicks OK button. The gain value is multiplied to the image colour map and the offset value is added to it. Both gain and offset helps in balancing the brightness and contrast of an image without affecting the original pixel values of an image [12].
- 3.2. **The band expression history** helps in storing the saved band calculator expressions from the band calculator dialog box. Even after closing the GUI, the saved expressions remain in the band history. The user is given a choice to delete an expression, delete entire history, refresh history or copy an expression from the history to use it again.
- 3.3. **The band information displays** the current image name, the band number it is comprised of or the band expression it is formed of, the description of the band and the original band name if the band is a derived band. A band can be a derived band only in two scenarios: it is the output of a band calculator expression or it is the output of spatial sub setting of an image. This information changes as the user switches from one tab to other.

The GUI is very user friendly as it provides the user with the options of zoom, pan, save, open, print, fit to window and convert. These options help in analysing images in a better way. The information regarding the use of these tools is provided in the help.

The zoom option helps in zooming in or out of the image using mouse scroll. Clicking again on zoom will deactivate zoom option. The pan option helps in hovering over the zoomed in image wherever you want and works in a similar manner like zoom. The print option helps in printing the current image on the screen. Save option saves the image but does not create a '.hdr' file for the same. In order to view the image in the GUI its '.hdr' file should be present. For this the user is provided with the convert option in the file menu. This option allows the user to decide the interleave as well as the image format and creates a '.hdr' file for the image in the same folder in which the original image is present and saves it. This converted image can be opened in the GUI using its '.hdr' file.

The GUI displays error message wherever user tries to perform an invalid operation. For example, gain and offset is applicable only to grey scale image. If the user tries to perform gain and offset operation over an RGB image then an error message is displayed indicating invalid operation and notifying the user with the correct operation. Along with these features, this software also comprise of certain tools. Detailed description of various tools of MASC software is provided in next section.

4. Detailed Description of Various Tools Available with MASC Software

Although MASC software has essentially been designed to perform 'mathematical and statistical operations on various bands' of remote sensing images. However, in order to enhance the utility of MASC software for users, various additional tools have also been added in MASC software. These tools are (a) Band Calculator, (b) Cursor Value, (c) Spectral Profile, (d) Image Sub-setting, and (e) Converter. Additional tools like Cursor Value Tool, Spectral Profile Tool, Image Sub-setting Tool, and Converter Tool along with key tool of MASC software (i.e. Band Calculator Tool) make this software a complete package for basis analysis of temporal or multispectral Remote Sensing Images.

4.1. Band Calculator Tool

The band calculator tool comprise of various mathematical and statistical functions [13]. The user can open band calculator dialog box (Figure 2) from Tools->Band Calculator, or they can directly click on the  icon on the tool bar. The user can also make use of the shortcut Ctrl + B.

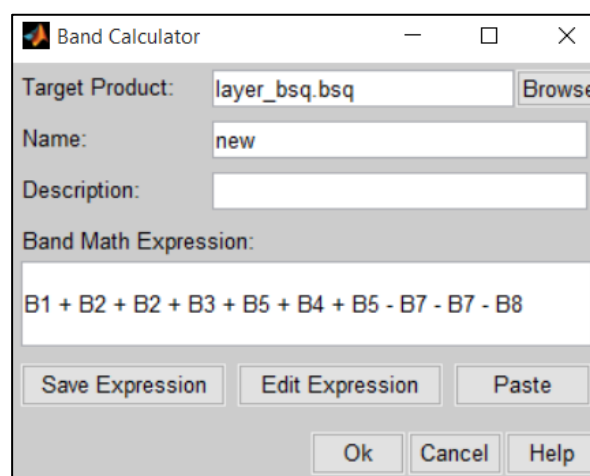


Figure 2: Band Calculator dialog box

After entering the required details, clicking on the edit expression will open the expression editor (Figure 3) as follows:

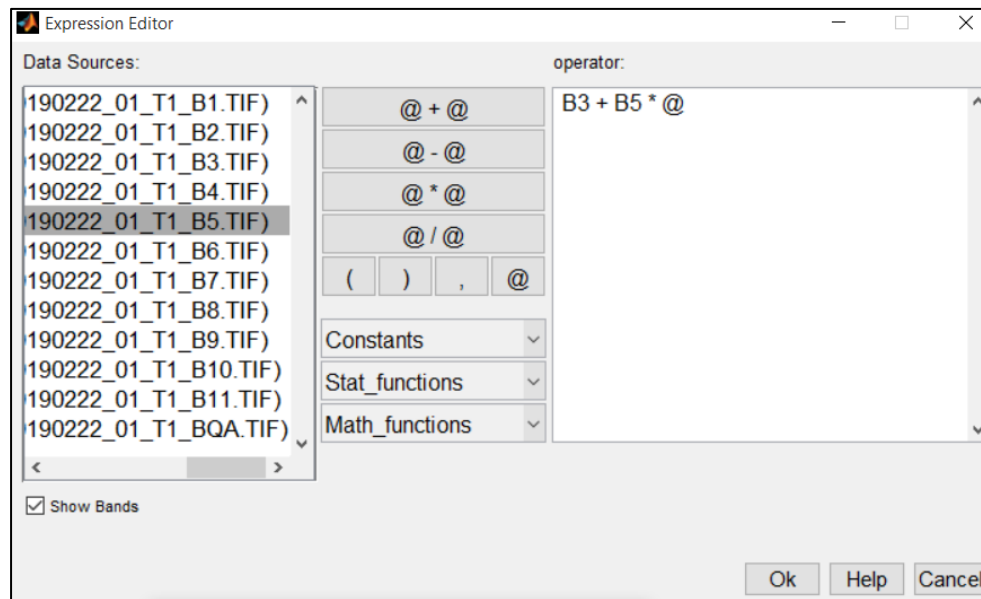


Figure 3: Band Expression Editor

The band expression editor is an expression generation tool that generates a band expression which will be evaluated further [13-16]. It is provided with a list of commonly used constants, statistical and mathematical functions along with all the basic arithmetic operators and special symbols. The help option displays a page which is an instruction manual for the users to understand the working of the editor. If a wrong expression has been formed, an error dialog box is displayed on the screen.

4.2. Cursor Value Tool

Simply opening the band calculator, writing the expression and getting the output will not give the surety that the user is getting the correct result. For this, the GUI is provided with a cursor value option which gives the pixel value of the current cursor position along with the pixel values of the neighboring pixels. The cursor value displays the pixel value of the current pixel rectangle. It is capable of displaying a single pixel value as well as the values of neighboring pixels.

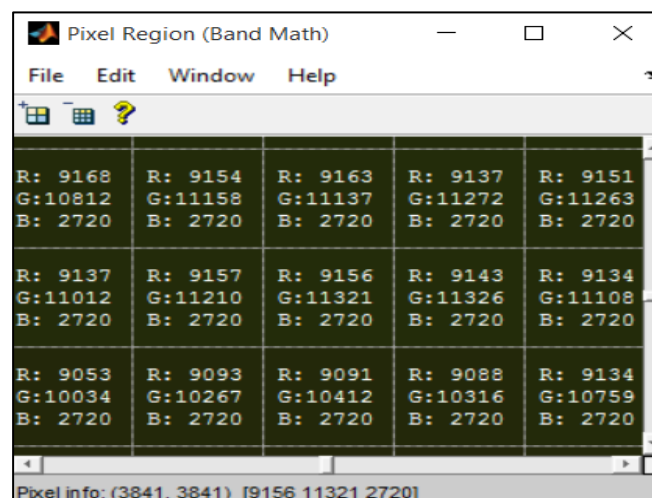


Figure 4: Pixel Region Value Box

The pixel region dialog box (Figure 4) displays the current rectangle pixel values and the bottom left corner displays the image coordinate along with the pixel values of the coordinate on which the cursor is pointing in the dialog. It displays the pixel values of RGB, grey scale and also 8-bit, 16-bit, 32-bit unsigned integer and also double values [17].

4.3. Image Sub Setting

The spatial sub setting of an image is possible with the help of image sub setter. The user can either directly select the subset area as shown in Figure 5(a) or he/she can enter the lines and sample range for sub setting as shown in Figure 5(b). The subsetted image will be displayed after clicking OK button.

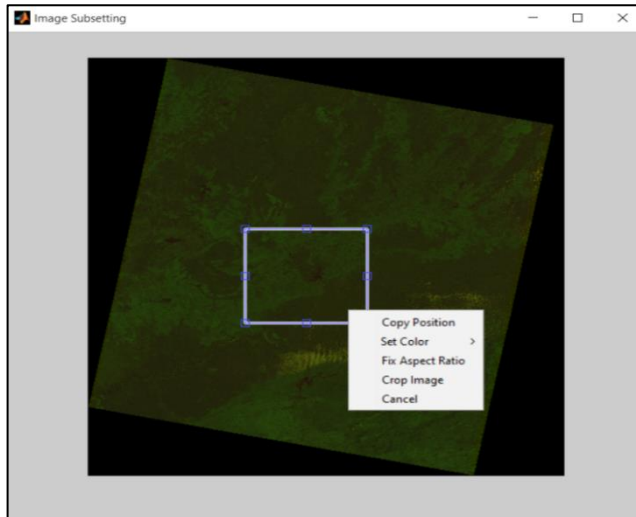


Figure 5(a) DirectSub setting from an image

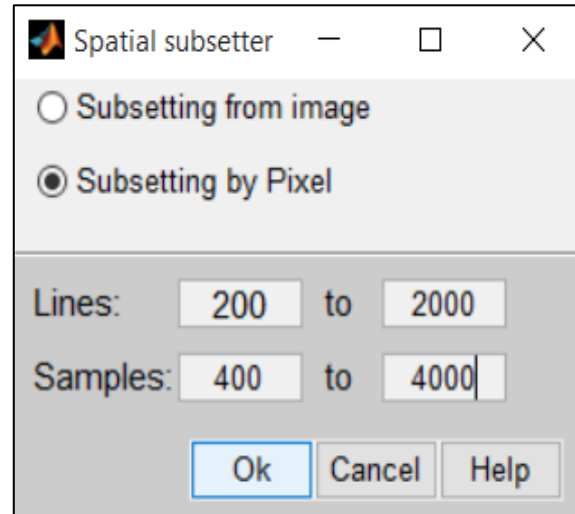


Figure 5(b) Sub setting by pixel

In 5(a) the user can drag using mouse the area he wants to select, right click and select crop. The area selected will be displayed in a new window. Whereas in 5(b), 'lines' is rows and 'samples' is columns. The user can set the range of lines and samples to get the image within this range. The subsetted image is displayed in a new tab. An error message is generated if the user inputs wrong data or the data which is not within range.

4.4. Spectral Profile Tool

The spectral profile (Figure 6) is a graph which is displayed for an image which is loaded into the GUI. The x-axis of the graph represents all the image bands in the image and the y-axis represents their corresponding pixel values.

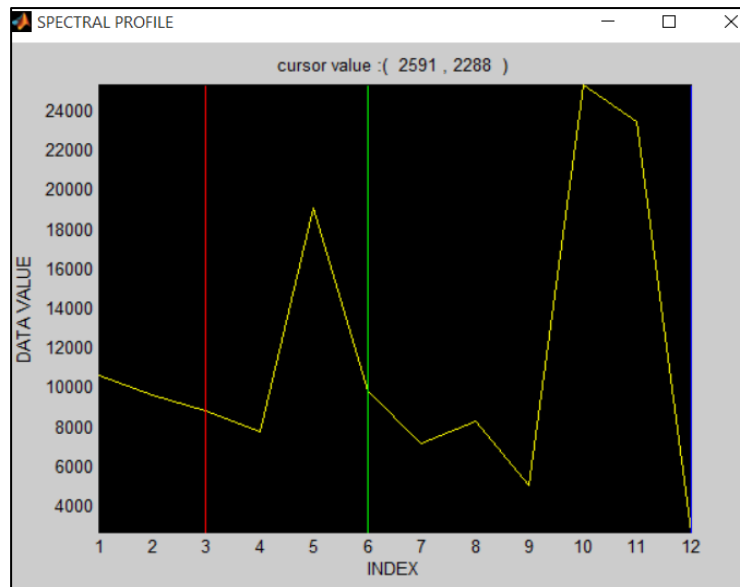


Figure 6: Spectral Profile

4.5. Converter Tool

The user can generate an image using image subsetter or band calculator and now he/she can save this image in his own binary and image format using the converter tool in the convert image dialog box (Figure 7). The user can give name to the file and this image will get stored in the required interleave and image format. The valid image formats are: .tif, .png, .jpg, .bsq, .bip and .bil.

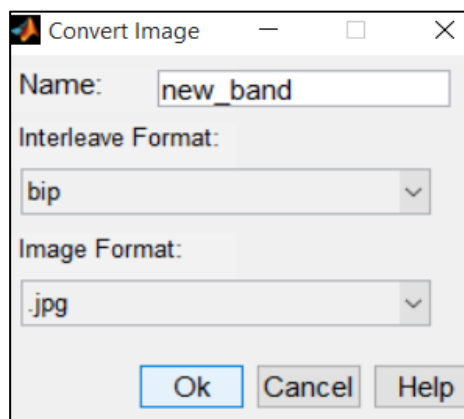


Figure 7: Convert Image Dialog Box

5. Opening an Image in GUI

When the software window loads onto the screen the first task is to open an image in the panel. The image should be an optical image along with a '.hdr' file. As the image appears, the tools and operations which can be applied on the image also appear on the toolbar. The '.hdr' file is a header file which contains information about the image like lines, samples, bands, band name, interleave format, etc. This information is fetched and the image is displayed as a 3-D matrix if RGB and a 2-D matrix if grey scale. Every image is stored inside the computer's memory in some binary format. This format cannot be displayed. It has to be converted into a matrix form for the viewer to see.

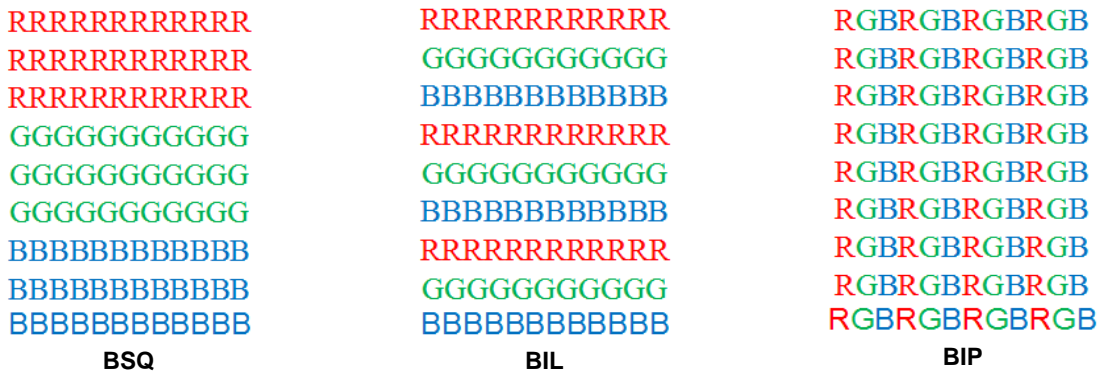
5.1. Binary Image Formats

This tool performs operations on optical image bands which consist on non-complex data. Basically there are three ways in which an image is stored in a binary format. They are namely: BSQ, BIL and BIP [18-19].

BSQ: It stands for Band Sequential. In this format the bands are stored one after the other. The first band will be stored first followed by the second and the third band.

BIL: It stands for Band Interleaved by Line. In this format the first line comprise of the first band. The second line comprises of the second band and the third line comprise of the third band. And this pattern is repeated till the end.

BIP: It stands for Band Interleaved by Pixel. As the name suggests, first pixel is the first pixel of the first band, second pixel is the first pixel of the second band third pixel is the first pixel of the third band and this pattern is repeated till the end.



BSQ, BIL and BIP are just storage formats and they don't disturb the basic arrangement of pixels in an image band. Therefore when the user wants to view the image, the R,G and B pixel values are fetched from the above and are stored as follows:



Figure 8: RGB pixel values are stored in the form of a 3-D matrix

This 3-D matrix of pixels is displayed on the screen.

6. Calculations performed by band calculator on images

On getting the expression using the band calculator expression editor in 'MASC' GUI the expression will be evaluated. Each band will be extracted in a 2-D matrix and the operations between two bands will be performed on each of the corresponding pixel in each band. The band expression $b1+b2+b3$ will be evaluated as shown in Figure 9 [20].

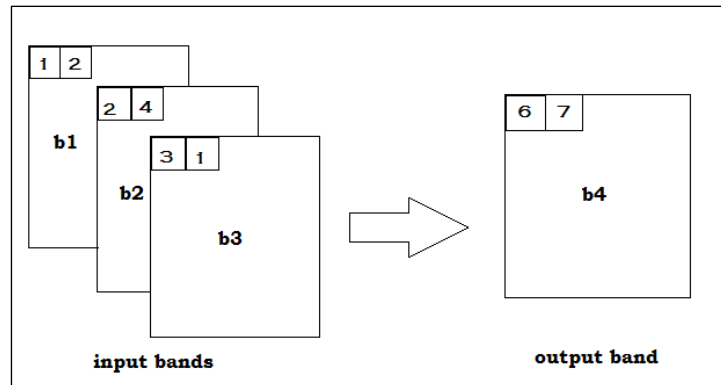


Figure 9: Input and output bands after performing band operation $b1+b2+b3$

Hence, all the corresponding pixels will be added together to give the new band b4 in the above example. The output will always be a grey scale image. The band calculator will similarly perform other mathematical and statistical operations on bands considering corresponding band values as operands.

6.1. Band Expression Evaluation Algorithm

The simple expressions can be evaluated using stack. But for evaluating band expressions which comprise of trigonometric and statistical functions, the simple expression evaluation algorithm needs to be expanded. This is possible with the help of stack in MATLAB 2013a. MATLAB performs operations on images. A simple addition operation can be performed on all the pixels of an image simultaneously. Thus, this feature of MATLAB avoids looping and reduces the time taken by the algorithm. This algorithm is implemented using stack [20-21].

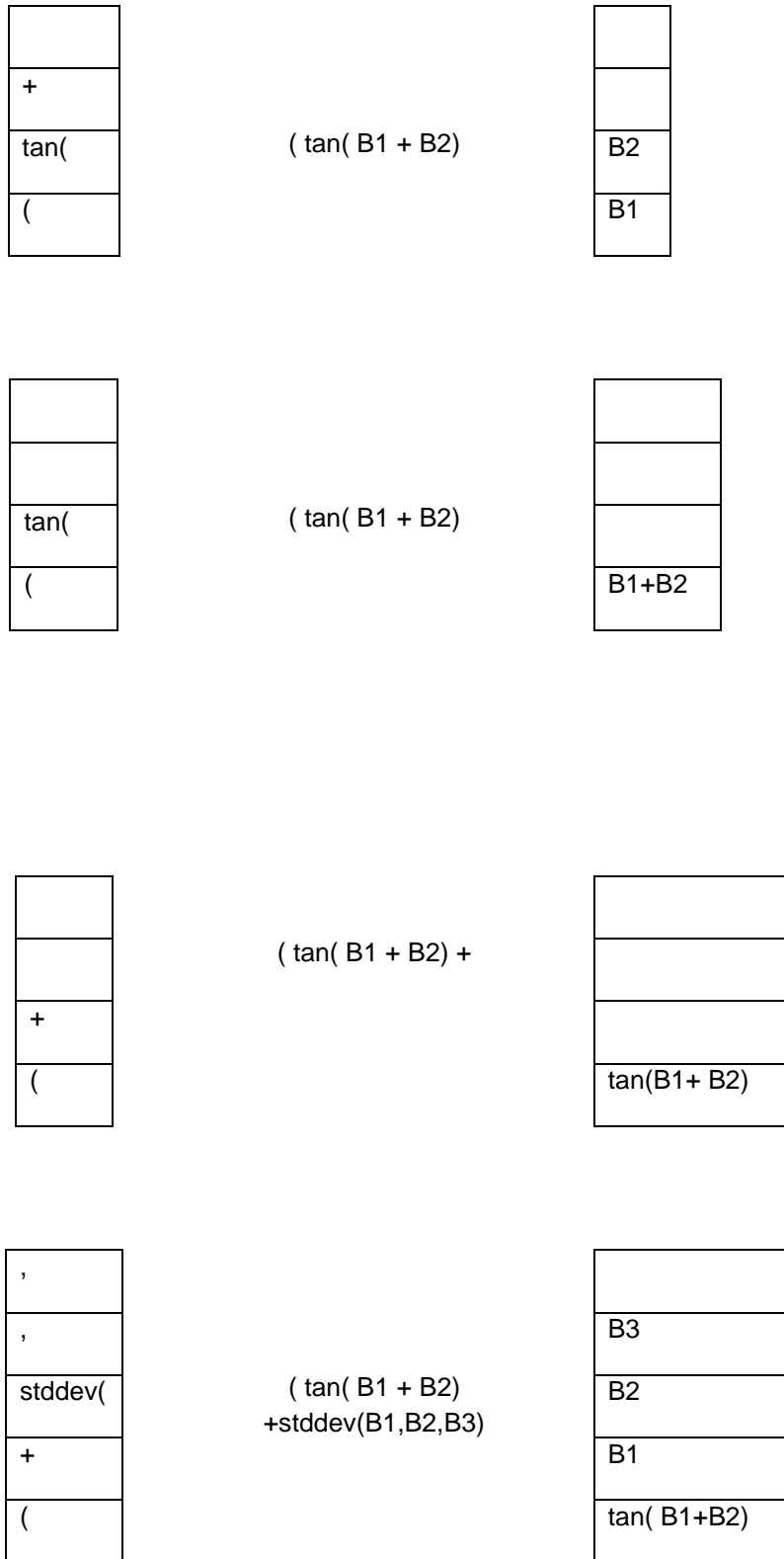
A band expression can involve any size of data. For example:

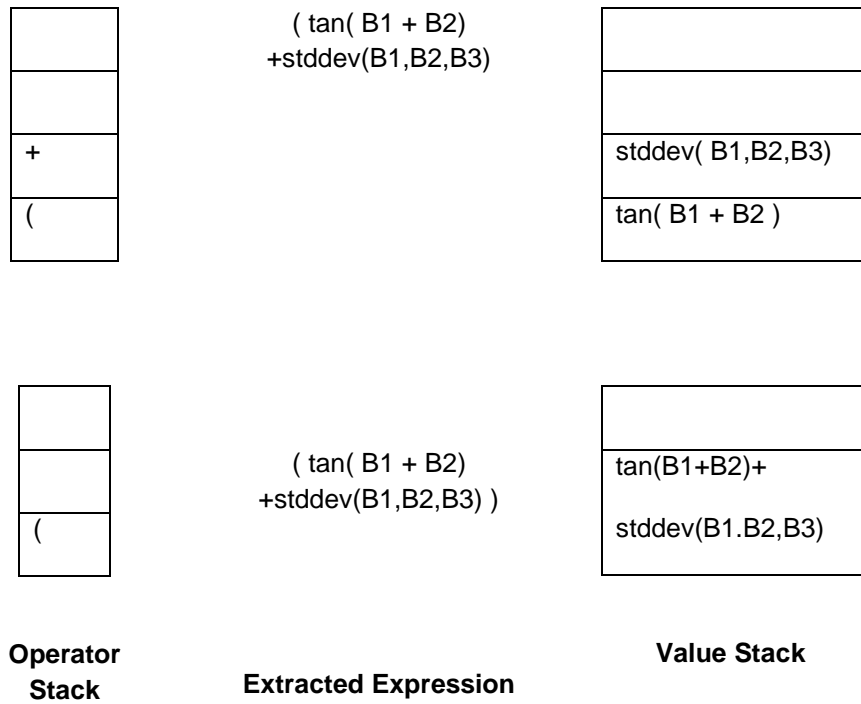
$$B1 + B2 - B3 * 0.5$$

In the above expression, the band B1, B2 and B3 belong to the same image and hence have the same size, but the constant 0.5 is a single value which is to be multiplied with every element of B3. While implementing stack we usually prefer numerical arrays. But numerical arrays contain numerical scalars as elements. Therefore, it is impossible to store a different number of elements in different slices of same dimensions. Instead of using numerical arrays **MASC** uses cell arrays as they contain variables of any type and dimensions as elements.

Let us consider a sample expression:

$\tan(B1 + B2) + \text{stddev}(B1, B2, B3)$





The band editor reads the expression as:

('tan(' 'B1' '+' 'B2' ') '+' 'stddev(' 'B1' ',' 'B2' ',' 'B3' ') '')

All the operators, functions, brackets and commas are pushed into the operator stack and all the variables and constants are pushed into the value stack and the expressions are evaluated according to the following order of precedence:

Table 1: Operator/ Functions Precedence Table

Precedence Number	Operators/ Functions
1.	(), statistical functions , mathematical functions
2.	*, /
3.	+, -

7. Supported Operators and Functions

In MASC GUI, the following operators and functions will be supported for performing operations on image bands.

7.1. Arithmetic Operators

Table 2: Arithmetic Operators in Band Calculator

Arithmetic Operator	Description
+	adding X and Y. If X and Y are image bands, every element of X will be added with every corresponding element of Y. If on adding the bands the result exceeds the given range then the value is divided by the maximum range value and brought within the range. If X is a band and Y is a constant then Y will be added to every element of X. Normal addition operation is performed if X and Y both are constants.
-	subtracting X and Y. If X and Y are image bands, every element of Y will be subtracted from every corresponding element of X. If on subtracting the bands the result is not within the given range then the value is divided by the maximum range value and brought within the range. If X is a band and Y is a constant then Y will be subtracted from every element of X. Normal subtraction operation is performed if X and Y both are constants.
*	multiplying X and Y. If X and Y are image bands, every element of X will be multiplied with every corresponding element of Y. If on multiplying the bands the result exceeds the given range then the value is divided by the maximum range value and brought within the range. If X is a band and Y is a constant then Y will be multiplied to every element of X. Normal multiplication operation is performed if X and Y both are constants.
/	dividing X and Y. If X and Y are image bands, every element of X will be divided by every corresponding element of Y. If the divisor is zero then the dividend will not be divided. If X is a band and Y is a constant then Y will divide every element of X. Normal division operation is performed if X and Y both are constants.

7.2. Mathematical Constants

Mainly two constant values can be used directly.

PI= 3.14159265358979323846

E =2.7182818284590452354

Some of the other constant values which are commonly used are also available like **0.5, 0.0, 1.0, 2.0, 273.15**.

Users can give their own constant values also by giving input from the keyboard.

7.3. Mathematical Functions

Table 3: Mathematical Functions in Band Calculator

Mathematical Function	Description
sqrt(X)	Returns square root of X
pow(X ,Y)	X raised to the power of Y
exp(X)	Returns Euler's number e raised to the power of X
exp10(X)	Returns the value of 10 raised to the power of X
log(X)	Returns the natural logarithm (base e) of X
log10(X)	Returns the common logarithm, the logarithm with base 10 of X
sin(X)	Returns the trigonometric sine of an angle X in radians
sinh(X)	Returns the hyperbolic sine of an angle X in radians

cos(X)	Returns the trigonometric cosine of an angle X in radians
cosh(X)	Returns the hyperbolic cosine of an angle X in radians
tan(X)	Returns the trigonometric tangent of an angle X in radians
tanh(X)	Returns the hyperbolic tangent of an angle X in radians
sech(X)	Returns the hyperbolic secant of an angle X in radians
cosech(X)	Returns the hyperbolic cosecant of an angle X in radians
rad(X)	Converts X from decimal degree to radian
deg(X)	Converts X from radian to decimal degree
abs(X)	Returns the absolute value of X
sign(X)	Returns the sign of A, always one of -1, 0, +1
floor(X)	Returns the largest (closest to positive infinity) double value that is less than or equal to X and is equal to a mathematical integer
round(X)	Returns the rounded value.
ceil(X)	Returns the smallest (closest to negative infinity) double value that is greater than or equal to X and is equal to a mathematical integer
rint(X)	Returns the double value that is closest in value to X and is equal to a mathematical integer. If two double values that are mathematical integers are equally close, the result is the integer value that is even
nan(X)	Returns true if X is a Not-a-Number (NaN) value, false otherwise

7.4. Statistical Functions

Table 4: Statistical Functions in Band Calculator [22-24]

Statistical Function	Description
min(X , Y,....)	Returns the smallest of the elements provided as comma separated list. If a single value is present then the minimum of a 3x3 kernel is calculated for each pixel with all the surrounding pixel values equal to 0. [25]
max(X , Y,....)	Returns the largest of the elements provided as comma separated list. If a single value is present then the maximum of a 3x3 kernel is calculated for each pixel with all the surrounding pixel values equal to 0. [26]
stddev(X , Y , ...)	Returns the standard deviation of the elements provided as comma separated list. If a single value is present then the standard deviation of a 3x3 kernel is calculated for each pixel with all the surrounding pixel values equal to 0.
coef_var(X , Y , ...)	Returns the coefficient of variation of the elements provided as comma separated list
mean(X,Y,...)	Returns the mean of all the elements provided as comma separated list
kurtosis(X,Y,...)	Returns the kurtosis of all the elements provided as comma separated list [27]
skewness(X,Y,...)	Returns the skewness of all the elements provided as comma separated list [28]
meanabsdev(X,Y,...)	Returns the meanabsdev of all the elements provided as comma separated list
variance(X,Y,...)	Returns the variance of all the elements provided as comma separated list. If a single value is present then the variance of a 3x3 kernel is calculated for each pixel with all the surrounding pixel values equal to 0.

7.5. Formulae for the Statistical Functions

$$Mean = \bar{x} = \frac{1}{N} \sum_{j=0}^{N-1} x_j$$

$$Variance = \frac{1}{N - 1} \sum_{j=0}^{N-1} (x_j - \bar{x})^2$$

$$\text{StandardDeviation} = \sqrt{\text{Variance}}$$

$$\text{Skewness} = \frac{1}{N} \sum_{j=0}^{N-1} \left(\frac{x_j - \bar{x}}{\sqrt{\text{Variance}}} \right)^3$$

$$\text{Kurtosis} = \frac{1}{N} \sum_{j=0}^{N-1} \left(\frac{x_j - \bar{x}}{\sqrt{\text{Variance}}} \right)^4 - 3$$

$$\text{MeanAbsoluteDeviation} = \frac{1}{N} \sum_{j=0}^{N-1} |x_j - \bar{x}|$$

$$\text{CoefficientofVariation} = \frac{\text{StandardDeviation}}{\text{Mean}}$$

8. Few Examples of Results Obtained for some Operations

Band Calculator is used to give results which are enhanced versions of original image in the form of a grey scale image. Following are few of the band calculator operation results:

8.1. Expression 1

B1+B2+B3+B4+B5+B6+B7

The above expression gives the following result for an image layer stacked (say) with 12 bands and adding the first 7 bands (Figure 10).

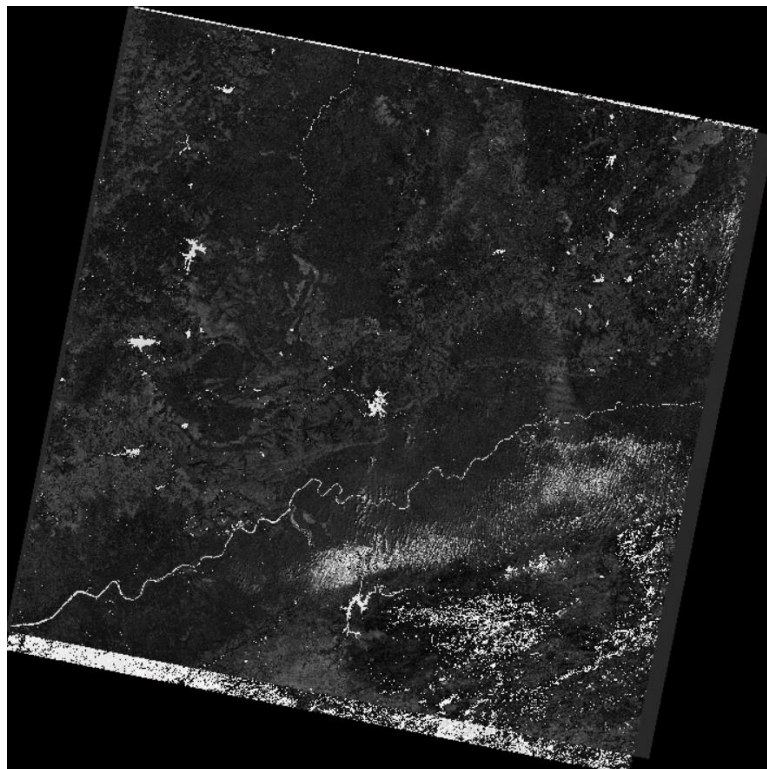


Figure 10: Result of Band Calculator expression $B1+B2+B3+B4+B5+B6+B7$

The pixel values at position let's say (3841, 3841) for bands are:

B1: 10799
 B2: 9922
 B3: 9156
 B4: 8179
 B5: 19399
 B6: 11321
 B7: 7890

Now addition is performed as follows:

Step 1: $10799+9922=20721$
 Step 2: $20721+9156=29877$
 Step 3: $29877+8179=38056$
 Step 4: $38056+19399=57455$
 Step 5: $57455+11321=68776$
 Step 6: $3240+7890=11130$

Since the data we are adding is 16 bit data, in step 5, the addition of 57455 and 11321 gives 68776, this value is out of range as 16-bit data lie between 0 to 2^{16} and the highest 16-bit value is 65535. Since 68776 exceeds 65535 we take the modulus of 68776 by the total number of values in 16 bit data i.e. 65536 giving the remainder 3240 which is the desired value. This value is correct as the 16-bit data can only be within this range and taking the modulus will bring the exceeded value within range.

8.2. Expression 2

$B1+B3*2-B5/B8$

The above expression will be solved according to the order of precedence (as mentioned in 8.1). Evaluating the expression gives the following result (Figure 11).

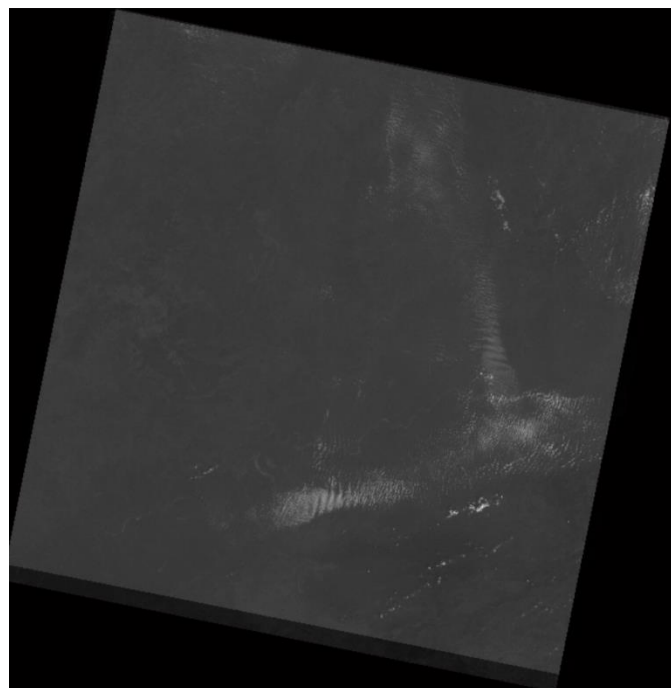


Figure 11: Result of Band Calculator expression $B1+B3*2-B5/B8$

At position (3841, 3841)

Step 1: $B3 * 2 \rightarrow (9156 * 2 = 18312.0000)$

Step 2: $B5 / B8 \rightarrow (19399 / 8780 = 2)$ (**Note: Dividing 16-bit data will give only a 16-bit value**)

Step 3: $B1 + (B3 * 2) \rightarrow (10799 + 18312 = 29111.0000)$

Step 4: $(B1 + (B3 * 2)) - (B5 / B8) \rightarrow (29111 - 2 = 29109.0000)$

Hence 29109.0000 is our answer which is a double value because constant 2 is multiplied to B3 and hence converts the entire expression to double.

8.3. Expression 3

tan (b8)

The band calculator can perform trigonometric operations as well. The tan of the pixel value gives the following result (Figure 12).



Figure 12: Result of band calculator expression $\tan (B8)$

The output value at (3841, 3841) is which is the tan of value 8780 is -0.934339974512928. It first converts the 16-bit number to double and thereafter calculate its tan.

8.4. Expression 4

stddev(B6)

Standard deviation is defined as a quantity expressing by how much the members of a group differ from the mean value for the group. The standard deviation for several bands is calculated by finding

the standard deviation of the comma separated bands in the function `stddev()`. If standard deviation is calculated for single band, then the standard deviation of a 3*3 kernel is calculated with the target pixel being the central pixel. This 3*3 kernel is used for calculating the standard deviation of the entire image matrix. The border pixels of the matrix are set to 0.

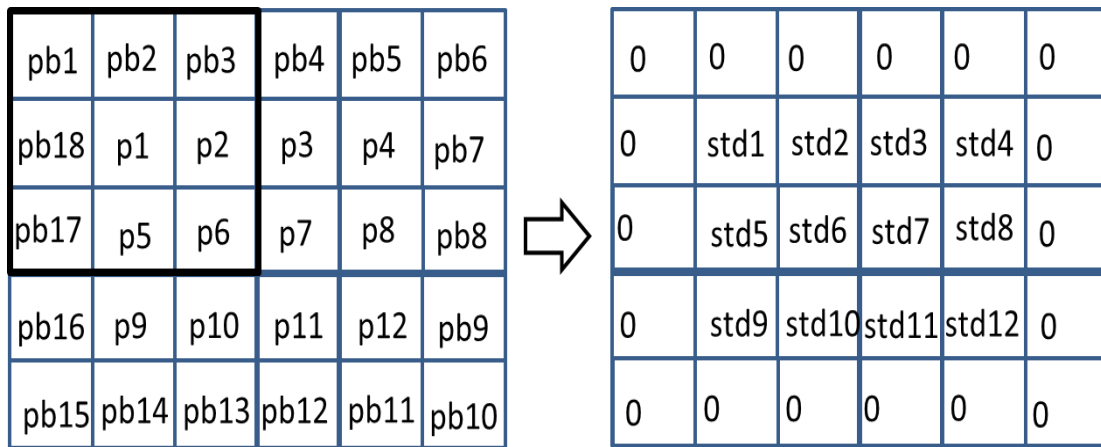


Figure 13: standard deviation calculation for a single band

This 3*3 kernel moves in the horizontal and vertical direction. The standard deviation value is set at the central position inside the kernel. In the above Figure 13 the currently selected kernel is indicated by black box and the value at p1 will be replaced by the standard deviation of the values within the kernel.

The following is the result for calculating the standard deviation for a single band (Figure 14).

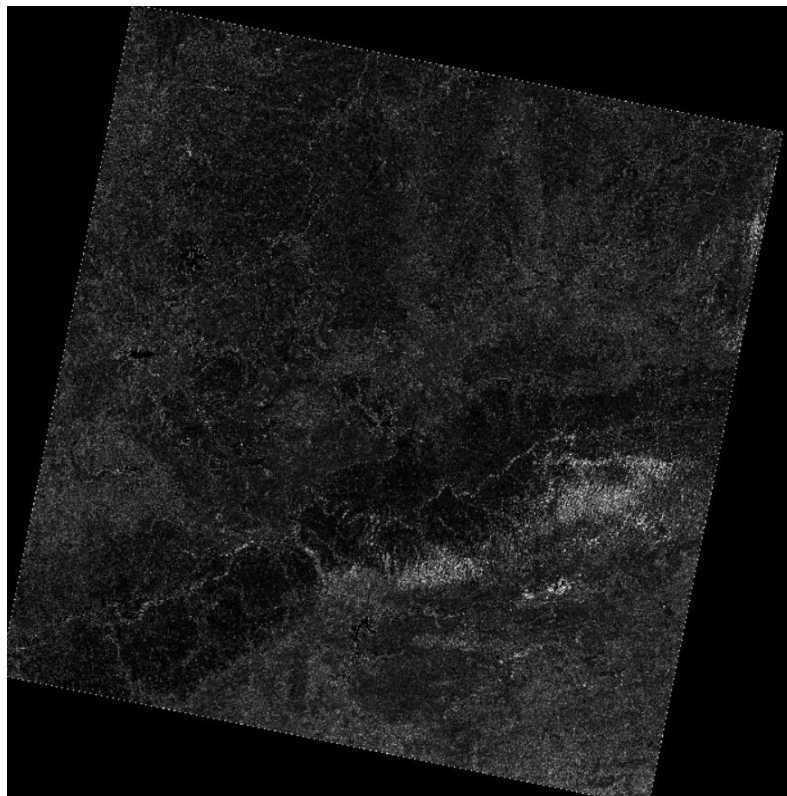


Figure 14: Result of band calculator expression `stddev(B6)`

The pixel dialog box for the band B6 for position (3841, 3841) being the central position in the kernel of 3*3 is as follows (Figure 15):

11158	11137	11272
11210	11321	11326
10267	10412	10316

Figure 15: 3*3 kernel for position (3841, 3841) in band B6

On calculating the standard deviation of this block we get the value 4.588731e+02 which is the desired pixel value we get at position (3841, 3841).

8.5. Expression 5

Skewness (B4, B8, B5, B3)

Skewness is defined as measure of the asymmetry of the probability distribution of a real-valued random variable about its mean. The skewness value can be positive, zero, negative, or undefined. The skewness of bands is calculated pixel by pixel in a similar manner. We have taken bands B4, B8, B5 and B3 of our layer stacked image and applied the skewness function to them. Skewness will be calculated for corresponding pixels of the 4 bands at each pixel position to give the final output as follows (Figure 16):

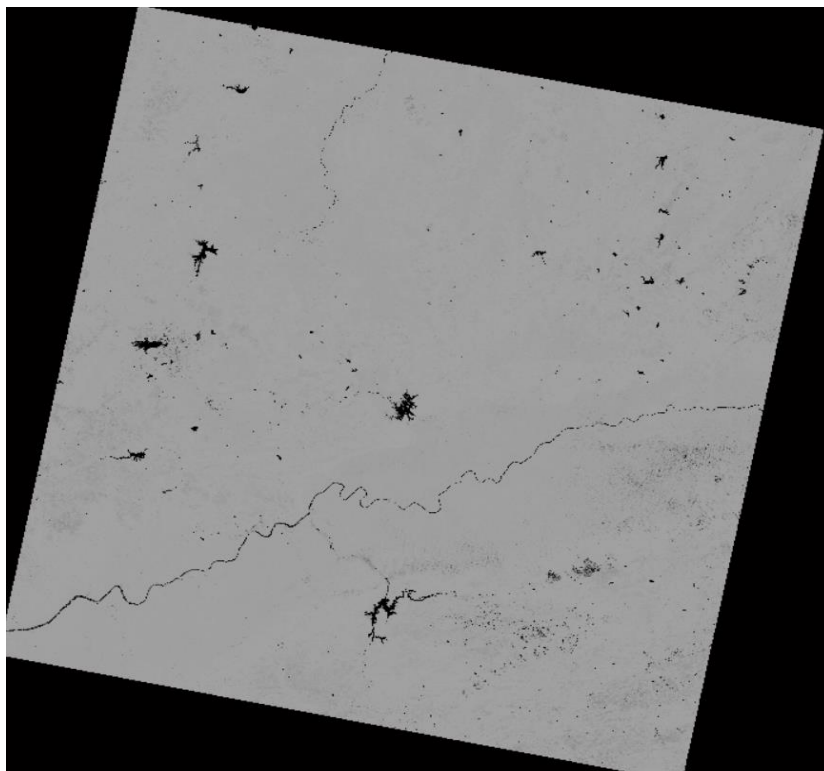


Figure 16: Result of band calculator expression skewness (B4, B8, B5, B3)

The result can be checked with the pixel value at sample position (3841, 3841) in the above image with the help of pixel evaluator. Hence, the skewness at this position is 1.134977957760603.

9. Conclusion

In this paper an attempt has been made to discuss various features of 'MASC' software along with its functioning. Paper explained the basic working of 'band calculator expression evaluator' algorithm and presented the results obtained by band calculator. The results obtained have been cross checked by the pixel evaluator which fetches the pixel value from the image on the screen. These values may be cross-verified by a user with the expected values to be obtained as results. Besides 'band calculator', paper also highlighted other features of 'MASC' software which make the software user friendly and more robust. Authors expect that this paper will be able to boost users' interest in open source free downloadable GUI based 'MASC' Image Processing Software for performing various mathematical and statistical operations on multi-temporal and multi-spectral remote sensing images. Availability of 'MASC' Image Processing Software will be very useful for students of those schools, colleges and institutes where sufficient funding is not available, but students wish to work with freely available multi-temporal and multi-spectral remote sensing images acquired by various satellites. It is expected that proper utilization of various tools of 'MASC' software will certainly enhance students' understanding about remote sensing data by providing option for better interpretation of multi-temporal and multi-spectral remote sensing images. **The exe file of the software can be obtained by sending an email to masc.freeware@gmail.com.** A *.EXE downloadable file will be send to the interested student/researcher. Any queries, suggestions and feedbacks can also discussed by sending an email to masc.freeware@gmail.com.

References

- [1] Centre for Remote Imaging Sensing and Processing. *Principles of Remote Sensing*. [<https://crisp.nus.edu.sg/~research/tutorial/image.htm>]
- [2] Humboldt State Geospatial Online. *Introduction to remote sensing: Image Bands*. [http://gsp.humboldt.edu/OLM/Courses/GSP_216_Online/lesson3-1/bands.html]
- [3] Humboldt State Geospatial Online. *Introduction to remote sensing: Natural and False Color Composites*. [http://gsp.humboldt.edu/OLM/Courses/GSP_216_Online/lesson3-1/composites.html]
- [4] MathWorks: MATLAB 2013a
- [5] MathWorks Help Center. *Create Standalone Application from MATLAB*. [<https://in.mathworks.com/help/compiler/create-and-install-a-standalone-application-from-matlab-code.html>]
- [6] MathWorks Help Center. *Enhance Multispectral Color Composite Images*. [<https://in.mathworks.com/help/images/enhancing-multispectral-color-composite-images.html>]
- [7] Yair Altman. 2011. *Undocumented Secrets of MATLAB-Java Programming*. Chapman and Hall, p.701.
- [8] Mahmut Sinecen. 2016. *Digital Image Processing with MATLAB*. Intech. 43
- [9] Haris Papasaika. *Digital Image Processing Using MATLAB*. [<https://pdfs.semanticscholar.org/ff38/489bbc62d765c8621b32e121ec2814e4fb1f.pdf>]
- [10] Miguel A. Veganzones. *Load ENVI hyperspectral image data with MATLAB*. [<http://www.ehu.es/ccwintco/uploads/d/dc/LoadHypercubesMatlab.pdf>]

- [11] MathWorks File Exchange. *Envi file reader/writer*.
[<https://in.mathworks.com/matlabcentral/fileexchange/27172-envi-file-reader-writer>]
- [12] MathWorks Help Center. *colormap*. [<https://in.mathworks.com/help/matlab/ref/colormap.html>]
- [13] SeaDas Tools. *Band Math Expression Editor*. [<https://seadas.gsfc.nasa.gov/help/visat/ExpressionEditor.html>]
- [14] L3 Harris Geospatial documentation center. *Band Math*.
[<https://www.harrisgeospatial.com/docs/BandMath.html>]
- [15] L3 Harris Geospatial documentation center. *IDL Tips for Use with Band Math*.
[<https://www.harrisgeospatial.com/docs/IDLTipsForUsingBandMath.html>]
- [16] SNAP Tutorials. *Band Math*. [<https://step.esa.int/main/doc/tutorials/snap-tutorials/>]
- [17] MathWorks Help Center. *Pixel Region Tool*.
[<https://in.mathworks.com/help/images/ref/impixelregion.html#d117e168577>]
- [18] Jensen, J.R. 1996. Digital Image Data Formats. *Introductory Digital Image Processing: A remote sensing perspective*. Prentice-Hall, pp.60-61.
- [19] LK Tan, *Image file formats*. Biomedical Imaging and Intervention Journal. 2006.
- [20] MathWorks Help Center. *Matrices and Arrays*.
[https://in.mathworks.com/help/matlab/learn_matlab/matrices-and-arrays.html]
- [21] Geeks for Geeks. *Expression Evaluation*[<https://www.geeksforgeeks.org/expression-evaluation/>]
- [22] Vijay Kumar and Priyanka Gupta. 2012. Importance of Statistical Measures in Digital Image Processing. *International Journal of Emerging Technology and Advanced Engineering*, 2(8), pp.2250-2459.
- [23] Motoyoshi, I., Nishida, S., Sharan, L., and Adelson, E. H. 2007. Image statistics and the perception of surface qualities. *Nature*, 447, pp. 206-209.
- [24] L3 Harris Geospatial documentation center. *Statistics*.
[<https://www.harrisgeospatial.com/docs/Statistics.html#Pixel>]
- [25] MathWorks Help Center. *min*. [<https://in.mathworks.com/help/matlab/ref/min.html>]
- [26] MathWorks Help Center. *max*. [<https://in.mathworks.com/help/matlab/ref/max.html>]
- [27] L3 Harris Geospatial documentation center. *Kurtosis*.
[<https://www.harrisgeospatial.com/docs/KURTOSIS.html>]
- [28] L3 Harris Geospatial documentation center. *Skewness*.
[<https://www.harrisgeospatial.com/docs/SKEWNESS.html>]

Case Study

Workforce and its Impact on the Development of Geospatial Technologies to Support the Delivery Management of Urban Infrastructure: Current Status and Future Needs- A Case Study of Riyadh City, Saudi Arabia

Mohammed Alqarni

Riyadh Municipality, Riyadh, Kingdom of Saudi Arabia

Correspondence should be addressed to Mohammed Alqarni, mhalqarni@alriyadh.gov.sa

Publication Date: 17 October 2020

DOI: <https://doi.org/10.23953/cloud.ijarsg.482>

Copyright © 2020 Mohammed Alqarni. This is an open access article distributed under the **Creative Commons Attribution License**, which permits unrestricted use, distribution, and reproduction in any medium, provided the original work is properly cited.

Abstract Geospatial technologies have created new opportunities for handling spatial information and are becoming more frequently used in many fields. As with other information and communication technologies, receiving growing attention in many disciplines where exerted efforts have been made to take full advantage of their rapid developments. Today, geospatial tools are employed in various fields related to urban management and planning, where they have become important tools in improving decision making. This, in turn, has led to a substantial demand for a qualified workforce able to harness the potential of these technologies. This study focuses on geospatial technology workforces working in the agencies responsible for service delivery in residential neighbourhoods in the city of Riyadh. The Delphi technique was used to understand the needs of the workforce and to highlight the aspects that can support users of these technologies to improve related activities. The study found that there is a shortage of qualified professionals who can bring about the desired outcomes regarding the potential offered by the use of these technologies. Issues of awareness, capacity-building and retention of qualified employees, along with lack of incentives, pose similar problems preventing the development of relevant activities. The results provide a number of strategies that may contribute to positive changes that can be implemented to overcome the challenges.

Keywords *Awareness; Capacity Building; Geospatial Technology; Training; Workforce*

1. Introduction

There is no doubt that the rapid developments in various technologies have played positive role in improving geospatial use and the availability of geospatial data in different contexts. These developments have contributed to providing support to decision makers, where can be used as a common platform to incorporate various database types, represented spatially, into one integrated system to facilitate decision-making. Despite the potential benefits offered by these technologies, the success of their use depends significantly on a qualified workforce who have a combination of specialised skills and competencies. In the city of Riyadh, several public and private sector agencies, concerned with residential infrastructure delivery, depend on the use of geospatial technologies to support administrative workflows and improve the planning processes and decision-making. This takes

on many forms based on the nature of the tasks that fall within the scope of their responsibilities. Although government support has had an impact on enhancing the implementation of these technologies, the development of their use in the context of residential infrastructure delivery is still limited. This study focuses on the human aspects and provides a comprehensive understanding of workforce issues that limit the development of geospatial technologies in the agencies, and the extent of its impact on the development of their activities. It also explores how to address and overcome these issues to achieve the benefits offered by these technologies.

1.1. Background

The rapid development of geospatial technology tools and their capability to improve decision-making have contributed to increasing their use; this has been largely linked to recent developments in the ICT domain. Several studies have discussed the issues of a geospatial workforce. These studies clearly show that the demand for a more qualified geospatial workforce is increasing. They also indicate that the rapid growth in the utilisation of geospatial tools, and the increased availability of spatial data, have created an increasing demand for a workforce having various skills and high expertise in all areas of the geospatial industry (Becony  et al., 2008; Solem and Schlemper, 2008; Disera, 2011; Musakwa, 2017).

Numerous shortcomings have been associated with the availability of a qualified workforce able to harness the potential of geospatial technologies. Understanding the needs of a geospatial workforce is considered a vital component to develop the use of these technologies, where a team of staff with the necessary knowledge, qualifications and skills is required. In fact, the geospatial workforce is made up of a number of individual specialists equipped with multiple skills. With the advancements of ICT, this field is no longer confined to professionals and specialists in geospatial related disciplines. Currently, there are diverse geospatial technology usages entwined with information technologies and other disciplines, which has created difficulties in categorising the needs of the workforce, who are going to use these technologies with a specific set of skills (Marble, 2006; Pettit and Pullar, 2009; Dangermond, 2011; Pfeffer et al., 2015).

Recognising the importance of this, efforts have been undertaken to introduce geospatial technologies as part of the curriculum at different stages of educational institutions systems to meet the needs of current and future workforce. However, this remains a low priority in both developed and developing countries due to a number of technological, pedagogical, administrative and curricular challenges (Favier and Schee, 2014; Chen and Wang, 2015; Starkenburg et al., 2018). As is the case in many countries, the progress of geospatial education in Saudi Arabia has not developed at the same pace as the utilisation of this technology, this is due to a number of administrative challenges and other factors associated with awareness regarding the importance in this field (Al-Garni, 2005; Aina, 2009). In fact, progress in establishing effective strategies and pedagogical practices focusing on geospatial technology education is still being made (Perkins, 2015). This reflects the difficulty in suggesting a unified policy for teaching geospatial technology, where it is often viewed as a field that integrates with many disciplines in different academic departments. Therefore, the academic curricula could not be generalised in order to meet the demand for a geospatial workforce. This, in turn, reflects a decrease in actual enrolment rates of students in geomatics majors. It has also affected the future of the geospatial workforce, which remains undefined as a clear employment category in many countries (Tejpal et al., 2012; Donert, 2015).

The accelerated growth of the geospatial industry calls for further job analyses to be conducted to understand the different occupations associated with geospatial technologies in different contexts, and to provide suitable education and training (Bishop and Grubestic, 2016). Indeed, the use of geospatial technologies is not without its shortcomings, as they may not be accepted by various users due to the lack of necessary skills. Research carried out by Crawford and Young (2008) confirms that the existence of training opportunities, along with educational programmes, has important implications in

meeting the demand of a multidisciplinary workforce who have knowledge and the broad skillset required to master the use of geospatial technology. Giuliani et al. (2013) add that providing suitable levels and quality of education and training, a necessary infrastructure, along with an understanding of the value of geospatial data in decision-making are essential components for capacity building. Meanwhile, Beerens (2006) suggests that capacity building should include not only professionals operating in the field of geospatial, but also managers and other decision makers who are responsible for relevant legislation and institutional arrangements. This, therefore, can help to raise awareness of the geospatial industry in general and making investments in capacity building is imperative to generate the required workforce. Thus, providing a well-trained workforce requires financial investment and considerable resources for successful geospatial technology development.

2. Data Used and Methods

This study seeks to highlight the issues that affect the geospatial workforce in the agencies responsible for planning the delivery of residential infrastructure. The main question that this study aspires to answer is to identify what are the issues faced by geospatial workforce and how are they being addressed. Indeed, answering this question will require taking into account the differences in the activities of geospatial technology, and the aims of their use in each agency. Accordingly, studying and dealing with these issues in a comprehensive manner is critical to determine the most appropriate ways they can be addressed. The Delphi technique was adopted as a means of gathering opinions on the key issues that face a geospatial workforce in their workplaces and to obtain a consensus on the most appropriate ways to address them.

Delphi preparation	Round 1	Round 2	Round 3
- Selection of a panel of participating experts.	(An exploration phase)	(An evaluation phase)	(An evaluation phase)
- Development of the first-round questions.	Face to face semi-structured interview	A structured questionnaire	A structured questionnaire
- Arrangement for conducting the first round.	(Sample size: 20)	(Sample size: 18)	(Sample size: 18)

Figure 1: The Delphi process

The study involved 24 experts representing relevant agencies chosen through purposive sampling. The expert panel consisted of the decision-makers and department managers who are responsible for geospatial activities in agencies concerned with the delivery of residential infrastructure, along with officials representing the national committee for geographic information systems and the e-government programme. The aim was to include experts representing all agencies concerned with the delivery of residential infrastructure and other government agencies that provide the support for working with these technologies (see Table 1). A total of 20 experts agreed to participate in the study, of those 20 only 18 completed the final round. The study was conducted in three iterative rounds in which qualitative data were collected in the first round and quantitative data in subsequent rounds. Qualitative data were collected using semi-structured face-to-face interviews, while quantitative data were collected through questionnaires in electronic format and in hard copy form to experts who did not provide an email address, or who had asked for a printed version. In the first round, all the questions asked in the interviews were open questions to encourage experts' free expression of views and raise issues that were significant to them. The data collected was analysed by using thematic analysis. The most commonly recurring themes were identified, and which served as a basis for the following rounds. The second and third round questionnaire was formulated using the themes

generated from the first round. The analysis of the data obtained in these rounds was based on measures of central tendency (mean) to measure the responses to each item, with the level of dispersion (interquartile range IQR) used to determine the level of consensus of expert opinions (Hsu and Sandford, 2007).

Table 1: Agencies concerned with the delivery of residential infrastructure and other that provide the support for working with geospatial technologies

No	Organisation or Agency
1	Riyadh Municipality
2	The General Department of Education
3	Saudi Post
4	General Directorate of Health Affairs
5	The Branch of Ministry of Islamic Affairs
6	General Directorate of Civil Defence
7	Public Security Department
8	Saudi Telecom Company
9	National Water Company – Riyadh
10	Saudi Electricity Company – Riyadh
11	The High Commission for the Development of Riyadh
12	The National Committee for Geographic Information Systems
13	E-Government Programme (YESSER)

For this research, an IQR of 0 to 1 indicates consensus achieved, which illustrates the difference between the first and third quartiles of the distribution of data ($IQR = Q3 - Q1$). Consensus was reached for 24 of the 28 strategies after the second round while in the third round, consensus was reached for all strategies and, consequently, no further rounds were required.

3. Results and Discussion

3.1. Data Analysis

3.1.1. The First Round

This round sought to elicit experts' views about issues associated with geospatial workforce and the need to improve performance. Semi-structured interviews were used as a tool for data collection. The reason for using the interview method was to enable the researchers, through open discussions with the panel of experts, to explore the issues closely and consider how they can be addressed. The results would then assist in the creation of themes for the following rounds.

Three main themes were identified from the first-round of data analysis. The first theme refers to the issues associated with a lack of awareness among decision makers and relevant employees in the agencies. The views of the experts showed that there are different levels of awareness about the roles and potentials that can be achieved by geospatial technologies, which made developing the use of these tools consistently difficult. As a consequence, this may pose an obstacle to taking full advantage of the benefits that can be brought about by these technologies towards improving decision-making in the context of service delivery.

In addition, the experts frequently expressed that capacity building is an issue faced by most agencies, especially in light of the absence of common strategies and training programmes and the limited role of academic institutions. The difficulty in providing financial support for the rehabilitation of staff and developing the skills necessary to deal with these technologies were also mentioned. The experts also recognised that there is a shortage of a qualified workforce, despite an increasing need. According to

the experts' responses, most of the agencies working in service delivery rely on employees from the relevant consulting offices in this area for the development and use of geospatial technology tools. This gives an indication of the lack of qualified employees who have the required technical qualifications, which in turn affects the development of the implementation of these technologies as well as their uses. At the same time, it has been pointed out that a lack of rehabilitation and continuous development programmes opportunities for employees, and dissatisfaction with the current level of training, have contributed to the low level of use of these technologies for performing daily tasks.

The drain of skilled experienced employees, especially from the public sector, whether at the end of contracted projects or because of a desire to earn better wages was another theme mentioned by the experts. They believe that finding solutions for the retention of such employees is vital. Along with this, the lack of incentives for users of geospatial tools, especially in government agencies, was also raised during interviews. The experts argued that this has affected the development of the required skills of specialist employees as well as encouraging non-specialists to use the tools.

3.1.2. The Second and Third Round

The second round was based on the results from the first round and a review of the relevant literature; a number of strategies were developed to address the issues raised with the aim of obtaining expert opinions regarding the importance of each strategy. In this round, experts were asked to determine the importance of each strategy, using a 5-point Likert-type scale anchored by 1 (not important) and 5 (very important). To enhance this, they were also asked to place comments and add suggestions based on their experiences. The third round sought to achieve further consensus and bridge the gap between the differences in opinions provided in the second round. The strategies, along with rating a summary of the responses obtained from the experts in the second round were also presented. This was to enable the experts to consider the replies given by others in the previous round, and a review of their assessment to reach a final consensus and a common agreement on the final strategies.

The analysis in the first round highlighted the main issues of workforce that have accompanied the utilisation of geospatial technologies in the agencies that provide residential infrastructure. The difference in the level of awareness among decision-makers and employees of these technologies on how to take advantage of the tools available and what they could offer was one of the important issues that hindered the development of their use in context of residential infrastructure delivery. Table 2 below presents the items that achieved a high consensus level within the expert panel, which included a number of activities that aim to raise awareness about the importance of the use of geospatial technologies tools in decision-making related to service delivery.

Table 2: Average rating of the importance of level of the items related to the activities of raising awareness

No	Item	Mean	IQR
1	Holding annual conferences and exhibitions.	4	0
2	Offering free training on the use of multiple geospatial tools and applications.	4.3	1
3	Conducting regular workshops for employees from various agencies.	3.8	0.75
4	Forming specialised communities for practitioners and interested parties.	4.3	1
5	Organising informal meetings between specialists from different sectors to discuss challenges and exchange experiences.	3.8	1
6	Raising awareness through school curricula in various stages of education.	4.1	1
7	Using audio-visual media and social media.	4.3	1
8	Issuing electronic and printed publications.	3.7	0.75

It can be noted that despite reaching a consensus on the elements described in the table above, there is a variance in the mean averages. The elements that had mean averages ranged between (4 and 4.3) can be described as limited activities in the Saudi context. They are also considered a reflection

of the limited opportunities of various agencies to learn about the potential of these technologies for raising the level of awareness. However, it must take into account that undertaking such activities requires wide participation from several sectors along with the agencies concerned with residential service delivery.

Such activities for raising awareness, as referred to by the experts, could contribute to overcoming the associated human behavioural issues in terms of rejecting the use of such technologies. However, the rapid developments in these technologies have created technical difficulties for their users and keeping pace with these changes remains an obstacle for many users in these agencies. The shortage of a skilled workforce within the agencies directly also affected the implementation of these technologies. In this regard, experts were asked to identify the appropriate measures for capacity building to keep pace with the variables of these accelerating technologies. Table 3 below shows that there was agreement on all items that describe these measures.

Table 3: Average rating of the importance level of the items related to capacity building activities

No	Item	Mean	IQR
1	Expanding the educational base through the provision of different degree levels and development of relevant departments and courses in universities and other educational institutions.	4.3	1
2	Increasing employment opportunities for nationals.	4.7	0
3	Raising the job merits for experienced employees in this area.	4.6	1
4	Providing a good job description for specialised employees.	4.3	1
5	Reducing dependence on consulting companies for project implementation and management.	3.8	0.75
6	Providing training and capacity building programmes.	4.5	1

As shown in the table above, the mean values of the items are in the rating average of the importance level of between 4.3 and 4.7 (very important and important), except for the item related to reducing dependence on consulting companies in the implementation of these technologies, which scored the lowest at 3.8 (moderately important). This gives an indication that the experts were not sure whether it is possible to rely on employees in those agencies to undertake all tasks related to geospatial activities. This may in line with their opinions communicated in the first round regarding the shortage of experienced employees in the geospatial field. Therefore, continuing the development of employees and enhancing their skills in handling the variables of these technologies are key elements for achieving optimal utilisation of their implementation. In this respect, the experts' consensus was reached on the items related to improving employees' capabilities as so listed in Table 4 below.

Table 4: Average rating of the importance level of the items related to improving the employees' capabilities in using geospatial technologies

No	Item	Mean	IQR
1	Designing training programmes based upon job needs.	4.7	1
2	Developing specific programmes based on employees' needs.	4.1	1
3	Obliging employees to attend a specific number of annual training hours to develop their skills.	4	0.75
4	Exploiting competencies within different sectors for conducting on-the-job training.	4.3	1
5	Diversity in the provision of training programmes (for example, distance training programmes).	3.8	0.75
6	Raising the level of coordination among the various agencies to conduct joint training.	4	0.75
7	Preparing a list of training programmes and giving employees the right to	3.7	0.75

No	Item	Mean	IQR
	choose the appropriate programmes to develop their skills.		
8	Providing scholarships for employees.	4.2	1
9	Collaborating with academics in preparing and implementing training programmes.	4.3	1
10	Providing financial and moral merits to encourage employees to attend training and relevant professional development.	4.1	1

Similarly, there were also high levels of consensus for items concerning the addressing of challenges of retaining qualified and highly skilled employees in the field of geospatial technologies in those agencies. Table 5 shows the rating average of the importance level of those items, where its noted that they are located within the range between very important and important.

Table 5: Average rating of the importance level of the items related to addressing the challenges of retaining qualified and highly skilled employees in the field of geospatial technologies

No	Item	Mean	IQR
1	Creating an appropriate and healthy work environment.	4.6	1
2	Capacity building and skills development through enhancing training and rehabilitation programmes.	4.5	1
3	Offering promotions and annual increases by the due date.	4.3	1
4	Granting opportunities to further develop professional capacity.	4.3	1
5	Providing incentives and financial support to the best performing employees.	4.6	1

3.2. Discussion

The issues of lack of awareness, training and qualified capacities are among the key issues that face geospatial workforce development, and these pose a challenge to the success of the employment of geospatial tools for planning tasks and improving decision-making related to residential infrastructure delivery. This is the case in many countries; although there has been a growth in the geospatial industry, these issues are still major obstacles towards realising the benefits of the implementation of these technologies (Róiste, 2014). In the context of the study, it can be noted that there are different levels of awareness, whether among decision makers or employees in these agencies around the importance of their utilisation to support cooperation and coordination in the activities of infrastructure delivery. This, in turn, has negatively impacted the achievement of optimal benefits from their implementation, making it imperative upon such agencies to take a structured approach towards raising the level of awareness about the advantages of integration in utilising these technologies, which is consistent with what have been reported by other researchers (Dangermond, 2011; Marsden, 2015).

The results derived from the study show that there is a need for an approach in which all agencies related to the geospatial as well as educational and media sectors participate in raising the level of awareness and knowledge about geospatial potential. This includes ways to take advantage of them not only within professional circles but also amongst the broader public. The measures agreed by experts in this regard are in line with Sullivan's (2007) results, which stressed that the participation of professional and academic sectors in raising awareness and delivering a sound knowledge of the benefits of geospatial technology would improve the understanding and use of these technologies. Such an approach for raising awareness may contribute to overcoming the associated behavioural attitudes issues related to dealing and interacting with new technologies. It may also help with stimulating the acceptance of change in the approach adopted to delivering residential infrastructure. In addition, it offers an opportunity for the exchange of experiences and discussing various issues and

challenges among specialists and interested parties, which in turn support the optimal use of these technologies. Similarly, the promotion of such efforts, especially those directed at the initial stages of education, may enhance the attraction of students to geospatial education pathways and contribute to bridging the gap in the shortage of qualified professionals in this field (Róiste, 2014). However, this requires finding a balance between market demands and different geospatial educational programmes which is difficult to achieve especially in the Saudi context, due to an inadequacy of information that defines the skills and disciplines required for these professions.

In this context, the majority of agencies included in this study were dependent on contracts with consulting companies in this area to carry out tasks related to geospatial activities, and this reflects the shortage of a workforce capable of dealing with these technologies. The current study suggests that improving geospatial educational opportunities and capacity building in these agencies will be an important in addressing this challenge. These results are consistent with a study by Aina (2009), which emphasises the need to expand the training and education in geospatial technologies to develop qualified workforce that meets the expansion in the implementation of these technologies. However, this must be paired with the provision of suitable work opportunities and setting a clear professional identity for graduates, especially in the public sector, which does not provide appropriate job descriptions for geospatial graduates within the classification of governmental jobs. Thus, following a structured approach to address these issues, there is a need for the participation of relevant sectors to determine the functional requirements of the workforce and the actual shortage in disciplines, as well as the determination of training and education areas necessary for the success of these endeavours.

Furthermore, and in the light of the difficulty of recruiting skilled employees who have expertise in the field of geospatial technologies, there is also a need for the continuous development of the workforce in these agencies. The results in this study stressed the importance of developing programmes and plans for the training of the workforce to meet the needs of the skills required to perform their tasks. It has also indicated the importance of diversity and flexibility in training choices and tools as well as the participation of the relevant sectors in implementing these programmes. This, in turn, may provide extensive opportunities for skills development and knowledge sharing. It may also help agencies to overcome funding shortfalls in their implementation. In addition, it can be utilised in the rehabilitation of non-specialised professionals and thus contributes to reducing the burden on the limited workforces available in these agencies. However, those programmes must be balanced in the sense that they include both technical and theoretical aspects and keep pace with the rapid development of these technologies.

Moreover, the results of the study show that capacity building activities are also one of the measures considered very important to retain a qualified workforce in these agencies. Nevertheless, this necessitates setting the systems that help limit the service termination of the workforce after they receive training. The results in this context highlighted the importance of improving employment conditions, wages and providing rewards in addition to moral support. However, this must be coupled with provide a good working environment to attract a qualified workforce. Furthermore, giving them more confidence to lead geospatial activities and reduce the total dependence on employees of consulting companies that perform some of the tasks related to geospatial activities, especially in the public sector. This necessitates the need to improve the systems of contracting with these companies, in that the transfer of their staff after implementing their assigned tasks to them creates a gap in the provision of a qualified workforce to perform the same duties. Therefore, training and raising the efficiency of the workforce must be one of the terms stipulated in contracts to ensure that the implementation of the projects will not be affected after their end. This in turn will play a role in reducing re-employment and training resulting from the loss of expertise, and this may positively affect the development of use of these technologies in various agencies.

4. Conclusion

Geospatial workforces with various specialisations are considered an important element in the development of geospatial activities. The success of utilising this technology is essentially associated with users' knowledge and skills along with the ability to optimally employ their potential. This study draws attention to the issues associated with geospatial workforces in the agencies accountable for providing residential services. It reveals that the current geospatial workforce is lacking, and that the agencies are inadequately prepared to address this issue. The causes are multiple and include limited awareness, capacity building as well as the ability to retain a qualified workforce. The study provides a robust view built on consensus and mutual acceptance among the relevant agencies to determine the most suitable solutions for addressing these issues. However, more efforts need to be made in facing the challenges of introducing such technologies into the working environment and the consequential changes in organisational structures and processes. At the same time, concerted efforts and sustained support on a consistent and continuous basis, within clear and specific programmes, are needed to overcome the obstacles that may arise when implementing the strategies.

Acknowledgments

This study was a part of PhD research. Author would like to express sincere thanks to all who contributed in any way to the production of this study.

References

- Aina, Y.A. 2009. Geomatics education in Saudi Arabia: Status, challenges and prospects. *International Research in Geographical and Environmental Education*, 18(2), pp.111-119.
- Al-Garni, A.M. 2005. Future of geo-sciences can be seen everywhere in the Kingdom. *GIS Development*, (1), pp.32–34.
- Beconytė, G., Govorov, M., Ningal, T.F., Paršeliūnas, E. and Urbanas, S. 2008. Geographic information e-training initiatives for national spatial data infrastructures. *Technological and economic development of economy*, 14(1), pp.11-28.
- Beerens, S. 2006. Building capacity in geo-information handling: addressing diversified needs. *International Archives of the Photogrammetry, Remote Sensing and Spatial Information Science*, 36, pp.45-50.
- Bishop, W. and Grubestic, T.H. 2016. *Geographic Information: Organization, Access, and Use*. Springer.
- Chen, C.M. and Wang, Y.H. 2015. Geospatial education in high schools: curriculums, methodologies, and practices. In *Geospatial Technologies and Geography Education in a Changing World*, pp.67-76. Springer.
- Crawford, C.A.G. and Young, L.J. 2008. Geostatistics: what's hot, what's not, and other food for thought. In *Proceedings of the 8th International Symposium on Spatial Accuracy Assessment in Natural Resources and Environmental Sciences, Shanghai, PR China*, pp.8-16.
- Dangermond, J. 2011. Book Review: *Geospatial Technology and the Role of Location in Science*, Henk J. Scholten, Rob van de Velde, and Niels van Manen (Eds.). Vol. 96 of the GeoJournal Library series. Published by Springer Science+ Business Media BV 2009. *Applied Spatial Analysis and Policy*, 4(2), pp.139-140.

Disera, D. 2011. The Geospatial Workforce Shortage. *Transmission & Distribution World*, 63, pp.22-22.

Donert, K. 2015. Digital earth–digital world: strategies for geospatial technologies in twenty-first century education. In *Geospatial Technologies and Geography Education in a Changing World* pp.195-204, Springer.

Favier, T.T. and van der Schee, J.A. 2014. The effects of geography lessons with geospatial technologies on the development of high school students' relational thinking. *Computers & Education*, 76, pp.225-236.

Giuliani, G., Ray, N., and Lehmann, A. 2013. Building regional capacities for GEOSS and INSPIRE: A journey in the Black Sea catchment. *International Journal of Advanced Computer Science and Applications*, 3(3), pp.19–27.

Marble, D.F. 2006. Who are we? Defining the geospatial workforce. *Geospatial Solutions*, 16(5), pp.14-21.

Marsden, R. 2015. A web based information system for planning support in Barnsley. *Applied Spatial Analysis and Policy*, 8(2), pp.131-153.

Musakwa, W. 2017. Perspectives on geospatial information science education: an example of urban planners in Southern Africa. *Geo-spatial Information Science*, 20(2), pp.201-208.

Gupta, J., Pfeffer, K., Ros-Tonen, M. and Verrest, H. 2015. Setting the Scene: the Geographies of Urban Governance. In *Geographies of Urban Governance*. pp.3-25. Springer.

Pettit, C.J. and Pullar, D., 2009. An online course introducing GIS to urban and regional planners. *Applied Spatial Analysis and Policy*, 2(1), pp.1-21.

Róiste, M. 2014. Filling the gap: The geospatial skills shortage in New Zealand. *New Zealand Geographer*, 70. pp.179-189.

Hong, J.E. 2016. Identifying skill requirements for GIS positions: A content analysis of job advertisements. *Journal of Geography*, 115(4), pp.147-158.

Perkins, R. 2015. Applied geospatial technologies in higher education. *Geospatial Technologies and Geography Education in a Changing World*, pp.77-88.

Solem, M., Cheung, I. and Schlemper, M.B. 2008. Skills in professional geography: An assessment of workforce needs and expectations. *The Professional Geographer*, 60(3), pp.356-373.

Starkenbug, D., Waigl, C.F. and Gens, R. 2018. Nurturing a Geospatially Empowered Next Generation. *Emerging Trends in Open Source Geographic Information Systems*, pp.50-72. IGI Global.

Sullivan, D. 2007. Developing a plan for the national coordination of geospatial technology education: a community college perspective. Master Dissertation. Corvallis: Oregon State University.

Tejpal, M., Jaglan, M. S., and Sharma, K. 2012. Significance of geospatial technology and status of its education and training in India. *International Journal of Geomatics and Geosciences*, 2(3), pp.731–737.

Research Article

Land Use Management in Colombo Municipal Council Area

T.D.C Pushpakumara¹, K.G.M. Ranga²¹Senior Lecturer, Department of Civil Engineering, University of Moratuwa, Sri Lanka²Engineer, Department of Civil Engineering, University of Moratuwa, Sri LankaCorrespondence should be addressed to T.D.C Pushpakumara, pushpakumara@uom.lk

Publication Date: 28 October 2020

DOI: <https://doi.org/10.23953/cloud.ijarsg.494>

Copyright© 2020 T.D.C Pushpakumara, K.G.M. Ranga. This is an open access article distributed under the **Creative Commons Attribution License**, which permits unrestricted use, distribution, and reproduction in any medium, provided the original work is properly cited.

Abstract Colombo city is the commercial capital and the largest city in Sri Lanka. It is located on the west coast of the island and adjacent to the Greater Colombo area which includes Sri Jayawardenepura Kotte. It is the financial Centre of the island as well as a popular tourist destination. As the vast development in the city and the increase of the need of people, People used to gather in the city as well as around the city. So the land requirement of the city is being increased in various ways. So that monitoring the land use against the land use requirement is essential to identify the land use changing patterns in the city. The objective of this study is to detect the land use changes in the Colombo city Municipal Council area between years 2000 and 2016 using spatial data, non-spatial data of Colombo city and analysis data using GIS software.

Keywords *Land use; GIS; Management; Monitoring; Changing Pattern*

1. Introduction

A Geographical Information System (GIS) is a system for capturing, storing, analyzing and managing data and associated attributes, which are spatially referenced (Lyengar, 1998). The concept of the GIS system was begun with the study of John Snow about the cholera that had been distributed through the London city. Then onward in 1962, the world's first true operational GIS was developed by the federal Department of Forestry and Rural Development in Ottawa, Canada by Dr. Roger Tomlinson. Today GIS is being used in various purpose such as scientific investigations, resource management, asset management, environmental impact assessment, urban planning, cartography, criminology, history, sales, marketing, and logistics etc. Land use management is benefited by GIS in many ways as interpretation of results are clear and easiness of understanding (Trung, 2006). Three land use decision elements have been used at regional scale such as (1) the distribution of land cover, population, and human activities over the landscape, or infrastructure; (2) the social organizations present in a region, or structure, and (3) the ideas, values, and attitudes that people have about the particular uses of the land, or superstructure (Smith et al., 1995). In the prospective of proper planning and utilization of natural resources and their management, land use and land cover is very important (Asselman et al., 1995). Geographic Information System (GIS) and Remote Sensing (RS) are now providing new tools for advanced ecosystem management (Sreenivasulu et al., 2014) and also use of satellite data is to take advantage of increasing amounts of geographical data available in conjunction with GIS to assist in interpretation (James R. et al., 1976). Land use of Sri Lanka will increase day by

day with the population increase (Mapa, 2002). It will affect to most of the urban cities, mainly Colombo city which is the largest city of the country as well as commercial capital. With the development of the country needs of people will increase and demand of land will increase. As a solution for the demand of the lands in Colombo city, proper land use management plan has to be made and changing of land use patterns and trends should be monitored. So this study is to identify the land use patterns in Colombo municipal area and forecast the future demand in Colombo city lands.

Colombo city is located on the west coast of the island and adjacent to the Greater Colombo area which includes Sri Jayawardenepura. Because of the natural harbor located in Colombo a lot of sailors were attracted to the country by identifying the advantage of the country. As a result of that country was attacked by Portuguese, Dutch and British successively. As a result of that colonial rulers built Colombo city by giving their priority to the Colombo port area. Afterwards the city was developed mainly concentrated among the port area and towards the northern highland area of Mattakkuliya where housing and warehouses were located. The eastern flood plain remained undeveloped while the southern area and coastal belt of the city attracted the middle and high income inhabitants. The present administrative demarcation is coming from evolutionary development on the Colebrook reforms introduced in 1833 during the British colonial rule. They divided the country into 5 provinces as it is easy to manage. Based on the complexity of the country, again they introduced new provinces to the country in year 1845 to 1889. Finally, it was divided into 9 provinces and no further divisions were carried out in provinces wise until present. Again the country had been divided into 20 districts, and with the time it was changed to 25 districts. Boundaries of these districts have been changed time to time.

In 1991 every district had been divided into sub division called Assistant Government Agent. Later on those division areas were called Divisional secretarial areas and which have been again divided in to Grama Niladhari divisions. These Grama Niladhari divisions are made, of either a collection of small villages or, of a part of a larger village. And again every district was divided in to Municipal Councils, Urban Councils and Town Council by considering the state of the area. In Colombo district there are 13 divisional secretaries, 557 Grama Niladhari divisions, 5 Municipal Councils, 5 Urban Councils, 3 Pradeshiya sabha areas (Source: Census and Statistics, 2012).

In this research it is going to be analyzed Colombo Municipal Council area land use patterns to carry out a better development plan in the city. Approximately 15% of the total urban population of the country lives in Colombo Municipal Council area. Land area of the CMC area is 37.3 squares Kilo meters and consist with two divisional secretariats. Which are Colombo D.S. Division with 35 Grama Niladhari divisions, and Thimbrigasyaya with 20 Grama Niladhari Division. Colombo CMC area consist 5 electorate areas. Which has been divided into 47 wards and 15 postal zones for administrative purposes and as the core area of the country, Colombo city has subjected to vast land use changes because of population increase in the city. The development of the port; the construction of roads and railway lines radiating from Colombo to all parts of the island; the rapid growth of the export trade based on plantation agriculture; the concentration of industrial, commercial, communicational, business and financial, administrative, health, educational, recreational functions in Colombo, attracted migrants to the city. So that the increase of hotels in the city area has been increased. As the almost all the main branches of companies are situated in the city population flow from different areas, cities, villages etc. has been increased.



Figure 1: Colombo Municipal Council Map

2. Objectives

The main objective of the study is to identify the changing pattern of land use in Colombo Municipal Council in Sri Lanka. In order to achieve this main objective, the following specific objectives are also to be achieved.

- To identify the pattern of urbanization.
- To study the main factors of the change in land use.
- To identify the temporal pattern of the land use changes.
- To forecast the future trends and changes in land us

3. Methodology

Case study of the selected area and scope of the research was identified. Study area limited to the Colombo Municipal Area as the current issue is highly effect on that area. Research proposal and literature review were prepared and Data was collected from relevant agencies. Then Data analysis was carried out using GIS software. Flow chart of the methodology is shown in Figure 2.

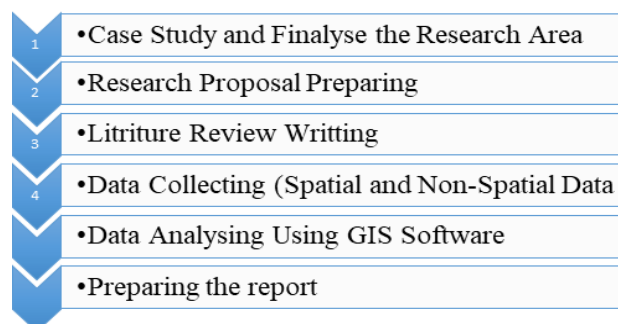


Figure 2: Flow Chart for Methodology

3.1. Data Collecting

In this research, it has collected two types of data to analyses the task. Which are spatial data, non-spatial Census and statistic data. Spatial data was obtained by Obtain by Urban Development Authority. Census data was obtained by Census and static Department. Spatial data that was collected is 2001- 2014. Land use shape files from Urban Development Department. Census and Statistic data of 2001, 2012 from Senses and Static Department.

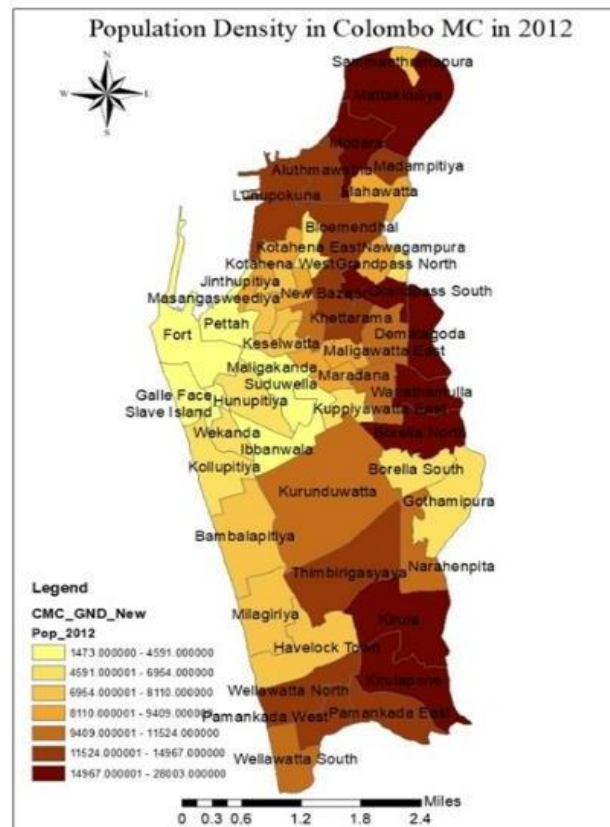


Figure 3: Population Density in CMC area

4. Results and Discussions

Land Extend in Colombo Municipal Council is shown in Table 1. It was divided in to two DS Division namely Colombo and Thimbirigasyaya. Thimbirigasyaya has higher extended than Colombo. The next outcome is population; Population distribution is changing in vast range in the area. High population density is appearing in Kirula, Kirulapone, Grandpass South, Modara, Mattakkuliya, Wanathamulla East, Borella North. Around 15000 to 28000 of population live in these areas. Least distribution of the city is around 1473 to 4591. The least population is identified in Fort area is 1473 (Table 2). The other consideration is Land use pattern; Land use pattern in 2014 at Colombo Municipal Council, Formal law density residential unit, Commercial, Industrial and Transport Units and Formal High Density Residential Units are shown in Figures 4, 5, 6, 7 and Table 3 respectively.

Table 1: Land Extent in Colombo MC

D S Division	Area Sq.km
Colombo	14.59
Thimbirigasyaya	18.29

Table 2: Land use in Colombo MC Area

Land use Type	Area (hectare)
Agricultural land	14.59
Commercial , industrial and transport Units	110441.55
Construction Sites	1310.27
Forest	4499.61
Formal high density residential	220199.72
Formal low density residential	195114.78
Other Natural and Semi- Natural area including wetland	7334.23
Urban Greenery	59289.01
Vacant land not obviously being prepared for construction	15641.61
Water bodies	9028.16

Table 3: Building Units in Colombo Municipal Council

	Colombo	Thimbirigasyaya	Total	Percentage
Single Stories	42881	34040	76921	62.83
Two Stories	15057	11955	27012	22.06
More than two stories	1483	1178	2661	2.17
Attached House/ Anex	2472	1178	3650	2.98
Flat	3001	2380	5381	4.39
Luxury Apartment	505	402	907	0.74
Twin House	389	307	696	0.56
Row House/ Line Rome	1857	1473	3330	2.72
Hut/Shanty	598	475	1073	0.876

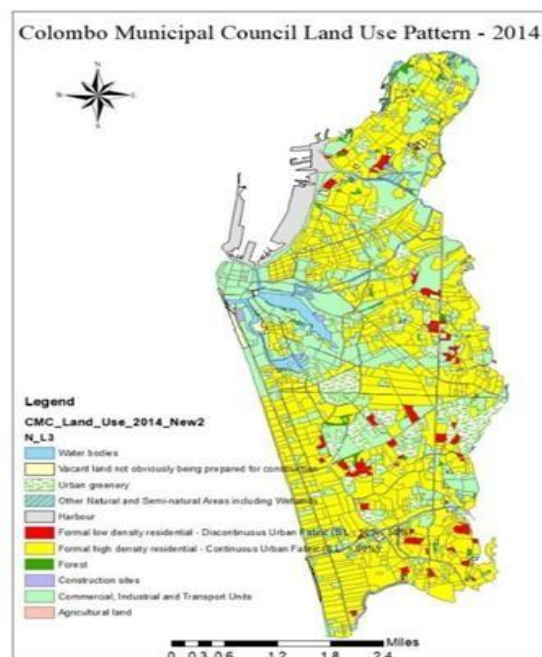


Figure 4: Land use pattern at Colombo Municipal Council

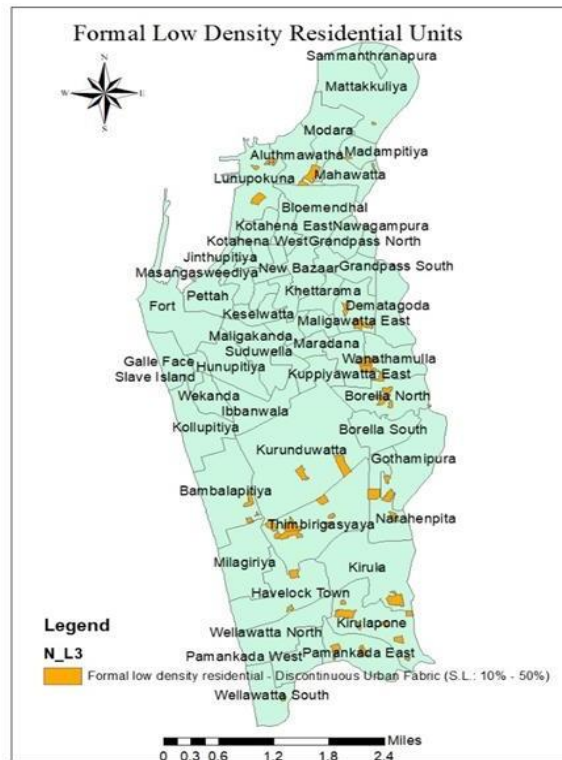


Figure 5: Formal Low Density Residential Units

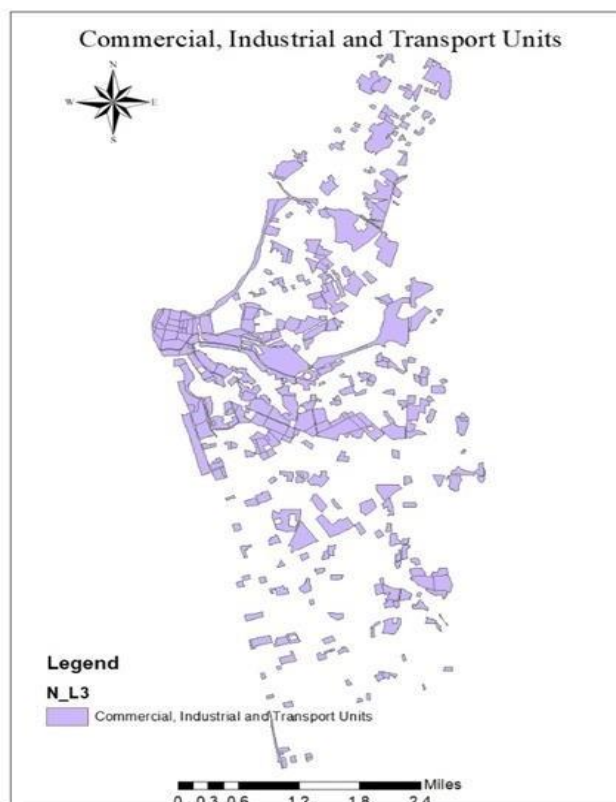


Figure 6: Commercial, Industrial and Transport Units

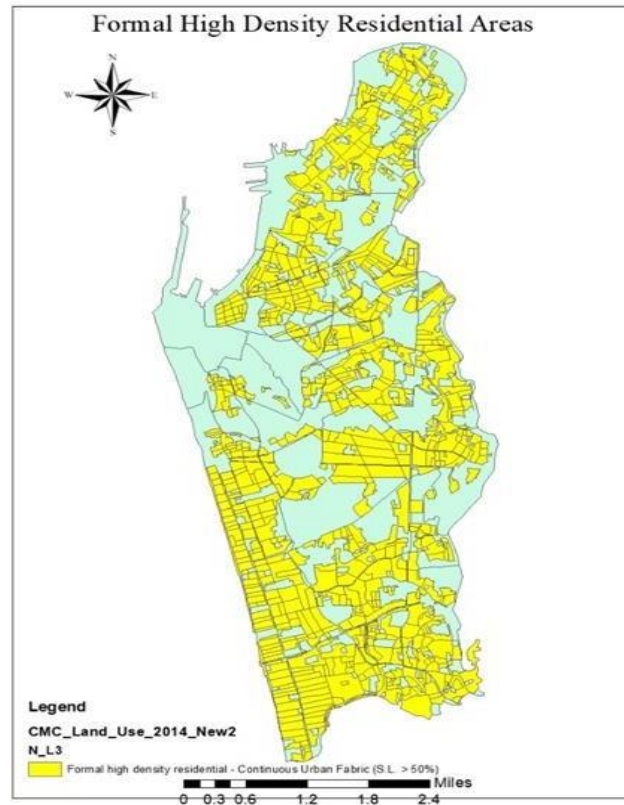


Figure 7: Formal high Density Residential Units

5. Conclusion

Most of urban centers are concentrated at west coast and Southern part of Sri Lanka. Suburbanization process can be identified very fast in Colombo city and surrounding cities around Colombo. When we consider the land use changing pattern in Colombo Municipal Council, we can see high density residential are high in the city while less agricultural land present in the city. No of one story houses, Dwelling, Shanties are a major issue as which reduce the land value of the city. As we can see 62% from the total buildings are single story buildings. Single house more than two story buildings are less than 3 present. As we compared with the population increase of the city near future the city will be over dense and proper rules and regulation have to be amended.

References

Asselman, N.E.M. and Middelkoop, H. 1995. Floodplain Sedimentation: Quantities, Patterns and Processes. *Earth Surface Processes & Landforms*, 20(6), pp. 481-499.

James R. Anderson, Ernest E. Hardy, John T. Roach, and Richard E. Witmer. 1976. A Land Use and Land Cover Classification System for Use with Remote Sensor Data. Geological Survey Professional Paper No. 964, U.S. Government Printing Office, Washington DC, 28.

John Snow, Map as a Lifesaving Tool: Map of Cholera, <https://www.giscloud.com/blog/map-as-a-lifesaving-tool/>

Lyenger, J.V. 1998. Application of Geographical Information System. *Journal of International Information Management*, 7(2), pp.101-117.

Mapa, R., Kumarage, D., Gunarathne, W.D.L., Dassanayake, A.R. 2002. Land Use in Sri Lanka: Past, Present and the Future. *17th World Congress of Soil Science*, 14-21 August, Thailand.

Roger Tomlinson. 1999. *GIS and LIS in Canada*, Chapter 15, In *Mapping a Northern Land: The Survey of Canada 1947-1994*, Gerald McGrath and Louis Sebert eds. McGill-Queen's University Press.

Smith, C.L., Steel, B.S., List, P.C., and Cordray, S. 1995. Making Forest Policy, Integrating GIS with Social Processes. *Journal of Forestry*, 93, pp.31-36.

Sreenivasulu, G., Jayaraju, N., Lakshmi Prasad, T. 2014. Land Use and Land Cover Change Detection Study at Pennar River Estuary, Nellore District, Andhra Pradesh, Southeast Coast of India. *Journal of Geotechnical Engineering*, 1(1), pp.1-9.

Trung, N.H. Tri, L.Q. van Mensvoort, M.E.F. and Bregt, A.K. 2006. Application of GIS in Land use planning A case study in the Coastal Mekong Delta of Vietnam. *International Symposium on Geoinformatics for Spatial Infrastructure Development in Earth and Allied Sciences*.

The Coebrooke–Cameron Reforms <http://countrystudies.us/sri-lanka/13.htm>, U.S. Library of Congress.

Research Article

Analysis and Prediction of Landslide using Drone Image and GIS Techniques- Case Study Aranayaka Area

T.D.C. Pushpakumara¹, P.P.G.P. Madushanka²

¹Senior Lecturer, Department of Civil Engineering, University of Moratuwa, Sri Lanka

²Engineer, Department of Civil Engineering, University of Moratuwa, Sri Lanka

Correspondence should be addressed to T.D.C Pushpakumara, pushpakumara@uom.lk

Publication Date: 24 December 2020

DOI: <https://doi.org/10.23953/cloud.ijarsg.497>

Copyright© 2020 T.D.C Pushpakumara, P.P.G.P. Madushanka. This is an open access article distributed under the **Creative Commons Attribution License**, which permits unrestricted use, distribution, and reproduction in any medium, provided the original work is properly cited.

Abstract Occurrence of Landslides has become a major impact considering the damage a landslide can do in a quick time. Among the natural hazards the country is exposed up to now, severe landslides are the upcoming major issue since it can affect to the lives of people too. In this case study from Aranayaka area, a method is developed to analyses and identify landslide prone areas. The methodology of the research includes collecting terrain data, building a model using geographic information system (GIS), satellite image processing, preparation of a landslide susceptibility potential map and giving recommendations on the landslide hazards. Among the factors that influence a landslide such as drainage, bedrock condition, slope angle range, land forms and etc. (published by National Building Research Organization), the foremost controllable and mostly varying factor. In this research, landslide prone areas are identified using the land use data. Identification of landslide hazards plays an important role in disaster management and risk controlling since a severe landslide can affect several aspects such as human lives, agricultural aspects, economic activities and transportation. This paper includes the background of the entire research that has developed up to current situation. This method can be used around the world as well as in the country.

Keywords *Land Slide; GIS; Drone image; Satellite Image; Disaster Management*

1. Introduction

Landslides occur mainly during monsoon and inter-monsoon seasons are the most pressing natural disaster in the Central Highland of Sri Lanka. 42% of the total populations of the country in 10 administrative districts consider being prone to land slide (Somarathne, 2015).

Geological, topographical map and plant cover maps, satellite images and the information about rainfall information processing in GIS environment and many parameters such as lithology, slope, slope aspect, annual rainfall, land use, distance to waterway, distance to the fault, and distance to road were used for some of previous studies (Shahabi et al., 2012).

National building research organization (NBRO), Sri Lanka has published six factors inducing landslides as (I) bedrock geology, (II) hydrology & drainage, (III) surface overburden, (IV) slope angle range, (V) land use, and (VI) land forms. Among these factors, hydrology & drainage and land use are

recognized as major factors since those need to be monitored time to time and update landslide susceptibility map (Pushpakumara et al., 2013 and Donnarumma, 2013).

A reliable prediction of a natural disaster leads to the safety of lives comfort. According to the facts recorded, 60% of the major disasters have happened in Asia-pacific region. Hence Asia-Pacific region is considered as the most disaster prone area in the world (Report on Disaster management Asia, 2019). The research includes an analysis and prediction of landslides using remote sensing and GIS techniques in Aranayake area.

Each inducing factor has been weighted considering the weightages published by NBRO. Because of the lack of a high quality satellite image of the considered area high quality drone image is used as main data source and digitized using GIS software to extract the land uses. The land uses are categorized as low, medium and high hazardous and by taking intersection with other causative factors, the landslide susceptibility map is generated (Karsli et al., 2008).

2. Data and Methodology

Figure 1 includes the selected area in Aranayake including the area of previous landslide and also considering the different land use patterns.

A socio-economic analysis was done to gather people's intention about the weather condition of the area after the landslide, economic growth of the area after the landslide, what were the main land uses of the area and whether they think those land uses was a main reason for the landslide.



Figure 1: High Quality Drone Image

Since there was no incident of a landslide in this area, no one noticed any clue of a landslide during the rain. Some people have been aware of an incident due to the heavy rain but not evacuated from the area because there was no evacuation plan. According to the survey, people have avoided the permanent evacuation because of the misleading behavior of the officials. This report strongly recommends that it is very urgent to practice successful emergency evacuation plan and informing the warning of a landslide as early as possible.

Weighted maps for causative factors other than land use are shown in Figure 2a, Figure 2b, Figure 2c, Figure 2d and Figure 2e. All the factors have been given a certain weight according to their influence for occurring of landslides as shown in Table 1.

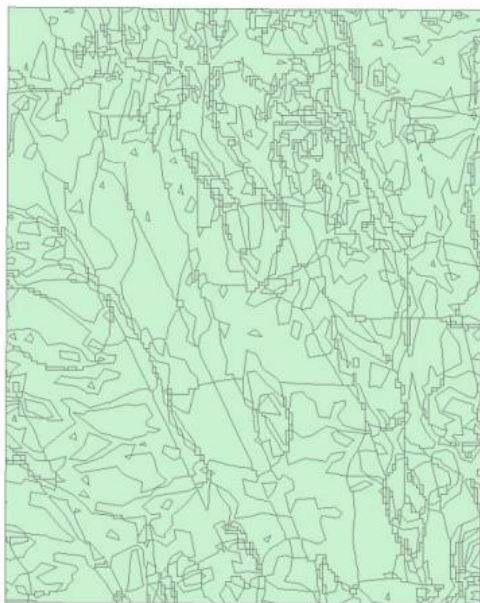


Figure 2a: Bed Rock Geology

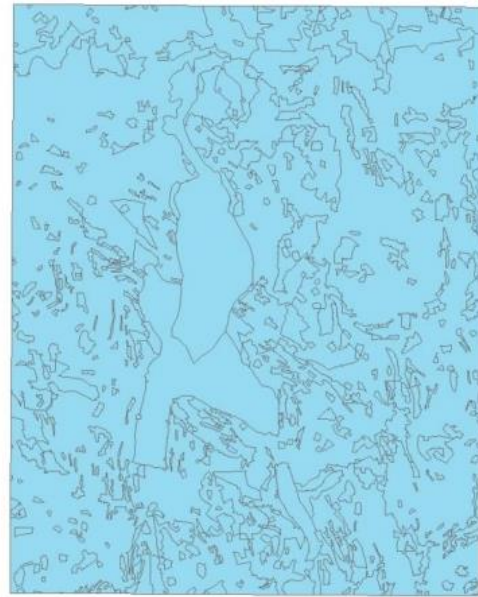


Figure 2b: Hydrology and Drainage



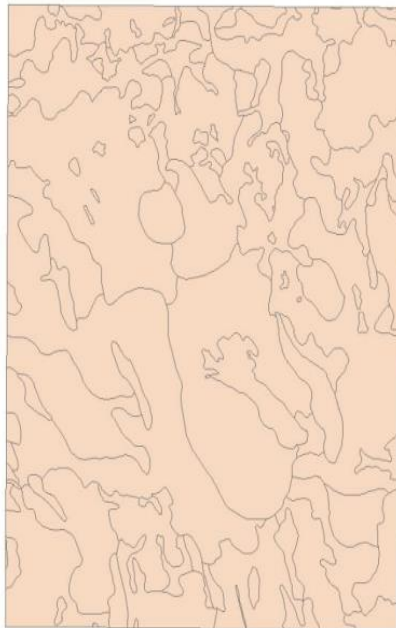
Figure 2c: Overburden



Figure 2d: Land Forms

The previous methodology was to get a panchromatic and a multispectral IKONOS images and analyses them using spatial analysis tool in ArcGIS software to obtain a true color image to recognize the land use patterns (Hari et al., 2018). But due to unavailability of satellite images, the method was slightly changed. The data available was a high quality drone image of the considered area. So that

the image was digitized manually and obtained the distribution of land uses such as Water bodies, Paddy, Rubber, Scrubs, Building, Coconut, Home gardens, Forest area, Grasslands and Tea in the selected area.



0 0.225 0.45 0.9 Kilometers

Figure 2e: Slopes

Table 1: Weights for Causative Factors of Slope Failures

Slope	Maximum Weighting
1 Bedrock Geology	20
2 Hydrology & Drainage	20
3 Surface Overburden	10
4 Slope Angle range	25
5 Land use	15
6 Land forms	10
Total	100

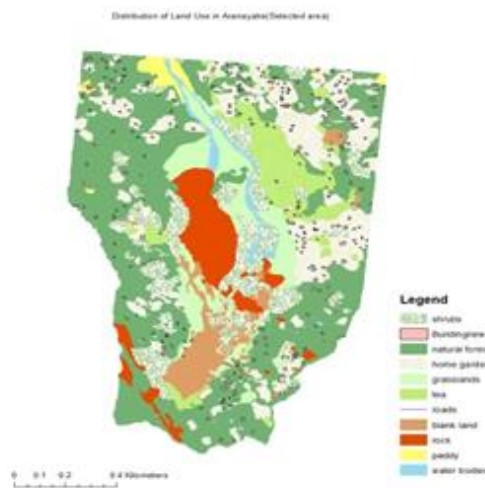


Figure 3: Land use Map

Table 2: Weights for categories of land uses

Linguistic Racing	Score	Factor Classes
Very low	3	Coconut, Forest, Well Manager
Medium	8	Paddy, Rubber, Scrub, Home Garden poor
Very High	15	Water Bodies Grasslands, Buildings

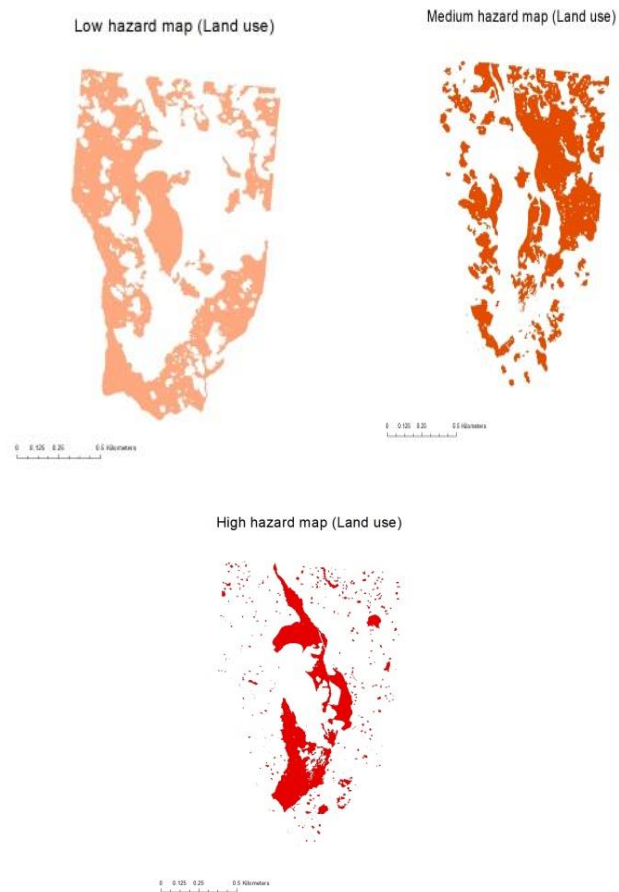


Figure 4(a): Hazard category maps considering Tea as poorly managed

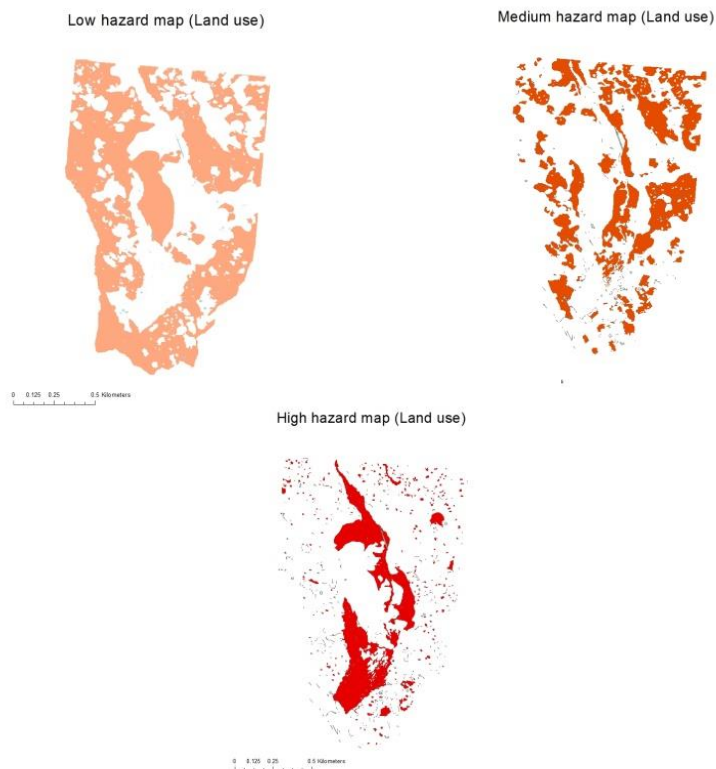


Figure 4(b): Hazard category maps considering Tea as well managed

The contribution of each land use for landslides is different. In the literature, NBRO has considered tea as two aspects as well managed and poorly managed. So that it was essential to consider both aspects since influence from each aspect is different from each other. According to the clarification done by NBRO, three weightages have been given for three categories. The clarification is shown in Table 2. Therefore, three maps were produced consequently for poorly managed tea and well managed tea. Each three maps are shown in Figure 4a and 4b, Figure 5a and 5b.

In case of obtaining the final intersected maps, these two maps were made intersection with other maps of landslide causative factors taken from NBRO. This was done using GIS analysis tools and these two maps can be presented to predict the landslide susceptibility according to the land use distribution of the area (Shahabi et al., 2012). Table 3 shows the arrays of weights of the hazard zonation which are defined by the National Building Research Organization.

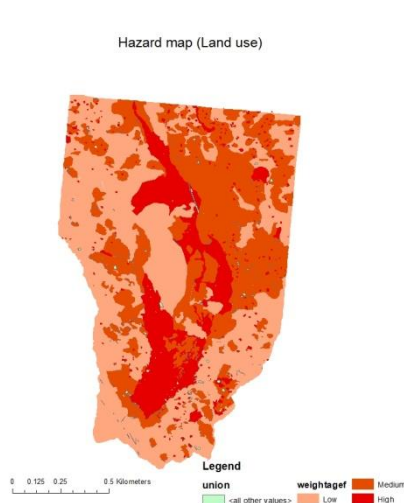


Figure 5(a): Hazard category map considering Tea as poorly managed

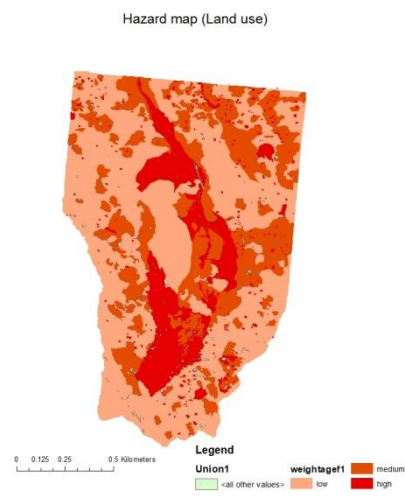


Figure 5(b): Hazard category map considering Tea as well managed

Table 3: arrays of weights for the hazard zonation

Total Score	Slope Failure Probability
>70	Higher hazards
55-70	Medium hazards
40-55	Low hazards
40>	Not likely

Conclusion

This research is proposing a methodology to analysing and predicting landslides using remote sensing and GIS techniques. And it was based on a high quality drone image of Aranayake area. But the accuracy of the research can be improved by using a high resolution satellite image. If a high resolution satellite image was available, a supervised classification and an unsupervised classification can be conducted to obtain a true colour image and a final classified map of different land uses where the land uses are classified by the software.

But due to unavailability of a satellite image to that required resolution, a high quality drone image was used to get the land use map of the selected area. This modelling method can be extended to the whole country to analyse and predict landslides based on the land use factor (Rathnayake, 2014).

References

Donnarumma Angelo, Revellino Paola, Grelle Gerardo and Guadagno Maria Francesco. 2013. Slope Angle as Indicator Parameter of Landslide Susceptibility in a Geologically Complex Area. In: Margottini C., Canuti P., Sassa K. (eds) *Landslide Science and Practice*. Springer, Berlin, Heidelberg.

Hari G., Hara Sudhan, Ganesh R. Aravid, Palani K. Thanaraja. 2018. Multispectral Analysis of satellite image using heuristic Algorithm. *International Conference on Communication and Signal Processing (ICCSP)*, pp1010-1013.

Karsli Fevzi, Atasoy Mustafa, Yalcin Ali, Reis Selçuk, Osman Demir and Gokceoglu Candan. 2008. Effects of land-use changes on landslides in a landslide-prone area (Ardesen, Rize, NE Turkey). *Environmental Monitoring and Assessment*, 156, pp.241-55.

Lynn M. Highland A Guide to Understanding Landslides, The Landslide Handbook, United States Geological Survey, and Peter Bobrowsky, Geological Survey of Canada Hydrology & Drainage.

Pushpakumara T.D.C. and Kodagoda K.G.H.N.R.P. 2013. Analyzing and Predicting of land Slide prone areas as Remote Sensing and GIS techniques. In: *International Conference on Building Resilience- Individual, Institutional and Societal Coping Strategies to Address the Challenges Associated with Disaster Risk Ahungalla, Sri Lanka*.

Rathnayake. 2014. *GIS based Landslide Forecasting Model: A Case Study in Kalutara District*. Master Thesis. Digital library, University of Peradeniya.

Report on Disaster management Asia, Economic and Social Council, Committee on Disaster Risk Reduction. United Nations, 2 July, 2019. ESCAP/CDR/2019/1. www.unescap.org.

Shahabi H., Ahmad B.B. and Khezri, S. 2012. Landslide Susceptibility Mapping Using Image Satellite and GIS Technology. *International Journal of Engineering Research & Technology*, 1(6).

Somarathne M. 2015. Challengers to Overcome: An Overview of Recent Landslides with Reference to Meeriabedda Landslide, NBRO Symposium, 2015, Innovations for Resilient Environment.

Thom A. Bogaard and Roberto Greco. 2015. Landslide hydrology: from hydrology to pore pressure. *WIREs Water*, 3(3) pp.439-459.

Tasseti, N. et al. 2008. Use of Remote Sensing Data and GIS Technology for Assessment of Landslide Hazards in Susa Valley, Italy. *EARSel eProceedings 7*, pp.59-67.

Research Article

Analysis of Land Use Pattern for Tourism Management using GIS

T.D.C. Pushpakumara¹, W.M.S.K. Peris²¹Senior Lecturer, Department of Civil Engineering, University of Moratuwa, Sri Lanka²Engineer, Department of Civil Engineering, University of Moratuwa, Sri LankaCorrespondence should be addressed to T.D.C Pushpakumara, pushpakumara@uom.lk

Publication Date: 30 November 2020

DOI: <https://doi.org/10.23953/cloud.ijarsg.495>

Copyright© 2020 T.D.C Pushpakumara, W.M.S.K. Peris. This is an open access article distributed under the **Creative Commons Attribution License**, which permits unrestricted use, distribution, and reproduction in any medium, provided the original work is properly cited.

Abstract Over the past few decades Sri Lankan tourism has been a story of untapped potential. The responsible parties have been unable to expand the footprint of tourism due to the lack of vision, coordinated planning and strategic commitment to the actions undertaken to accomplish a country's goal. Beyond question, the present tourism industry occupies an integral part of the economy of Sri Lanka. As a result, the negative impact of rapid and uncontrolled tourism development has become an inevitable critical issue. Regarding the indicated facts, this paper offers a remarkable aspect of tourism management defining proper land use patterns via GIS (Geographical Information Systems) for the identified tourism destinations in order to develop the tourism industry further on a both environmentally sustainable and economical platform. The study discusses the capabilities and shortcomings that are possible to encounter, brief description on GIS contribution and also the author's perspective relating to the future tourism strategic plan. Rooted in a GIS based analysis, the author anticipates to design a general framework to evaluate the proper land use systems as well as an infrastructure in effective transformation towards eco-tourism in Welipenna area through Bentota and Meegama river along with novel suggestions in conclusion.

Keywords *Eco Tourism; Land Use Planning; Tourism Development; GIS; Management*

1. Introduction

Sri Lanka has a fast-growing tourism industry and has always been a vast attractive tourist destination over the years (Fernando, 2016). Tourism is the third largest export earner in the economy and contributes about 5% of GDP. According to the latest data released by the Sri Lanka Tourism Development Authority (SLTDA) tourist arrivals have reached approximately 2 million which is a growth of 18% over the past couple of years despite of serious setbacks such as the partial closure of the main airport which highly affected immigration, devastating floods in the southern half of the country which obstructed the access to many resort areas and dengue epidemic in the outskirts of the commercial capital Colombo which resulted an adverse international media publicity that had a negative impact on forward bookings. Except the climatic woes came across, since the cessation of the three decades lasted civil war, the clouds of threatening insecurity has been blown away, rapidly elevating the tourism industry. However, it has not yet been able to utterly unleash the potential of Sri Lankan tourism. The struggling efforts of SLTDA to develop diverse, unique and quality tourism services and products converting Sri Lanka into the Asia's foremost tourism

destination globally has not yet been quite productive although the current position that SL tourism holds in the world is somewhat satisfactory. Opportunities are not captured enough to increase investment and employment effectively. And the Hence in order to expand tourism, a long-term vision and a fruitful mission are required and should be executed not only concerning the economic benefit but also considering the environmental sustainability. This is where sustainable tourism comes on the stage. It dominates an important role in conserving the natural assets while approaching the mentioned objective in transforming the story of untapped potential into a story of utmost success.

Tourism is in fact the fastest growing and the largest industry in the world with an estimated 11.5% of world GDP (Gross Domestic Product) and employing about 12.5% of the world's work force, according to the latest studies of UNWTO (United Nation World Tourism Organization). Moreover, they believe that tourism can be the key to many global solutions for challenges like climate change, poverty reduction, and waste reduction, preserving nature and moving the world to a more sustainable planet which is unthoughtful of many people involved in the industry. Thus, more attention is paid to the concept of sustainable tourism over the past years. (Safran, September 2015)

Sustainable tourism is defined as an industry which less affects the environment and local culture without exposing the fragile ecosystems to a risk of catastrophe whilst thriving the opportunities to enhance tourism targets. The positive of sustainable tourism is to ensure an optimistic development for local people, tourism companies and tourists themselves as well. In simple words, it is the concept of visiting a place as a tourist and departing the place as it was before without any sort of disturbance.

The Global Sustainable Tourism Council is the global leader promoting sustainable tourism. The progress so far encouraging the concept is quite appreciable and noted in many parts around the world. But it is questionable how far we have contributed to this concept as a country that has been able to draw the World's attention in tourism. The foundation and the uniqueness of the Sri Lankan travel experience lie in the inherent breath-taking beauty of the nature specially in hill country and the coastline. Not concerning the very fact might lead to disastrous consequences which would put Sri Lankan tourism at stake. Certain areas in the country already experience this harmful impact due to the rapid non-eco-friendly projects performed in order to develop tourism. When launching the very concept as an actual mission, there are various conflicts to be dealt with and obstacles to overcome. Among them land issues can be considered as one of the top most affective facets in tourism development. (Van Nostrand Reinhold, 1991)

Land management is an essential factor in tourism development. It is the process of optimal use of land resources ensuring maximum utilization. Land is needed for tourism infrastructure and facilities and for tourism associated businesses and services. With the increasing tourist arrivals, there is a mounting pressure to manage land use in high tourism potential areas. Thus, one should have a broad understanding about the demand for lands in order to unravel the tourism land issue. The overall demand for land can be roughly depicted by considering the land: man ratio. With the growth of population, the land: man, ratio has gradually decreased causing a crisis between man and nature. Furthermore, it has given rise to deforestation and invasion of conserved land such as natural habitats and sanctuaries threatening the bio-diversity and biological equilibrium. Since land is used for multiple major purposes such as housing, irrigation, agriculture, etc. and there is only a limited amount of lands available it's rather a hardship to acquire lands for a minor purpose like tourism. Apart from that, lack of land use planning is also partly responsible for the shortage of lands. Land use planning is a widely followed technique mainly to improve the quality life in urban areas which helps to increase overall efficiency of the area. Since resources are limited, they have to be used wisely. Therefore, land use planning and resource allocation must be applied in tourism management as well (Dredge, 1999). Since the success of any tourism business is determined by tourism planning, tourism development and research and tourism marketing.

Geographic Information Systems is a rapidly expanding field enabling the development of applications that manage and use geographic information in combination with other media (Verka, 2008). GIS technology offers great opportunities for the development of modern tourism applications using maps. This technology integrates common database operations such as query with the unique visualization and geographic analysis benefits offered by maps. The integration of tourism data and GIS data is a big challenge for the tourism industry, today. So, using these functions, providing proper land use patterns for tourism industry is a major target of this study. There are lots of cases where GIS has been used to bring significant value in tourism land use planning. The following cases have been selected in order to emphasize remote localities or situations where tourism development is only at the consideration stage and where issues of land uses are on the planning stage at the moment. The significant value of GIS technology therefore, is in its ability to provide desk-top mapping through the graphical display and manipulation of data in order to identify patterns or relationships based on particular criteria. In this way enhanced (value-added) information becomes available for further analysis or to assist in a decision-making process. So, the main purpose of this research is to find proper land use patterns for Sri Lankan tourism industry from GIS functions by covering all tourism destinations. Access to land or a place is a primary requirement for tourism management. Land is needed for tourism infrastructure and facilities, and for tourism-associated businesses and services. So, if there are not enough public lands for tourism, we should have a proper land use management system to develop tourism industry in Sri Lanka.

When considering about the relation between tourism management issues about land use and GIS application followings can be mainly identified to be managed.

- Tourist attracted areas in Sri Lanka.
- Visitor flow management (to identify principal tourist activities within a destination or among destinations).
- Facility inventory and resources use (to identify issues of environmental justice, to identify conflicts, complementary land uses, tourist activities, natural resources).
- Assessing impacts of tourism development (to demonstrate tourism impacts on its surrounding).

GIS was used as an integrating system and analysis tool for the assessment and prediction of parcel-based land-use change. It appears that building permits and cadastral data contain timely and valid information on land use changes. They are the major alternatives of data sources for analysing changes. This is particularly important for tourist destinations, as they are often too small to be analysed using traditional land use change analysis techniques. GIS has advantages over traditional methods in integrating different data sources, performing spatial analysis, and mapping the results into land use studies. The Murrells Inlet study shows that the use of GIS in conjunction with building permits and parcel data can provide adequate information on corridor change, land use change, timing, and spatial change. It is admitted that there are some limitations of this study. These limitations are mainly due to the data constraints and parcel properties. Obtaining the status of building permits (already built or not yet built) and improving data quality are critical to deriving the accurate information of parcel-based land-use change. These things about land use planning can be identified from this report (Jeffery S. Allen, 1999).

In 2005 Bas Boers was conducted to examine the potential of STIP as a tourism planning approach to address sustainability criteria. By integrating social and natural resource data, STIP aims to plan (spatially identify) infrastructure at sustainable sites rather than planning tourism development along existing transport structures that are not necessarily sustainable. Although the generated maps for two visitor segments are the most sustainable trail development sites, some issues still need to be resolved. First, the reviewed literature shows a lack of understanding of "network morphology" and "network connectivity" in terms of visitor satisfaction in specific and sustainable tourism development in general. Further research on these topics is required to come to sustainable trail networks.

Second, there is no statistical technique to analyse visitor preferences simultaneously at a substantial, spatial and temporal coherence level. Consequently, spatial and temporal visitor preferences were not taken into account in the illustrated road networks. The integration of spatial-temporal preferences is a prerequisite for sustainable development of the trail. Third, current GIS do not allow calculation of minimum cost paths while zonal constraints are applied. Therefore, the concept of sustainability could not be fully implemented. However, this "sustainability" constraint may be resolved by adjusting the minimum cost path algorithm (McAdam, 1999)

Given the above limitations and the poor quality and availability of case study data, no conclusions should be drawn regarding the development of sustainable tourism infrastructure in SFR. This does not mean that STIP has no potential as a tourism planning tool. The STIP's three-phase GIS-based methodology allows (to some extent) the inclusion of sustainability criteria in tourism planning. Provided that identified limitations are overcome, STIP allows visitors to guide them to preferred attraction and service facilities, using routes that: consider the experience needs of visitors; minimizing adverse effects on resources; and were developed in accordance with PA development goals. Thus, a higher level of visitor satisfaction can be achieved and maintained, while development-related costs and benefits can be channeled to the right places.

Analysis procedure, using visitor survey data, rendered a 'nature' and 'culture' visitor segment. Segment specific preferences and associated behaviour served, next to natural resource conditions and managerial objectives, as input for the development of carrying capacity and visitor opportunity zones.

Also, another case study on the Land Use Pattern of Kanyakumari District- Using GIS concluded how to decide the type of field patterns and an appropriate area for profitable utilization of land cover features which leads to efficient vegetation. Thus, the work had been carried out for the land use pattern analysis in Kanyakumari District. The analysis had been carried out with the NDVI classification of the respective study area. As such the entire land use had been visualized with the help of ArcGIS mapping software. Land use is the most observable of all environmental changes and assessment of any changes in ecosystem can be observed through the analysis (Vinodhini Shanmugapriya, 2016)

In 2003 Yianna Farsari has done a literature retrieval on GIS applications in tourism has revealed that most applications are concentrated rather on recreation (resources management and planning for national parks) than tourism. Those having as object tourism are primarily focused on identifying the most suitable location for tourism development. Very little attention, if any, is paid on the management and planning needs of already developed, popular destinations. Moreover, regarding sustainable tourism, applications are rather at the side as a consequence of resources management than the objective of the application. GIS applications related to sustainable tourism are mostly concerned with social participation. There is an apparent lack of integrated systems to support planning and management for sustainable tourism. This lack is even more apparent regarding the sustainable management of mass tourism in popular destinations. So, idea of tourism destinations and land patterns using GIS can be identified from this article.

Tourist attractions within the Western region are predominantly beach and water sports oriented, apart from in the Colombo City zone. Other attractions are Urban Tourism, Beach Tourism, Resorts, Entertainment, Night life, Eco and Nature tourism as well as facilities for Golf, Fishing, Surfing, Windsurfing and other Water Sports (Sailing, Boating and Yachting; Kayaking and River Rafting Scuba Diving), Nature tourism and Cultural/ Spiritual Tourism.

It is estimated that 325,000 indirect employment opportunities had been created through tourism within the Western region in 2014. The estimated direct employment was 129,400. By 2020, it is projected that direct employment would increase to 199,200.

As mentioned in SLTDA tourism employment will be increased rapidly in hotels and restaurants sector rather than other sectors. This is well implemented from following Table 1 and Table 2 information.

Considering above literature review and facts Sri Lankan government need to focus on one eco-tourism and cultural tourism therefore, it is need to study following objectives.

(a) *Eco tourism*

- Promotion of nature tourism in the Forest City Zone
- Development of marine infrastructure in the Western Province in order to find natural transport mode.
- Development of Dedduwa river mouth and surrounding area that has many potential attractions with wetland, lakes, irrigation canals and abandoned paddy fields.

(b) *Cultural Tourism*

- The Megapolis Region possesses a vast array of tangible and intangible assets that are of an archaeological, architectural, religious and aesthetic value for tourists and for nature lovers.

2. Research Methodology

The methodology of the research as follows. First the literature review was done based on the tourism land use patterns. Then the common factors that affect for tourism land use management was determined. In Sri Lanka there are so many places that are popular with their attraction in tourism industry and also there are proposed projects such as Megapolis tourism development. In this study it was selected the location mostly considering on calm and quiet environment-based eco-tourist attraction. So, giving a platform for land use pattern for tourists attracted hotels near Welipenna area through Meegama and Bentota River in Kalutara district using GIS is the main idea of my study.

Following steps were followed using the collected data and the analysis was done using Arc GIS 10.3 to find suitable places where tourists are attracted for Nature and Medical cluster in Welipenna area.

After doing the literature survey on tourism attractions, Meegama river area close to Welipenna Expressway exit has been selected according to the ease of access through the southern expressway from the Bandaranaike International Airport according to the topic related to calm and quiet environment-based attraction.

Even though a DEM map was created it is difficult to do the study for the whole area because the area is spread over a broad scope. Therefore, few locations that are suitable for tourism hotels were selected for the study and it may be considered as a case study of the area (Figure 1)

According to the 2012 census & statistic data total population of the area is 7068 and forecasted population of the area for 8608 is which is going to increase by 1540 within 18 years (Figure 2) and Welipenna area has poor population concentration in the Western Region (Figure 3). So, with this Eco-tourism development, we can increase the living standards of people in this area.

Most important parameters that are affected to select this location are as follows.

- Ease of access through southern express way to Location.
- Welipenna service area is the only highway service area available in Sri Lanka and tourist hotel agents can take them there.
- Boat rides can be provided from the Welipenna exit to hotels through Meegama River and Bentota river.
- Good connectivity between other tourist attractive destinations.
- Suitable Hotel locations have analyzed by using Arc GIS software and it was done according to selected GN districts. They are Kurudippita, Henpita, Dippita, Galmatta, Lewanduwa and Welipenna GN divisions.



Figure 1: Selected Area for Study

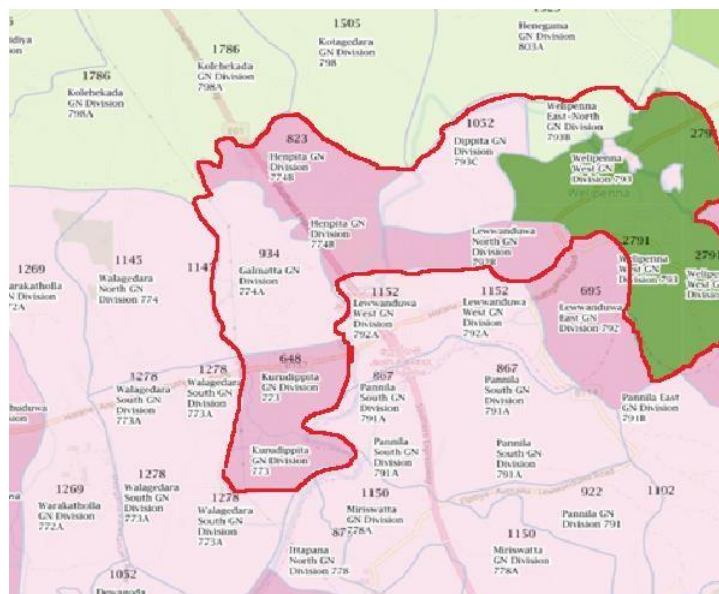


Figure 2: Existing Human Settlement Pattern

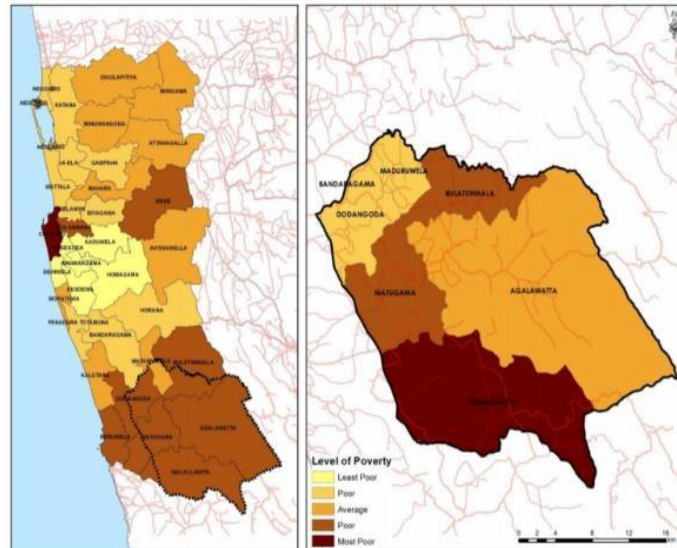


Figure 3: Poverty Level of the Area

2.1. Land Use Pattern

Suitable Hotel locations have analyzed by using Arc GIS software and it was done according to selected GN districts. They are Kurudippita, Henpita, Dippita, Galmatta, Lewanduwa and Welipenna GN divisions.

Most of the lands in Welipenna are occupied by the Rubber and paddy Plantation which accounted 58.16% of the total land area, which offers tremendous opportunity for high value Eco friendly development. A sizable 10.06% of the land is under Forest Cover that needs to be protected. Only 25.24% of the Welipenna area is classified under Homestead and Buildup areas (Table 3).

Table 3: Existing Land Use Pattern

Land Use	Area	Percentage
Rubber	777.33	29.51
Forest	264.99	10.06
paddy	754.68	28.65
Home Land	664.85	25.24
Tea	120.12	4.56
Water Bodies	36.08	1.37
Coconut	16.07	0.61

2.2. Proposed Hotel Developments

(a) Leisure and Recreational Hotels

Propose recreational activities to attract local and international visitors to the area. This will include recreational facilities such as golf, hotels and luxury residences constructed in high ground areas. Luxury and semi-luxury hotels are proposed to the areas which have capabilities to provide endemic cultural experience of the country.

- To attract and keep stay more local and international tourists to the area.
- To increase the connectivity among the tourist attracted places within the region
- To provide opportunities to experience the beauty of nature in a calm and quiet environment.

(b) Medical Tourism Cluster

Proposed to provide Ayurvedic and Western Medical facilities those who seek special medical treatment, which is only possible away from work and make trips to other surrounding tourism attracted places. The importance of promoting alternative medicine i.e. Ayurveda, homeopathy, acupuncture to the western market and promoting western medicine mainly to the ASIAN region.

- To become a global natural tourist attracted destination in South Asia.
- To promote Ayurvedic tourism among foreign countries.
- Benefit the local communities

3. Results

The optimal location was then identified via Arc GIS and the following map illustrates a glimpse of the region in Welipenna including the highway expressway exit (Figure 4). Best locations for tourism hotels are identified and Following Tables (4, 5, 6) and Figure 5 show the observed information.

Table 4: Collected Information

Even	Information
Population	7068
Land Area	2634.12 acres
Avg. Temperature	26.9 C
Avg. Rainfall	3610 mm per year
Warmest Month	April
Coolest Month	January

Table 5: Preferred location for Hotel Development

Location	Access way to boat ride	Distance from Welipenna (Km)
Kurudippita	Boat Ride	2.0
Galmatta	Road(Henpita Rd)	2.3
Henpita	Boat ride	3.2
Lewwanduwa	Road(B157)	4.3
Dippita	Boad ride	5.2
Welipenna North	Boat ride	6.8
Welipenna West	Road (B157)	4.2

Table 6: Derived locations and Access paths for each Hotel developments

Proposed Hotel Development	Selected G N Division	Access Way
Leisure and Recreational Hotels	Henpita	Boat Ride
Medical Tourism Cluster	Dippita	Boat Ride

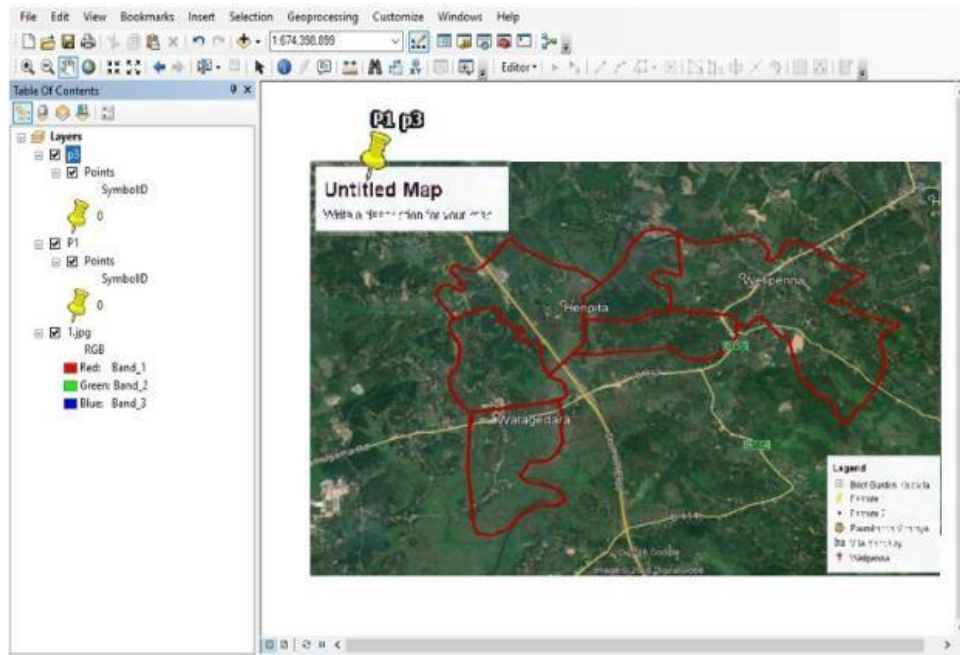


Figure 4: GIS Map Indication

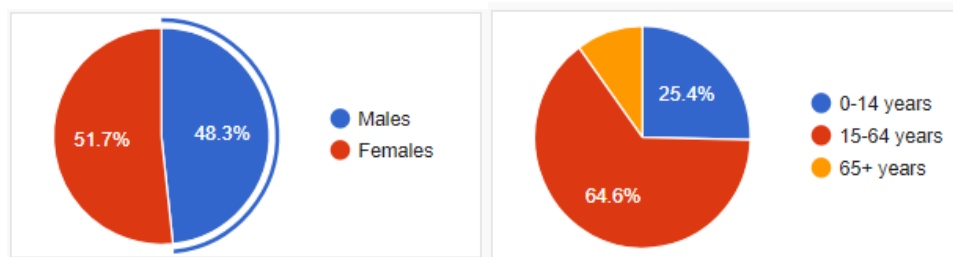


Figure 5: GIS Population Variance

3.1. Connectivity pattern

Road transportation is the dominant mode of travel to Welipenna area as it has no direct Railway connection to the area. Vital national Expressways is Southern Expressway. Welipenna highway exit located along these corridors and tourists can reach to hotels Using boat service through Meegama River (Table 7).

Table 7: Connectivity Pattern Distances

Origin – Designation	Distance (Km)
Bandaranayke international airport to Welipenna Highway Exit	95.1
Welipenna Exit to Megama river	0.3
Boat ride to Hotel	2-6

3.2. Social and Cultural Importance of the Study Area

Most of the social facilities are concentrated in to the upper part (Mathugama) of the area as rest of area mostly concentrated with the forest. Lot of archaeological sites are distributed around the area which provide high potentials for tourism activities (Figure 6)



Figure 6: Connectivity of regions

4. Discussion

After identifying proposed developments and locations analysis part was done by comparing distances to the locations and access ways. Most of GN divisions have both access from by roads and through Meegama river. By considering ease of access and distances Henpita GN division is suitable for Leisure and Recreational Hotels and Dippita is suitable for Medical Tourism Cluster. Finally, We can identified that the Welipenna area is most suitable to develop calm and quite environment based eco-friendly tourist attractive places for future development of Sri Lankan tourism industry.



Figure 7: Tourism Management Style for the study

5. Conclusion

The GIS-based land use analysis has been applied in a variety of situations in present. The idea is to develop a method using GIS because, GIS can play a role in auditing environmental conditions, examining the relevance of sites for proposed developments, identifying conflicts of Interest and Modelling Relationships. The systematic assessment of environmental impact is often hampered by information deficiencies, but also by tools for integration, manipulation, visualization and analysis of data. So, with the help of this GIS applications, research introducing a new land use pattern for calm and quite environment-based tourism management in Welipenna in Kalutara District using GIS and its integration with the principles of Eco tourism development in Sri Lanka (Figure 7)

Future work

- The suitability of the Land use pattern for Develop and manage tourism industry in other regions of the country.
- Possibility of using this method as well as in other tourist categories such as Urban Tourism, Beach Tourism, Resorts, Entertainment.
- Development of Eco-Tourism Hotels and activities in according to this land use pattern and tourism management style.

References

- Bas Boers, M. and Stuart Cottrel. 2007. Sustainable Tourism Infrastructure Planning: A GIS-Supported Approach. *Tourism Geographies*, 9(1), pp.1-21.
- Dredge, D. 1999. Destination Place Planning and Design. *Annals of Tourism Research*, 26(4), pp. 772-791.
- Fernando, S., Bandara, J.S., and Smith, C. 2016. Tourism in Sri Lanka. In M.C. Hall & S.J. Page (Eds.), *The Routledge Handbook of Tourism in Asia*, pp.251-264, Abingdo, Oxon, UK: Routledge.
- Jeffery S. Allen, K.S. (n.d.). *A GIS-based Analysis and Prediction of Land-Use Change in A Coastal Tourism* Presented at the 1999 World Congress on Coastal and Marine Tourism Vancouver, British Columbia, Canada.
- McAdam, D. 1999. The Value and Scope of Geographical Information Systems in Tourism Management. *Journal of Sustainable Tourism*, pp.77-92.
- Safran, Patrick. 2015. *Understanding Land Issues and Their Impact on Tourism Development: A Political Economy Analysis of Pohnpei, Federated States of Micronesia*.
<http://www.sltda.lk/sites/default/files/tourism-strategic-plan-2017-to-2020.pdf>
- The Mega Police Western Region Master Plan
<http://www.slembassykorea.com/eng/download/Megapolis%20Master%20Plan.pdf>
- Van Nostrand Reinhold, Tourism Planning: An Integrated and Sustainable Development Approach. Edward Inskeep, 115 Fifth Avenue, New York, 10003. 1991, p.508.
- Verka Jovanovic. S.U. and Angelina Njegus 2008. The application of GIS and its components in tourism. *Yugoslav Journal of Operations Research*, 18(2), pp.261-272.

Vinodhini E. Shanmugapriya, Veda S. Samhitha, and Geetha, P. 2016. A Case Study on the Land use Pattern of Kanyakumari District Using GIS. *IOSR Journal of Applied Geology and Geophysics*, 4(4), pp.36-41.

Yianna Farsari, P.C. (n.d.). GIS-based support for sustainable tourism planning and policy making. Foundation for Research and Technology Hellas, Institute of Applied and Computational Mathematics, Regional Analysis Division, Heraklion, Crete, Greece.

Research Article

Development on Water Transport System in Sri Lanka with Available Water Resources

T.D.C. Pushpakumara¹, U.L.P. Nimesh²

¹Senior Lecturer, Department of Civil Engineering, University of Moratuwa, Sri Lanka

²Engineer, Department of Civil Engineering, University of Moratuwa, Sri Lanka

Correspondence should be addressed to T.D.C Pushpakumara, pushpakumara@uom.lk

Publication Date: 14 December 2020

DOI: <https://doi.org/10.23953/cloud.ijarsg.496>

Copyright© 2020 T.D.C Pushpakumara, U.L.P. Nimesh. This is an open access article distributed under the **Creative Commons Attribution License**, which permits unrestricted use, distribution, and reproduction in any medium, provided the original work is properly cited.

Abstract Traffic congestion is an enormous problem at peak hours in western province. Existing transport system is not capable to overcome these complexity situations. Therefore, Srilankan government needs to find out different mode of transport to save time and money and finally economy of the country. In the past history, there was a rich water transportation system over the country. Specially, the western province has a well-distributed network of inland waterways, comprising of main rivers, streams, canals, lakes, and tanks. Most of the time, the existing waterways were used for freight transportation (timber, sand, brick, and tiles. compare to Public transportation. The study is to determine the efficient use of waterways for the public transportation focusing the travel time and fuel consumption. The existing water way network was map and find availability of other network connectivity using ArcGIS and Google Earth Pro software. Then compare it with an existing public transportation mode (bus) and checked the suitability of usage of water transportation as an alternative to reduce the existing traffic congestion problem. And proposed water way transport system, that capable of potential and strategic way to reduce the traffic congestion problem in Colombo and its sub urban areas.

Keywords *ArcGIS; Inland Water Transportation; Public Transportation Modes; Traffic Congestion*

1. Introduction

Traffic Congestion is a massive problem in congested towns of Sri Lanka. Especially, in the western province, people lose their time and money due to traffic congestion at peak hours. The average speed of a vehicle has dropped below 10kmph in peak time. The present transport system is not sustaining congestion and traffic delay at peak hours. Several alternative policies have implemented to overcome the situation for public and private transportation. However, it was not come in to satisfactory level. On the other hand, the existing transport system can cause to increase environmental pollution. Therefore, water transportation system is a high potential and environment-friendly alternative to address the issues. It is low cost, fuel-efficient, flexible and safer transport method. The water transportation mode is remarkable solutions for most part of the world and used in Asia, Africa, America, and Europe countries. They use their inland waterways to transport passengers and freight. However, water transport is a rare In Sri Lanka (Animansa and Danimi, 2014). Approximately 90% of land lies in the wet zone in western province. The average annual rainfall is

over 2500 mm (reference). There is significant waterway network Such as Canals, rivers, and tributaries in the area. The Portuguese constructed s the canal system in Colombo area for freight transport. The canals were established from Colombo to Hendala, and also linked Bolgoda Lake in the south to Kotte Lake. Dutch era has contributed to distribute the canal system in the entire country. The most well-known among these was the 02-mile long Colombo-Puttalam waterway which was constructed in 1900. They have built a Canal system and linked the old canal system in Negombo. They introduced the boat service and the boat called padda boat (reference). British time, they used waterways to transport the production of tea, coffee, rubber, and graphite (Ganga, 1981)

Colombo is the capital and largest city of Sri Lanka. Under the Megapolis project, an inland water transportation service in the western province is being developed. It is one effective solution to reduce traffic congestion in the province. Three water transport lines have been identified to develop under this project. Wellawatta- Battaramulla Line (IW1), Fort- Union Place Line (IW2) and Mattakkuliya Hanwella Line (IW3). These lines will establish on Rivers, canals, and marshes in the region. The system for traffic demand analysis (STRADA) was the transport demand model which was used for the Megapolis transport project. The boats are stopped in jetties and those are similar to bus halts in road transportation. According to the modelling, those jetties are located in places which the most demanded and suitable locations with average speed of a boat is 18km/h (Final Report, 2017). Recently, the effective boat service has been implemented by Sri Lankan Navy to transport students and staff of the Open University the route Nawala, Nugegoda to Wellawatta and extended the service from Wellawatta to Battaramulla along the Kirulupone canal (Wijayapala, 2010)

Although, the water transportation is considered as an environment-friendly transport mode, it might be badly affected for the environment such as solid waste disposal, air pollution, operational oil pollution. The solar powered and electric boat can be used to minimize the pollution that occurred by the inland water transportation system. It may be possible to introduce some limitation such as number of boat enters to the system and introduce speed limits to ensure safety of the passengers. In other hand water turbulence and disturbance of inland fishing activities need to be carefully considered before planning of water transport system (Sulaiman et al., 2011). There were few guidelines and methods to design the navigational channel. Among those, mostly used guidelines are introduced by PIANC (Permanent International Association of Navigation Congresses). There are several factors will consider before design a channel.

Such as, the dimension and speed of the ship, maneuvering characteristics, allowances of sedimentation and shoaling etc. ArcGIS and Google earth pro software can be used acquire more accurate and reliable data for analyzing and designing waterway works. These techniques can have used to update data time to time.

2. Methodology and Results

The digital data of Sri Lanka were found from the Survey Department of Sri Lanka. By using ArcGIS software, Separated the western province polygonal layers including the existing waterways and land usage layers (Figure 1). The study area of 10km radius from Colombo fort was taken as case study due to more traffic congested and it can be simplifying to other area as well (Senanayake et al., 2013).

The study selected bus routes which operate in the study area and proposed the terminal point of the waterway network considering land usage of the area and developed the existing waterway network by adding the connectivity. Some of the small new waterway paths need to be added to increase the path between selected terminal. Shorted path between those terminals will be considering when selecting waterway network.

Some canals' widths are small and not able to travel a boat. Therefore, these kinds of waterway need to be modified. Mostly the adding segments were created on the lake, paddy field, and none build-up

area. However, in some places, to create the connectivity of waterway, the small segments had to be placed on the building area.



Figure 1: Existing Waterways in Western Province

Subsequently, these layers were converted to Keyhole Markup Language (KML) format using ArcGIS software and the generated files were opened in Google Earth Pro software. The existence of these routes along waterways was spatially verified and modified by visual analysis with existing features in the satellite imagery at Google Earth Pro. Then compare travel time via inland waterways and existing public transport mode (buses). During peak hours, the study found the travel time via the public road transportation system between selected terminal stations in the study area (Table 1).

Table 1: Average Travel Time by Public Transport (Bus) in Peak hour in Some Selected Routes

Starting Station	Ending station	Peak Hours 7.30-8.30 a.m. Minutes	Peak hour 530-6.3p.m Minutes	Average Travel Time in Minutes
Fort	Narahenpita	40	40	40
Fort	Elakanda	52	55	53
Kotahena	Maharagama	62	65	63
Pettah	Elakanda	45	48	46
Kollupitiya	Wellampitiya	50	55	52
Wellawatta	Narahenpita	36	40	38
Pettah	Kaduwela	70	74	72

To find the travel time via waterways, firstly, waterways were divided into a small segment and measure each segment distance (Figure 2).

Secure speed for all ships that are used in inland water transport must be maintained, sufficient and successful steps taken to prevent a collision are taken and stopped within the same range as the prevailing circumstances and conditions (Navigation Rules and Regulation Handbook, 2014).

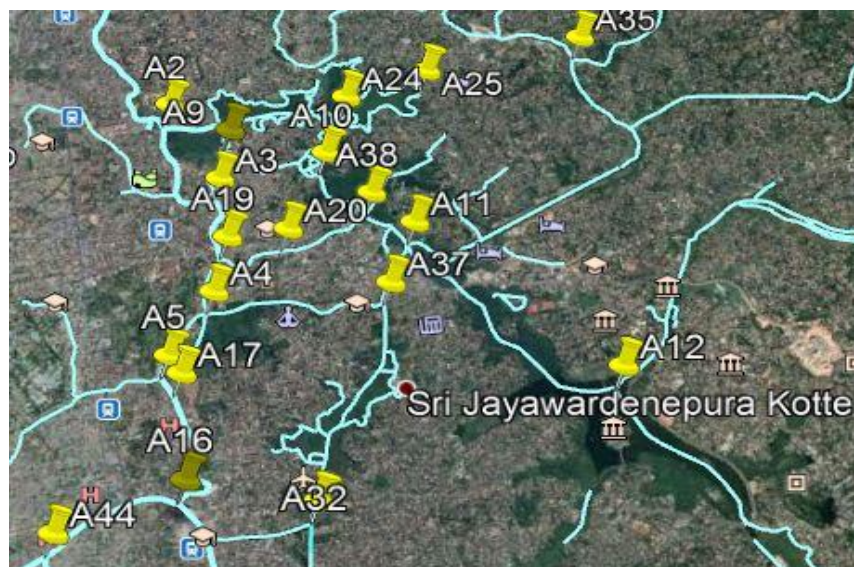


Figure 2: Segment-Wise Divided Waterway Network

When concern about low water levels and the risks involved, the speed will be reduced to 5 knots or less (Transport Safety Victoria, 2019). Regarding all these aspects, the average speed of vessels used in inland water bodies is selected as 7 knots (13km/h). Therefore, the time to be travelled through the inland waterway between the selected terminals was determined by estimating the average speed of vessels as 13 km / h (Table 2).

Table 2: Travel Time through Waterway Network

Starting Station	Ending station	Distance trough water way(Km)	Travel Time Minutes
Fort	Narahenpita	10.3	48
Fort	Elakanda	10.2	47
Kotahena	Maharagama	18.15	84
Pettah	Elakanda	10.2	47
Kollupitiya	Wellampitiya	11.8	54
Wellawatta	Narahenpita	4.4	20
Pettah	Kaduwela	20.6	95

Subsequently, by comparing the travel times via waterways and public road transportation, selected the waterways which could be saved more than 10 minutes compared to public road transportation system (Table 3).

After that, compared the boat fare and bus fare. The fuel consumption was found to be 4.8 l / h for the speed 13 km/h and the power requirement 5.5 hp/ t by assuming the engine burns 0.25 l / h for each horsepower for a boat with an 8 m waterline length and a 3175 kg service condition displacement (Gulbrandsen, 1982). The fuel consumption can be estimated to travel between the selected terminals by using the diesel value in December 2019 (SL Rs.104). Since calculating the cost of transporting the fuel between each terminal, the researcher calculated the passenger's boat charges for transport between each Terminal by adding 30 % to the fuel consumption. Then, separately calculated the boat fare for a Passenger, when the boat capacities are 10, 15 and 25 passengers. The present bus fare between each bus terminal could be finding out by the National Transport Commission (NTC). Table 4 shows a significant reduction of the boat fare per passenger when the number of passengers accommodated by a boat is increased. Further, the boat fare of the passenger is raised relative to the bus fare, when the distances between the start station and end station are increased. In addition to that, the researcher needed to get a rough idea about the initial cost that has to be paid to develop the

existing waterways according to the travel requirement. Assuming the boat beam is 3m, the minimum canal width was calculated to travel along the waterway.

$$W_T = 2W_{BM} + 2\sum W_i + W_{Br} + W_{Bg} + \sum W_p \quad (1)$$

W_T is the final width of the channel, W_{BM} is required channel width for maneuvering of the sail safety in favorable environmental an operational condition, W_i are additional channel widths due to ship speed and wave, W_{Br} and W_{Bg} are the ban clearance sides of navigational channel and W_p is the passing distance. Considering all these factors, final canal's width would be 33m (El-Sersawy and Ahmed, 2005)

Subsequently, the canal width was widened along the proposed waterway paths included in the waterway network (Figure 3) then, to get an idea about initial construction cost; the land area that has to be acquired for the proposed waterways was measured by using existing satellite imagery at Google Earth Pro. Mainly, the researcher has divided those lands into with buildings and without buildings. After, the rough idea can be getting by concerning the percentages of those areas from the total canal area (Table 5)

Table 3: Comparison the Travel Time between Public Transport and Water Transport

Starting Station	Ending station	Travel Time by public Transport (P T)	Travel Time by Water Transport (WT)
Wellawatha	Narahenpita	10.30	48.0
Pettah	Abatale	10.20	47.0
Borella	Jayawwrdanapura	18.15	84.0
Battaramulla	Mattakuliya	10.20	47.0
Pettah	Kaduwela	20.6	95.0

Table 4: Bus Fares in December 2019 with the suggested Boat Fares and Distance between among each Selected Terminal in the Study Area

Starting Station	Ending station	Distance Between each Station (km)	Bus Fair Sri Lankan rupees (Rs)	Suggested boat fare (SL Rs.) with a 30% profit from Fuel consumption to transport		
				10 Passengers	15 Passengers	25 Passengers
Fort	Narahenpita	10.30	19.0	52.0	34.0	21.0
Fort	Elakanda	10.20	32.0	51.0	34.0	20.0
Kotahena	Maharagama	18.15	47.0	91.0	61.0	36.0
Pettah	Elakanda	10.20	32.0	54.0	34.0	20.0
Kollupitiya	Wellampitiya	11.80	28.0	59.0	39.0	24.0
Wellawatta	Narahenpita	4.40	14.0	22.0	15.0	9.0
Pettah	Kaduwela	20.60	39.0	103.0	69.0	41.0
Fort	Rajagiriya	8.98	19.0	45.0	30.0	18.0
Seemamalakaya	Mattakuliya	8.98	32.0	45.0	30.0	18.0
Kalanimulla	Seemamalakaya	14.66	36.0	73.0	49.0	29.0
Pettah	Abatable	10.54	32.0	53.0	35.0	21.0
Pettah	Gothatuwa	9.81	23.0	49.0	33.0	20.0
Kiribathgoda	Angulana	30.07	52.0	151.0	100.0	60.0
Mattakuliya	Soysapura	22.35	47.0	112.0	75.0	45.0
Town Hole	Salmal Uyana	12.35	39.0	62.0	41.0	25.0
Slave Island	Angoda	12.00	32.0	60.0	40.0	24.0
Kotahena	Nugegoda	15.10	39.0	76.0	50.0	30.0

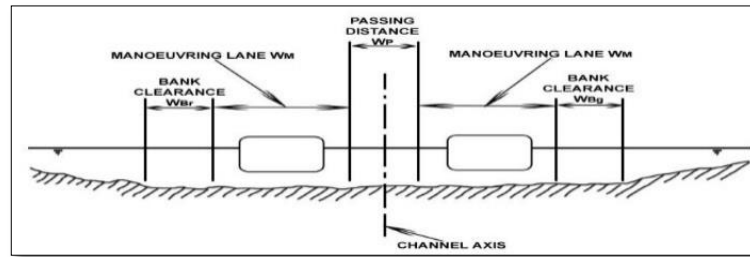


Figure 3: Element of Channel Width

Table 5: The building area and without buildings area measuring and it is comparison with total required waterway area

Starting Station	Ending station	Total waterway area	Land with building area as a percentage from the total area(%).	Land without Building Area as a percentage from the total area (%)
Fort (Colombo)	Narahenpita/ Borella	339900	18.12	15.04
For Kotahena	Elakanda Maharagama	336600 598950	16.25 9.25	9.27 10.34
Pettah	Elakanda	336600	16.25	9.27
Kollupitiya	Welampitiya	389400	11.82	8.48

3. Discussion and Recommendation

According to the comparison of travel time through waterways and public transportation (bus), water transportation is effective than the existing public transportation. In here, the boat speed was taken as 13km/h for safe travel. But it can be increased. Due to the manoeuvring effect, the researcher has limited the boat speed to 13km/h. But when it moves freely (no boat crossing), the boat speed can be increased over 13km/h. So it would be caused to reduce travel time furthermore. As the researcher found, there are few waterway routes that can be used to save the travel time more than 10 minutes at peak time. Therefore, if there is an idea to implement the water transportation system in the Colombo area, it is better to consider these waterway routes as an initial step. Here the boat fares were calculated, considering fuel consumption as 4.8 l / h for the speed of 13 km/h and adding the 30% by the cost of fuel consumption. Table 3 shows, when the number of passengers accommodated by a boat is increased, the boat fares are reduced. It is suitable to accommodate more passengers. Here the Table 6 shows, these waterway routes save travel cost more than Rs.15.00 than the existing public transport mode. Furthermore, boat fares can be reduced by using fuel saving boats. And also, if the electrical boat can be used, the negative effect for the environment due to boat transportation can be minimized and it would be a cost-effective and environment friendly method. Furthermore, compared to the Bus service, the maintenance cost of boat service is low and the initial cost of boat service is lower than the bus service. Subsequently, the researcher has measured the land that has to be acquired for water way to get the draft idea about the initial construction cost. According to that, table shows, the coverage of built-up area is below 25% (1/4) from the total land area which is about to expand (for the expansion of canal width) by the proposed waterway network. The remaining land area (75% - 3/4) comprises from canal (above 50% - 2/4) and non-built-up area (below 25% - 1/4) (Figure 4). Since the built-up area is comparatively low (1/4); the land acquisition process, demolishing process and compensation process are effective in terms of cost and time. Hence the proposed waterway network can be positioned as a feasible project. According to the comparison of travel time and travel cost between the existing public transport method (bus) and waterway transport method, Table 7 shows the significantly effective waterways that can be used to travel among those terminals and it can save time and cost. If water transportation will be added to the transport method in the western province to reduce traffic congestion at peak hours, these waterways can be effectively used.

The proposed waterway network has potential to reduce the traffic congestion in Colombo and its sub urban areas. And also inland water transportation network can be mentioned as a city beautification element. It can attract local and foreign tourists and the water network can be promoted for tourism related activities. The infrastructure facilities of the city area and its sub urban areas will develop in accordance with the initiation of proposed waterway transportation network. The proper maintenance of the water transportation network can preserve the environmental condition and eco system of the canal network by preventing the garbage disposal and wastewater disposal to the canal network.

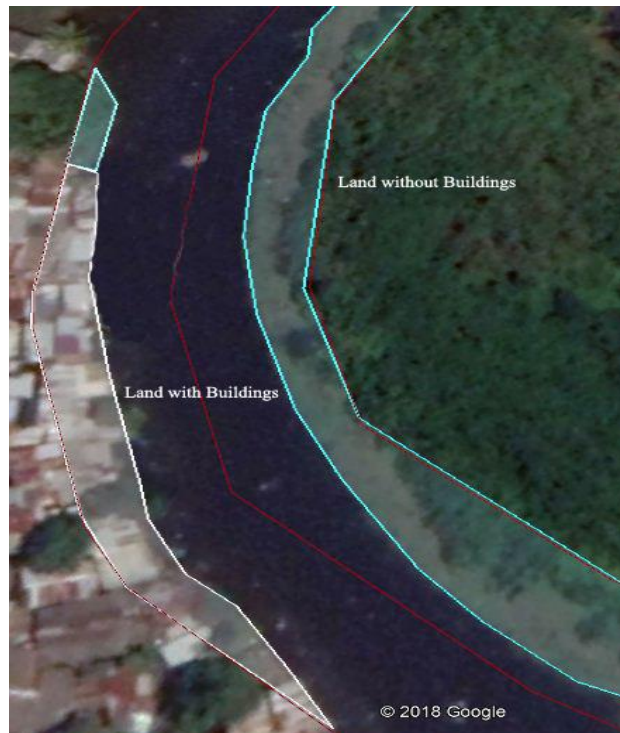


Figure 4: The Building area and without Building Area

Table 6: Comparison between Bus and Boat Fare

Starting Station	Ending Station	Bus Fare(SL Rs)	Boat Fare 25 passenger	Difference Between Bus and Boat Fare
Battaramulla	Pettah	39.0	23.0	16.0
Battaramulla	Mattakuliya	42.0	24.0	18.0

Table 7: Comparison of Travel Time and Travel Cost between existing Public Transport Method and Waterway Transport Method

Starting Station	Ending Station	Travel Time Difference	Travel Fare Difference
Wellawatta	Narahenpitiya	18.0	60.0
Pettah	Ambatale	11.0	11.0
Borella	Jayawadanagama	16.0	12.0
Battaramulla	Mattakuliya	12.0	17.0

4. Conclusion

Considering the travel time and travel cost, it is effective to do a detailed study for the area within a 10km radius from the Colombo fort to propose an inland water transportation network. The selected bus routes which operate in the study area was used to get the terminal point of the waterway network and then considering these points and land usage of the study area and developed the existing waterway network by increasing the connectivity. Therefore, some small new waterway paths had to be added. The existence of these routes along waterways was spatially verified and modified by visual analysis them with existing features in the satellite imagery at Google Earth Pro.

The analysis of travel time comparisons, fuel consumption rate comparisons and fare comparisons the proposed project has more advantages and a considerable level of feasibility. As well as the land acquisition and upgrades of the existing waterway network recorded a less amount of impact. Overall, the proposed waterway transportation can be found as a potential and strategic way to reduce the traffic congestion problem in Colombo and its sub urban areas.

Apart from the solution for the traffic congestion, the inland waterway network is an element of city beautification, magnet for tourist attraction and motivation for environmental preservation.

References

- Animansa B. and Danimi G.I. 2014. Living in high-rise: An analysis of demand for condominium properties in Colombo. *African Journal of Estate and Property Management*, 1(3), pp.56-61.
- El-Sersawy, H. and Ahmed, A.F. Inland Waterways Design Criteria and Its Applications in Egypt. In *Ninth International Water Technology Conference, IWTC9, 2005*, pp. 905-918.
- Final Report, Pre-Feasibility Study, Inland Water Based Transport Project (Phase I) Western Province Sri Lanka. Ministry of Megapolis and Western Development Sri Lanka Land Reclamation and Development Corporation in collaboration with Western Region Megapolis Planning Project, April 2017, pp. 4-90.
- Ganga, K. 1981. Spread of the Canal Network. *Economic Review*, August, pp.3-13.
- Gulbrandsen, O. *Bay of Bengal Programme, Development of Small- Scale Fisheries*. The Ministry of Fisheries, Sri Lanka, 1982, pp.1-34.
- Navigation Rules and Regulation Handbook*. Department of Homeland Security United States Coast Guards, Aug. 2014, pp.1-8.
- Sulaiman, O.O., Saharuddin, A.H., Kader, A.S.A., and Laily, A.R.N. 2011. Safety and Environmental Risk and Reliability Model for Inland Waterway Collision Accident Frequency. *International Journal of Energy, Environment and Economics*, 5(4), pp.461-477.
- Senanayake, I.P., Puswewala, U.G.A. and Pushpakumara, T.D.C. 2013. A GIS Based Analysis on Use of Inland Waterways for Public Transportation in the Western Province of Sri Lanka. *Engineer-Journal of the Institution of Engineers, Sri Lanka*, 46(2), pp.1-11.
- Transport Safety Victoria, State Government of Victoria, Australia. *Safe passenger transport and boating for all Victorians*, Available: <https://transportsafety.vic.gov.au/> [Dec. 02, 2019]
- Wijayapala, R. 2010. Canal transport turns Colombo into another Venice. Sunday, October 10, *Sunday Observer Plus*, pp.2-5.